UNIVERSITY OF NEWCASTLE UPON TYNE

DEPARTMENT OF CIVIL ENGINEERING

THE INFLUENCE OF COHESION ON SEDIMENT MOVEMENT IN CHANNELS OF CIRCULAR CROSS-SECTION

by

ENRIQUE M. ALVAREZ-HERNANDEZ

Thesis submited in fulfilment of the requirements for the Degree of Doctor of Philosophy in Civil Engineering.

December 1990

To My Family

ACKNOWLEDGEMENTS

I like to express my gratitude to the Department of Civil Engineering, University of Newcastle upon Tyne, for providing the experimental facilities. I also appreciate the support of the Science and Engineering Research Council (SERC).

I am especially grateful to Dr. C. Nalluri, under whose guidance this study was conducted, and who has generously given his time, assistance and valuable comments during the experimental work and during the writing of this thesis.

I also wish to express my appreciation for the technical support provided by the staff of the Hydraulics Laboratory of the Civil Engineering Department, especially Mr.A. Jefferson and Mr. Peter Dawer. Thanks are also due to Mr. T. Edmonds for his invaluable help in the operation of the computer and laser equipment.

Special acknowledgments are due to the University of Santiago of Chile (USACH) for their unconditional support by granting a leave of absence, during all these years. I specially wish to express my gratitude to Mr. Luis Gomez, Director del Departamento de Obras Civiles and to Mr. Hernan Ayarza, Vicerrector Academico, for their encouragement and support.

I am also indebted with The British Council for providing the grant that made possible for me to come to Newcastle, and also for all the support, which I received from them during and after the period of the grant.

Finally I like to express my deep gratitude to my wife, Rosita for her love, patience and understanding, and to my parents Ramon and Teresa for their unconditional support and encouragement.

ABSTRACT

The presence of sediment deposits in sewers causes loss of their hydraulic capacity. This could eventually lead to various operational problems such as surcharging, surface flooding and premature operation of overflows with the consequent increase of pollution of water courses.

The present study has covered hydraulics, deposition, erosion and sediment transport in channels of circular cross-section, all with sediment bed. Throughout the programme comparisons between cohesive and non-cohesive sediment results were made. Velocity, turbulence and shear stress distributions obtained for various bed thicknesses showed dependency on the shape effects (bed thickness, bed roughness, flow depth and slope) of the channel. Bed shear stresses predicted using Einstein-Vanoni's separation technique were comparable to the measured values.

Initiation of erosion experiments with uniform non-cohesive sediments yielded lower threshold values of mean shear stress than those published for wide channels (i.e., Shields' curve). However, when sand and cohesive additives (china clay, oil, petroleum jelly, etc.) were used in the experiments a substantial increase of the critical shear stress was observed. This increase was dependent on the amount and concentration of the cohesive additive.

A link between laboratory and field (actual sewer sediment behaviour) however, was essential in order to relate the experimental results to sewers. As a result of chemical and rheological studies (Williams and Williams, 1988) of UK sewer samples a synthetic sewer sediment was suggested (Laponite RD clay, sand and water in various proportions) for flume testing. The experimental results showed that for a given clay-gel concentration there is an optimum proportion of sand to clay-gel to achieve maximum resistance to erosion. It was found that only freshly deposited weak sediments (less cohesive Type C sediment) will erode at shear stresses of around 2.5 N/m^2, whereas slightly consolidated (Type A - Crabtree, 1988) sediment will erode at around 6 to 7 N/m^2. Transport experiments using cohesive and non-cohesive sediments resulted in lower shear stresses for non-deposition conditions compared to those corresponding to wide rectangular channels.

The study resulted in establishing the hydraulics (though limited) of sewers with deposited beds, erosion thresholds of non-cohesive (uniform and non-uniform mixtures) sediments and cohesive sewer sediment of different degrees of strength. Additionally, it has been possible to establish the transport rates of cohesive sediments (during high flows) over fixed (consolidated) sediment beds likely to be deposited during low flows (DWF). This led to a better understanding of erosion and transport processes of cohesive sediments.

CONTENTS

5. SUMMARY OF CONCLUSIONS AND RECOMMENDATION FOR FURTHER WORK

LIST OF FIGURES

CHAPTER FOUR

FIGURE 4.57: COMPARISON WITH MAYERLE'S EQUATION FOR RECT. CHANNELS NON-DIMENSIONAL VELOCITY PARAMETER Sediment Transport Over Fixed Beds - Limit Deposition Condition

FIGURE 4.58: COMPARISON WITH KITHSIRI'S EQUATION FOR RECT. CHANNELS NON-DIMENSIONAL VELOCITY PARAMETER Sediment Transport Over Fixed Beds - Limit Deposition Condition

FIGURE 4.59: COMPARISON WITH MAYERLE'S RESULTS FOR RECT. CHANNELS NON-DIMENSIONAL SHEAR STRESS Sediment Transport Over Fixed Beds - Limit Deposition Condition

FIGURE 4.60: COMPARISON WITH KITHSIRI'S EQUATION FOR RECT. CHANNELS NON-DIMENSIONAL SHEAR STRESS Sediment Transport Over Fixed Beds - Limit Deposition Condition

LIST OF TABLES

CHAPTER FOUR

TABLE 4.14: INITIATION OF EROSION EXPERIMENTS (SYNTHETIC SEWER SEDIMENT)

(Laponite Clay-Sand-Water Mixtures)
Sand size 600-1180 um (0.89 mm)
D = 154 mm E = 18.4 mm (smooth bed)

TABLE 4.15: INITIATION OF EROSION EXPERIMENTS (SYNTHETIC SEWER SEDIMENT)

(Laponite Clay-Sand-Water Mixtures)
Sand size 90-150 um (0.12 mm)
D = 154 mm E = 18.4 mm (smooth bed)

TABLE 4.16: SUMMARY OF SYNTHETIC SEWER SEDIMENT EXPERIMENTS

Laponite clay-sand-water sediment erosion studies
D = 154 mm E = 18.4 mm (smooth bed)

TABLE 4.17: TRANSPORT EXPERIMENTS OVER LOOSE BED (NON-COHESIVE SEDIMENT)

Flume 154 mm dia. E = 18.4 mm

TABLE 4.18: TRANSPORT EXPERIMENTS OVER FIXED BED - NO DEPOSITION

CONDITION NON-COHESIVE SEDIMENT

Flume 154 mm dia. E = 18.4 mm (smooth bed)

TABLE 4.19: TRANSPORT EXPERIMENTS OVER FIXED BED - NO DEPOSITION

CONDITION NON-COHESIVE SEDIMENT

Flume 154 mm dia. E = 18.4 mm (rough bed k = 2.3 mm)

TABLE 4.20: CONSTANTS IN EQUATION 4.33

TABLE 4.21: TRANSPORT EXPERIMENTS OVER FIXED BED - NO DEPOSITION

CONDITION COHESIVE SEDIMENT20% clay gel c = 24 g/l
80% sand d = 0.9 mm
Flume 154 mm dia. E = 40.8 mm (smooth bed)

TABLE 4.22: TRANSPORT EXPERIMENTS OVER FIXED BED - NO DEPOSITION

CONDITION Cohesive Sediment:20% clay gel c = 30 g/l
80% sand d = 0.9 mm
Flume 154 mm dia. E = 40.8 mm (smooth bed)

CHAPTER ONE

INTRODUCTION

The presence of sediment deposits in sewers has been shown (CIRIA, 1987) to occur in many older combined sewer and surface water drains. It is suggested that up to 25,000 Km of sewers and drains may be affected nationally. Sediment deposition in sewers causes loss of their hydraulic capacity, which eventually leads to various operational problems such as surcharging, surface flooding, premature operation of storm sewage overflows (SSO), with the consequent increase of pollution of water courses, etc., and it is estimated that this may cost the country some £ 60 millions a year.

It is believed (WRc, 1986) that a large proportion of the pollutant load discharged during storm events (operation of SSO) is derived from the erosion and re-entrainment of material that has previously been deposited in the sewer system. Although river pollution from SSO is generally infrequent and of a transient nature, it often may be of sufficient magnitude (in terms of concentration, load and frequency of discharge) to be the critical factor limiting the ecology of many urban water courses.

Therefore there is a need (CIRIA, 1987) for re-examination of the current state of knowledge of the processes of sediment movement (deposition, re-entrainment and transport) in sewers and of the design approaches.

An important factor in the design of sewerage systems is the minimum gradient at which pipes need to be laid. Under the current design practice these minimum gradients are determined using the self-cleansing velocity criterion. The British Standard Code of Practice CP 8005 (1986) on sewerage recommends the use of a minimum velocity of 0.75 and 1.0 m/s when assuming the sewer to be running at half full and full pipe flow respectively, and suggest that this velocity should be exceeded for a short period at least once a day.

Several studies (Macke, 1982, May, 1982, Novak & Nalluri, 1984, Mayerle, 1988) have shown that the self-cleansing condition cannot simply be defined in terms of a fixed velocity, but there is a need to take into account the size, concentration and density of sediment in the system and the diameter of the pipe. Several equations that include these new factors have been proposed. However, due to the lack of quantitative knowledge about the occurrence of sediments in sewers these design methods are not widely used.

Having realized the extent of the sediment associated problems in sewers, the Water Research Centre (WRc) and the Water Authorities Association (WAA) have set out the framework (WRc-WAA Sewerage Rehabilitation Manual, 1986) within which the future rehabilitation and operational strategies will be developed for existing sewerage systems in the UK. Their main objective is to develop an appropriate level of understanding of the total system.

As result of the study of these matters the need for further research was indicated . A collaborative research effort was initiated by the WRc's River Basin Management (RBM) programme with simultaneous work on various areas of the sediment related problems in sewers at several institutions in the UK, including characterization of sewer sediments (WRc), sediment sampling and testing (University College of Swansea/WRc), field monitoring on the effect of re-entrainment of sediments and field monitoring of sediment loads (Dundee Institute of Technology), sediment rheology and transport (Swansea/Dundee), laboratory studies to clarify scale effects of non-cohesive sediments (Hydraulic Research Ltd.), laboratory studies on the influence of cohesive additives (University of Newcastle upon Tyne), sediment and pollutants (University of Birmingham), sediment in tanks (University of Manchester), etc., which will contribute towards the development of an improved sewer flow quality model.

The present work, which forms part of the RBM programme, financed by the Science and Engineering Research Council (SERC), has been carried out at the University of Newcastle upon Tyne. The work relates only to the influence of cohesion on the erosion and transport of sewer sediments.

Recent studies on sewer sediment characteristics carried out with samples from seven different locations in the U.K. (Crabtree 1988) indicated that the pollutant load discharged from storm sewage overflows is mostly cohesive in nature. Therefore the results from laboratory studies with non-cohesive sediment

may need to be applied with caution to combined sewerage systems. The presence of cohesive sediment and intermittent nature of flow in sewers cause (see Crabtree 1988) the formation of stationary sediment deposits specially during low flows or Dry Weather Flows (DWF). For this reason it was decided to carry out this study in flumes of circular cross-section with flat sediment beds. The sediment bed was formed with uniformly graded sand and a cohesive additive. Several additives such as china clay, oil, petroleum jelly, laponite clay, etc. were used in the search for a synthetic sewer sediment. The main problem was to relate the behaviour of the synthetic sewer sediment to the actual sewer sediment.

The main objectives of the present study were:

1) To identify the influence of cohesive additives to the erosion threshold of non-cohesive sediments.

2) To establish the hydraulic parameters and frictional characteristics critical to the re-entrainment and transport of deposited sediments.

3) To relate the above performance characteristics to the properties of sediments occurring within combined sewers.

In order to achieve these objectives an experimental programme with uniform flows was proposed to be conducted in two smooth flumes of circular cross-section (154 and 302 mm diameters) with flat sediment beds. In the initial stages of the project

non-cohesive (i.e., uniformly graded sands) sediment experiments were carried out to assess shape effects (compared with wide channel theory) on the threshold of erosion and on the transport capacity of the flow. This provided a basis of comparison for the cohesive sediment studies. It was also necessary to measure channel roughness, velocity and shear stress distributions and turbulence levels in order to characterize the flow through this particular cross-section, and assess its implication on sediment movement.

Chemical and rheological studies (Williams and Williams 1988) were carried out with sewer samples collected from different locations in the U.K. (Crabtree 1988). As a result a synthetic sewer sediment (with similar rheological properties to actual sewer sediment) formed by mixing Laponite RD clay, sand and water was suggested for flume testing in the laboratory. A large number of initiation of erosion experiments covering the entire range of combinations (varying the concentration of the clay gel and the proportion of sand) of the synthetic sewer sediment was carried out in the 154 mm diameter flume. These mixtures were mimicking from freshly deposited (Type C with low cohesion) to slightly consolidated (Type A with high cohesion) sewer sediments. Transport experiments over fixed (limit deposition condition) and loose (alluvial) beds were carried out using non-cohesive sediments as well as the synthetic sewer sediment, in order to assess the influence of cohesion in the transporting capacity of a flow.

The contents of this thesis are organized as follows:

Chapter 1 is the present introductory summary. Chapter 2 contains a brief analysis of the literature on the sediment movement in channels (alluvial and rigid beds, cohesive and non-cohesive sediments) considered relevant to the present work. Chapter 3 shows a detailed description of the laboratory equipment and a description of the experimental procedures adopted during the conduction of the laboratory work. In Chapter 4 the main results are presented in tabulated and graphic form for the various sets of experiments (hydraulic characteristics, initiation of erosion, and sediment transport). The experimental data is analysed and comparisons are made between the results obtained from cohesive and non-cohesive sediment, and between wide channels and channels of circular cross-section. Chapter 5 contains further discussion and conclusion of the results of each set of experiments and some recommendations for further work are presented.

Finally there are 9 Appendixes, which include:

a) Notation (list of symbols used)
b) An extensive list of references
c) Plates (set of photographs from the laboratory)
d) Velocity profiles data
e) Turbulence intensity measurements
f) Initiation of erosion, non-cohesive sediment data
g) Initiation of erosion, synthetic sewer sediment data
h) Laser Doppler Velocimetry, operation of the IFA-550
i) Einstein-Brook-Vanoni's wall separation technique

CHAPTER TWO

SEDIMENT MOVEMENT IN CHANNEL - A LITERATURE REVIEW

2.1 NON-COHESIVE SEDIMENTS

2.1.1 Alluvial Channels

2.1.1.1 Rectangular Wide Channels

Many investigators have studied the problems of sediment movement in open channels and only those directly related to the present work will be briefly described here.

a) Threshold of Motion

The limiting condition marking the boundary between the state of motion and the state of rest of the sediment particles on the bed cannot be defined with precision. At any given condition some particles will move, others will not, due to the statistical nature of the problem.

In 1936 Shields found that the parameters $\frac{1}{\psi} = \frac{\tau_{oc}}{\rho(S_s - 1)gd_{50}}$ the entrainment function, and $Re_* = \frac{u_* d_{50}}{\nu}$ the Reynolds number of the particle, were related so that the plot $\frac{1}{\psi}$ Vs. Re_* falls on a single line (see Fig. 2.1). Based on experimental data Shields plotted a curve that separates the state of motion from the state of sediment at rest on the bed. The curve represents the threshold of motion of an alluvial channel.

Although experiments plotted on Shields' diagram (see Fig. 2.1) show a fair amount of scatter they support Shields' general conclusions and it is widely accepted as a criterion for initiation of sediment movement. The curve has the form:

$$\frac{\tau_{oc}}{\rho(S_s - 1)gd} = fct\left(\frac{d\ u_*}{\nu}\right) \qquad (2.1)$$

where τ_{oc} is the critical shear stress, d the particle size, ρ_s the density of the sediment, ρ the fluid density, ν the kinematic viscosity, S_s the relative density of the sediments, and $u_* = \sqrt{\frac{\tau_o}{\rho}}$ the shear velocity.

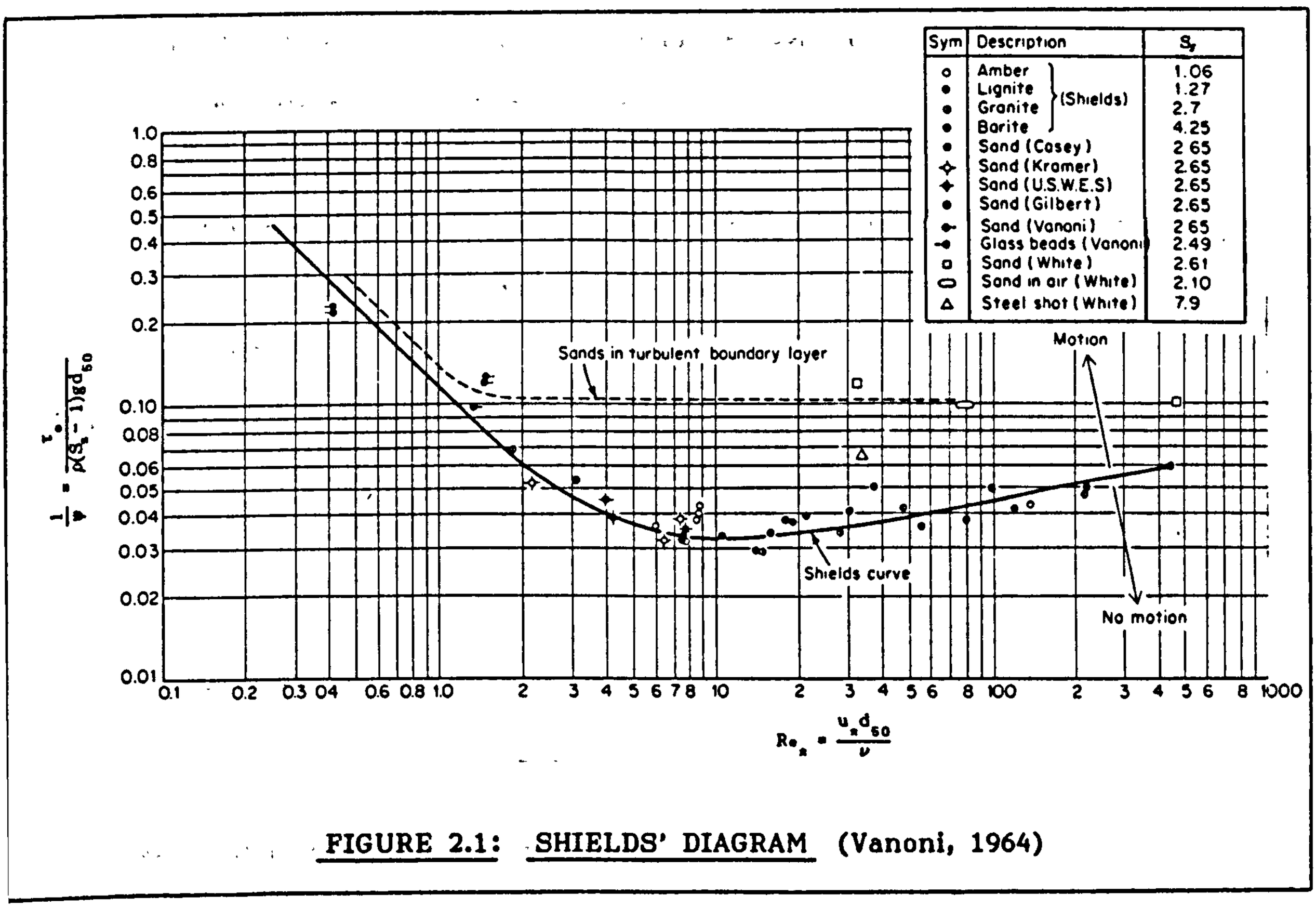

FIGURE 2.1: SHIELDS' DIAGRAM (Vanoni, 1964)

A large proportion of the scatter can be attributed to the confusion in the definition of critical shear stress. Many investigators simply defined critical conditions at some arbitrary point in the critical movement process with no regards to the amount of sediment movement. This made the definitions very subjective.

There is no flow stage at which all bed surface particles are suddenly placed in motion. On the contrary, bed movement takes place gradually over a range of shear stresses as the flow velocity is increased.

Other factors also influence grain movement such as shape and size of sediment particles, the degree of exposure to the flow and the effect of flow turbulence.

Sometimes the threshold velocity (V_c), which is the mean velocity of the flow for incipient motion, is used to define critical conditions.

For $Re_x > 500$ Eq. 2.1 can be written as:

$$\frac{\tau_{oc}}{(\rho_s-\rho)gd} = 0.056 \qquad (2.2)$$

For loose sediment bed Manning's n can be assumed:

$$\frac{1}{n} = \frac{26}{d^{1/6}} \qquad (2.3)$$

where d is the particle size in (m).

Combining Eqs. 2.2 and 2.3 with Manning's equation yields:

$$\frac{V_c}{\sqrt{gd}} = 1.96\,(S_s - 1)^{1/2}\left(\frac{d}{R}\right)^{-1/6} \qquad (2.4)$$

where V_c is the critical velocity, d the particle size, S_s the relative density of the sediment, and R the hydraulic radius.

Bogardi (1968) suggested, for critical conditions, the relation:

$$\frac{V_c}{\sqrt{gY_o(S_s - 1)}} = 1.7\left(\frac{Y_o}{d}\right)^{-0.405} \qquad (2.5)$$

Rearranging the terms, Eq. 2.5 can be expressed in the form:

$$\frac{V_c}{\sqrt{gd}} = 1.7\,(S_s - 1)^{1/2}\left(\frac{d}{Y_o}\right)^{-0.095} \qquad (2.6)$$

Grass (1970) showed that for any area of flat bed there will be a random distribution of critical shear stresses. Some bed particles are more exposed and easily detached than others. For a given flow there will be a random distribution of shear stresses (turbulent nature of the flow) acting on the bed. Thus, there are two independent distributions of shear stress and when they start to overlap the weakest grains will begin to move.

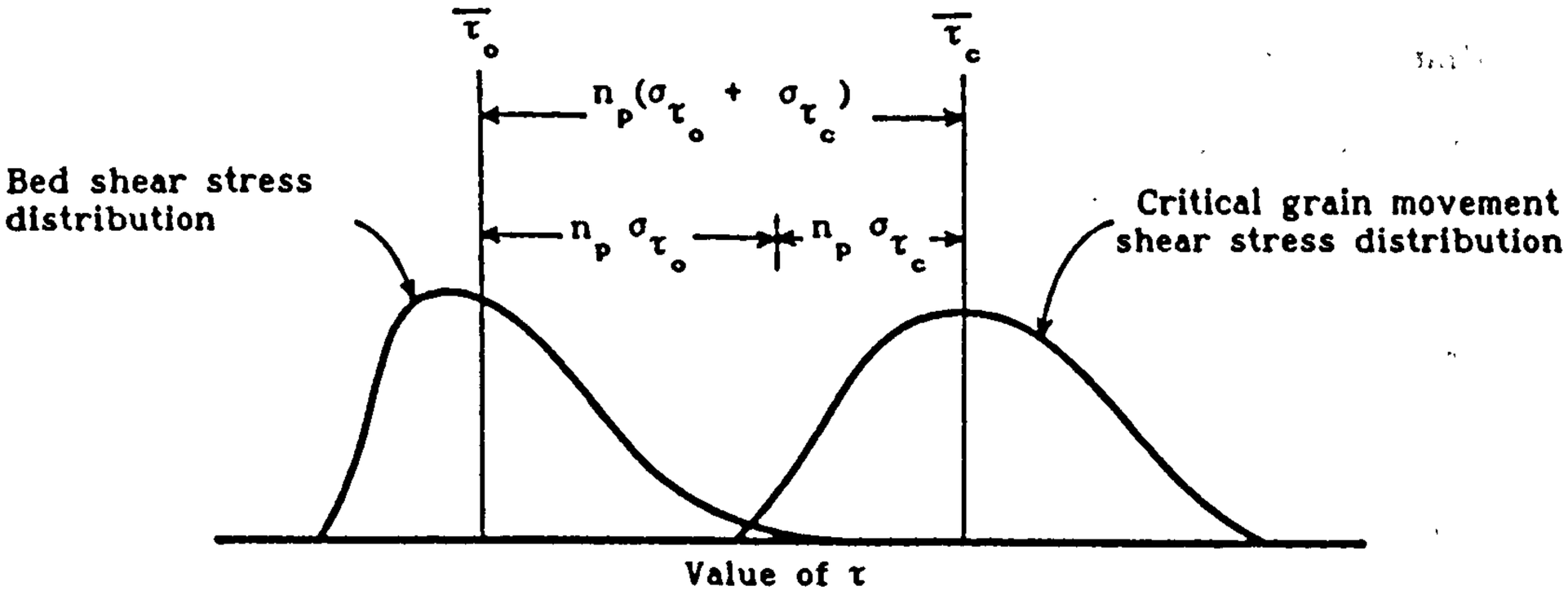

FIGURE 2.2: OVERLAP OF THE SHEAR STRESS DISTRIBUTIONS
(after Grass, 1970)

Grass (1970) defined quantitatively critical movement in terms of the overlap (see Fig. 2.2) of the two distributions as the multiple "n_p" of the sum of the standard deviation of the two distributions that separate the two mean values.

b) Bed Load

The first approach to the study of the movement of bed sediment in channels was published by du Boys in 1879 in which a bedload relation was suggested in the form:

$$q_s = C_s\ \tau_o\ (\tau_o - \tau_{oc}) \qquad (2.7)$$

where τ_o is the mean shear stress, τ_{oc} the critical shear stress for incipient motion and C_s a coefficient dependent on sediment size.

Kalinske (1947) took into consideration turbulent fluctuations of the velocity at the bed, which were assumed to be normally distributed, and presented the following equation for the computation of bed load:

$$\frac{q_s}{u_* d} = 10\left(\frac{1}{\psi}\right)^2 \qquad (2.8)$$

where q_s is the volume rate of sediment transported per unit width, u_* the shear velocity, and d the sediment size. Even though spherical grains were assumed, sometimes non-uniform sands were represented by their median diameters.

Einstein in 1942 developed his well known formula (Eq. 2.9) based on physical reasoning and on dimensional considerations. Equation 2.9 relates bed load transport with properties of the grain and of the flow causing the movement. Einstein employed statistical reasoning to an even greater extent than Kalinske did, and he finally concluded that,

$$\phi = \frac{q_s}{w_s d} = f\left(\frac{1}{\psi}\right) \qquad (2.9)$$

where ϕ is known as Einstein bed load function, w_s is the particle fall velocity, d is the particle diameter and $\frac{1}{\psi}$ is Shields' entrainment function. This result is very similar to that of Kalinske where the latter uses the shear velocity (u_*) instead of the particle's fall velocity (w_s).

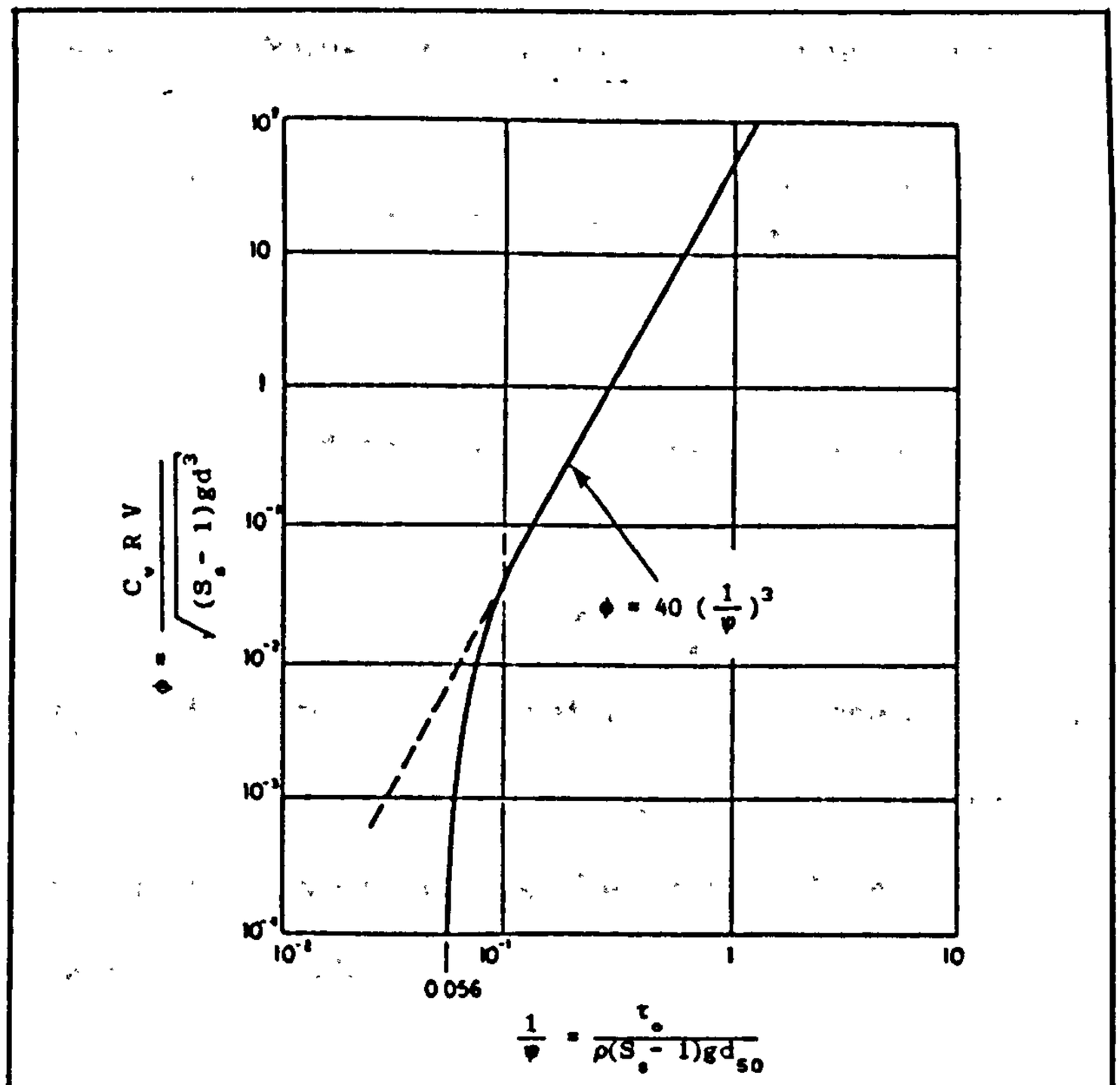

FIGURE 2.3 BROWN'S CURVE

Brown (1950) using many experimental data (sand size ranges: 0.315 mm < d_{50} < 28.6 mm and 1.25 < S_s < 4.2) presented the empirical relation:

$$\phi = 40\ (\frac{1}{\psi})^3 \qquad (2.10)$$

valid for ϕ < 0.4

The lower part of the plot (see Fig. 2.3) curves away to the asymptote $\frac{1}{\psi}$ = 0.056, which represents the threshold condition of Shields' data (Eq. 2.2).

Meyer-Peter and Muller in 1948 presented the formula,

$$\frac{\gamma R(n'/n)^{3/2}S}{d} - 0.047(\gamma_s - \gamma) = 0.25\sqrt[3]{\rho}\,\frac{(g_s')^{2/3}}{d} \qquad (2.11)$$

which is widely used for sand mixtures. Equation 2.11 was obtained as the best fit of experimental data with sand size ranges: 0.4 mm < d_{50} < 28.6 mm and 1.25 < S_s < 4.2, and wide channels, where γ_s is the specific weight of the sediment, n and n' are Manning's total roughness coefficient and grain roughness coefficient respectively, g_s' is the bed load rate in weight per unit time per unit width.

In their computations, Meyer-Peter et al. (1948) kept the hydraulic radius constant and divided the energy slope into two components. One taking the portion of the energy loss due to grain resistance (S') and the other due to bed form (S"),

$$S = S' + S" \qquad (2.12)$$

Whereas Einstein divided the hydraulic radius for the same reasons keeping the slope fixed as:

$$R = R' + R" \qquad (2.13)$$

Therefore in Eq. 2.11 the term $(n'/n)^{3/2}S = S'$ represents the energy loss due to grain resistance, which is responsible for sediment transport.

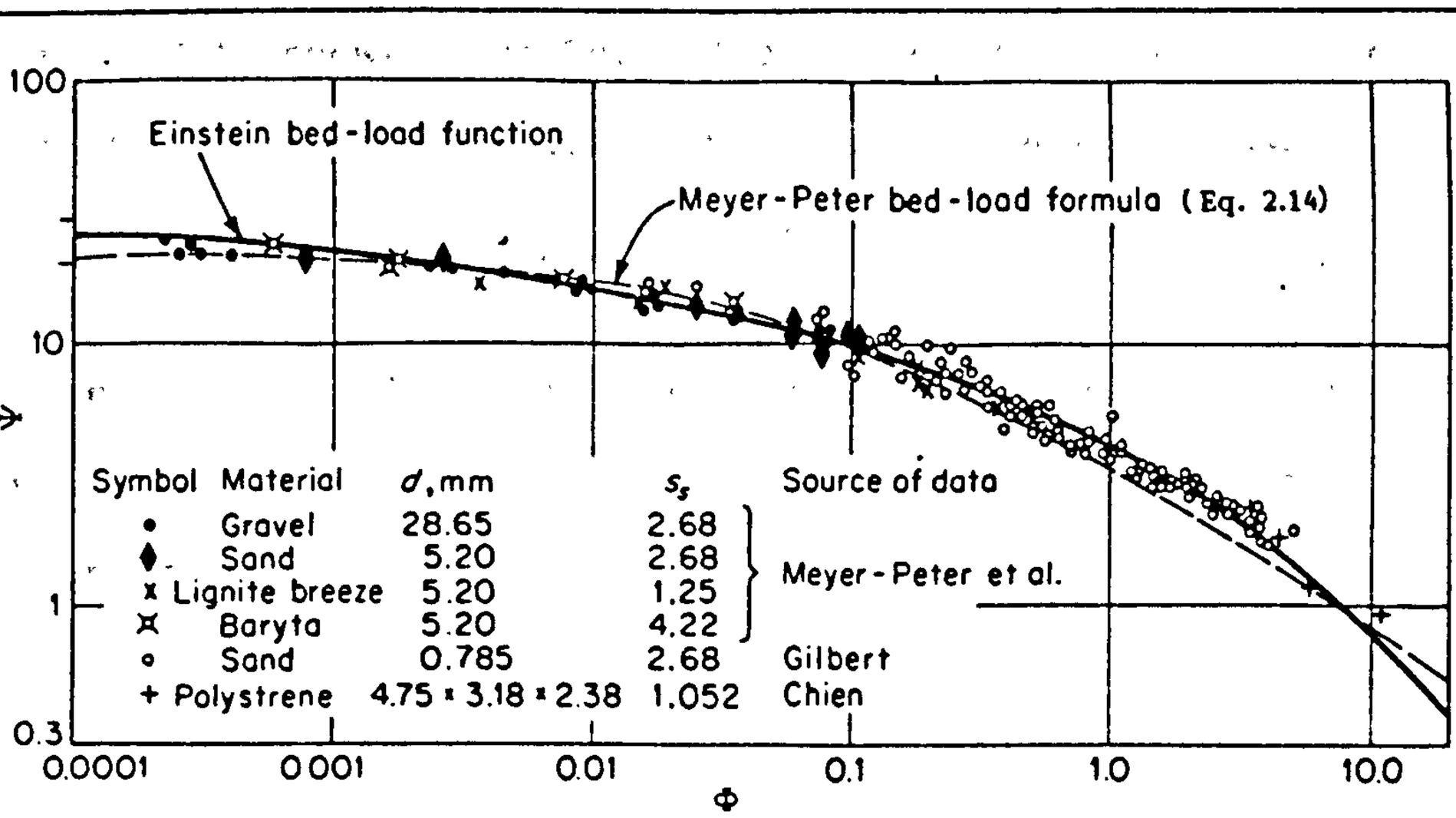

FIGURE 2.4: COMPARISON OF THE BEDLOAD EQUATION OF EINSTEIN AND MEYER-PETER ET AL. (CHIEN 1954)

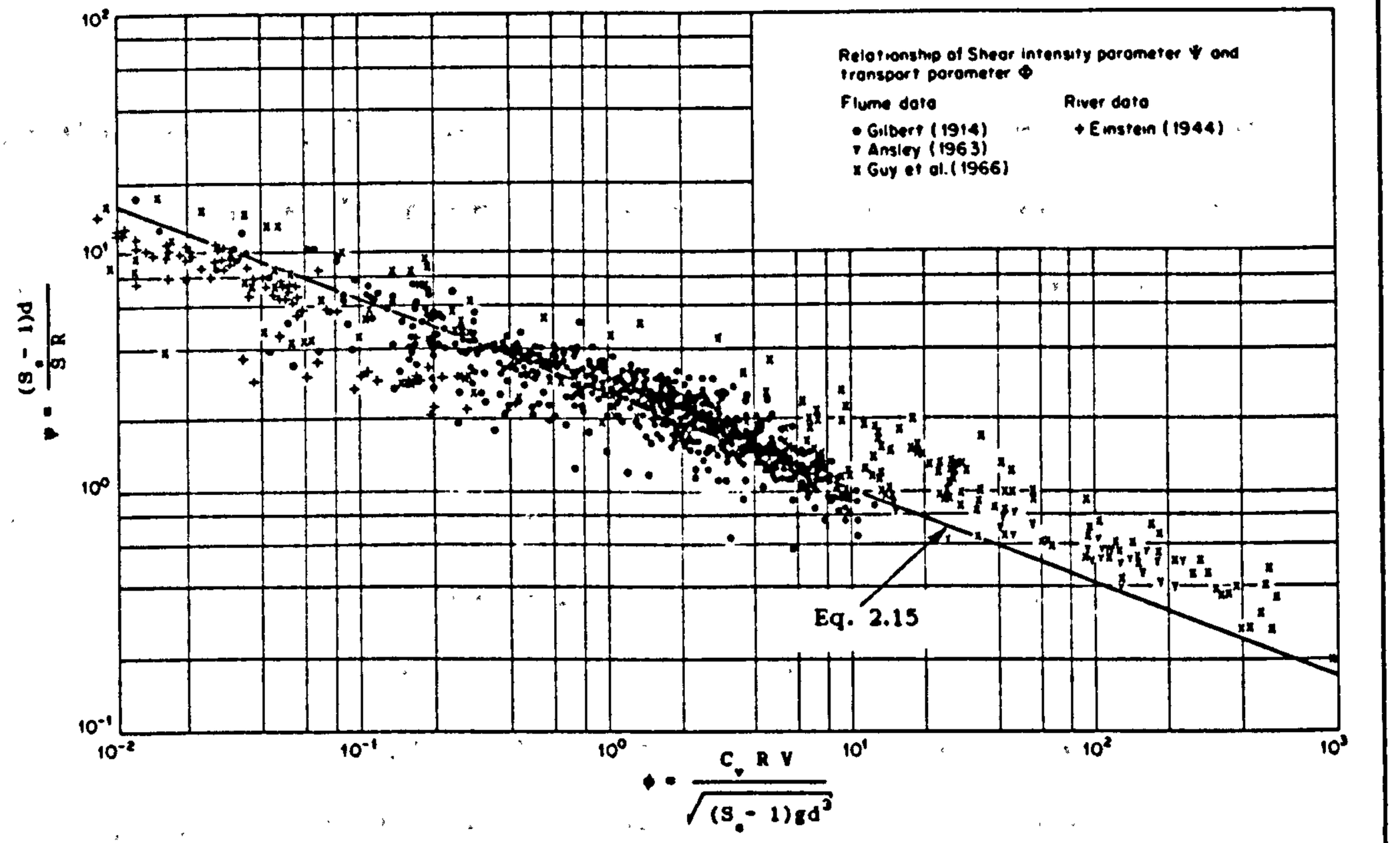

FIGURE 2.5: TRANSPORT VS. FLOW INTENSITY PARAMETERS OPEN CHANNEL FLOW DATA (Graf and Acaroglu, 1968)

Chien in 1954 showed that Eq. 2.11 gives results comparable to those of Einstein (see Fig. 2.4) and that it can be written as:

$$\phi = \left(\frac{4}{\psi} - 0.188\right)^{3/2} \qquad (2.14)$$

Graf and Acaroglu (1968) analysed several laboratory (open and closed conduits) and field data and obtained the following relation (see Fig. 2.5):

$$\phi = 10.39 \left(\frac{1}{\psi}\right)^{2.52} \qquad (2.15)$$

with

$$\phi = \frac{C_v \, R \, V}{\sqrt{(S_s - 1) g d^3}} \qquad (2.16)$$

known as the transport parameter and

$$\psi = \frac{(S_s - 1) d}{S \, R} \qquad (2.17)$$

as the flow intensity parameter where C_v is volumetric sediment concentration, R the hydraulic radius, V the mean flow velocity, S_s the relative density of sediment, S the channel slope and d the particle size.

Einstein and Meyer-Peter and Muller equations are widely used for bed load calculations. However, there are several other equations available in the literature such as those of Bagnold (1956), Yalin (1963), Engelund and Hansen (1967), Ackers and White (1973), etc., to which the interested reader is referred to.

c) Bedform classification

The type of bedform is generally dependent on the flow regime (i.e., Froude number) and on the type and size of sediments. Once the shear stress is sufficient to cause transport "ripples" will start to form on the bed. As the shear stress is increased the ripples will grow into larger "dunes", which will be migrating downstream. Dunes and ripples differ in their relative sizes (with respect to flow depth). The random element present in bed formation is considerable. Thus individual waves of the bed formation (at any instant) are not identical in their size and shape and the dimensions of dunes and ripples refer to the average (along the channel axis) values.

A typical bedform sketch is shown in Fig. 2.6 where Y_o is the normal depth with respect to the average bed level, L is the dune length, Δ is the height of the dunes and V is the mean flow velocity.

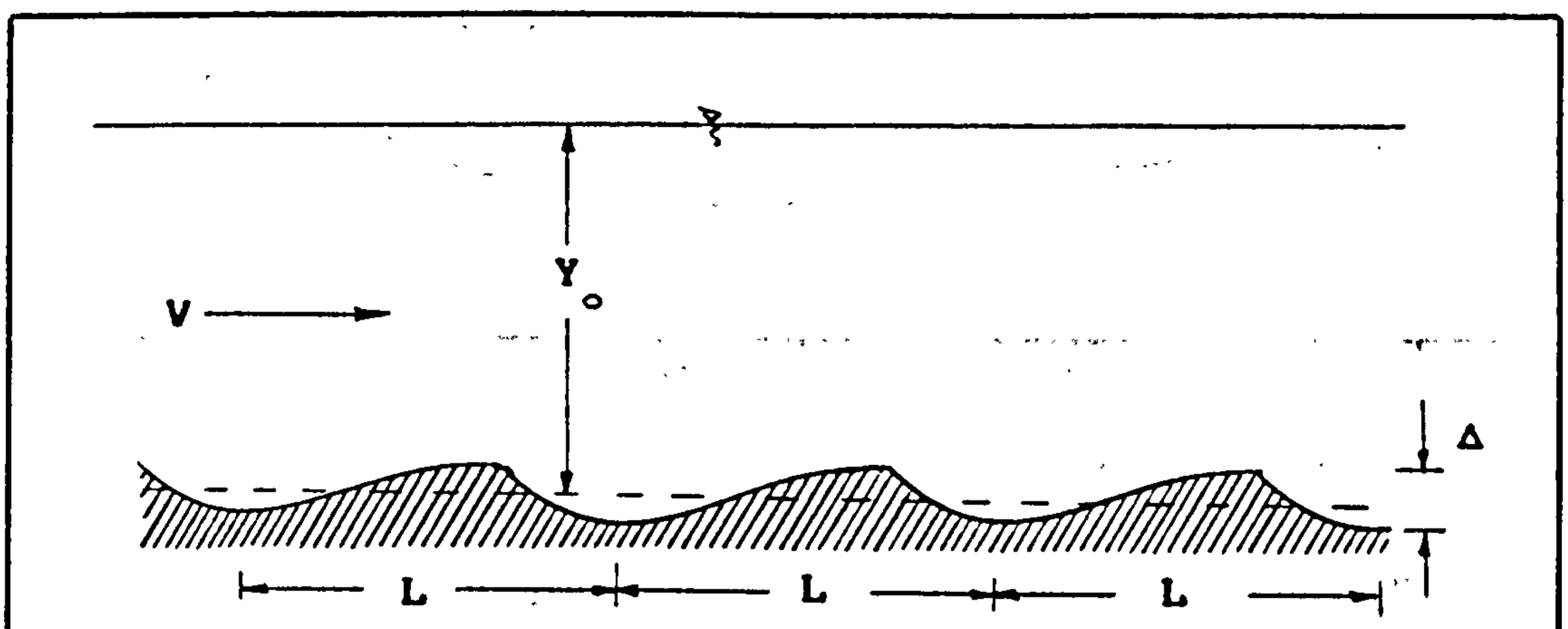

FIGURE 2.6: TYPICAL BEDFORM IN ALLUVIAL CHANNELS

There is a large number of investigators in the literature who have studied bed formation in alluvial channels and presented relations for their prediction. Only a few of them are presented here.

Shields (1936) correlated bed formation with shear stress and classified bedforms (see Fig. 2.7) according to the flow intensity parameter and particle Reynolds number.

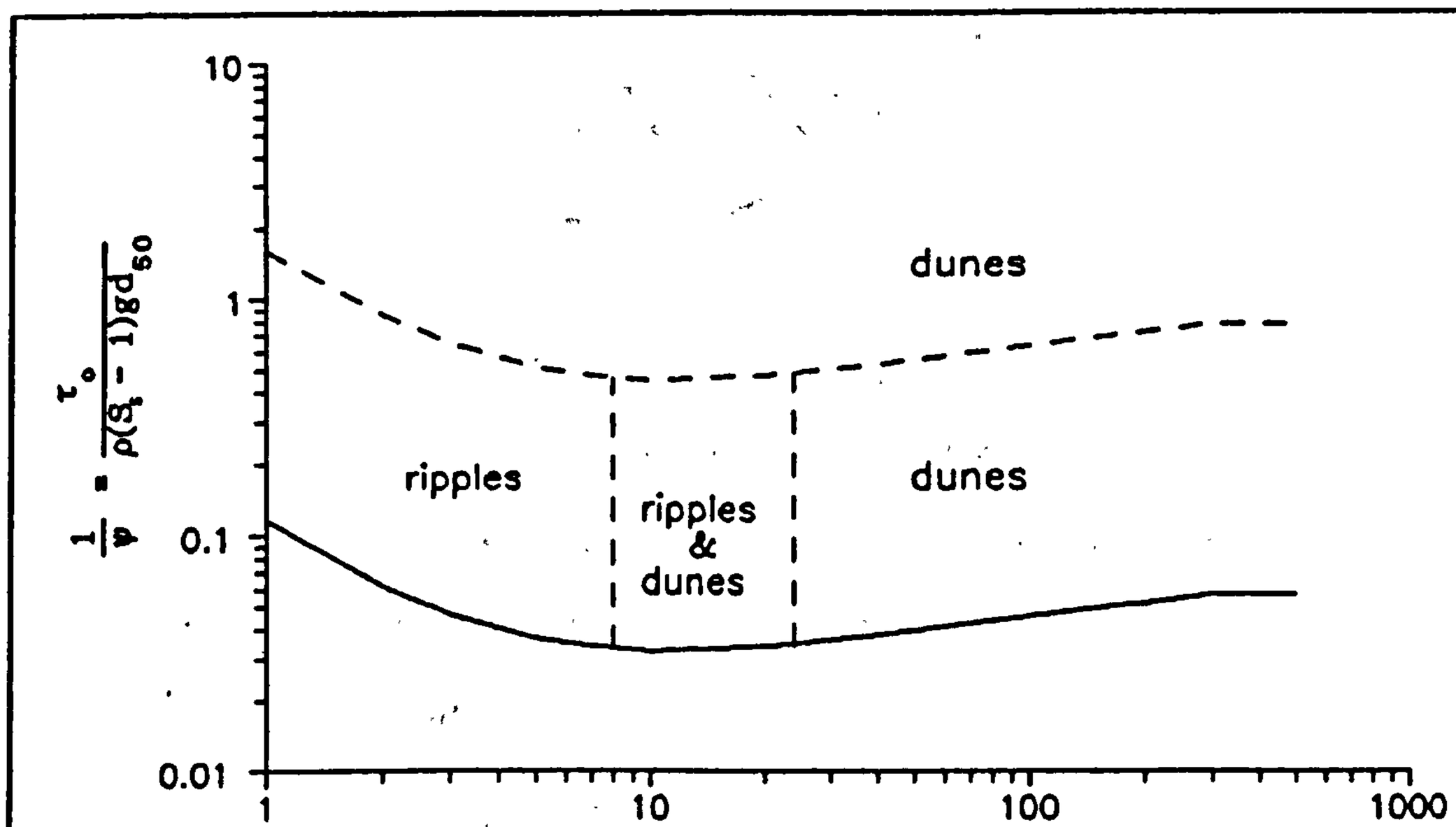

FIGURE 2.7: SHIELDS' DIAGRAM WITH BEDFORM CLASSIFICATION

Simons et al. (1963) using experimental and field data suggested the use of the stream power ($\tau_o V$) for the classification of bedforms. In Fig. 2.8 the stream power is plotted against the fall diameter (obtained from settling experiments) and the various types of bed formation are shown.

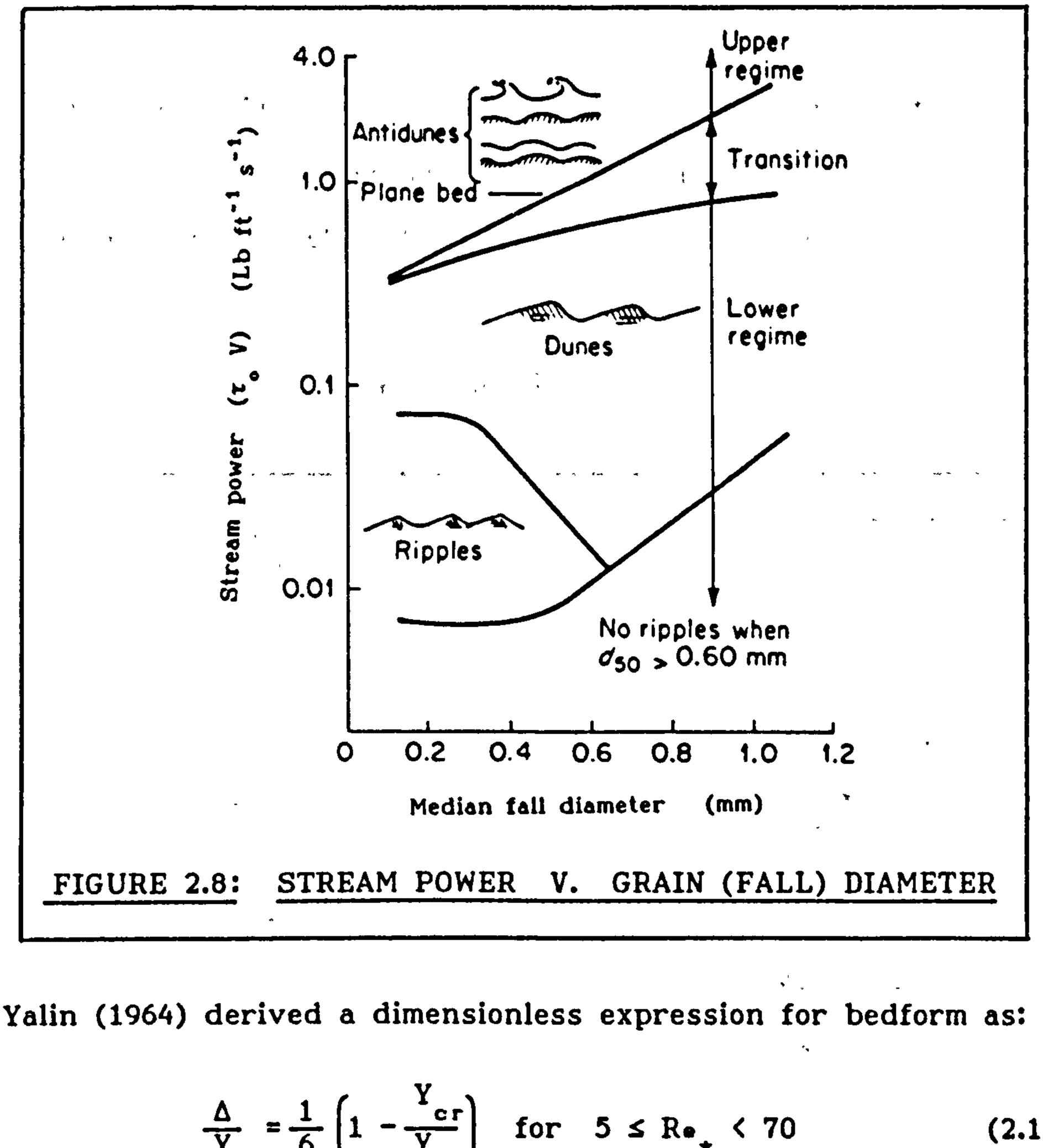

FIGURE 2.8: STREAM POWER V. GRAIN (FALL) DIAMETER

Yalin (1964) derived a dimensionless expression for bedform as:

$$\frac{\Delta}{Y_o} = \frac{1}{6}\left(1 - \frac{Y_{cr}}{Y_o}\right) \quad \text{for} \quad 5 \leq Re_* < 70 \qquad (2.18)$$

where Δ is the bedform height, Y_{cr} the flow depth for incipient motion and Y_o the uniform flow depth.

In 1985 Yalin presented an expression for the length (L)) of the ripples:

$$\frac{L}{d} = f(Re_*, \Xi) \qquad (2.19)$$

where Ξ is a dimensionless particle number given by:

$$\Xi = \frac{(S_s - 1)}{\nu^2} g (d_{50})^3 \qquad (2.20)$$

From his experiments he obtained a family of curves for each value of Ξ. By successive approximation a coefficient α was obtained, for which all data formed a single pattern (see Fig. 2.9), as:

$$\alpha = 3.38\ \Xi^{-0.25} \qquad (2.21)$$

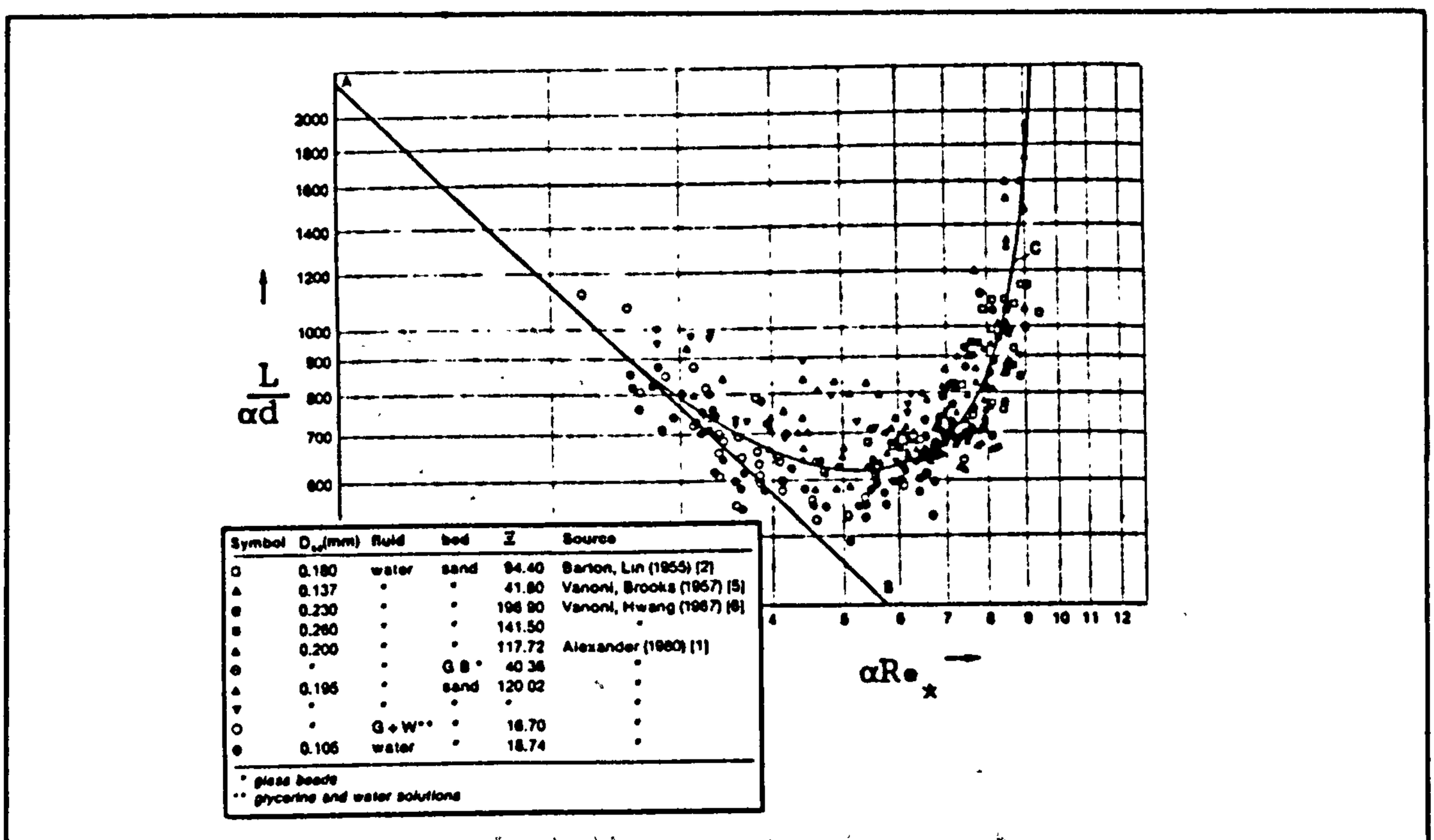

FIGURE 2.9: RELATIVE RIPPLE LENGTH VS. PARTICLE REYNOLDS NUMBER (Yalin, 1985)

Thus, Eq. 2.19 becomes:

$$\frac{L}{\alpha d} = f(\alpha Re_*) \qquad (2.22)$$

The ripple height may be predicted using Eq. 2.21 and Fig. 2.9, for a given sand and flow characteristics.

Znamenskaya (1969) presented a generalized empirical relation for bedforms classification (see Fig. 2.10) based on the flow characteristics, i.e., the Froude number of the flow, the mean velocity of the flow V, and the type of bed material w_s.

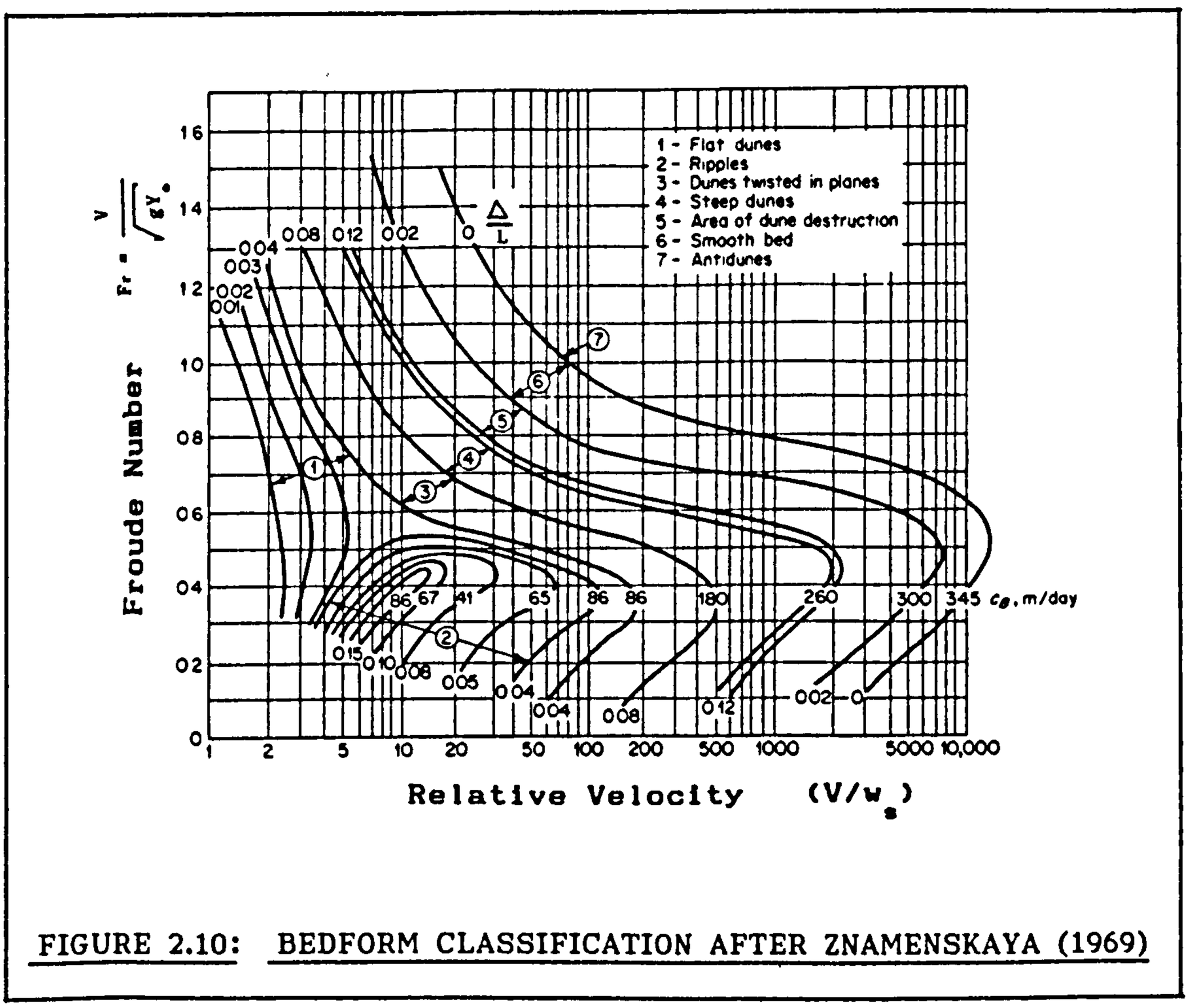

FIGURE 2.10: BEDFORM CLASSIFICATION AFTER ZNAMENSKAYA (1969)

The Froude number was defined as:

$$Fr = \frac{V}{\sqrt{gY_o}} \tag{2.23}$$

where Y_o is the normal depth with respect to the average bed level and V is the mean flow velocity. The plot in Fig. 2.10 (Znamenskaya, 1969) permits the prediction of the type of bedforms, the bedforms steepness ($\frac{\Delta}{L}$) and the velocity (c_B) at which the bedforms travel for any given sand size and flow conditions.

Van Rijn (1984) presented a classification of bedforms using two dimensionless parameters (see Fig. 2.11). One is a dimensionless particle number, D_* given by:

$$D_* = \left(\frac{(S_s - 1)g}{\nu^2} \right)^{1/3} d_{50} \tag{2.24}$$

where d_{50} is the particle mean diameter, ν is the kinematic viscosity, and S_s is the relative density of the sediments. The other one is a transport parameter, T expressed as:

$$T = \frac{(u_*')^2 - (u_{*cr})^2}{(u_{*cr})^2} \tag{2.25}$$

where u_*' is the shear velocity related to grain only, and u_{*cr} is the critical shear velocity from Shields' diagram. The shear velocity is given by:

$$u_*' = \left(\frac{g^{1/2}}{C'} \right) V \tag{2.26}$$

where V is the mean flow velocity, and C' is Chezy coefficient

related to grain as:

$$C' = 18 \log\left(\frac{12\ R_b}{3\ d_{90}}\right) \qquad (2.27)$$

in which R_b is the hydraulic radius of the bed, and d_{90} is the particle diameter of bed material not exceeded by 90% by weight of the particles.

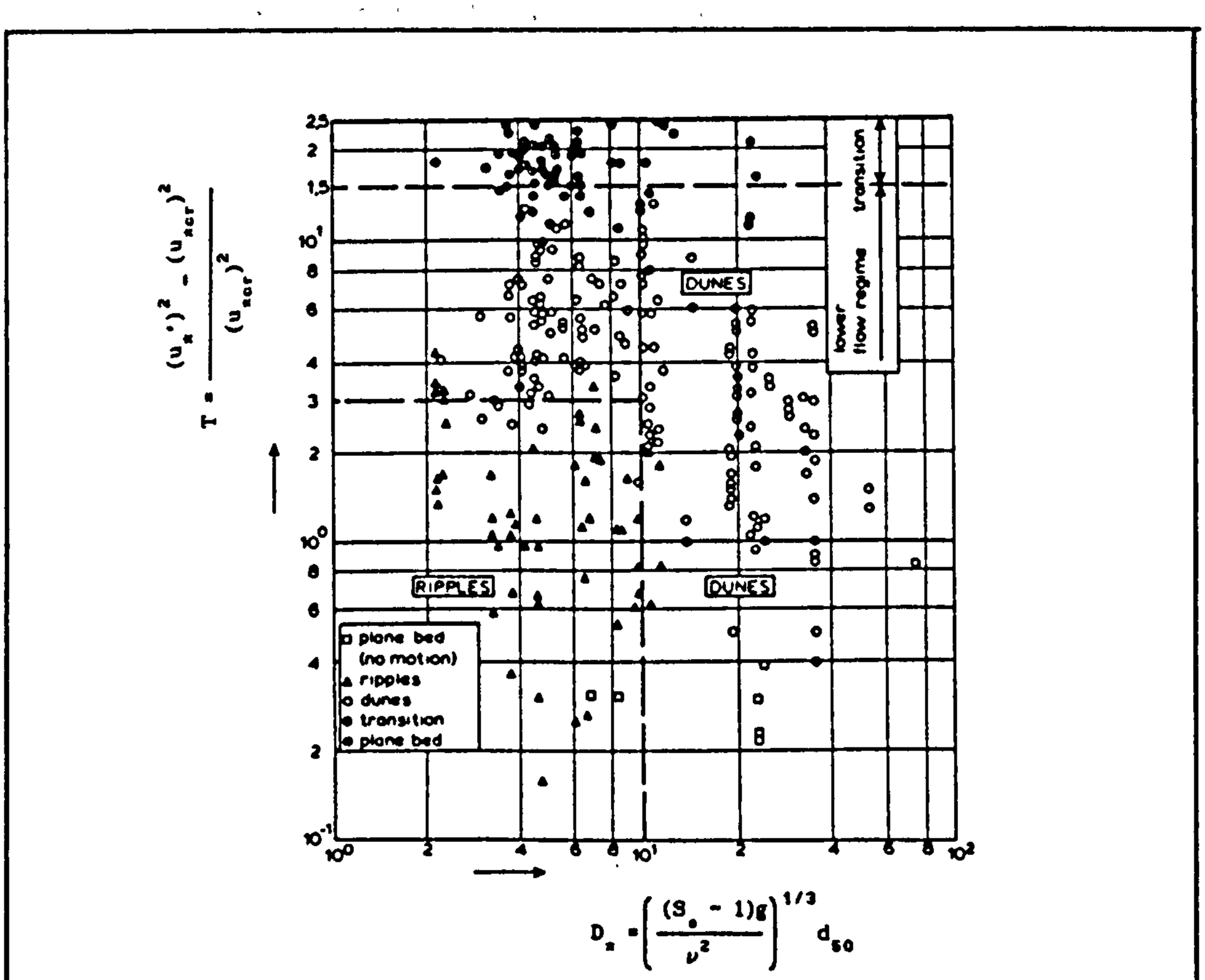

FIGURE 2.11: CLASSIFICATION OF BEDFORMS (Van Rijn, 1984)

Van Rijn (1984) after analyzing a large quantity of experimental (bedforms) data concluded that the dimensionless grain number D_* had negligible influence on bedform dimensions. He presented best-fit equations for prediction of bedform dimensions as:

$$\frac{\Delta}{Y_o} = 0.11 \left(\frac{d_{50}}{Y_o}\right)^{0.3} \left(1 - e^{-T/2}\right) (25 - T) \qquad (2.28)$$

where Δ is the dune height, Y_o is the normal depth, d_{50} is the particle mean diameter, and T is the transport parameter as defined in Eq. 2.25. And for dune length an approximate relation was given (Van Rijn, 1984) as:

$$L = 7.3\ Y_o \qquad (2.29)$$

where L is the dune length and Y_o the normal depth.

2.1.1.2 Channels of Circular Cross-section

a) Sediment Transport

The mechanism governing the movement of sediment through channels of circular cross-section is quite different from that of alluvial channels. However, certain similarities are found for the case of pipe channels where sediment transport takes place over a loose sediment bed (i.e., pipe partly filled with sediment).

There are many investigators in the literature who have dealt with sediment transport in pipes. Most of them studied sediment transport under full pipe flow conditions (heterogeneous mixtures) for industrial applications such as conveyance of coal and ores, disposal of tailings, ashes, and other waste products, transportation of raw materials in industrial processes, etc.

Acaroglu (1969) observed the various phases occurring during transportation of sediment (d = 2 mm) in a pipe (see Fig. 2.12). It began with inert sediment bed for low velocities, followed by initiation of motion for higher velocities, and then by sediment transport with bed formation for even higher velocities. A further velocity increment caused plane bed, and finally suspension (heterogeneous flow) occurred for very high velocities.

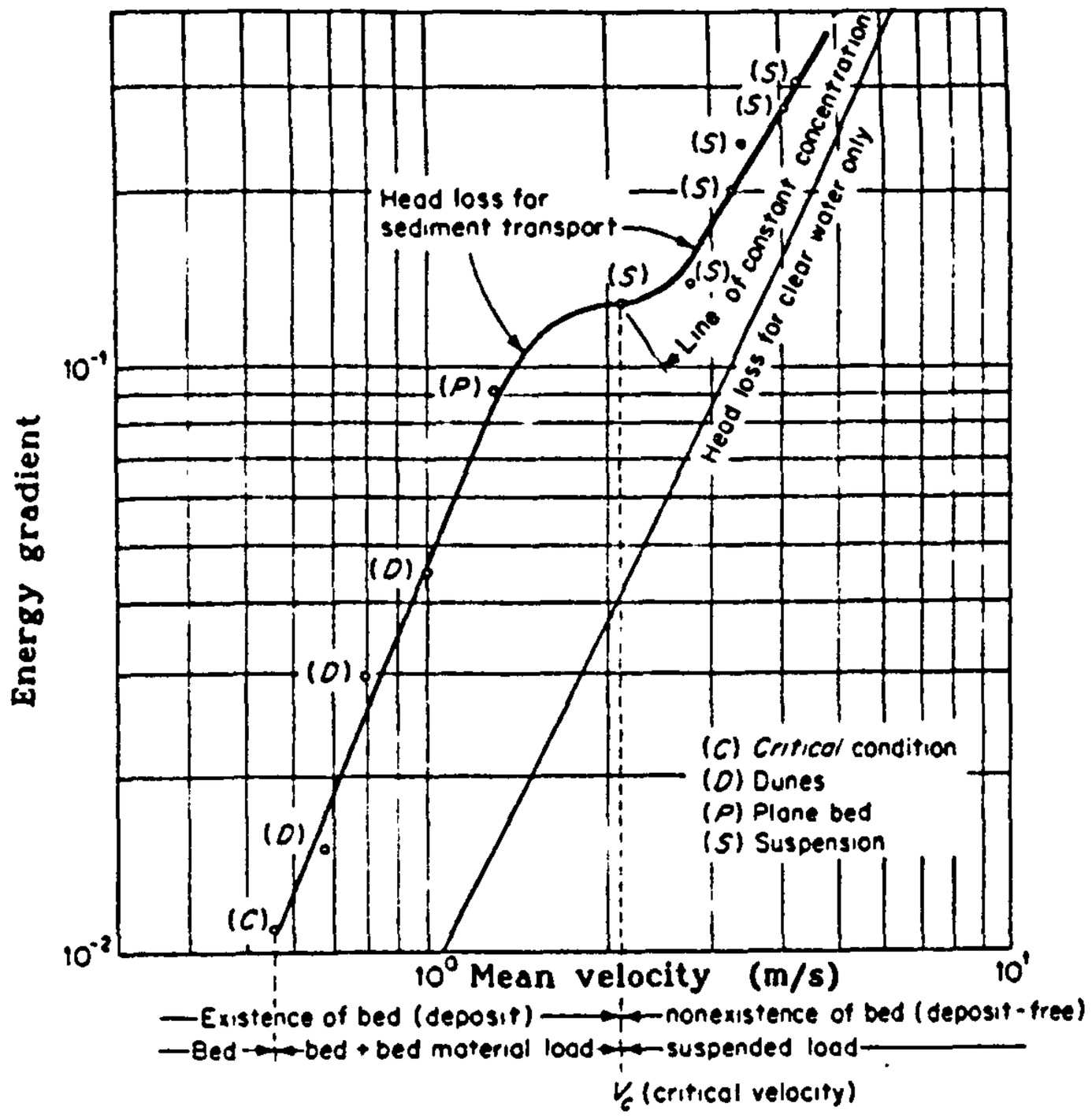

FIGURE 2.12: ENERGY GRADIENT VS. VELOCITY IN PIPES (Acaroglu, 1969)

For full pipe flow conditions Craven (1954) investigated sediment movement for various bed thicknesses using two pipe diameters 5.55" (141 mm) and 2" (51 mm). Sediments utilized were uniform quartz sand, sizes 0.25, 0.58 and 1.62 mm. He presented a relation between sediment thickness ratio (Y_s/D) and a sediment concentration parameter (see Fig. 2.13):

$$\frac{Q}{D^{2.5}\sqrt{(\gamma_s - \gamma)/\rho}} \left(\frac{Q_s}{Q}\right)^{-1/3} \geq 5.0 \qquad (2.30)$$

where Q_s is the absolute volume rate of sediment transport and Q is the volume flow rate. Craven concluded that for no deposition to occur this parameter (Eq. 2.30) should exceed 5.0.

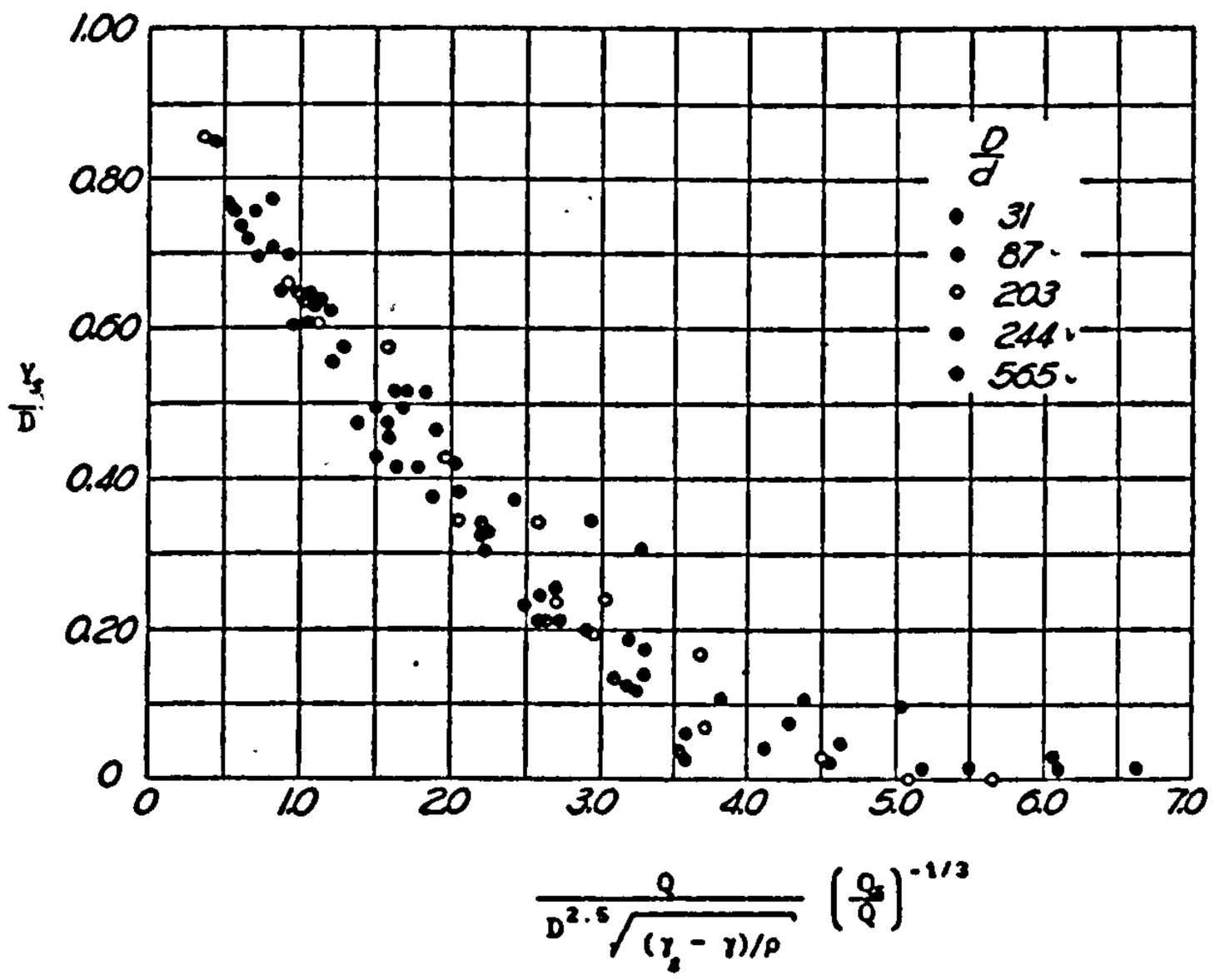

FIGURE 2.13: SEDIMENT BED THICKNESS RATIO VS. SEDIMENT CONCENTRATION PARAMETER (Craven, 1953)

An extension of Craven's investigation was presented by Ambrose (1953) who considered the general case of sediment movement under open channel flow conditions. In his experimentation in pipes with sediment beds cases II (full pipe flow conditions), and III (open channel flow conditions), he employed the same rig and sediment as Craven. Ambrose (1953) found a relation between water depth ratio and the transport function (see Fig. 2.14):

$$\frac{Q}{g^{2/5}\, D^2\, Q_*^{1/5}(S_* - 1)^{2/5}} = f\left(\frac{Y_o}{D}\right) \qquad (2.31)$$

However, the small amount of data limits the application of this function.

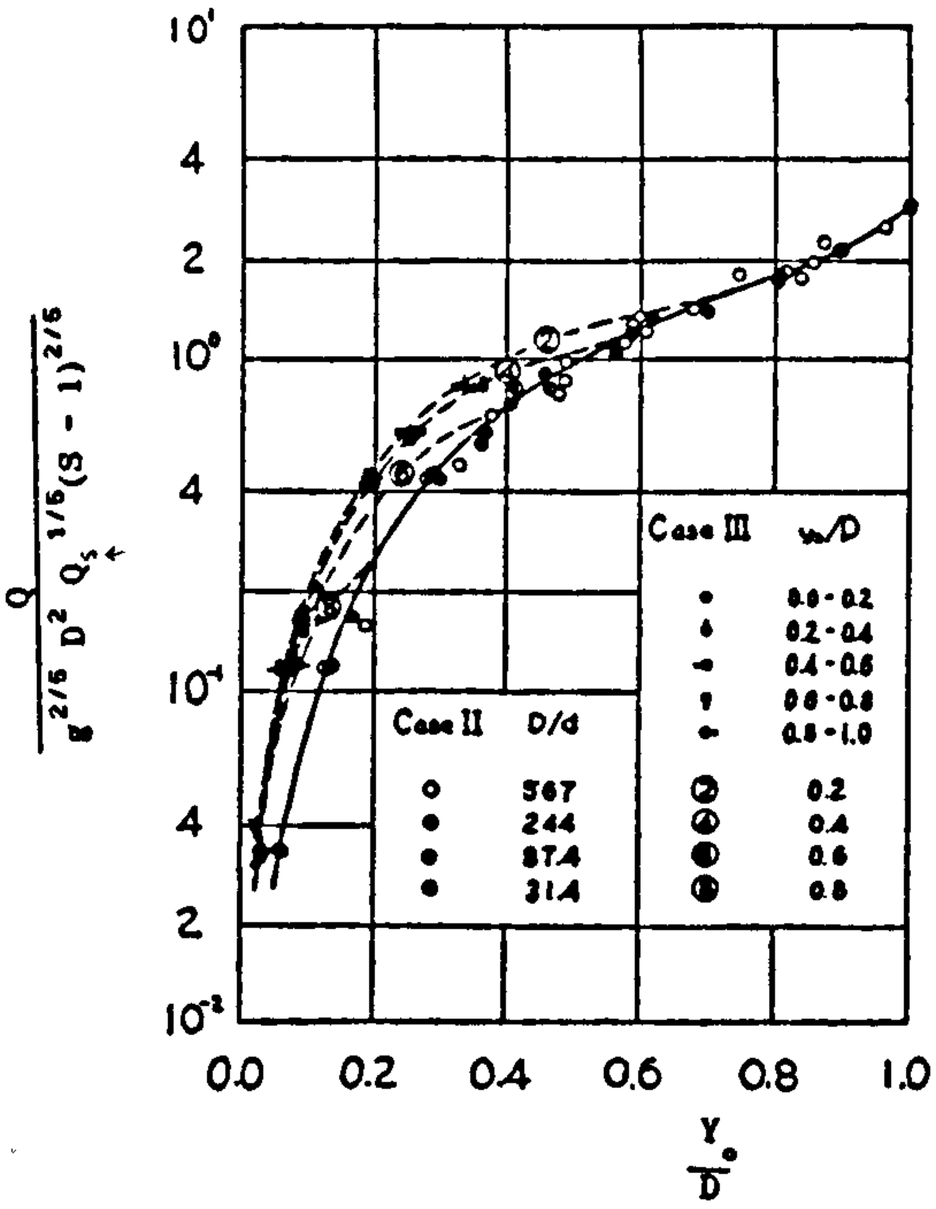

FIGURE 2.14: TRANSPORT FUNCTION V. RELATIVE DEPTH (Ambrose, 1953)

Durand and Condolios (1956) carried out sediment transport experiments in pipes with diameters ranging from 40 to 580 mm, uniform sand sizes between 0.2 and 25 mm, relative densities between 1.6 (plastic) and 3.95 (corondum) and sediment concentrations between 50 and 600 g/l. From their experimental results they suggested a dimensionless sediment transport parameter:

$$\varphi_D = K_D \left(\frac{V^2}{gD(S_s - 1)} \sqrt{\frac{gd(S_s - 1)}{w_s^2}} \right)^{-3/2} \qquad (2.32)$$

where K_D is an empirical coefficient, d is the particle size, D is the pipe internal diameter, S_s is the sediment relative density, and w_s is the particle fall velocity.

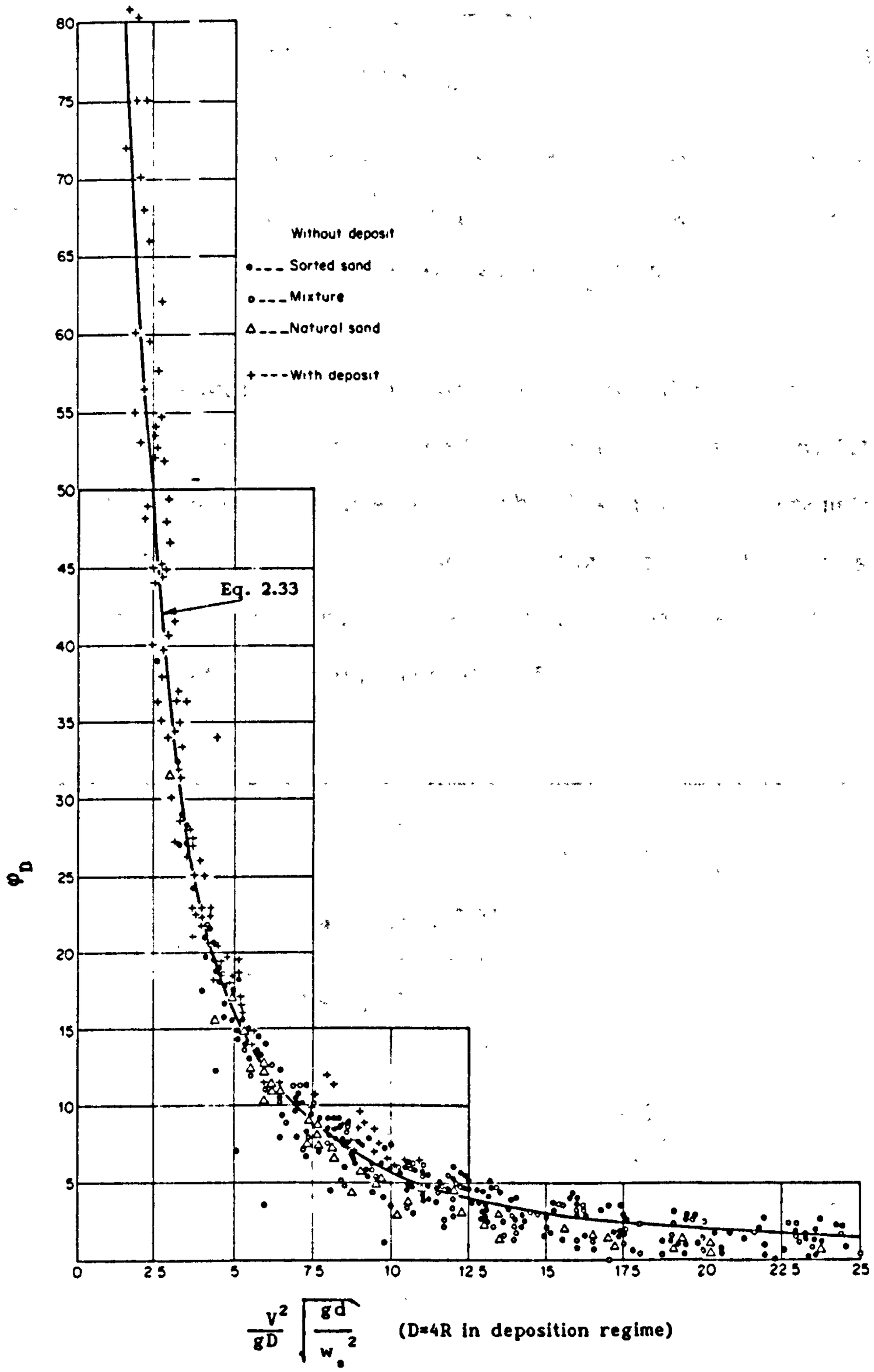

FIGURE 2.15: DIMENSIONLESS SEDIMENT TRANSPORT PARAMETER OF DURAND-CONDOLIOS (after Gibert, 1960)

For sands (S_s=2.65) Eq. 2.32 becomes:

$$\varphi_D = 176 \left(\frac{V^2}{gD} \sqrt{\frac{gd}{w_s^2}} \right)^{-3/2} \qquad (2.33)$$

For deposited bed conditions the diameter was replaced by the hydraulic radius (i.e., $R = \frac{D}{4}$). Much of their data was plotted (see Fig. 2.15) by Gibert (1960) for sand (S_s=2.65).

Graf and Acaroglu (1968) using total load data from open channels, rivers and pipes obtained a general relation (Eq. 2.15) between the transport parameter and the flow intensity parameter. Equation 2.15 is plotted in Fig. 2.16 together with closed conduit data only, for sand sizes ranging between 0.091 to 2.78 mm and relative density around 2.65.

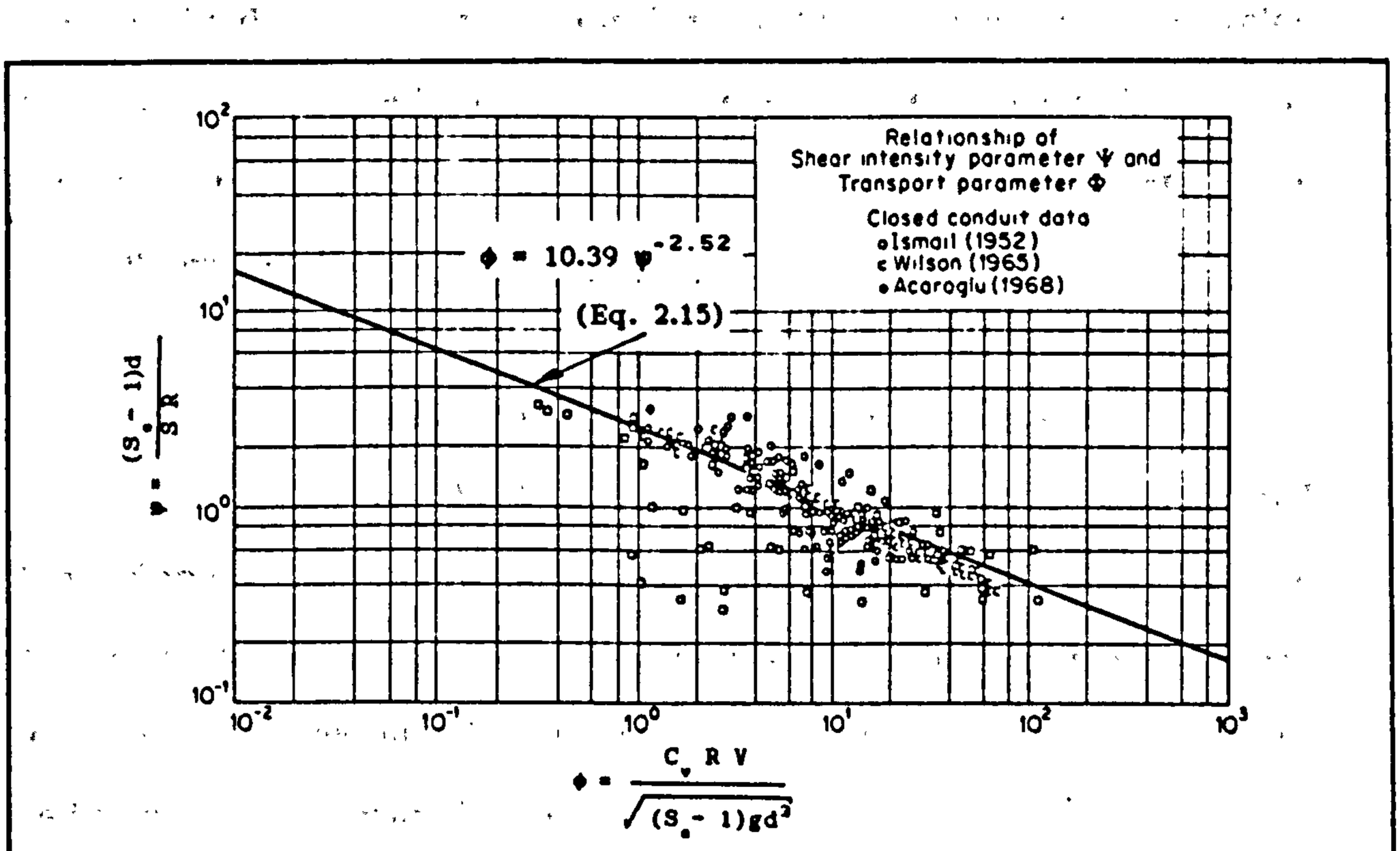

FIGURE 2.16: TRANSPORT VS. FLOW INTENSITY PARAMETERS CLOSED CONDUIT DATA (Graf and Acaroglu, 1968)

Even though there is some degree of scatter, Eq. 2.15 explains well the data for closed conduit flow as it is shown in Fig. 2.16. However, as it can be seen in Fig. 2.5, there is less scatter for the open channel flow data, which cover a larger experimental range. This reflects the fact that Eq. 2.15 was derived from a wide range of experimental data from open channel flow conditions (field and laboratory studies) as well as from closed conduits.

b) Bedforms

Bedforms were observed by many investigators during the low flow conditions with deposited sediment bed in the conduits. However, not many have actually measured the bedforms. A pipe with a previously deposited non-cohesive sediment bed will develop various types of bed formations. These will depend on the shear stress exerted by the flow, the size of the sediments and the rate of sediment transport.

Once the shear stress is sufficient to cause transport "ripples" will start to form on the bed. As the shear stress is increased the ripples will grow into larger "dunes", which will be migrating downstream. A further increase in the shear stress will lead to the formation of larger isolated dunes as the entire sediment bed is eroded away.

Perrusquia (1988) conducted experiments with various depths of sediment bed in a concrete pipe (225 mm diameter) using two sand sizes (0.5 and 1.0 mm). The first part of his work dealt with plane bed as flow resistance was studied. He concluded that Einstein-Vanoni's wall separation technique (Vanoni-Brook, 1957) gave satisfactory results.

In the second part of the work (Perrusquia, 1988) bedforms were studied. Several methods for predicting bedform dimensions such as those of Engelund and Hansen (1972), Fredsoe (1982) and van Rijn (1984), have been shown to be acceptable, with some modifications, for estimating bed formation in pipes with a flat sediment bed.

2.1.2 Rigid Bed Channels

Here there is no erosion of the channel boundary. The sediment is fed from external sources. Such are the familiar cases of lined canals and sewers.

a) Initiation of Movement

Pedroli (1963) experimented with two rectangular channels (300 and 600 mm wide) with rigid smooth beds. Uniform sands (S_s = 2.65) were used ranging from 1.1 mm to 11.1 mm in size. The volumetric concentration ranged between 2.2×10^{-5} and 10^{-2}. For incipient motion the following equation was obtained:

$$\tau_{oc} = 0.00144\ \rho_s g \left(d_{50}\right)^{2/5} S^{1/4} \qquad (2.34)$$

where τ_{oc} is the critical shear stress in (N/m^2), d_{50} is the mean diameter in (m), ρ_s is the density of the sediment in (Kg/m^3), and S is the channel slope.

Novak and Nalluri (1975) conducted initiation of erosion experiments in two circular flumes (152 mm and 305 mm diameter) and one rectangular flume 305 mm wide. The range of sand size was 0.6 to 50 mm. The relative density varied between 1.18 (diakron) and 11.74 (lead) and the Reynolds numbers between 1.63×10^4 and 1.61×10^5. A general equation for the threshold condition was given as:

$$\frac{V_c}{\sqrt{gd}} = 0.61\ (S_s - 1)^{1/2} \left(\frac{d}{R}\right)^{-0.27} \qquad (2.35)$$

where V_c is the critical velocity for incipient motion, d is the particle size, and R the hydraulic radius.

Eq. 2.35 is plotted in Fig. 2.17 together with Shields' curve (Eq. 2.4) and Bogardi's curve (Eq. 2.6) for alluvial channels, for comparison. Novak-Nalluri's data fell below the alluvial channels curves (Shields' and Bogardi) , as was expected due to the lower frictional resistance of smooth rigid boundary and the lack of group effect (sheltering, armouring, etc.).

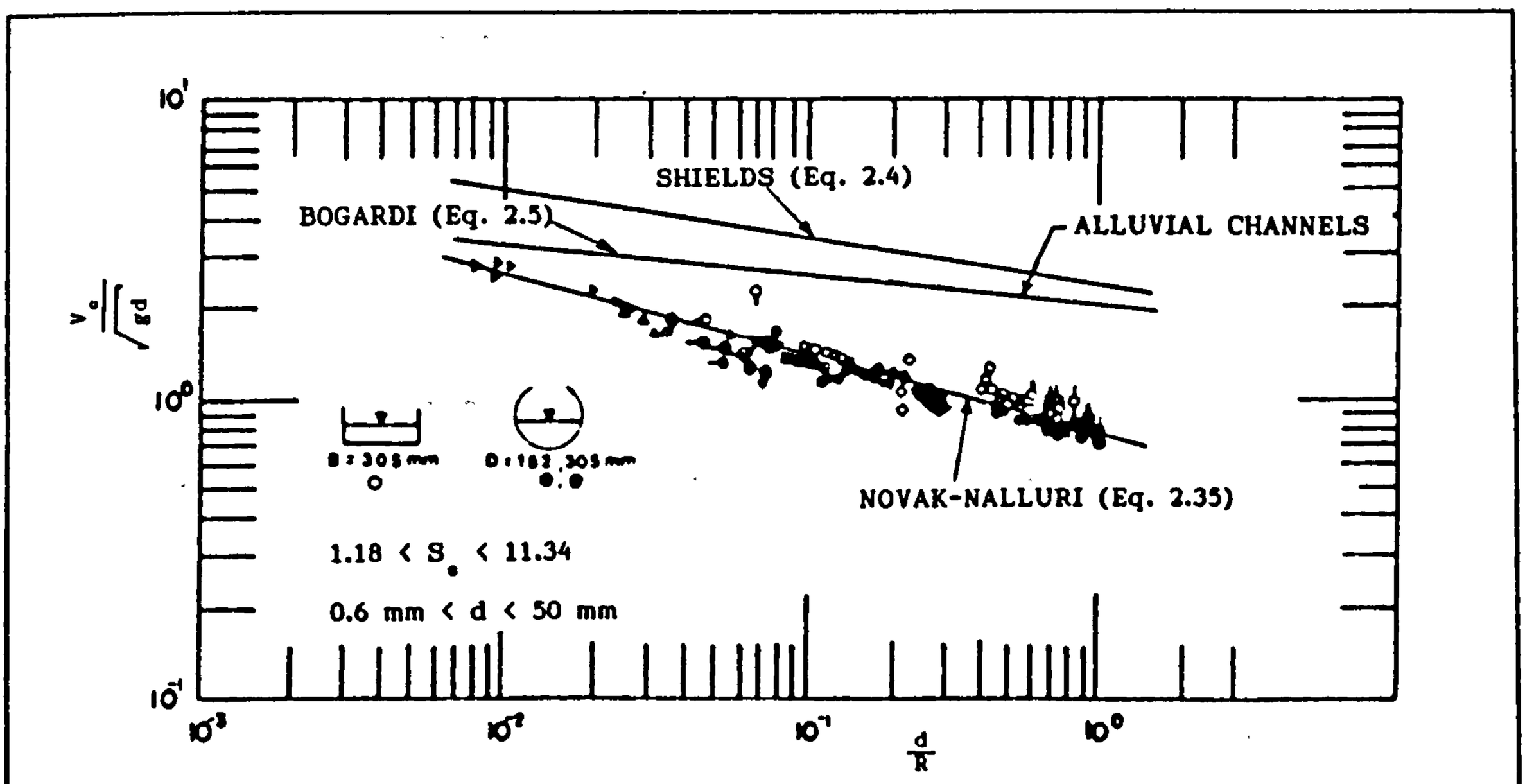

FIGURE 2.17: CRITICAL VELOCITY PARAMETER VS. RELATIVE SAND SIZE (NOVAK & NALLURI, 1975)

b) Sediment Transport with Limit Deposition Condition

The limit deposition velocity (V_L) refers to the velocity for which the transported particles are just about to deposit on the channel invert. It is the minimum velocity required to prevent deposits forming at a given sediment transport rate.

Ambrose (1953) carried out an experimental study in smooth pipes (50.8 mm and 152.4 mm diameters) to complement that of Craven (1953). Uniform sands sizes 0.25, 0.58 and 1.62 mm were used. He obtained a transport function (Eq. 2.36) for his Case I for "impending deposition" (limit deposition) and concluded that for,

$$\frac{Q}{g^{2/5}\ D^2\ Q_s^{\ 1/5}(S_s - 1)^{2/5}} \leq 2.9 \qquad (2.36)$$

where Q_s is absolute volume rate of transport, no deposition will occur in the pipe.

Pedroli (1963) from his experiments in rectangular channels with rigid smooth beds suggested a sediment transport equation, which expressed in S.I units yields:

$$\frac{\tau^{8/5}\ g^{3/5}\ d^{1/5}}{\gamma^{8/5}\ \nu^{1/5}} = 1.6 + 0.069\ \frac{g_s}{\gamma_s\ \nu} \qquad (2.37)$$

where g_s is the mass rate of sediment per unit width (Kg/sm), τ is the shear stress in (Kgf/m^2), d_{50} is the particle size in (m), ν is the kinematic viscosity of water in (m^2/s) and γ_s the specific gravity of the sediment in (Kgf/m^3) (old metric units!).

Novak and Nalluri (1975) additionally studied the limit deposition criterion in their experiments. They used graded sands of uniform size ranging from 0.15 to 2 mm and volumetric sediment concentration from 1.7×10^{-5} to 2.4×10^{-3}. An expression for limit deposition criteria, using Einstein's transport and flow parameters, was presented:

$$\phi = 11.6\ \psi^{-2.04} \tag{2.38}$$

Replacing channel slope S by Darcy's equation for head loss,

$$S = \frac{\lambda V^2}{8gR} \tag{2.39}$$

Eq. 2.38 can be written as:

$$\frac{V_L}{\sqrt{8g(S_s - 1)R}} = 0.632 \left(\frac{d}{R}\right)^{0.175} C_v^{0.325}\ \lambda^{-0.662} \tag{2.40}$$

where V_L is the limit deposition velocity, C_v the volumetric sediment concentration, d the particle size, S_s the density of the sediment, R the hydraulic radius, and λ the overall friction coefficient.

Similarly May (1989) did rearrange Graf-Acaroglu's expression for sediment transport (Eq. 2.15) and obtained:

$$\frac{V}{\sqrt{8g(S_s - 1)R}} = 0.732 \left(\frac{d}{R}\right)^{0.252} C_v^{0.248}\ \lambda^{-0.624} \tag{2.41}$$

where R is the hydraulic radius, λ the overall friction coefficient for the pipe, and V the mean flow velocity.

Although Eq. 2.40 was derived for limit deposition criterion in pipes, it shows certain similarities to Eq. 2.41, which is another form of Graf-Acaroglu's general equation (Eq. 2.15) for sediment transport in pipes and open (alluvial) channels.

In Fig. 2.18 Novak-Nalluri Eq. 2.38 is plotted together with Pedroli's data and Graf-Acaroglu Eq. 2.15 for comparison. It is apparent that for the same value of flow intensity parameter (ψ), a higher value of transport parameter (ϕ) applies in cases of channels of fixed smooth beds. As in the case of alluvial beds a great deal of the flow energy is dissipated by the bedforms, the sediment transport capacity of the flow is diminished.

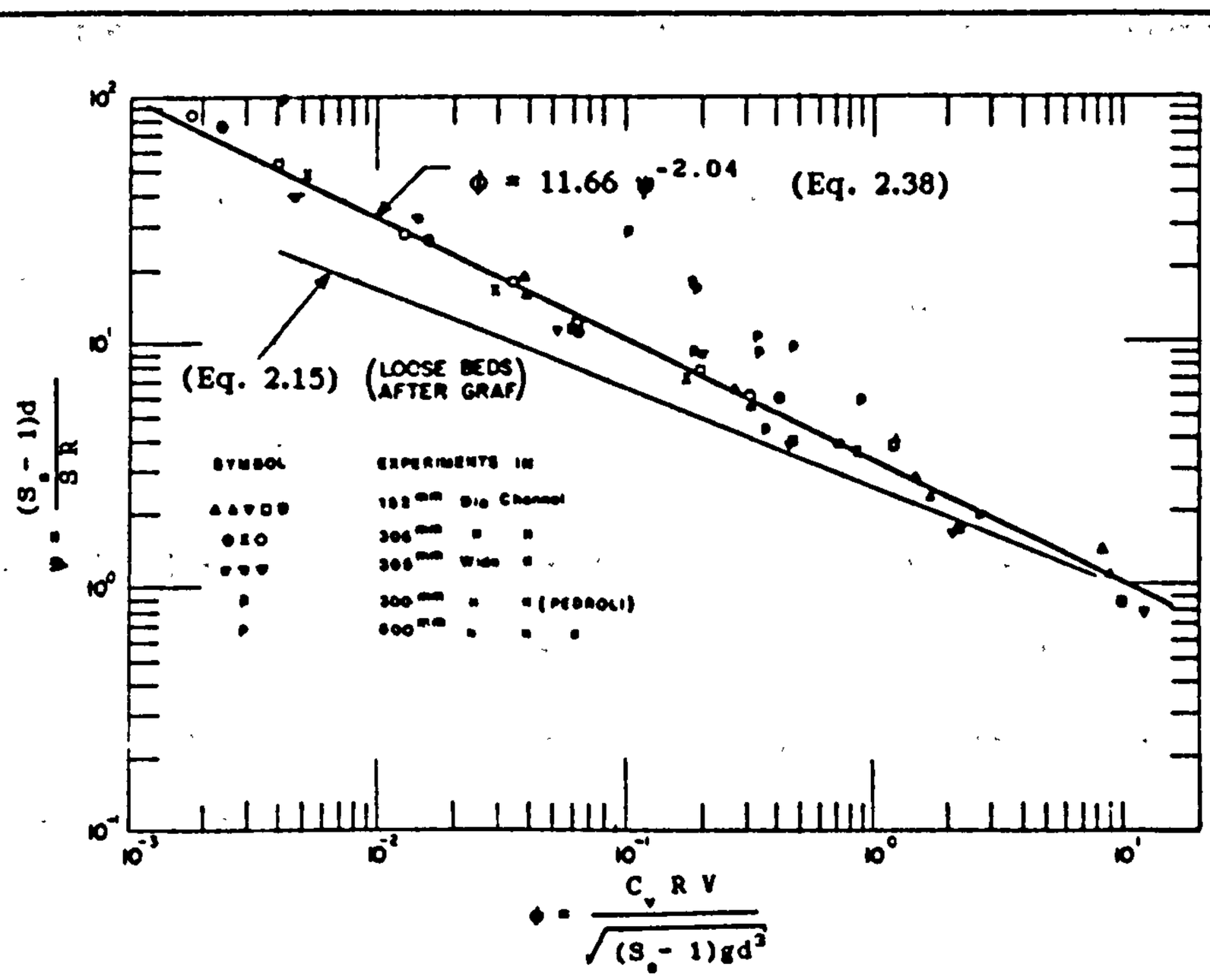

FIGURE 2.18: TRANSPORT VS. SHEAR INTENSITY PARAMETERS (Novak & Nalluri, 1975)

May (1975) re-analysed Laursen's data (1956) for limit deposition criterion in smooth pipes (51 and 152 mm diameters). Sand sizes ranged between 0.25 and 1.6 mm. The best-fit relation obtained was:

$$\frac{V_L}{\sqrt{2g(S_s - 1)y}} = 7.0\ C_v^{1/3} \qquad (2.42)$$

where V_L is the mean velocity in the pipe at limit deposition, y is the flow depth, C_v is the volumetric sediment concentration, and S_s is the relative density of the sediments.

Robinson and Graf (1972) carried out transport experiments in two smooth pipes (102 and 152 mm diameters) flowing full. They used two sediment sizes, 0.45 and 0.88 mm. The volumetric sediment concentration (C_v) was varied between 10^{-3} and $7x10^{-2}$. A relation for the limit deposition criterion was obtained as:

$$\frac{V_L}{\sqrt{2g(S_s - 1)D}} = \frac{0.928\ C_v^{0.105}\ d^{0.056}}{1 - \tan\theta} \qquad (2.43)$$

where d is the sediment size in (mm), $\tan\theta$ is the slope of the pipe (θ positive for an upwards sloping pipe), S_s the relative density of the sediment, V_L the velocity at limit deposition, and D the pipe diameter.

May (1982) conducted tests on limit deposition criterion at Hydraulics Research Ltd. using two smooth pipes (77 mm and 158 mm diameters). He employed three sediment sizes, 0.6 mm, 5.8 mm and

7.9 mm, and the volumetric sediment concentrations ranged between 120 and 2110 ppm. He suggested the best-fit equation:

$$C_v = 0.0205\left(\frac{D^2}{A}\right)\left(\frac{d}{R}\right)^{0.6}\left(1 - \frac{V_c}{V_L}\right)^4\left(\frac{V_L}{g(S_s - 1)D}\right)^{3/2} \qquad (2.44)$$

where D is the pipe diameter, A is the cross-sectional area, R is the hydraulic radius of the flow, C_v is the volumetric sediment concentration, V_L is the mean velocity in the pipe at limit deposition, and V_c is the threshold velocity from Novak and Nalluri (Eq. 2.35).

Macke (1982) conducted transport experiments in smooth pipes with diameters 192, 290 and 445 mm. Two sand sizes were used, 0.16 mm and 0.37 mm. He plotted his data (see Fig. 2.19) together with the data of other investigators. Two regions are indicated, Region I, which relates to the transport of sediments over loose (alluvial) beds channels, and Region II, which relates to the transport of sediments over fixed bed channels (limit deposition criterion).

For the transport over loose beds Macke (1982) obtained (see Fig. 2.19, Region I)) the best-fit Equation:

$$Q_s^* = Q_s\, \rho g(S_s - 1)w_s^{3/2} = 0.000164\, \tau_o^3 \qquad (2.45)$$

where Q_s^* is a sediment transport parameter in $\left(\frac{N}{s}(\frac{m}{s})^{3/2}\right)$, w_s is the fall velocity of the particle in (m/s), and τ_o the mean shear stress in (N/m^2).

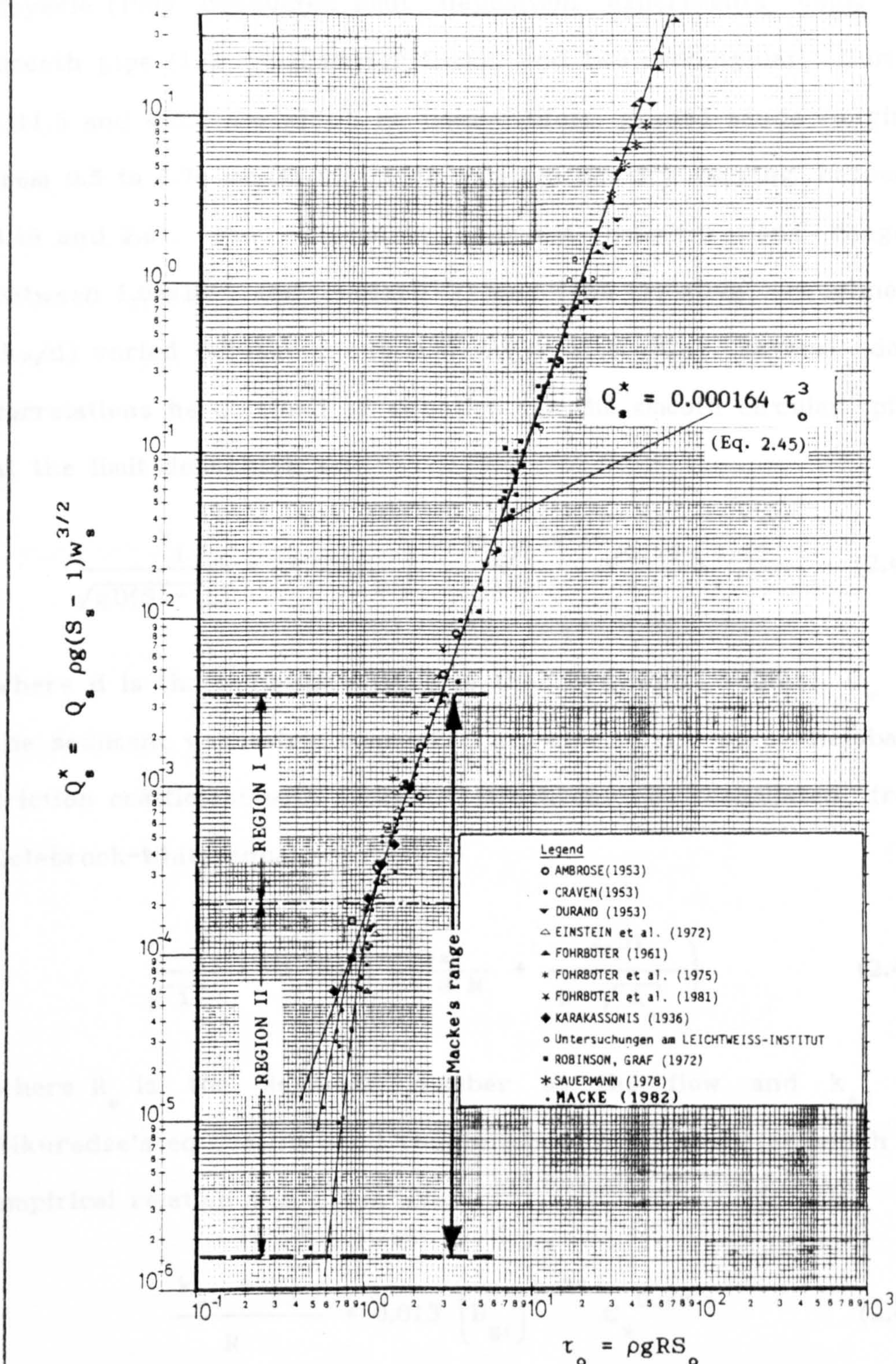

FIGURE 2.19: TRANSPORT PARAMETER VS. MEAN SHEAR STRESS FOR PIPES (Macke, 1982)

Mayerle (1988) conducted limit deposition experiments using a smooth pipe (152 mm diameter flume) and two rectangular flumes (311.5 and 462.3 mm wide). He used uniform graded sands ranging from 0.5 to 8.74 mm in size with relative density varying between 2.49 and 2.61. The volumetric sediment concentrations ranged between 1.03×10^{-5} and 3.03×10^{-3}, and the relative roughness (k_s/d) varied between 0 and 0.87. After attempting several data correlations he obtained an equation for the smooth circular pipe at the limit deposition as:

$$\frac{V_L}{\sqrt{gD(S_s - 1)}} = 14.43 \left(D_{gr}\right)^{-0.14} \left(\frac{d}{R}\right)^{-0.56} C_v^{0.18} \lambda_s^{0.18} \qquad (2.46)$$

where d is the sediment size, R is the hydraulic radius, C_v is the sediment volumetric concentration, and λ_s is Darcy-Weisbach friction coefficient with sediment, which can be calculated from Colebrook-White equation:

$$\frac{1}{\sqrt{\lambda_s}} = -2 \log \left(\frac{k_{ss}}{14.8\ R} + \frac{2.51}{R_e \sqrt{\lambda_s}} \right) \qquad (2.47)$$

where R_e is the Reynolds number of the flow and k_{ss} is Nikuradse's equivalent sand roughness with sediment for which an empirical relation was given as:

$$\frac{k_{ss} - k_s}{R} = 0.013 \left(D_{gr}\right)^{0.24} C_v^{0.40} \qquad (2.48)$$

with $r^2 = 0.21$, k_s being Nikuradse's equivalent sand roughness with clear water.

Parameter D_{gr} is the non-dimensional grain diameter defined as:

$$D_{gr} = \left[\frac{g\ (S_s - 1)}{\nu^2}\right]^{1/3} d \qquad (2.49)$$

The non-dimensional grain diameter D_{gr} is identical to the parameter D_* (Eq. 2.24), used by Van Rijn (1984) in his classification of bedforms. It is also equivalent to Yalin's particle number Ξ, (Eq. 2.20) as they are related by:

$$\Xi = \left(D_{gr}\right)^3 \qquad (2.50)$$

For rectangular channels Eqs. 2.46, 2.47 and 2.48 become:

$$\frac{V_L}{\sqrt{gd(S_s - 1)}} = 11.59\left(D_{gr}\right)^{-0.14}\left(\frac{d}{R_b}\right)^{-0.43} C_v^{0.15}\ \lambda_{bs}^{0.18} \qquad (2.51)$$

with $r^2 = 0.93$,

$$\frac{1}{\sqrt{\lambda_{bs}}} = -2\ \log\left(\frac{k_{sb}}{11.55\ R_b} + \frac{2.51}{R_{eb}\sqrt{\lambda_{eb}}}\right) \qquad (2.52)$$

$$\frac{k_{bss} - k_{bs}}{R_b} = 0.0245\left(D_{gr}\right)^{0.40} C_v^{0.44} \qquad (2.53)$$

with $r^2 = 0.38$, respectively. where V_L is the mean flow velocity at limit deposition conditions, R_b is the bed hydraulic radius, d is the particle size, S_s is the sediment relative density, C_v is the sediment volumetric concentration, D_{gr} is the non-dimensional grain diameter, λ_{bs} is the bed friction coefficient with sediment, and k_{sb} and k_{ssb} are the equivalent bed roughnesses with clear water and with sediment respectively.

Based on Eqs. 2.46 to 2.53, Nalluri and Mayerle (1989) proposed a method for evaluation of the necessary velocities for non-deposition in channels of rectangular and circular cross-section.

Kithsiri (1990), using the same experimental facilities as Mayerle (1988), extended the range of relative roughness up to 2.5. He conducted limit deposition experiments using a rectangular flume 311.5 mm wide. He used uniform graded sands ranging from 1 to 8.4 mm in size with relative density varying between 2.61 and 2.63. The volumetric sediment concentrations ranged between $1.x10^{-5}$ and $4.3x10^{-3}$. Kithsiri (1990) obtained the following equations:

$$\frac{V_L}{\sqrt{gd(S_s - 1)}} = 4.96\left(D_{gr}\right)^{-0.02}\left(\frac{d}{R_b}\right)^{-0.61} C_v^{0.08}\,\lambda_{bs}^{0.5} \qquad (2.54)$$

with $r^2 = 0.966$, and

$$\frac{k_{ssb} - k_{sb}}{R_b} = 0.0927\left(D_{gr}\right)^{0.64} C_v^{0.61} \qquad (2.55)$$

with $r^2 = 0.683$. where V_L is the mean flow velocity at limit deposition conditions, R_b is the bed hydraulic radius, d is the particle size, S_s is the sediment relative density, C_v is the sediment volumetric concentration, D_{gr} is the non-dimensional grain diameter, λ_{bs} is the bed friction coefficient with sediment, and k_{sb} and k_{ssb} are the equivalent bed roughnesses with clear water and with sediment respectively. From Eqs. 2.52, 2.54 and 2.55 the required velocities for non-deposition condition in rectangular channels can be estimated.

Using his own data Kithsiri proposed a new method based on determining the minimum shear stress required for non-deposition condition. The method is based on the following best fit equations:

$$\frac{\tau_b}{\rho(S_s - 1)gd} = 3.24\left(D_{gr}\right)^{-0.02}\left(\frac{d}{R_b}\right)^{-1.23} C_v^{0.17}\,\lambda_{bs}^{1.98} \qquad (2.56)$$

with $r^2 = 0.966$, and

$$\frac{\tau_b}{\rho(S_s - 1)gd} = 2.29\left(D_{gr}\right)^{-0.04}\left(\frac{d}{R_b}\right)^{-1.23} C_v^{0.16}\,\lambda_{bs}^{1.91}\left(\frac{k_{bss} - k_{bs}}{d}\right)^{0.04} \qquad (2.57)$$

with $r^2 = 0.972$ and

$$\lambda_{bs} = 0.694\,\lambda^{0.88}\,C_v^{0.02}\,D_{gr}^{0.06} \qquad (2.58)$$

with $r^2 = 0.965$, where τ_b is the bed shear stress at limit deposition conditions, R_b is the bed hydraulic radius, d is the particle size, S_s is the sediment relative density, C_v is the sediment volumetric concentration, D_{gr} is the non-dimensional grain diameter, λ_{bs} is the bed friction coefficient with sediment, and k_{sb} and k_{ssb} are the equivalent bed roughnesses with clear water and with sediment respectively.

Using Mayerle's data Kithsiri obtained a set of equations for determining the minimum shear stress required for non-deposition condition as:

$$\frac{\tau_b}{\rho(S_s - 1)gd} = 13.91\left(D_{gr}\right)^{-0.27}\left(\frac{d}{R_b}\right)^{-0.86} C_v^{0.29}\,\lambda_{bs}^{1.36} \qquad (2.59)$$

with $r^2 = 0.928$, and

$$\frac{\tau_b}{\rho(S_s - 1)gd} = 39.12\left(D_{gr}\right)^{-0.28}\left(\frac{d}{R_b}\right)^{-0.99} C_v^{0.36}\ \lambda_{bs}^{1.68}\left(\frac{k_{bss} - k_{bs}}{d}\right)^{-0.15} \quad (2.60)$$

with $r^2 = 0.945$ and

$$\lambda_{bs} = 0.791\ \lambda^{0.82}\ C_v^{0.05}\ D_{gr}^{0.02} \quad (2.61)$$

with $r^2 = 0.919$, where τ_b is the bed shear stress at limit deposition conditions, R_b is the bed hydraulic radius, d is the particle size, S_s is the sediment relative density, C_v is the sediment volumetric concentration, D_{gr} is the non-dimensional grain diameter, λ_{bs} is the bed friction coefficient with sediment, and k_{sb} and k_{ssb} are the equivalent bed roughnesses with clear water and with sediment respectively.

Finally using his own data and Mayerle's data Kithsiri proposed a method based on determining the minimum shear stress required for non-deposition condition. The method is based on the following best fit equations:

$$\frac{\tau_b}{\rho(S_s - 1)gd} = 12.93\left(D_{gr}\right)^{-0.21}\left(\frac{d}{R_b}\right)^{-0.98} C_v^{0.29}\ \lambda_{bs}^{1.5} \quad (2.62)$$

with $r^2 = 0.918$, and

$$\frac{\tau_b}{\rho(S_s - 1)gd} = 32.03\left(D_{gr}\right)^{-0.22}\left(\frac{d}{R_b}\right)^{-1.08} C_v^{0.35}\ \lambda_{bs}^{1.79}\left(\frac{k_{bss} - k_{bs}}{d}\right)^{-0.14} \quad (2.63)$$

with $r^2 = 0.929$ and

$$\lambda_{bs} = 0.851\ \lambda^{0.86}\ C_v^{0.04}\ D_{gr}^{0.03} \quad (2.64)$$

with $r^2 = 0.964$, where τ_b is the bed shear stress at limit deposition conditions, R_b is the bed hydraulic radius, d is the

particle size, S_s is the sediment relative density, C_v is the sediment volumetric concentration, D_{gr} is the non-dimensional grain diameter, λ_{bs} is the bed friction coefficient with sediment, and k_{sb} and k_{ssb} are the equivalent bed roughnesses with clear water and with sediment respectively.

The empirical equations for transport over loose (alluvial) beds as well as for transport over fixed beds (limit deposition criterion) that have been presented in this chapter show certain similarities. However, they still differ in their predictions. This reflects the difficulties involved in this type of experiments. Therefore care should be taken to apply them within their respective experimental ranges.

2.1.3 Sewer Design Considerations

Once the design discharge for a sewer reach has been estimated a pipe diameter and slope have to be selected. The British Code of Practice (BS-CP8005) indicates that sewers shall be laid at such gradients that will produce high enough cleansing velocities to prevent deposition of sediment in the invert of the pipe. The self-cleansing velocities (0.75 and 1 m/s, assuming half full pipe flow and full pipe flow conditions, respectively) shall occur at least once a day.

In practice two different approaches are used. One approach considers the minimum velocity to attain self-cleansing conditions, as recommended by the BS-CP8005. The other approach considers the minimum shear stress required to prevent deposition, as used in some European countries.

As the main parameter responsible for erosion and transport of sediment is the shear stress it seems more appropriate the use of the minimum shear stress criterion. Combining Manning's resistance equation

$$V = \frac{1}{n} R^{2/3} S_o^{1/2} \qquad (2.65)$$

with the shear stress equation

$$\tau_o = \rho g R S_o \qquad (2.66)$$

yields for mean velocity:

$$V = \frac{1}{n} R^{1/6} \sqrt{\frac{\tau_o}{\rho g}} \qquad (2.67)$$

and for the shear stress

$$\tau_o = \frac{\rho g}{R^{1/3}} \left(\frac{V^2 n^2}{S_o} \right) \qquad (2.68)$$

Substituting the hydraulic radius for the diameter ($R = \frac{D}{4}$) in Eq. 2.67 the mean velocity (V) has been plotted (see Fig. 2.20) against pipe diameter (D) for various mean shear stresses. The computations were made assuming concrete pipe (Manning's n = 0.013) and half full pipe uniform flow. The curves were plotted in logarithmic scales to obtain straight lines.

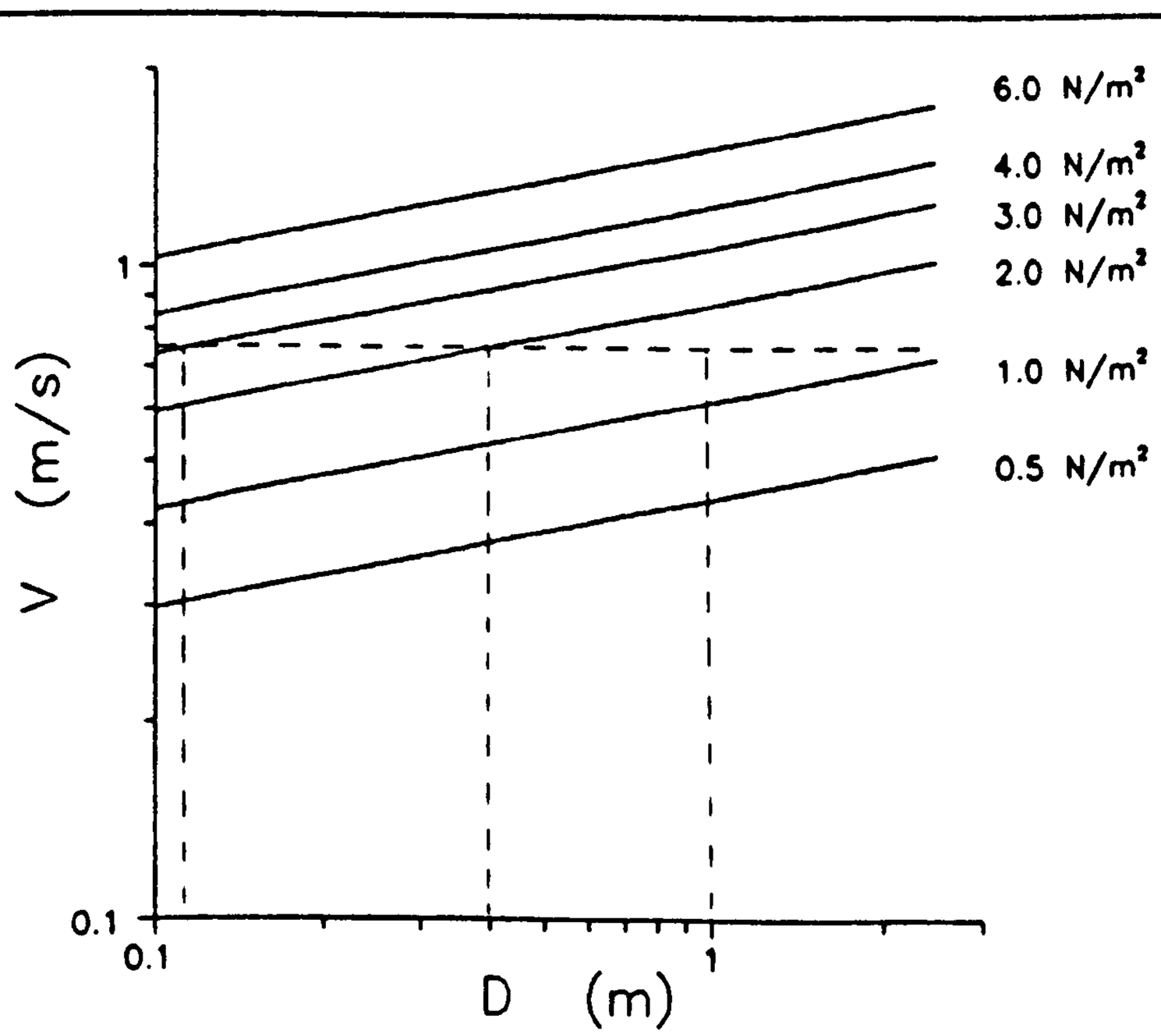

FIGURE 2.20: SELF-CLEANSING VELOCITY CRITERION

Assuming concrete pipe (n = 0.013) and half full flow (Y /D = 1/2)

The use of the self-cleansing velocity criterion (0.75 m/s) has two drawbacks. First, smaller diameter pipes will tend to be over-designed (i.e., with shear stresses higher than necessary). For example 125 mm pipe (see Fig. 2.20) will have a mean shear stress of 3 N/m^2. And second, larger diameter pipes will be under-designed (i.e., with shear stresses lower than required for non-deposition conditions). For example a 2.5 m diameter pipe (see Fig. 2.20) will only have about 1 N/m^2.

In Fig. 2.21 the shear stress (τ_o) has been plotted (for various flow velocities) against pipe diameter (D), assuming concrete pipe, n = 0.013, and half full uniform flow (Eq. 2.68).

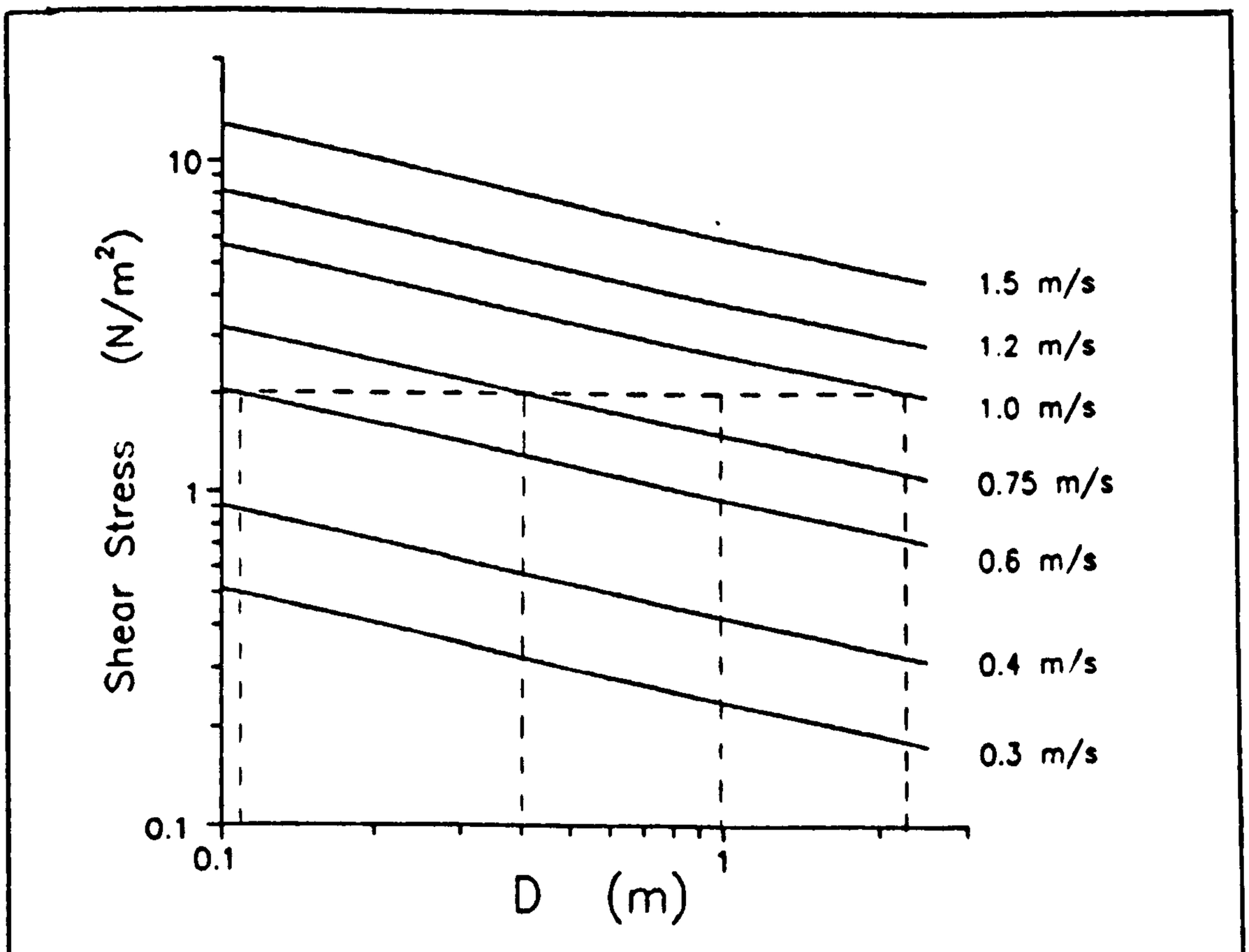

FIGURE 2.21: MINIMUM SHEAR STRESS CRITERION

Assuming concrete pipe (n = 0.013) and half full flow ($Y_o/D = 1/2$)

In Fig. 2.21 it is apparent that by limiting the shear stress flow velocities will depend on pipe diameter. For example, if a design shear stress of 2 N/m^2 is selected, a 125 mm diameter pipe (see Fig. 2.21) will have a velocity of 0.6 m/s, a 400 mm diameter pipe 0.9 m/s and a 2.25 m diameter pipe 1 m/s.

The use of higher self-cleansing velocities (1 m/s) results in safer and yet over-designed sewers. A 100 mm diameter pipe will have about 5.7 N/m^2 in the example (see Fig. 2.20). This does not solve the problem of improving sewer design.

The preceding studies mentioned above made clear that sediment concentration is a very important factor in the determination of the self-cleansing velocity. However, the British Code of Practice does not take sediment concentration into account.

One application of the results of sediment transport studies is in sewer design (without deposition). Sewers are designed under the assumption that a sewer carry non-cohesive sediments only. However, from field studies (Crabtree, 1989) the presence of cohesive additives (fat, bitumen, organic material, etc.) has been observed, which increases the complexity of the problem even more.

2.2 COHESIVE SEDIMENT STUDIES

In this section a brief description of the properties of cohesive sediments, classification of clay minerals and rheology is presented. It is followed by a review of the recent investigations published on the initiation and transport of cohesive sediments.

2.2.1 Cohesive Sediment Properties

Cohesive sediments are characterized by several properties such as sensitivity, swelling, consolidation, flocculation, etc., which will be explained in this section. Past studies and research on sediment transport in pipe and channels were mostly related to non-cohesive sediment. Whereas the movement of non-cohesive sediment depends on the physical properties of the particles such as size, shape and density, in cohesive sediment the resistance to erosion depends on the strength of the cohesive bond between the particles. The most important factors determining cohesive sediment behaviour are its mineral composition, water content, degree of saturation and structure or fabric.

2.2.1.1 Classification of clay minerals

There are two main groups of atomic bonds that hold atoms together, primary bonds (ionic, covalent, and hydrogen and hydroxyl) and secondary bonds (van der Waals Forces and Electric bonds).

Almost all minerals with sheeted structure, which are encountered in the very fine soil fraction belong to the group known as clay minerals. This group can be divided into three classes.

a) Kaolinites

The structure of kaolinite is almost a perfect two-layer clay lattice based on a single sheet of silica tetrahedrons combined with a single sheet of alumina octahedrons. These sheets are held together tightly by hydrogen bonds and the structure is non-expandable. It has a low cation exchange capacity as exchangeable ions are located in the broken edges of the kaolinite plates.

b) Illites

Illites are characterized by a basic non-expanding three-layer clay structure consisting of a sheet of aluminium octahedrons between and combined with two sheets of silica tetrahedrons. In the octahedral sheet there is partial substitution of aluminium by magnesium and iron, and in the tetrahedral sheet there is partial substitution of silicon by aluminium. The combined sheets are linked together by weak bonding due to potassium ions (the only external exchangeable ions) held between them. Illites have a small cation exchange capacity.

c) Montmorillonite or Natural Smectites

Montmorillonites are characterized by a neutral three-layer structure. In the octahedral sheet there is partial substitution of aluminium by magnesium. The space between the combined sheets is occupied by water molecules and exchangeable cations other than potassium. The great amount of chemical substitution makes them very sensitive to their chemical environment and thus very important in the equilibria between solids and solution. Considerable swelling of montmorillonite can occur due to additional water being adsorbed between the combined sheets. The structure is held together by van der Waal forces, which are weak compared with the primary bonds that hold the atoms in the unit layer together. As a result cleavage parallel to the unit layer is favoured leading to the formation of the characteristic flakes of these minerals.

2.2.1.2 Structure of clay particle

A single particle of clay may consist of many sheets piled one on another. Clay particles are likely to be plate-shaped or to exhibit flat terraced surfaces. These flat surfaces carry residual negative electrical charges. However, the broken edges of the plates or the edges of the terraces may carry either positive or negative charges, depending upon the environment.

In clay the largest proportion of the inorganic component is crystalline, which is defined by the crystal chemistry. The most

important crystalline components (in clay) are the hydrous aluminosilicates, which have distinctive properties due to their structure, shape and very small particle size. These minerals are responsible for most of the qualities that characterize clay.

A high value of specific surface suggests that a large proportion of the total number of atoms making up a particle forms the surface of the particle, and that the particles consist, in general, of thin plates whose diameter may be as great as several hundred times the plate thickness.

A few water molecules dissociate into ions H+ and hydroxyl OH-. Impurities present in water dissociate as well into positively charged cations and negatively charged anions. Since the plane surface of the clay minerals carry negative electrical charges, the cations (including the H+ provided by the water itself) are attracted toward the surface of the plates (i.e., are adsorbed by the clay mineral).

Adsorbed ions are not permanently attached to the clay mineral. They may be replaced by other ions (i.e., cation exchange). Water adjacent to the negatively charged faces of the mineral may itself undergo alteration. Depending on the location and nature of the adsorbed cation and by the spacing of the crystal lattice of the clay mineral, water molecules may become organized into a pattern that is known as adsorbed water. Adsorbed water together with the adsorbed ions constitute the adsorption complex.

2.2.1.3 The Electric Double Layer

Adsorbed cations tend to accumulate near the surface of the clay particle due to the electrostatic attraction by the surface. Simultaneously they have a tendency to diffuse away from the surface towards the bulk of the solution, where their concentration is low. Thus a diffuse atmosphere of counter-ions is formed around the clay particle charge having the greatest density near the surface and decreasing density with increasing distance from it (Van Olphen, 1963). This is what is known as the electric double layer (see Fig. 2.22).

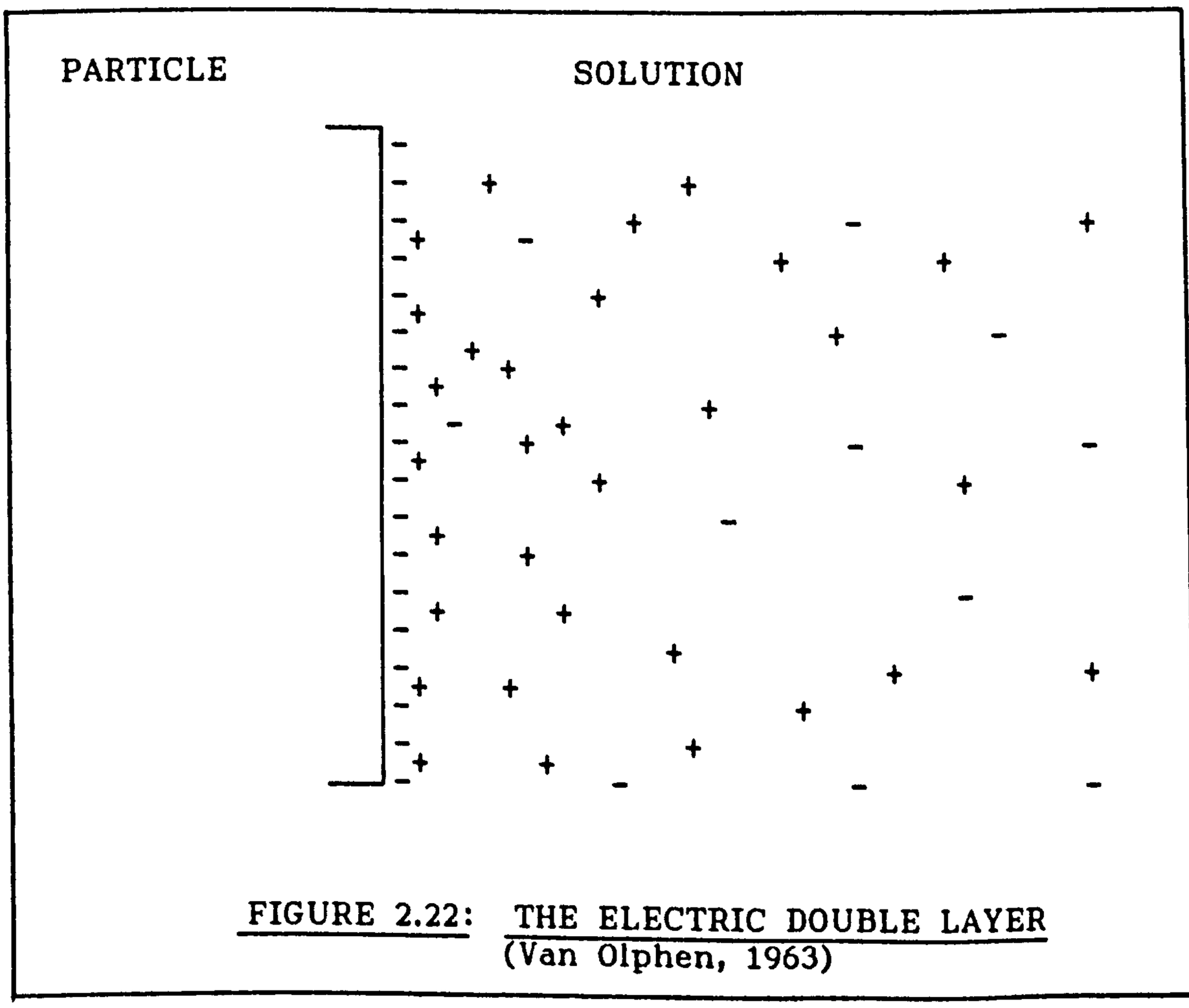

FIGURE 2.22: THE ELECTRIC DOUBLE LAYER
(Van Olphen, 1963)

The extension of the double layer in the solution decreases with increasing electrolyte concentration. When two clay particles carrying double layer approach each other they repel (double layer repulsion). Van der Waal forces between the particles must be of comparable magnitude in order to compete with the double layer repulsion (see Fig. 2.23).

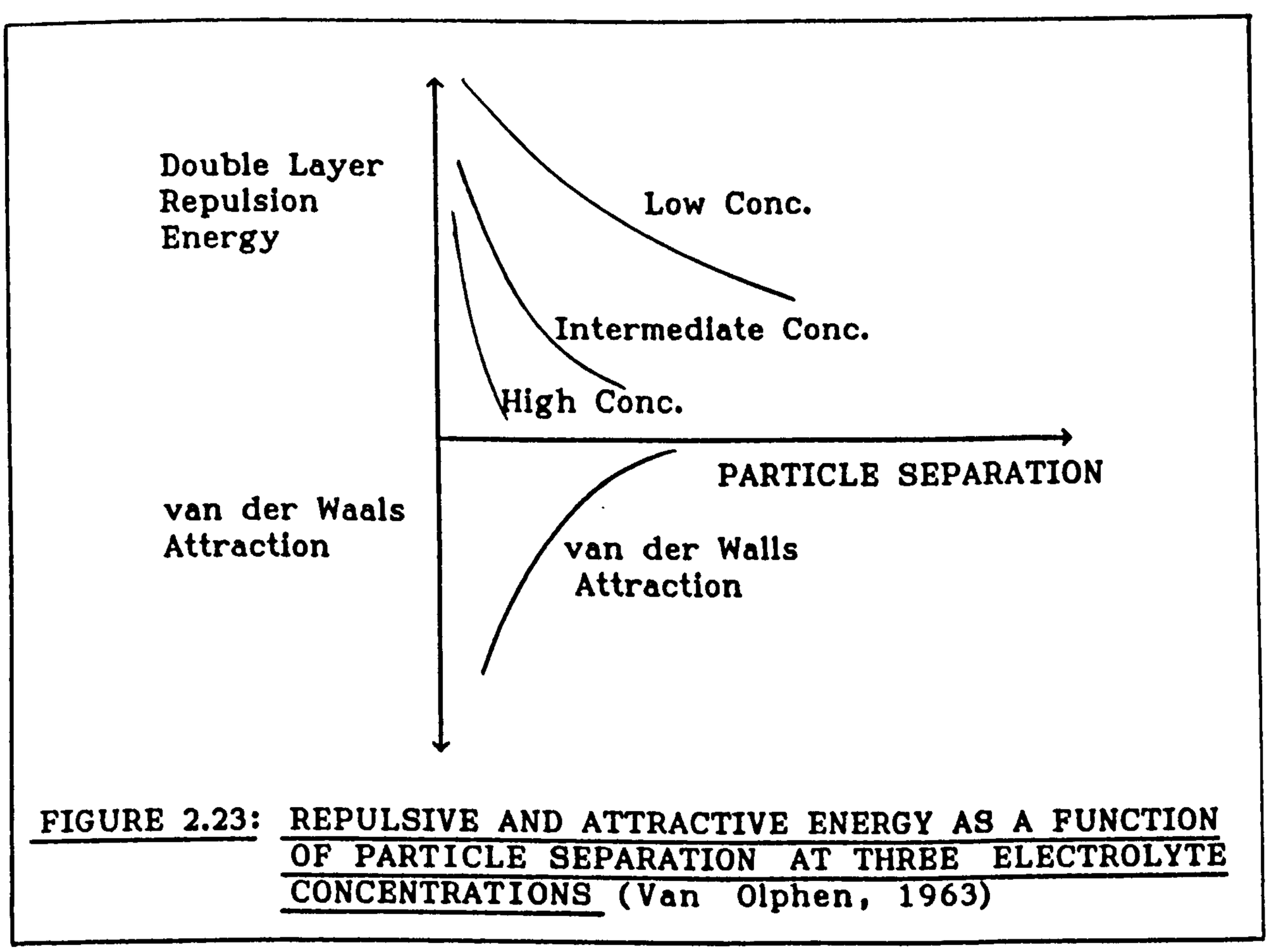

FIGURE 2.23: REPULSIVE AND ATTRACTIVE ENERGY AS A FUNCTION OF PARTICLE SEPARATION AT THREE ELECTROLYTE CONCENTRATIONS (Van Olphen, 1963)

2.2.2.4 Fabric of clay soils

The orientation in space of the fabric elements of which the soil is composed, is sometimes very important to the engineering properties of clay. When fabric elements display a mutual

parallelism they are said to have preferred orientation. This may be caused by deposition, growth or deformation.

According to Terzaghi (1967) some sediments or soils are composed of individual grains of silt and flocculated clay arranged in an arching skeleton enclosing large voids (honeycomb structure). This structure is a consequence of the forces associated with the surface of clay acting during sedimentation.

If clay particles are introduced into distilled water, the particles will be kept apart from each other by the repulsive force attributable to the negative charge of each particle. As the gravity force acting on each particle is negligibly small, the particle will either settle down very slowly or remain in suspension exhibiting Brownian movement. However, as natural water contains electrolytes some of the particles will attract and adsorb ions of opposite sign. Such particles can then be attracted to others forming up flocs large enough to settle down to the bottom by the action of the gravity force (i.e., flocculation takes place).

Sediment deposited by a flowing medium such as water is likely to show monoclinic symmetry of fabric. On the other hand sediment deposited in a static medium the fabric may be expected to have axial symmetry. The chemical composition of the fluid affects sediment fabric as well (flocculation, for example).

Three different modes of particle association must be considered in the flocculating system. Single crystal clay mineral platelets may associate in an edge-to-edge, edge-to-face, face-to-face or random pattern. Three different combinations of the two double layers are involved, and the total van der Waal attraction energies are different for the three modes of association.

Sometimes if the broken ends of the plates forming the particle carry positive charges, the particles in the flocs may have an edge-to-face structure (Fig. 2.24). In other circumstances the flocs may consist of particles in an essentially parallel structure (Fig. 2.25).

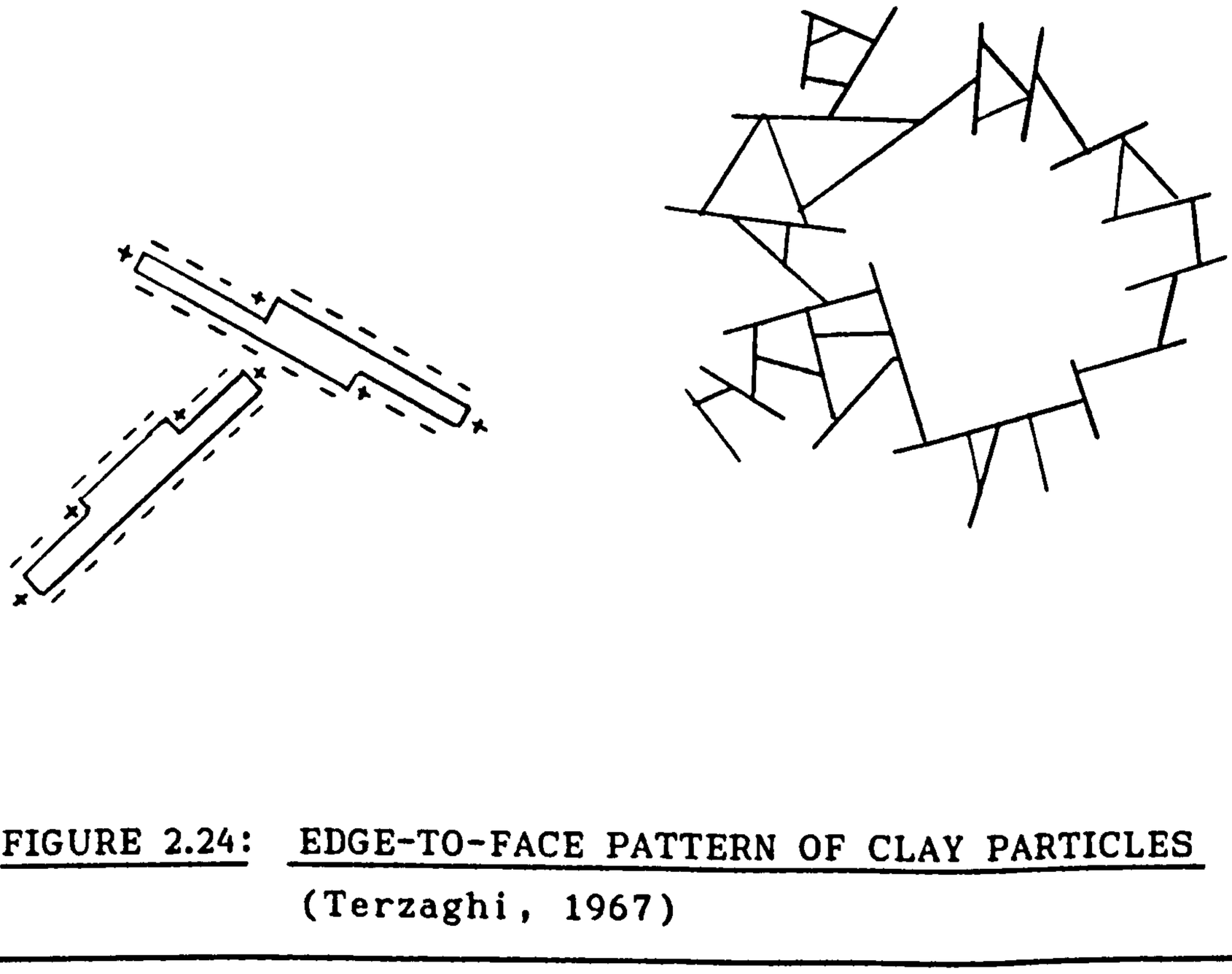

FIGURE 2.24: EDGE-TO-FACE PATTERN OF CLAY PARTICLES
(Terzaghi, 1967)

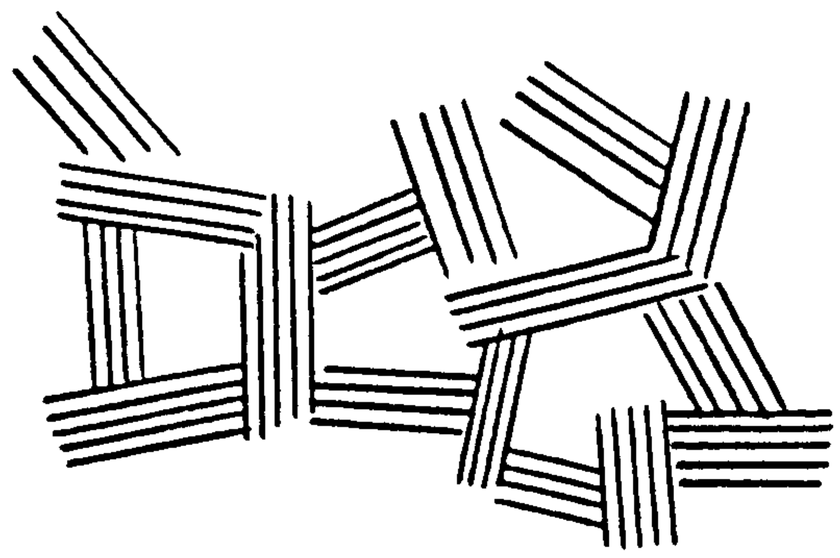

FIGURE 2.25: PARALLEL PATTERN OF CLAY PARTICLES
(Terzaghi, 1967)

Most sediments also contain coarser particles, which alter the whole arrangement of the soils. When sediments are kept under pressure the water content of the sediments decreases and the particles are forced closer together. The soil is said to *consolidate*. If the soil remains in free water and the pressure is decreased then the water content and the volume of the sediment increases. This is known as *swelling*.

Sediment subjected to shear stress (by flowing water, for example) will develop a resistance to shear through the interference between flocs. This phenomenon is especially marked if most of the structure of the clay is arranged in an edge-to-face pattern. Resistance also would be offered by the

attraction at the contact between the edges and faces of the particles. All this interference and attraction constitute the shearing resistance of the sediment.

If a natural sediment is well remoulded, the flocs are disrupted and many of the clay particles become oriented in nearly parallel arrays. Thus the shearing resistance of the sediment might have been substantially reduced. This property is known as *sensitivity*. Some clays have such a high sensitivity that after remoulding they assume the character of a viscous fluid.

2.2.1.5: Rheology of Clay Suspensions

Rheological properties are very important in the determination of sediment behaviour. They are rather indirect criteria for determining particle association.

There are various types of shear stress-strain relationships the simplest one being *Newtonian Fluids* (see Fig. 2.26-curve A) where the shear stress is proportional to the rate of deformation,

$$\tau = \mu \left(\frac{dV}{dy}\right) \qquad (2.69)$$

where μ is the viscosity of the material that is independent of the shear stress applied, and $\left(\frac{dV}{dy}\right)$ is the rate of shear.

Many systems display a more complicated flow behaviour. These are generally known as *Non-Newtonian Fluids*. For example in Fig. 2.26-curve B a *Yield Stress* (τ_y) has to be applied before

any flow may occur after which there is a linear relation between the shear stress and the rate of shear,

$$\tau = \tau_y + \mu \left(\frac{dV}{dy}\right) \qquad (2.70)$$

and these systems are defined as *Ideal Plastics.*

Another very commonly observed behaviour in dispersed systems is shown in Fig. 2.26-curve C, which approximates the ideal plastic flow and is called *Bingham Plastic Flow.* By extrapolation of the linear part of the curve the *Bingham Yield Stress* (τ_{yb}) is obtained at the intersection with the shear stress ordinate. This Bingham yield stress is somewhat higher than the true measured yield stress τ_y.

A complication arises in dealing with disperse systems (clay solutions) as their flow diagrams are dependent on the previous shear history of the system. Some systems become more fluid (thinner) when stirred, but then slowly recover their original consistency (see Fig. 2.27) when left at rest. They are said to exhibit *thixotropy.*

The reduction of yield stress when stirred suggests that the shear causes a breakdown of the particle links of the flocculated structure. The recovering of the yield stress after a period of rest, shows that the links are re-established by the Brownian motion that bring the particles back together.

The different modes of association determine (Partheniades, 1965) the rheological behaviour of a system. An edge-to-edge or an edge-to-face association, for example increases the viscosity and rigidity (yield stress) of a concentrated clay suspension. This type of association lead to the formation of continuous, linked, card-house structures, which extend throughout the total available volume as an aqueous gel is formed, which behaves like a Bingham system.

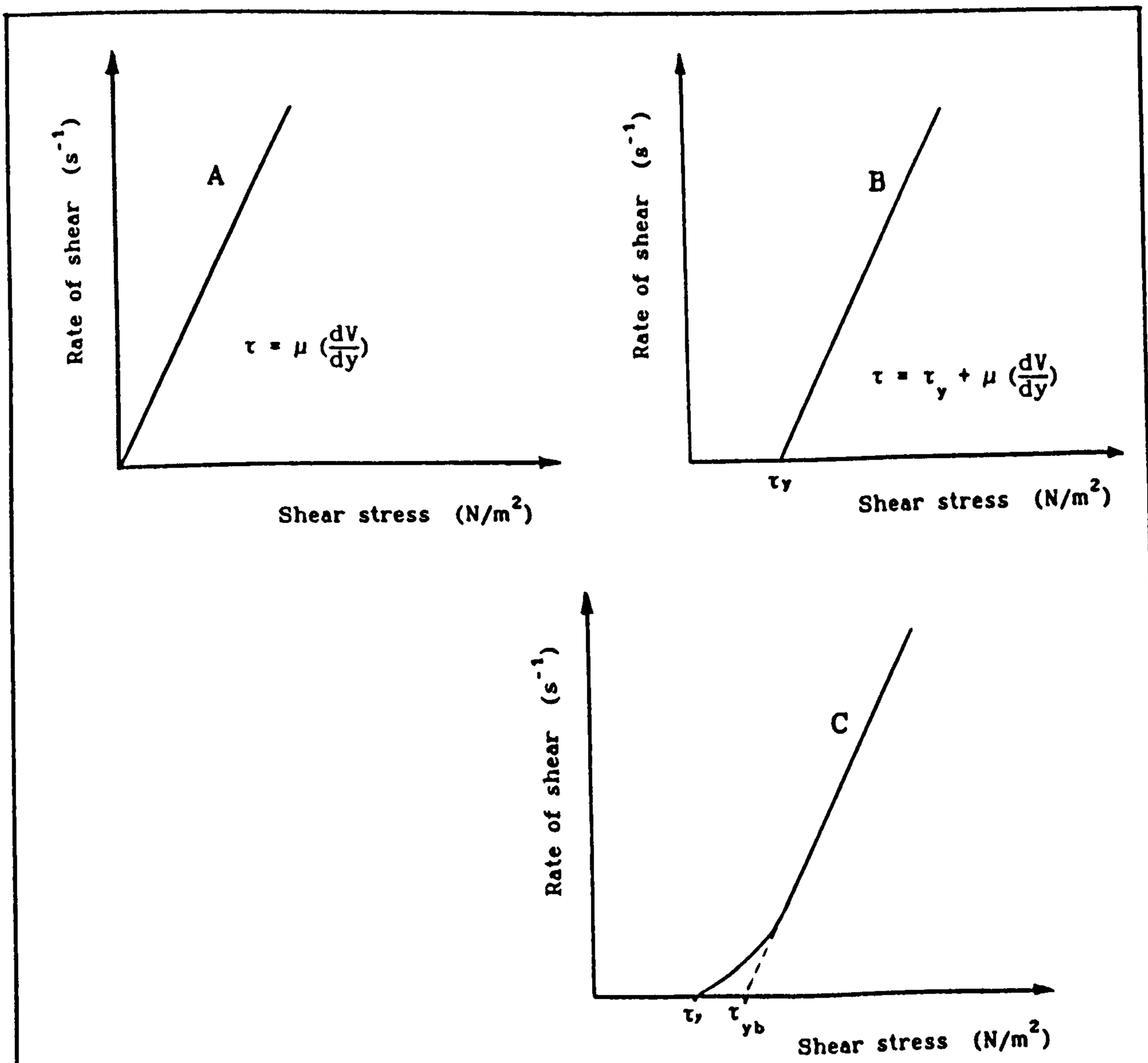

FIGURE 2.26: SHEAR STRESS VS. RATE OF SHEAR (clay solution)

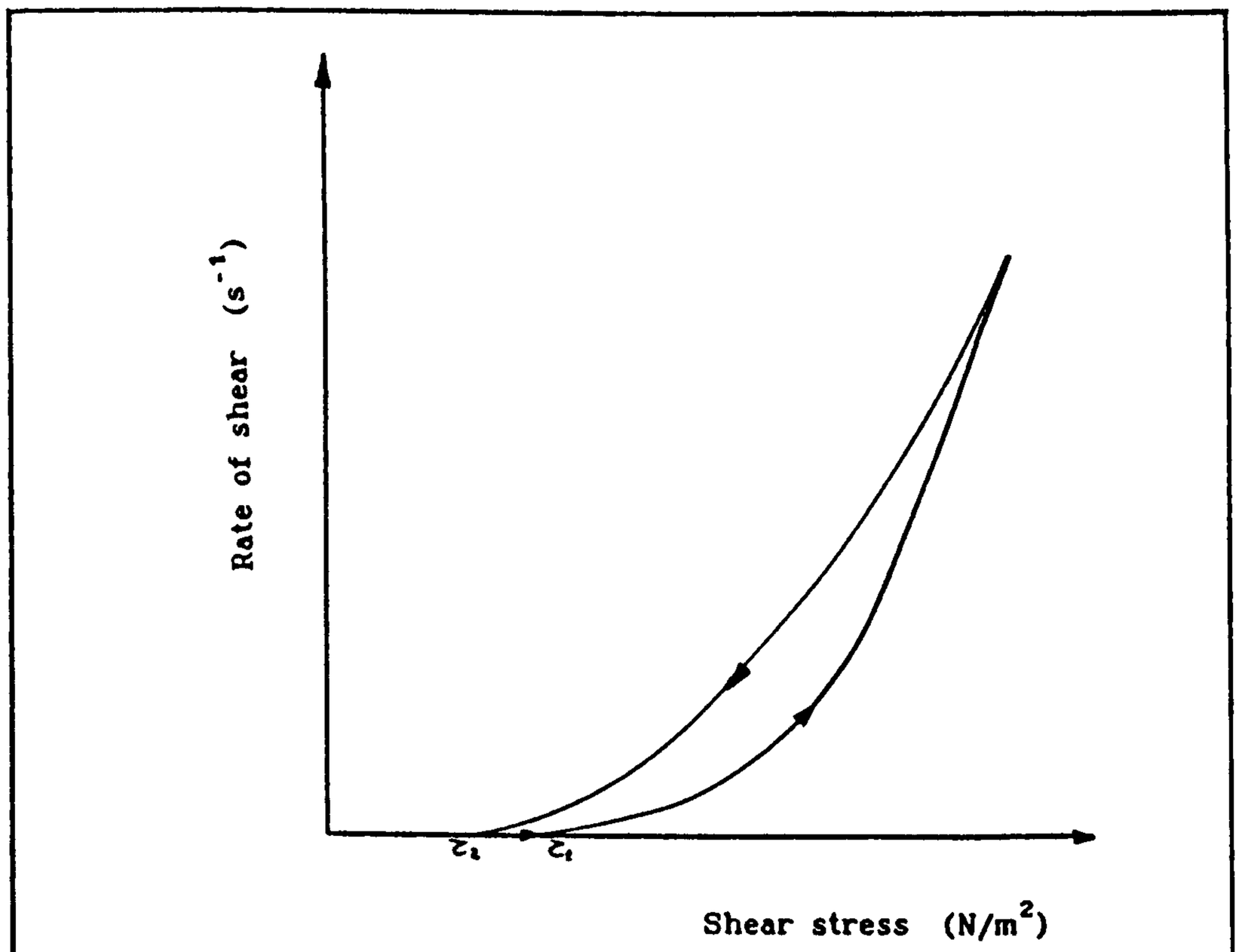

FIGURE 2.27: SHEAR STRESS V. RATE OF SHEAR (thixotropic solution)

2.2.2 Review of Laboratory Investigations on the Movement of Cohesive Sediments

In channels with cohesive sediment bed the values of Shields' function (ψ_c) for initiation of erosion are increased by the effect of cohesion. Erosion resistance in clay-water complex is principally governed by the electro-chemical forces. Thus apart from the shear stress caused by the eroding fluid other mechanical forces are not very important.

As more has been learned about soil properties, recently more effort is being directed towards the understanding of the interaction between water and fine particles, and to determine those hydraulic and soil properties, which control cohesive soil erosion and deposition. In this brief literature review only a general description of some of the main research works on the erosion of cohesive sediment (in chronological order) will be presented.

Laboratory research can be classified into two main groups: Consolidated clay beds and soft cohesive beds. Although the laws governing erodibility for both groups must be the same, the theoretical approaches and laboratory procedures can be quite different.

2.2.2.1 Consolidated Clay Beds

This group includes research on remoulded consolidated clays and the objectives are to study scour in terms of a critical shear stress and soil properties of the bed. Recently attempts have been made to include chemical parameters as it will be shown below. The equipment commonly used in these cases are: Re-circulating flumes, Submerged water jet and Rotating Cylinder Apparatus.

The earliest attempt to study erosion of cohesive material was reported by Dunn (1959). He carried out experiments with remoulded consolidated clay samples subjected to erosion by a submerged vertical water jet. The shear stress exerted by the submerged water jet was measured by a shear plate placed at the bottom of the cylinder. The critical shear stress was defined as that corresponding to the flow at which the water becomes cloudy and no subsequent clearing occurred. Dunn (1959) found a linear relation between critical shear stress and vane shear strength. The plasticity index, which ranged between 6 and 16, was also found (Dunn, 1959) to be good in estimating the critical shear stress.

Another earlier attempt correspond to Smerdon and Beasley (1959) who conducted experiments in an open flume with loosely placed soil without any strength measurements. They defined the critical shear stress as that corresponding to the point when the material

was in general motion. By correlating critical shear stress and plasticity index the following equation was obtained,

$$\tau_{oc} = 0.0034(PI)^{0.84} \tag{2.71}$$

where τ_{oc} is the critical mean shear stress in [lb/ft^2] and PI is the plasticity Index. The values of critical shear stress obtained with Eq. 2.71 are 10 to 15 times smaller than the corresponding values obtained by Dunn (1959).

Moore et al. (1962) experimented with a rotating-cylinder test apparatus to study the relative scour resistance of cohesive sediments. They found the depth of scour to be proportional to the logarithm of time during which erosion took place. Masch et al. (1963), using this apparatus defined the critical shear stress as the shear stress corresponding to the point at which appreciable quantities of sediment came loose from the sample and water in the annulus became cloudy.

Espey (1963) using the same type of apparatus, obtained a range of shear stresses at the stage of severe failure between 8.6 and 96 N/m^2, depending on the interpretation of the data. No attempt to correlate critical shear stress with soil properties was made.

Abdel-Rahman (1963) run experiments with artificially compacted clay and mixtures of clay and sand in an open flume. His objective was to establish a relationship between the mean

erosion depth and the mean bed shear stress and relate it to the soil shear strength as well. Shear stresses ranged between 0.7 and 4 N/m^2 and the plasticity index was 23 (%). Considering that for the same plasticity index Smerdon and Beasley (1959) gave a critical shear stress of 0.2 N/m^2, it seems that the shear stresses applied by Adbel-Rahman (1963) were beyond the critical conditions even though he did not define a critical shear stress as such.

Strong erosion was observed (Abdel-Rahman, 1963) at the beginning of the experiment with suspended and bed load but the erosion rate decreased and finally stopped with time. The time taken to reach the state of no erosion did not seem to be dependent on the shear stress. The stopping of erosion with time could be a result of the laboratory conditions that made the actual shear stress acting on the sediment bed diminish with time. Actually Abdel-Rahman (1963) does mention the presence of a gluey layer developed on the bed surface when reaching the steady state condition.

Enger (1963) carried out experiments in an open recirculatory flume, where 8 inches diameter samples were inserted in the middle of the flume. He found some relations for the critical shear stress and the moisture content at which the soil sample was compacted.

Lyle and Smerdon (1965) included the void ratio, which is an indication of the soil compaction. Their results clearly showed an increase in critical shear stress with a decrease in void ratio (see Fig. 2.28). The critical shear stress was also found to be directly related to the plasticity index.

Grissinger (1966) attempted to study the influence of some soil properties such as, bulk density, antecedent moisture content, type and orientation of clay minerals, percentage of clay, and water temperature. Instead of defining an arbitrary critical shear stress the determination of the soil erodibility was given in terms of mass erosion rate.

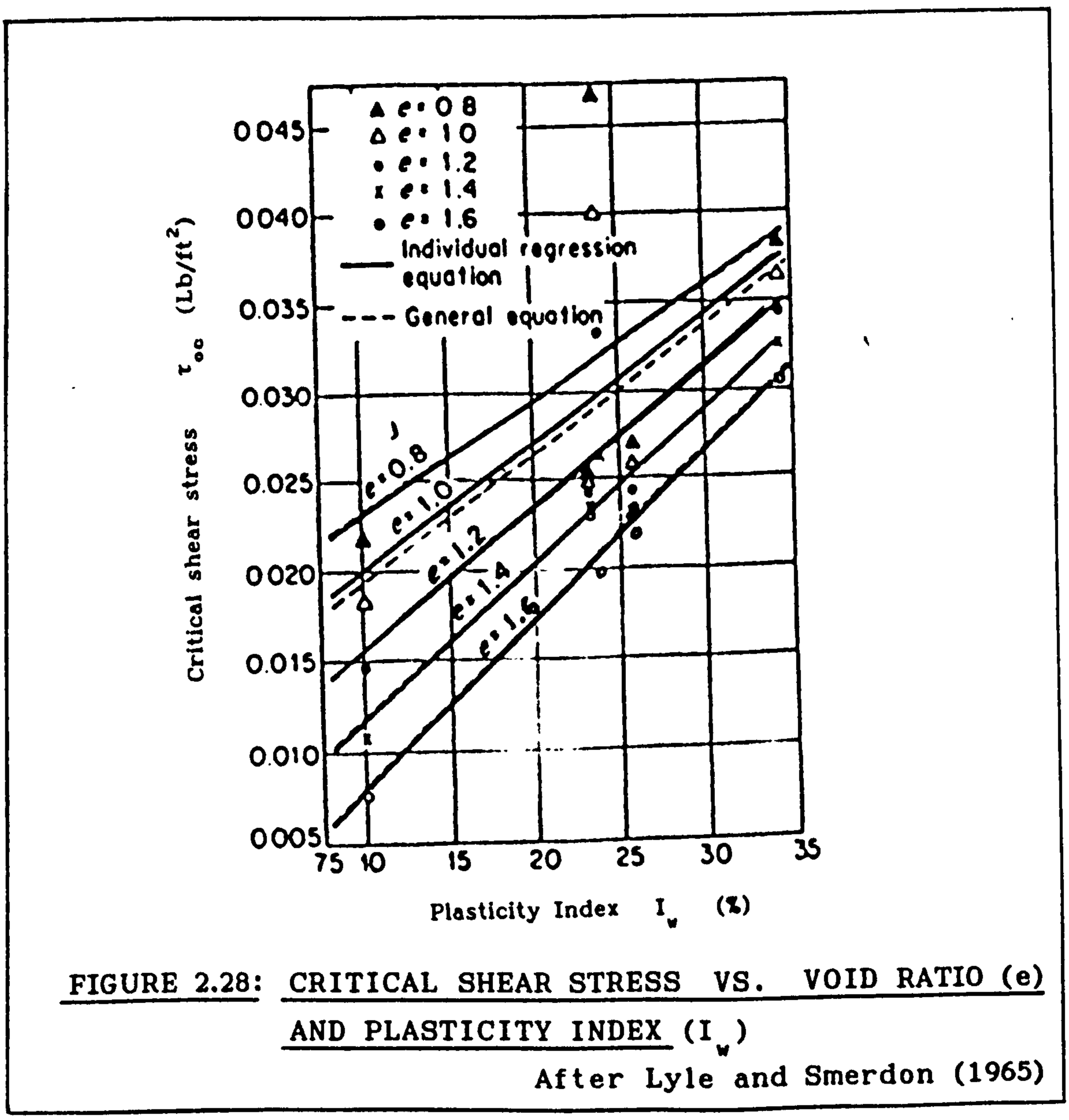

FIGURE 2.28: CRITICAL SHEAR STRESS VS. VOID RATIO (e) AND PLASTICITY INDEX (I_w)

After Lyle and Smerdon (1965)

It was found (Grissinger, 1966) that the orientation of the clay particles has a pronounced effect on erodibility. Erosion rates decrease with increasing degree of orientation. He also observed that the erodibility of the soil decreased by increasing the clay content, with one exception (montmorillonite) which could be attributed to swelling.

The antecedent moisture content (prior to testing) was found (Grissinger, 1966) to have a significant effect on erodibity on all the soil samples tested with the exception of kaolinite. He also found erosion rates to increase with increasing water temperature, and to decrease slightly with increasing bulk density although this last result was not very conclusive.

Kelly and Gularte (1981) carried out erosion experiments in a water tunnel with remoulded illite clay samples, subjected to high shear stress. The parameters studied were shear stress, salinity, water content, and temperature. The shear stress was measured with a shear plate, pH was kept constant (8.5), the velocity was measured with a propeller fibre optic current meter and a laser photocell was used to measure the amount of material in suspension. Their main objective was to test the applicability of the Rate Process Theory to the erosion of cohesive soils.

The Rate Process theory is based on the assumption that atoms and molecules make up flow units, which are continuously attempting to move but there are some energy barriers, that restrain their

movement, separating equilibrium positions. The fact that the erosion rates are temperature dependent makes it possible to apply the rate process theory. Thus a flow unit needs external energy, assumed to come from thermal energy and applied potentials, to cross an energy barrier. Therefore, to apply rate process theory to the erosion of cohesive soils a deformation mechanism was postulated (Kelly and Gularte, 1981). For the case of erosion of soil with constant fabric, it was assumed that the rate at which flow units cross energy barriers in the direction of applied stress is proportional to the rate at which particles leave the soil surface, i.e., the rate of erosion.

Thus the proposed equations are,

$$E = \frac{R\ T_2\ T_1}{(T_2 - T_1)} \ln \left(\frac{\dot{\varepsilon}_2\ T_1}{\dot{\varepsilon}_1\ T_2} \right) \qquad (2.72)$$

$$V_f = \frac{2\ k\ T}{(\tau_2 - \tau_1)} \ln \left(\frac{\varepsilon_2}{\dot{\varepsilon}_1} \right) \qquad (2.73)$$

where E is the activation energy, R is a universal gas constant, T is the absolute temperature, $\dot{\varepsilon}$ is the erosion rate, k is Boltzman's constant, τ is the average shear stress, and V_f is the flow volume.

Finally from their experiments Kelly and Gularte (1981) concluded that the Rate Process Theory qualitatively described surface erosion on cohesive soils. Their results are shown in Figs. 2.29 and 2.30.

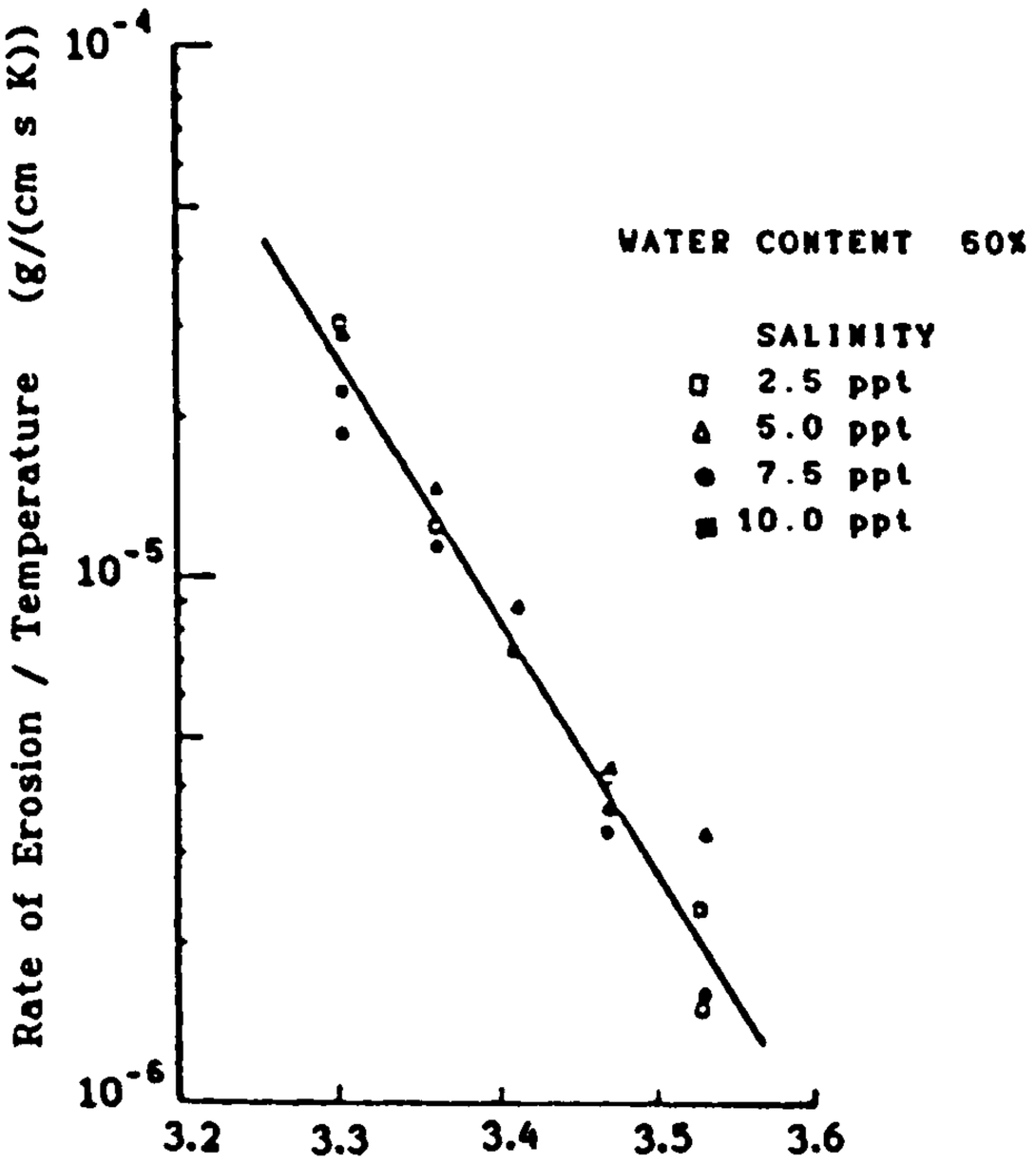

FIGURE 2.29: (RATE OF EROSION / TEMPERATURE) VS. INVERSE OF OF TEMPERATURE) (after Kelly and Gularte, 1981)

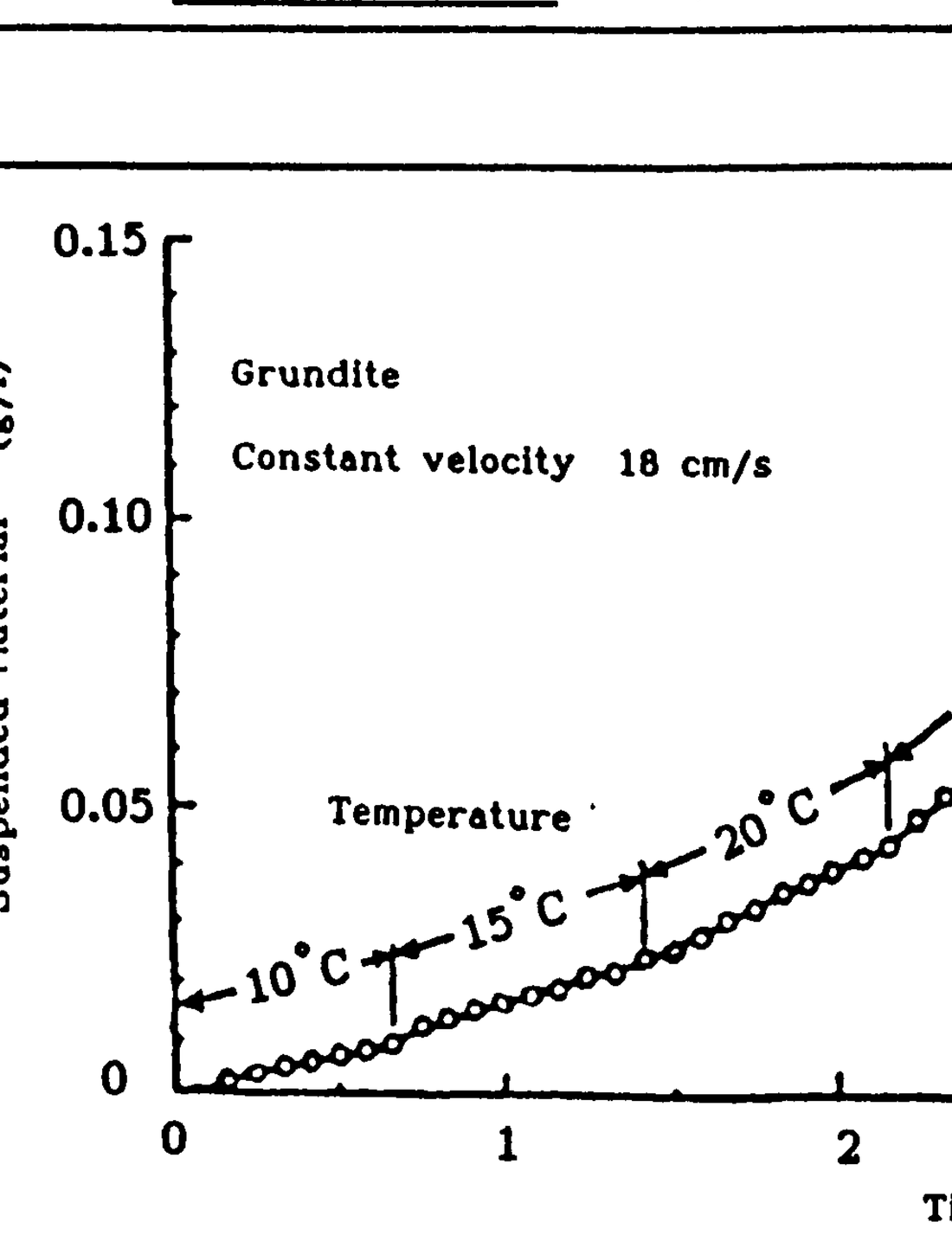

FIGURE 2.30: SUSPENDED MATERIAL VS. TIME
(after Kelly and Gularte, 1981)

Kamphuis and Hall (1983) performed experiments with artificially consolidated (48 to 350 KN/m^2) cohesive sediments in a flume-tunnel capable of providing high bed shear stresses (up to 26 N/m^2). Remoulded pure natural clay samples and clay-sand mixture samples were carefully consolidated in a specially designed press. Then each sample was placed in the flume and tested. The applied shear stress was determined from the velocity profile, and a relation between the critical shear stress (τ_{oc} in N/m^2) and the velocity at a height of 3 mm above the bed (u_{3c} in m/s) was obtained,

$$\tau_{oc} = 2.93\ u_{3c}^{1.75} \tag{2.74}$$

Eq. 2.74 was used instead of determining the velocity profile for every case. As in some tests the sample was immediately subjected to the critical shear stress and erosion began immediately, it was concluded that erosion depended on the shear stress and was not highly dependent on prior flow history.

The erodibility of the clay sample decreased with increasing consolidation pressure (see Fig. 2.31). This was explained (Kamphuis and Hall, 1983) to be a result of the decrease of the inter-particle spacing due to the consolidation pressure, which finally increases the inter-particle bonding forces.

Critical shear stresses were found (Kamphuis and Hall, 1983) to be proportional to the shear strength of the soil sample, i.e.,

unconfined compressive strength (Fig. 2.32) and vane shear strength (Fig. 2.33). The unconfined compressive strength, q_u in (KN/m^2), is an indirect measure of the shear strength of a soil, whereas the vane shear strength, S_v in (KN/m^2) is a direct measure of the shear strength of a soil as the relevant tests are performed in situ. Critical shear stresses were also found to increase with plasticity index (see Fig. 2.34) and clay content (see Fig. 2.31 & 2.34).

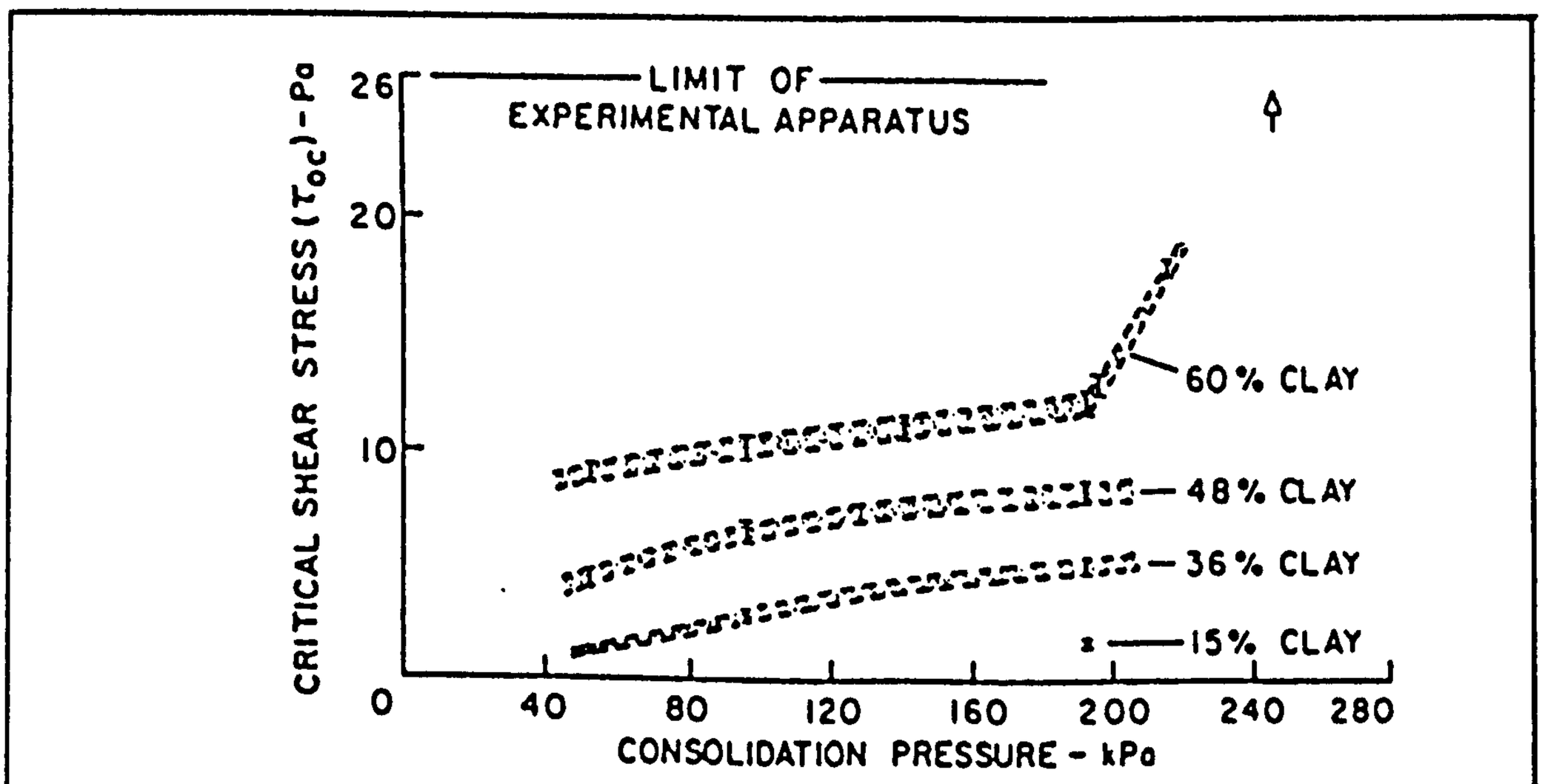

FIGURE 2.31: CRITICAL SHEAR STRESS VS. CLAY CONTENT AND CONSOLIDATION PRESSURE

(after Kamphuis and Hall, 1981)

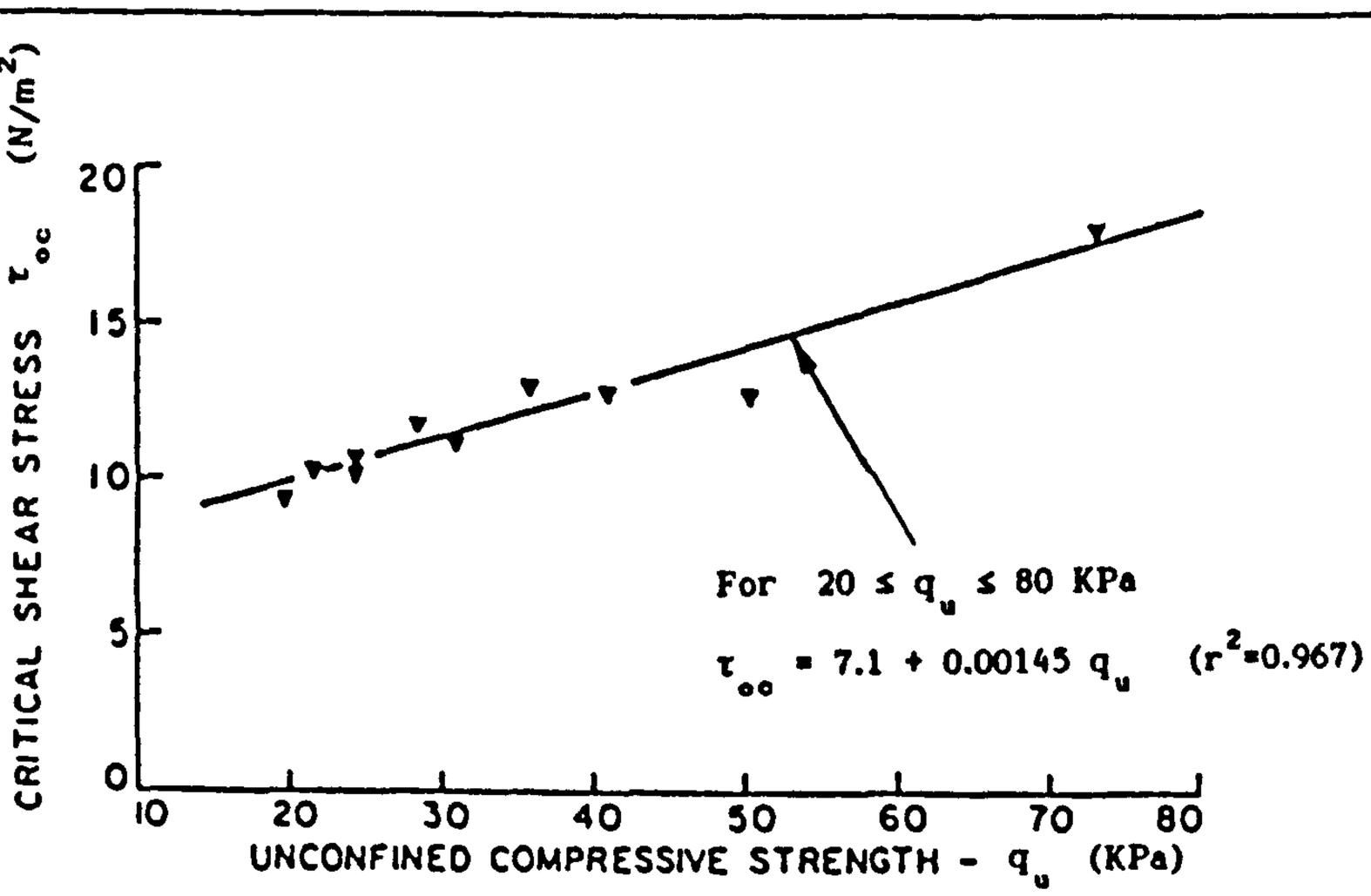

FIGURE 2.32: CRITICAL SHEAR STRESS VS. UNCONFINED COMPRESSIVE STRENGTH

(after Kamphuis and Hall, 1983)

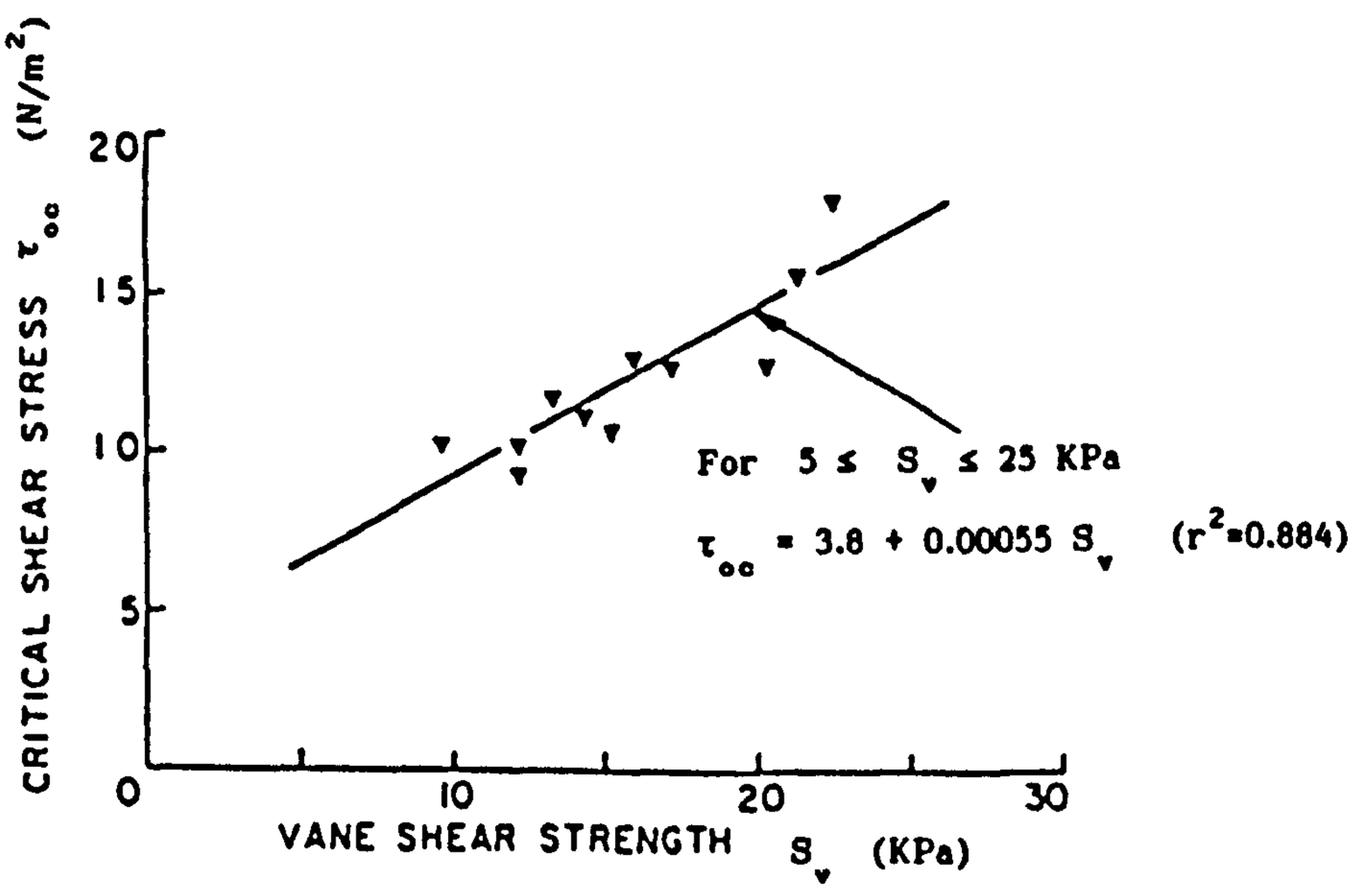

FIGURE 2.33: CRITICAL SHEAR STRESS VS. VANE SHEAR STRENGTH

(after Kamphuis and Hall, 1983)

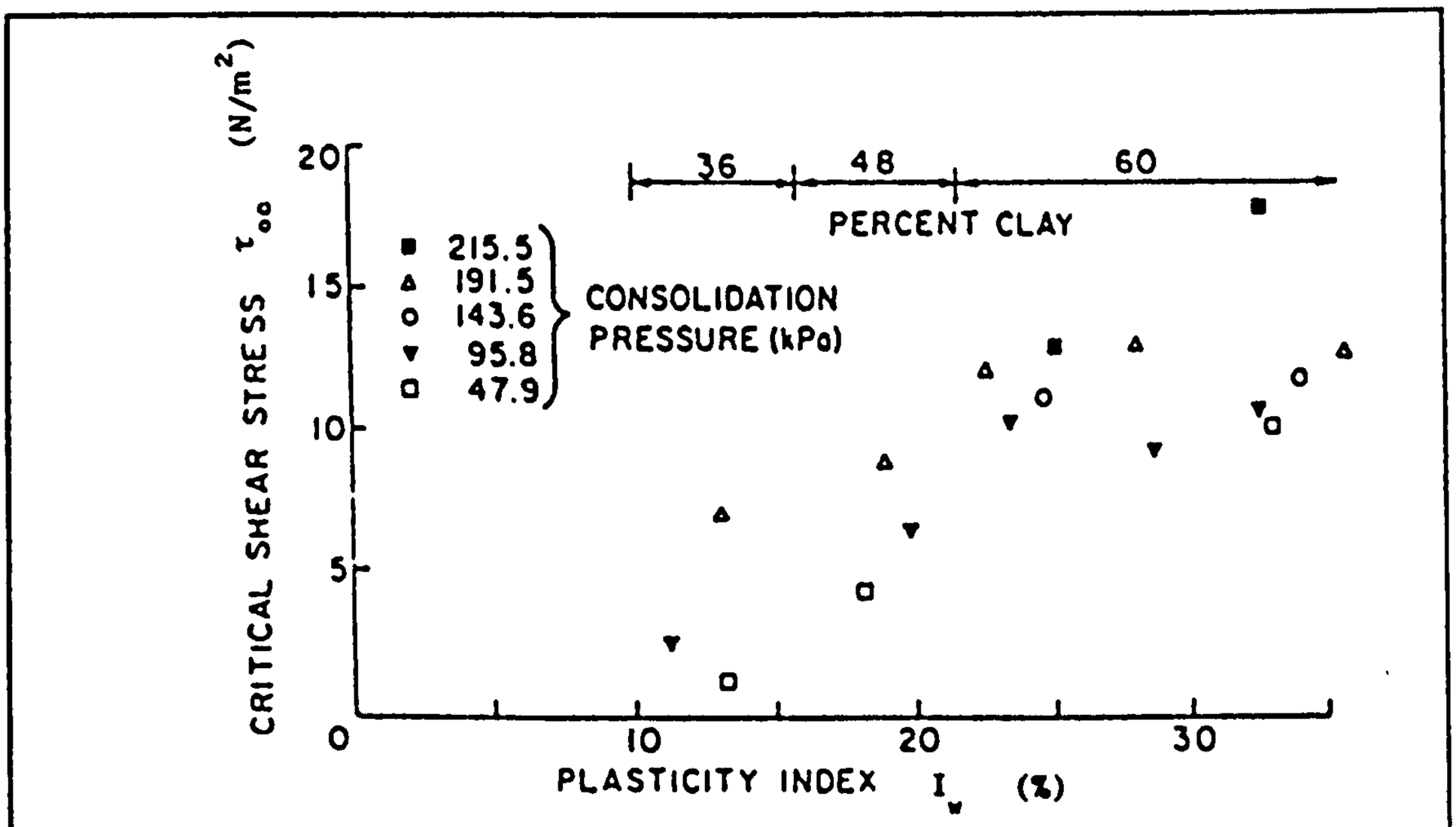

FIGURE 2.34: CRITICAL SHEAR STRESS VS. PLASTICITY INDEX

(after Kamphuis and Hall, 1983)

Raudkivi and Tan (1984) carried out erosion experiments on cohesive soils using a "circular couette flow device" (rotating cylinder apparatus), with various clays and electrolytes (eroding and pore water). The applicability of the rate process theory to the erosion of clay was demonstrated. It was concluded that there exists a strong dependence of the erosion rate on the pH-value and salt concentration of the electrolyte.

In Fig. 2.35 it can be seen that the erosion rate increases with pH-value. The increase in pH-value causes a compression of the

double layer as the edge-to-edge and face-to-face orientation become more prominent, thus the double layer repulsion forces are larger that the van der Waal forces.

It was also found (Raudkivi and Tan, 1984) that the presence of salt serves to compress the electric double layer of the edge-to-face orientation of clay particles that results in closer packing of clay particles. This leads to a stronger bonding and a higher erosion resistance (see Fig. 2.36). However, by further increasing salt concentration an upper limit of erosion resistance is reached. After that dispersion may occur depending on the type of clay.

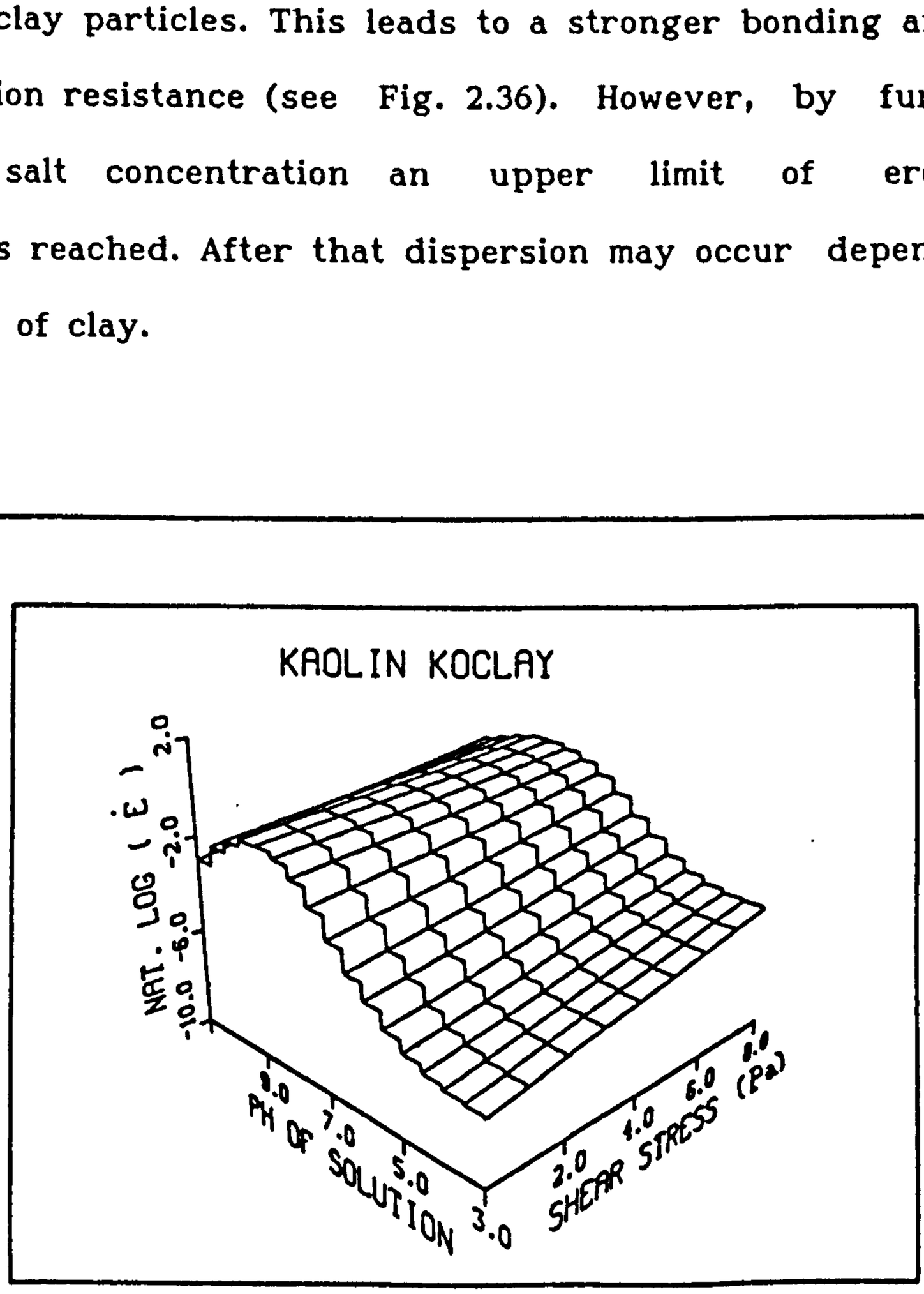

FIGURE 2.35: EROSION RATE VS. SHEAR STRESS AND pH OF SOLUTION

(after Raudkivi and Tan, 1984)

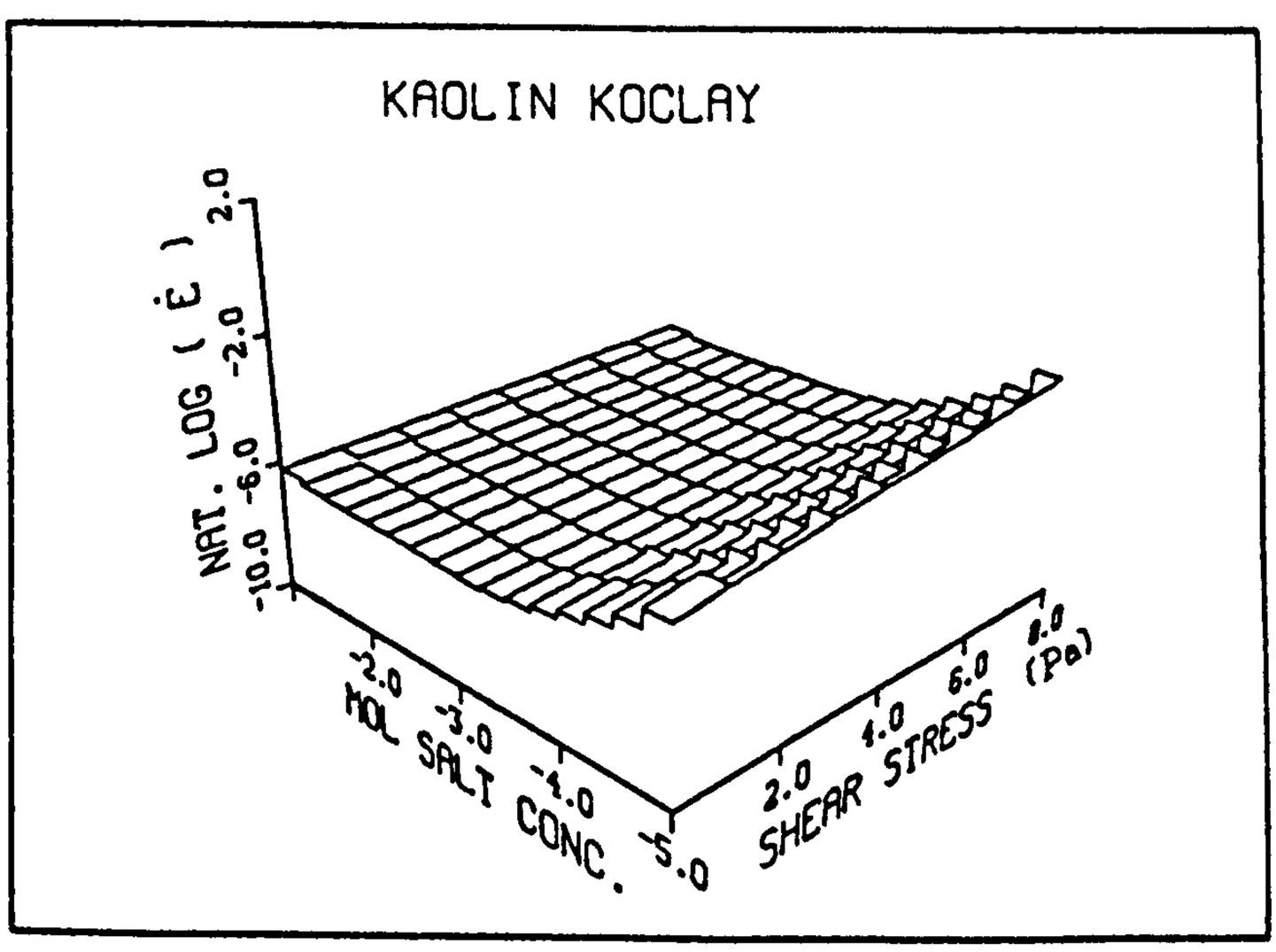

FIGURE 2.36: EROSION RATE VS. SHEAR STRESS AND MOLAR SALT CONCENTRATION

(after Raudkivi andTan, 1984)

2.2.2.2 Soft Cohesive Beds

This type of bed is either a freshly deposited mud or a low strength older deposit. Most of these investigations are directed towards understanding erosion, transport and deposition of fine cohesive sediments in estuaries.

In order to study deposition and re-suspension the laboratory equipment must be such that the flocs are not disrupted by mechanical effects (i.e., the pump in a recirculating flume). Recent investigators have implemented a special circular (annular) flume, where the flow is motivated by a rotating ring in contact with the water surface of the flume (Burt et al., 1985). In this type of flume the flocs are not disrupted, however other problems arise with the appearance of secondary currents and corrections have to be made in order to apply the results to straight channels.

Partheniades (1965) carried out flume experiments on erosion and deposition of fine estuarial cohesive sediments, with water at ocean salinity and constant depth. He used San Francisco Bay mud as bed material, which is composed of equal amounts of silt and clay with traces of sand and some organic matter. Two different types of bed were tested. The first one (Fig. 2.37-Series I) was a remoulded sample at field moisture content and the second one (Fig. 2.37-Series II) was flocculated and deposited in the flume directly from suspension at very low flow velocity.

Even though the shear strength of the first type of bed was about 100 times greater than that of the second one, the critical shear stresses were observed to be almost the same for both beds (see Fig. 2.37) 0.01 Lb/ft^2 (0.48 N/m^2) and 0.028 Lb/ft^2 (1.34 N/m^2) for Series I and Series II respectively.

Partheniades (1965, 1970) observed that the material is eroded from the bed in two different forms:

a) Erosion that takes place in small clusters of particles, when the applied shear stress does not exceed the bulk shear strength of the bed. The critical shear stress indicates the point at which the erosion rates start to increase very rapidly. Thus erosion might occur at very small shear stresses. However the critical shear stress will be determined by the flow that can carry the smallest eroded particles in suspension.

b) Erosion that takes place in layers, when the applied shear stress exceeds the bulk shear strength of the sediment. Then rapid mass erosion will take place.

It was also concluded that surface erosion rates depended strongly on the excess of the applied shear stress over the critical shear stress, and that the erosion rates are not affected by the concentration of suspended sediments.

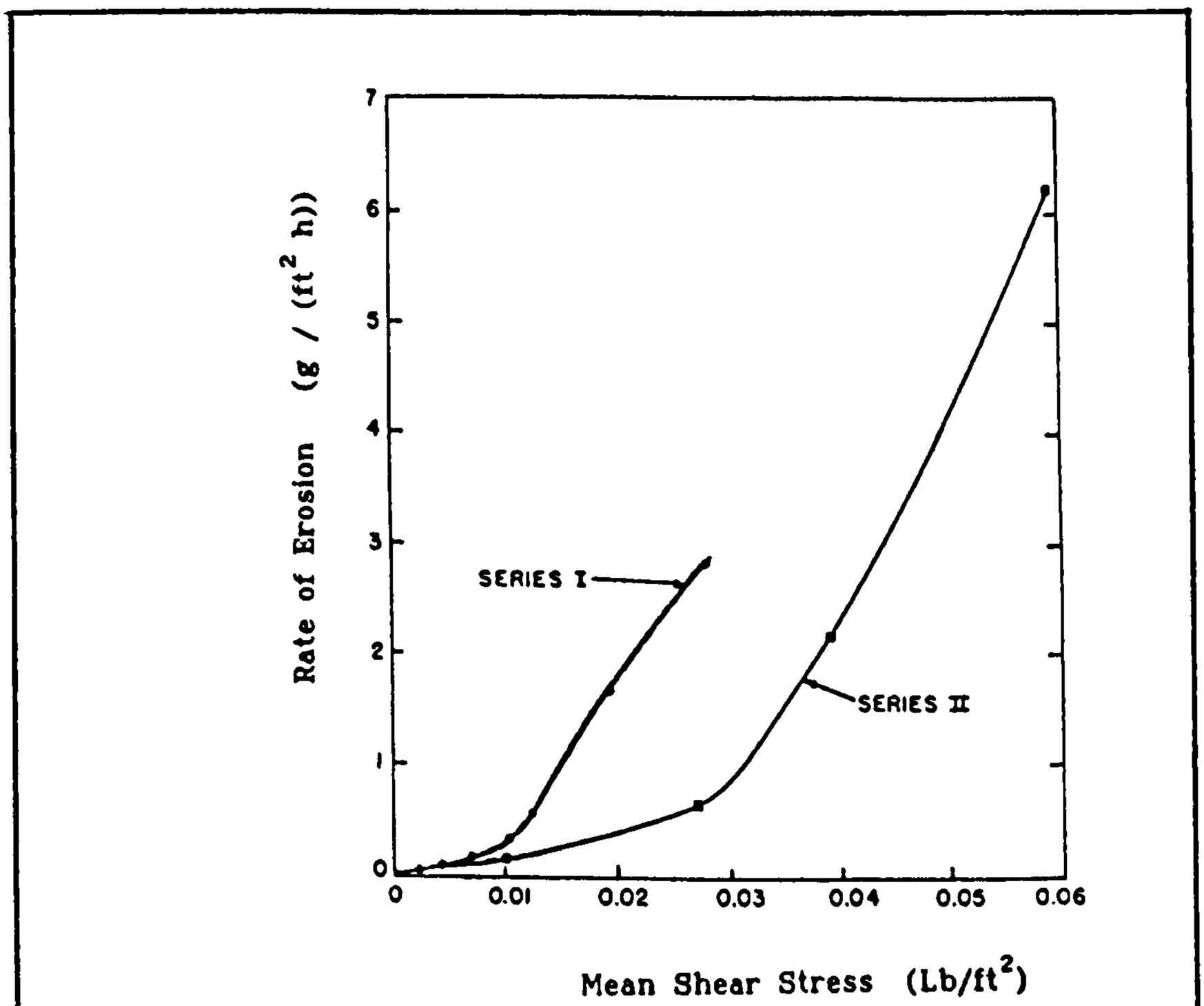

FIGURE 2.37: EROSION RATE VS. SHEAR STRESS
(after Partheniades, 1965)

Lambermont and Lebon, (1978) studied erosion of soft cohesive soils. Using experimental data from Migniot (1968) and Partheniades (1965) they derived expressions for the density distribution in sediment layers and for the erosion rate respectively, taking into account the action of the turbulent flow. From the results of ultra-centrifuge tests it was concluded that the density distribution of the sediment layer depends on the whole previous deposition and erosion history (see Fig. 2.38).

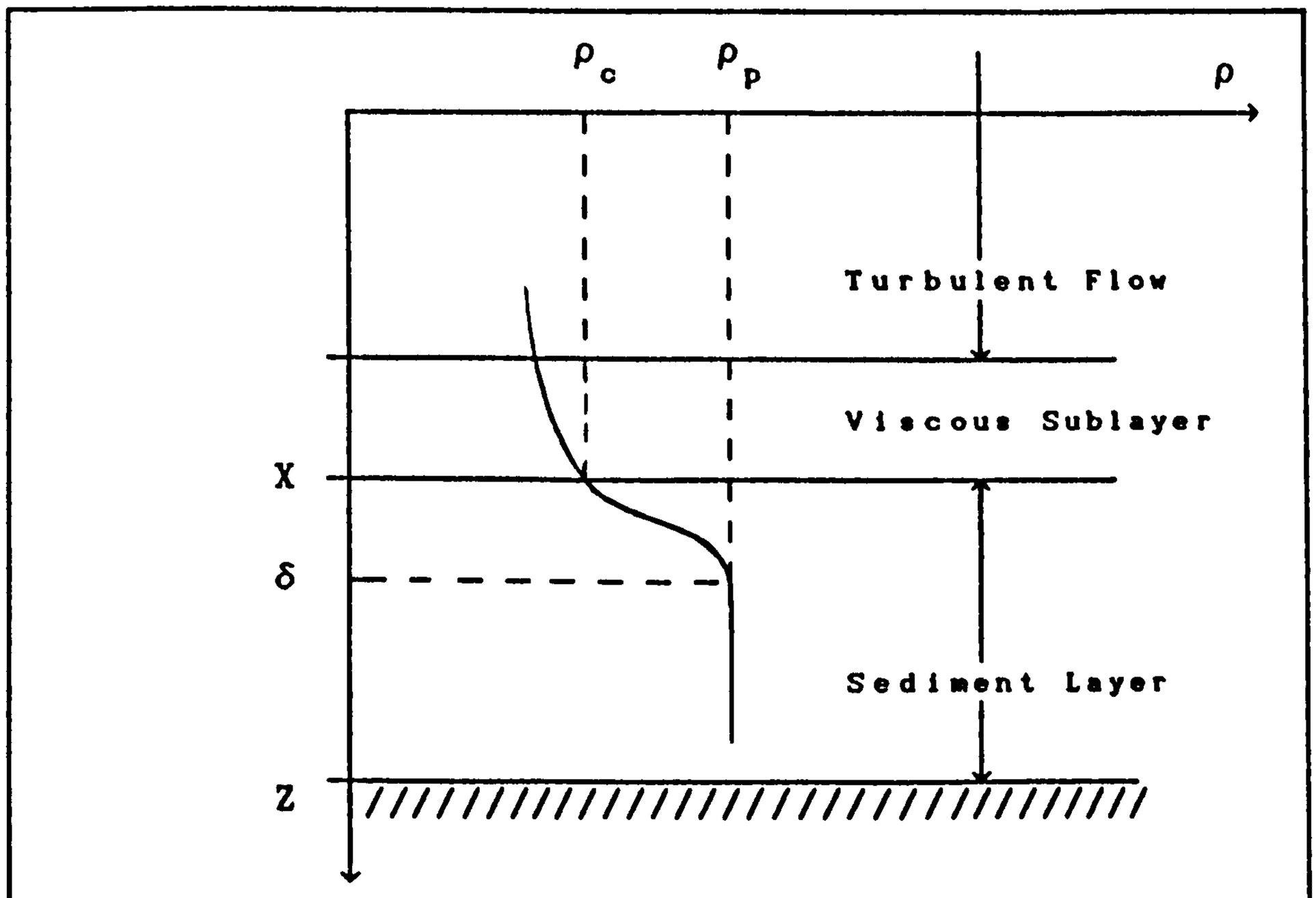

FIGURE 2.38: TYPICAL DENSITY DISTRIBUTION IN A SOFT SEDIMENT LAYER (Lambermont & Lebon, 1978)

A critical sediment density ρ_c was defined (Lambermont & Lebon, 1978) as the density at a depth X (bed-fluid interface) that would be eroded by a given shear stress, applied on the bed. This critical density was related to the sediment (Migniot, 1968) yield stress τ_y by the following equation,

$$\tau_y = n \rho_c^m \qquad (2.75)$$

where n and m are constants depending on the sediment characteristics. Migniot found m to be close to 5 and n between 10^{-12} and 10^{-15} when τ_y is expressed in N/m^2 and ρ in g/l. The shear velocity u_* was related to the yield shear stress as,

$$u_* = 0.01778\ G^{m/4}\ \tau_y^{1/4} \quad \text{for} \quad \tau_y \leq \frac{1.5}{G^m} \tag{2.76}$$

where G is a correction factor, that takes into account the decrease in density of the upper region of the sediment layer that is in contact with the fluid, whose value was expected to be between 1 and 5 and

$$u_* = 0.016\ G^{m/2}\ \tau_y^{1/2} \quad \text{for} \quad \tau_y > \frac{1.5}{G^m} \tag{2.77}$$

The shear stress was expressed as a function of the sediment density given by,

$$\tau_o = E_i \left(\rho_c\right)^{\beta_i} \tag{2.78}$$

where E_i and β_i are constants.

A differential equation for cohesive sediment bed was formulated, and by making several assumptions and simplifications (parabolic density distribution, constant coefficients of diffusion and sedimentation, temperature gradient in the bed neglected, etc.) an analytical solution for a stationary erosion rate was obtained. It was finally shown that the theory agreed very well with the erosion experiments of Partheniades (1965).

Thorn (1981) performed experiments on soft cohesive sediments and demonstrated that the critical shear stress is a function of the bed density as it is shown in Fig. 2.39.

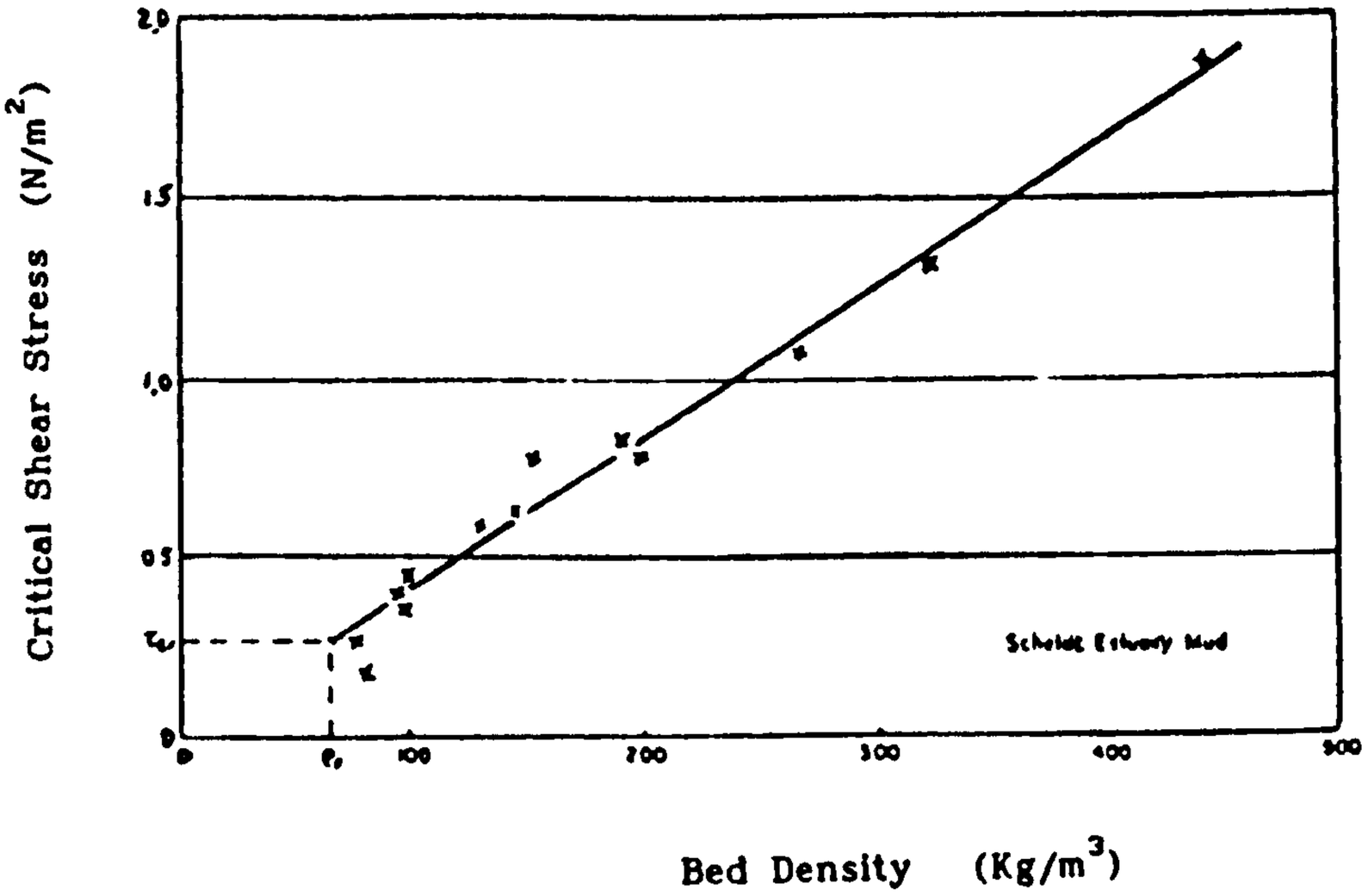

FIGURE 2.39: CRITICAL SHEAR STRESS VS. SEDIMENT DENSITY (after Thorn, 1981)

Parchure and Mehta (1985) carried out erosion experiments in a circular flume with soft cohesive sediments. An experimental procedure involving layer by layer erosion, under a range of bed shear stresses of successfully increasing magnitude was employed. The main objective was to study the erosion that occurs on the top active layer of estuarial beds, where the conditions are quite different from that of a uniform flow channel. The estuarial bed is formed by deposition of suspended fine particles forming layers of different densities.

The density of a bed layer is dependent on the depth and on the time the layers have been subjected to consolidation pressure. Therefore, the critical shear stress will vary with depth of the sediment bed. It was found (Parchure and Mehta, 1985) that erosion rates were proportional to the square root of the excess of applied shear stress over the shear strength of the bed, as it is shown in Fig. 2.40.

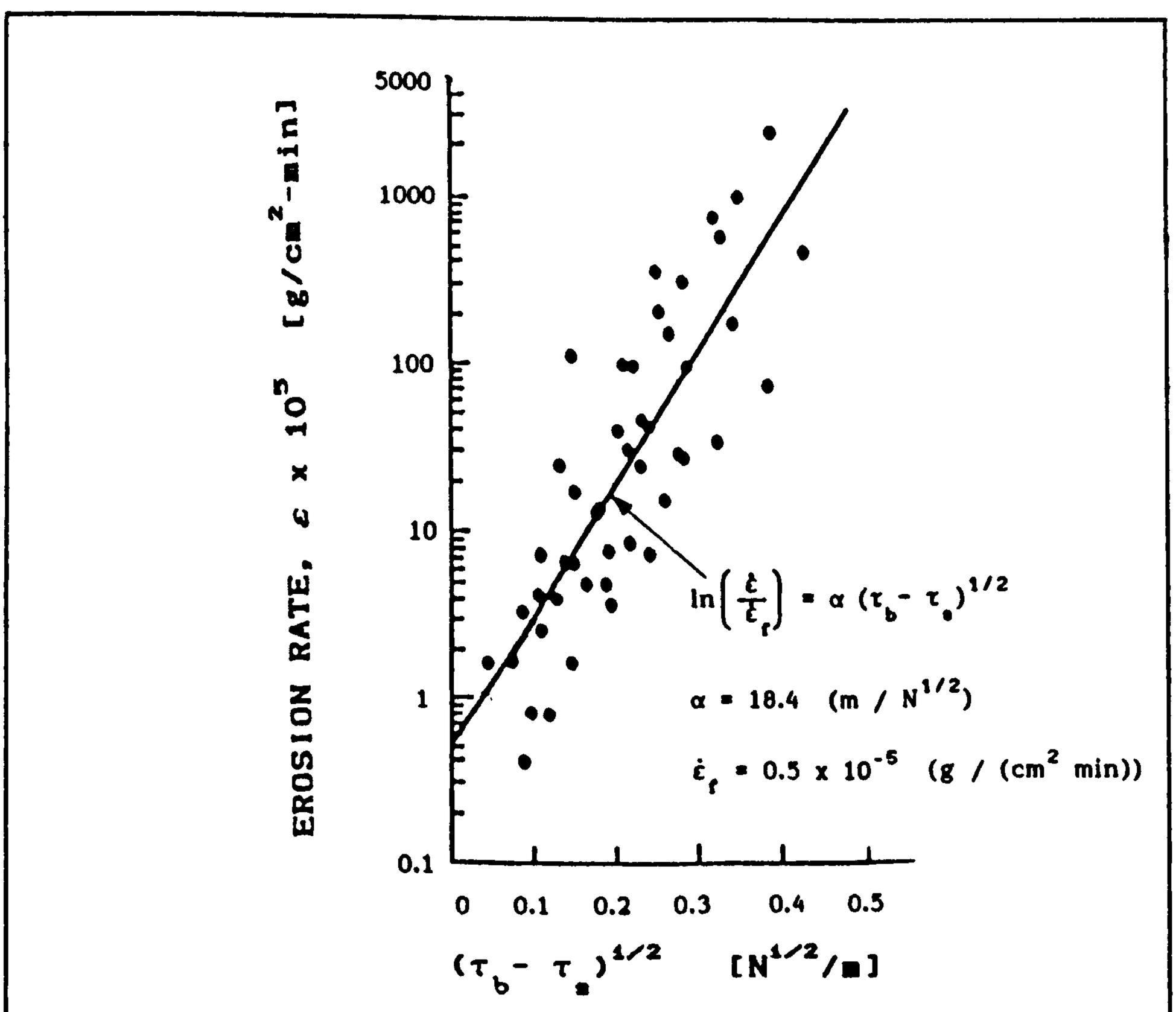

FIGURE 2.40: VARIATION OF $\left(\dot{\varepsilon} / \dot{\varepsilon}_f\right)$ WITH $(\tau_b - \tau_s)^{1/2}$
(after Parchure and Mehta, 1985)

An experimental study of the critical shear stress of cohesive sediments was carried out by Otsubo and Muraoka (1988) to relate critical conditions with rheological and settling properties of

the sediment. Natural and artificial mud samples (Kaolinite, bentonite and lake mud from various origins) were tested.

A tunnel of rectangular cross-section was used to test the samples. The threshold conditions were obtained through visual observation and from the rise in turbidity. Two critical shear stress values were defined (Otsubo and Muraoka, 1988). One was τ_{c1} (mud particles begin to be dislodged) and the other τ_{c2} (the sediment bed begins to be disintegrated). Yield stresses were obtained using a rotary viscometer. Settling tests were carried out for the sediment samples. Critical shear stress was found to be dependent on the viscosity and on the yield shear strength value (see Fig. 2.41).

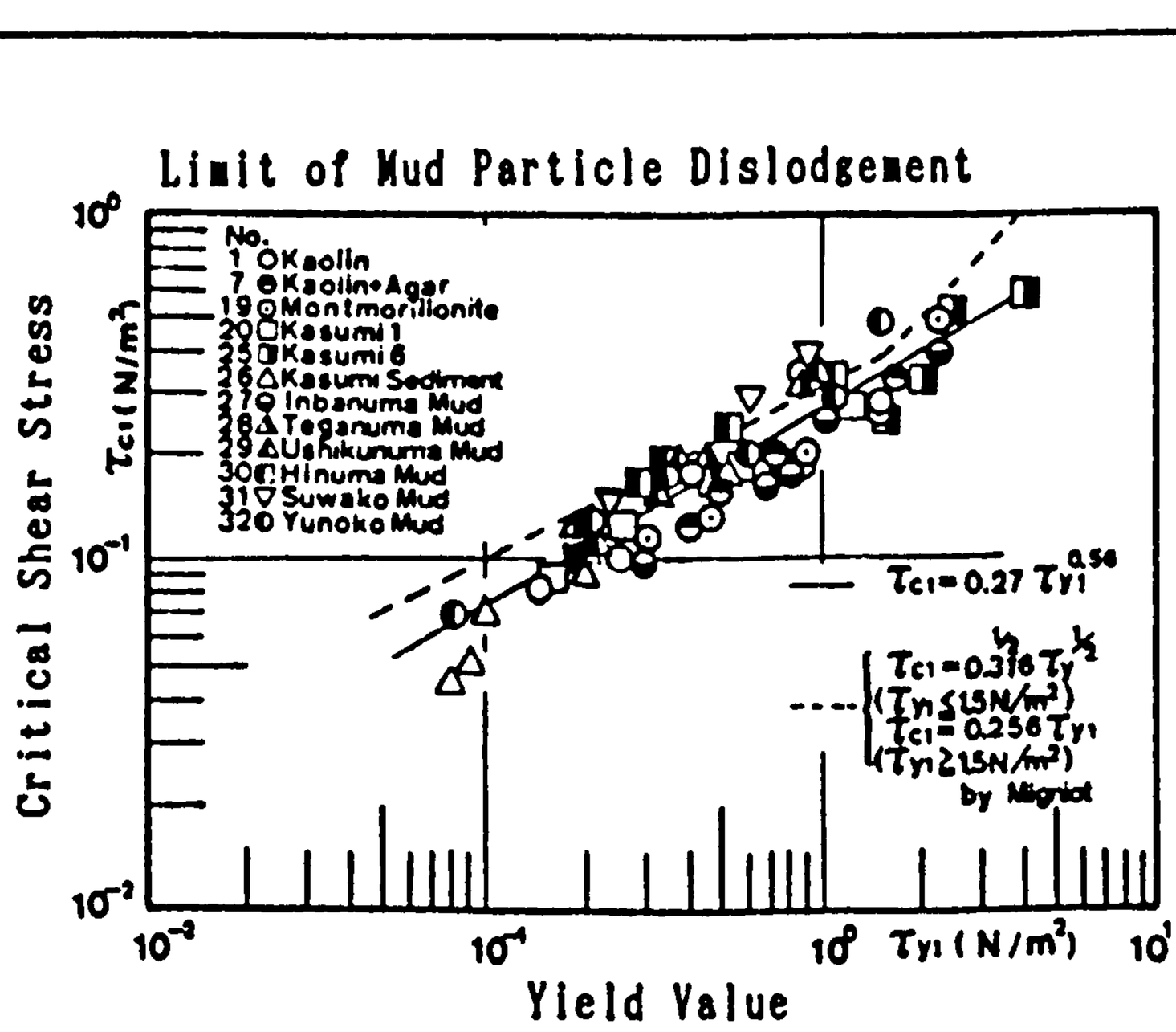

FIGURE 2.41: CRITICAL SHEAR STRESS VS. YIELD STRESS
(Otsubo & Muraoka, 1988)

The two limits of critical shear stress were explained by Otsubo and Muraoka (1988) as follows. In the first limit τ_{c1}, because of the turbulence the shear stress occasionally exceeds τ_y (at that moment some particles are dislodged, i.e., beginning of particle movement). The second limit occurs at τ_{c2} when the shear stress is almost equal to τ_y and is acting constantly on the bed causing its mass destruction (i.e., the limit of destruction of the bed).

The two limits were expressed as:

$$\tau_{c1} = 0.27 \left(\tau_y\right)^{0.56} \qquad (2.79)$$

$$\tau_{c2} = 0.79 \left(\tau_y\right)^{0.94} \qquad (2.80)$$

where τ_y is the yield stress in N/m^2.

A mathematical model, which simulates the transport of cohesive sediment was developed by Nicholson and O'Connor (1986). The model solves the complete three dimensional version of the diffusion-advection equation.

In the literature many other models have been presented (Odd & Owens 1972, Ariathurai & Krone 1976, Ariathurai et al., 1977, Rodger, 1980, Scarlatos, 1981, Onishi, 1981, Cole & Miles, 1983, Nicholson, 1983, Hayter & Mehta, 1984, etc., to which the interested reader is referred to. As these models deal mainly with estuarine sediments that are quite different from sewer sediments they will not be discussed here.

2.2.2.3 Concluding remarks

The study of erosion of cohesive materials is quite complex because not only it involves physical parameters such as shear stress or shear strength, but also chemical and physical bonding of the individual particles.

As shown in this chapter, arbitrary and subjective criteria were established to study and analyse erosion of cohesive sediments. In the experimental works described above, for the same conditions, different critical shear stress values are predicted with variations as great as 30 times. This can be attributed to experimental error, variation in experimental techniques, interpretation of sediment properties, and especially the different criteria used to define the critical shear stress. A better criterion is based on the definition of critical conditions described in terms of erosion rates.

However, in the last two decades the inclusion of various clay properties such as fabric, inter-particle bonding and clay colloid chemistry has brought more light to the understanding of the problem.

2.3 SEWER SEDIMENTS

In this section a classification of in-sewer sediments will be shown together with their chemical, physical and rheological properties. Based on these properties a synthetic sewer sediment (for flume studies purposes) will be presented.

Since both foul sewerage and surface water drainage systems are often combined it is necessary to study the complete system. The nature of sediment in sewers is quite complex due to the presence of many sources of sediment (grit, road surfacing materials, industrial processes, domestic sewage, soil, sand, etc.), and the spatial and temporal variation.

Because of the intermittent nature of the flow in sewerage systems it is nearly impossible to prevent deposition occurring. Thus the sediment is conveyed through the system in a series of deposition and re-entrainment cycles.

2.3.1 Classification of Combined Sewer Sediments

2.3.1.1 Sewer Sediment Types

A classification of combined sewer sediment based on field observation, sampling and analysis of sewer sediment deposits was made by Crabtree (1988) at the Water Research Centre (WRc), Swindon. The study was carried out at seven locations in the U.K., which were known to have significant sediment deposits.

TABLE 2.1: CLASSIFICATION OF COMBINED SEWER SEDIMENT
(after Crabtree, 1988)

TYPE A	coarse, loose, granular, predominantly mineral material found in the invert of pipes.
TYPE B	as TYPE A but concreted by the addition of fat, bitumen, cement, etc. into a solid mass
TYPE C	mobile, fine grained deposits found in slack flow zones, either in isolation or above TYPE A material.
TYPE D	organic pipe wall slimes and zoogloeal biofilms found in the invert of fast flowing pipes without any other sediment deposits and around the mean flow level along the pipe walls.
TYPE E	fine grained mineral and organic deposits found in Storm Sewage Overflow (SSO) storage tanks.

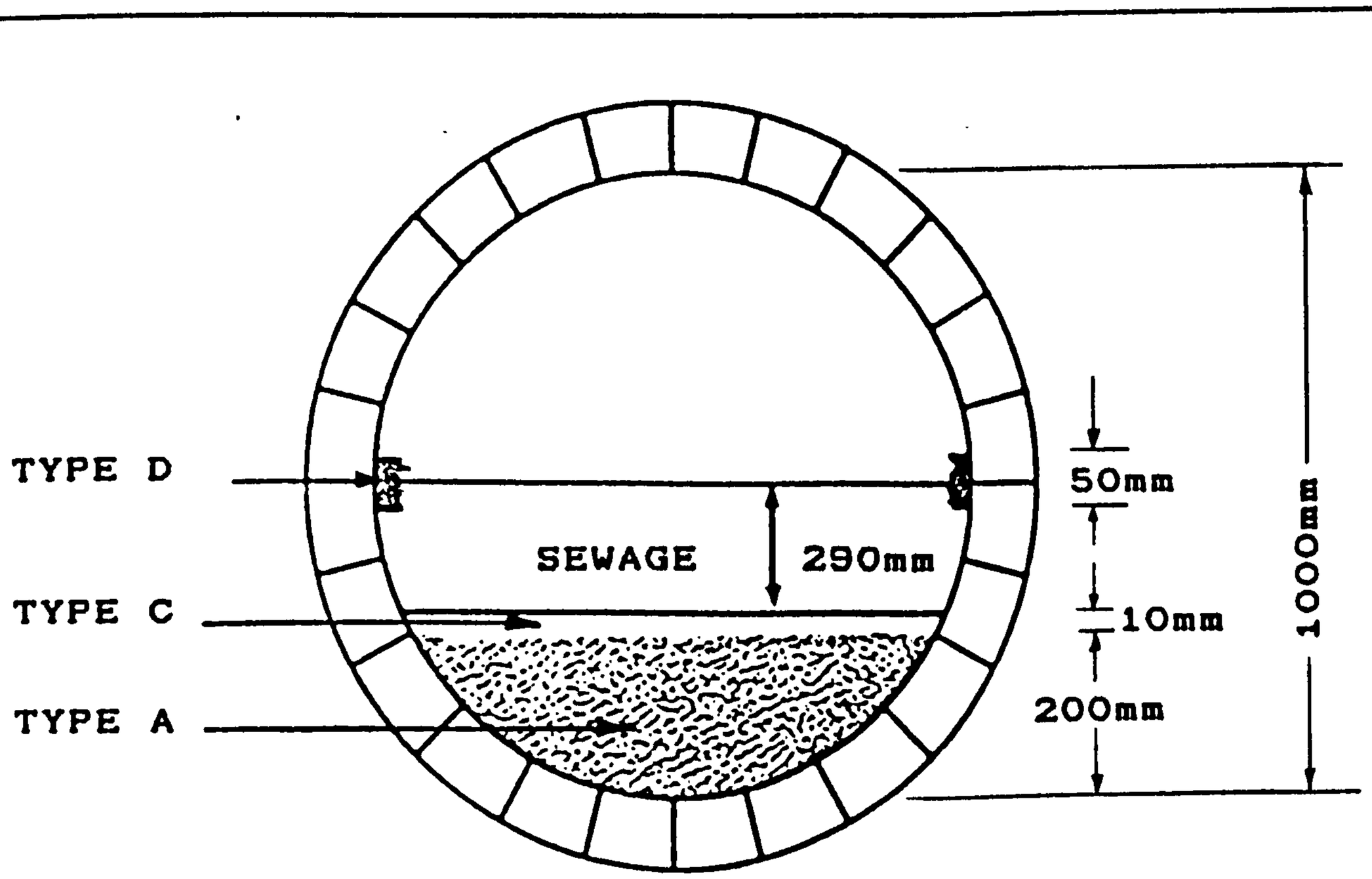

FIGURE 2.42: COMBINED SEWER SEDIMENT CLASSIFICATION TYPICAL SECTION (Crabtree, 1988)

Based on observations of the nature and appearance of sewer sediment during sampling and on the provenance and location of the deposits within the sewerage system five categories of sediment were suggested (see Table 2.1 and Fig. 2.42).

2.3.1.2 Physical Characteristics

Although particle size analysis of the samples (see Table 2.2) did not show a clear distinction between Types A, C and E, a general classification was made. The coarsest material was Type A. Type C was predominantly silt, clay and fine sands.

2.3.1.3 Chemical Characteristics

The results of chemical analysis of the samples showed a high degree of variability in pollutant strength within each class. However, sediment types could still be ranked according to the

TABLE 2.2: PHYSICAL CHARACTERISTICS OF SEWER SEDIMENT TYPES (Crabtree, 1988).

Parameter		Sediment Type			
Percentage Particle Size		A	C	D	E
Gravel (2.0 - 50.0mm)	Mean	33	0	6	9
	Maximum	90	0	20	80
	Minimum	3	0	1	4
Sand (0.063-2.0mm)	Mean	61	55	62	69
	Maximum	87	71	83	85
	Minimum	3	5	1	1
Silt and Clay (< 0.063mm)	Mean	6	45	32	22
	Maximum	30	73	52	80
	Minimum	1	29	17	1
Wet bulk density $x10^3$ Kg/m^3		1.72	1.17	1.21	1.4
% Total Solids		73.4	27.0	25.8	48.0

average pollutant strength as follows: Type D, Type C, Type E and Type A in decreasing order. Table 2.3 shows the average polluting load of the bulk wet sediment for each class type, expressed in terms of both mass and volume of deposits.

Table 2.3 shows the average associated pollutant loads related to the various types of sewer sediments. A relative comparison with normal crude sewage is shown in Table 2.4, which illustrates the very high pollutant strength of Type D deposits compared with the other types. Obviously the total polluting load could only be released under extreme flow conditions when all sediment deposits are eroded.

TABLE 2.3: SEWER SEDIMENT TYPE AVERAGE ASSOCIATED POLLUTANT LOADS (after Crabtree, 1988)

Pollutant Parameter		SEDIMENT TYPE			
		A	C	D	E
COD	mass	16.9	20.5	49.8	23.0
	volume	29.1	24.0	60.3	33.6
$BOD_{4\ hour}$	mass	0.3	0.5	0.4	0.4
	volume	0.5	0.6	0.5	0.6
BOD_{5day} (ATU)	mass	3.1	5.4	26.6	6.2
	volume	5.3	6.3	32.2	9.1
Ammonia (NH_4-N)	mass	0.1	0.1	0.1	0.1
	volume	0.2	0.2	0.1	0.2
Organic Nitrogen	mass	0.6	1.0	0.7	0.7
	volume	1.0	1.2	0.8	1.1

mass = grams per Kg wet bulk sediment.
volume = Kg of pollutant per m^3 of wet bulk sediment (conc.).

2.3.1.4 Rheological Characteristics

A rheological study was carried out with samples of sediment types A, B, C and E (Williams and Williams, 1988) in order to assess the cohesivity of the different types of sediments. Determinations of critical yield stresses (τ_y) were carried out on 11 samples of sediment by using applied stress rheometry. The critical yield stress corresponded to the yield point (i.e., the onset of structural failure).

TABLE 2.4 RELATIVE POLLUTING LOAD OF THE SEWER SEDIMENT TYPES COMPARED WITH CRUDE SEWAGE (on bulk wet sediment pollutant load basis - Crabtree, 1988).

SEDIMENT TYPE	RELATIVE STRENGTH	
	$BOD_{4\ hour}$	$BOD_{5\ Day}$
A	3	8
C	5	14
D	4	67
E	4	16
Crude Sewage	1	1

Note: To obtain the relative comparison in Table 2.4 the values for crude sewage used were:

$$BOD_{4hour} = 0.1\ g/Kg$$
$$BOD_{5Day} = 0.4\ g/Kg$$

All samples were classed as non-Newtonian substances that exhibited elastico-viscous behaviour. The results summarized in Table 2.5 are to be interpreted with caution because of the small number of samples and the considerable variation of τ_y for

different samples reflecting the differences in physico-chemical and biochemical properties of those sediment samples.

TABLE 2.5: VALUES OF CRITICAL YIELD STRESS FOR SEWER SEDIMENT SAMPLES (Williams 1988).

SEDIMENT TYPE	τ_y (N/m^2)
A	>800
A	620
A	425
A	400
B	>800
B	>800
C	98
E	>800
E	>800
E	200
E	25

According to their report (Williams and Williams, 1988) all samples presented a degree of cohesion from the weak Type C sediment to the highly cohesive Type B material.

2.3.2 Synthetic Sewer Sediment for Flume Studies

From their rheological investigations Williams and Williams (1988) suggested the use of Laponite clay (synthetic smectite collied Laponite RD) for flume studies. Laponite RD clay can be mixed with sand to provide the rheological characteristics

required of a synthetic sewer sediment (see Table 2.6). Laponite clay RD forms thixotropic gels in aqueous systems and has the chemical composition:

SiO_2 59.5%, MgO 27.3%, LiO 0.8%, and Na_2O 3.8%

TABLE 2.6: VALUES OF CRITICAL YIELD STRESS (LAPONITE RD-SAND-WATER MIXTURES, Williams and Williams, 1988).

Solids Conc. (g/ml)	Proportion (by weight) clay %	Proportion (by weight) sand %	Density ρ (Kg/m^3)	Rigidity Modulus G (N/m^2)	Yield Stress τ_y (N/m^2)
0.172	2.7	14.5	1042	410	17.5
0.220	2.5	19.5	1106	220	16.0
0.278	2.3	25.5	1200	500	23.0
0.410	2.2	37.8	1300	600	30.0
0.487	1.9	47.0	1380	1300	43.0
0.548	1.8	53.0	1440	2300	58.0

Table 2.6 shows that by appropriate laponite clay-sand-water mixture the sewer ranges of τ_y and G are easily reproduced. Therefore it was suggested (Williams and Williams, 1988) to conduct erosion experiments in flumes of circular cross-section, utilizing these Laponite clay-sand-water mixtures as bed material.

This synthetic sewer sediment, which mimics the rheological properties of some sewer sediments, simplifies the inherent complexity of natural sewer sediments. These complexities arise from the interaction of physical, chemical and biological factors. However, the non-linear dependence of yield stresses on solids concentration (Williams and Williams, 1988) has implications for the interpretation of flume erosion studies as well as for the design of sewers. The variation in density with sediment depth (consolidation process) determines that the superficial layer of sediment (freshly deposited) is the weakest one. Therefore it is not possible to relate the onset of erosion with the bulk density of the sediment but with the rheological properties of the superficial layer. The current design practice of self-cleansing sewer allows for a minimum shear stress between 2 and 6 N/m^2, which would only flush the freshly deposited bed of sewer sediment.

Work on rheological studies of natural cohesive sewer sediment is now in progress (Ashley et al., 1988). Their main objective is to increase the understanding of the nature and behaviour of sewer sediments, and in the long term to integrate in situ rheological measurements with the study of local flow field. It is also expected to improve mathematical models of sediment behaviour in combined sewers, such as MOSQITO, which would be developed into an enhanced version of the present sewer flow quality model.

CHAPTER THREE

EXPERIMENTAL EQUIPMENT AND PROCEDURES

3.1 GENERAL LAYOUT

The experimental work was carried out in two channels of circular cross-section with flat sediment bed one 154 mm and the other 302 mm in diameter. However most of the work was carried out in the 154 mm diameter flume, which could be operated not only under open channel flow conditions but also under pressure (i.e., full pipe flow conditions), thus increasing the range of shear stresses up to 15 N/m^2 necessary to cover the range of critical shear stresses on cohesive sediment beds.

3.1.1 The 154 mm diameter flume

This is a 154 mm diameter flume of circular cross-section and 20.5 m long (see Fig. 3.1 and plate 1a) with tilting facility, the longitudinal slope ranging from zero to 1/200. Channel slope can be varied by a screw jack located near the downstream end of the flume. The flume has a re-circulating system with an independent tank to avoid any possible contamination of the laboratory main water supply.

The upstream half of the flume length, (about 10 m) is used as an approach length and in the other 10.5 m there is a false flat bed on the invert of the pipe (see Fig. 3.2).

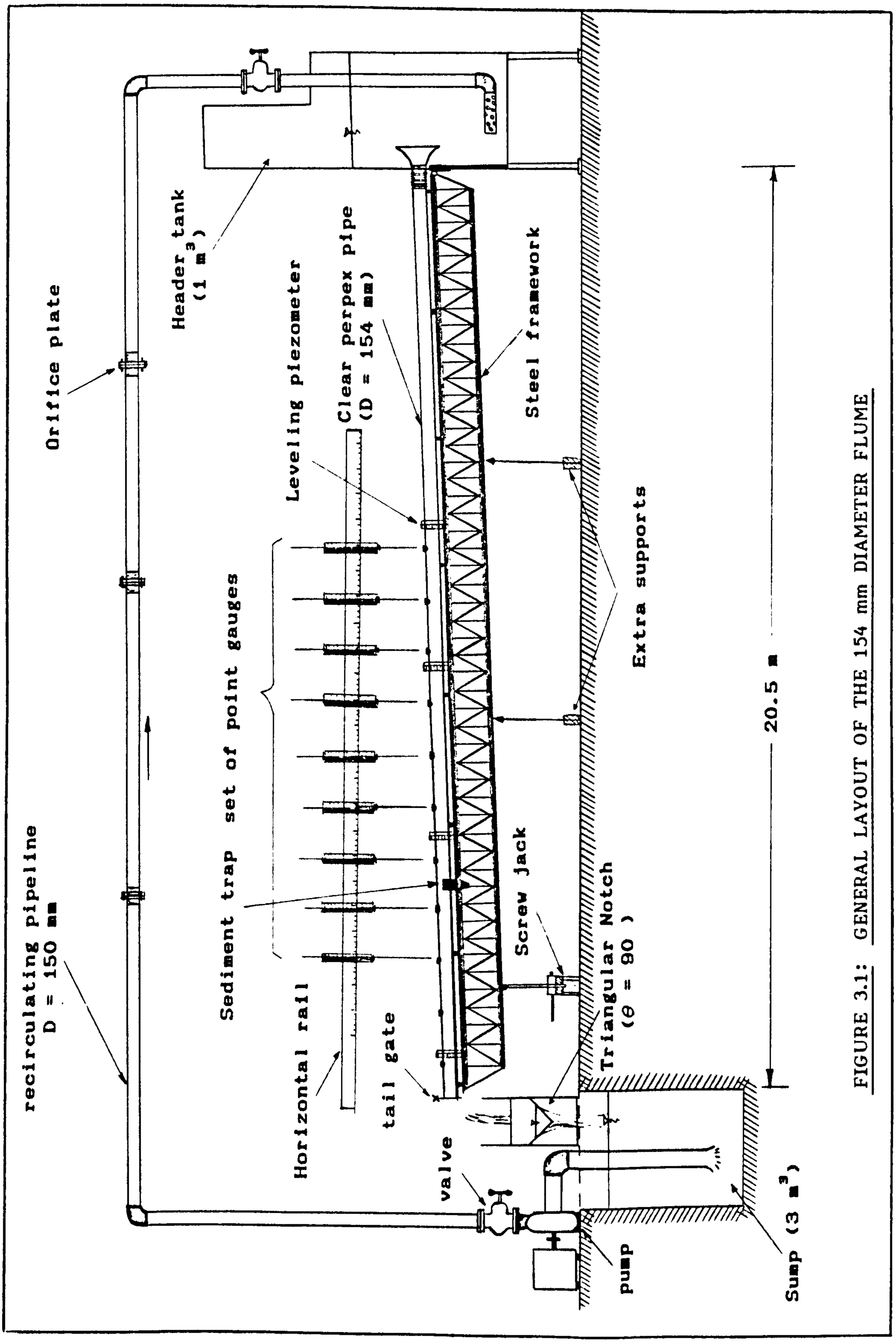

FIGURE 3.1: GENERAL LAYOUT OF THE 154 mm DIAMETER FLUME

The sediment bed thickness is varied from 10.6% to 39% of the diameter, by a modular system of layers made of uPVC sheets. The test section covered 2 m (4 m for transport experiments). The false bed was artificially roughened by glueing uniform size sand of the appropriate size on its surface (using either epoxy resin or double sided adhesive tape).

Access windows 100 mm diameter were opened on the top side of the pipe in order to have access to the sediment and to measure bed and water level using a set of 9 point gauges located (permanently) along the flume approximately every 1 m apart and supported from a horizontal rail suspended from the laboratory ceiling. The accuracy of the readings is +/- 0.1 mm. Bed slope and water surface slope can be determined by fitting a straight line to the point gauges readings using the least square method.

3.1.1.1 Measurement of Discharge

Water discharge was measured by a 90° triangular notch placed downstream of the flume using the calibration equation:

$$Q = 1.365\ h^{2.5} \qquad (3.1)$$

where Q is the flow rate in (m^3/s), and h is the water height above the V-notch vertex in (m). The discharge is computed with a maximum error of 1.3% (BS 3680). The discharge was regularly cross-checked by an orifice plate located in the returning pipeline of the re-circulating system.

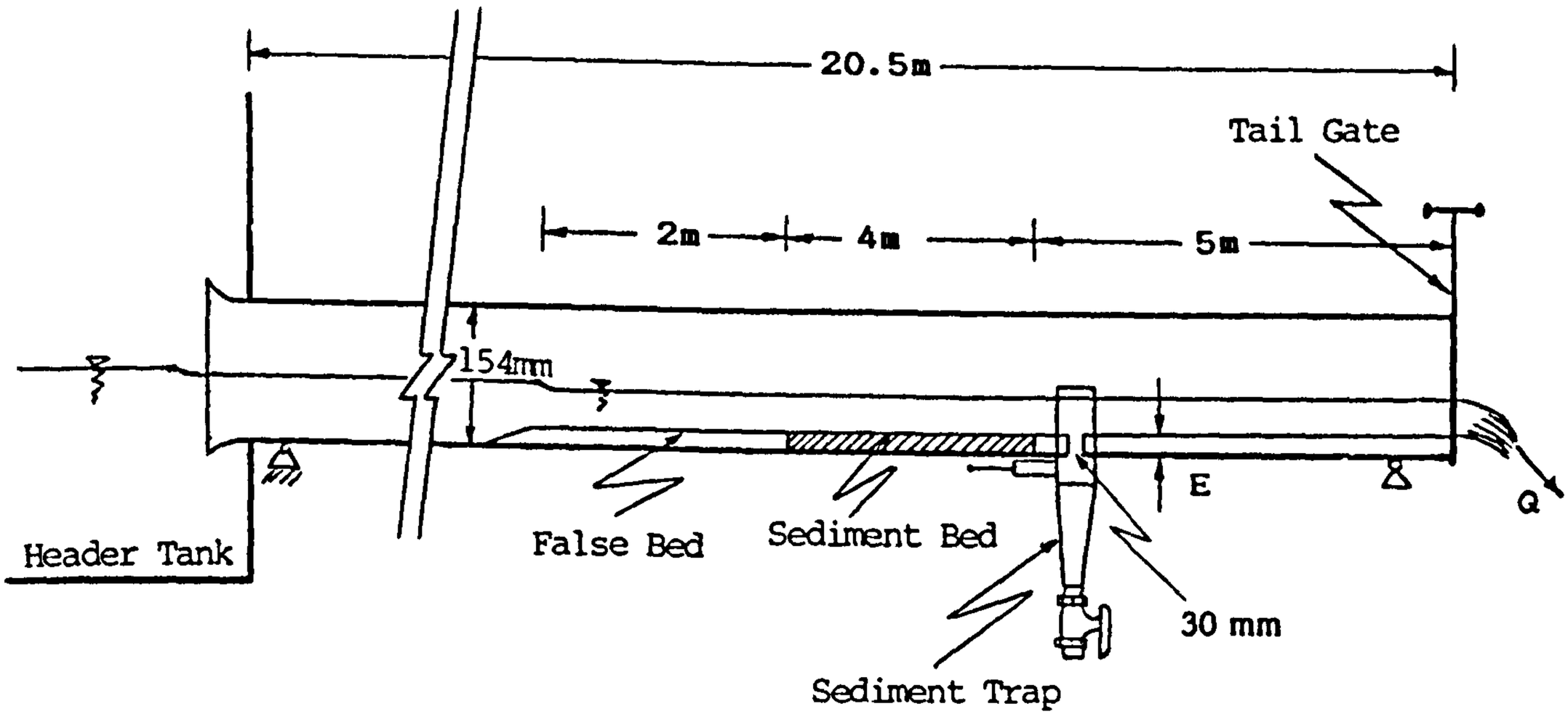

a) Side Elevation of the 154 mm Diameter Flume

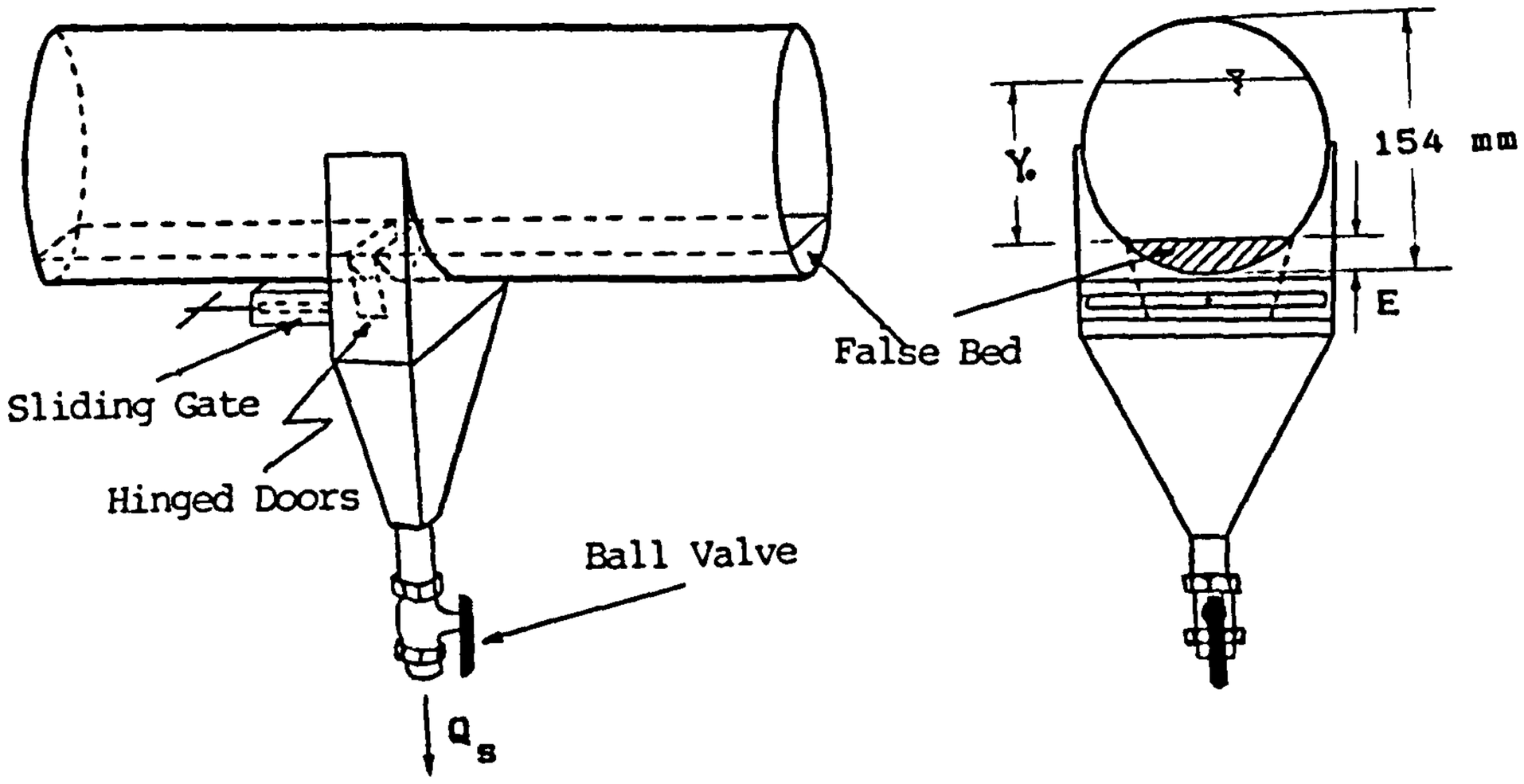

b) Details of Sediment Trap

FIGURE 3.2: DETAILS OF THE 154 mm FLUME

3.1.1.2 Longitudinal Alignment of the flume

Longitudinal alignment of the 154 mm diameter flume was carried out using a surveying theodolite and the necessary adjustment of the pipe support levels were made. The levelling then showed the longitudinal alignment to be within 0.5 mm of the straight line, which was considered acceptable (see Fig. 3.3). However, when the flume was filled up with water (full pipe flow condition) the levelling of the flume showed a substantial vertical deflection (about 12 mm) in the middle of the flume (see Fig. 3.3).

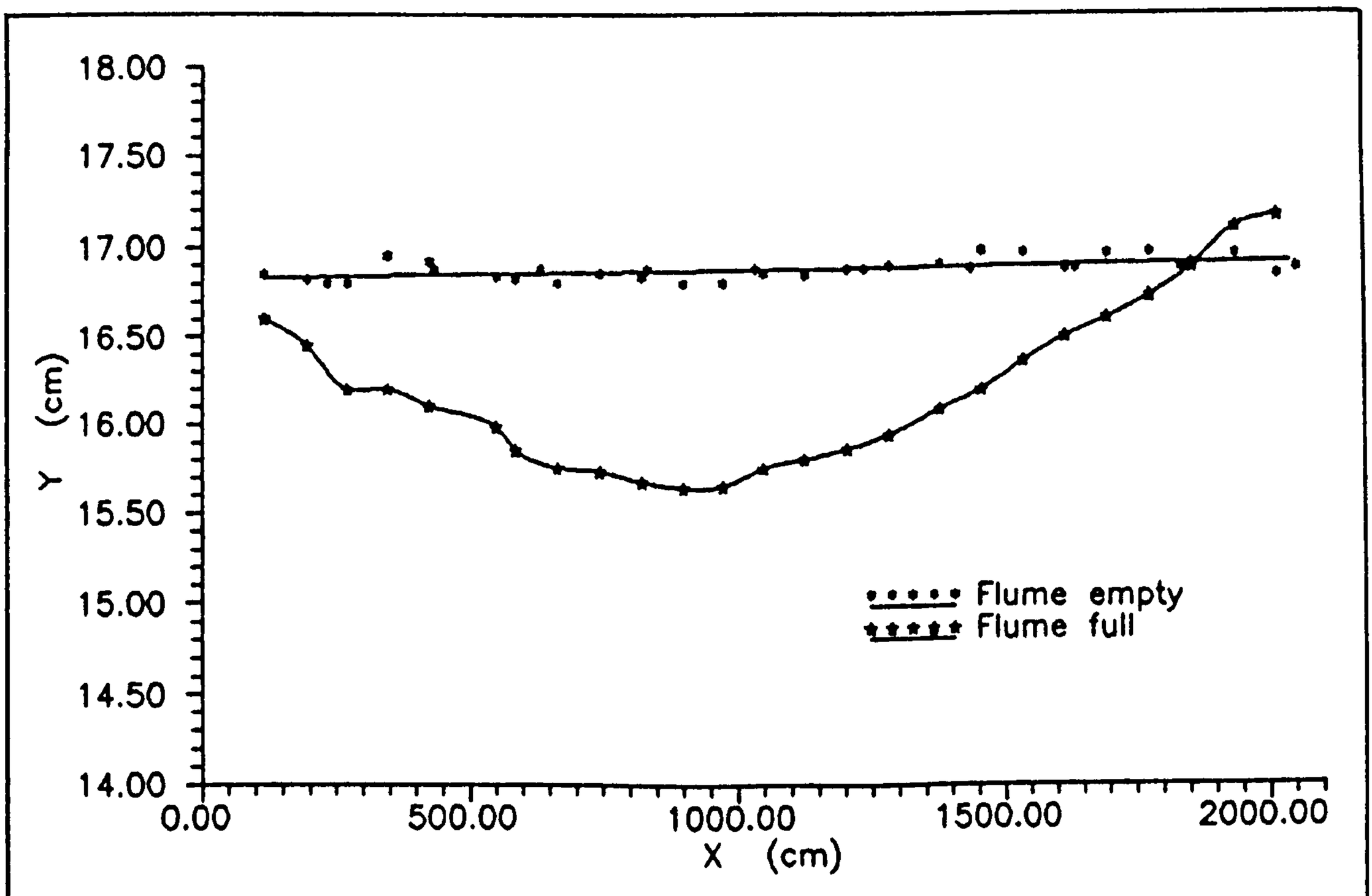

FIGURE 3.3: LEVELLING OF THE 154 mm DIAMETER FLUME

This was caused by the large span (17.26 m) between the supports of the flume framework. This vertical deflection is not acceptable at all because if the flume is in horizontal position the upstream half would have a slope of about 0.001 and the downstream half a negative slope of about -0.001, which would make it very difficult and unreliable to work with uniform flows.

Therefore a modification of the rig was necessary. Two additional sets of support were installed approximatelly at the two third points of the flume length (see Fig. 3.1). For each slope setting the supports have to be fastened before any water is allowed into the flume. Thus no flume slope changes are possible while water is running in the flume. Checking the alignment under full pipe flow conditions with the additional supports fastened gave satisfactory results as the alignment was within +/- 0.5 mm.

3.1.1.3 Measurement of Sediment Discharge

Bedload is measured using a sediment trap located at the downstream end of the test section (see Fig. 3.2 and Plate 2). For very high flows the bedload is measured by collecting the sediment in a sieve basket at the downstream end of the flume.

3.1.2 The 302 mm diameter flume

This is a modification of a rectangular flume 460 mm wide. A 302 mm diameter uPVC pipe was installed inside the rectangular flume and the necessary modifications were made to seal the

entrance to transform the flume into a flume of circular cross-section. In the test section (about 3 m) clear perspex pipe was installed in order to make visual observations and to use the laser Doppler velocimeter (LDV). The flume is 12 m long with tilting facility and a maximum longitudinal slope of 1/200 (see Fig. 3.4).

The channel slope is varied by a screw, which displaces the flume's wheeled supports (resting on steel wedges). The slope is computed from the difference in water level of two cylinders fixed at each end of the flume (11.223 m apart) and communicated by plastic tubing. The entire length of the flume has a flat false bed, with an actual testing section of about 3 m. The false bed is made of uPVC sheets, with which bed thicknesses are easily changeable.

3.1.2.1 Measurement of Discharge

The discharge is measured by using a rectangular notch (with side contraction) located at the downstream end of the flume The discharge (Q) in (m^3/s) is given by:

$$Q = \{1.777 + 0.245(\frac{h + 0.0012}{0.443})\}0.4495(h + 0.0012)^{3/2} \qquad (3.2)$$

where h is the water level above the crest of the weir in (m). The discharge is computed with a maximum error of 1.5% (BS 3680). Alternatively there are orifice plates located in each one of the two 100 mm diameter supply pipelines for cross-checking purposes.

Water surface slope is measured using a point gauge installed in a trolley, which can be moved along the entire length of the flume on a rail parallel to the flume. The accuracy of the readings is +/- 0.1 mm. To move the trolley about and insert the point gauge in the slots provided on the top of the pipe proved to be quite cumbersome, and in order to speed up measurements 6 point gauges were installed at fixed position along the flume.

3.1.2.2 Longitudinal Alignment of the Flume

Longitudinal alignment of the flume was carried out using a surveying theodolite and the necessary adjustment of the pipe and rail was made. The levelling was then within +/-1 mm of the straight line, which was considered acceptable. There was no noticeable vertical deflection when levelling the flume with water, as the flume length was only 12 m and the framework was solid and very rigid.

3.1.2.3 Measurement of Sediment Discharge

Bedload is measured using a sediment trap located downstream of the test section (see Fig. 3.4). In the case of very high flows the bedload is measured by collecting the sediment in a sieve basket at the downstream end of the flume.

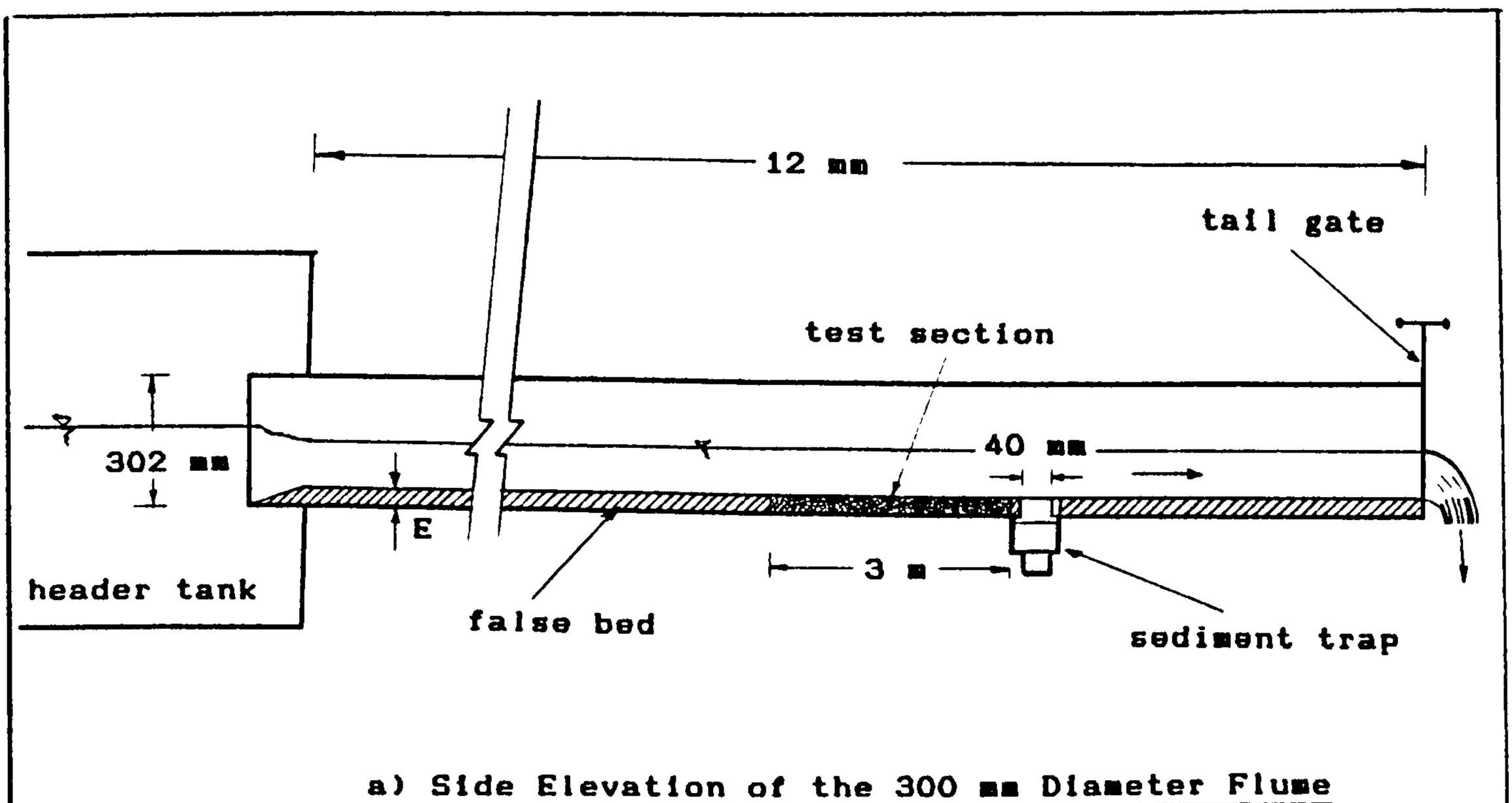

a) Side Elevation of the 300 mm Diameter Flume

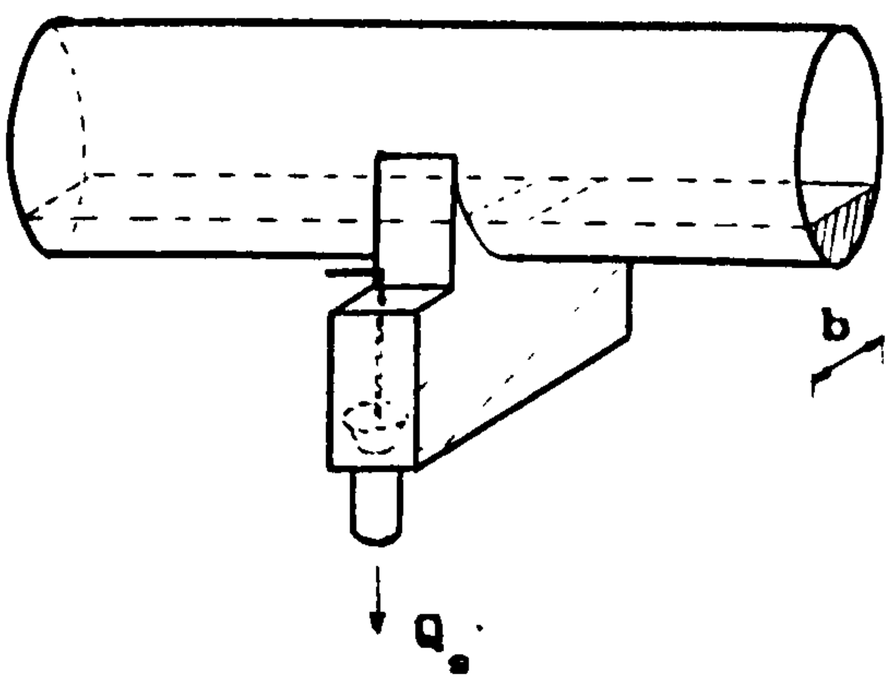

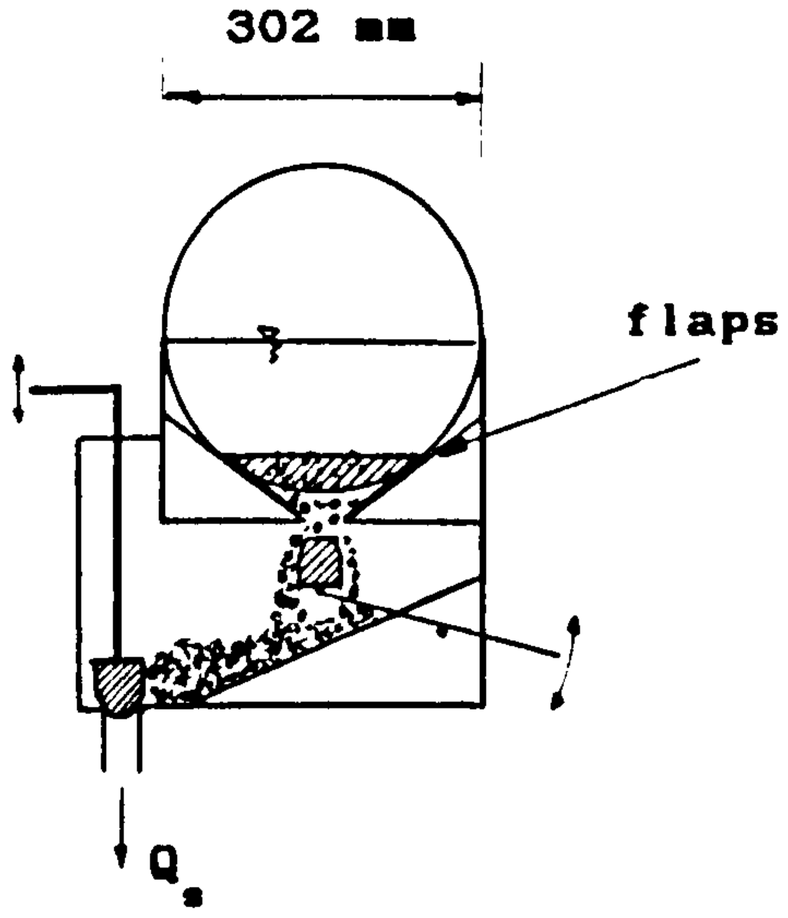

b) Details of Sediment Trap

FIGURE 3.4: LAYOUT OF THE 302 mm DIAMETER FLUME

3.2 ESTABLISHMENT OF UNIFORM FLOW

3.2.1 The 154 mm diameter flume

The steps to achieve uniform flow in the 154 mm diameter flume are (see Table 3.1):

a) An approximate channel slope is set using the slope scale at the screw jack, and the additional supports of the framework are fastened.

b) Bed level readings are taken using the set of point gauges and the actual slope is obtained by fitting a regression line to the bed level readings.

c) The pump is started and the delivery valve is gradually opened until the desired discharge is obtained (a discharge scale at the triangular notch well, gives a good approximation).

d) The tail gate opening is adjusted in such a manner as to achieve constant depth along the channel, using the set of piezometers (which should read the same). Once the flow is in equilibrium a reading of the notch level is taken at the point gauge well.

e) Then the readings of the water surface level along the flume are taken using the set of point gauges. A maximum and a minimum level at each position are taken. Then the surface slope is obtained by fitting a straight line to the readings (average). If the surface slope (S_f) is within 10 % of the bed slope (S_o) the

TABLE 3.1: TYPICAL UNIFORM FLOW COMPUTATION SHEET

WATER SURFACE SLOPE (24-2-88 b)

X (mm)	Y (mm)
11850	101.35
13035	98.95
13565	97.35
13960	94.40
14360	93.35
14755	91.45
15160	89.80
15610	88.35
16530	85.60

Regression Output:

Constant	145.39
Std Err of Y Est	0.7562
R Squared	0.9812
No. of Observations	9
Degrees of Freedom	7
X Coefficient(s)	-0.00363
Std Err of Coef.	0.000189

Surface slope = 0.003632

FLUME BED SLOPE (24-2-88)
(slope gauge = 155.0 mm)

X (mm)	Z (mm)	DEPTH (mm)
11850	68.30	33.05
13035	64.40	34.55
13565	62.10	35.25
13960	60.60	33.80
14360	59.30	34.05
14755	57.90	33.55
15160	56.50	33.30
15610	55.10	33.25
16530	52.20	33.40

Regression Output:

Constant	109.50
Std Err of Y Est	0.2300
R Squared	0.9980
No. of Observations	9
Degrees of Freedom	7
X Coefficient(s)	-0.00348
Std Err of Coef.	0.000057

Bed slope = 0.003486

UNIFORM FLOW COMPUTATIONS

d_{50} =	2.00	(mm)	(sand size)
D =	154.00	(mm)	(circ. cross-sect. flume dia.)
E =	18.40	(mm)	(sediment bed thickness)
So =	0.003486		(flume bed slope)
S_f =	0.003632		(surface slope)
dif =	4.2	(%)	(Difference)
S =	0.003576		(corrected slope)
Y_o =	33.90	(mm)	(Normal depth)
Y/D =	0.22		(depth ratio)
(Y+E)/D =	0.34		
T =	18.9	(°C)	(Temperature)
Q =	1.43	(l/s)	(Discharge)
τ_o =	0.8284	(N/m2)	(Mean shear stress)
V =	0.331	(m/s)	(Mean flow velocity)
n =	0.0149		(Manning's coefficient)
F_r =	0.615		(Froude number)
q_s =	0.0036	(g/min)	(Bed load)

flow is accepted as uniform. Otherwise the appropriate adjustment of the tail gate has to be made and the process repeated.

f) The effective slope of the quasi uniform flow is computed by applying a correction to the flume bed slope based on the uniformly varied flow equation,

$$\frac{dy}{dx} = \frac{(S_o - S_f)}{1 - Fr^2} \qquad (3.3)$$

where S_o is the flume bed slope, S_f the energy gradient, Fr the Froude number of the flow and $\frac{dy}{dx}$ the water surface slope (S_p).

For uniform flow conditions the three slopes should be equal ($S_o = S_f = S_p$). Assuming the flow is nearly uniform the effective slope can be expressed as:

$$S = S_o - (S_o - S_p)(1 - Fr^2) \qquad (3.4)$$

It is apparent in Eq. 3.4 that as the flow approaches uniform conditions the correction $(S_o - S_p)(1 - Fr^2)$ becomes smaller as the effective slope converges to the channel bed slope (S_o).

3.2.2 The 302 mm diameter flume

In this flume the procedure to achieve uniform flow is more or less the same as described above for the 154 mm diameter flume. However, as here the point gauges are fixed to the flume structure and the bed slope can be varied during operation it is much easier to achieve uniform flow conditions.

3.3 MEASUREMENT OF VELOCITY AND SHEAR STRESS DISTRIBUTIONS

3.3.1 Velocity Measurements

Velocity profiles were measured in various sections of the flume to check the uniformity of the flows. These measurements were also used for the determination of the shear stresses exerted on the bed by the flowing water. The velocity profiles were obtained using a Pitot tube, several 10 mm propeller current meters, and a Laser Doppler Velocimeter (LDV). The latter will be described in section 3.4.1.

3.3.1.1 Pitot Tube

A pre-calibrated Pitot tube connected to a high precision pressure difference reading device (+/- 0.1 mm water column) was employed. The internal and external diameters of the Pitot tube are 0.8 and 2.3 mm respectively. The velocity is given by:

$$u = 14 \sqrt{\Delta h} \tag{3.5}$$

where u is the local velocity in (cm/s) and Δh is the manometer deflection in [m] of water.

3.3.1.2 Propeller Current Meter

In order to speed up velocity measurements several propeller current meters (Nixon Ltd. and HR Ltd.) were used. The propeller diameter was 10 mm and the lowest position measured was 7.5 mm from the bed. The probes were factory pre-calibrated by means of

a towing tank rig, and were regularly cross-checked with the Pitot tube.

The range of velocities varied from 0 to 1.5 m/s (0 to 300 Hz) with a maximum absolute error of 0.015 m/s. The readings were taken from a digital counter that was set to give 10 seconds average. For each position eight readings were averaged (i.e., 80 seconds) to obtain the local mean velocity. The velocity of a current meter is given by an equation of the form:

$$u = a X + b \tag{3.6}$$

where u is the local velocity in (cm/s), X is the current meter frequency reading in (Hz), and a and b are constants (factory calibrated), which are given in Table 3.2.

TABLE 3.2: CALIBRATION OF CURRENT METER PROBES

Probe Number	Calibration Constants			
	N < 45 Hz		45 ≤ N < 270 Hz	
	a	b	a	b
DIXON LTD.				
1398	0.564	4.165	0.538	5.729
1398a	0.551	3.224	0.510	5.365
1399	0.566	3.486	0.543	4.483
1094	0.558	3.064	0.534	4.401
HR LTD.				
N1(43)	0.474	3.733	0.474	3.733
N2	0.236	8.778	0.236	8.778

The probes are cleaned with distilled water every time they are used in order to remove any debris, hairs, etc., which could affect their calibration. However, the probes are calibrated regularly (twice a year) to maintain the accuracy.

3.3.2 Measurements of Bed Shear Stress Distribution

3.3.2.1 Velocity Distribution Method

Theoretical investigations of Prandtl and von Karman and the experimental studies of Nikuradse (1933) on flow through pipes led to rational formulae for velocity distribution and hydraulic resistance for turbulent flows over flat plates and in circular pipes flowing full. As certain similarities exist between circular pipes and open channel flow, these formulas can be applied to open channel flow by changing the constant to include factors such as the free surface effect, the non-uniform shear stress distribution along the wetted perimeter, etc., and by using the hydraulic radius in place of the diameter (D = 4R).

From Prandtl mixing length theory the relation,

$$\frac{u}{u_*} = \frac{1}{\varkappa} \ln(y) + \text{constant} \qquad (3.7)$$

in which $u_* = \sqrt{\tau_o/\rho}$ is the shear velocity, u the velocity in x-direction at y-position, $\varkappa$ is von Karman's universal constant and τ_o the bed shear stress. For open channel flow Eq. 3.7 can be

expressed for smooth surfaces, as:

$$\frac{u}{u_*} = 5.75 \text{ Log}\left(\frac{9yu_*}{\nu}\right) \tag{3.8}$$

where ν is the kinematic viscosity and, for rough surfaces, as:

$$\frac{u}{u_*} = 5.75 \text{ Log}\left(\frac{30.2\ y}{k_s}\right) \tag{3.9}$$

where k_s is Nikuradse's equivalent sand roughness. For the position of maximum velocity (y=h) Eq. 3.9 can be written as,

$$\frac{u_{max}}{u_*} = 5.75 \text{ Log}\left(\frac{30.2\ h}{k_s}\right) \tag{3.10}$$

Subtracting Eq. 3.9 from Eq. 3.10 yields,

$$\frac{u_{max} - u}{u_*} = 5.75 \text{ Log}\left(\frac{h}{y}\right) \tag{3.11}$$

Equation 3.11 is valid for both, rough and smooth boundaries. Because Eq. 3.11 does not include the term k_s it is easier to use. Plotting $(u_{max} - u)$ Vs. $5.75 \text{ Log}\left(\frac{h}{y}\right)$ gives a straight line (universal velocity distribution law) and the shear velocity can then be obtained directly from the slope of the curve, and thus the local bed shear stress. In Table 3.3 (one velocity profile) for a typical case of computation of the local bed shear stress. The velocity profile and logarithmic velocity distribution for the particular case of Table 3.3 are shown in Fig. 3.5. By measuring several vertical velocity profiles across the width of the flume it was possible to obtain the distribution of shear stresses on the bed.

TABLE 3.3: TYPICAL SHEAR STRESS DISTRIBUTION COMPUTATION

VELOCITY PROFILE to obtain Shear Stress

154 mm diameter circular cross-section flume
(14-10-88a) X = 0 cm (centerline)

Flume Diameter	154	(mm)
Sand size	2.00	(mm)
Bed Thickness	18.40	(mm)
Slope	0.002350	
Discharge	5.59	(l/s)
Normal Depth	77.45	(mm)
(Y+E)/D	0.62	
Mean Shear Stress	0.929	(N/m^2)
Mean Velocity	0.512	(m/s)

Current Meter u = 0.510 N + 5.365 (48.5<N<267 Hz)
(#1398-A) (cm/s) (Hz)

y (mm)	N (Hz)	u (m/s)	umax-u (m/s)	-5.75LOG(y/h)
7.5	76.64	0.444	0.1331	4.18
10.0	81.65	0.470	0.1075	3.46
12.0	86.14	0.493	0.0847	3.01
14.0	88.93	0.507	0.0705	2.62
18.0	93.69	0.531	0.0462	1.99
22.0	96.24	0.544	0.0332	1.49
30.0	100.96	0.568	0.0091	0.72
40.0	102.75	0.577	0.0000	0.00
50.0	99.31	0.560	0.0175	-0.56
70.0	90.00	0.512	0.0650	-1.40

Regression Output:

Constant	-0.03473
Std Err of Y Est	0.001967
R Squared	0.997406
No. of Observations	5
Degrees of Freedom	3
X Coefficient(s)	0.040327
Std Err of Coef.	0.001187

Shear Velocity	$u_* = 0.0403$	(m/s)
Measured Bed Shear Stress	$\tau_{bm} = 1.626$	(N/m^2)
Predicted Bed Shear	$\tau_b = 1.386$	(N/m^2)
Mean Shear Stress	$\tau_o = 0.929$	(N/m^2)

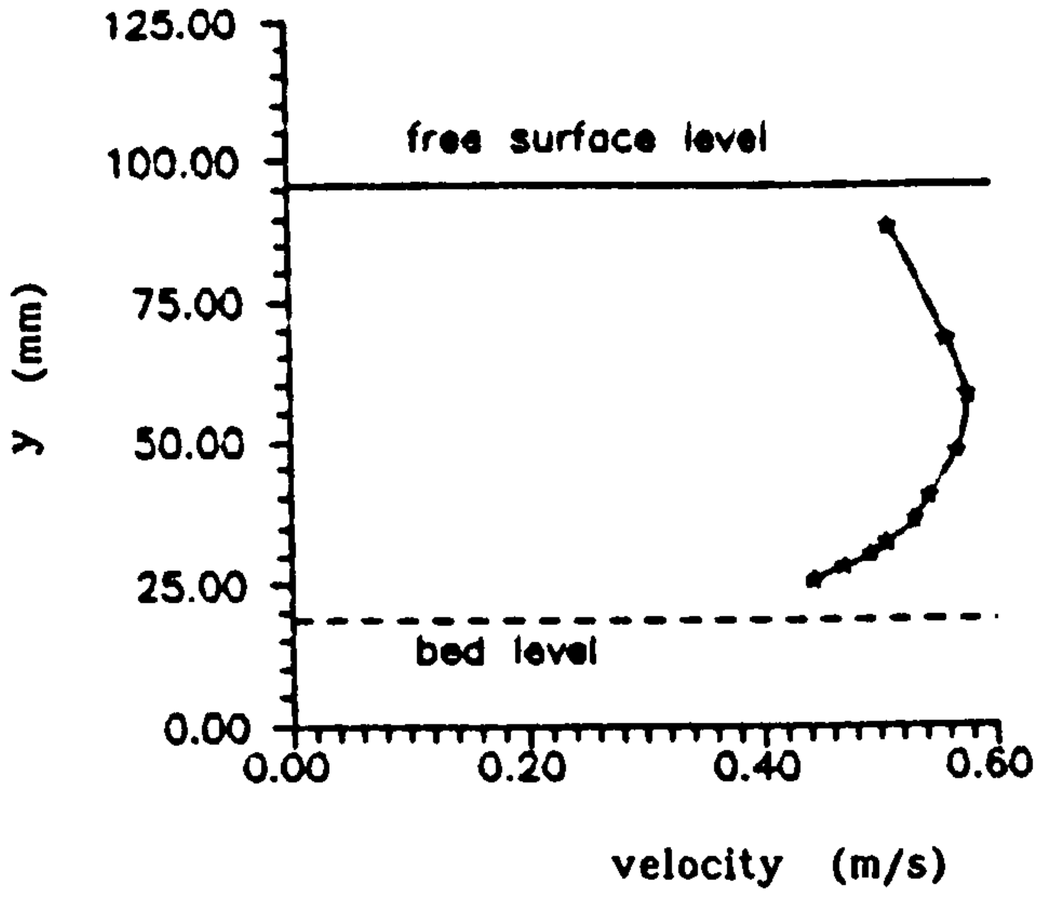

a)Velocity distribution

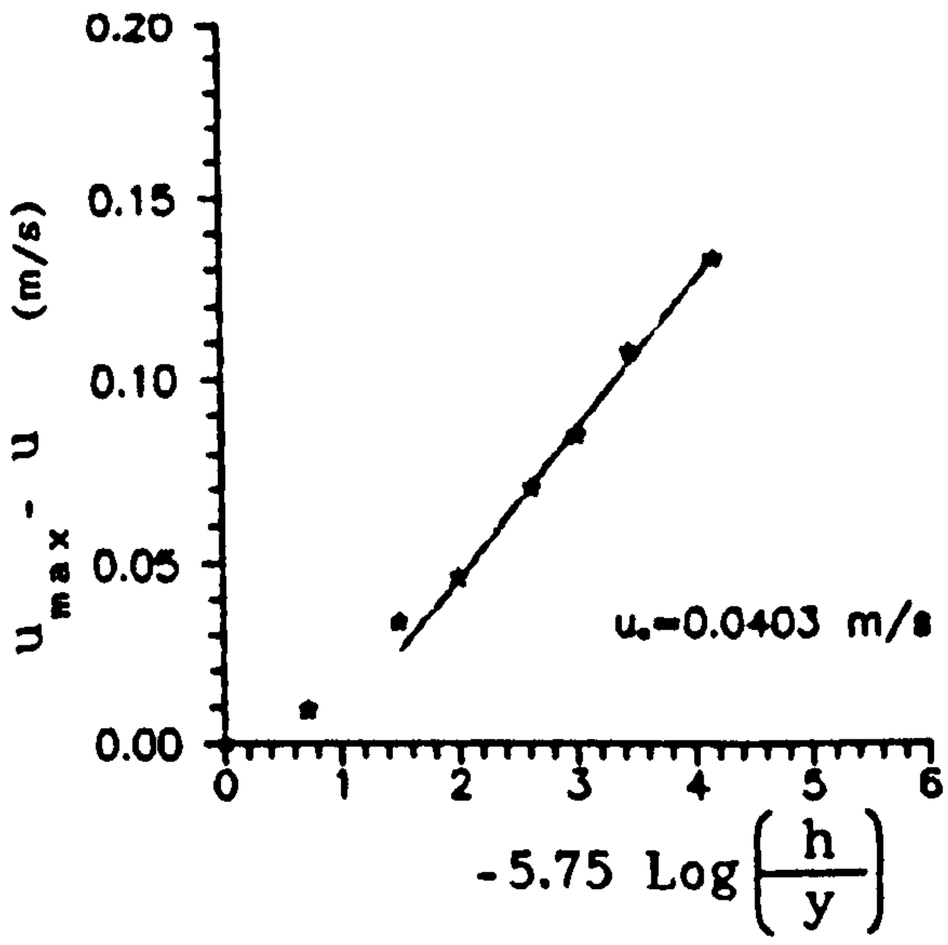

b) Log. Veloc. defect Distr.

FIGURE 3.5: TYPICAL VELOCITY DISTRIBUTION

154mm dia. flume (E=18.4mm)
S_o=0.00235 Q=5.59 l/s Y_o=77.5mm

3.4 MEASUREMENT OF TURBULENT INTENSITIES

The flow in channels is usually turbulent with large fluctuations in velocity that account for much of the dissipation of energy, mass transfer and heat transfer in turbulent liquids. Transfers of momentum between neighboring pulses of the fluid are very important, and it is well known that boundary shear stresses in turbulent flow, are much higher than the corresponding shear stresses for same fluid in laminar flow. The root mean square (RMS) of the velocity fluctuation $\sqrt{\overline{(u')^2}}$, is a measure of the intensity of turbulence in the x-direction.

With the advent of laser light with its unique properties of spatial and temporal coherence it was possible to use the Doppler effect to measure velocities of fluids by optical methods. This is known as LDV, and it is based on the measure of the rate of change-of-phase (i.e., frequency) of the lightwaves after scattering from particles moving with the fluid.

3.4.1 Laser Doppler Velocimeter (LDV)

A TSI LDV equipment with forward scatter mode and single component (see Plate 4) was used for measuring turbulence intensities. Figure 3.6 shows the LDV with laser source, optical system and photodetector. The optical system contains a beamsplitter, a prism for directing one of the two beams internally, a bragg cell module and front optics. The laser beam is split into two parallel beams 50 mm apart. The bragg cell

module together with the electronic frequency shifter introduce a fixed frequency difference (usually 0.1 MHz) between the two beams, the "frequency shift", which is used by the processor to distinguish between negative and positive flow directions. Then the two parallel beams pass through a 243 mm lens.

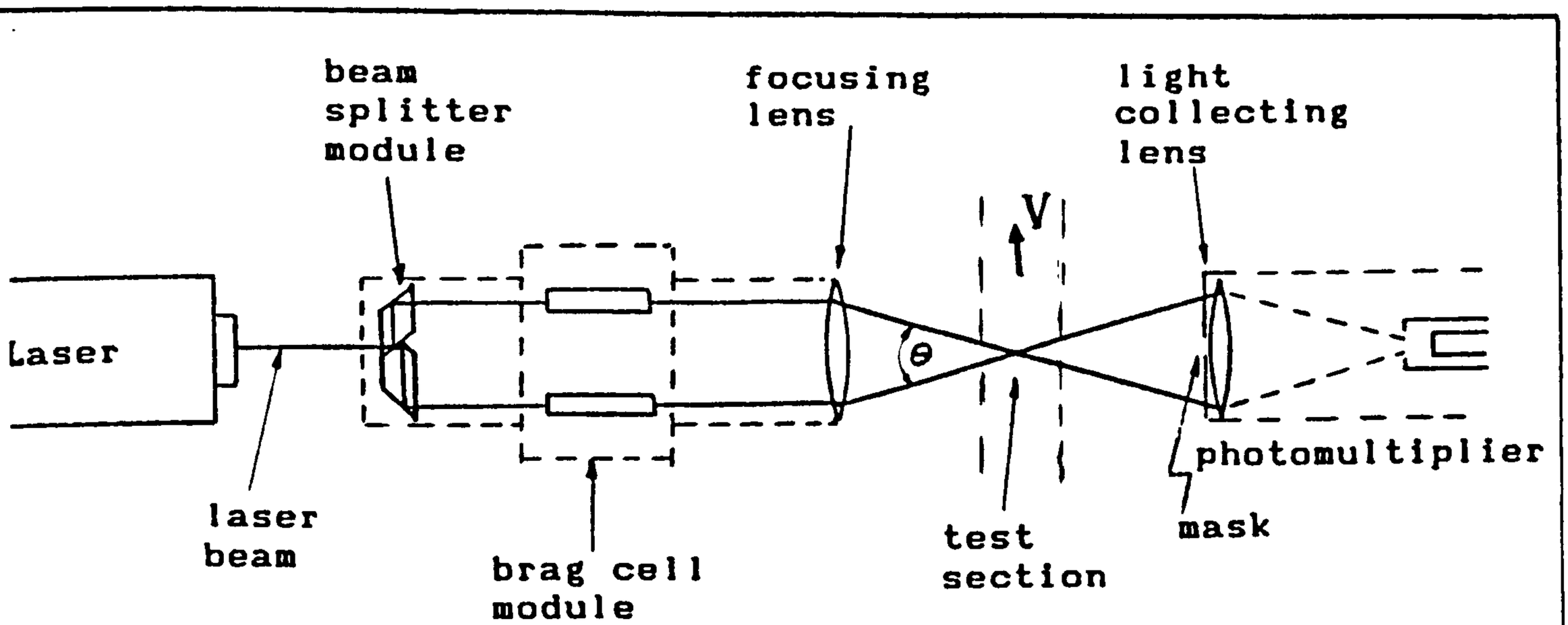

a) Laser Optical System

Laser	: He-Ne Laser
Wavelength	: 632.8 μm
Mode	: Forward scatter
Components	: Single component
Angle (θ)	: 11.66°
Focal Distance (f)	: 243 mm
Power	: 15 mW
Make	: TSI
Signal Processor	: IFA-550

b) Technical Specifications

FIGURE 3.6: LASER DOPPLER VELOCIMETER

At each position 50,000 velocity measurements were made in less than a minute. These data were logged and saved in floppy disk for later analysis using a TSI IFA-550 processor, which could compute RMS and do spectra analysis as well (see Fig. 3.7).

The measurements were taken in the following manner:

a) The alignment of the flume was checked

b) The laser equipment was installed in the flume.

c) A uniform flow was established (see Sec. 3.2)

d) The crossing point of the laser beams (measuring volume) was positioned at the centre of the flume, and the vertical position was measured and the positioning scale outside the flume was adjusted.

e) The receiving optics was focused and the Doppler signal was checked in the oscilloscope (multiparticle signal 1 to 3 volts in amplitude).

f) Using an IBM compatible computer and the IFA-550 processor a set of readings was taken and saved in floppy disk for subsequent analysis.

g) The laser was positioned at a higher position and the process from step "e" was repeated.

After completion of the measurements the raw data (floppy disks) were analysed using the IFA-550 processor and the computer, to obtain the velocity and turbulence intensity profiles. Sometimes

simultaneous measurements of velocity were taken using the laser velocimeter and a current meter for cross-checking purposes.

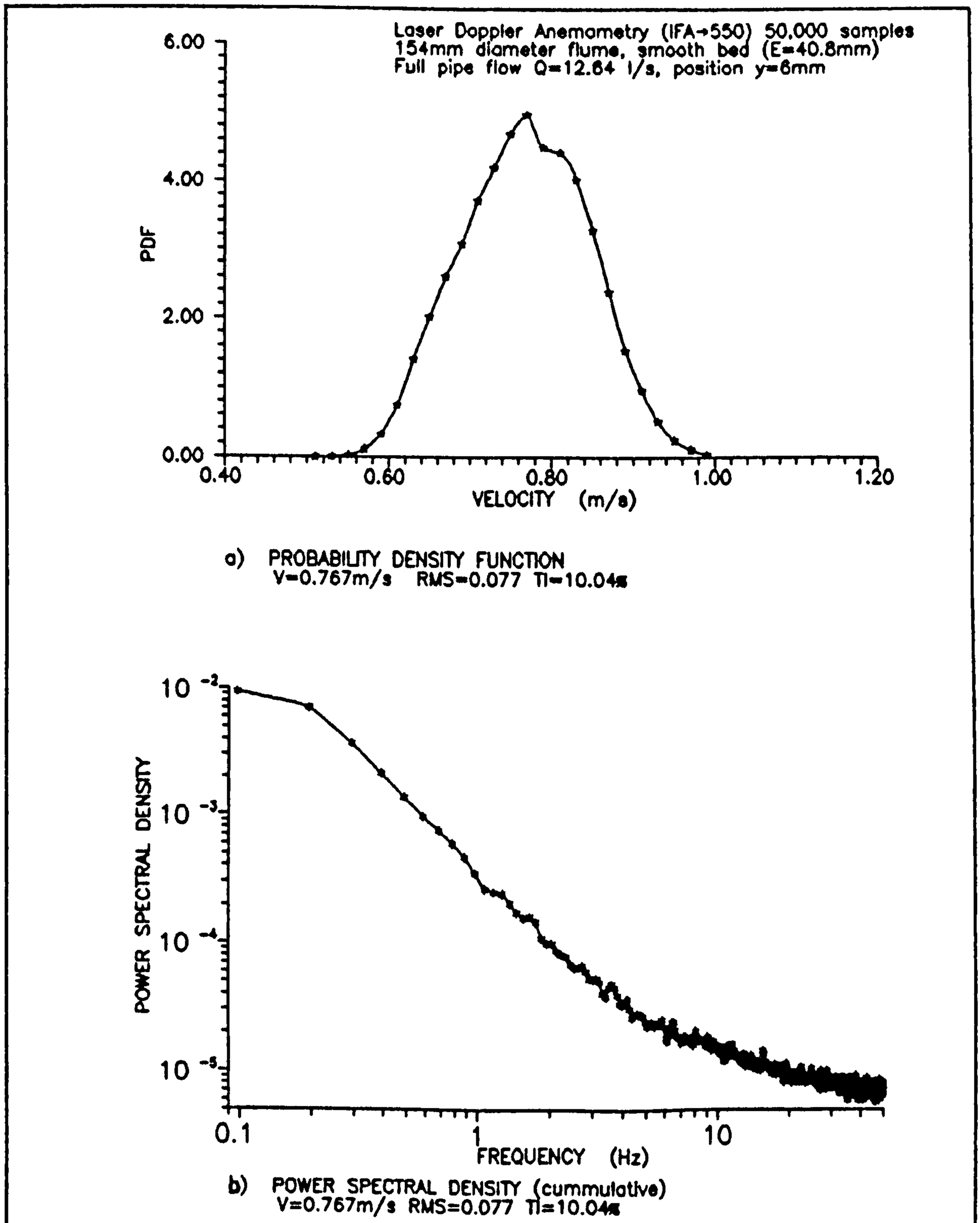

FIGURE 3.7: TYPICAL OUTPUT FROM THE IFA-550 SIGNAL PROCESSOR

3.5 DETERMINATION OF THRESHOLD OF MOTION

3.5.1 Non-cohesive Sediments

3.5.1.1 Preparation of Sediments

Uniformly graded sands received from the supplier were mechanically separated using BS sieves in order to improve their uniformity. From the sand supplied (see Fig. 3.8 and Table 3.4), with a mean size of 2.56 mm, two size fractions were obtained, one with d_{50}= 2.03 mm, i.e., the material retained between sieves 1.70 mm and 2.36 mm only (see Fig. 3.9-curve F), and the other with d_{50}= 2.86 mm, i.e., the material retained between sieves 2.36 mm and 3.35 mm only (see Fig. 3.12-curve G).

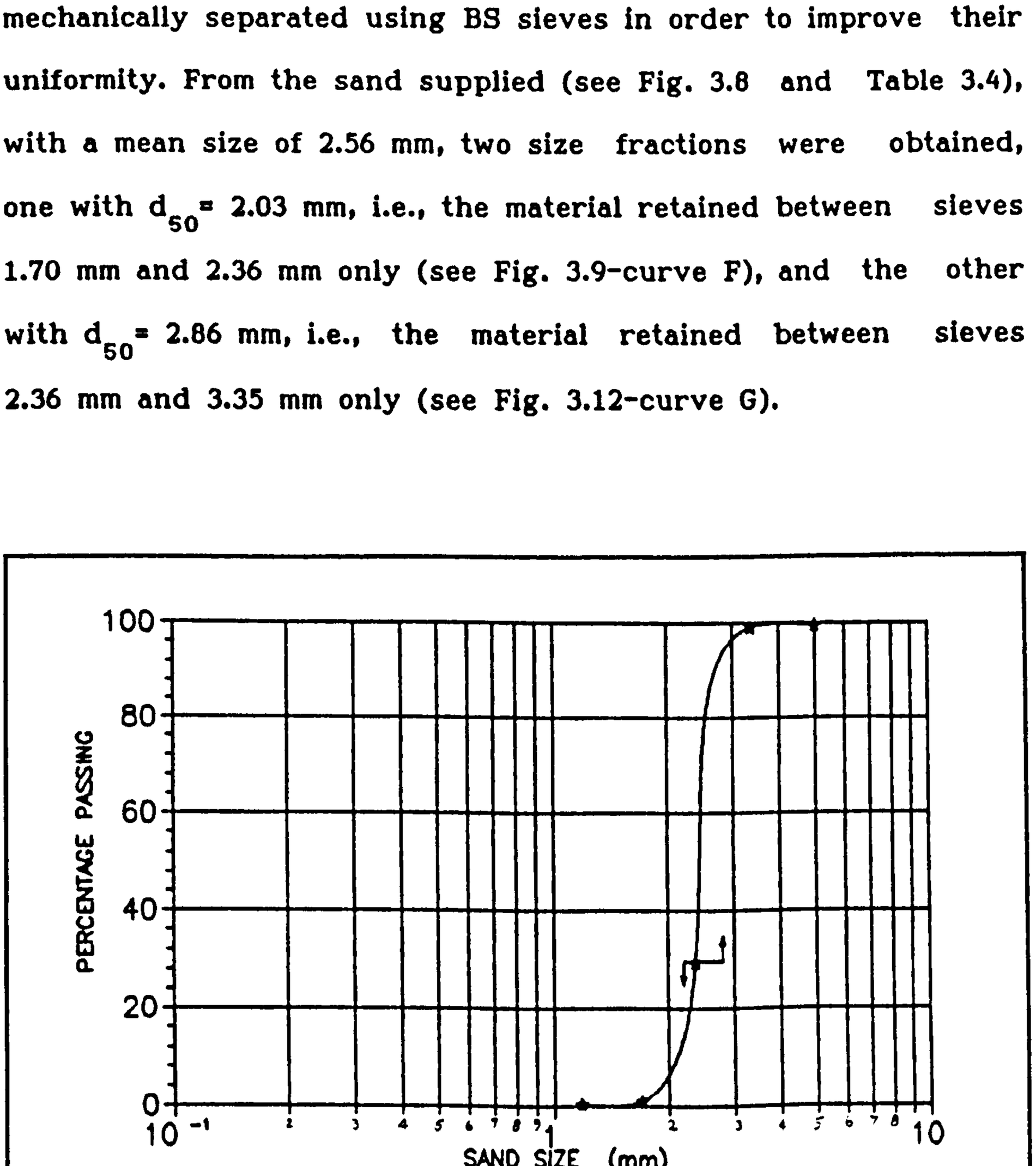

FIGURE 3.8: TYPICAL SAND SIZE DISTRIBUTION

Sand d_{50}= 2.56 mm to obtain two size fractions (2.03 and 2.86 mm)

TABLE 3.4: UNIFORM SAND CHARACTERISTICS

d_{50} (mm)	Sieve Size max.- min. (mm)	Density		Relative Density S_s
		Absolute (Kg/m^3)	Apparent (Kg/m^3)	
0.12	0.090 - 0.150	2542	1464	2.54
0.36	0.300 - 0.425	2484	1618	2.48
0.51	0.425 - 0.600	2609	1615	2.61
0.89	0.600 - 1.180	2593	1658	2.59
1.44	1.180 - 1.700	2574	1544	2.57
2.03	1.700 - 2.360	2507	1577	2.51
2.86	2.360 - 3.350	2548	1517	2.55
4.17	3.350 - 5.000	2479	1575	2.48

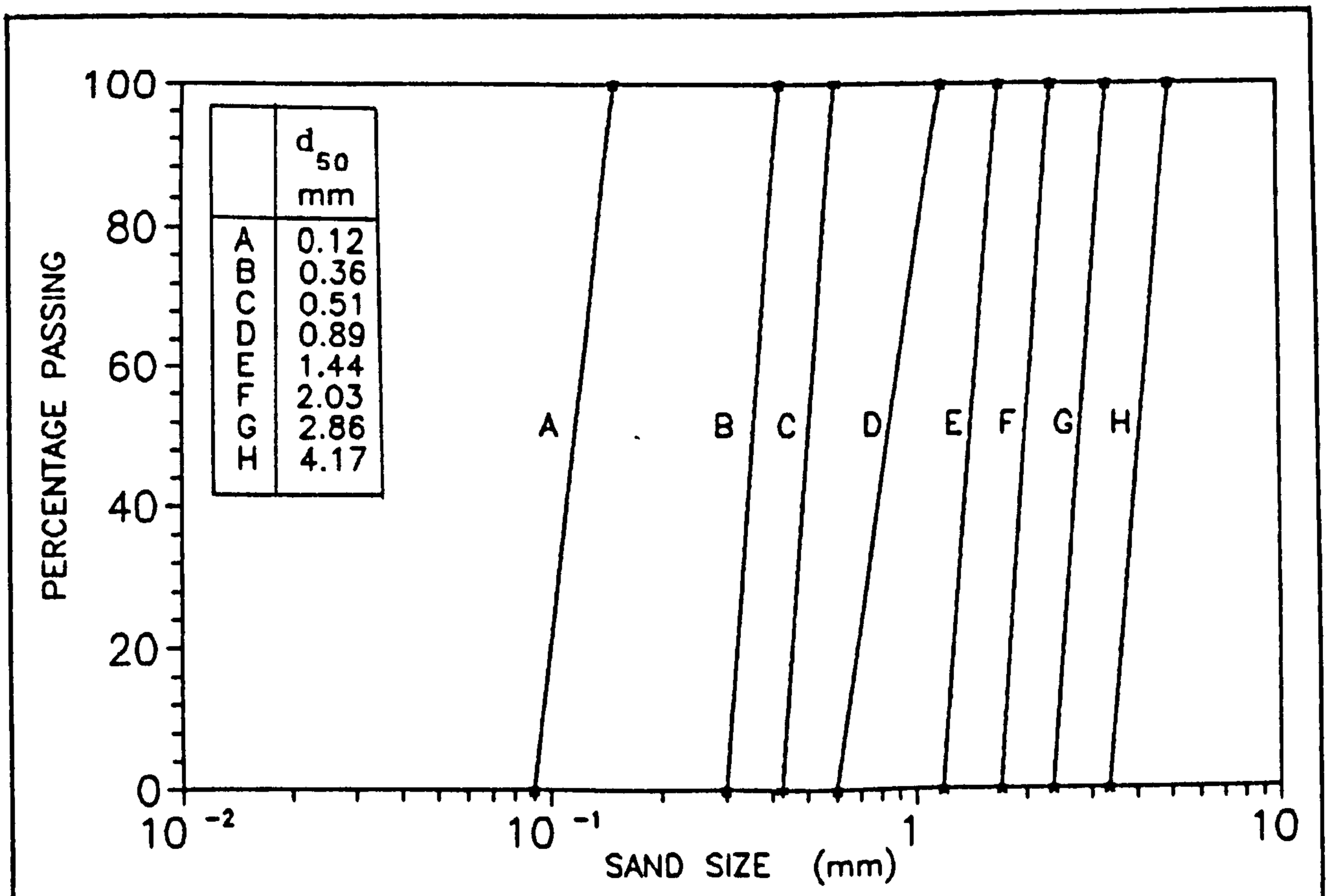

FIGURE 3.9: UNIFORM SANDS AFTER SEPARATION

(Each size fraction is limited by two consecutive meshes)

As it was mentioned in Chapter 2 many investigators used different criteria for defining critical conditions for initiation of motion . However, due to the turbulent nature of open channel and full pipe flows, there will always be some sediment transport for even the very small shear stresses. Therefore, a more scientific approach for defining critical conditions is that of relating critical shear stresses to erosion rates. In the present laboratory work critical erosion rates were defined in terms of a volumetric concentration ($C_v = 10^{-8}$).

3.5.1.2 Procedure to Determine Critical Conditions

1) A channel slope was selected for the flume.

2) The test section was filled with sand (of a given size) and levelled with the false bed.

3) The pump was started and the delivery valve slightly opened.

4) The flume was slowly filled up with water (tail gate fully closed).

5) The delivery valve was opened to obtain the desired discharge and the opening of the tail gate was gradually adjusted until a uniform flow was achieved (see Section 3.2).

6) The sediment trap was opened and the stop watch started. The flow was then left running for about 30 minutes.

7) The bedload sample collected in the trap was removed and put in a container into the oven to dry.

The sediment trap was further operated to collect two additional samples, then the flow was increased and the procedure repeated in order to measure the bedload for a higher shear stress. The entire process was repeated for higher flows, in order to have measurements for at least four shear stresses beyond the critical conditions.

A plot of sediment concentration C_v versus shear stress was prepared (see Fig. 3.10) with the data and the critical shear stress was obtained by extrapolation to $C_v = 10^{-8}$. The procedure described above was repeated for various slopes for each sand size.

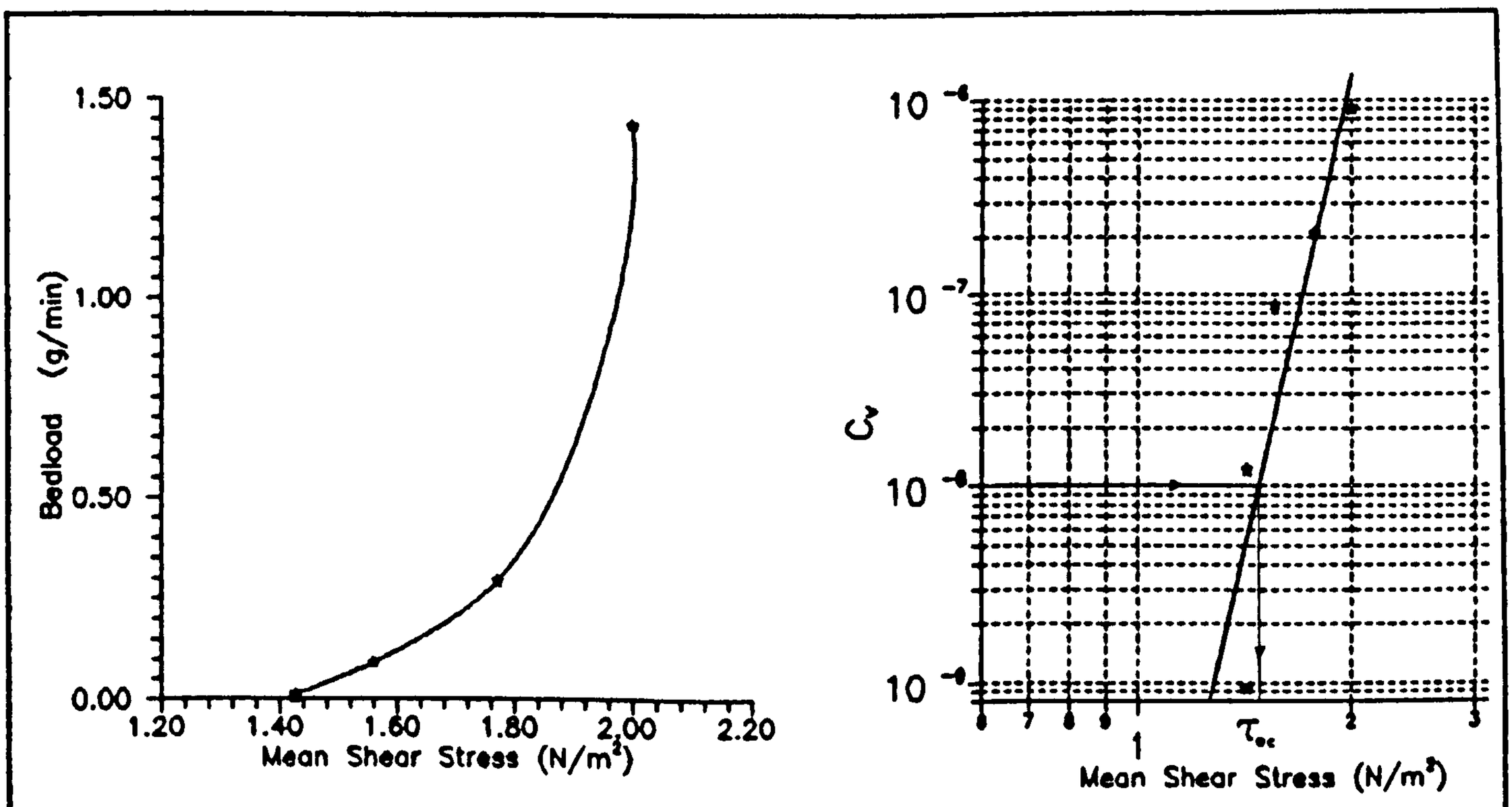

FIGURE 3.10: TYPICAL COMPUTATION OF CRITICAL SHEAR STRESS

Flume 154mm diameter (E=20mm)
S_o = 0.003762 d_{50}=4.17mm τ_{oc} = 1.5 N/m^2

3.5.2 Cohesive Sediments

3.5.2.1 Preparation of Cohesive Sediments

a) Preliminary Experiments

The same uniform sands mentioned in Sec. 3.5.1.1 were used as basic material for the preparation of cohesive sediments. Several cohesive additives such as china (kaolinite) clay, petroleum jelly (vaseline), gear oil and laponite clay were used. Sand was mixed with a small proportion of cohesive additive in order to form a sticky substance. The proportion of sand, and the type and concentration of the cohesive additive were used as parameters.

b) Synthetic Sewer Sediment Experiments

The synthetic sewer sediment (see Sec. 2.3.2) is formed mixing Laponite RD clay, sand and water, and the steps for preparing the mixture are:

1) Laponite RD clay powder is dissolved in water to the required concentration (18 - 40 g/l) to form a gel (colloidal solution). Due to the very fine size of the clay particles (0.025 μm) the container where the clay powder is dissolved has to be placed in an ultrasonic bath in order to achieve a homogeneous solution in a reasonable time (1/2 hour per litre of solution). Once the solution is prepared it is left to rest for an hour to let it buildup its molecular structure (with a clear gel appearance).

2) A known weight of sand is placed in a bucket. Then a known amount of clay gel is gradually added to the sand to form a mixture, which is constantly stirred until the desired sand/clay gel proportion is achieved. Then the mixture is left in an airtight container for at least one hour before placing it into the flume.

3) The sediment mixture is placed in the test section of the flume, and it is levelled with the false bed. Then it is left for at least 1 hour before any water is passed through the flume.

3.5.2.2 Determination of Critical Shear Stresses

a) Open Channel Flow Experiments

Once the sediment bed was ready for testing the procedure for determining critical shear stresses under open channel flow conditions is more or less the same as the one described in Sec. 3.5.1.2. However, cohesive sediment beds did not show any signs of erosion until the shear stresses were very close to critical conditions. The procedure was:

1) A channel slope was selected for the flume (S_1 in Fig. 3.11).

2) The pump was started and the delivery valve slightly opened.

3) The flume was slowly filled up with water (tail gate fully closed).

4) The delivery valve was further opened to obtain the desired discharge and the tail gate was gradually adjusted until a

uniform flow was achieved (see Sec. 3.2). The flow was left running for about 30 minutes.

By increasing the discharge in small increments at a time the process was repeated until either the first signs of erosion were apparent or the maximum depth of the flume was reached. In the latter case the flow was stopped, the flume drained and the slope of the flume was increased (S_2 in Fig. 3.11). This procedure was repeated until the first sign of erosion appeared on the bed. Then the sediment trap was operated to obtain the bedload for that flow.

In a similar manner the bedloads for several flows with higher shear stresses, were measured. As the shear stresses were very high near the critical conditions the sediment trap efficiency was considerably diminished. The rapid collapse of the sediment bed after exceeding the critical conditions did not allow much time to measure sediment rates. Therefore critical conditions had to be defined by visual observations most of the time.

b) Full Pipe Flow Experiments

Most of the cohesive sediments tested showed very high critical shear stresses (see Fig. 3.11), beyond that attained under open channel flow conditions. So it was necessary to carry out the tests under pressure (i.e., full pipe flow conditions).

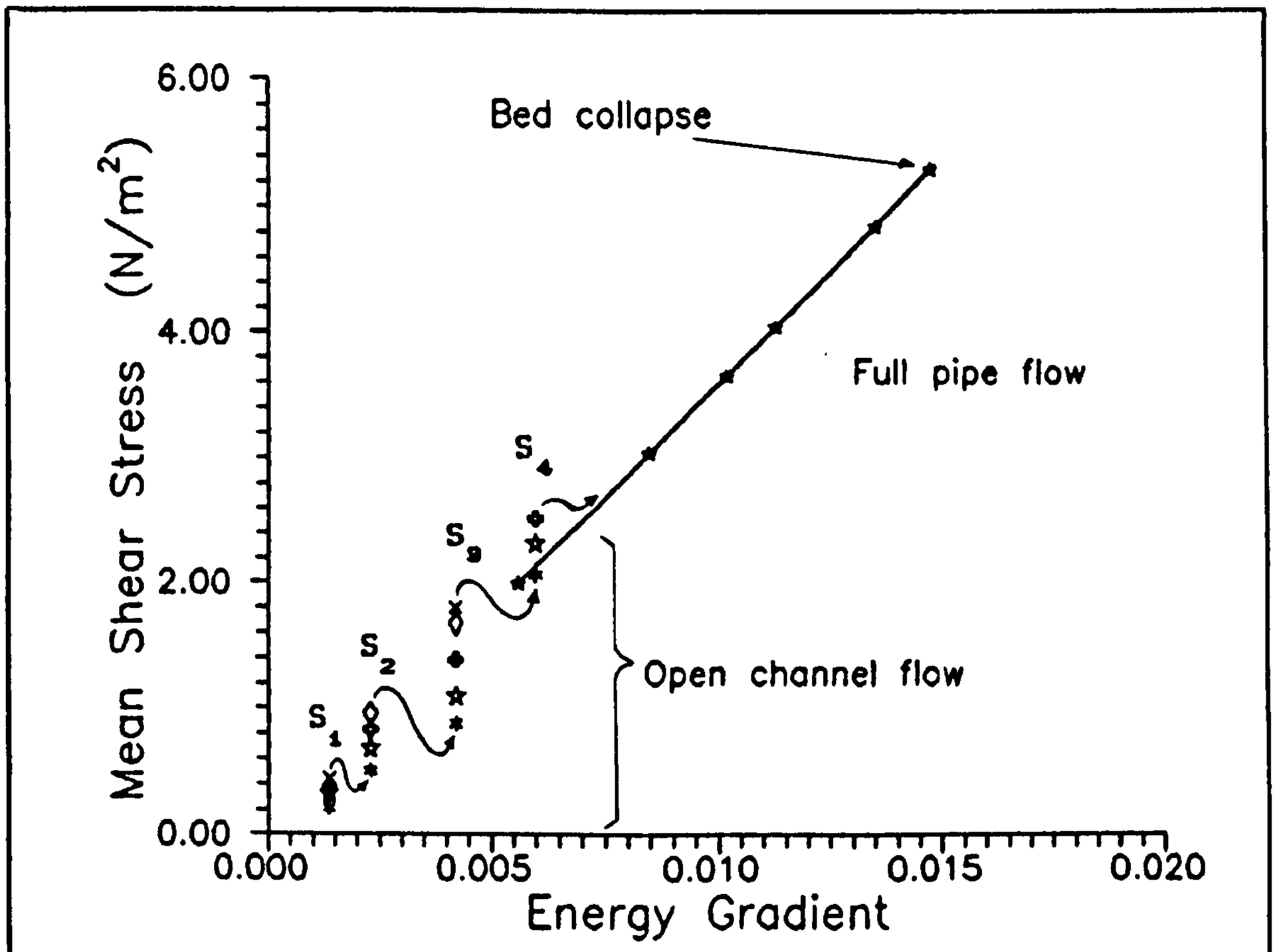

FIGURE 3.11: TYPICAL COHESIVE SEDIMENT EXPERIMENT

70 % uniform sand (d = 0.36mm)
30 % Laponite clay gel (24 g/l)

To run the test under full pipe flow conditions the following procedure was adopted:

1) The windows on the top of the pipe were sealed with the plastic watertight caps.

2) The pump was started and the delivery valve slightly opened. The flume was slowly filled up with water (tail gate fully closed).

3) The delivery valve was opened to obtain the desired discharge and the tail gate was gradually adjusted in such a manner as to keep a positive pressure along the flume. Then the flow was left to reach equilibrium conditions, and the pressure gradient was obtained from the readings of the piezometer bank. The flow was left running for about 30 minutes.

By increasing the discharge in small increments at a time, the process was repeated until the first signs of erosion were apparent. Then the discharge was still further increased until the stage of the collapse of the sediment bed was reached.

3.6 TRANSPORT EXPERIMENTS

3.6.1 Non-cohesive Sediments

3.6.1.1 Alluvial Beds

Transport experiments with a loose bed were carried out in the 154 mm diameter flume. The length of the test section was extended to 4 m, and a vibration sand feeder was installed in the flume to supply the amount of sediment being transported (see Fig. 3.12) at any time to maintain equilibrium conditions. The sediment rate is dependent on the frequency of the vibrator, the gap between the sand container mouth and the tray, and the inclination of the tray. In order to keep the sediment discharge constant it was necessary to maintain the level of sand in the hopper by refilling it often during operation.

Transport experiments were carried out for each uniform sand and bed thickness configuration under various uniform flow conditions. The false bed (uPVC) upstream and downstream of the test section was artificially roughened with uniform sand of the appropriate size, using double sided adhesive tape, which could be easily removed to change the sand size (bed roughness).

Three different sediment bed thicknesses were set up in the flume and various uniform sands were tested. For each run, after equilibrium conditions were reached, the flow was stopped (by closing the tail gate and the delivery valve) and the channel was slowly drained. Then bedforms were measured.

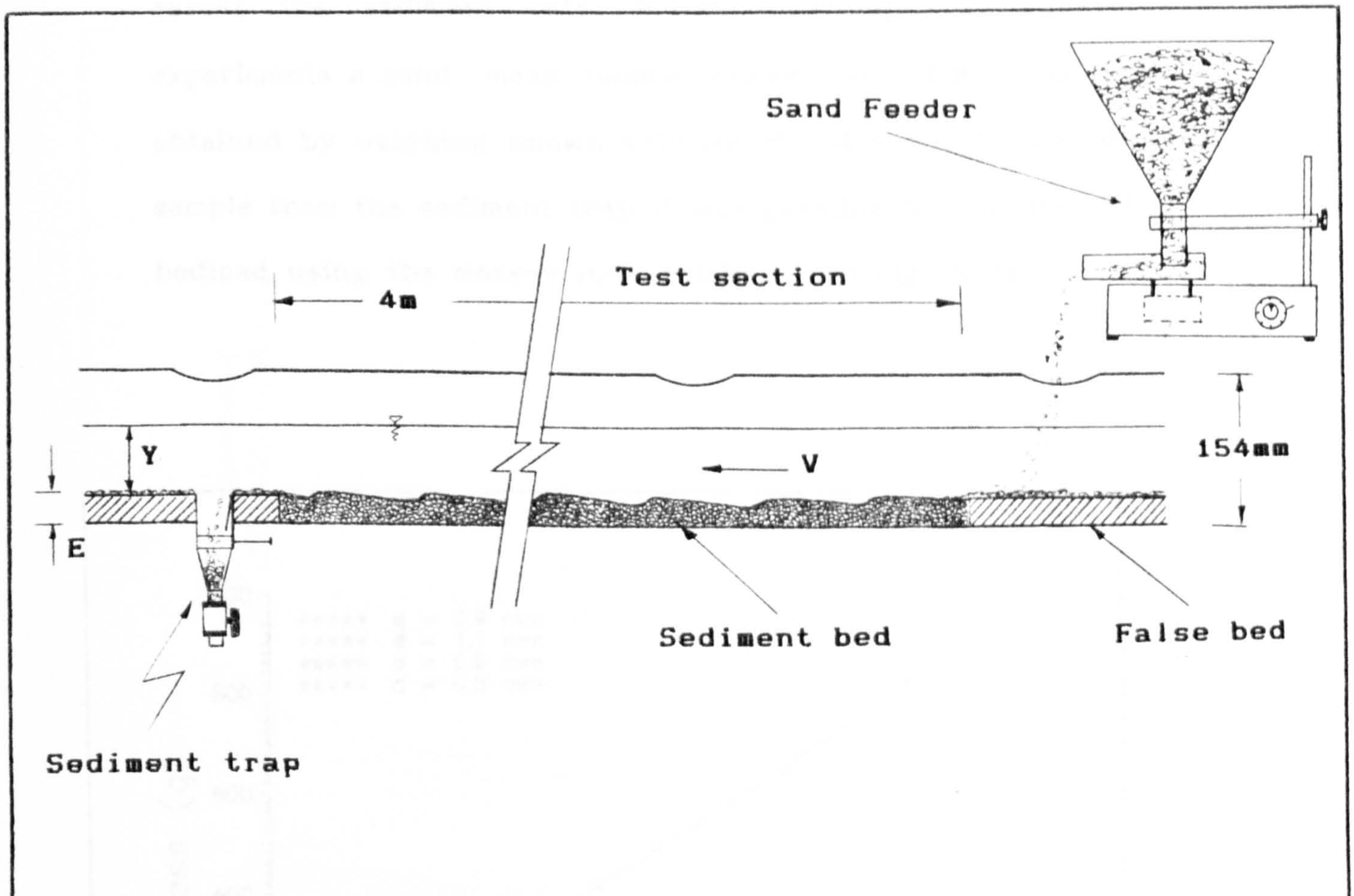

FIGURE 3.12: TRANSPORT EXPERIMENTS SET UP

Non-cohesive sediment (alluvial bed)
154 mm diameter flume

The procedure adopted to carry out the transport experiments over loose beds was:

1) The test section was filled up with a given sand and flattened in level with the false bed.

2) Uniform flow conditions (see Sec. 3.2) were set in the flume with a shear stress just over the threshold of motion.

3) The sediment feeder was started and adjusted to supply the estimated sediment rate.

4) The sediment trap was operated for a few minutes in order to assess the sediment rate. Before carrying out transport experiments a sand mass-volume curve (see Fig. 3.13) was obtained by weighing known volumes of wet sand. By taking a sample from the sediment trap if was possible to estimate the bedload using the mass-volume relation (see Fig. 3.13).

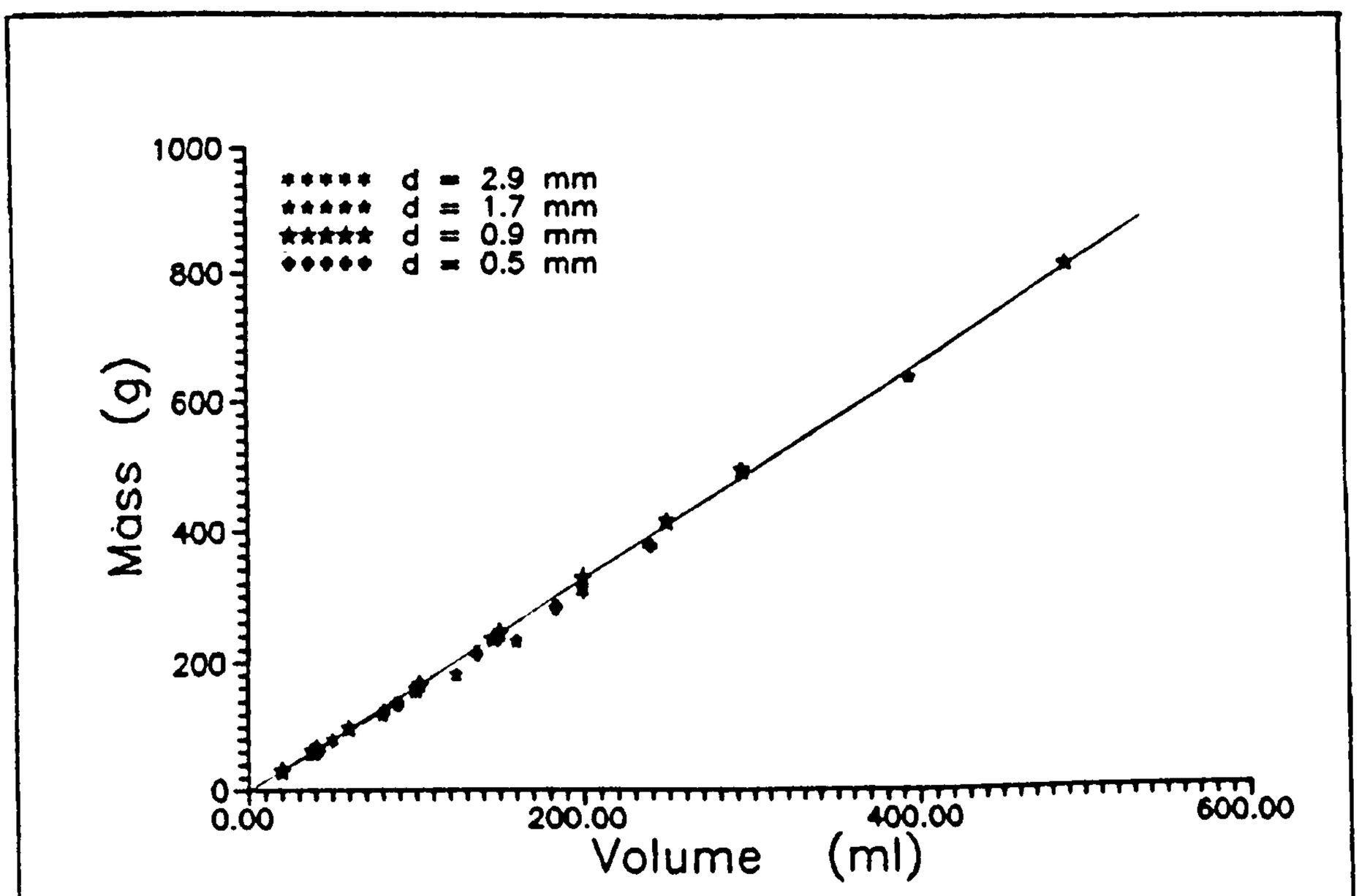

FIGURE 3.13: TYPICAL SAND MASS / VOLUME CURVE

Then the sand feeder was adjusted accordingly. This was repeated until the sediment rate reached equilibrium conditions (1/2 hour to 3 hours). The sediment feeding was constantly adjusted using the sediment trap information.

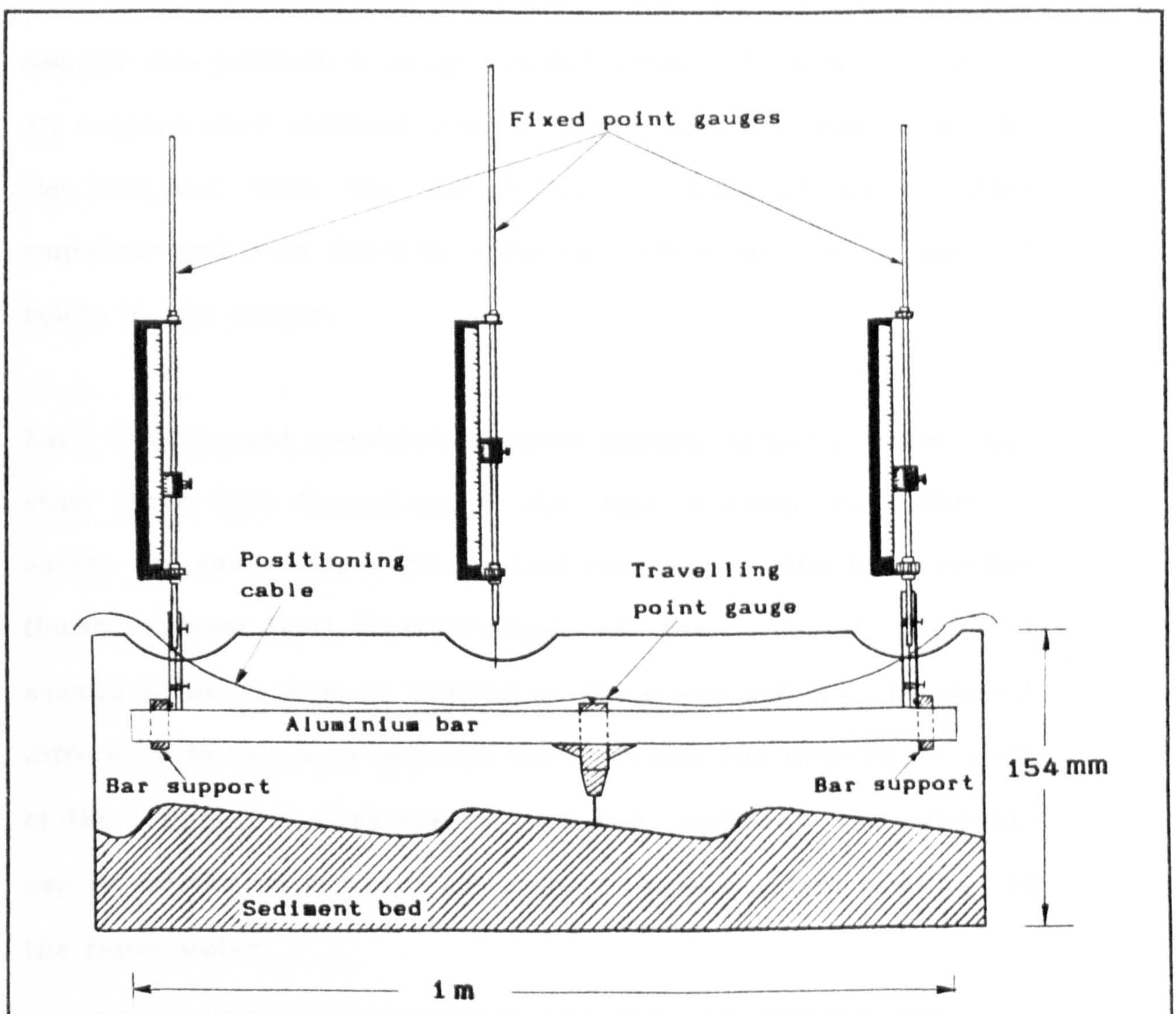

FIGURE 3.14: TRAVELLING POINT GAUGE FOR BEDFORMS MEASUREMENTS

5) After running for at least 30 minutes, the flow was gradually stopped (by closing the tail gate and the delivery valve) and the channel was slowly drained. Then using a travelling point gauge inside the pipe (see Fig. 3.14), bedforms were measured along the entire test section.

In order to measure suspended sediment a water sampler with a Pitot tube shape (see Fig. 3.15) was used. The volume of the sampler was calibrated using distilled water (9.904 ml at 20°C). All samples were obtained from a fixed position (3 mm from the flat bed) and then the sample was transferred to a glass container and oven dried in order to determine the weight of solids in the sample.

Each measurement consisted in three samples from upstream and other three from downstream of the test section, in order to assess the suspended sediment load coming from the test section (loose sediment bed). However, most of the sediment transport seemed to be in form of bedload as there was not any consistent difference in readings between the upstream and downstream ends of the test section. Therefore suspended sediment measurements can be attributed to the small sediment concentration existing in the flume water.

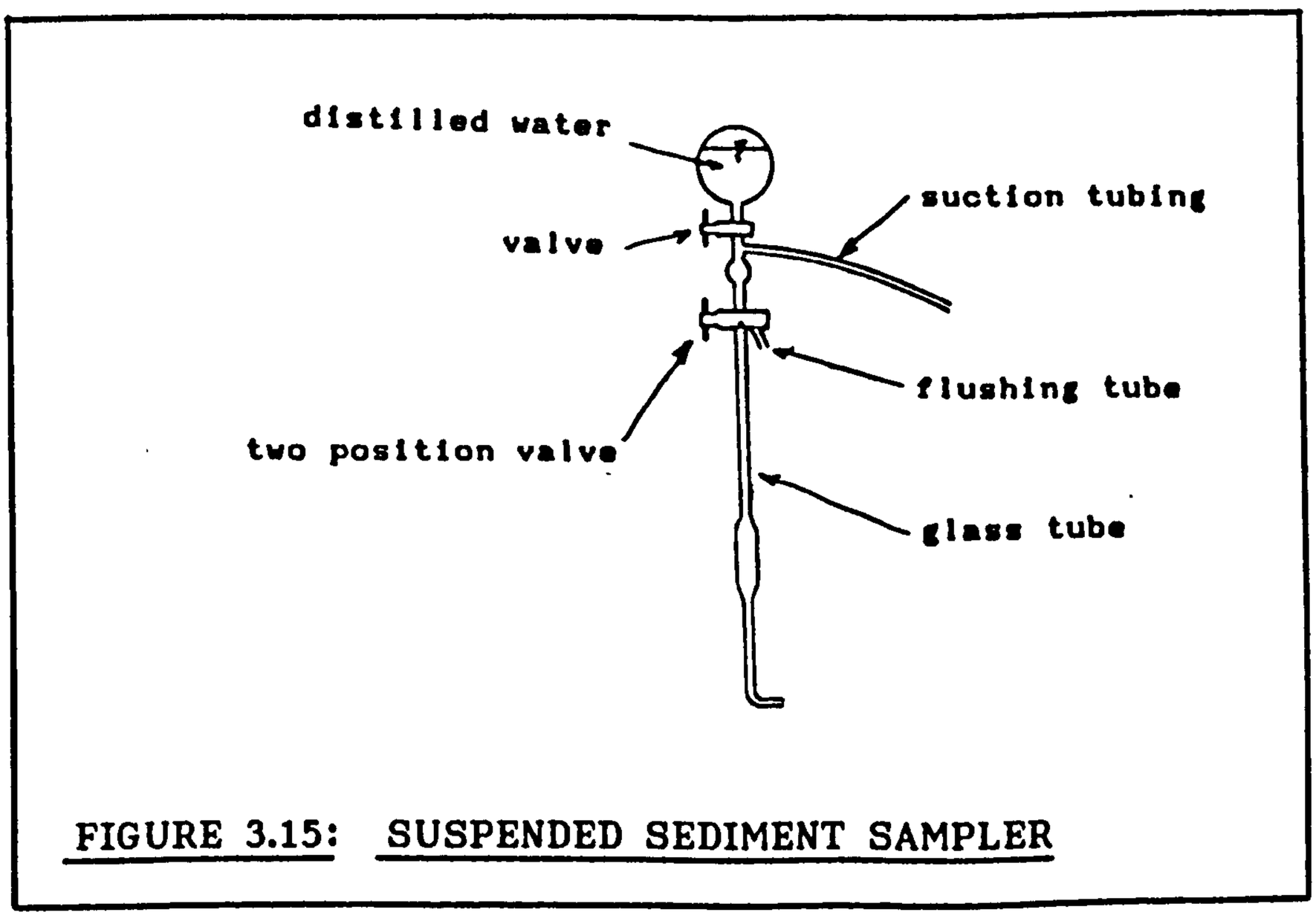

FIGURE 3.15: SUSPENDED SEDIMENT SAMPLER

In order to obtain a continuous reading of the suspended sediment concentration during the transport experiments an electro-optical turbidity meter (based on light attenuation principle) was also used. The monitor was previously calibrated using sand-water solutions of known concentration.

The probe consists of a light source (gallium-arsenide light emitting diode (LED)) and a sensor (phototransistor), both fitted with lenses and positioned side by side in a machined perspex holder. The probe is connected by a flexible lead to a control unit for signal integration and data logging operations. The instrument is based on pulsed light (Smith et al. 1980) thus eliminating the ambient light effects. The LED and the phototransistor both have a peak response in the near infrared light range of about 0.8 μm with narrow bandwidths. A 5 mm back silvered mirror is positioned at approximately 10 mm in front of the LED and sensor pair.

Suspended sediment loads were also detected on initiation of erosion experiments with cohesive sediments. The readings from the suspended sediment monitor showed a substantial increase during the rapid collapse of the bed.

3.6.1.2 Fixed Beds (Limit Deposition Conditions)

In this set of experiments the test section was covered with a uPVC layer (smooth surface) in level with the rest of the false bed. Because of the limited time available only one sediment thickness (E = 40.8 mm) was used.

a) Smooth Beds

The procedure adopted in the tests was to keep a given uniform flow in the flume and then increase the rate of sediment supply (sediment feeder) in steps, until sand particles begin to form deposits on the false bed. Then the sediment supply was slightly decreased and left running for a while (10 to 15 minutes). If no deposition was observed then the flow condition was taken to be at the limit of deposition. Only three sand sizes were tested (0.9, 2.0 and 5.7 mm) in this flume configuration.

b) Rough Bed

The entire false bed was artificially roughened with the appropriate uniform sand (0.9 mm) using double sided adhesive tape. Similar experiments as described above (Sec. 3.6.1.2 a) were carried out. Only one sand size (0.9 mm) was tested under this flume configuration.

3.6.2 Cohesive Sediments

3.6.2.1 Cohesive Sediment Bed

The test section (as in Sec. 3.6.1.1) was filled with the synthetic sewer sediment (prepared as described in Sec. 3.5.2.2.1 b). A few transport experiments with cohesive sediment beds were attempted in the 154 mm diameter flume.

A special sediment feeder was devised for using in transport experiments with cohesive sediment (see Fig. 3.16). This apparatus consisted of a steel cylinder, a piston, a slicer and a vibrator (rotating cam). The rate of sediment was controlled jointly by the displacement rate of the piston and by the energy of the vibration. The latter was needed to overcome the friction forces between the cylinder walls and the cohesive sediment. For a given sediment rate the more cohesive the sediment (i.e., higher clay concentrations) the higher vibration frequency was required to avoid stoppage.

Once the cohesive sediment bed was in place a procedure similar to that described in a previous section (Sec. 3.6.1.1) for transport over loose beds was adopted. However, very small bedloads were measured before critical conditions were reached. As soon as the critical conditions were exceeded the erosion rates increased very rapidly with the appearance of the first spots of erosion. Next a violent collapse and destruction of the entire sediment bed followed. There was no time to measure

sediment rates as the phenomenon took place very rapidly and sediment bed was washed away very quickly.

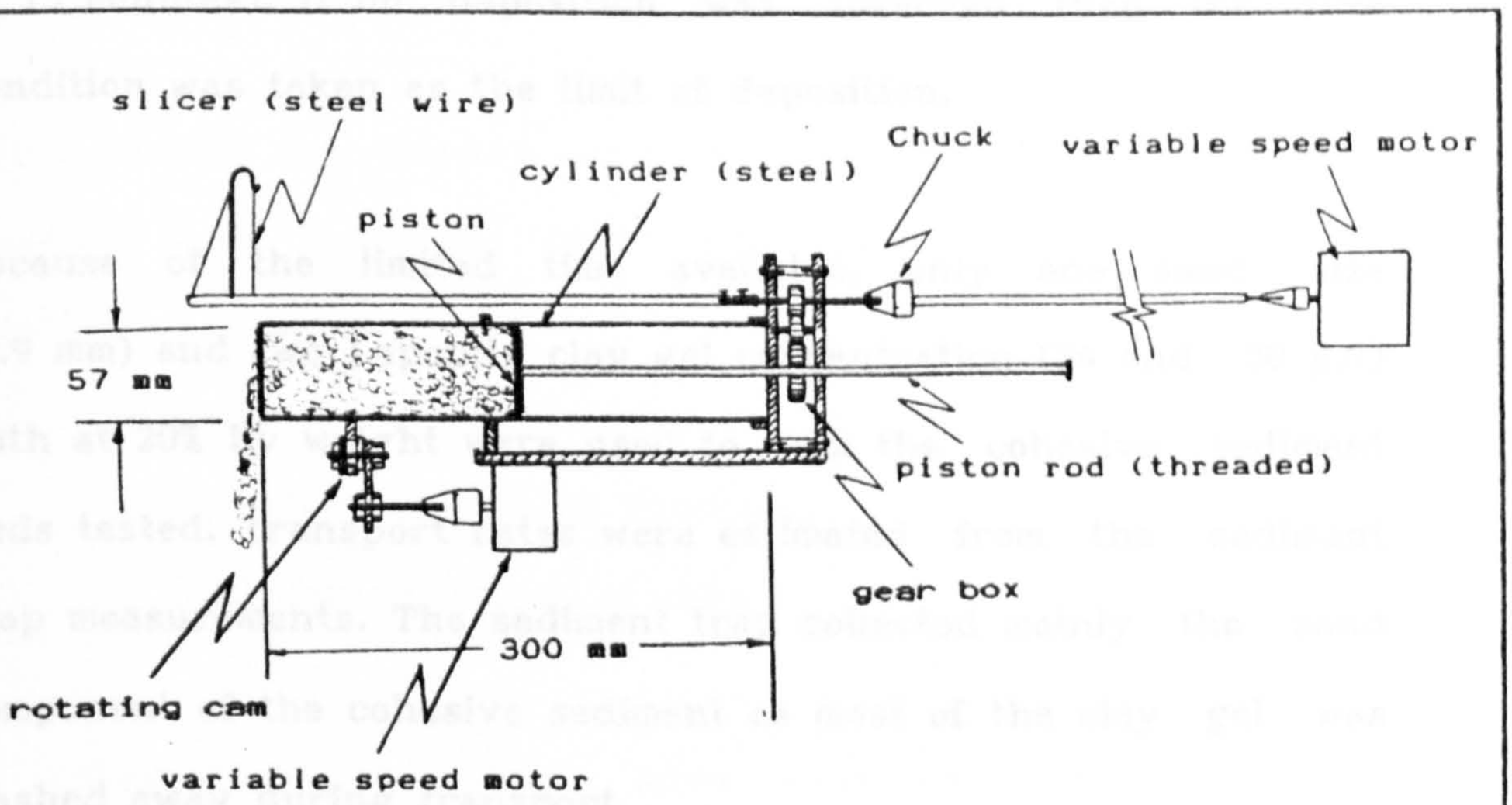

FIGURE 3.16: COHESIVE SEDIMENT FEEDER

Therefore it was not possible to establish equilibrium conditions of sediment transport over cohesive sediment beds. It was then decided to carry out the transport experiments with cohesive sediments over fixed beds only, using the limit deposition criterion.

3.6.2.2 Fixed Bed (smooth)

The procedure adopted in the tests (similar to that described in Sec. 3.6.1.2 a) was to maintain a given uniform flow in the flume

and increase the rate of sediment supply (cohesive sediment feeder, see Fig. 3.16) in steps, until sand particles begin to form deposits on the false bed. Then the sediment supply was slightly decreased and the flow was left running for a while (10 to 15 minutes). If no deposition was observed then the flow condition was taken as the limit of deposition.

Because of the limited time available, only one sand size (0.9 mm) and two Laponite clay gel concentration (24 and 30 g/l) both at 20% by weight were used to form the cohesive sediment beds tested. Transport rates were estimated from the sediment trap measurements. The sediment trap collected mainly the sand component of the cohesive sediment as most of the clay gel was washed away during transport.

4.2 HYDRAULIC CHARACTERISTICS

Experiments for determination of hydraulic characteristics of the flow were carried out in both the channels. As the configurations of the flumes changed with bed thickness and sediment size, it was necessary to study the hydraulic characteristics of the various flow conditions.

4.2.1 Frictional Characteristics (no sediment bed)

4.2.1.1 Full Pipe Flow Condition

In this series of experiments the cross-section of the flume was kept circular (i.e., no sediment bed) and the flume was run under full pipe flow conditions (see Sec. 3.5.2.2b). The pressure gradient was obtained from the piezometer bank, with a maximum error in the computation of the pressure gradient of about 3.8 %.

Darcy's equation for head loss can be written in terms of the discharge Q as

$$\lambda = \frac{\pi^2 \, g \, D^5 \, S_f}{8 \, Q^2} \qquad (4.1)$$

where D is the internal diameter of the pipe, S_f the pressure gradient, g the gravitational acceleration and λ the friction coefficient.

Colebrook-White equation for turbulent flow (transition zone) is:

$$\frac{1}{\sqrt{\lambda}} = -2 \log\left(\frac{k_s}{3.7 \, D} + \frac{2.51}{Re \sqrt{\lambda}} \right) \qquad (4.2)$$

where Re is Reynolds' number of the flow ($Re=\frac{V\ D}{\nu}$), and k_s is Nikuradse's equivalent sand roughness. Re-arranging the terms Eq. 4.2 can be expressed in the form:

$$k_s = 3.7\ D \left(10^{-1/(2\sqrt{\lambda})} - \frac{2.51}{Re\sqrt{\lambda}}\right) \qquad (4.3)$$

Eq. 4.3 was employed to estimate Nikuradse's equivalent sand roughness of a given flow. A summary of the results of flow resistance experiments under full pipe flow conditions (no sediment bed), in the 154 mm diameter flume is shown in Table 4.1. Negative values of k_s come from small experimental error in the determination of pressure gradients

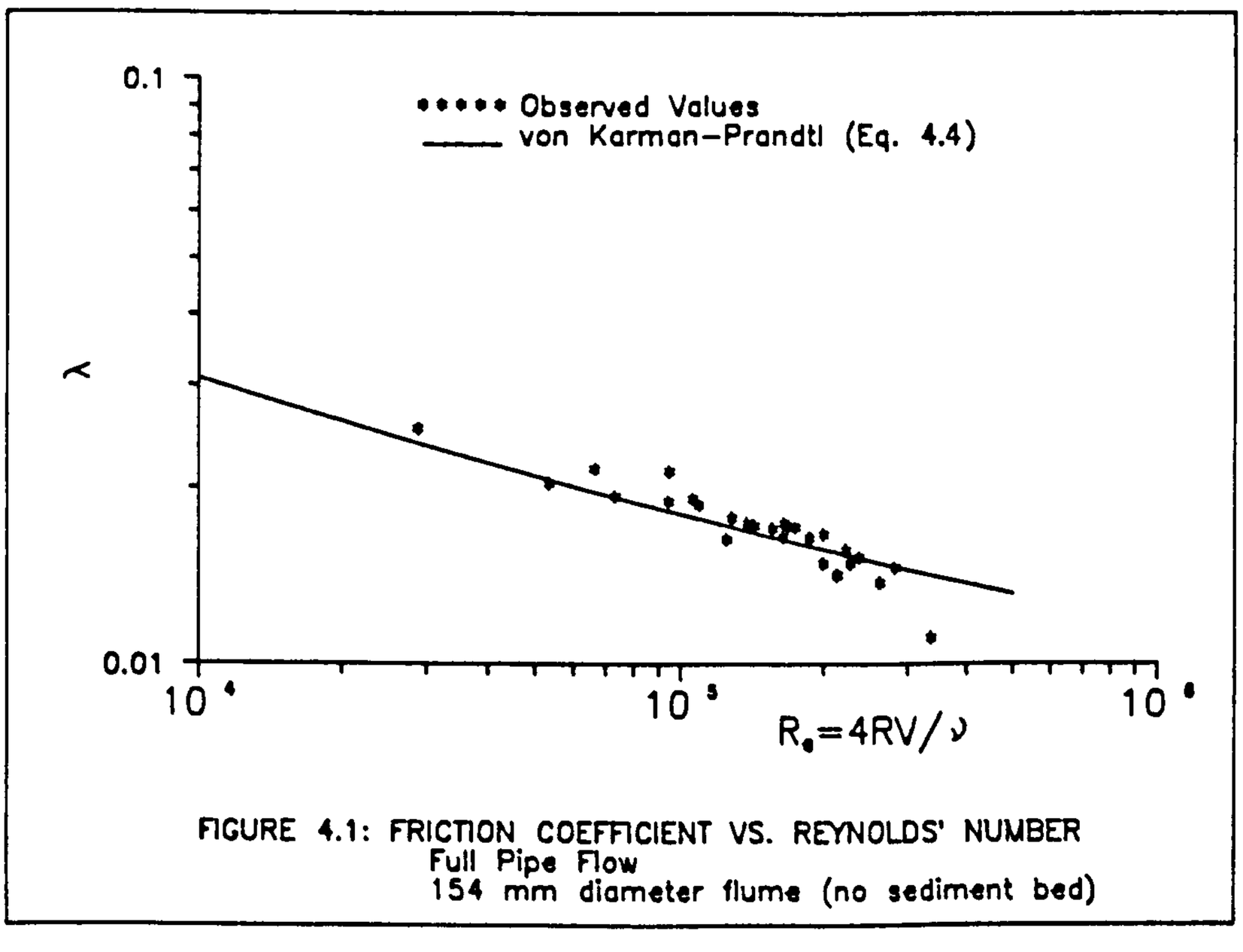

FIGURE 4.1: FRICTION COEFFICIENT VS. REYNOLDS' NUMBER
Full Pipe Flow
154 mm diameter flume (no sediment bed)

It was possible to estimate an average value for Nikuradse's equivalent sand roughness as 0.009 mm suggesting the pipe to be smooth. However, for Re ≥ 200,000 the situation is not very clear.

Nevertheless, in the sediment movement experiments the values of Re where always below 200,000. Therefore the von Karman-Prandtl equation for smooth pipe,

$$\frac{1}{\sqrt{\lambda}} = -2 \log\left(\frac{2.51}{Re\sqrt{\lambda}}\right) \qquad (4.4)$$

was utilized to compare the experimental results. The variation of Darcy-Weisbach friction coefficient with Reynolds' number is shown in Fig. 4.1 together with Eq. 4.4. The observed values fall around von Karman-Prandtl's curve for smooth pipes suggesting the flume to be smooth.

4.2.1.2 Open Channel Flow Conditions

A series of flow resistance experiments were carried out in the flumes (with no sediment bed), under open channel flow conditions. In each run uniform flow conditions were established (see Sec. 3.2) Expressing the diameter D in terms of the hydraulic radius R (for circular pipes D = 4 R) Eq. 4.1 can be rewritten as,

$$\lambda = \frac{8\ g\ R\ S_f}{V^2} \qquad (4.5)$$

where R is the hydraulic radius, S_f is the energy gradient, V is the mean flow velocity and λ is Darcy-Weisbach's friction coefficient. The equivalent sand roughness (Eq. 4.3) then becomes:

$$k_s = 14.8\ R\left(10^{-1/(2\sqrt{\lambda})} - \frac{2.51}{Re\sqrt{\lambda}}\right) \qquad (4.6)$$

Equation 4.6 gives Nikuradse's equivalent sand roughness of a representative hypothetical circular pipe (running full) that has the same energy gradient at the same discharge, as the open channel flow in question.

These two equations (Eqs. 4.5 and 4.6) were employed in the computations of the results of the flow resistance experiments under open channel flow conditions (Table 4.2). Average values for Nikuradse's equivalent sand roughness were estimated as -0.024 mm for the 154 mm diameter flume and 0.038 mm for the 302 mm diameter flume.

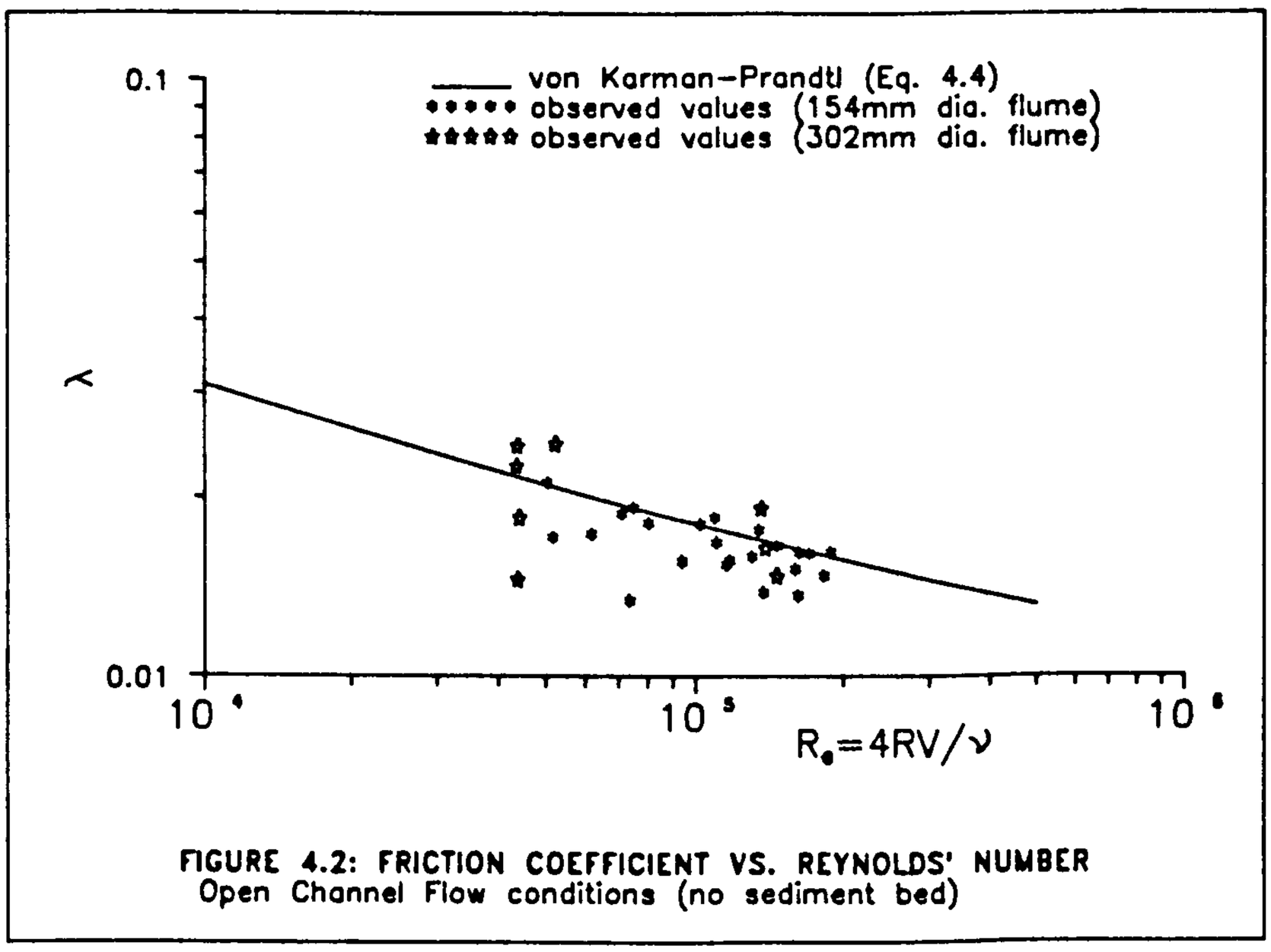

FIGURE 4.2: FRICTION COEFFICIENT VS. REYNOLDS' NUMBER
Open Channel Flow conditions (no sediment bed)

Figure 4.2 shows the variation of Darcy-Weisbach friction coefficient with Reynolds' number. The observed values fall around von Karman-Prandtl smooth pipe curve (Eq. 4.4) . However,

there is appreciable scatter as the substitution of D by 4R in Darcy's equation for head loss yields friction factors for the hypothetical equivalent pipe of circular cross-section.

From the same set of data average values for Manning's roughness coefficient, n, were estimated as 0.008 and 0.009 for the 154 mm and 302 mm diameter flumes respectively (see Fig. 4.3). These values correspond to a smooth boundary channel. The pieces of uPVC and perspex pipe making up the 302 mm diameter flume do not fit perfectly due to slight differences in their internal diameters. This explains why this flume shows higher roughness (k_s) and Manning's n values than the 154 mm diameter flume.

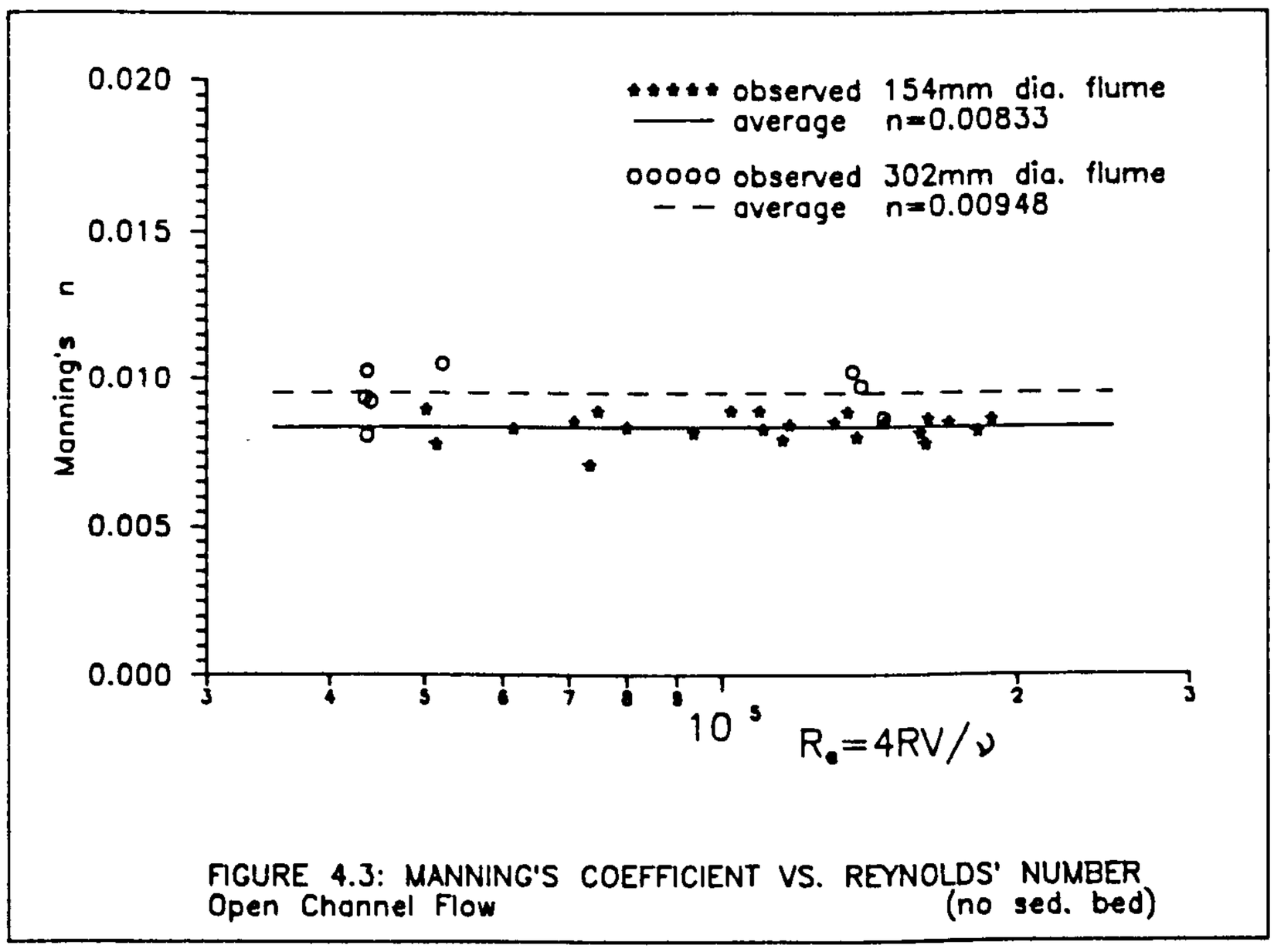

FIGURE 4.3: MANNING'S COEFFICIENT VS. REYNOLDS' NUMBER
Open Channel Flow (no sed. bed)

From the experimental results (full pipe and open channel flow conditions) it can be concluded that the flume walls are smooth.

This supports the assumption of smooth walls (see Fig. 4.4) made in the derivation of the equations (see Appendix I) utilized in Einstein-Vanoni wall separation technique (Vanoni-Brook, 1957). The cross-section is divided into two subsections, one corresponding to the rough bed and the other one to the smooth walls. As the velocity and headloss are assumed to be equal in both subsections, by applying von Karman-Prandtl equation for smooth boundary (Eq. 4.4) the friction coefficient for the wall can be found. Then by iteration the friction coefficient of the bed is obtained. The method is explained in Appendix I.

4.2.2 Frictional Characteristics (with flat sediment bed)

4.2.2.1 Full Pipe Flow Conditions

Friction experiments were carried out in the 154 mm diameter flume for each configuration (sediment bed thickness and bed roughness) under full pipe flow conditions using clear water. Nikuradse's equivalent sand roughnesses and friction coefficients were determined.

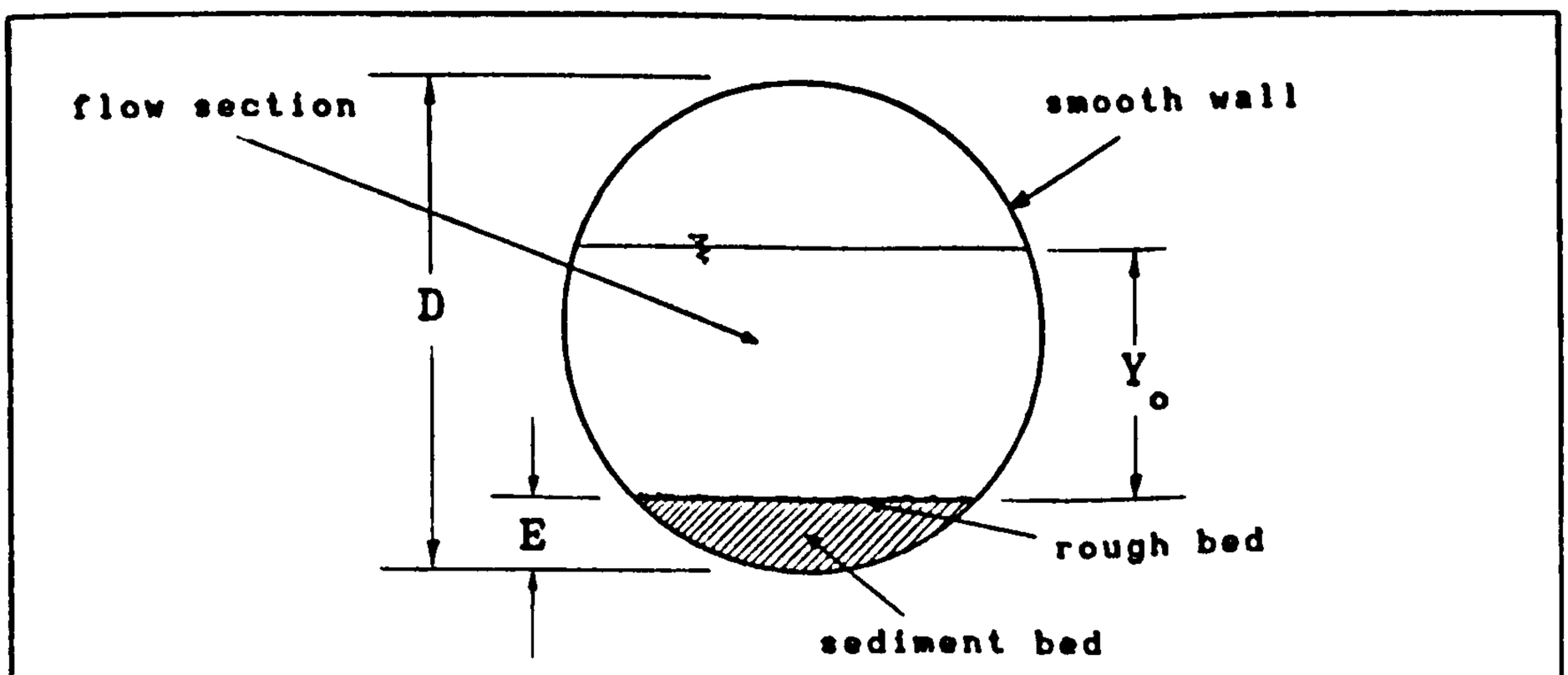

FIGURE 4.4: CHANNEL CROSS-SECTION WITH SEDIMENT BED

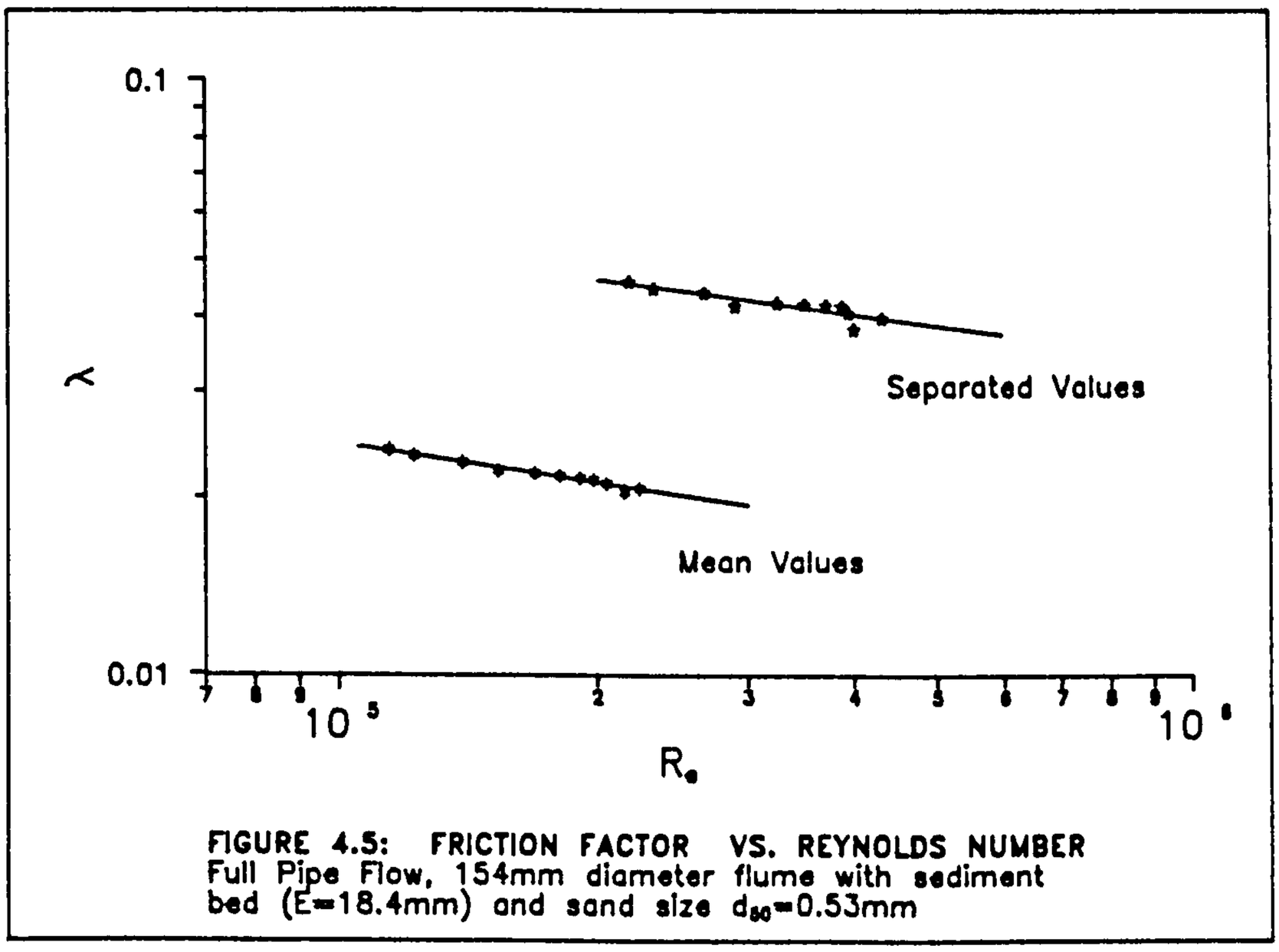

FIGURE 4.5: FRICTION FACTOR VS. REYNOLDS NUMBER
Full Pipe Flow, 154mm diameter flume with sediment bed (E=18.4mm) and sand size d_{50}=0.53mm

A typical plot of mean and bed friction coefficient against Reynolds' number can be seen in Fig. 4.5. The curve representing the overall values is more or less parallel to the curve representing the separated bed values. This occurs because the hydraulic radius remains constant (full pipe flow conditions).

4.2.2.2 Open Channel Flow Conditions

Results from friction experiments under open channel flow conditions are summarised in Tables 4.4 & 4.5 for the 154 mm and the 302 mm diameter flumes respectively. The experiments were carried out with clear water for various flume bed configurations (see Fig. 4.4).

As Reynolds number increases, curves of mean and separated values of friction coefficient seem to diverge (see Fig. 4.6), due to an

increase in water depth with increasing Reynolds number. Each flume has smooth walls and fixed rough bed that causes the overall friction coefficient to decrease as the water depth increases. Thus a larger difference between bed and overall friction coefficients (see Fig. 4.7a) is observed for high values of Reynolds number, R_e and relative depth, $(Y_o+E)/D$.

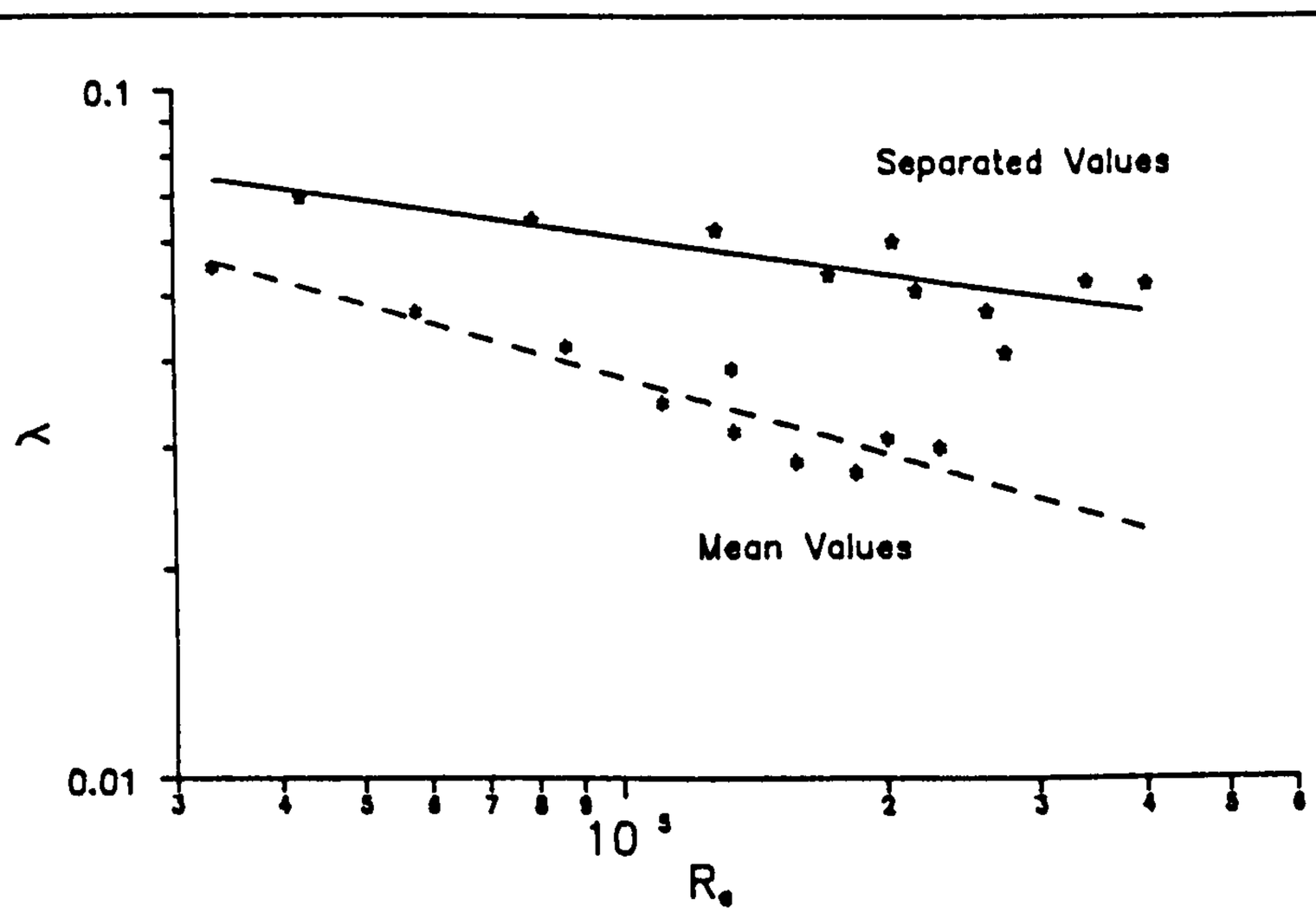

FIGURE 4.6: FRICTION COEFFICIENT VS. REYNOLDS NUMBER
Open Channel Flow, 302mm diameter flume with sediment bed (E=47.6mm) and sand size d_{50}=1.6mm

Whereas several bed thicknesses were implemented in the 154 mm diameter flume for the various sets of experiments, only one bed thickness was used in the 302 mm diameter flume. The main experimental work was carried out in the 154 mm diameter flume.

The ratio between separated and overall friction coefficient for open channel flow conditions, seems to be dependent on water depth ratio $(Y_o+E)/D$ (see Fig. 4.7a), and bed roughness as it is

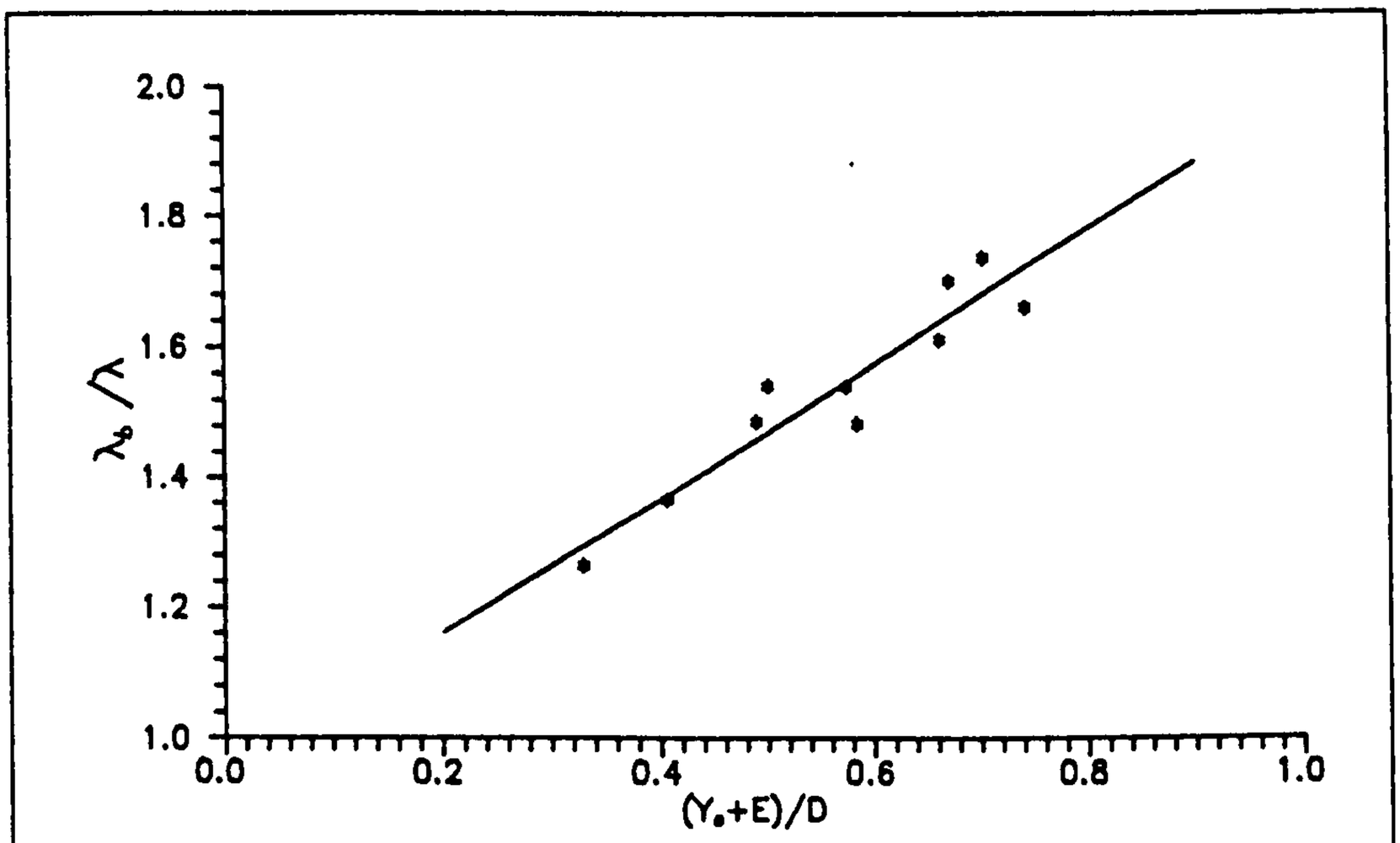

FIGURE 4.7a: RELATIVE FRICTION FACTOR VS. RELATIVE DEPTH
Open channel flow in 302mm diameter flume with sediment bed (E=47.6mm) and sand size d_{50}=1.6mm

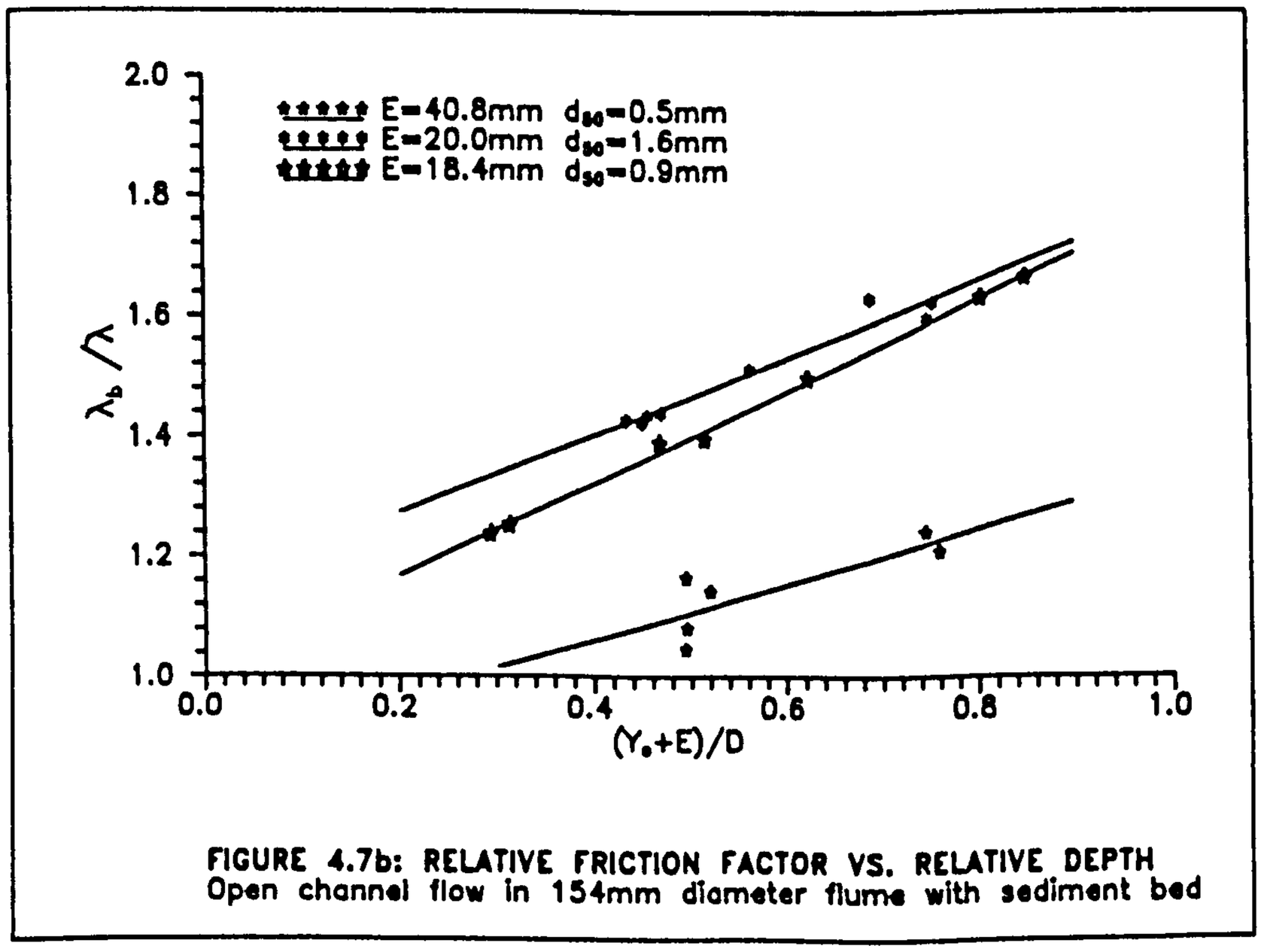

FIGURE 4.7b: RELATIVE FRICTION FACTOR VS. RELATIVE DEPTH
Open channel flow in 154mm diameter flume with sediment bed

shown in Fig. 4.7b for the 154 mm diameter, for which several bed thicknesses were tested. It is apparent that the larger ratios occur for full pipe flow conditions where they can easily exceed the value of 2 (see Table 4.3 for sand bed 1.6 mm and bed thickness 20 mm).

4.2.3 Velocity and Shear Stress Distributions

The shape of the channel flow-section varies considerably with sediment bed thickness and flow depth (see Fig. 4.4), and the velocity and shear stress distributions are influenced by the associated shape effects. Therefore, an attempt was made to measure these distributions in one of the flumes. To estimate shear stresses the universal velocity distribution law (see Sec. 3.3.2.1-Eq.3.11) was employed. Detailed velocity profiles were measured using a combination of Pitot tube, propeller current meter and a Laser Doppler Velocimeter (LDV).

The computation of a typical shear stress distribution is shown in Table 4.6 and Figs. 4.8 and 4.9. For each velocity profile in the cross-section, the local shear stress is computed as explained in Section 3.3.1.1. In Figures 4.11 a and b the corresponding shear stress distribution and the velocity contours are shown. This is a case of an open channel flow, which is more or less two dimensional in spite of small secondary currents (see Figs. 4.11 a) observed at the sides of the section near the free surface. The shear stress has a maximum at the centreline (see Figs. 4.11 b) of the section and decreases towards the sides.

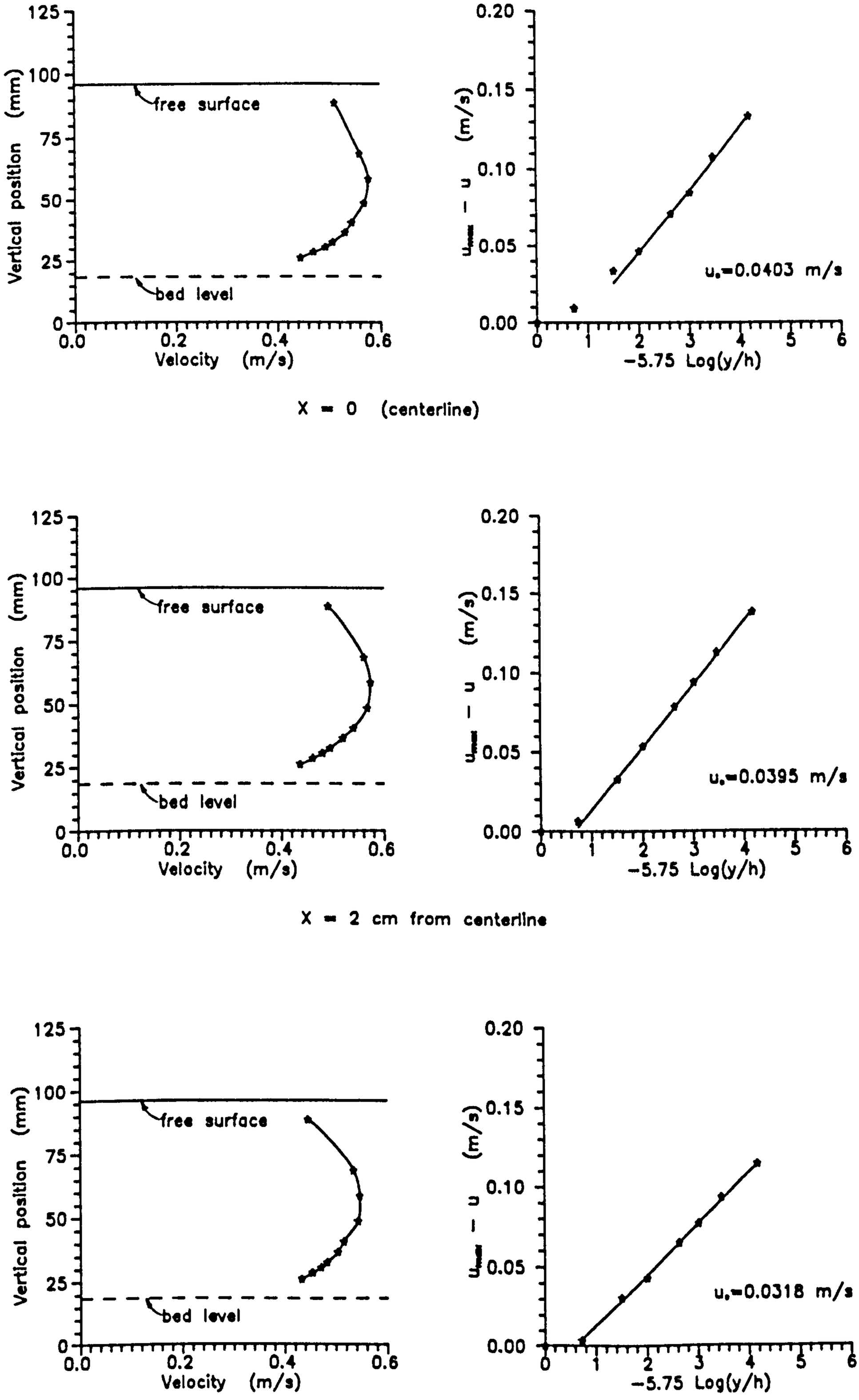

FIGURE 4.8: TYPICAL VELOCITY DISTRIBUTION CURVES
Open channel flow in the 154mm diameter flume

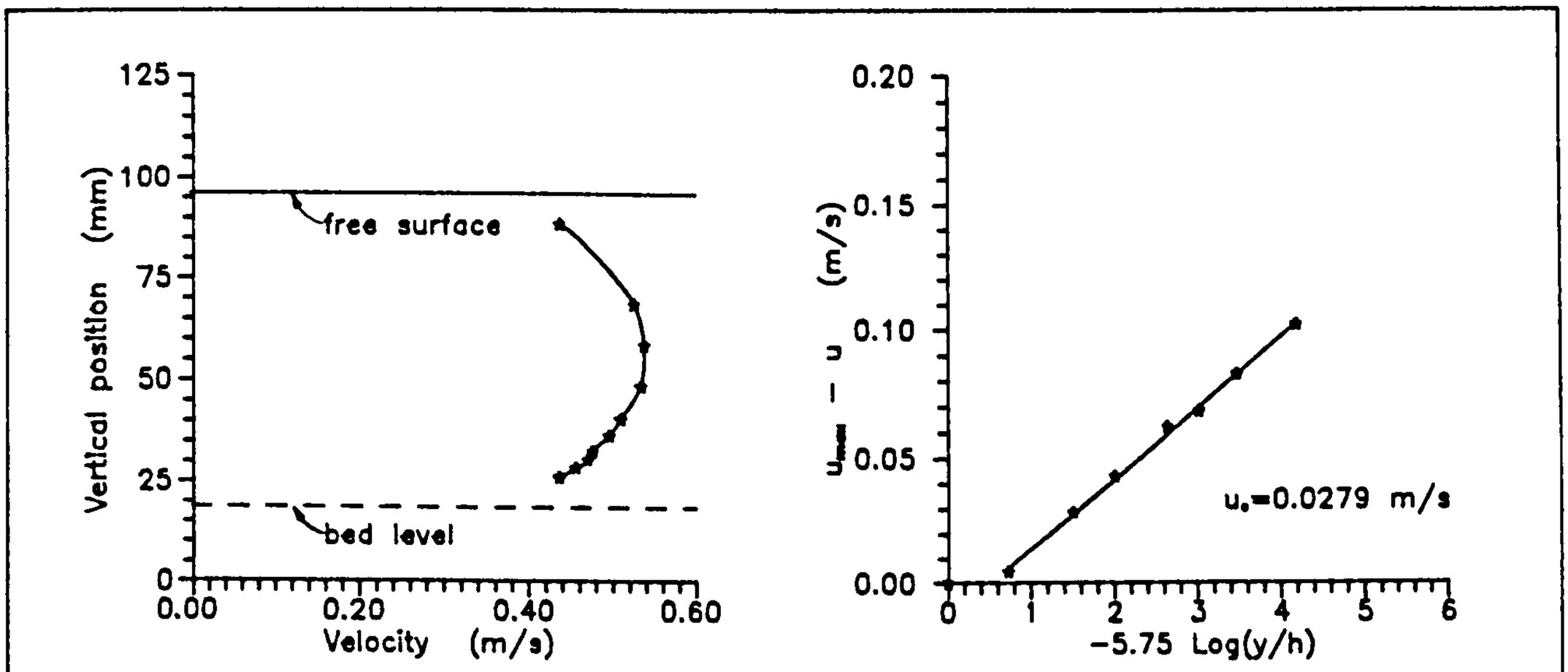

FIGURE 4.9: TYPICAL VELOCITY DISTRIBUTION CURVES
Open channel flow in the 154mm diameter flume

A large number of velocity profiles was measured under both full pipe and open channel flow conditions. A summary of the results is shown in Tables 4.7 and 4.8 for full pipe and open channel flow conditions respectively. However, only four typical cases of velocity and shear stress distributions are plotted in Figs. 4.10 to 4.13 covering the range from narrow depth uniform flow up to full pipe (pressurised) flow. For more details on the shear stress distribution measurements see Appendix D).

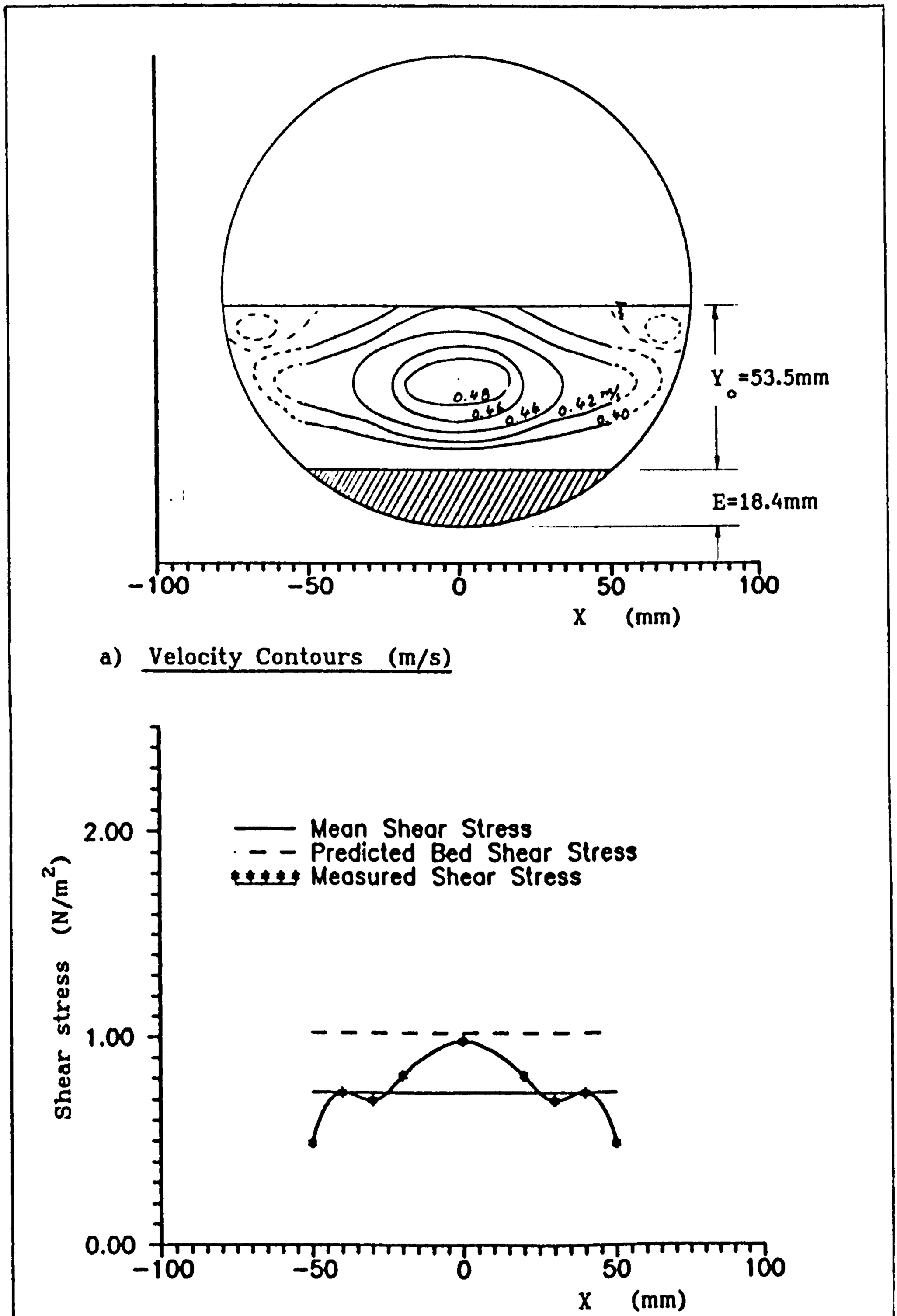

FIGURE 4.10: SHEAR AND VELOCITY DISTRIBUTION CURVES
154mm diameter flume (E=18.4mm) Y_o=53.5mm $(Y_o+E)/D$=0.47
Y_o/D=0.35 Q=3.10 l/s S_o=0.00229 sand size d_{50}= 0.53mm

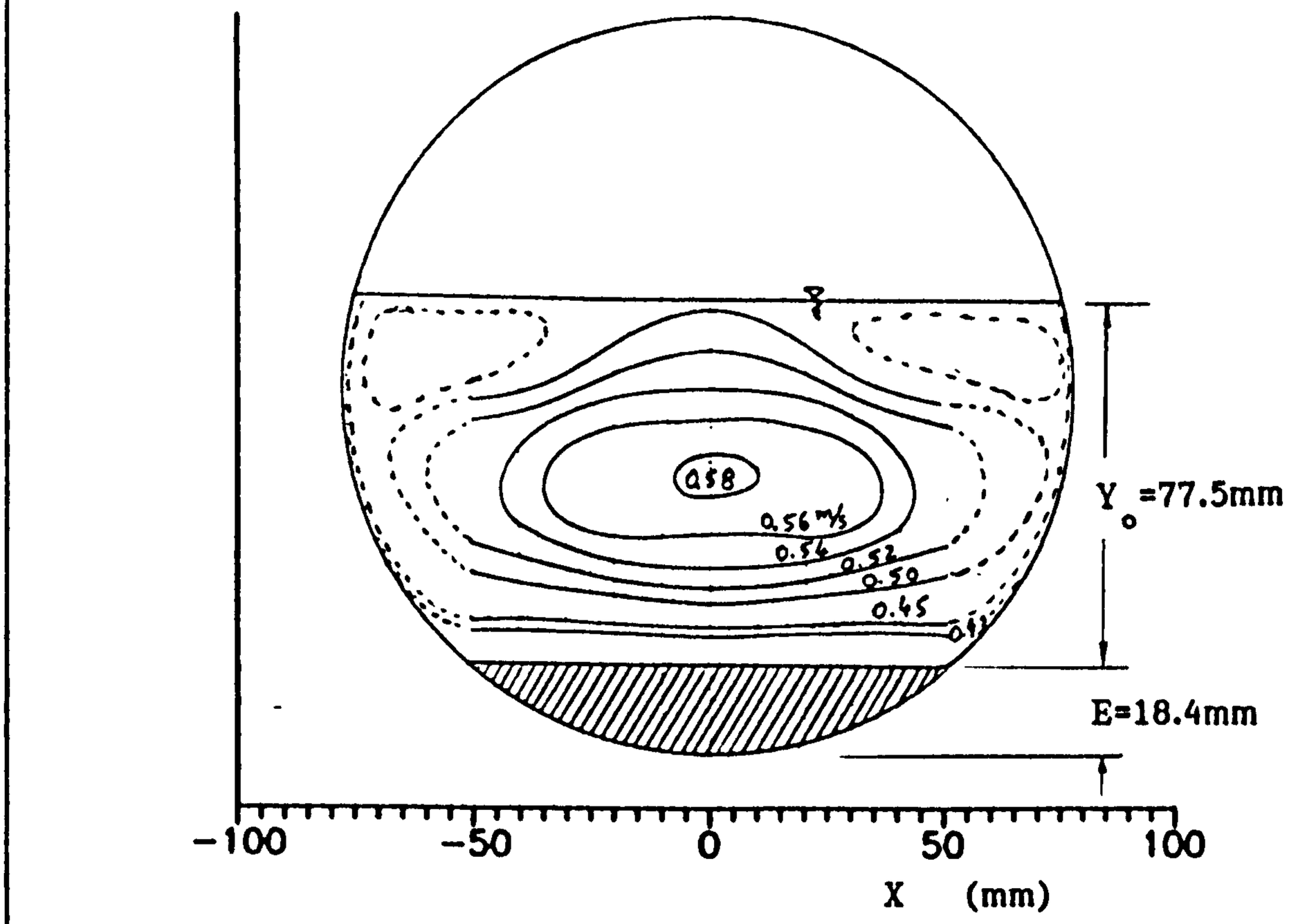

a) Velocity Contours

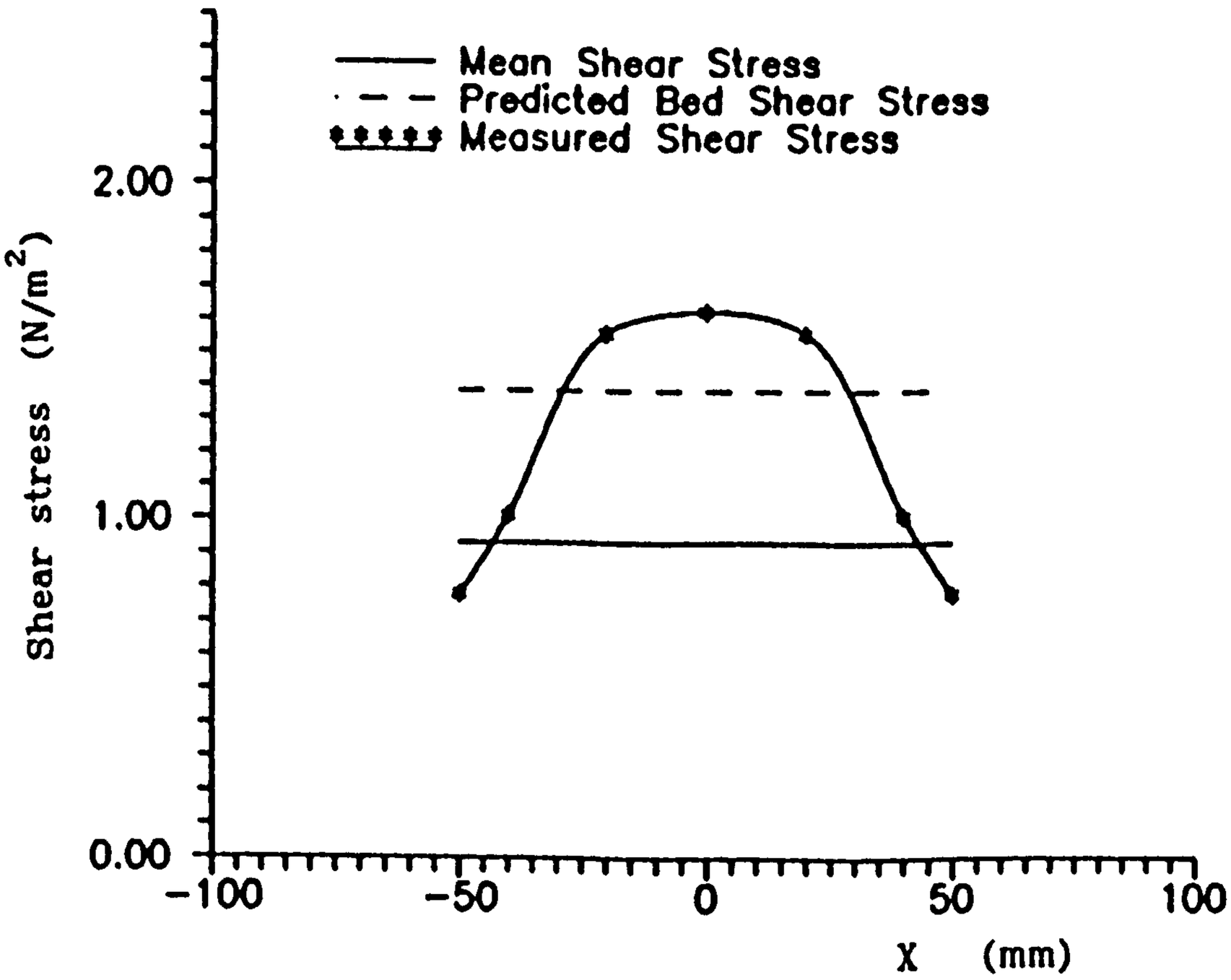

b) Bed Shear Stress Distribution

FIGURE 4.11: SHEAR AND VELOCITY DISTRIBUTION CURVES

154mm diameter flume (E=18.4mm) Y_o=77.5mm $(Y_o+E)/D$=0.62
Y_o/D=0.5 Q=5.59 l/s S_o=0.00235 sand size d_{50}= 0.53mm

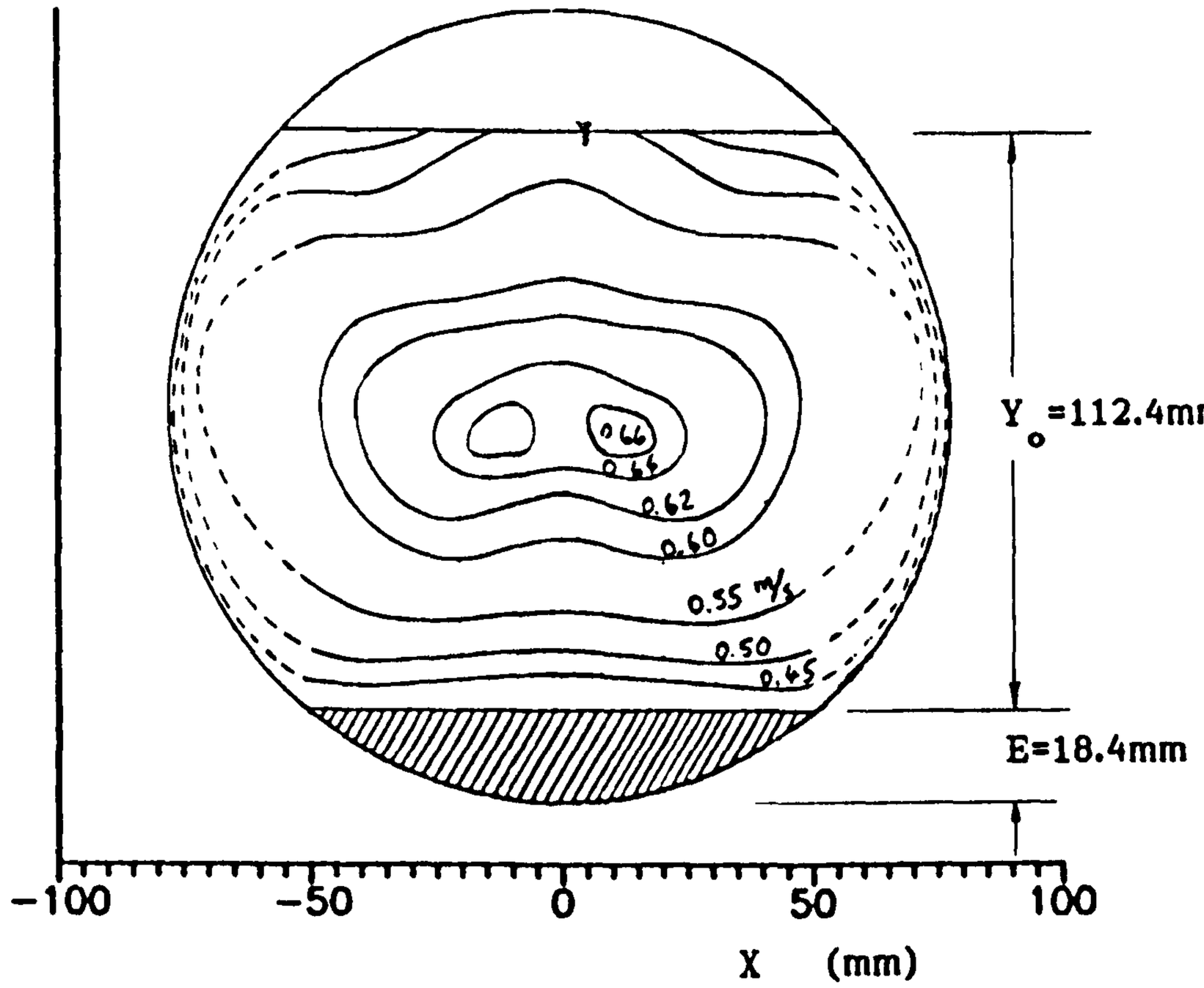

a) Velocity Contours (m/s)

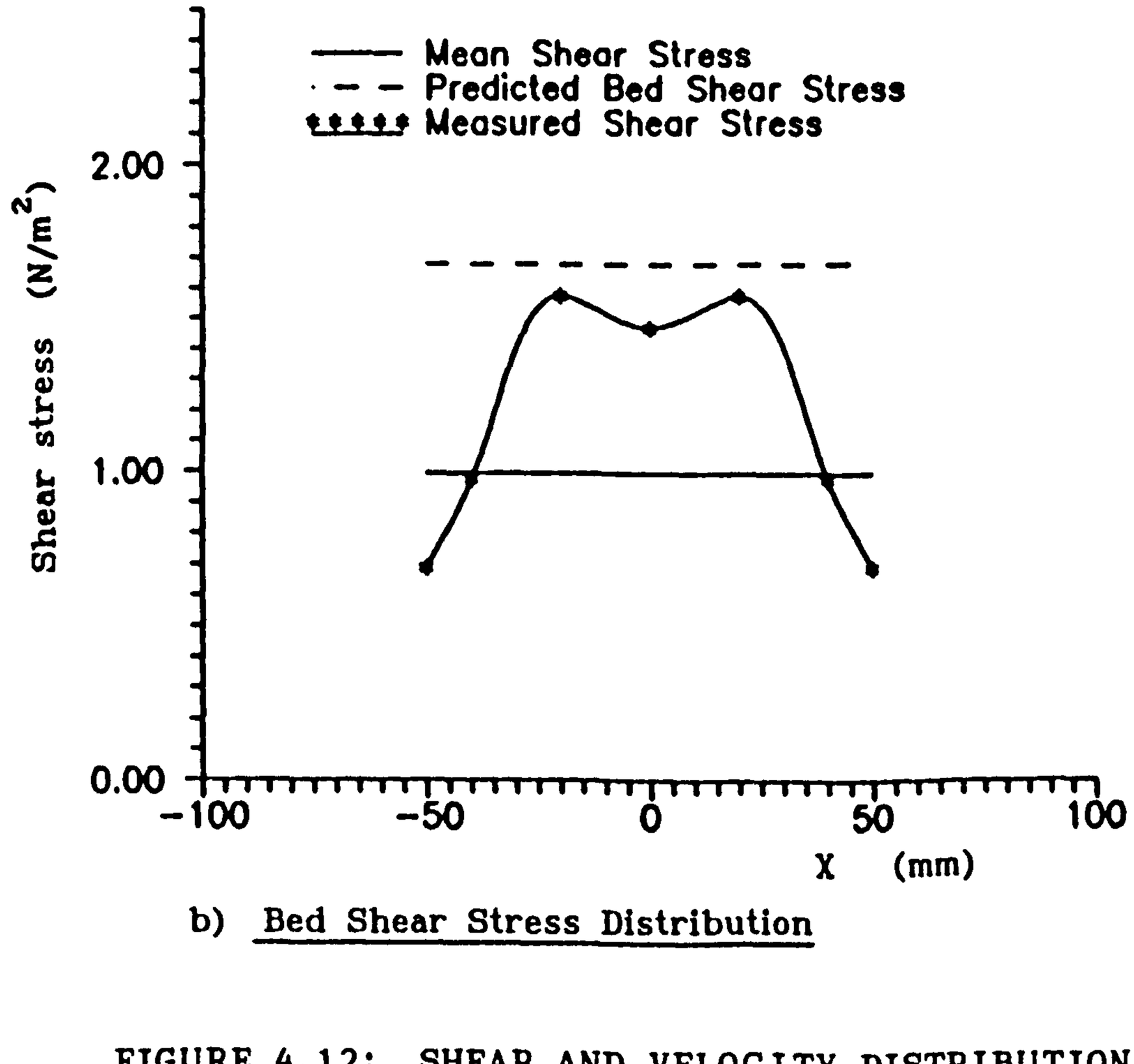

b) Bed Shear Stress Distribution

FIGURE 4.12: SHEAR AND VELOCITY DISTRIBUTION CURVES

154mm diameter flume (E=18.4mm) Y_o=112.4mm $(Y_o+E)/D$=0.85
Y_o/D=0.73 Q=8.62 l/s S_o=0.002278 sand size d_{so}= 0.53mm

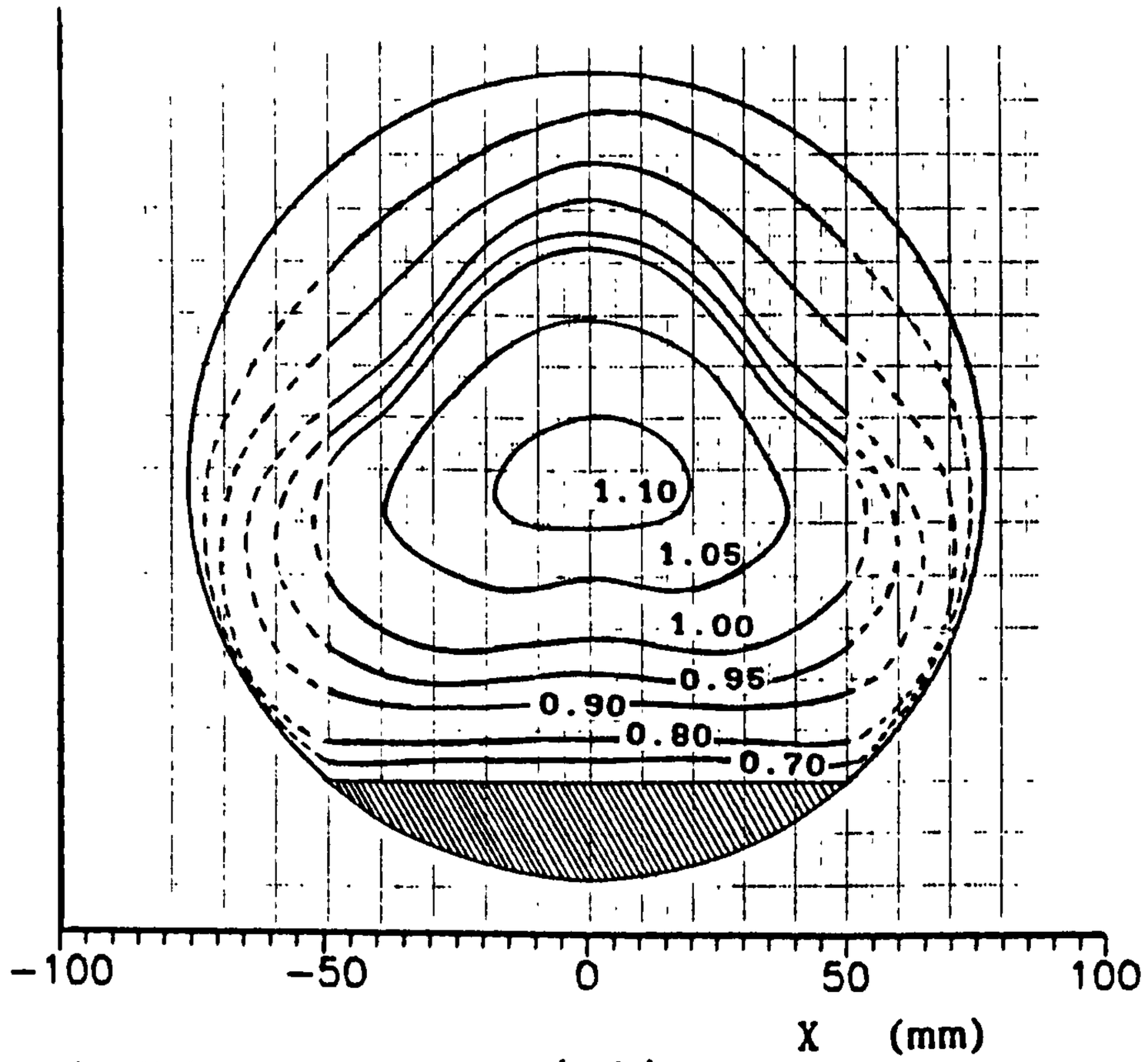

a) Velocity Contours (m/s)

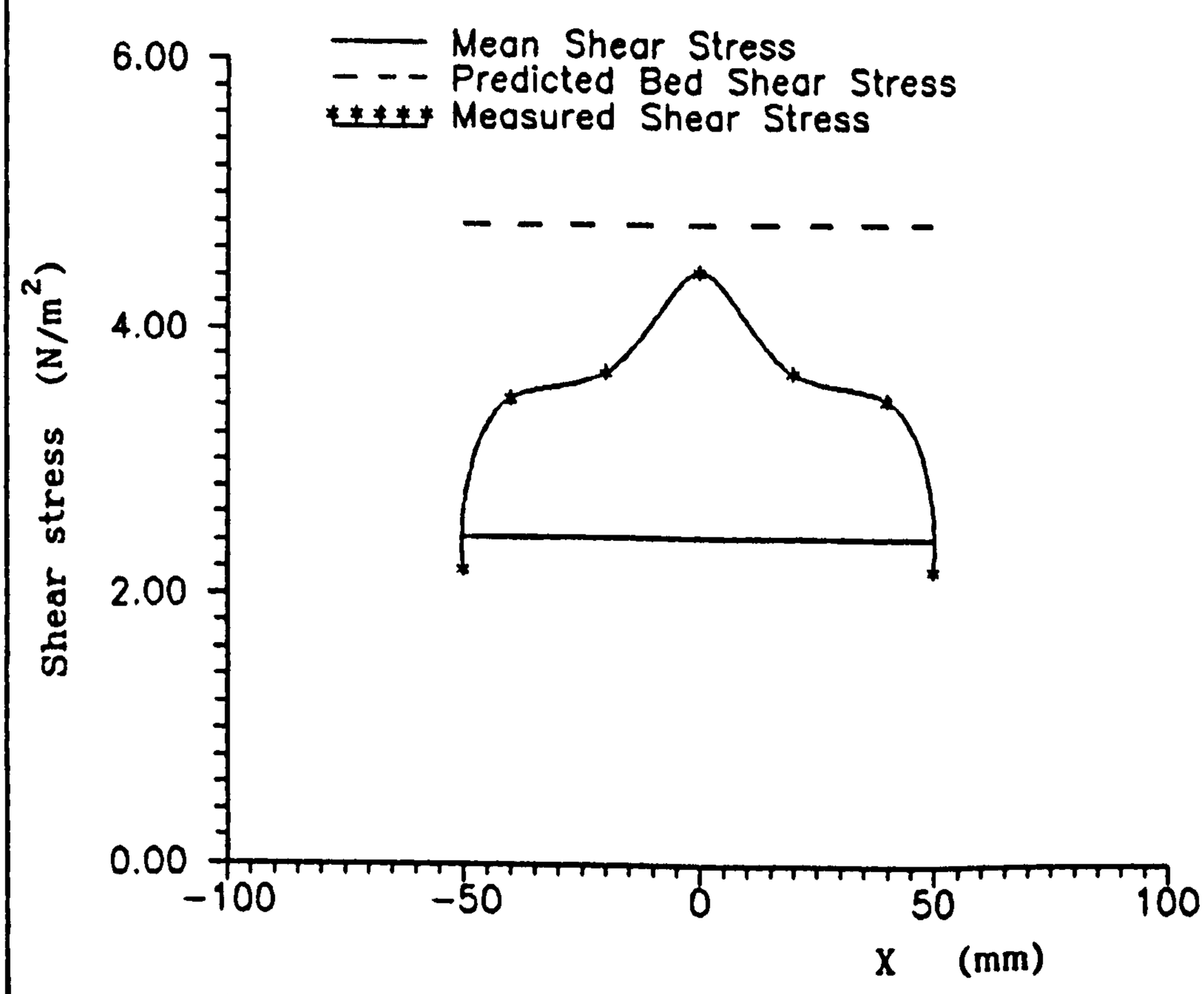

b) Bed Shear Stress Distribution

FIGURE 4.13: SHEAR AND VELOCITY DISTRIBUTION CURVES
154mm diameter flume (E = 18.4mm) Full Pipe Flow
$(Y_o+E)/D = 1$ Q = 15.84 l/s S_f = 0.006754 (smooth bed)

4.2.3.1 Velocity Distribution

The isovels for three cases of flow depth i.e., $(Y_o+E)/D$ between 0.47 and 0.85 (see Figs. 4.10a, 4.11a and 4.12a) confirm the existence of shape effects in the flumes described above. The velocity distribution is two-dimensional for low depths ($(Y_o+E)/D < 0.47$). When the ratio $(Y_o+E)/D$ is greater than 0.62 the flow shows three dimensional characteristics. Experiments with $(Y_o+E)/D = 1$ (pressurised flow) indicate that the velocity distribution reverts to two dimensional flow (see Fig. 4.13).

4.2.3.2 Shear Distributions

The bed shear stress distributions, no doubt, exhibit the influence of shape effects of the channel (see Figs. 4.10 to 4.15). In the case of the open channel flow condition $(Y_o+E)/D=0.62$ (see Fig. 4.11b), the maximum shear stress is located at the centre line of the channel. However, the existence of small secondary currents is suggested by the shape of the velocity contours (see Fig. 4.11a). A similar phenomena can be observed in Fig. 4.10 ($(Y_o+E)/D=0.47$), where the maximum shear stress is located at the centre line of the flume. Deeper flows ($(Y_o+E)/D > 0.62$) show the existence of important secondary currents, which are apparent in Figs. 4.12a and 4.12b where two peaks of shear stress can be seen at both sides of the section.

Bed shear stress distributions for various flow depths and one sediment bed thickness (E=18.4mm) are shown in Fig. 4.14. One maximum peak on the centre line with two secondary peaks on the

sides are observed for $(Y_o+E)/D \leq 0.47$, whereas two main peaks at each side of the centreline are observed for $1 > (Y_o+E)/D > 0.62$, these two peaks reflect the effects of secondary currents near the sides of the section.

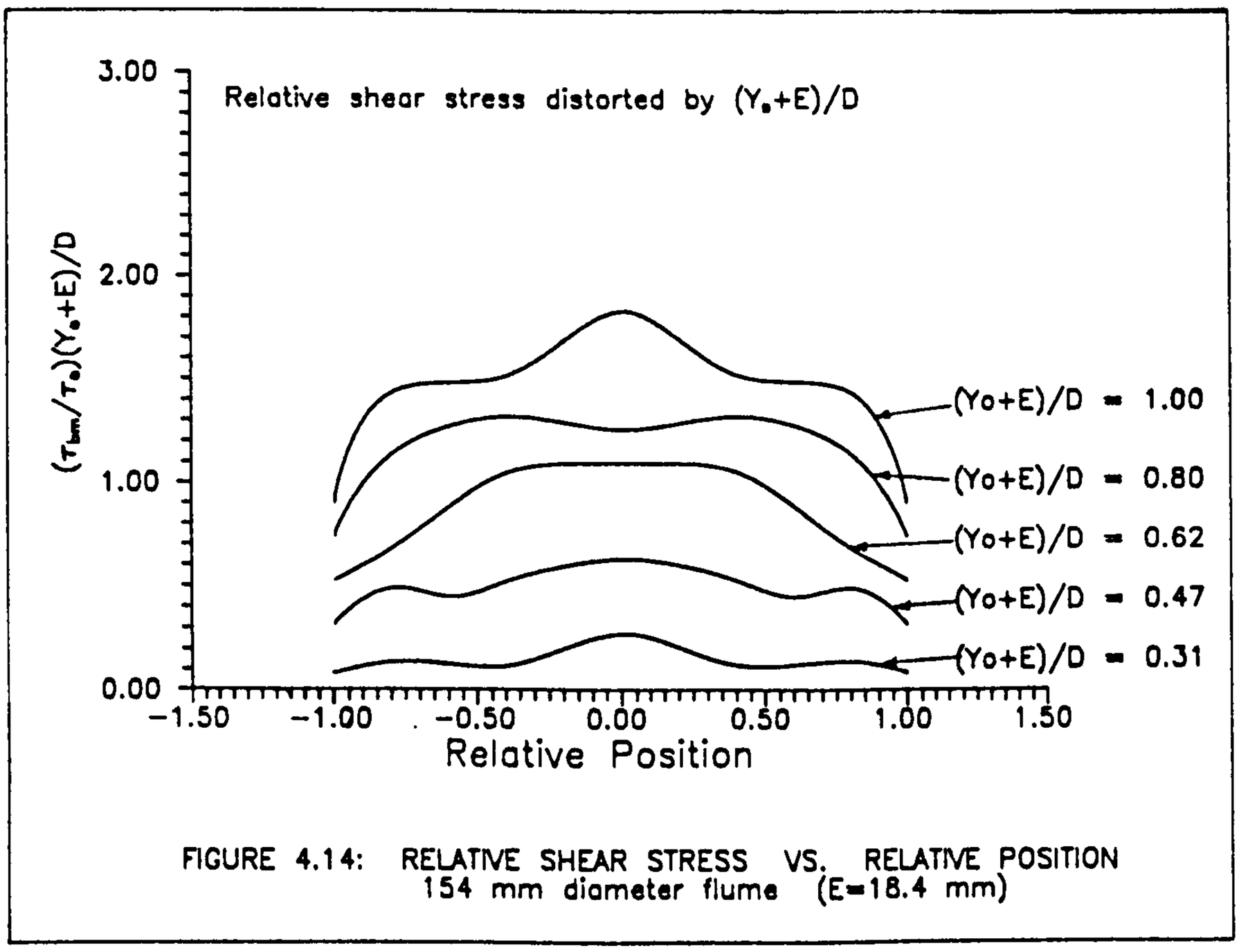

FIGURE 4.14: RELATIVE SHEAR STRESS VS. RELATIVE POSITION
154 mm diameter flume (E=18.4 mm)

On full pipe flow conditions one maximum peak is observed at the centre line of the flume cross-section. However, secondary currents (existence of two smaller peaks) also were observed specially for large bed thickness (see Fig. 4.15). Only a limited number of velocity and shear stress distribution profiles was measured in the largest bed thickness (i.e., E=60.3mm). In this case it seems that the flow changes from two dimensional characteristics for narrow flow depths ($Y_o/(D-E) < 0.37$) to three dimensional characteristics for greater depths. It must be pointed out however, that the sediment bed in this particular case is occupying around 39% of the diameter. As the flow became deeper secondary currents were observed in both sides of the

section. However, more measurements for a wide range of (Yo+E)/D are needed to achieve more conclusive results.

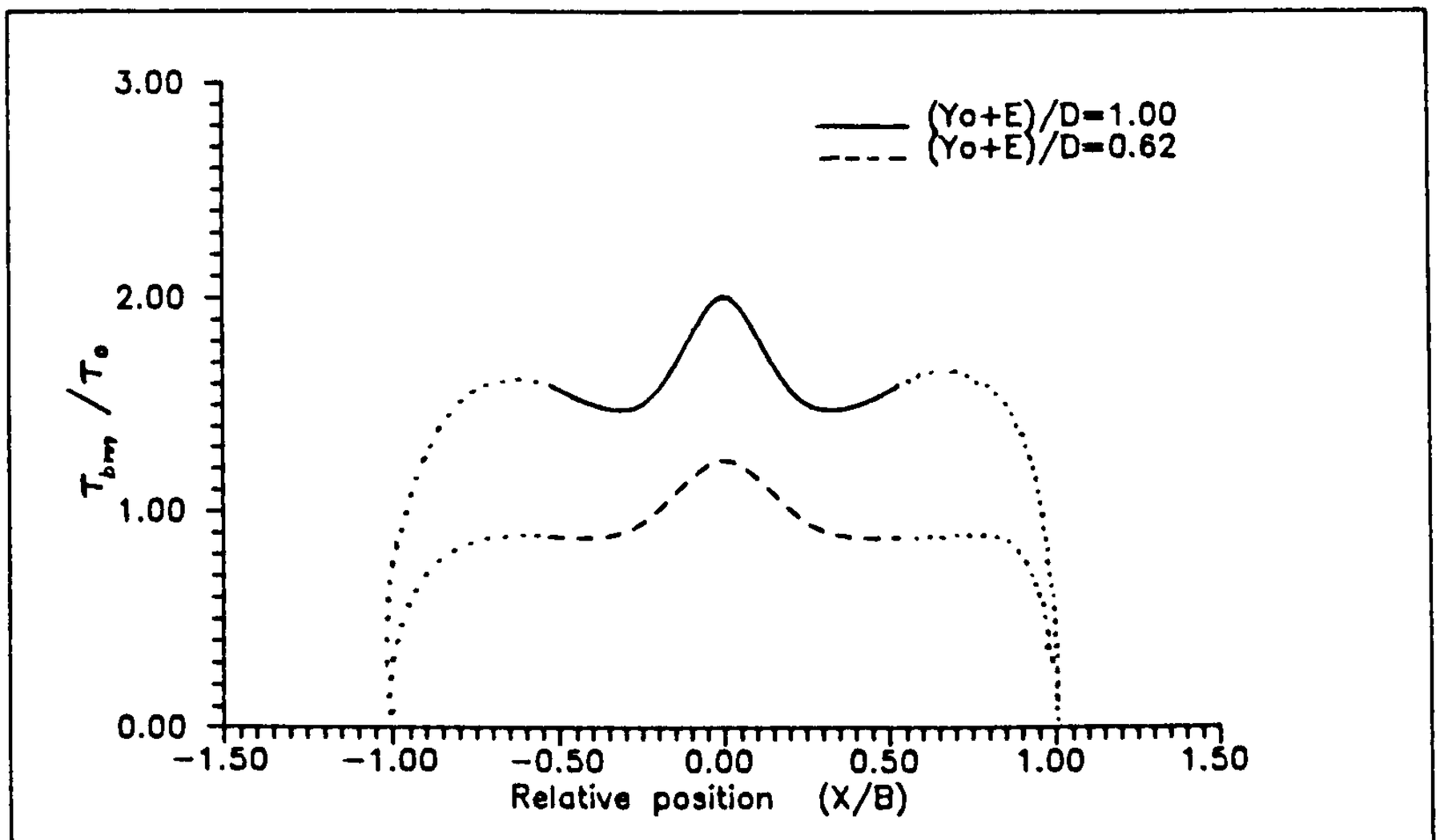

FIGURE 4.15: RELATIVE SHEAR STRESS VS. RELATIVE POSITION
Open channel flow in the 154mm diameter flume (E=60.3 mm)

Shear stress computations from velocity distributions show the measured bed shear stresses (τ_{bm}) exerted on the bed to be much higher (see Fig. 4.16) than the computed (i.e., $\tau_o = \rho g R S_o$) mean shear stresses. Bed and mean shear stresses are related by:

$$\tau_b = 1.56\ \tau_o^{1.21} \qquad (4.7)$$

which has a correlation coefficient r^2=0.96, and it is valid for E/D = 0.08 to 0.39. The measured bed shear stresses (τ_{bm}) compared reasonably well (see Fig. 4.17) with the predicted values (τ_b) by Einstein-Vanoni's separation technique. It must be pointed out that the predicted bed shear stress (τ_b) is an average value for the bed. Thus it is reasonable to expect the measured shear to be distributed around the predicted values.

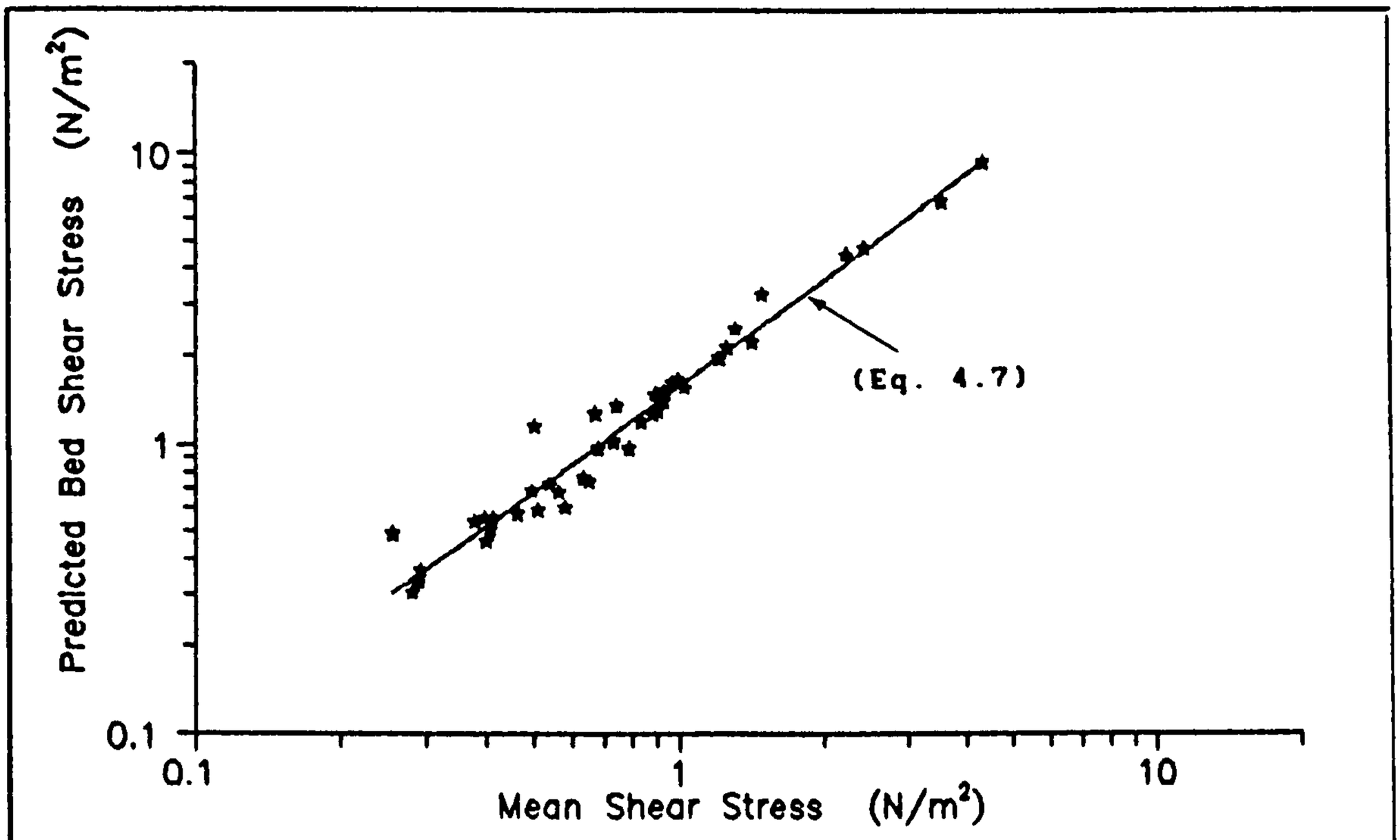

FIGURE 4.16: MEAN SHEAR STRESS VS. BED SHEAR STRESS
154 m diameter flume (E=12.5 to 60.3mm)

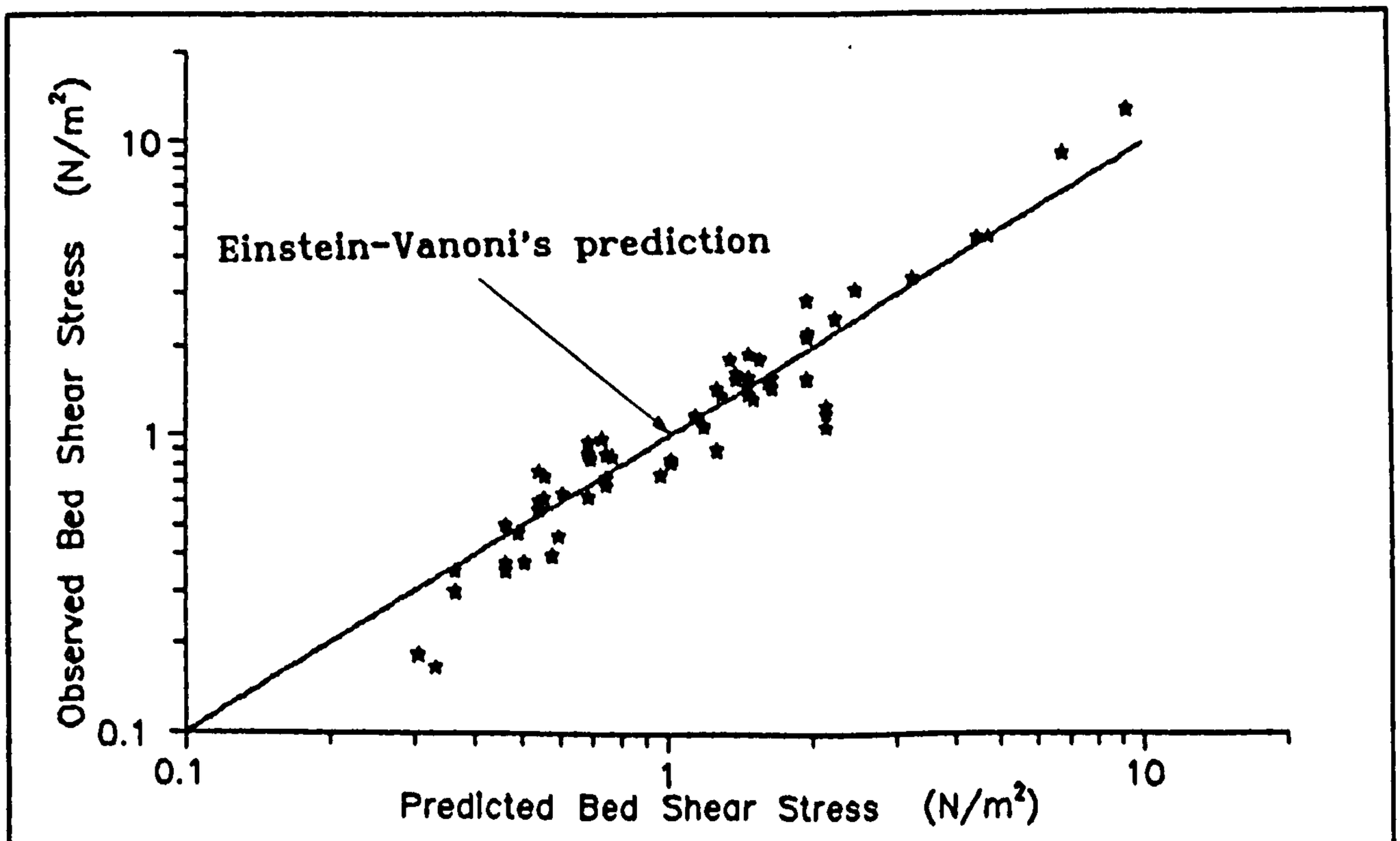

FIGURE 4.17: PREDICTED VS. OBSERVED BED SHEAR STRESS
154 mm diameter flume (E=12.5 to 60.3mm)
(Einstein-Vanoni's separation technique)

4.2.4 Turbulence Measurements

Turbulence measurements (u-component only) were carried out in the 154 mm diameter flume for various uniform open channel and full pipe flow conditions ($(Y_o+E)/D$ = 1/2, 3/4 and 1), and one sediment bed thickness (E=40.8mm). The objective of these experiments was to assess the effect of turbulence on the movement of sediment in the flume. A Laser Doppler Velocimeter (see Sec. 3.4 and Plate 4) in forward scatter mode with single component was used to measure velocity and turbulence profiles of each flow. The measurements were performed at the centre line of the flume only because of technical limitations of the laser supporting structure and the time availability.

Turbulence intensities measurements were classified into four groups according to their flow characteristics,

a) Smooth Bed - Open Channel Flow (series S1 to S8)
   - Full Pipe Flow (series SF1 to SF4)

b) Rough Bed - Open channel flow (series R1 to R6)
   - Full pipe flow (series RF1 and RF2)

In Tables 4.9 and 4.10 the flow characteristics of the 20 runs are summarised. A typical computation of turbulence intensities is shown in Table 4.11 and in Fig. 4.18. More details of turbulence intensities measurements and computations can be seen in Appendix E.

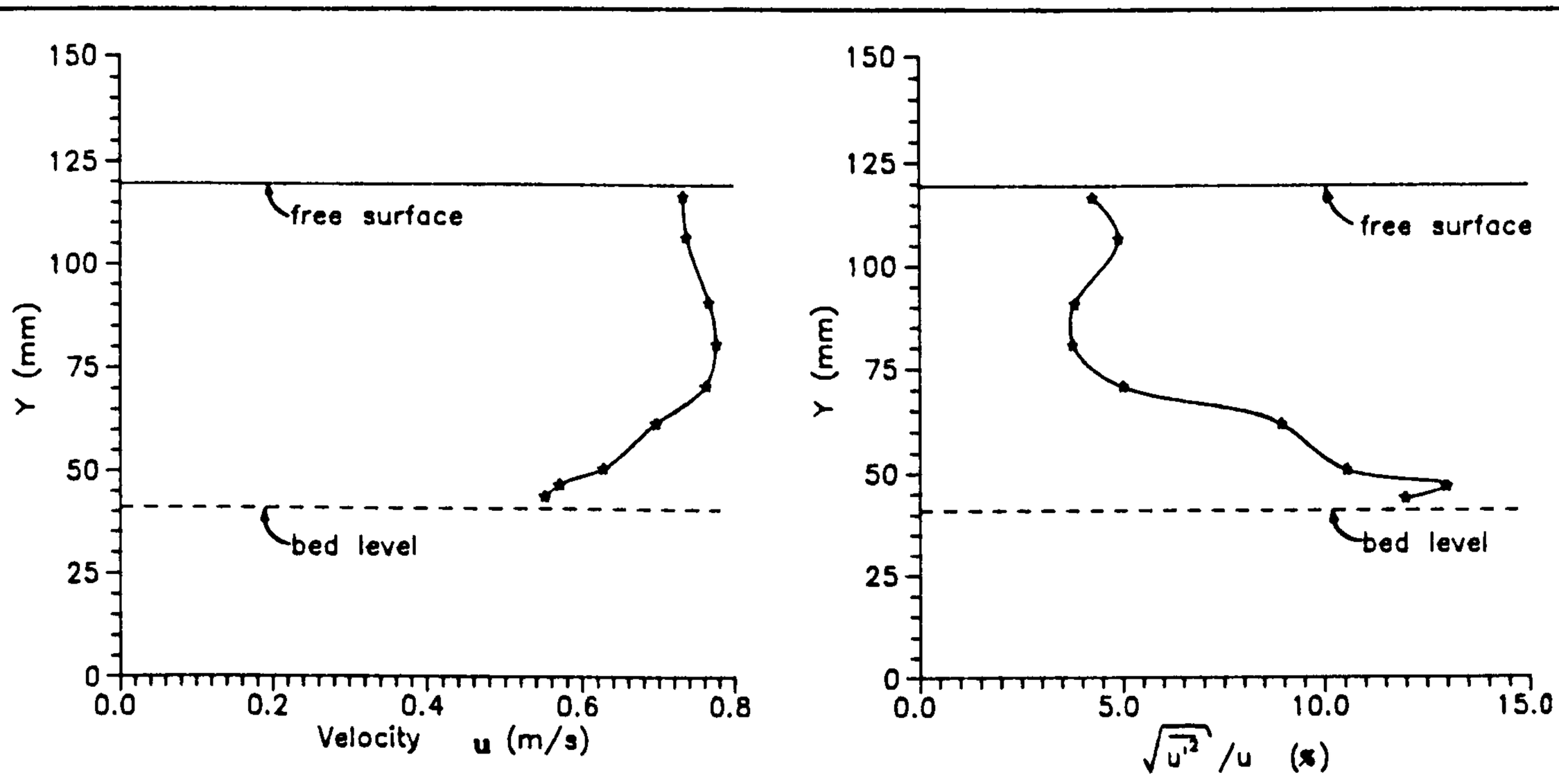

FIGURE 4.18: TYPICAL VELOCITY AND TURBULENCE INTENSITY PROFILES
Open channel flow in the 154mm diameter flume, rough bed (E=40.8mm) d_{50}=0.5mm

Plots of turbulence intensities $\left(\sqrt{\overline{u'^2}} / u\right)$ (where u is the time average velocity and u' is the velocity fluctuation) show their dependence on flow depth, bed roughness and slope (see Figs. 4.19 to 4.23. The near bed turbulence levels over rough boundaries are found to be larger than those over smooth boundaries. For example in Fig. 4.20 $(Y_o+E)/D = 3/4$) the turbulence intensity near the bed attained a value of around 13% on the smooth bed and around 16% on the rough bed. In Fig. 4.21 $(Y_o+E)/D = 1$) the values are 12% and 14.5% for the smooth bed and for the rough bed respectively.

Because of the physical limitations of the glass box used for measurements (to avoid the refraction problems inherent to circular cross-section flumes) with the LDV it was not possible

to obtain turbulence measurements in the upper 20% of the pipe diameter (see Fig. 4.21).

Turbulence levels are found to be higher near the bed for all cases (see Figs. 4.19 to 4.23). Turbulence intensities seem to be dependent mainly on flow depth and bed roughness. In Fig. 4.23 full pipe flow cases are shown. It can be seen that the turbulence levels are higher in the case of rough beds (RF1 and RF2) than those corresponding to the smooth bed cases (SF1 to SF4). It also can be observed that the minimum levels of turbulence are found around a relative depth (y/Y_o) = 0.5, i.e., at the centre of the flow section. The maximum levels of turbulence are found near the flume bed. Secondary peaks of turbulence levels are found near the free surface in case of open channel flow, and near the pipe soffit in case of full pipe flow conditions.

On erosion experiments with cohesive sediments (Sec. 4.3.2) the sediment bed surface is quite smooth before reaching critical conditions but it becomes rougher with the presence of erosion spots as the flow approaches critical conditions. The appearance of erosion spots causes an increase in turbulence levels, which in turn is responsible for the magnification of the erosion spots (i.e., increase in k_s). This causes higher turbulence levels which further increases the bed roughness and so forth. Finally an accelerated destruction of the sediment bed was observed to take place (Sec. 4.3.2.2).

The appearance of the first spots of erosion is the event that triggers off the erosion process. On the sediment bed the weakest area that is subjected to the highest transient (turbulence) shear stress begins to be eroded i.e., first spots of erosion. However, further work is essential to identify fully the effect of turbulence on sediment movement. Because of the limited available time, this could not be achieved.

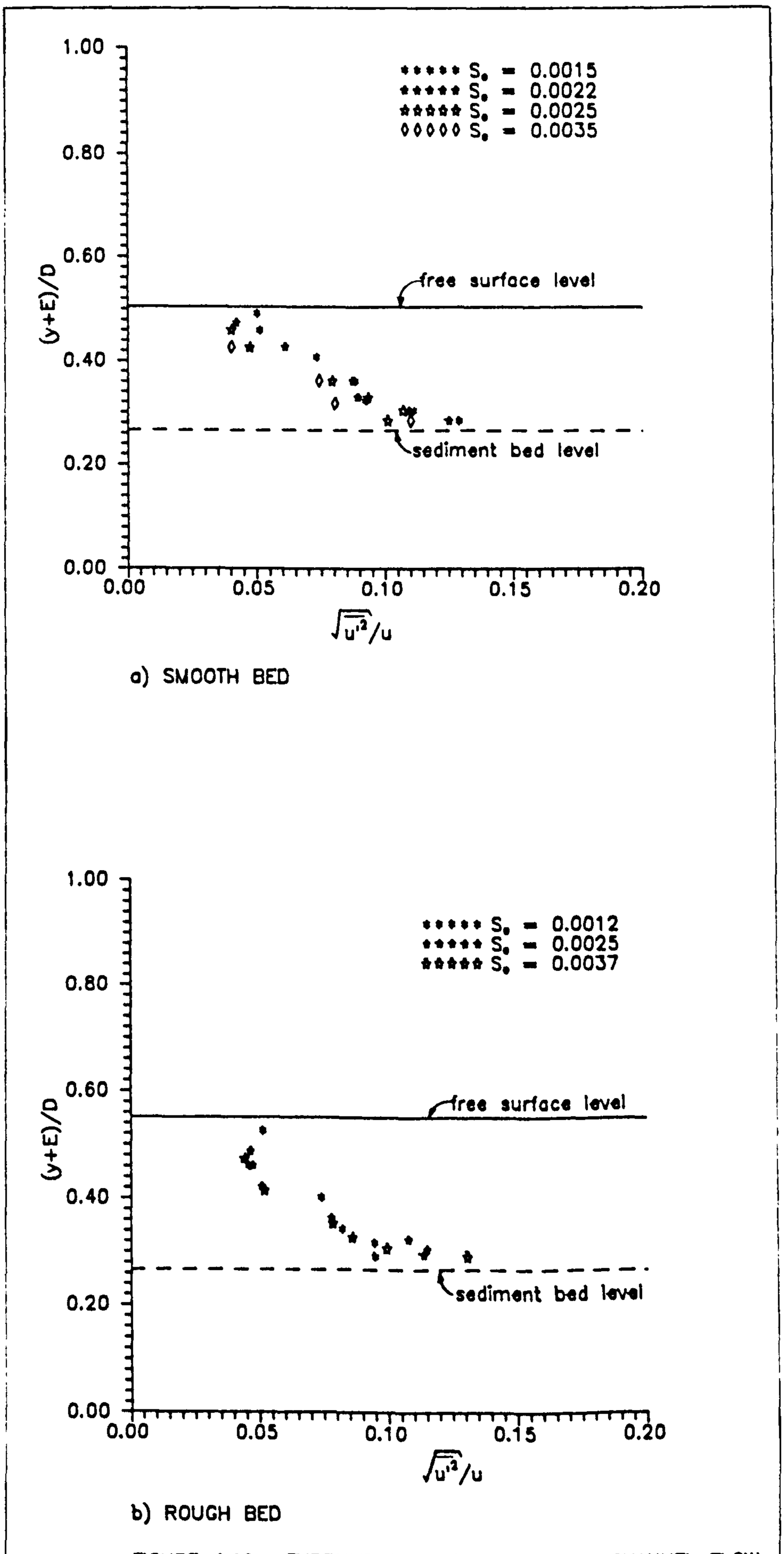

FIGURE 4.19: TURBULENCE PROFILE IN OPEN CHANNEL FLOW
D = 154 mm (Yo+E)/D = 0.49–0.55

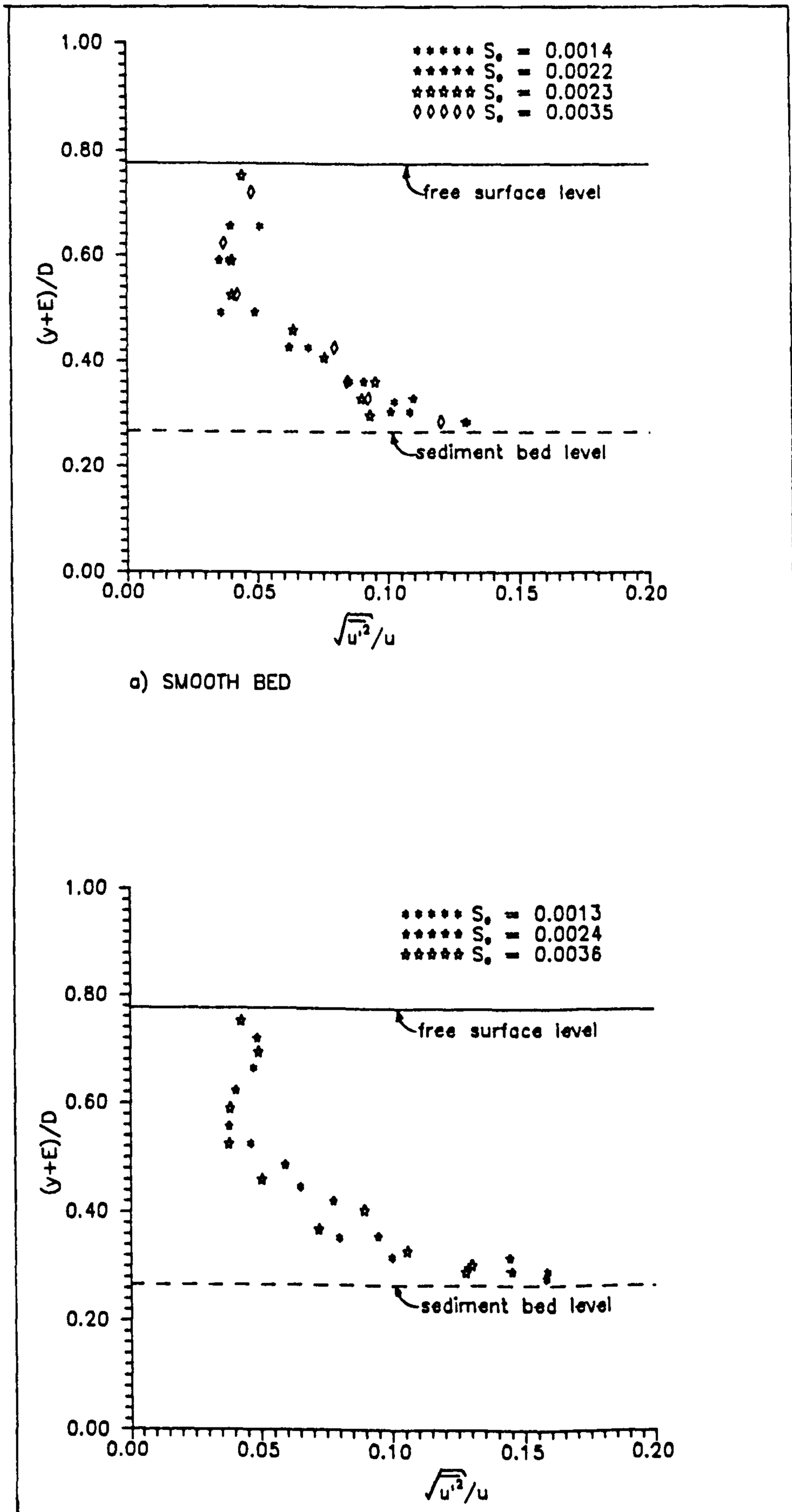

FIGURE 4.20: TURBULENCE PROFILES IN OPEN CHANNEL FLOW
D = 154 mm E = 40.8 mm (Yo+E)/D = 0.70–0.78

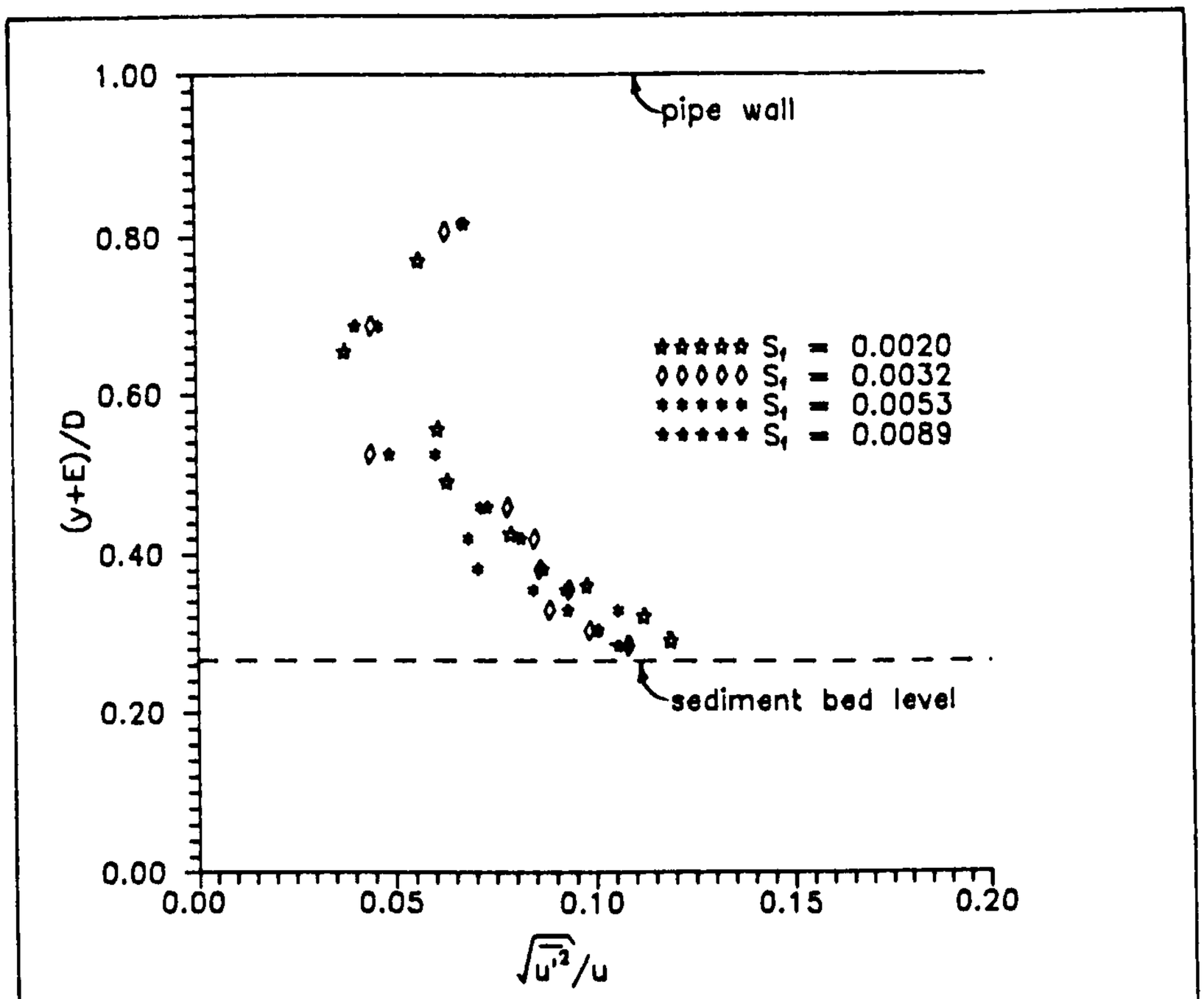

a) SMOOTH BED

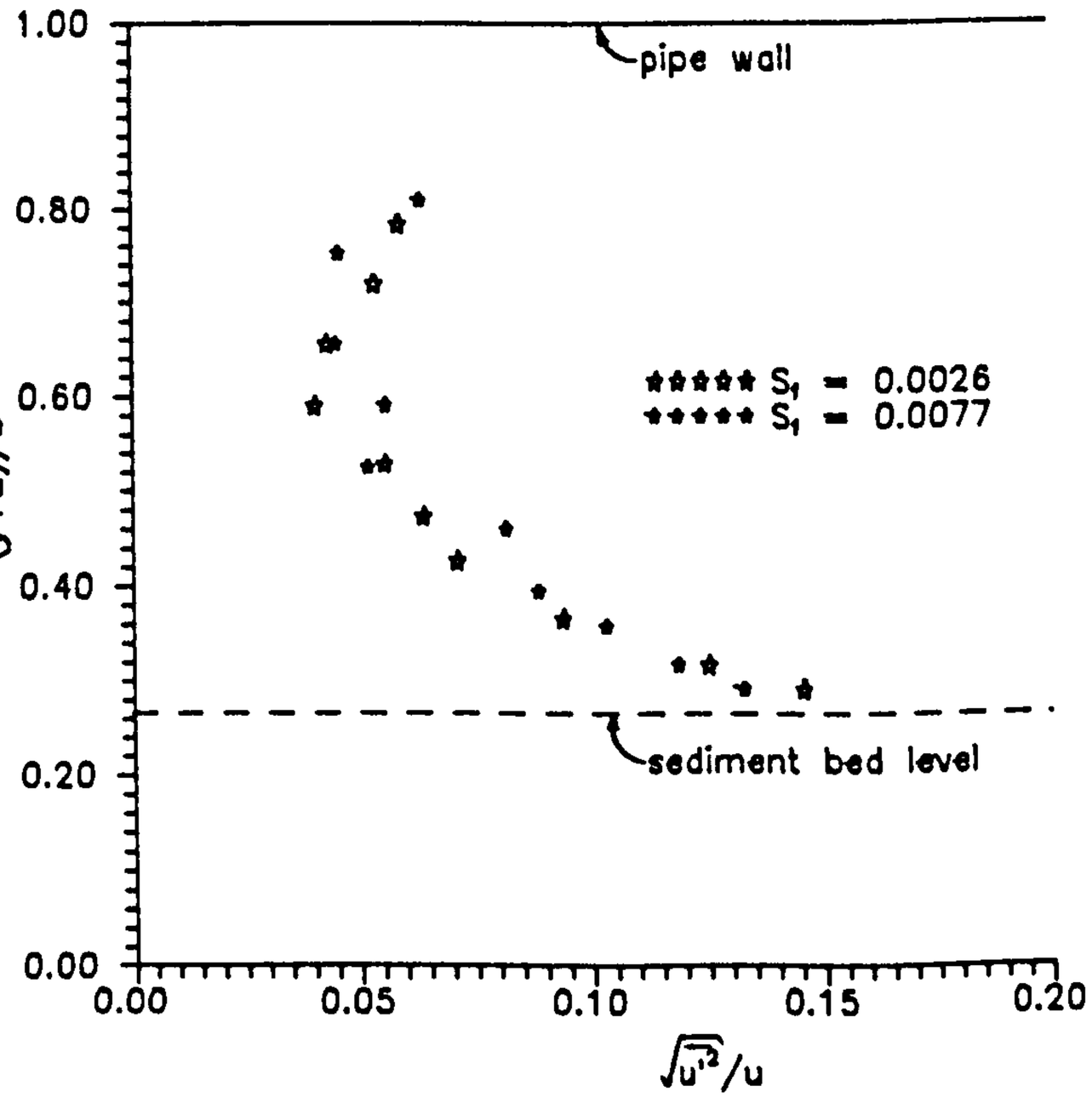

b) ROUGH BED

FIGURE 4.21: TURBULENCE PROFILES IN FULL PIPE FLOW
D = 154 mm E = 40.8 mm (Yo+E)/D = 1

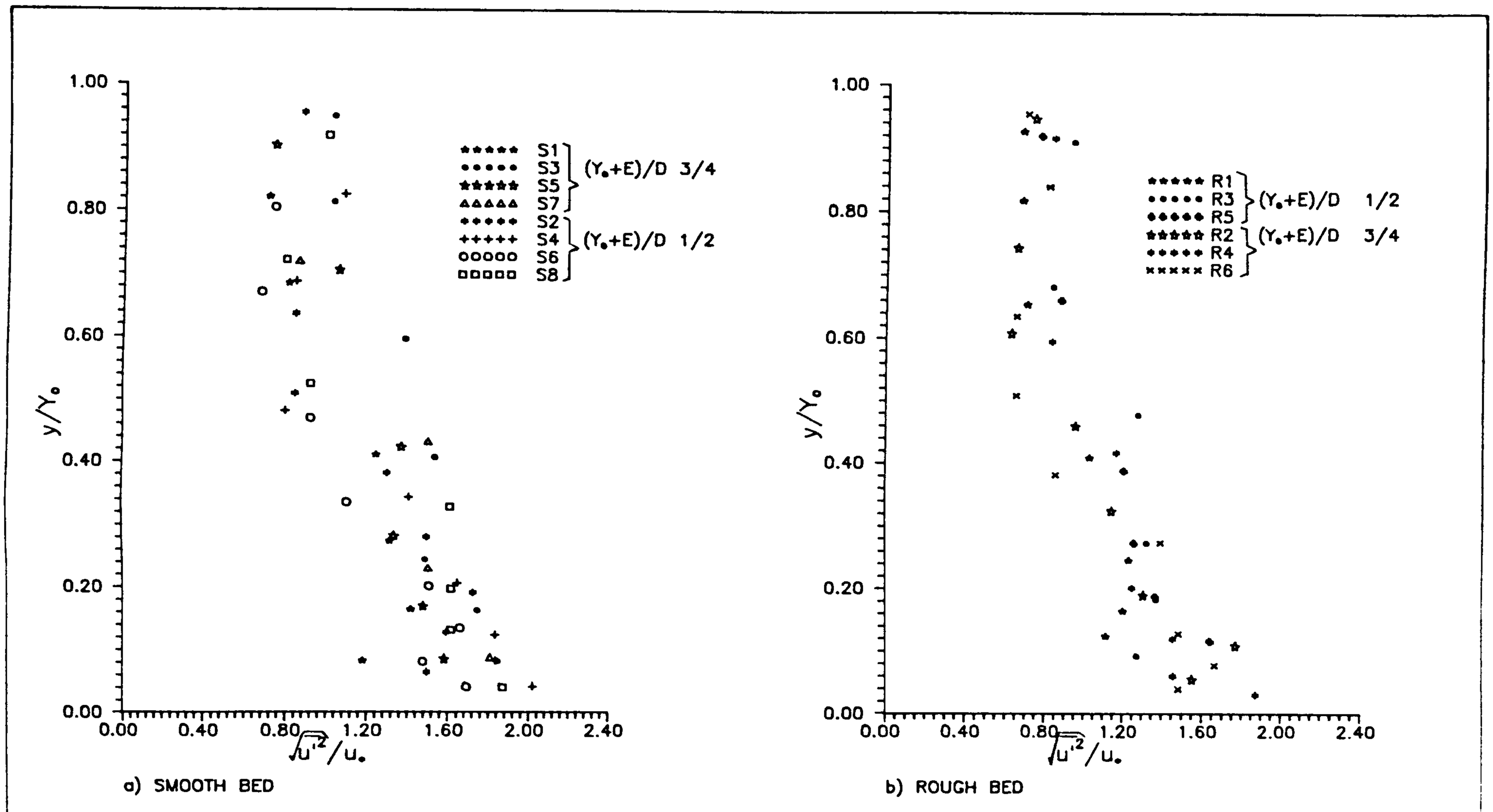

FIGURE 4.22: TURBULENCE INTENSITY ($\sqrt{\overline{u'^2}}/u_*$) VS. RELATIVE DEPTH ($y/Y_0$)
OPEN CHANNEL FLOW 154 mm diameter flume (E=40.8mm)

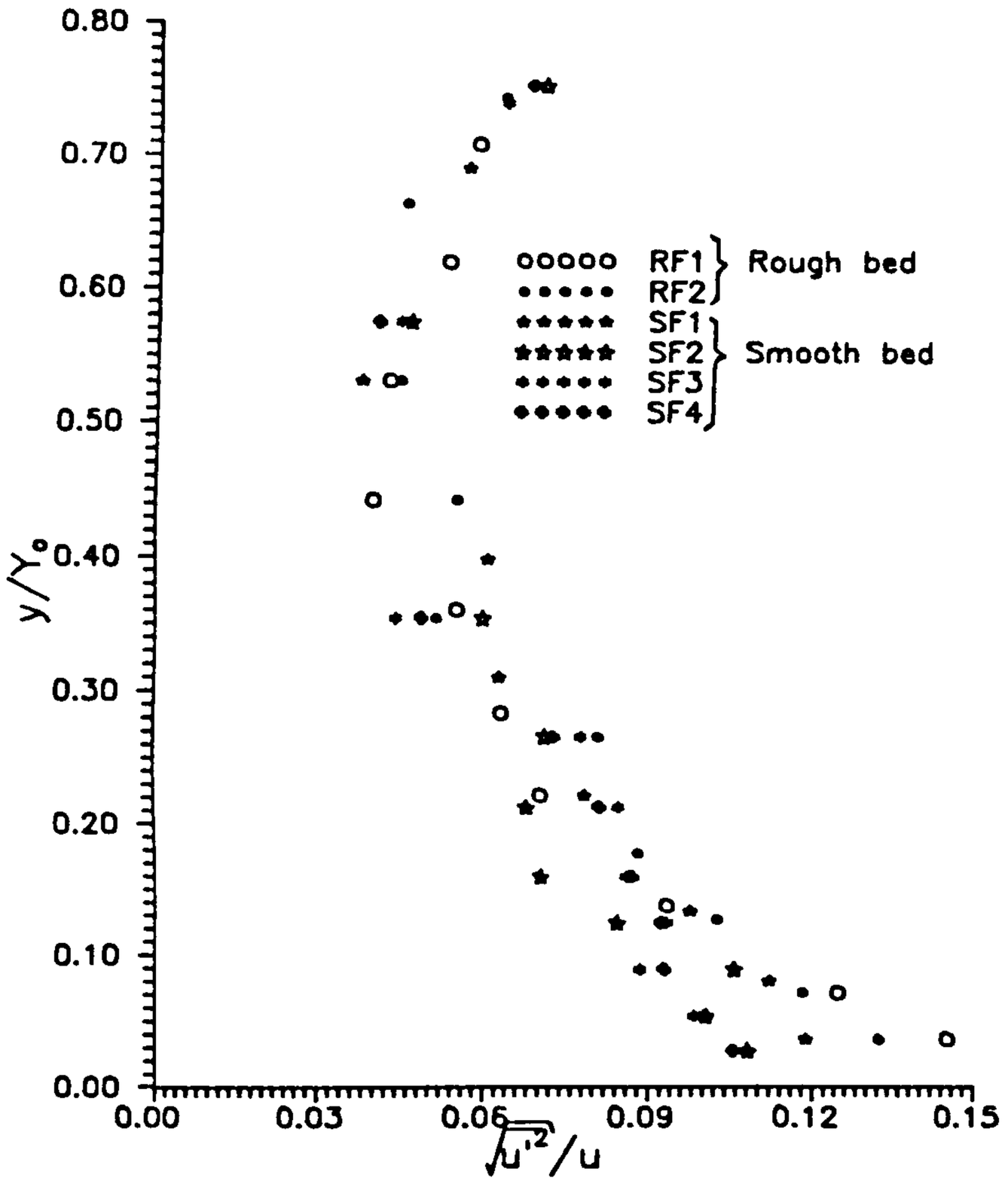

a) Normalized by Local Velocity

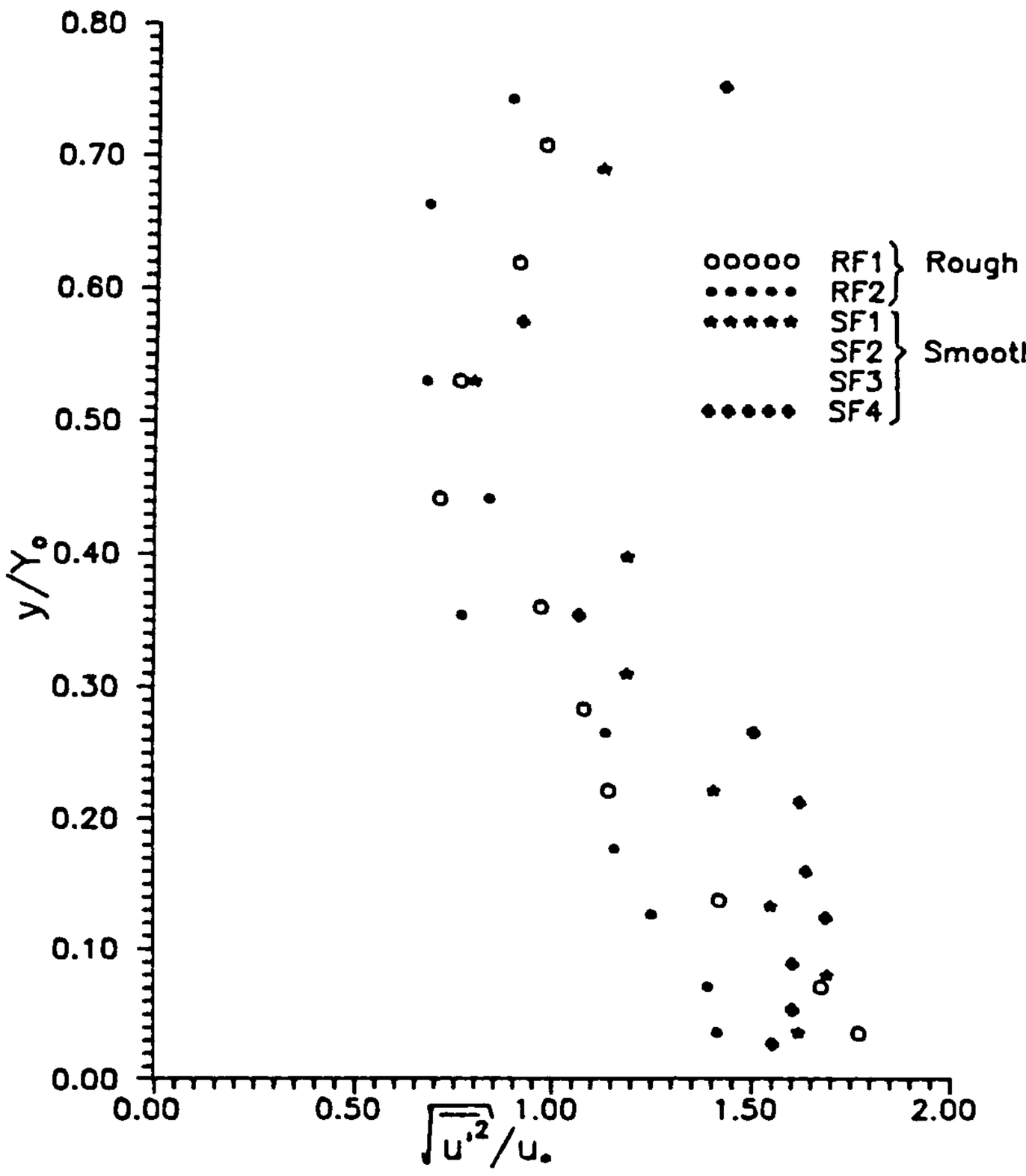

b) Normalized by Shear Velocity

FIGURE 4.23: TURBULENCE INTENSITY VS. DEPTH RATIO (y/Yo)
FULL PIPE FLOW (154 mm diameter flume ε = 40.8 mm)

4.3 SEDIMENT MOVEMENT EXPERIMENTS

4.3.1 Initiation of Erosion of Non-cohesive Sediments

4.3.1.1 Selection of parameters

Initiation of motion of sediment particles can be determined by such characteristic parameters as: the water density (ρ), the dynamic viscosity of the water (μ), the mean size of the particles (d), the flow depth (Y_o), the shear velocity of the flow (u_*), particle shape factor (SF_p), channel shape factor (SF_c), the density $(\rho)_s$ and buoyant specific weight $(\gamma_s - \gamma)$ of the sediment, in which (γ_s) is the specific weight of the sediment and (γ) is the specific weight of the water. A functional relation can be written in the form:

$$F\{\rho, \mu, \rho_s, d, Y_o, u_*, SF_p, SF_c, (\gamma_s - \gamma)\} = 0 \qquad (4.8)$$

Using Buckingham π-theorem with selected basic parameters as, d, ρ and u_* (which obviously have independent dimensions). Thus 6 dimensionless parameters can be found by applying the π-theorem.

$$\pi_1 = \frac{u_* d}{\nu} = Re_* \qquad (4.9)$$

known as the particle size Reynolds number (Re_*). It reflects the influence of viscosity and thus it is a characteristic of the relative motion of a grain in fluid.

$$\pi_2 = \frac{\rho u_*^2}{(\gamma_s - \gamma)} = \frac{1}{\psi} \qquad (4.10)$$

known as the entrainment function or mobility number ($1/\psi$). It

reflects the influence of the submerged weight. It characterizes the ratio of the dynamic forces acting on the grain to grain weight.

$$\pi_3 = \frac{Y_o}{d} \tag{4.11}$$

known as the flow depth ratio ($\frac{Y_o}{d}$). It reflects the influence of the flow depth on sediment movement. However, when the product RS (hydraulic radius and channel slope) is kept constant (i.e., for a given critical shear stress) the shear stress near the bed is practically not dependent on flow depth. This is why many equations for initiation of erosion do not include the flow depth parameter.

$$\pi_4 = \frac{\rho_s}{\rho} = S_s \tag{4.12}$$

known as the relative density of the sediment (S_s). It characterizes the influence of inertia forces, which are important to the properties of individual grains. However, as in general the interest is focused on mass grain motion S_s is not an important dimensionless parameter.

$$\pi_5 = SF_p \tag{4.13}$$

known as the shape factor of the particles (SF_p), which is another dimensionless variable. In case of uniform size sediment (spherical particles, or uniform sand size, for example) the particle shape factor is constant ($SF_p \cong 1$).

$$\pi_6 = SF_c \tag{4.14}$$

known as the shape factor of the channel cross-section (SF_c). It is another dimensionless parameter, which is important in cases

where the shape of the cross-section changes with flow depth (i.e., channels of circular cross-section).

Two dimensionless parameters T/P (surface width/wetted perimeter, see Fig. 4.24) and Y_o/P (normal depth/wetted perimeter, see Fig. 4.25) can be used to characterize channel shape. In Fig. 4.24 the relative flow depth $(Y_o+E)/D$ is plotted against T/P for various sediment bed thicknesses. The influence of sediment bed thickness on the parameter T/P decreases as the relative

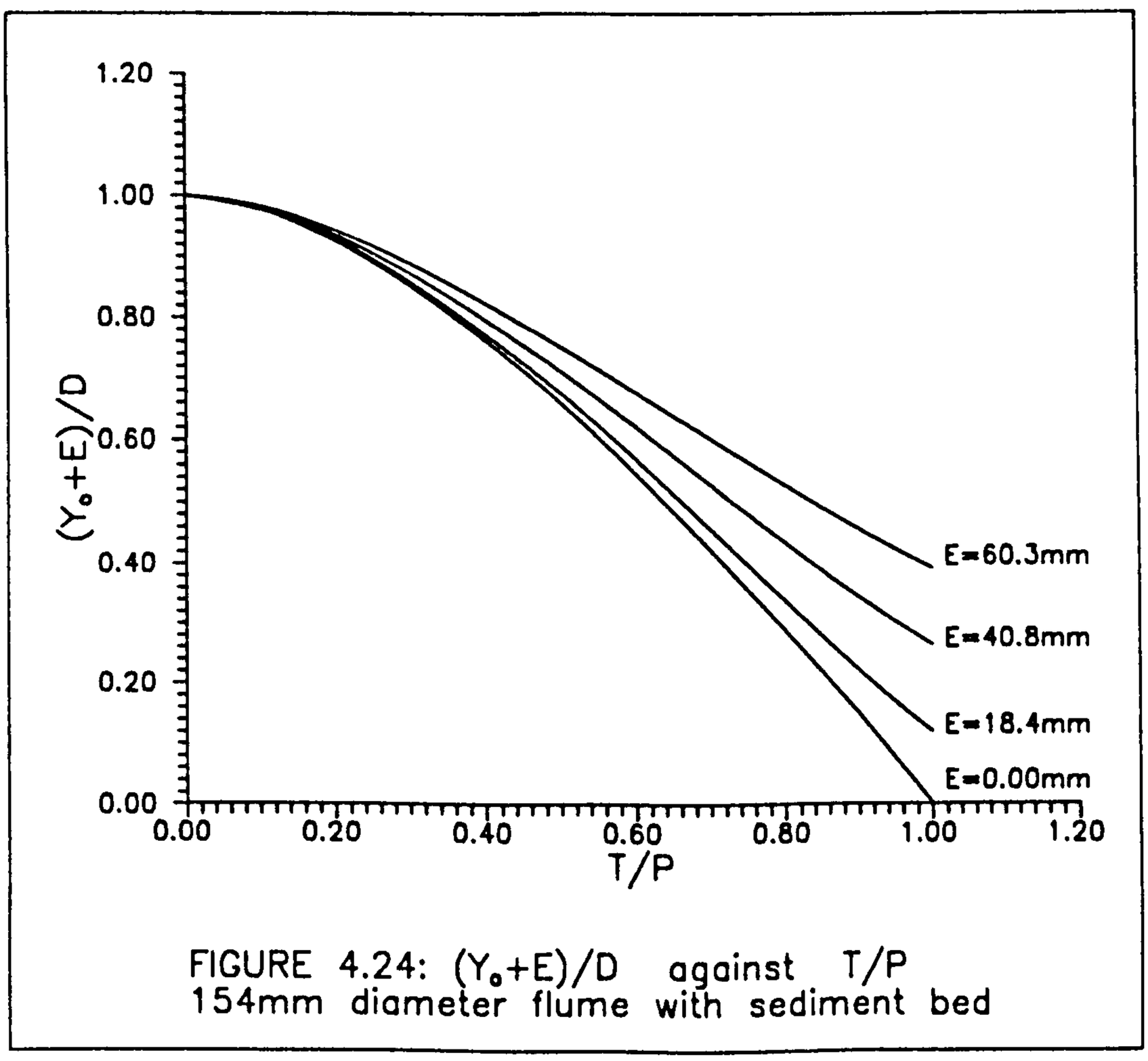

FIGURE 4.24: $(Y_o+E)/D$ against T/P
154mm diameter flume with sediment bed

depth increases. For full pipe flow conditions the parameter T/P remains constant (T/P=1) independent of sediment bed thickness. Therefore, the channel shape effects would not be well represented by the parameter T/P.

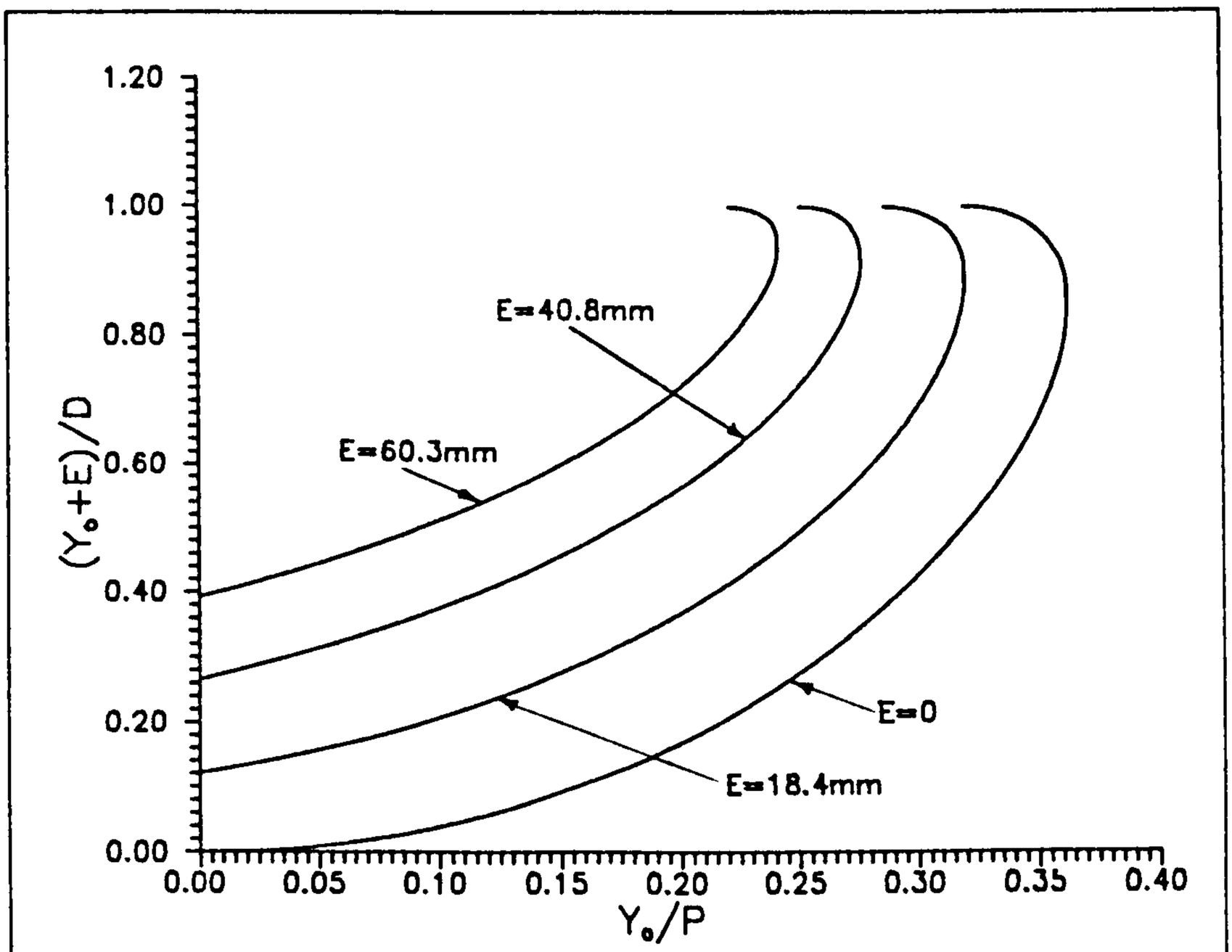

FIGURE 4.25: $(Y_o+E)/D$ against Y_o/P
154mm diameter flume with sediment bed

In Fig. 4.25 the relative flow depth $(Y_o+E)/D$ is plotted against Y_o/P for various sediment bed thicknesses. It can be seen that the parameter Y_o/P is dependent on flow depth and on sediment bed thickness. Four curves for various sediment bed thickness (0, 18.4, 40.8 and 60.3mm) are plotted. Each curve has a maximum at relative depth $(Y_o+E)/D$ = 0.877, 0.909, 0.936, and 0.961 for sediment bed thicknesses 0, 18.4, 40.8 and 60.3mm respectively. Further increases in relative depth results in decreasing values of Y_o/P. For full pipe flow the values of the parameter Y_o/P are 0.318, 0.286, 0.25 and 0.22 for sediment bed thicknesses 0, 18.4, 40.8 and 60.3mm respectively.

Flow depths near full pipe showed instabilities in uniform flow conditions. For this reason the flow depths were limited to $(Y_o+E)/D \leq 0.85$ (i.e., below the point of maximum Y_o/P) in the experiments. Thus the parameter Y_o/P may be used to represent the channel shape effects. Additionally Y_o/P was considered to analyse the shape effect (Nalluri-Adepoju, 1984) on resistance to flow in smooth open channels of circular cross-section. Therefore the parameter Y_o/P will be used to characterize shape effects in the analysis of the experimental results. The phenomenon of initiation of erosion may be described by:

$$\frac{\rho u_*^2}{(\gamma_s - \gamma)} = f\left(\frac{u_* d}{\nu}, \frac{Y_o}{P}\right) \qquad (4.15)$$

which is equivalent to Eq. 2.1, presented in Chapter 2:

$$\frac{\tau_{oc}}{\rho(S_s - 1)gd} = f\left(\frac{u_* d}{\nu}\right) \qquad (2.1)$$

where no channel shape effects were considered as those studies (Shields, 1936) were concerned with wide rectangular channels only.

In the literature the concept of critical velocity is also used to describe incipient motion. The corresponding dimensionless parameter (critical Froude number of the particle) can be expressed as:

$$F_{dc} = \frac{V_c}{\sqrt{(S_s - 1)gd}} \qquad (4.16)$$

where V_c is the critical velocity for initiation of motion of sediment particles. F_{dc} takes into account the density and size

of the particles. A single critical velocity value would be expected for each particular sediment. However, for a given mean velocity the shear stress exerted on the particles is directly proportional to channel slope. Thus one value of F_{dc} for each particle size and channel slope may be expected. The critical Froude number of the particle is also likely to be influenced by the channel shape (i.e., Y_o/P), as it will be shown below.

4.3.1.2 Uniformly Graded Sands Experiments

Initiation of erosion experiments under uniform flow conditions with non-cohesive sediments were carried out as described in Sec. 3.5.1.2. A wide range of uniform sand sizes (d_{50} = 0.12 - 4.1 mm) was used. The objective of these experiments was to obtain a basis of comparison for the cohesive sediment studies.

In every experiment a uniform size sand constituted the flat sediment bed (modeling deposited sewer sediment bed). Initiation of erosion was achieved by small increments of the shear stress (maintaining uniform flow conditions). Several bedload samples were taken for various flows beyond critical conditions. Critical shear stresses were determined by extrapolation to zero bed load from the C_v vs. τ_o curves (see Fig. 3.10). A summary of the results of these experiments is shown in Table 4.12 a, and in Figs. 4.26 and 4.27 (for more details see Appendix F).

The results suggest that for channels of circular cross-section with flat sediment bed critical conditions occur at lower (see

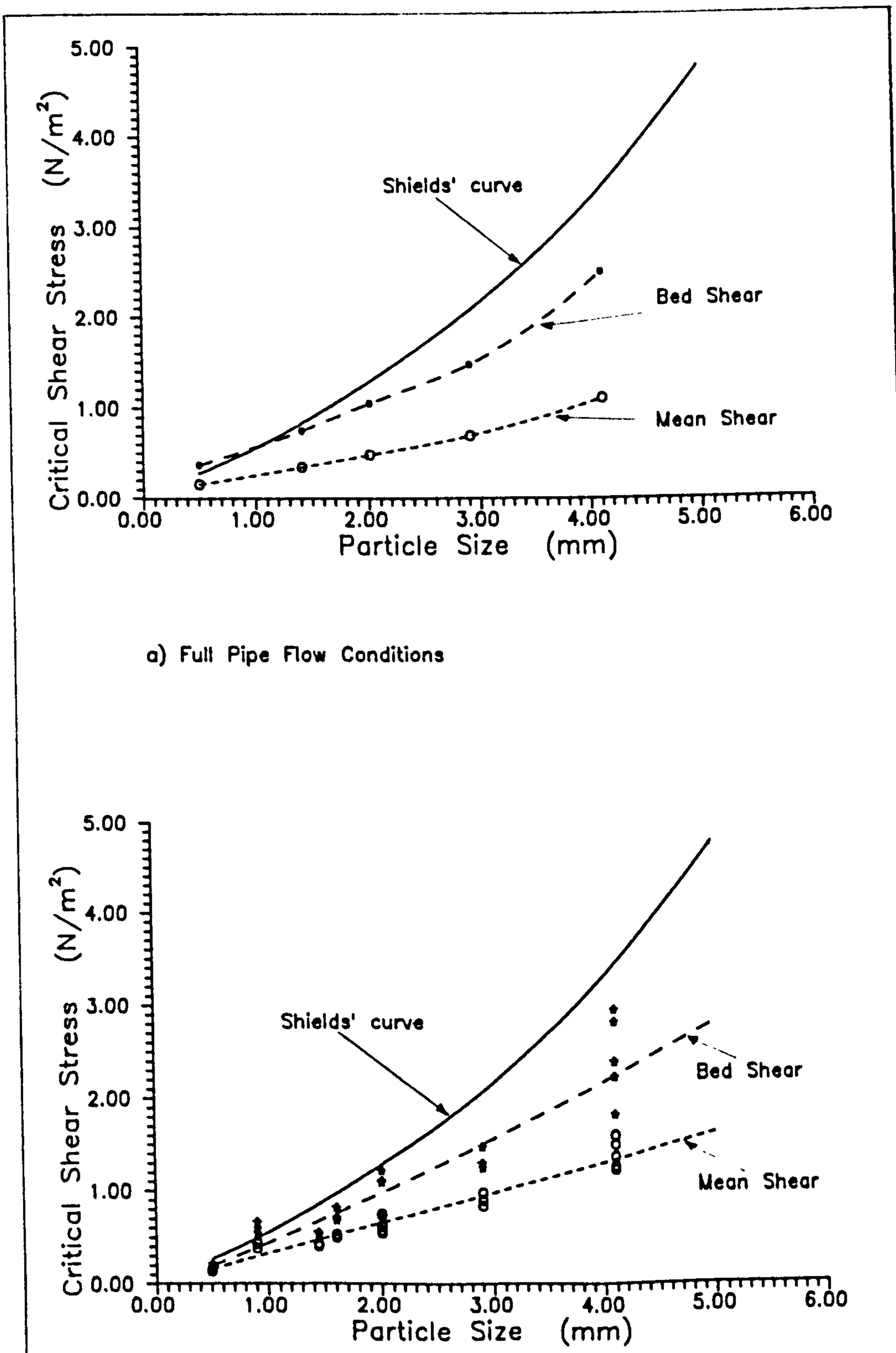

a) Full Pipe Flow Conditions

b) Open Channel Flow Conditions

FIGURE 4.26: CRITICAL SHEAR STRESS VS. PARTICLE SIZE
Non-cohesive sediments (154 mm diameter flume)
Loose bed E = 18.4 – 20.0 mm

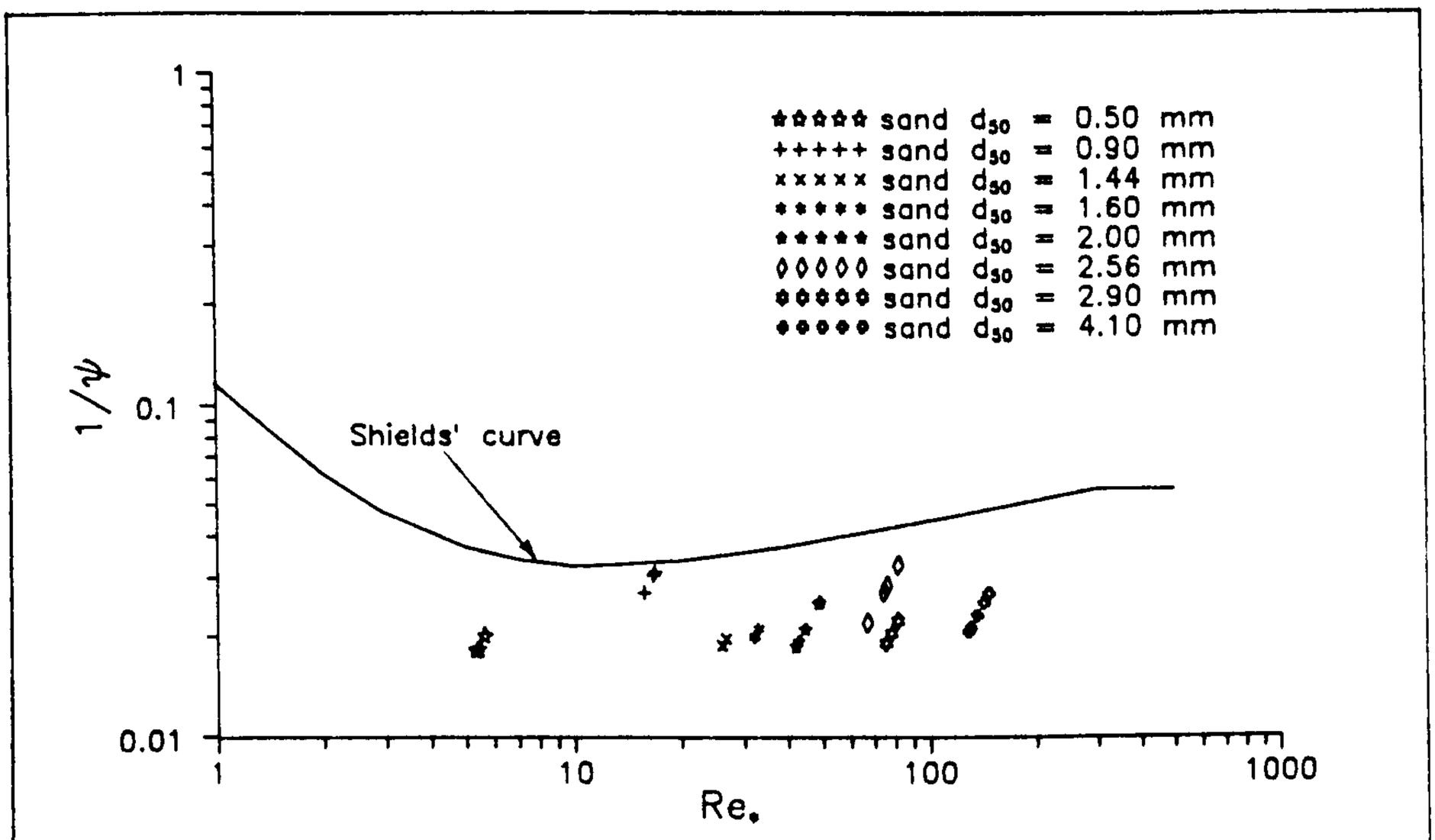

a) Mean Shear Stress Values

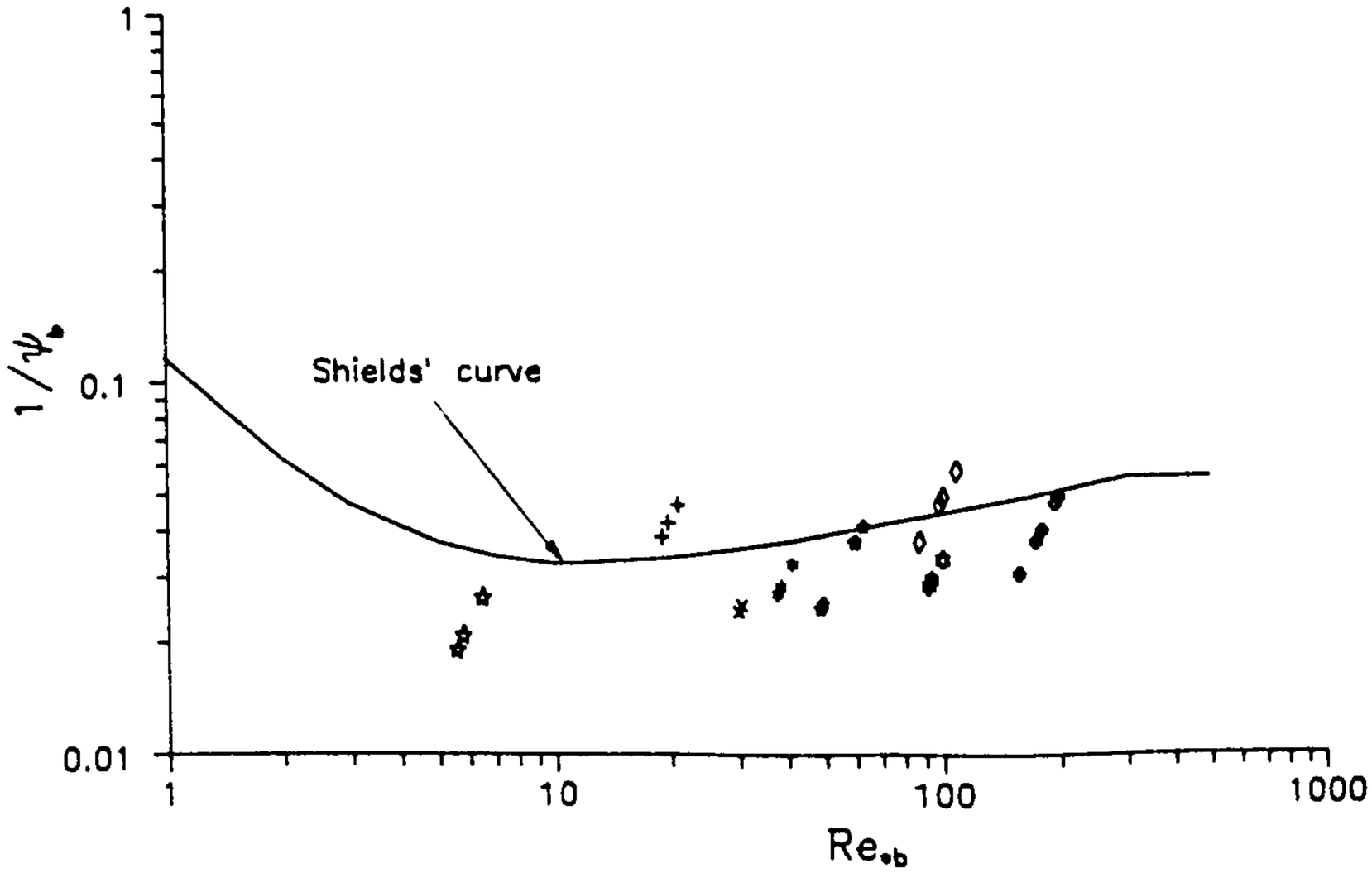

b) Bed Shear Stress Values

FIGURE 4.27: SHIELDS' DIAGRAM FOR INITIATION OF MOTION OF NON-COHESIVE SEDIMENTS in the 154 mm diameter flume E = 18.4 – 20 mm (loose sediment bed)

Fig. 4.26 and 4.27a) values of mean shear stresses (τ_o) than those of Shields for wide channels. However, separated critical bed shear stresses (τ_b) (computed using Einstein-Vanoni's separation technique) are found to be comparable to Shields' results (see Fig. 4.26 and 4.27). The scatter can be explained by the presence of secondary currents and turbulence levels.

An attempt was made to analyse the influence of channel shape on critical shear stress. In Figures 4.28a and 4.28b critical shear stresses are plotted against the shape factor parameter Y_o/P for experiments with bed thicknesses 18.4 and 20 mm respectively. A variation in critical shear stress with channel shape is observed for flow depths above half full pipe (i.e., larger size sands d_{50}= 2.00, 2.56, 2.90 and 4.10 mm). Figs. 4.28a and 4.28b suggest that for a given sand size the required shear stresses to initiate sediment movement are lower for flow depths above half full pipe (i.e., smaller channel slopes).

As it was mentioned before (Sec. 4.2.3) the velocity and bed shear stress distributions showed a marked dependence on flow depth (see Fig. 4.14). For flow depth above half full pipe there are secondary currents that enhance the eroding capabilities of the flow. In addition turbulence levels near the bed (rough beds) were found to be higher for flows depths above half full pipe (see Sec. 4.2.4), which also encourages erosion. The combined effects of secondary currents and turbulence is apparent in Figs. 4.28a and 4.28b as the points above the half full pipe show a decrease in critical shear stress with increasing flow depth.

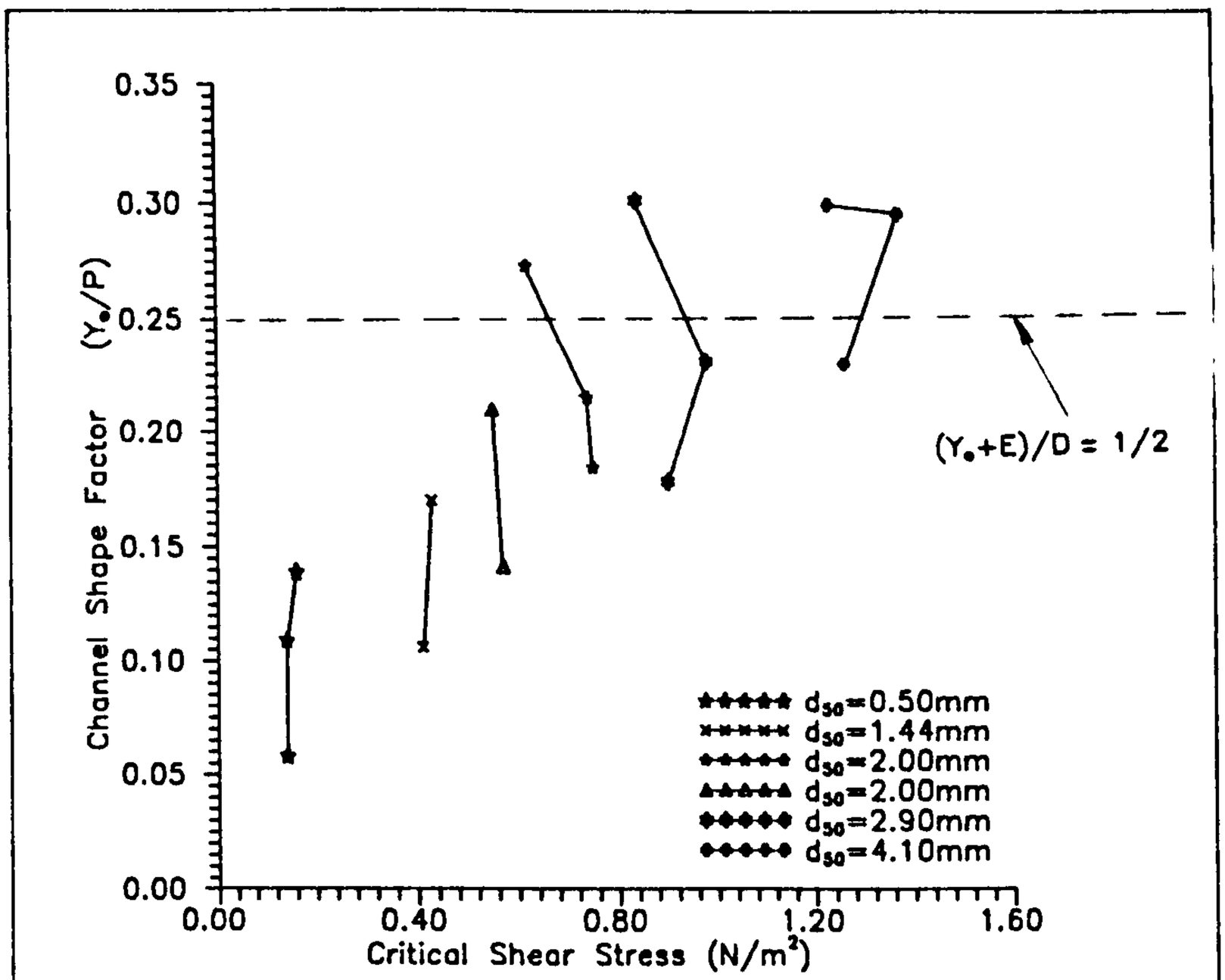

FIGURE 4.28 a; CRITICAL SHEAR STRESS VS. SHAPE FACTOR
154 mm diameter flume (E=18.4mm)
Non-cohesive sediments, loose bed

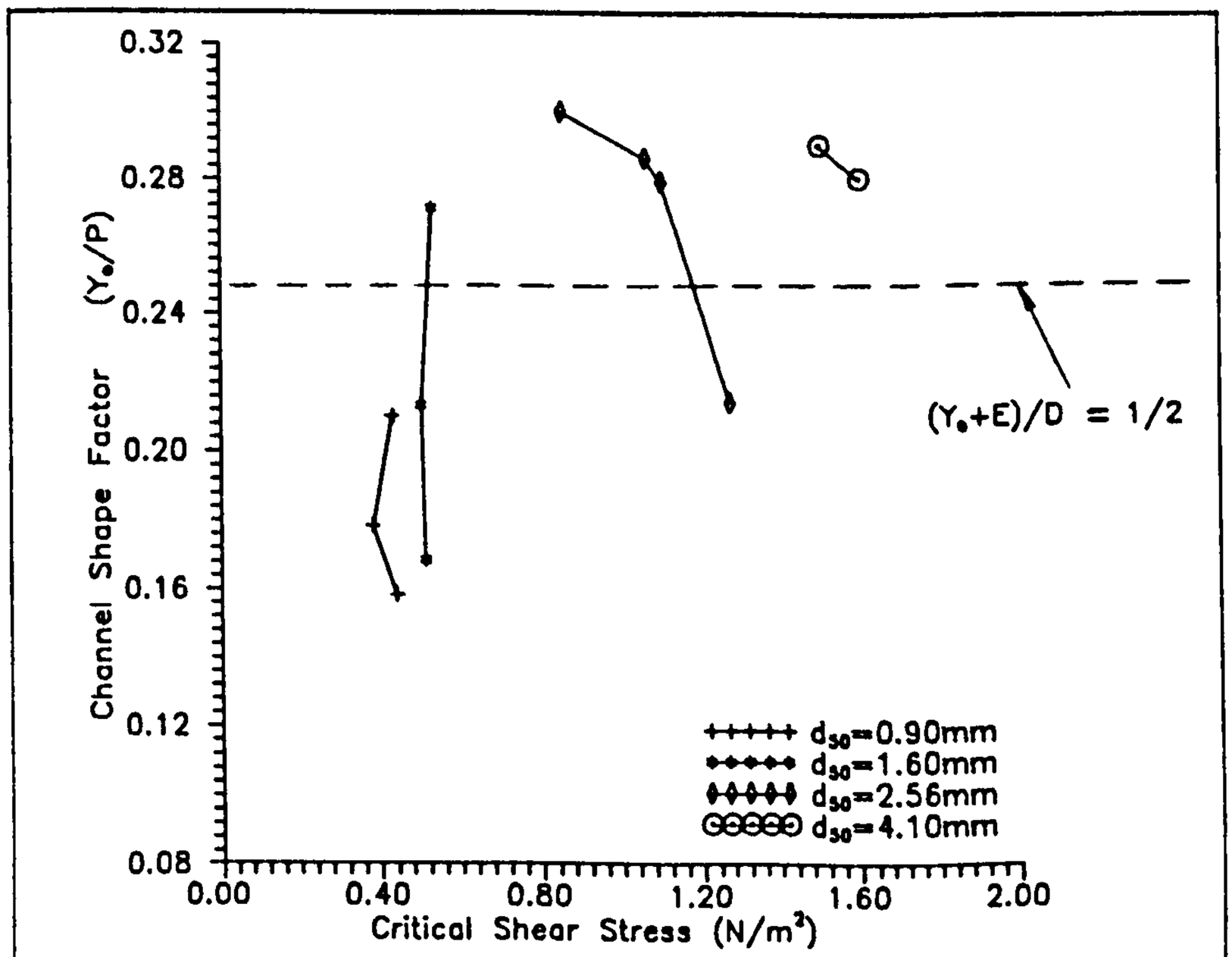

FIGURE 4.28 b: CRITICAL SHEAR STRESS VS. SHAPE FACTOR
154 mm diameter flume (E=20.0mm)
Non-cohesive sediments, loose bed

Nevertheless, due to the limited experimental data (3 or 4 slopes for each sand size only) it was not practical to fit a general relation between the critical shear stress and the shape factor.

On the other hand, however, smaller sand sizes (i.e. d_{50}= 0.50, 0.90, 1.44 and 1.60) did not show any considerable variation in critical shear stress with shape factor. This is because the flow depths used in these experiments were below half full pipe flow, which suggests that channel shape effects on critical conditions are noticeable only for flow depths above half full pipe.

The influence of sediment bed thickness on critical shear stress was studied by determining the critical conditions for two sand sizes (0.53 and 0.89 mm) in three bed thicknesses (16.3, 40.8 and 60.3 mm). The critical shear stresses (see Table 4.12a) obtained by extrapolation to zero bedload (i.e., C_v=10^{-8}) did not show any consistent dependency on bed thickness.

This may be due to the experimental error in the sediment rate values. As in the initiation of erosion experiments the sediment rates commonly measured were quite small, the sediment trap required longer measuring times (hours) with the consequent variation of water temperature. Even though the bedloads were averaged over three different measurements they still represent an average value in a given time interval, for the average flow conditions. However, as it is shown in Section 4.3.3.2 (Fig. 4.41 & 4.42), there are indications that the transport rate, for a given shear stress, increases with sediment bed thickness.

A multiple correlation was performed with the data and the entrainment function was found to be best described (see Fig. 4.29) by:

$$\frac{\tau_{bc}}{\rho(S_s - 1)gd} = 0.77 \left(\frac{Y_o}{P}\right)^{0.17} (\lambda_b)^{0.90} \left(\frac{Y_o + E}{D}\right)^{0.38} \qquad (4.17)$$

where τ_{bc} is the computed bed shear stress, ρ is the density of the water, S_s is the relative density of the sediments, g is the acceleration due to gravity, d is the particle size, Y_o is the normal flow depth, P is the wetted perimeter, λ_b is the computed bed friction factor, E is the sediment bed thickness and D is the channel diameter. Eq. 4.17 is valid for sand sizes $0.5 \leq d \leq 4.1$ mm, relative density $2.48 \leq \rho \leq 2.61$, and sediment bed thickness $E/D \cong 0.12$ (tested in the 154 mm diameter flume). Eq. 4.17 shows the importance of the channel shape in determining the critical conditions.

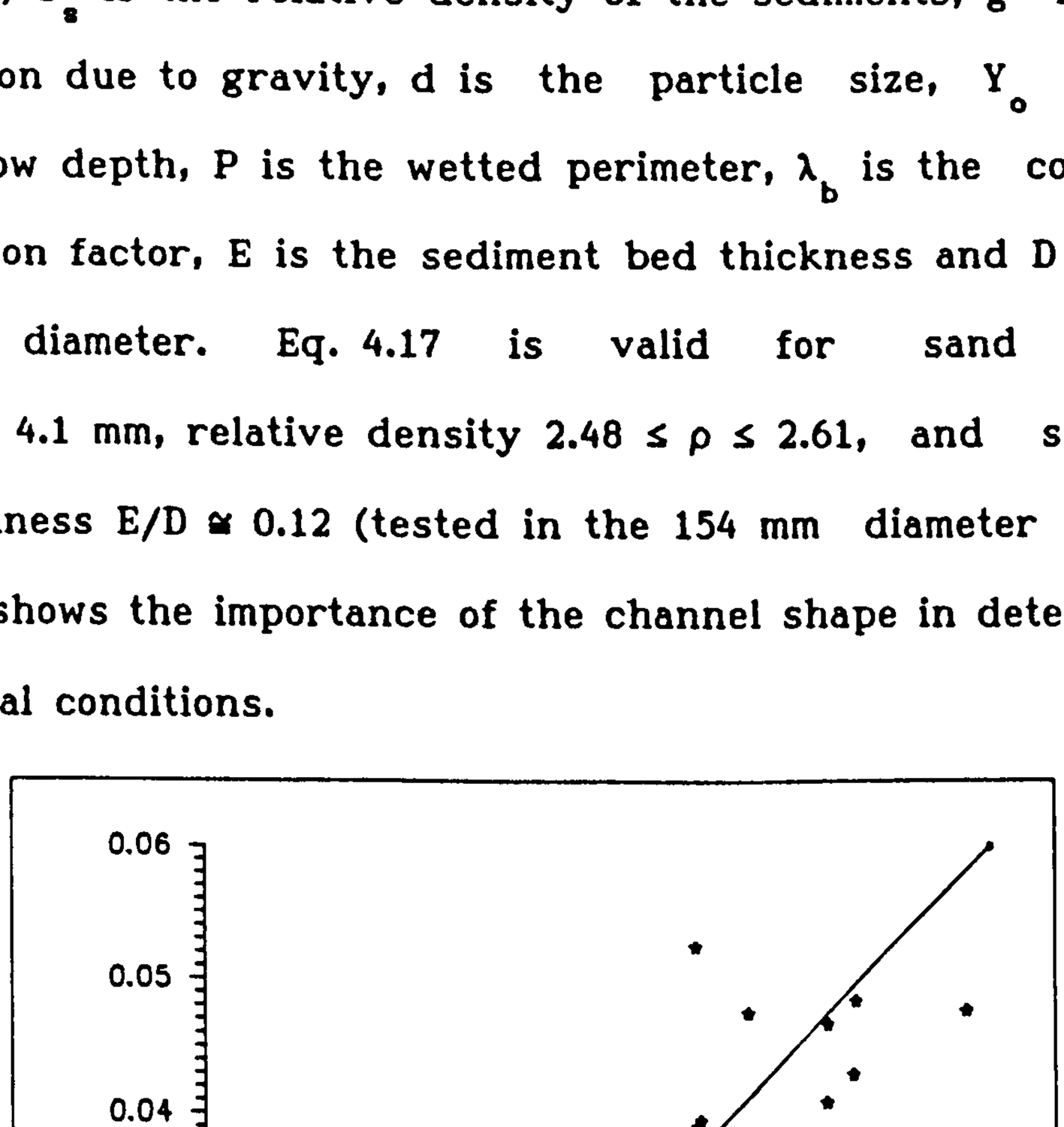

FIGURE 4.29: INITIATION OF EROSION EXPERIMENTS
Multiple regression of entrainment function

The critical Froude number of the particle (F_{dc}) was plotted against particle Reynolds number (Re_*) in Fig. 4.30a. Although there is considerable scatter a trend of increasing F_{dc} with Re_* can be observed as:

$$F_{dc} = \frac{V_c}{\sqrt{(S_s - 1)gd}} = 1.568\ Re_*^{0.077} \qquad (4.18)$$

with r^2=0.47, where V_c is the mean flow velocity for incipient motion, S_s is the relative density of the sediment, d is the particle size and g the acceleration due to gravity. Equation 4.18 was derived from experimental data with sand sizes $0.5 \leq d_{50} \leq 4.1$mm, relative density $2.48 \leq \rho \leq 2.61$, and sediment bed thickness E/D≅0.12, in a 154 mm diameter flume. The scatter in Fig. 4.30 may be explained by the channel shape, which influences critical velocity in a similar manner as it influences critical shear stress (previously discussed).

A better fit-regression was obtained (see Fig. 4.30b) correlating the dimensionless velocity with the shape factor (Y_o/P) the friction factor (λ), which shows that the shape factor is important in determining critical velocities. The expression obtained can be written as:

$$\frac{V_c}{\sqrt{(S_s - 1)gd}} = 1.69 \left(\frac{Y_o}{P}\right)^{0.22} (\lambda_b)^{-0.13} \qquad (4.19)$$

with r^2=0.69, which is valid for sand sizes $0.5 \leq d_{50} \leq 4.1$mm, relative density $2.48 \leq \rho \leq 2.61$, and sediment bed thickness E/D≅0.12 (tested in a 154 mm diameter flume).

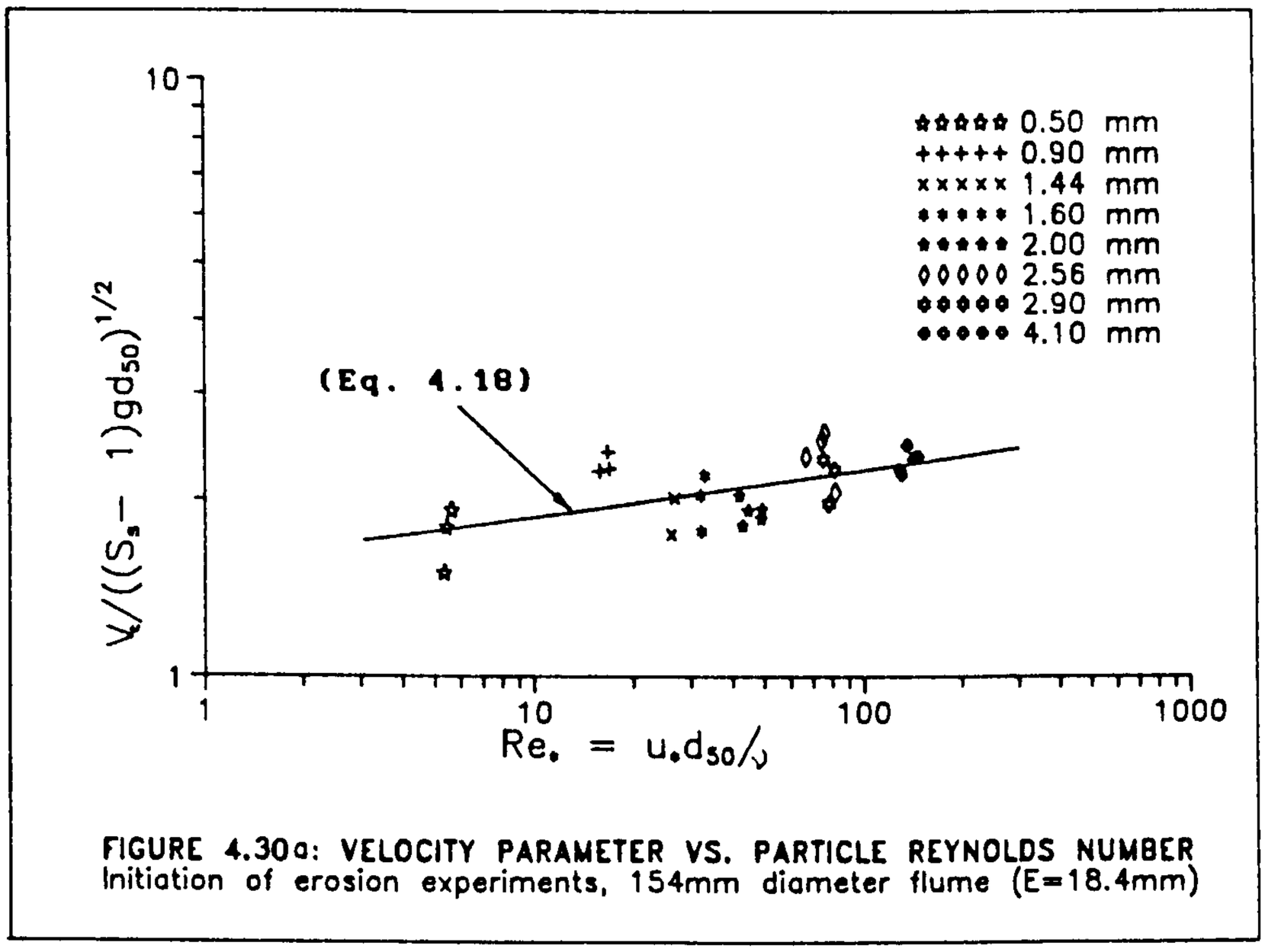

FIGURE 4.30a: VELOCITY PARAMETER VS. PARTICLE REYNOLDS NUMBER
Initiation of erosion experiments, 154mm diameter flume (E=18.4mm)

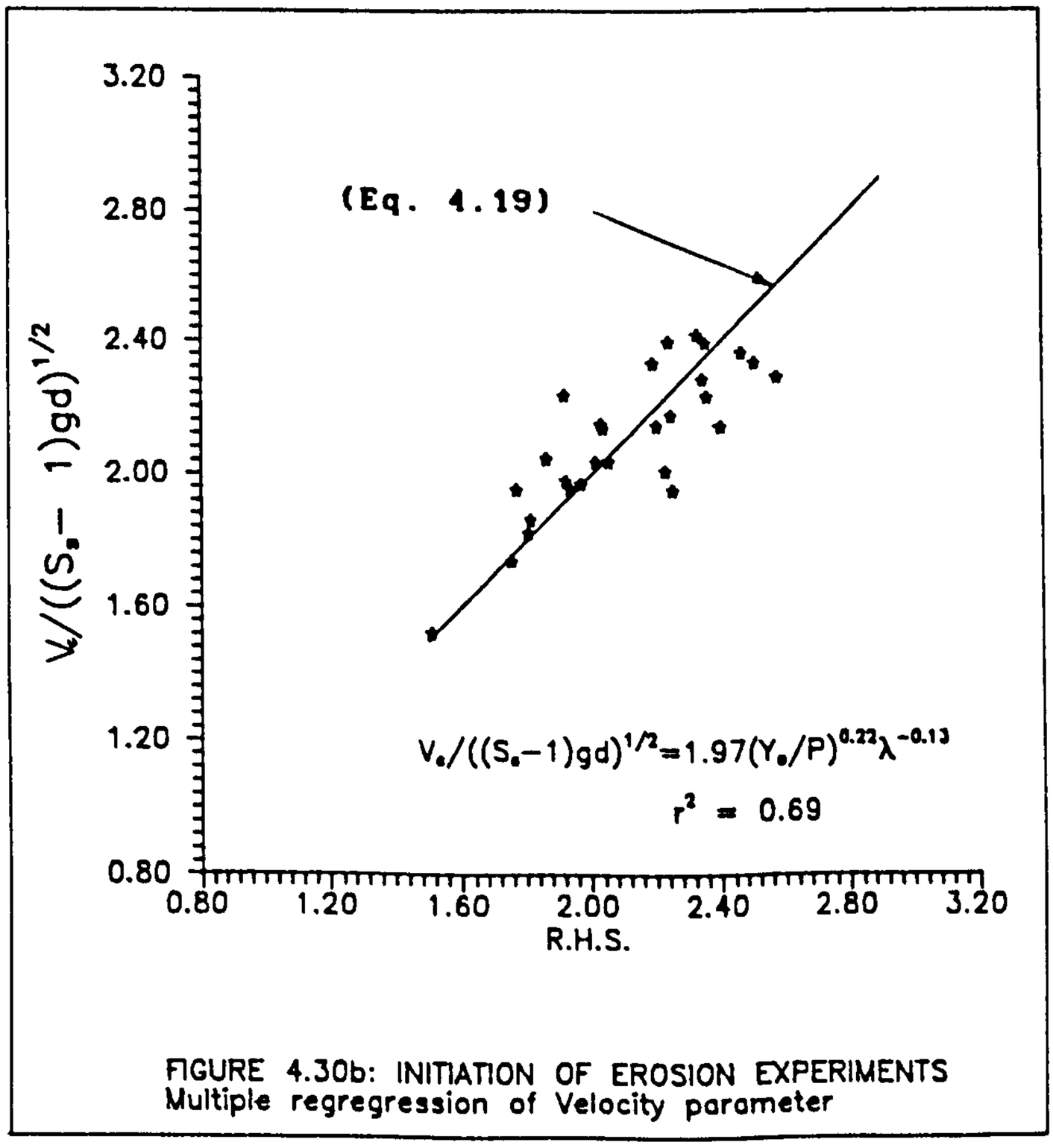

FIGURE 4.30b: INITIATION OF EROSION EXPERIMENTS
Multiple regregression of Velocity parameter

4.3.1.3 Graded Sand Beds

Initiation of erosion experiments were also carried out using mixed size sands as detected in type A and type C sediments granulometry (see Fig. 4.31). The experimental procedure was similar to that described for uniform sands. However, the sediments collected in the sediment trap were later separated by size fractions and the bedload for each fraction size was obtained. The critical shear stress was then determined by extrapolation to zero bed load. Because of the very small size of Type C sand (d_{50}= 0.12 mm) it was not practical to separate it into size fractions.

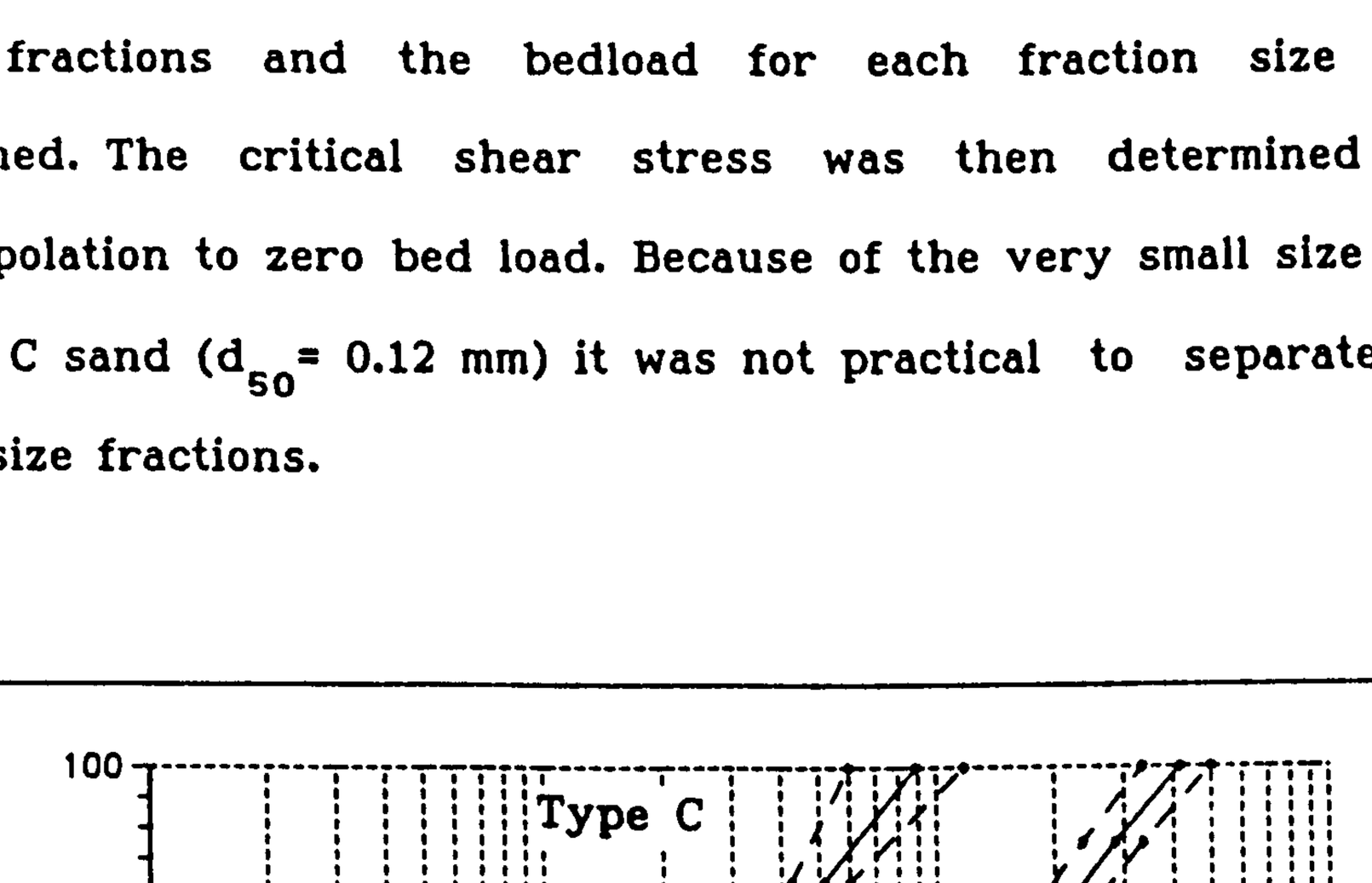

FIGURE 4.31: SIZE DISTRIBUTION OF TYPE A AND C SEDIMENT USED IN THE LABORATORY

The results obtained for Type A sand are shown in Table 4.12 b. A comparison of these results (Table 4.12b) with those obtained

using uniformly graded sands suggests the existence of interaction between the particles of different sizes (armouring and sheltering). The smaller size fractions show higher critical shear stresses and the larger size fractions lower critical shear stresses than those shear stresses corresponding to their respective uniform sizes.

4.3.2 Initiation of Erosion of Cohesive Sediments

4.3.2.1 Preliminary Experiments

The project was initially conceived to study the influence of cohesion on the movement of non-cohesive sediment in channels of circular cross-section. Therefore erosion experiments were carried out in the 154 mm diameter flume using sand with various additives such as china clay, oil, petroleum jelly, etc.

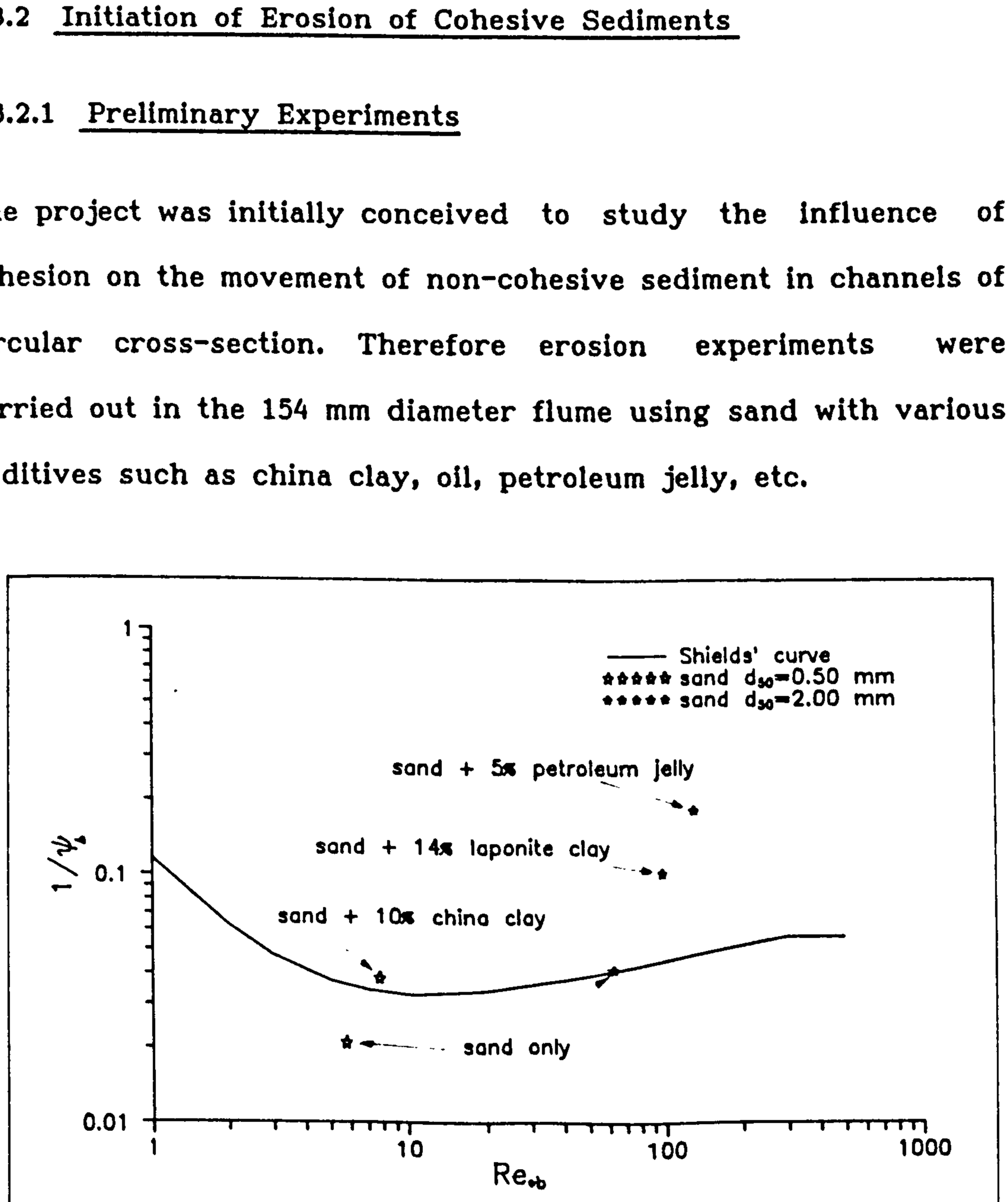

FIGURE 4.32: SHIELDS' DIAGRAM FOR INITIATION OF MOTION OF SAND WITH COHESIVE ADDITIVES
154 mm diameter flume (E = 18.4 mm)

All open channel flow tests were conducted in a manner similar to non-cohesive sediment tests (Sec. 4.3.1.2). However, sediments with cohesive additives required much higher shear stresses for initiation of erosion than non-cohesive sediments. This caused a sharp drop in the efficiency of the sediment trap. Also the mode of transport did not allow to establish sediment rates systematically. Critical shear stresses were then obtained most of the times by visual observation only.

The presence of cohesion in sediments has a marked influence on the incipient motion of the sediment beds (see Fig. 4.32). First the critical shear stresses are dramatically increased by several orders of magnitude (depending on the type and concentration of the cohesive additive). Second the mode of erosion is entirely different. Whereas a gradual entrainment process occurred in non-cohesive sediment beds, a violent collapse (see Fig. 4.33) of the entire sediment bed took place on cohesive sediment beds when the corresponding critical conditions were exceeded. It was observed that the cohesive sediment bed is eroded in clusters of various sizes that behave like non-cohesive sediment particles being carried downstream by the flow.

4.3.2.2 Sewer Sediment Analogues

The experimental results indicated an increase in critical shear stresses with the cohesive strength of the sediments. The type and concentration of the cohesive additive determined the critical conditions of a given sediment bed (see Fig. 4.32). The

interpretation and quantification of this effect in sewers depended on the mechanical, rheological and chemical properties of the actual sewer sediment.

An important objective of the project was to relate cohesive sediment behaviour in the laboratory to actual sewer sediment. However, as no practical information on the actual properties of in-sewer sediment was available it was not possible to generalize the results obtained with the various additives tested. It is necessary to relate the properties of the sediments used in flume experiments to the properties of sewer sediments in order to extrapolate the flume results. This forced a change in direction of the project concerning the selection of an artificial sewer sediment, as field and laboratory characterization of sewer sediments became essential.

From their laboratory study of real sewer sediments (see Sec. 2.3.2) from various locations in the U.K., Williams and Williams, (1988) suggested a synthetic sewer sediment for flume studies. This synthetic sewer sediment has rheological and chemical characteristics similar to that of actual sewer sediments. The sediment is a mixture of Laponite RD clay, sand and water (see Sec. 2.3.2).

Preliminary initiation of erosion experiments were carried out using similar synthetic sediment mixtures to those tested at Swansea (Williams and Williams, 1988). The test ranges for

initiation of erosion experiments were defined as follows:

Concentration of Laponite clay gel	18 - 40 g/l
Sand/clay gel ratio	0 - 100% by weight
Sand sizes (d_{50})	0.12 - 2.9 mm

A large number of erosion experiments using the synthetic sewer sediment for a wide range of combinations was carried out.

a) First spots of erosion beginning to appear
Q = 20.5 l/s, V = 1.18 m/s, τ_o = 3.7 N/m^2

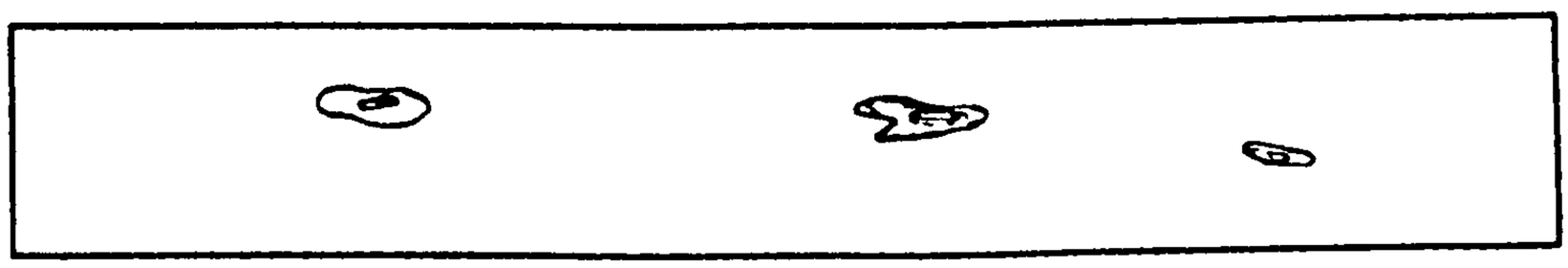

b) First spots of erosion increasing in size
Q = 22.2 l/s, V = 1.28 m/s, τ_{o1} = 4.09 N/m^2

c) Bed failure progressing very rapidly...(bed collapse)
Q = 23.3 l/s, V = 1.34 m/s, τ_{o2} = 4.55 N/m^2

Sample: 50% Laponite clay gel (c=25g/l)
50% Sand (90 - 150μm)

FIGURE 4.33: TYPICAL EROSION PATTERN OF THE SYNTHETIC SEWER SEDIMENT (154mm diameter flume E=18.4mm)

The same erosion pattern was observed in all cohesive sediment experiments. It started with some isolated spots of erosion, at mean shear stress τ_{01} followed by a sudden collapse of the bed for a small increment of the shear stress, at shear stress τ_{02} (see Fig. 4.33 and Plates 6 & 7). This process was also accelerated by the local turbulence produced by the macro roughnesses created by the eroded spots (see section 4.1.4).

It must be pointed out however, that the cohesive behaviour described above was observed only when the cohesive additive was present in adequate proportion. Depending on sand size this could vary between 5 to 15 % by weight. All sand particles need to be wetted by the clay solution before the cohesive bond can develop. It was also observed that for low clay concentration and small sand size mixtures a very small erosion process was taking place well before the appearance of the first spots of erosion and the collapse of the bed. This occurred as the surface layer of sand was slowly being detached particle by particle. This erosion process was only detected by operating the sediment trap for a long time. This phenomena could not be easily seen with the naked eye and did not seem to have any significance on the collapse of the bed.

The results show that for a given clay gel concentration there is an optimum sand/clay-gel proportion (see Figs. 4.34 and 4.36 and Tables 4.13 to 4.15) to achieve maximum resistance to erosion. Critical shear stresses were found to increase with clay gel concentration. Very often the critical shear stresses were beyond

the maximum values obtainable under open channel flow conditions and the tests had to be carried out under full pipe flow conditions (see Sec. 3.5.2.2).

For a given sand size the mean critical shear stress is found to be directly proportional to clay gel concentration. However, there seems to be an overall maximum critical shear stress value of around 6 - 7 N/m^2 (see Figs. 4.35 and 4.37).

The upper limit of 40 g/l of laponite clay gel used as cohesive additive in the experiments represents freshly deposited beds in sewers with slight consolidation (Type A sediment, Crabtree, 1988). The clay gel concentration of 18 g/l mixed with very fine sand represents a weak cohesive sewer sediment (Type C sewer sediment, Crabtree, 1988) with a maximum mean critical shear stress of around 2.5 N/m^2.

Table 4.16 shows a summary of the results covering the entire ranges of sand sizes and clay gel concentration tested. Only the optimum proportion (maximum critical shear stress) of sand and clay-gel is shown (Table 4.16) for each clay gel concentration used (see Figs. 4.35 and 4.37). More details of the individual runs can be found in Appendix G.

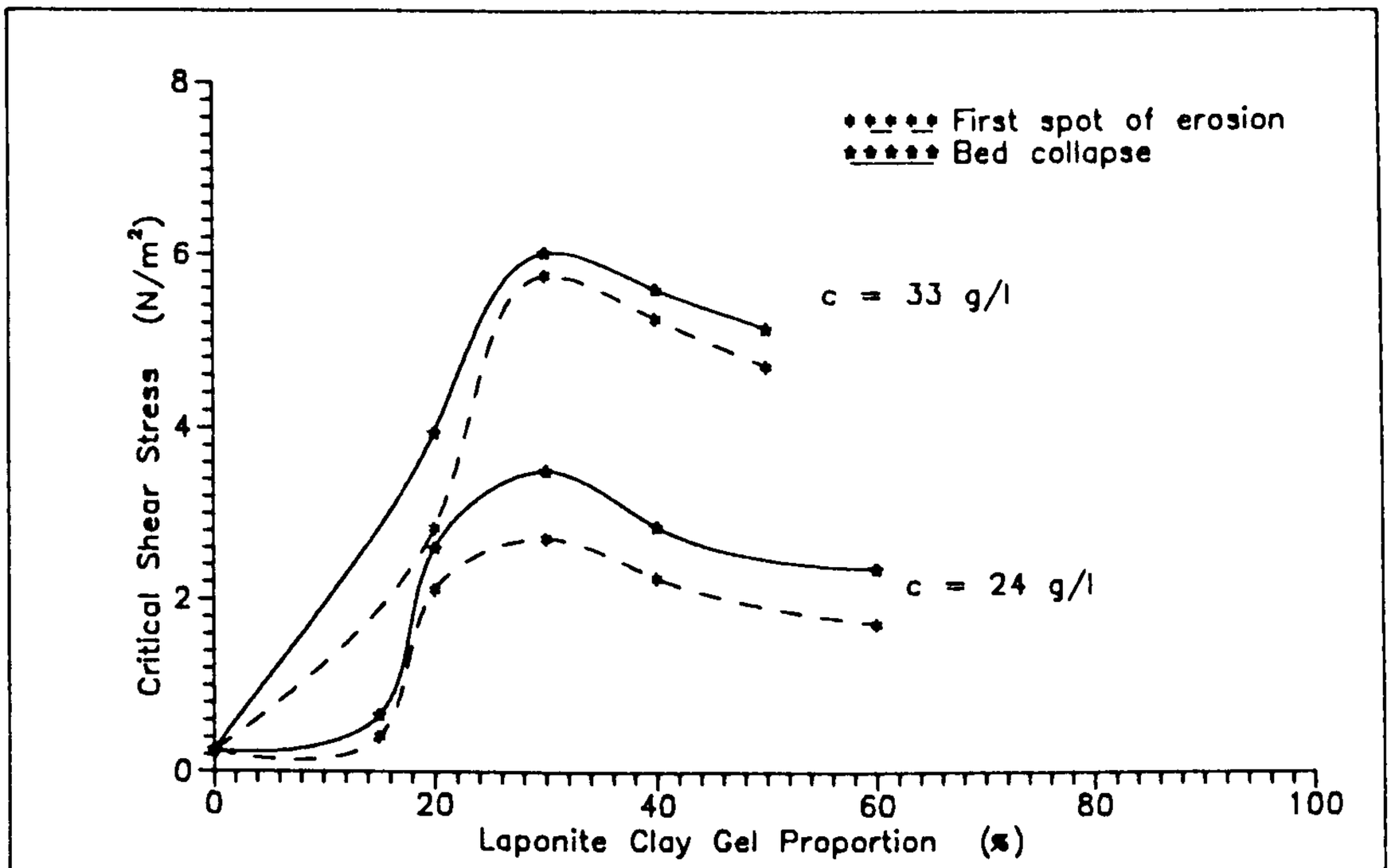

FIGURE 4.34: CRITICAL SHEAR STRESS VS. CLAY GEL – SAND PROPORTION
Mixture: sand d_{50}=0.89mm and clay gel conc. 24 and 33g/l

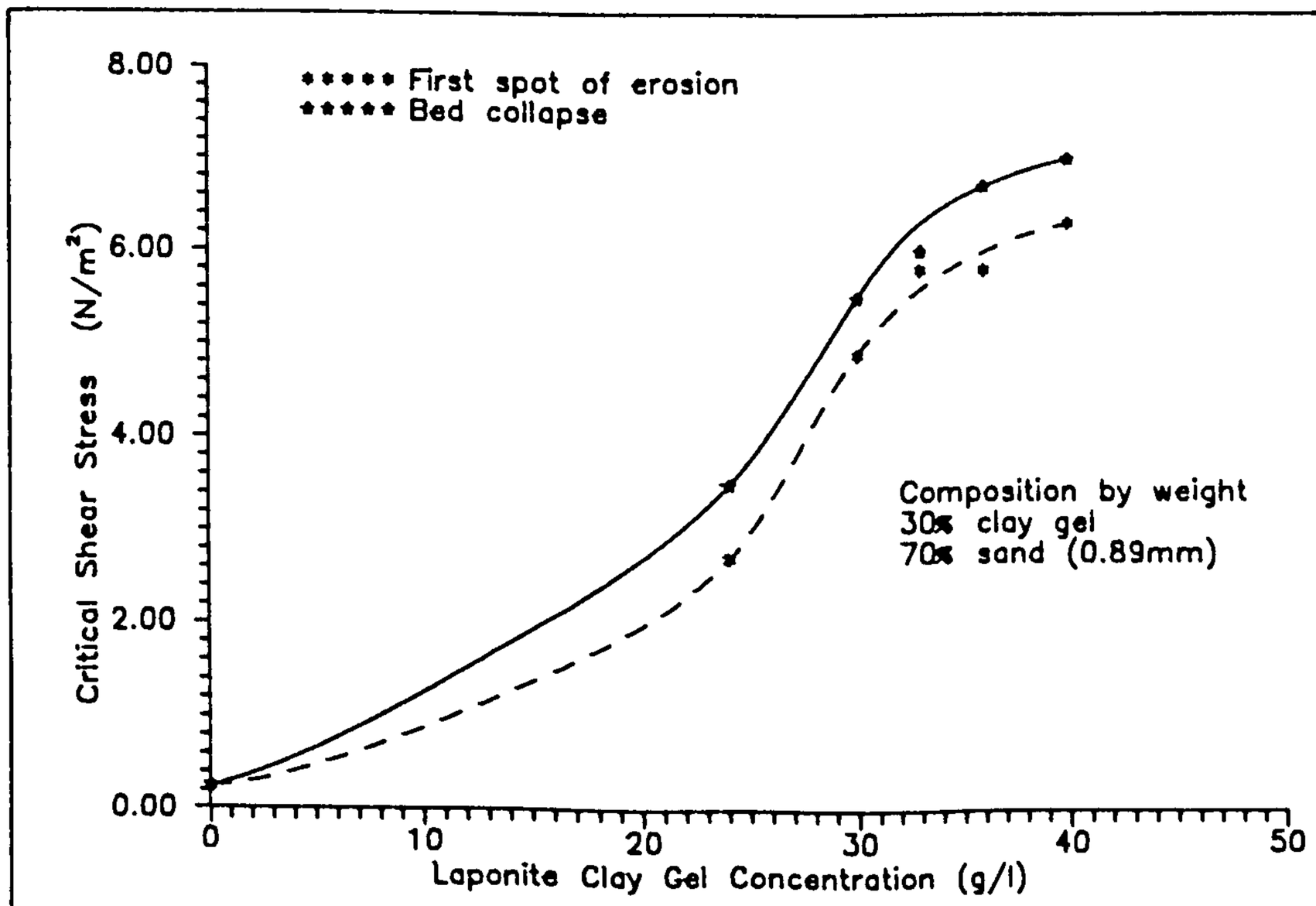

FIGURE 4.35: CRITICAL SHEAR STRESS VS. CLAY GEL CONCENTRATION
Optimum sand – clay gel proportion values (sand d_{50}=0.89mm)

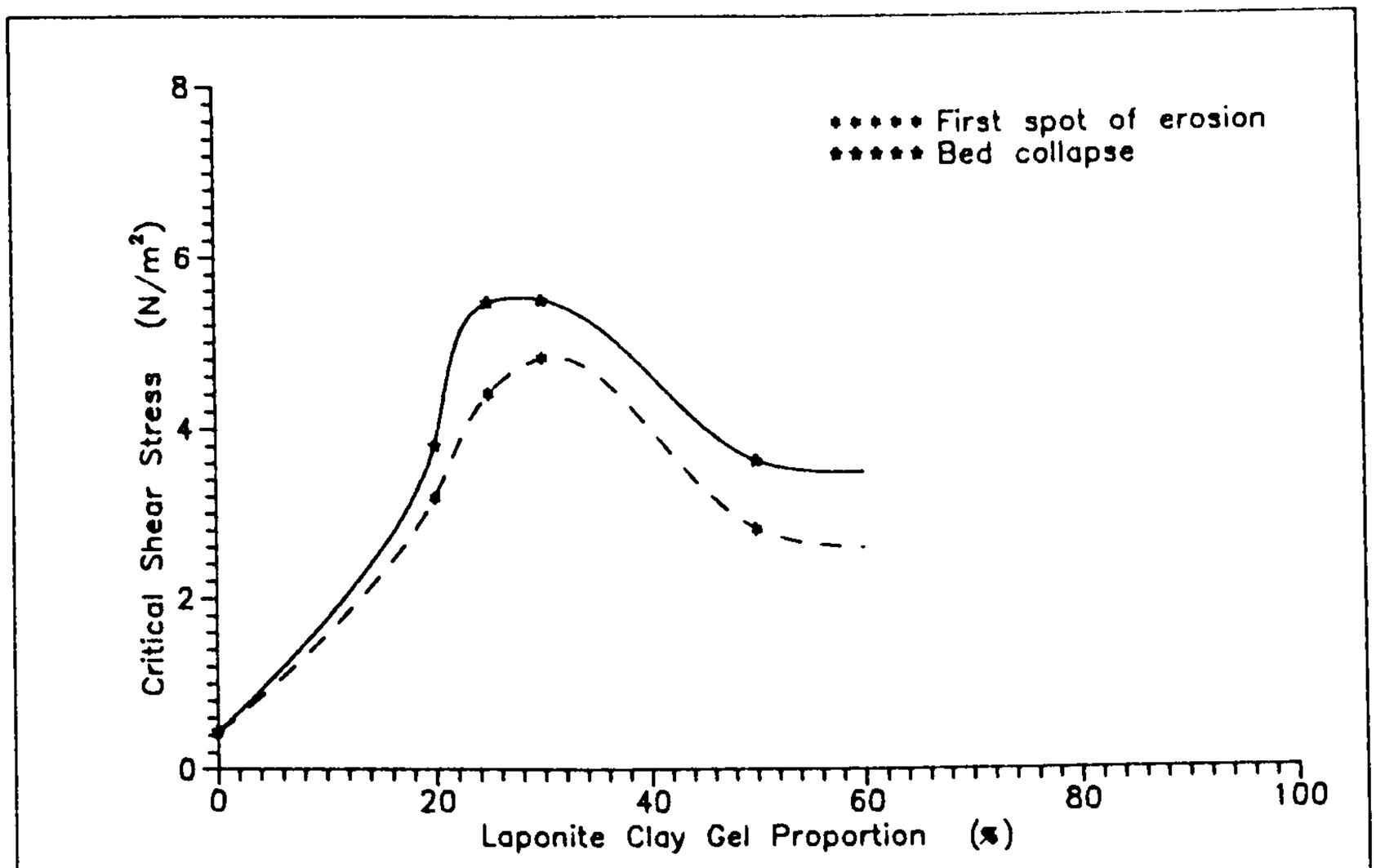

FIGURE 4.36: CRITICAL SHEAR STRESS VS. CLAY GEL – SAND PROPORTION
Mixture: sand d_{50}=1.44mm and clay gel concentration 30g/l

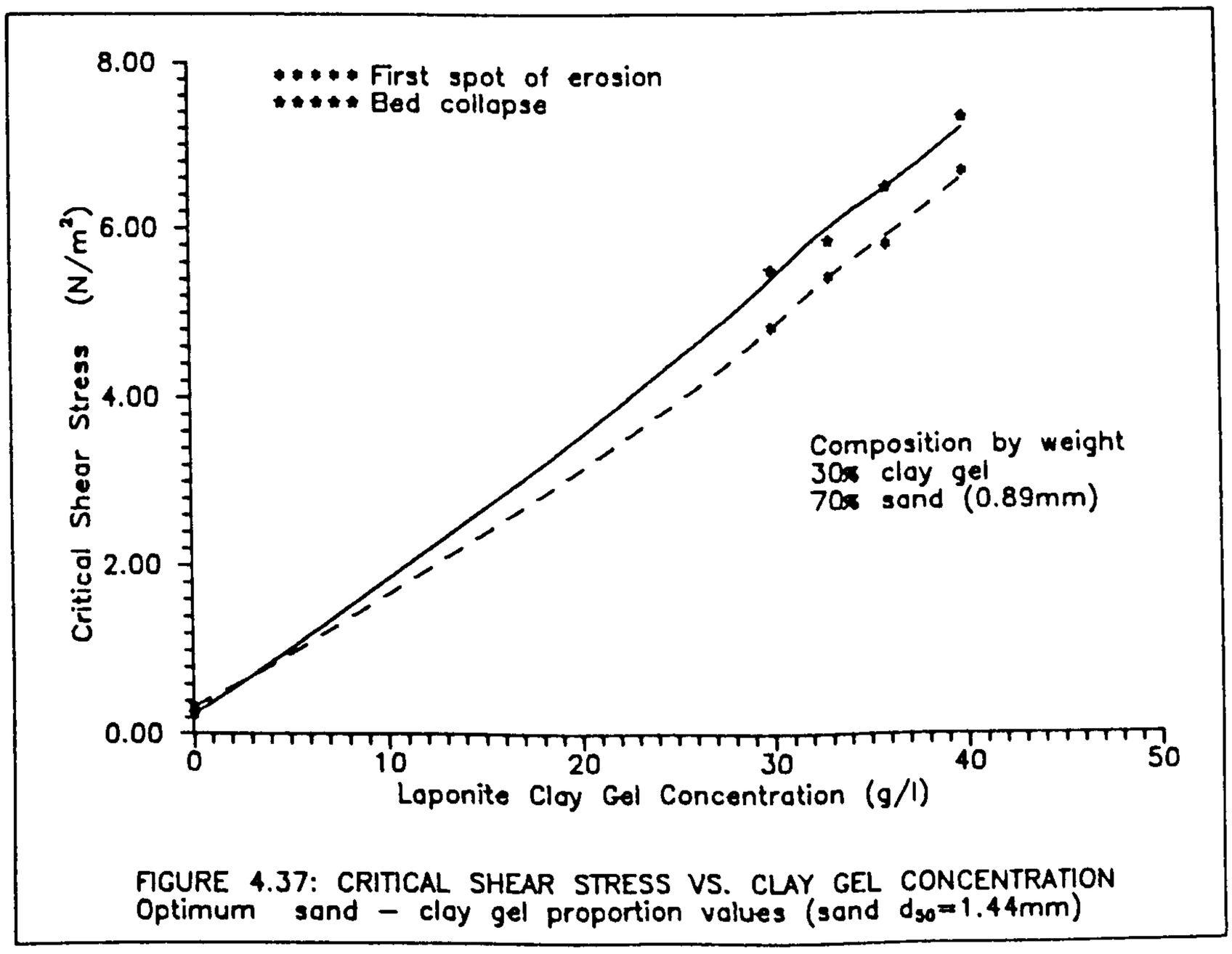

FIGURE 4.37: CRITICAL SHEAR STRESS VS. CLAY GEL CONCENTRATION
Optimum sand – clay gel proportion values (sand d_{50}=1.44mm)

4.3.3 Transport Experiments over Loose Beds

4.3.3.1 Selection of Parameters

Conducting a similar dimensional analysis as Sec. 4.3.1.1 the relevant dimensionless parameters describing sediment transport are selected. The transport of sediment particles by water can be determined by such characteristic parameters as: the water density (ρ), the dynamic viscosity of the water (μ), the mean size of the particles (d), the flow depth (Y_o), the shear velocity of the flow (u_*), particle shape factor (SF_p), channel shape factor (SF_c), the density ($\rho)_s$ and buoyant specific weight ($\gamma_s - \gamma$) of the sediment, in which (γ_s) is the specific weight of the sediment and (γ) is the specific weight of the water, and the bedload (q_s) in volume per unit width per unit time. A functional relation can be written in the form:

$$F\{\rho, \mu, \rho_s, d, Y_o, u_*, SF_p, SF_c, (\gamma_s - \gamma), q_s\} = 0 \qquad (4.20)$$

Buckingham π-theorem was employed with the selected basic parameters d, ρ and u_* (which obviously have independent dimensions), and 7 dimensionless parameters were found. Thus the functional relation can be expressed as:

$$F1\left\{\frac{u_* d}{\nu}, \frac{\rho u_*^2}{(\gamma_s - \gamma)}, \frac{Y_o}{d}, \frac{\rho_s}{\rho}, SF_p, SF_c, \frac{q_s}{u_* d}\right\} = 0 \qquad (4.21)$$

For similar reasons to that of the previous section (Sec. 4.3.1.1) the parameters Y_o/d, S_s, and SF_p can be excluded from the analysis and SF_c can be represented by (Y_o/P).

Thus the functional relation (Eq. 4.21) becomes:

$$F2\left\{\frac{u_* d}{\nu}, \frac{\rho u_*^2}{(\gamma_s - \gamma)}, \frac{Y_o}{P}, \frac{q_s}{u_* d}\right\} = 0 \qquad (4.22)$$

in which $q_* = \frac{q_s}{u_* d}$ is Kalinske's transport parameter (Kalinske, 1947). Einstein (1942) in his probabilistic bedload model used the dimensionless parameter:

$$\phi = \frac{q_s \rho^{1/2}}{\sqrt{(\gamma_s - \gamma) d^3}} \qquad (4.23)$$

where ϕ is the well known Einstein (1942) transport parameter, q_s is the bedload in volume per unit time per unit width, ρ is the water density, γ_s is the specific weight of the sediment, γ is the specific weight of the water and d is the diameter of the particles. The bedload q_s can be replaced in terms of the volumetric concentration C_v to obtain Eq. 2.16 as:

$$\Phi = \frac{C_v V R}{\sqrt{(S_s - 1) g d^3}} \qquad (2.16)$$

The functional relation can then be written as:

$$F4\left\{Re_*, \frac{1}{\psi}, \frac{Y_o}{P}, \phi\right\} = 0 \qquad (4.24)$$

4.3.3.2 Non-cohesive Sediments Experiments

Transport experiments using sand of various sizes were carried out in the 154 mm diameter flume. The bed was formed with loose sand and subjected to erosion under uniform flow conditions. Dried sand of the proper size was fed from the upstream end of the sediment bed at a constant rate using a vibration sediment

feeder (see Fig. 3.12). The input sediment rate was adjusted to match the rate of transport of the flume. After reaching equilibrium conditions (sediment transport) the flow was slowly stopped and the channel drained. Then using a moveable point gauge (see Fig. 3.14) inside the pipe the bed formation was measured along the entire sediment bed. The results obtained are summarised in Table 4.17. A comparison of the experimental results with those corresponding to wide channel is shown in Figs. 4.38 to 4.40.

In Fig. 4.38 the data is plotted in Kalinske's diagram in terms of the dimensionless transport rate (q_*) and the relative shear stress (τ_c/τ_o). The data plotted in Fig. 4.38 show considerable scatter, which is greatly reduced by using the separated values (τ_b , τ_{bc} and u_{*b} computed employing Einstein-Vanoni's separation technique). The data does follow a definite trend, which can be described by:

$$\frac{\tau_{bc}}{\tau_b} = 0.738 \exp\left\{ \frac{-5.61\ q_s}{u_{*b}\ d_{50}} \right\} \qquad (4.25)$$

where q_s is the bedload in volume per unit time per unit width, u_{*b} is the shear velocity related to the bed, and τ_b and τ_{bc} are the bed shear stress of the flow and the critical bed shear stress of the particle respectively. Equation 4.25 was derived from experimental (uniform open channel flow) data obtained in a 154 mm diameter flume and it is valid for sand sizes $0.53 \leq d_{50} \leq 2.9$ mm and sediment bed thicknesses $0.08 \leq E/D \leq 0.391$.

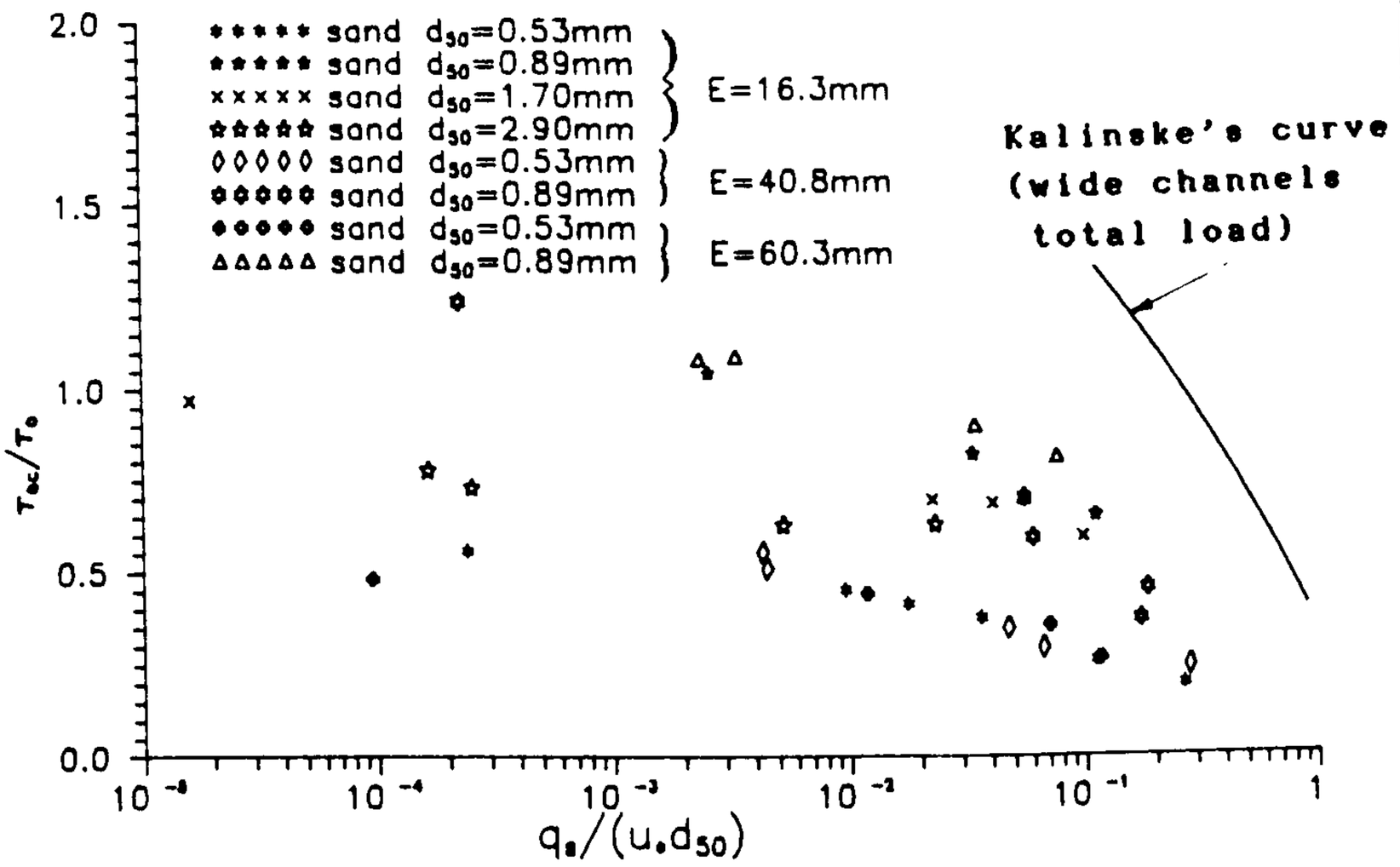

a) MEAN VALUES

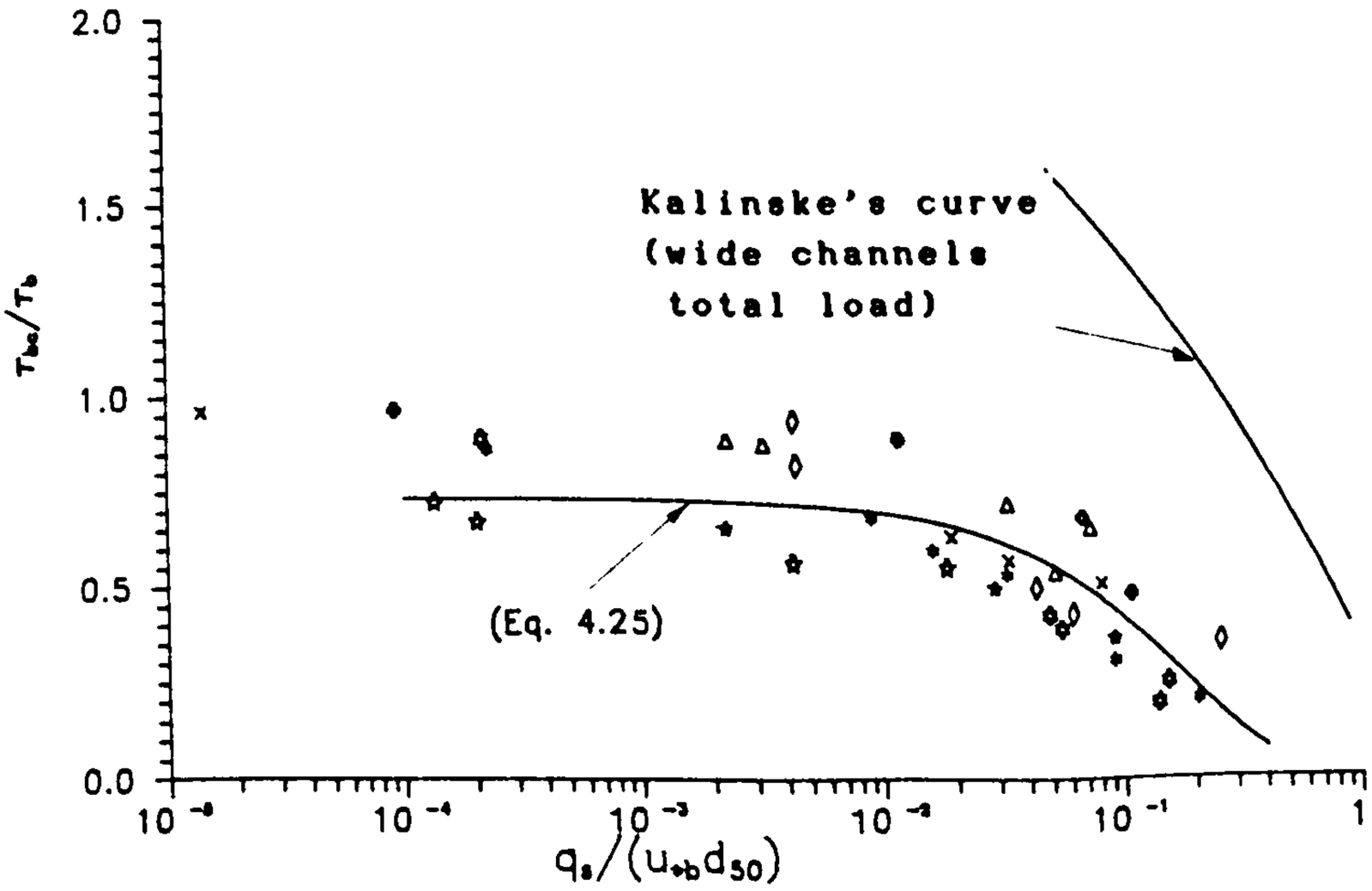

b) SEPARATED VALUES

FIGURE 4.38: NON-COHESIVE SEDIMENT TRANSPORT OVER LOOSE BEDS KALINSKE DIAGRAM (154 mm diameter flume with sediment bed)

The data does not agree with Kalinske's curve (see Fig. 4.38), because first, Kalinske takes into consideration total load, and second his critical conditions are different to the ones used by the author. Kalinske defined critical conditions for a rather high level of sediment transport (i.e., $\frac{g_s}{u_* d} = 0.25$), which also included suspended loads. This is equivalent to a sediment volumetric concentration (C_v) of about 10^{-4} and in the present study the critical conditions were defined at $C_v \cong 10^{-8}$.

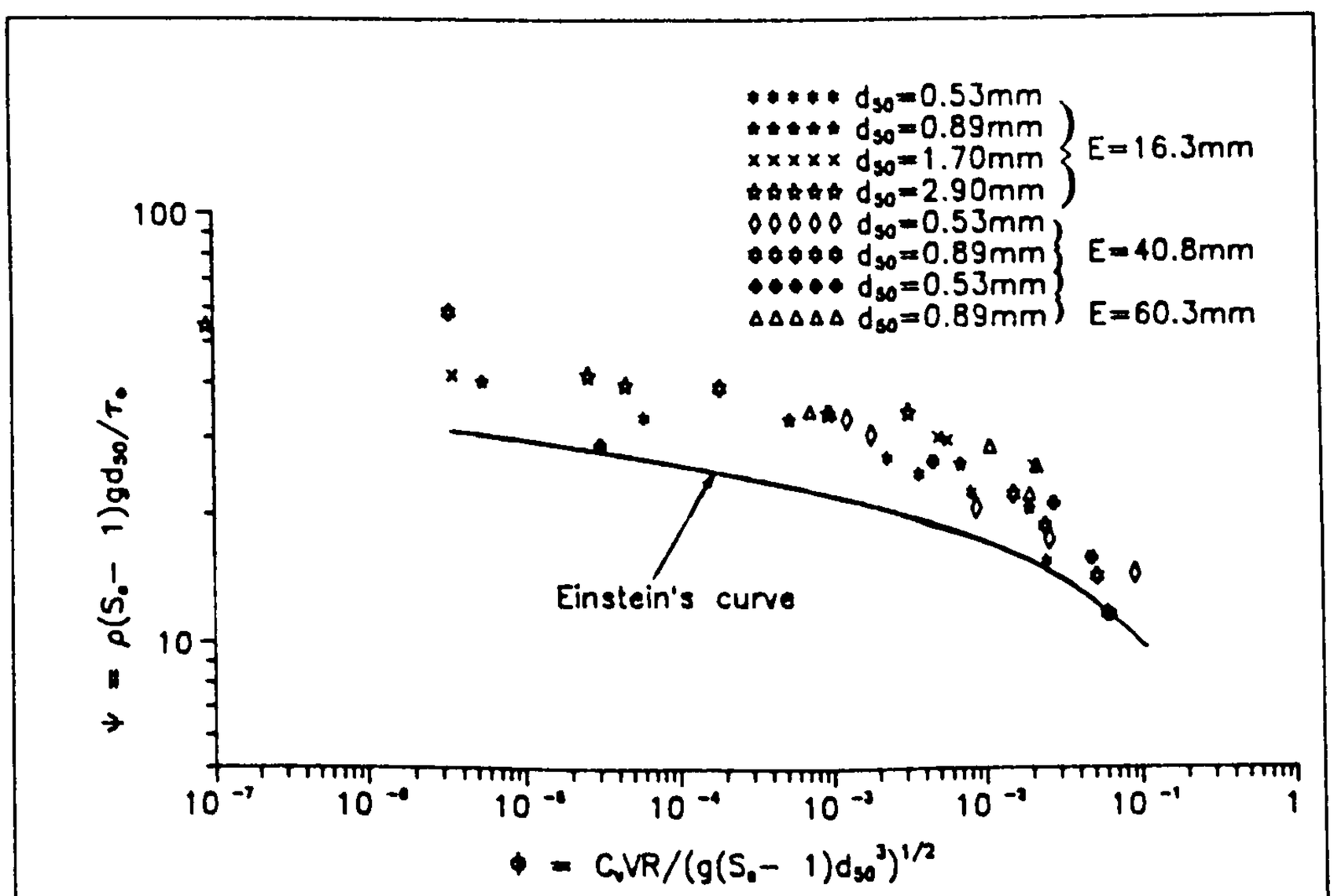

FIGURE 4.39: SEDIMENT TRANSPORT OVER LOOSE BED
Einstein Bedload Function (154mm diameter flume)
Mean values

The data is plotted (Fig. 4.39) in terms of the transport parameter ϕ (Eq. 2.16) and the flow intensity parameter, ψ (Eq. 2.17) in an Einstein bedload diagram using mean values (τ_o, R, ϕ and ψ). The points fall above Einstein bed-load curve. The agreement is not good especially for the low flows. However, when

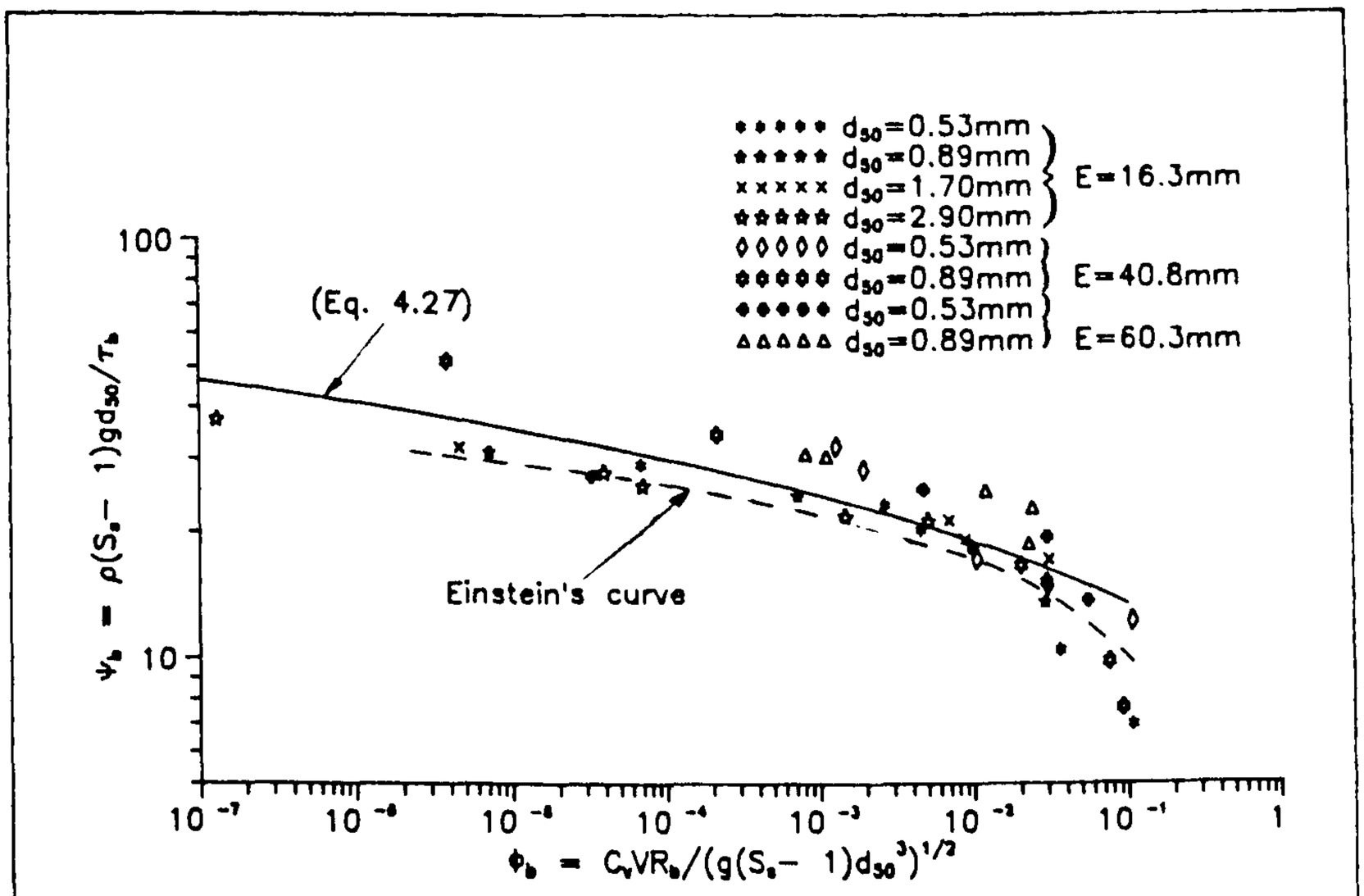

a) LOGARITHMIC EQUATION FIT

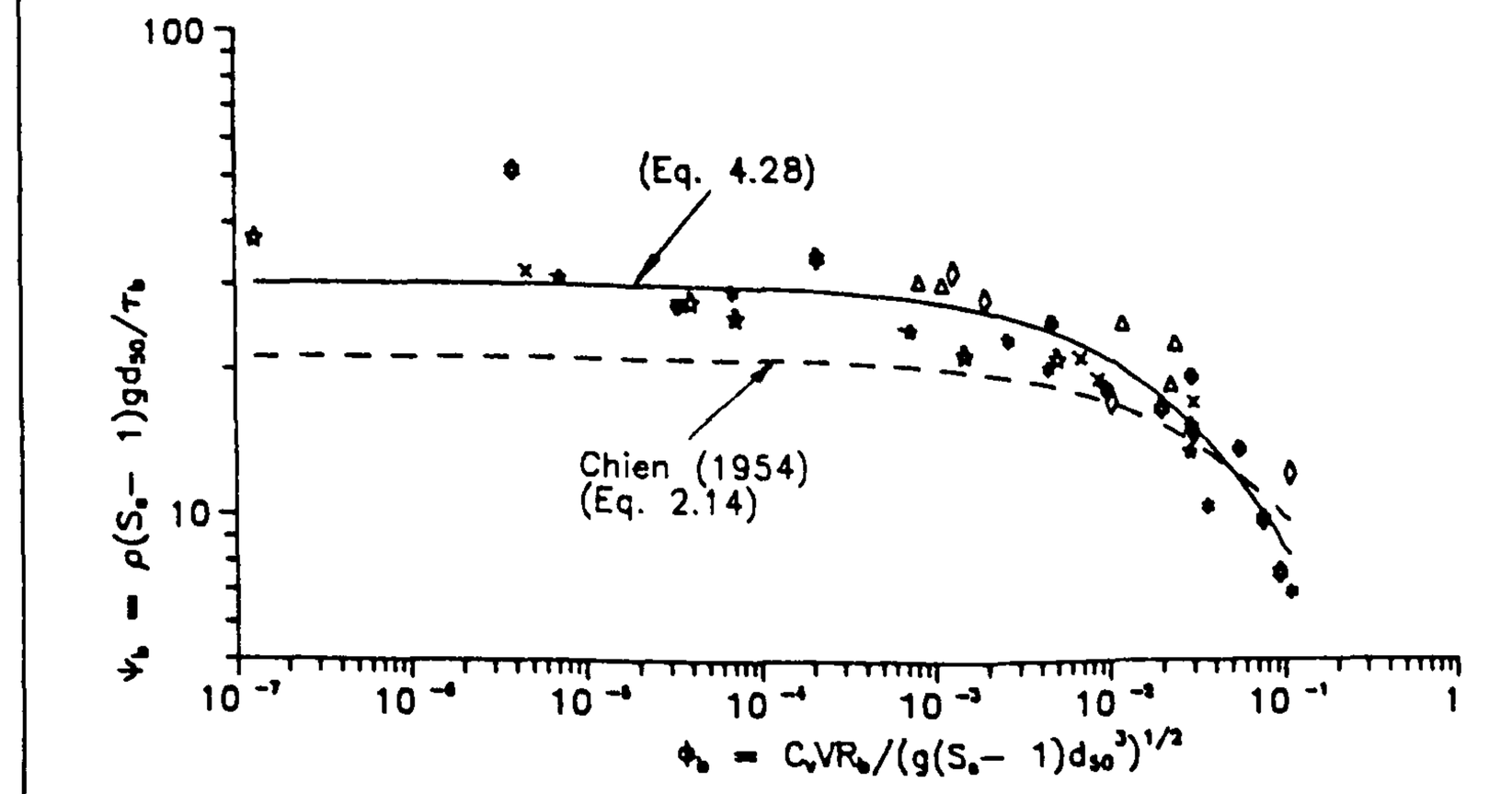

b) NON-LINEAR EQUATION FIT

FIGURE 4.40: SEDIMENT TRANSPORT OVER LOOSE BED
Einstein Bedload Function (154mm diameter flume)

separated bed values (τ_b, R_b, ϕ_b and ψ_b) are used the data is closer to Einstein bed-load curve, but it is still above it. This suggests that in channels of circular cross-section with sediment bed the transport capacity is greater than in wide rectangular alluvial channels under similar hydraulic conditions (see Fig. 4.40-a).

By using the method of least square a power equation was fitted to the data as:

$$\psi_b = 9.931\ \phi_b^{-0.123} \tag{4.26}$$

which has a low correlation coefficient (r^2=0.62). The subscript b indicates that the values of the shear intensity and transport parameters are computed using the values relevant to the bed (i.e., Einstein-Vanoni's separation technique). Using a logarithmic equation yields:

$$\psi_b = -2.47\ \ln \phi_b + 7.4 \tag{4.27}$$

which has a better correlation (r^2=0.70) as it is apparent in Fig. 4.40-a). A curve which resembles Eq. 2.14 (Chien, 1954) can also be fitted to the data as:

$$\psi_b = \frac{1.937}{(\phi_b^{2/3} - 0.188)^{1.644}} \tag{4.28}$$

which shows a better correlation (r^2=0.82) and does represent the data better (see Fig. 4.40b). Equations 4.26 to 4.28 were derived from experimental (uniform open channel flow) data obtained in a 154 mm diameter flume and it is valid for sand sizes $0.53 \leq d_{50} \leq 2.9$ mm and bed thicknesses $0.08 \leq E/D \leq 0.391$.

The influence of sediment bed thickness on sediment transport is illustrated in Figs. 4.41 and 4.42, where the bedload is plotted against bed shear stress for the various bed thicknesses used, for the sand sizes 0.53 and 0.89 mm respectively. It is apparent in Fig 4.41 that for similar levels of shear stress the transport rate (weight per unit time per unit width) increases with bed thickness. Although in Fig. 4.42 (d_{50}= 0.89 mm) there is not a clear distinction between the curves corresponding to bed thickness 16.3 and 40.8 mm, the general trend is the same. However, as the bedload decreases (towards critical conditions) there is not a clear relation between critical shear stress and sediment bed thickness as the curves tend to cross and overlap.

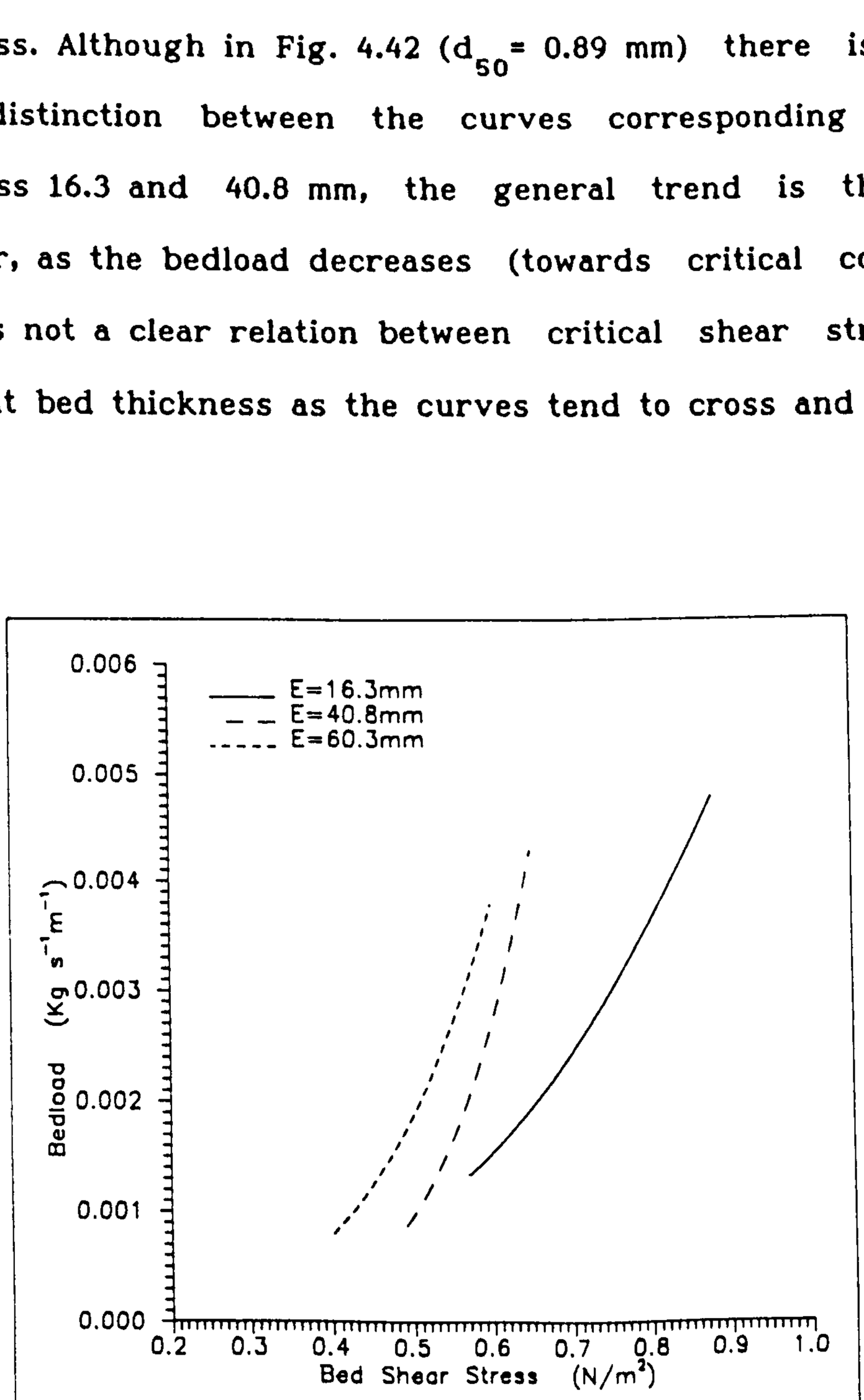

FIGURE 4.41: BEDLOAD VS. SHEAR STRESS AND SEDIMENT BED THICKNESS, sand d_{50}=0.53mm 154mm diameter flume

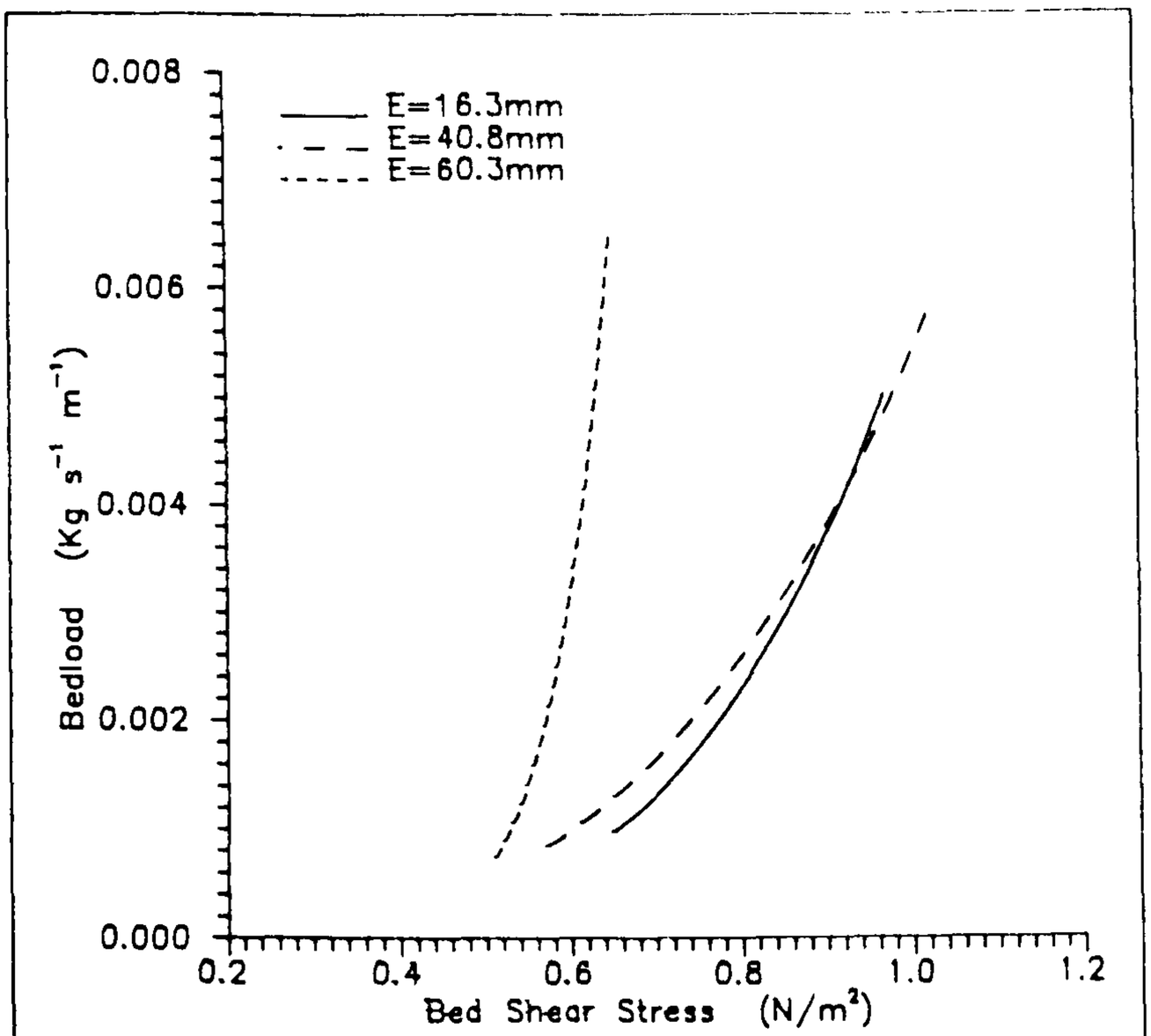

FIGURE 4.42: BEDLOAD VS. SHEAR STRESS AND SEDIMENT BED THICKNESS, sand d_{50}=0.89mm 154mm diameter flume

4.3.3.3. Bedforms

a) Classification of Bedforms

Sand dunes and ripples were observed for the various flow conditions (see Plate 8). In spite of the small amount of data available an attempt has been made to compare the measured bedforms characteristics with other studies (Figs. 4.43 to 4.46).

In Fig. 4.41 the data is plotted in a Shields' diagram. According to Shields (see Fig. 2.7 in Sec. 2.1.1.2c) the bedforms are in the transition zone between ripples and dunes. Obviously all points fall above Shields' curve as the shear stresses exceed the critical conditions.

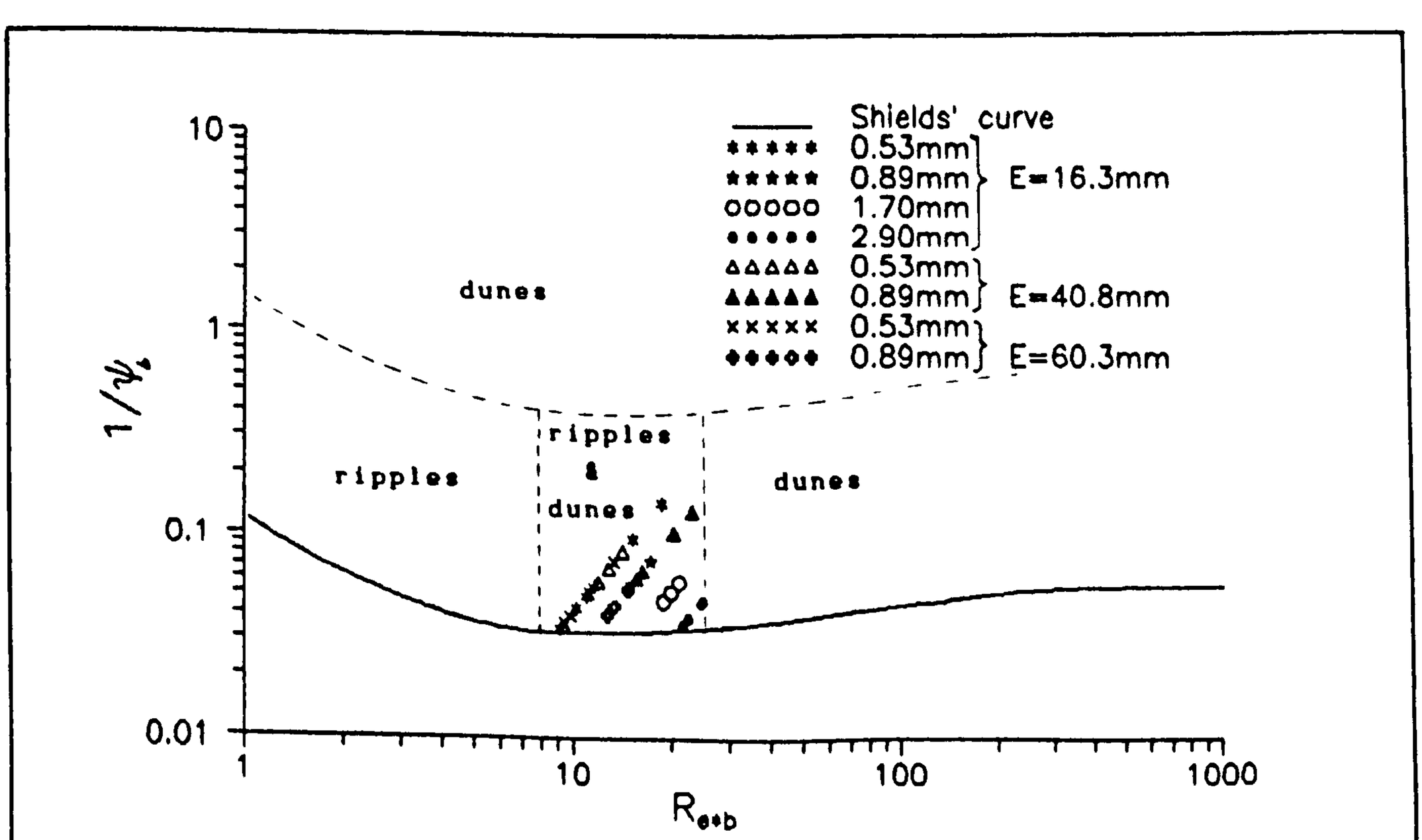

FIGURE 4.43: SHIELDS' DIAGRAM - BEDFORMS CLASSIFICATION (Sediment Transport Over Loose Beds (154mm dia. flume with sediment bed)

Ripples and dunes were observed on experiments with sand sizes 0.53 and 0.89 mm . However with sand sizes 1.7 and 2.9 mm larger bedforms were observed; sometimes the whole test section was occupied with one or two wavelengths (see Table 4.17).

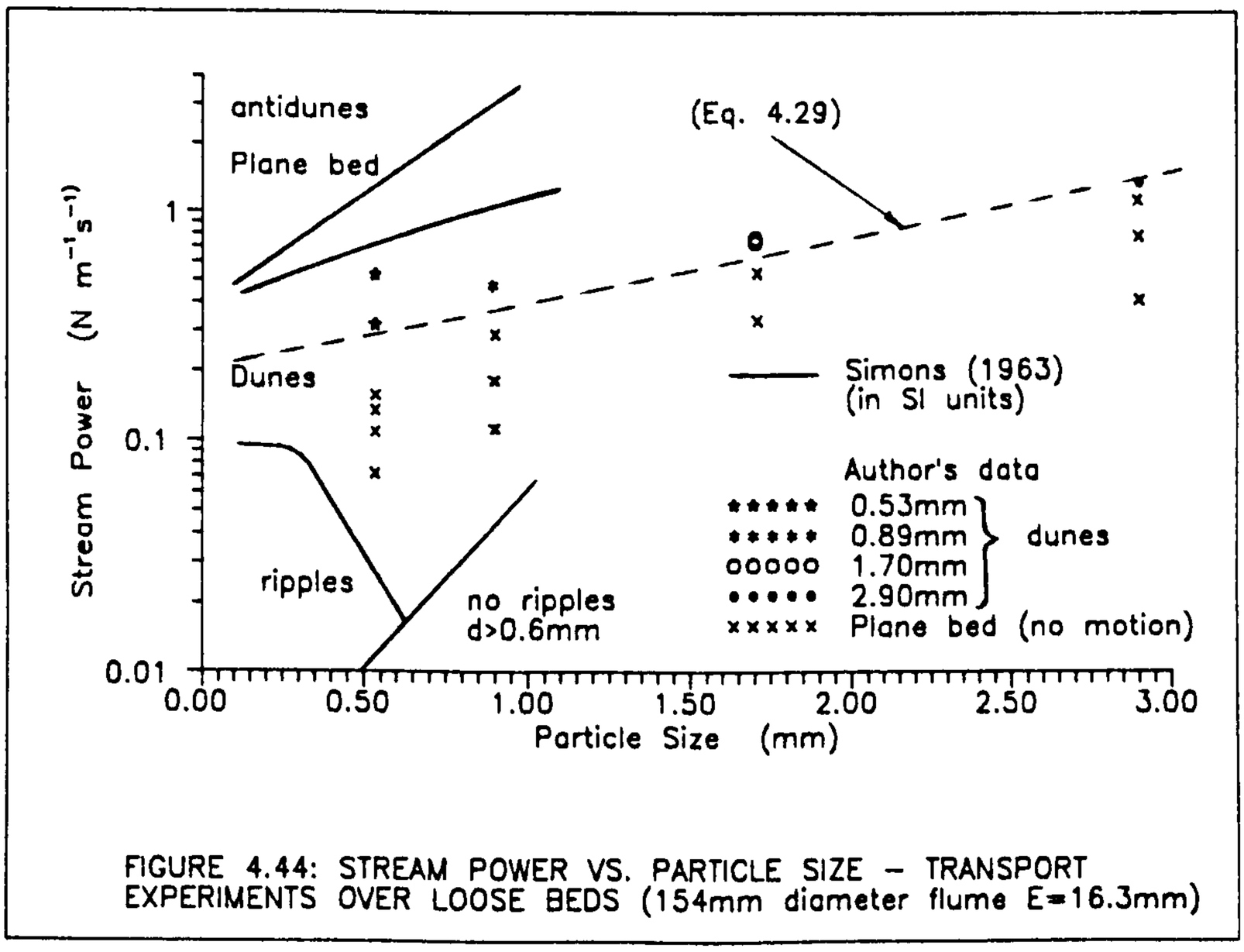

FIGURE 4.44: STREAM POWER VS. PARTICLE SIZE – TRANSPORT EXPERIMENTS OVER LOOSE BEDS (154mm diameter flume E=16.3mm)

Fig. 4.44 shows a plot of stream power ($\tau_b V$) against sand size (d_{50}) for a sediment bed thickness of 16.3 mm. In order to compare the results with those obtained by Simons et al. (1963) (Fig. 2.8), the values were converted to S.I. units (see Fig. 4.44). The data fall in the zone of dunes (0.53 and 0.89 mm sands) of Simons et al. (1963). However, he uses the median fall diameter instead of the mean particle size (d_{50}). The boundary (dashed line in Fig. 4.44) delimiting the zone of plane bed (after initiation of erosion) from the zone of bedforms (dunes)

is given by:

$$\tau_b V = (1/5)\ 10^{284d} \qquad (4.29)$$

where d is the particle size in (m), τ_b the bed shear stress in (N/m^2) and V the mean flow velocity in (m/s). Equation 4.29 was derived from experimental (uniform open channel flow) data obtained in a 154 mm diameter flume and it is valid for sand sizes $0.53 \leq d_{50} \leq 2.9$ mm and relative sediment bed thickness E/D=0.08.

The results obtained with 0.53 and 0.89 mm sand, which were tested with three different bed thicknesses suggest that the boundary between plane bed (after initiation of motion) and dunes is dependent on sediment bed thickness. As the bed thickness increases the boundary seems to go down towards Simons' values (see Fig. 4.44) for wide channels.

Another classification of bedforms is that of Van Rijn (1988). He uses the dimensionless grain number D_* (Eq. 2.24) and the transport parameter T (Eq. 2.25) that were described in Sec. 2.1.1.2c. The observed values are plotted in Fig. 4.45 and it can be seen that for sand sizes 0.89 and 1.7 the limit between plane bed (no motion) and dunes is between $T \approx 0.25$ and 0.45. However, for the smaller sand (d_{50}= 0.53mm) that limit corresponds to $T \approx 1.8$ and for the larger sand (d_{50}= 2.9mm) is $T \approx 0.6$. This agrees with the observations of Van Rijn (1988). Obviously the boundary separating the state of plane bed (no motion) and the zone of dunes is dependent on particle size as do

the critical conditions for initiation of motion. According to Van Rijn classification no ripple should be formed with the sands used in the tests.

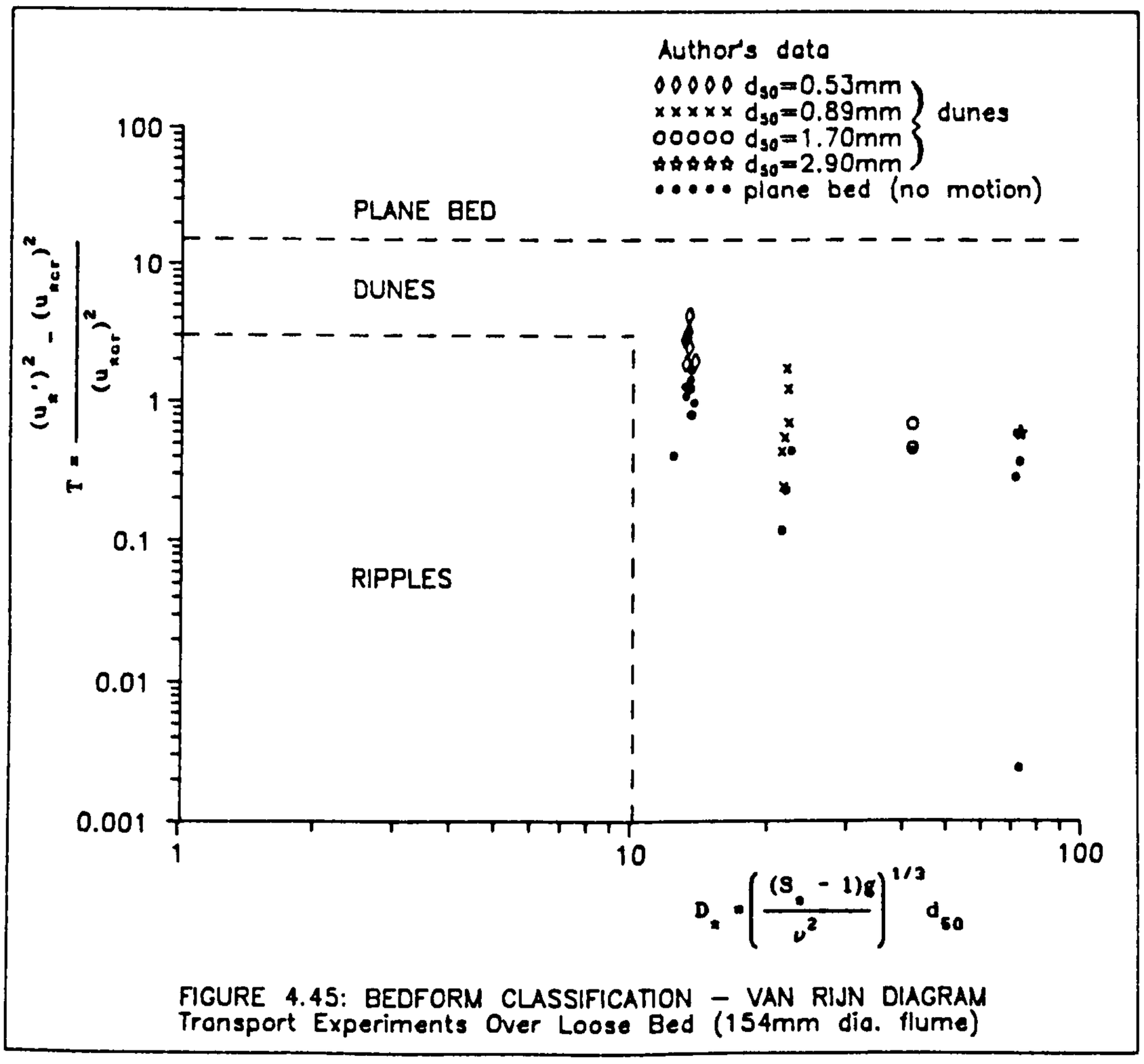

FIGURE 4.45: BEDFORM CLASSIFICATION – VAN RIJN DIAGRAM
Transport Experiments Over Loose Bed (154mm dia. flume)

b) Bedforms Dimensions

Bedforms, as mentioned in Sec. 2.1.1.1-c, consist of statistically periodic irregularities, which influence the behaviour of the flow and transported material. In spite of the limited number of measurements, an attempt was made to quantify bedform dimensions in channels of circular cross-section with sediment bed.

The bedforms height (Δ) and length (L) given in Table 4.17 are the averages values of the measurements made along the flume on the entire test section after each run was stopped. After trying several correlations an expression for dune height was found as:

$$\frac{\Delta}{Y_o} = 1.349 \left(\frac{d}{Y_o}\right)^{0.397} \left(\frac{Y_o}{P}\right)^{0.383} T^{-0.09} \qquad (4.30)$$

in which Δ is the dune height (as defined in Sec. 2.1.1.1-c), Y_o is the normal depth, d is the particle mean size, P is the wetted perimeter and T is van Rijn transport parameter. Equation 4.30 (see Fig. 4.46a) gave a good correlation (r^2=0.959) and was based on experiments with uniform sand sizes 0.53 and 0.89mm, for

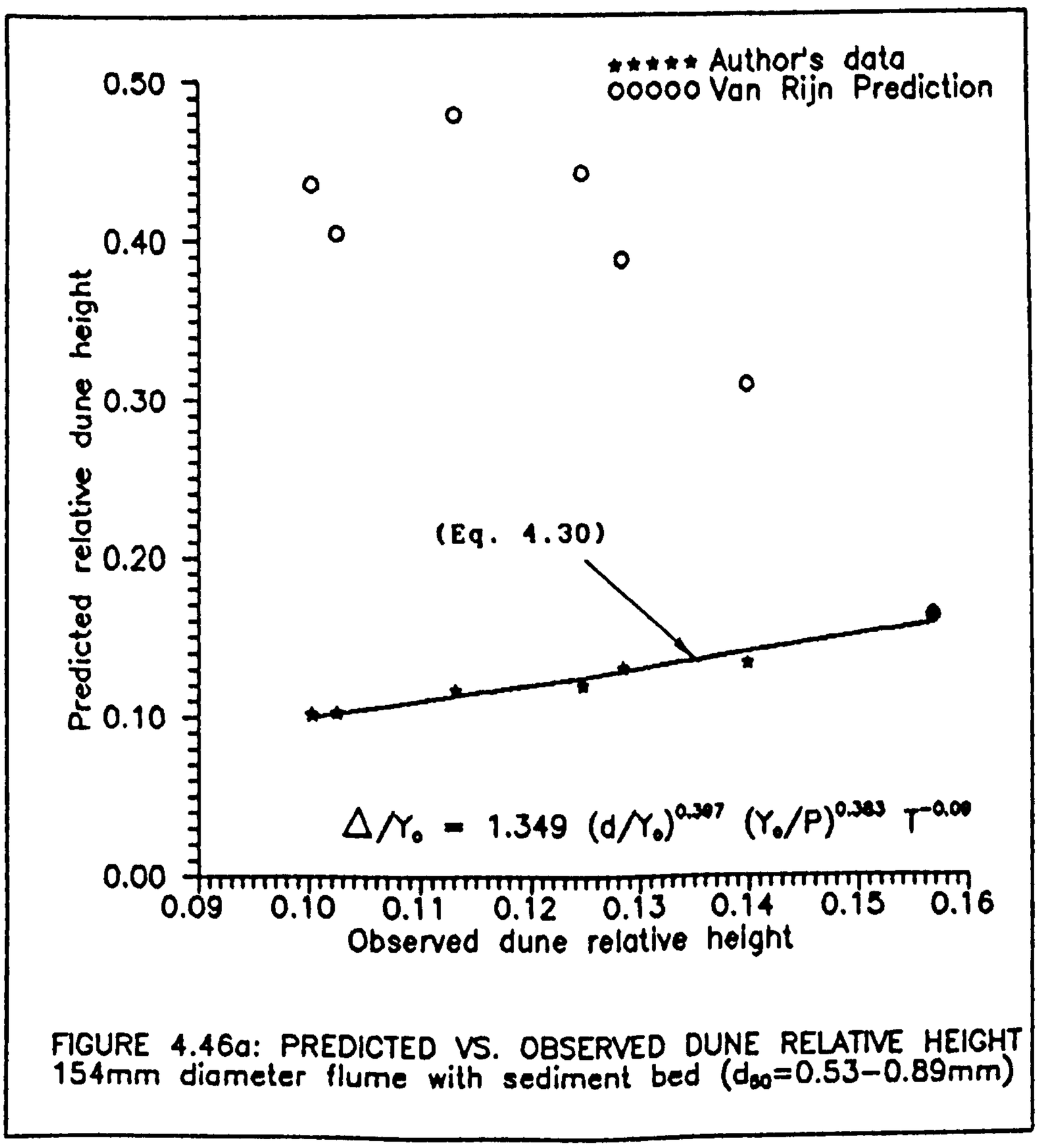

FIGURE 4.46a: PREDICTED VS. OBSERVED DUNE RELATIVE HEIGHT 154mm diameter flume with sediment bed (d_{50}=0.53–0.89mm)

relative sediment bed thickness $0.08 \leq E/D \leq 0.39$, in a 154 mm diameter flume. Neither the transport parameter T nor the dimensionless grain size D_* were found to be important in determining dune height, which corroborates Van Rijn (1988) observations. However, Van Rijn (Eq. 2.28) predicts greater dune heights, and this can be explained by the channel shape, as Van Rijn's equation was developed for alluvial wide channels.

For the length of the bedforms the relation obtained was:

$$L = 0.345 \left(\frac{d}{Y_o}\right)^{-0.39} \left(\frac{Y_o}{P}\right)^{0.78} T^{-1.04} \qquad (4.31)$$

where L is the dune wave length in (m) (as defined in Sec. 2.1.1.1-c), Y_o is the normal depth in (m), d is the particle mean size in (m), P is the wetted perimeter in (m) and T is Van Rijn dimensionless transport parameter. Equation 4.31 (see Fig. 4.46b) gave a correlation coefficient r^2=0.84 and was derived from experiments with uniform sand sizes 0.53 and 0.89mm, relative sediment bed thickness $0.08 \leq E/D \leq 0.39$, in a 154 mm diameter flume.

Van Rijn predicted values (Eq. 2.29) are plotted together (Fig. 4.46b) with the data for comparison. Except for one case Van Rijn predicts greater dune length, which illustrates the variation in bedforms between an alluvial wide channel and a pipe channel with loose sediment bed. According to Van Rijn dune length is only dependent (Eq. 2.29) on flow depth.

In pipe channels with sediment bed the size of the sediment and the channel shape are found to be important in the determination of dune dimensions, height and length.

In the limited number of transport experiments over loose beds in pipe channels some similarities to wide alluvial channels (in the mode of transport and bedformation) were observed. In order to achieve more conclusive results more experiments, with a wider range of bed widths, sediment sizes, and flow depths, are required.

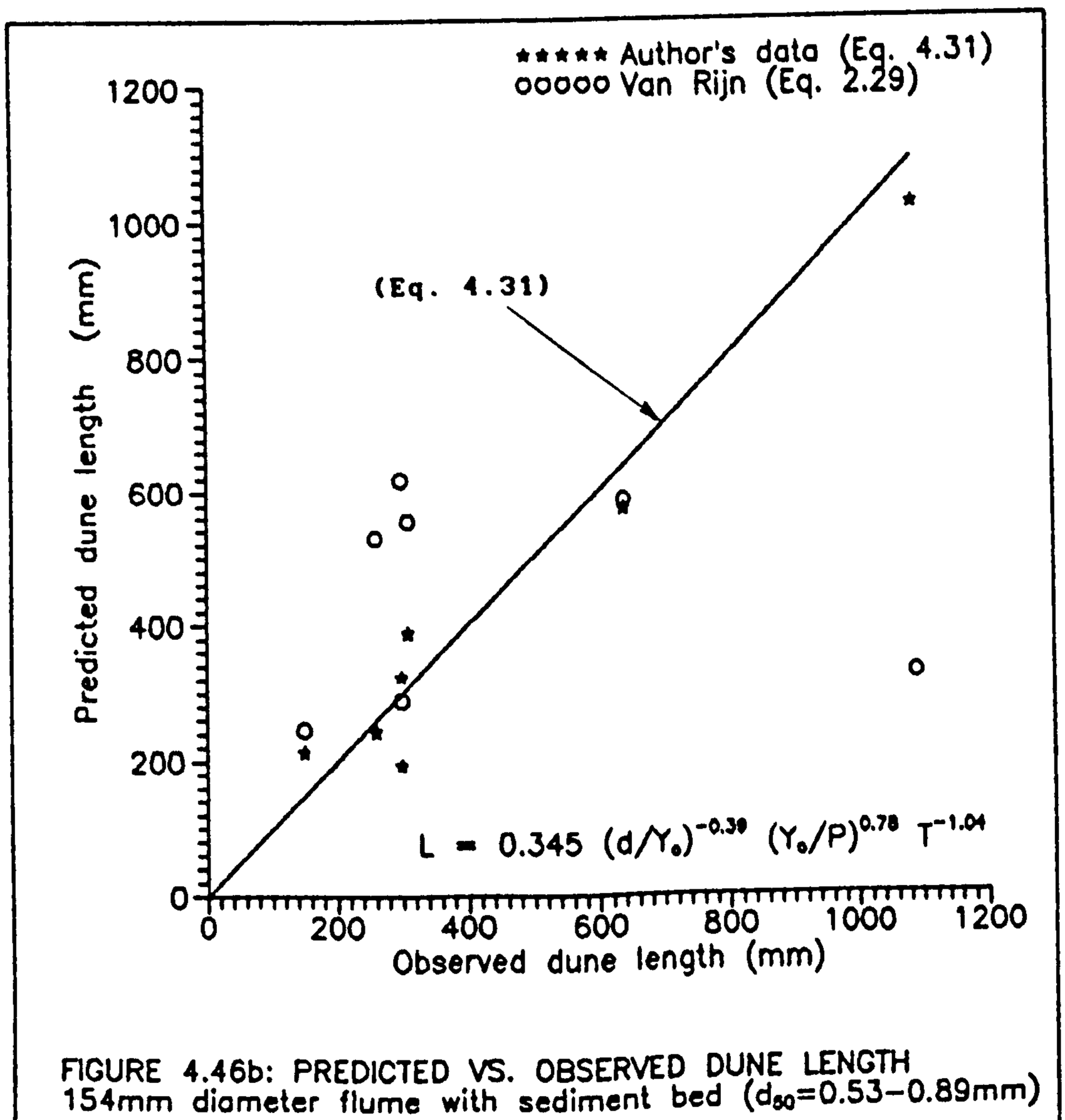

FIGURE 4.46b: PREDICTED VS. OBSERVED DUNE LENGTH
154mm diameter flume with sediment bed (d_{50}=0.53–0.89mm)

4.3.3.4 Cohesive Sediments Experiments

In transport experiments with cohesive sediment a special sediment feeder was devised (see Sec. 3.6.2.2, Fig. 3.16 and Plate 3). The experimental technique similar to that described for non-cohesive sediment transport (Sec. 4.3.3.2) was not found to be suitable for the synthetic sewer sediment. The breaking up of cohesion once the bed started to erode did not allow the establishment of equilibrium conditions of transport.

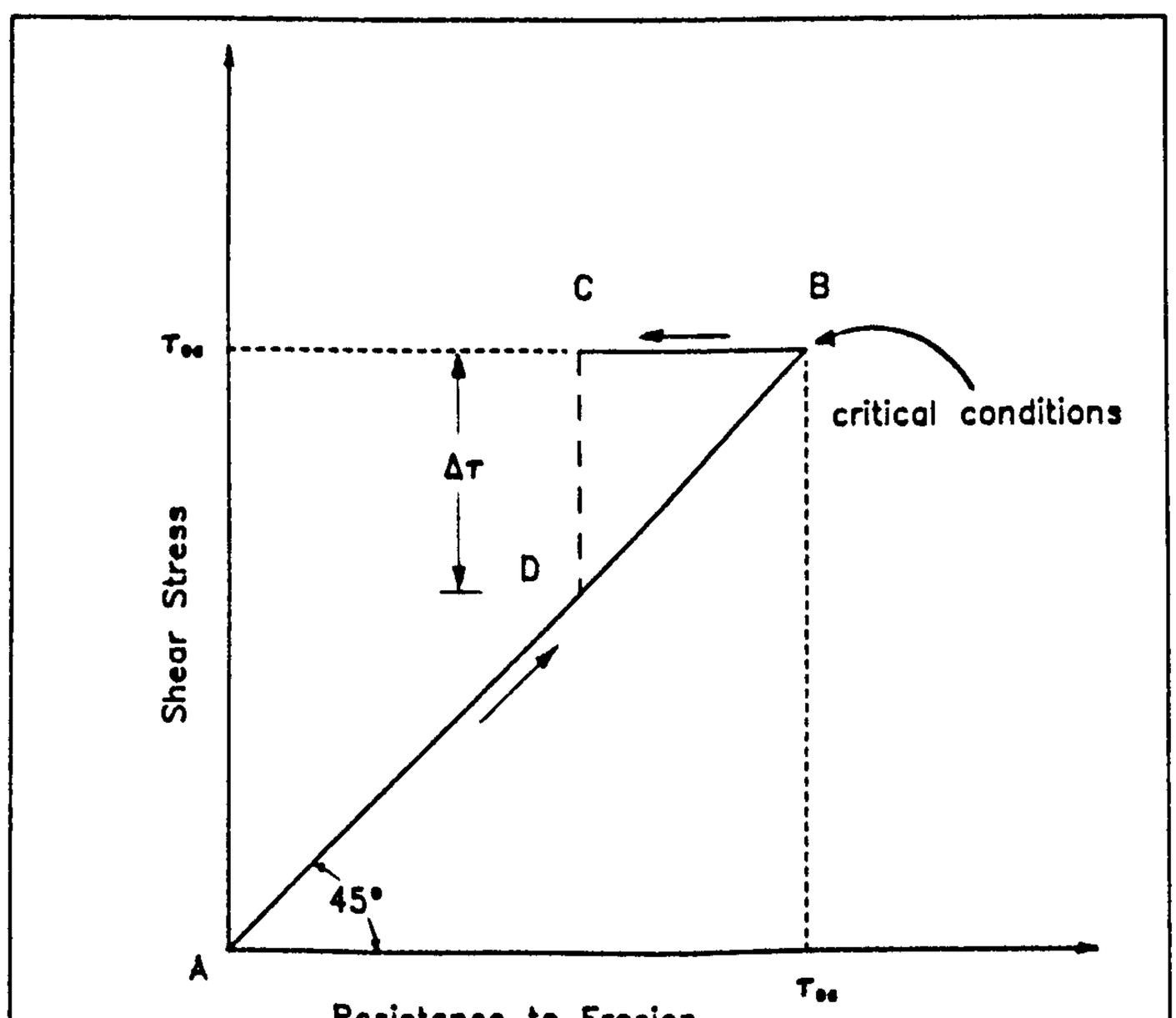

FIGURE 4.47: MECHANISM OF EROSION OF COHESIVE SEDIMENT BEDS (synthetic sewer sediment)

During the initial stages of erosion experiments (from A to B in Fig. 4.47) the shear strength of the sediments balances the shear stress exerted by the flowing water, and no erosion takes place.

When critical conditions are reached (point B in Fig. 4.47) the structure of the sediment bed suffers a rapid change as clusters of particles are removed exposing more area to the eroding flow. The new exposed sediment material is remoulded by the turbulent flow and as a result the shear strength of the sediment bed is highly reduced (point C in Fig. 4.47). It is this deficiency in shear strength that causes the sediment bed to be disintegrated.

Well before reaching critical conditions the shear stress exerted on the bed (τ_o) is larger than the critical shear stress (τ_{oc}) of the loose sand (incorporated in the cohesive bed) by several orders of magnitude. It is to the (excess) shear stress ($\tau_o - \tau_{oc}$) to which the sand particles are abruptly subjected to, once they are detached from the cohesive sediment bed. This is the effective shear stress that will move the sand particles once the erosion process is started.

The sand particles are detached from the bed as the cohesive bond is lost. The erosion process takes place both in clusters of particles and loose particles that are detached from the bed. Because of the high (excess) shear stress ($\tau_o - \tau_{oc}$) exerted on the bed during the critical conditions this process is very violent, as observed during the experiments. It was not possible to achieve equilibrium conditions of sediment transport. Any attempt to supply the necessary amount of sediment at the upstream end of the test section, made no difference. The sediment was carried in suspension and the sediment bed continued to be eroded modifying the geometry of the channel cross-section.

Therefore in order to maintain a stable sediment bed (i.e. the original flume configuration) it was decided to carry out transport experiment over fixed false beds. Thus the influence of cohesion on sediment transport could be assessed.

4.3.4 Transport Experiments Over Fixed Beds

4.3.4.1 Selection of Parameters

From the previous dimensional analysis (see Sec. 4.3.3.1) several dimensionless parameters (Re_*, $1/\psi$, Y_o/P , ϕ) were found to be related to the transport of sediment over loose beds. Additionally three more parameters are relevant:

a) The relative particle sand size, d_{50}/R , which now becomes important as the movement of individual particles is relevant to the limit deposition criterion.

b) The sediment volumetric concentration, $C_v = g_s' \, b/(\rho_s g Q)$ where g_s' is the transport rate of sediment in weight per unit time per unit width, Q is the water discharge, ρ_s is the density of the sediments, b is the channel bed width, and g the acceleration due to gravity.

c) Darcy-Weisbach friction coefficient, λ_s of the flow with sediment. Therefore the functional relation can be written as:

$$F\left(Re_*, \frac{1}{\psi}, \frac{Y_o}{P}, \phi, \frac{d_{50}}{R}, C_v, \lambda_s\right) = 0 \qquad (4.32)$$

4.3.4.2 Non-cohesive Sediment Experiments

The limit deposition criterion as discussed earlier (see Sec. 2.1.2-b) was employed in these experiments. For a given uniform flow sediment was fed to the flow in increasing amounts until the point of deposition was reached (see Sec. 3.6.1.2).

Because of the limited time available, only one bed thickness (E = 40.8 mm) in the 154 mm diameter flume was used in the experiments. Three sand sizes were tested (0.9, 2.0 and 5.7 mm). Two sets of experiments were carried out, one with smooth bed (see Table 4.18), and the other with artificially roughened bed (see Table 4.19).

In spite of the small size of the data, clear trends can be observed in Fig. 4.44. The transport parameter (ϕ) is plotted against the flow intensity parameter (ψ). A power fitting of the form

$$\psi = a\ \phi^{b} \tag{4.33}$$

was attempted, where a and b are constant to be obtained from the data. In Table 4.20 the values of the constants for each sand size are shown.

In Fig. 4.48 it can be seen that many observed values fall above Graf-Acaroglu's curve (Eq. 2.15) derived from open channels, closed conduits and field data. This suggests that the transport capacity of flows in channels of circular cross-section (limit deposition condition) with a sediment bed is greater than that of

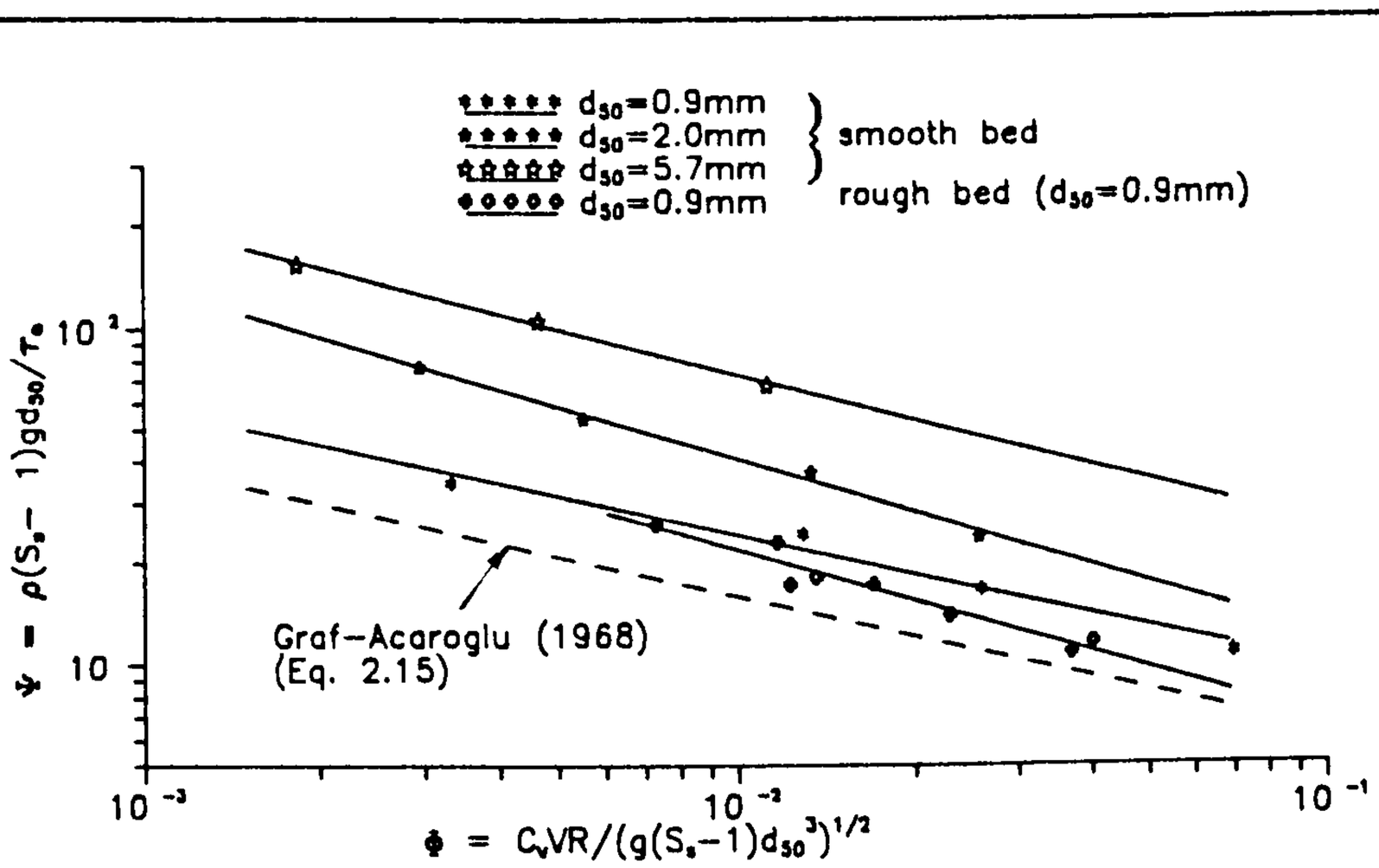

a) MEAN VALUES

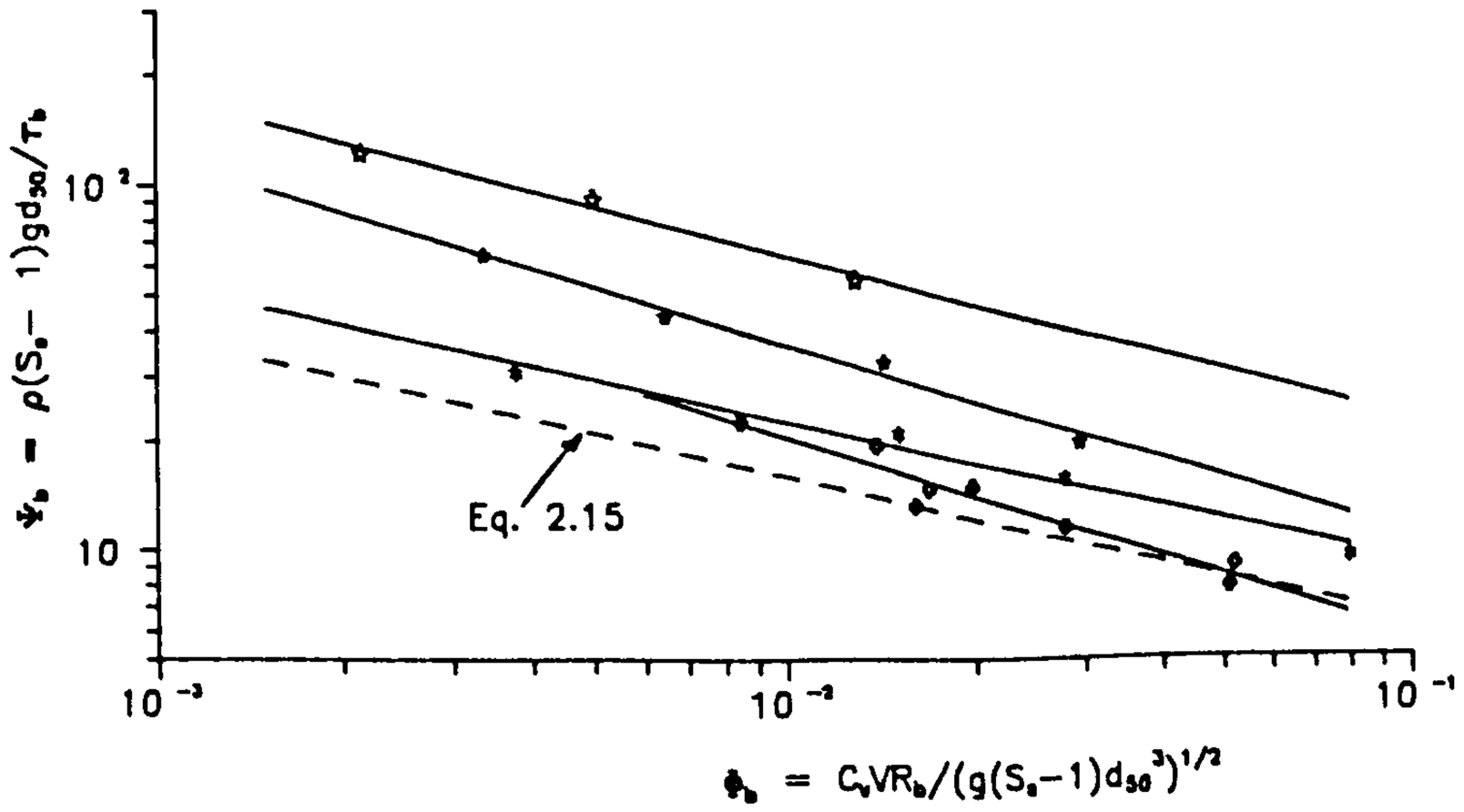

b) SEPARATED VALUES

FIGURE 4.48: NON–COHESIVE SEDIMENTS TRANSPORT OVER FIXED BEDS LIMIT DEPOSITION CONDITION (154mm diameter flume E=40.8mm)

similar flows in alluvial channels. This can be explained by the difference in bed roughness. In rigid bed channels bed roughness is uniform and smaller compared with alluvial beds where bedforms also occur. The existence of secondary currents (turbulence) due to the channel shape also encourage sediment transport by helping to keep the particles in motion.

In Fig. 4.48 it is apparent that for a given level of shear stress, on smooth bed experiments, there is more transport for the larger sand. This is due to the greater exposed area of the larger particles, which are subjected to the drag forces of the flow. The curves corresponding to 0.9 mm sand for rough and smooth beds (Fig. 4.48) show a variation in slope, and a decrease in transport rate for increasing bed roughness.

A multi-regression analysis (see Fig. 4.49) was performed with the data. The entrainment parameter ($1/\psi$) was expressed in terms of the volumetric concentration (C_v), relative sand size (d_{50}/R) and the friction coefficient (λ_s). Using the mean values (mean shear stress) the equation representing the phenomena is:

$$\frac{1}{\psi} = \frac{\tau_o}{\rho(S_s - 1)g d_{50}} = 3.42\, C_v^{0.66} \left(\frac{d_{50}}{R}\right)^{-1.32} (\lambda_s)^{0.78} \qquad (4.34)$$

with a correlation coefficient $r^2 = 0.978$ (see Fig. 4.49-a).

Using the separated values (computed bed shear stress) the equation representing the phenomena becomes:

$$\frac{1}{\Psi_b} = \frac{\tau_b}{\rho(S_s - 1)gd_{50}} = 1.60\, C_v^{0.64} \left(\frac{d_{50}}{R_b}\right)^{-1.27} (\lambda_{sb})^{0.62} \qquad (4.35)$$

with a correlation coefficient $r^2 = 0.977$ (see Fig. 4.49-b). In order to consider the effects of channel shape the parameter (Y_o/P) is incorporated in the analysis and equations 4.34 and 4.35 become:

$$\frac{\tau_o}{\rho(S_s - 1)gd_{50}} = 1.01 C_v^{0.65} \left(\frac{d_{50}}{R}\right)^{-1.34} (\lambda_s)^{0.58} \left(\frac{Y_o}{P}\right)^{-0.18} \qquad (4.36)$$

with a correlation coefficient $r^2 = 0.979$, and

$$\frac{\tau_b}{\rho(S_s - 1)gd_{50}} = 0.26 C_v^{0.63} \left(\frac{d_{50}}{R_b}\right)^{-1.32} (\lambda_{sb})^{0.35} \left(\frac{Y_o}{P}\right)^{-0.4} \qquad (4.37)$$

with a correlation coefficient $r^2 = 0.983$ respectively. The inclusion of the parameter (Y_o/P) slightly improves the correlation. The channel shape influences sediment transport over fixed beds in channels of circular cross-section.

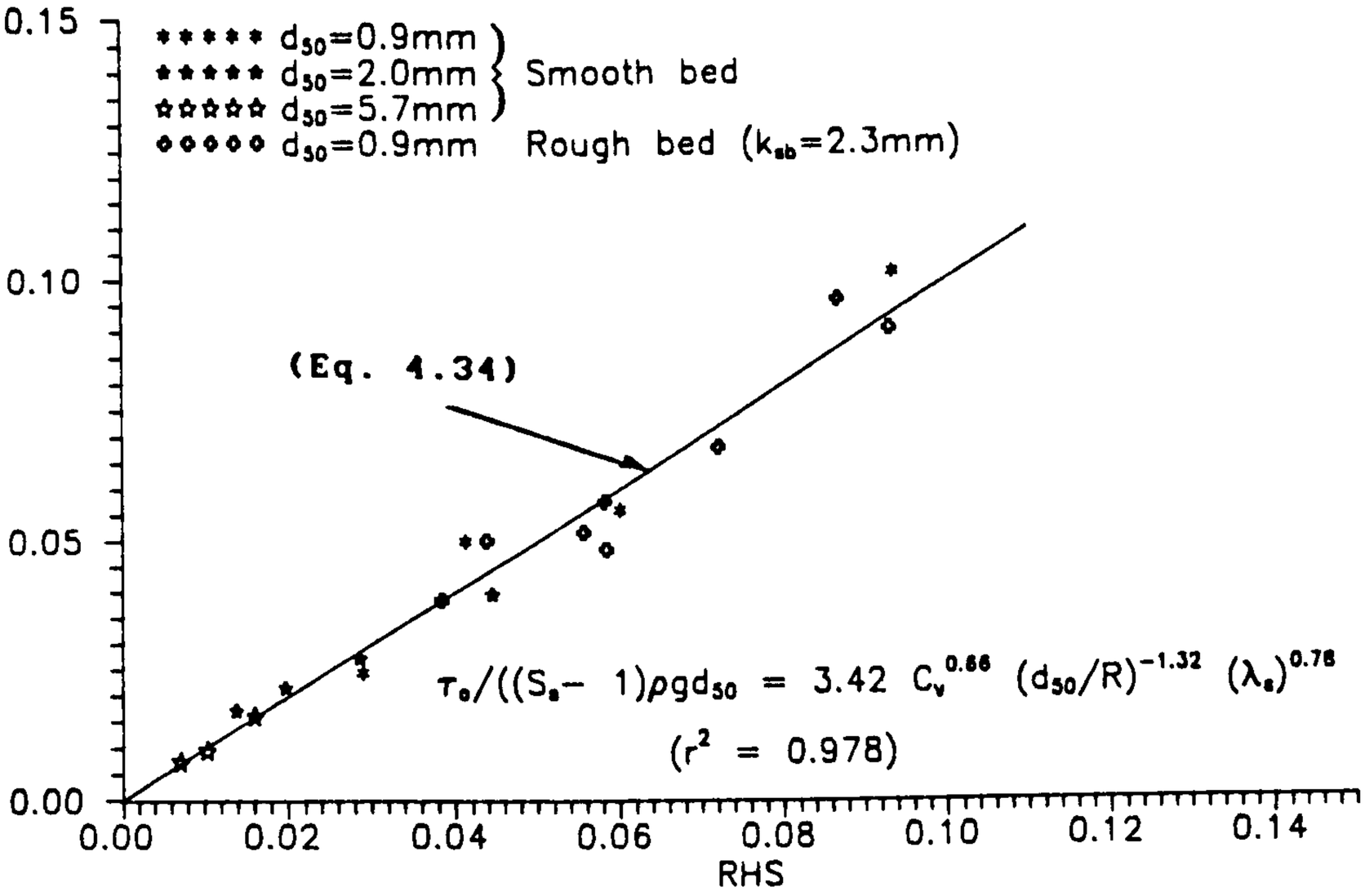

a) MEAN VALUES

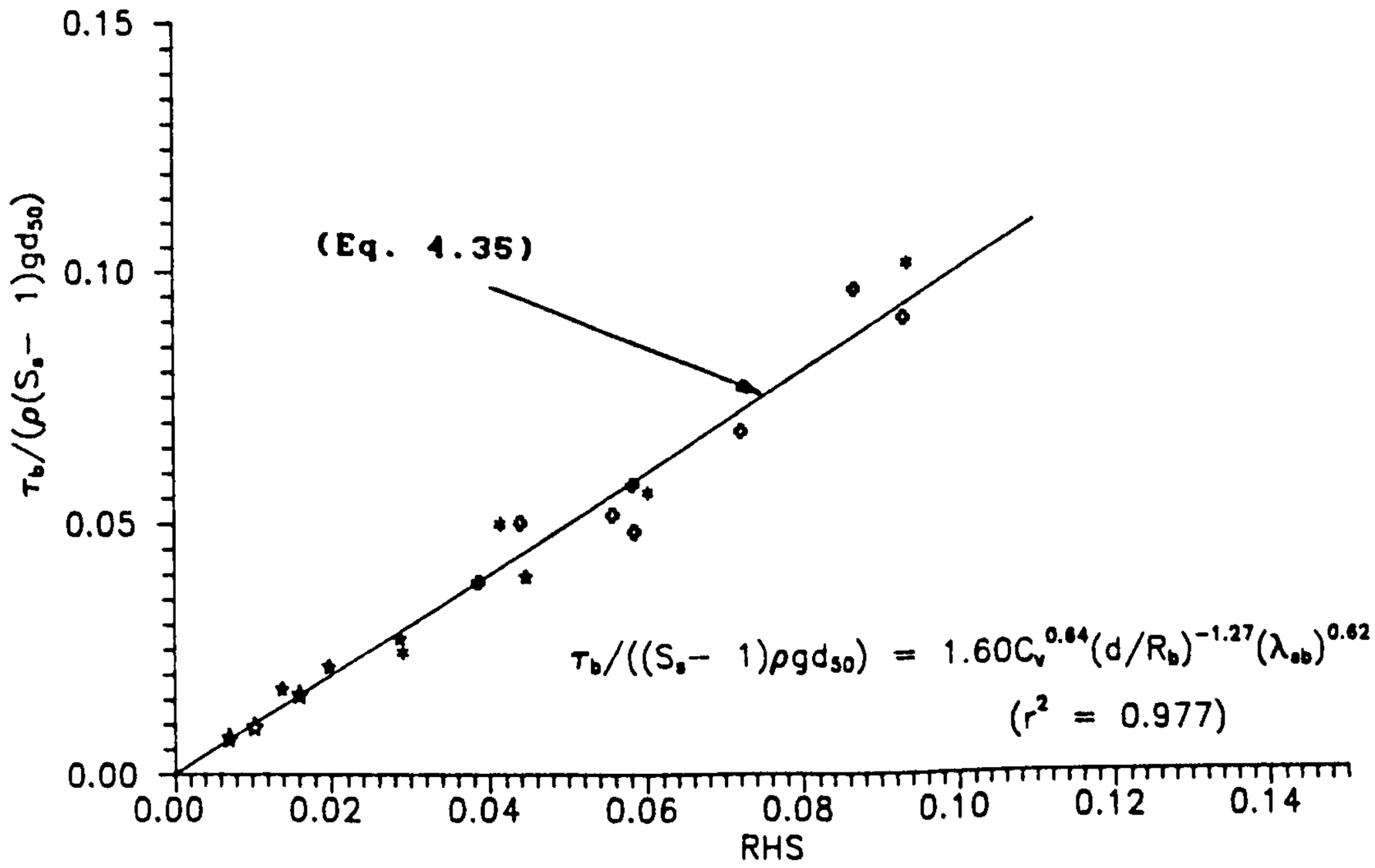

b) SEPARATED VALUES

FIGURE 4.49: SEDIMENT TRANSPORT OVER FIXED BEDS
Limit Deposition Condition – 154mm diameter flume
with fixed sediment bed (E=40.8mm).

4.3.4.3 Cohesive Sediment Experiments

Cohesive sediment transport experiments over fixed smooth beds were carried out as explained in Sec. 3.6.2.2. The rigid bed would represent a consolidated sewer sediment bed, Type B sediment (Crabtree 1988).

The limiting deposition criterion was used in the experiments in a similar manner to that explained in the previous section (Sec. 4.3.4.2). Only the 154 mm diameter flume was used in these experiments. The smooth false bed (E 40.8 mm) was made of uPVC sheets. Two different cohesive sediment mixtures were prepared using sand size 0.9 mm (80% by weight) and Laponite clay gel (20%) at concentration of 24 and 30 g/l respectively. The results of these experiments are summarised in Tables 4.21 and 4.22.

The transport parameter (ϕ) is plotted against the flow intensity parameter (ψ) in Fig. 4.50. A power curve was fitted to the data (using mean values) to obtain:

$$\psi = 4.63\ \phi^{-0.332} \qquad (4.38)$$

with a correlation coefficient $r^2 = 0.939$. For separated bed values (computed bed shear stress) the following equation (see Fig. 4.50-b) is obtained:

$$\psi = 4.15\ \phi^{-0.322} \qquad (4.39)$$

with a correlation coefficient $r^2 = 0.882$. The coefficients obtained for equations 4.38 and 4.39 are very similar to those of equation Eq. 4.31 (see Table 4.20) for non-cohesive sediment

transport over fixed beds. This suggests that cohesive sediment, once in motion, behaves like non-cohesive sediment.

Shields' function ($1/\psi$) was expressed in terms of the volumetric concentration (C_v), relative sand size (d_{50}/R) and the friction coefficient (λ_s). Using the mean values (mean shear stresses) a multi-regression was performed and the best fit equation representing the phenomena was found (see Fig. 4.51-a) to be:

$$\frac{1}{\psi} = \frac{\tau_o}{\rho(S_s - 1)gd_{50}} = 0.17\ C_v^{0.39} \left(\frac{d_{50}}{R}\right)^{-0.34} (\lambda_s)^{-0.34} \qquad (4.40)$$

with a correlation coefficient $r^2 = 0.913$. Using the separated values (see Fig. 4.51-b) the equation obtained was:

$$\frac{1}{\psi_b} = \frac{\tau_b}{\rho(S_s - 1)gd_{50}} = 0.96C_v^{0.46}\left(\frac{d_{50}}{R_b}\right)^{-0.77}(\lambda_{sb})^{-0.41} \qquad (4.41)$$

with a correlation coefficient $r^2 = 0.953$. To include the effects of channel shape on sediment transport the parameter (Y_o/P) is incorporated in the analysis and equations 4.40 and 4.41 become:

$$\frac{\tau_o}{\rho(S_s - 1)gd_{50}} = 2.70C_v^{0.39}\left(\frac{d_{50}}{R}\right)^{0.29}(\lambda_s)^{-0.43}\left(\frac{Y_o}{P}\right)^{0.57} \qquad (4.41)$$

with a correlation coefficient $r^2 = 0.914$, and

$$\frac{\tau_b}{\rho(S_s - 1)gd_{50}} = 1.15\ C_v^{0.46}\left(\frac{d_{50}}{R_b}\right)^{-0.82}(\lambda_s)^{-0.41}\left(\frac{Y_o}{P}\right)^{-0.07} \qquad (4.42)$$

with a correlation coefficient $r^2 = 0.953$ respectively.

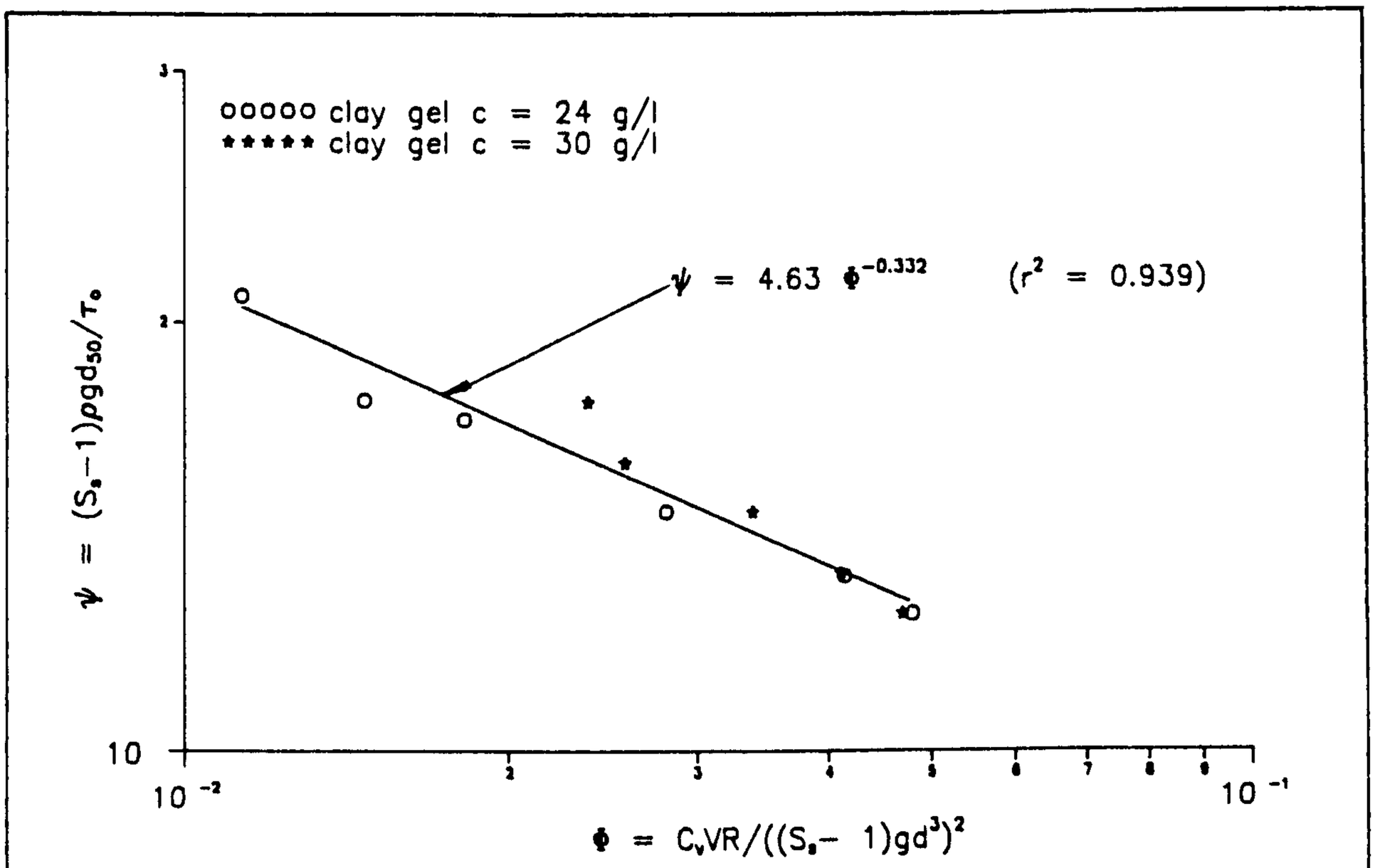

a) MEAN VALUES

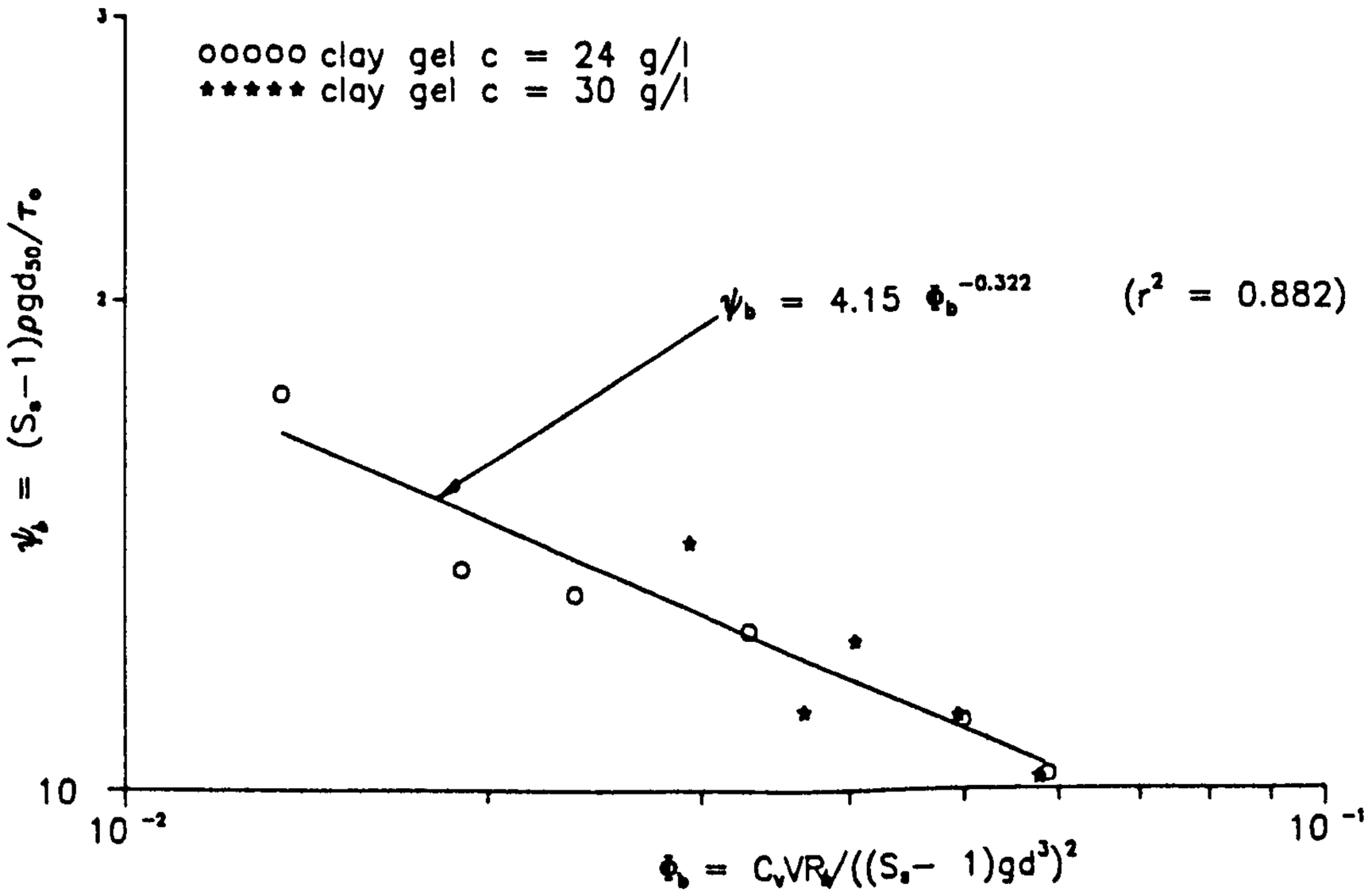

b) SEPARATED VALUES

FIGURE 4.50: SEDIMENT TRANSPORT OVER FIXED SMOOTH BED
Einstein bedload diagram – Limit Deposition Condition
154mm dia. flume (E=40.8mm) 20% clay gel, 80% sand (0.9mm)

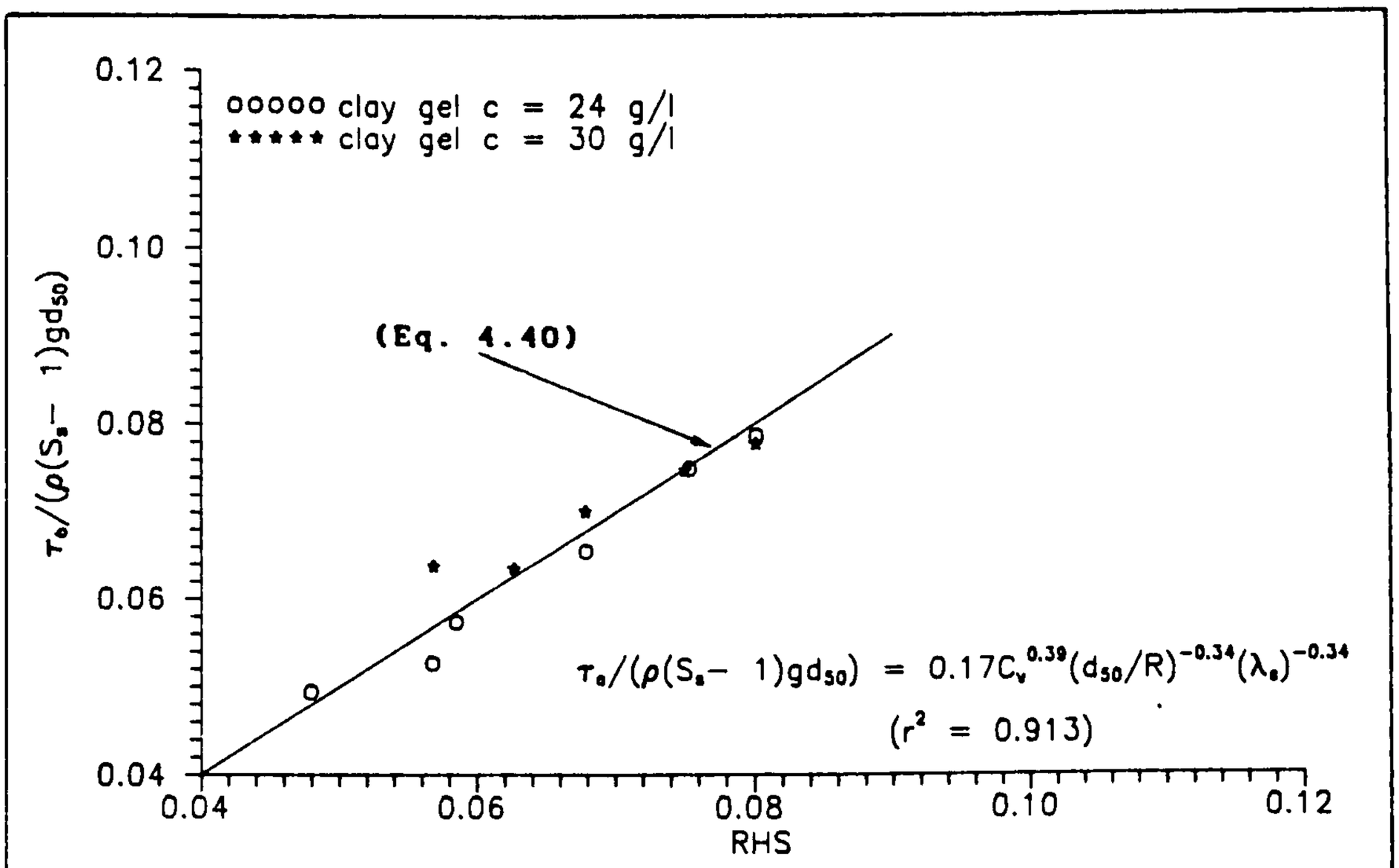

a) MEAN VALUES

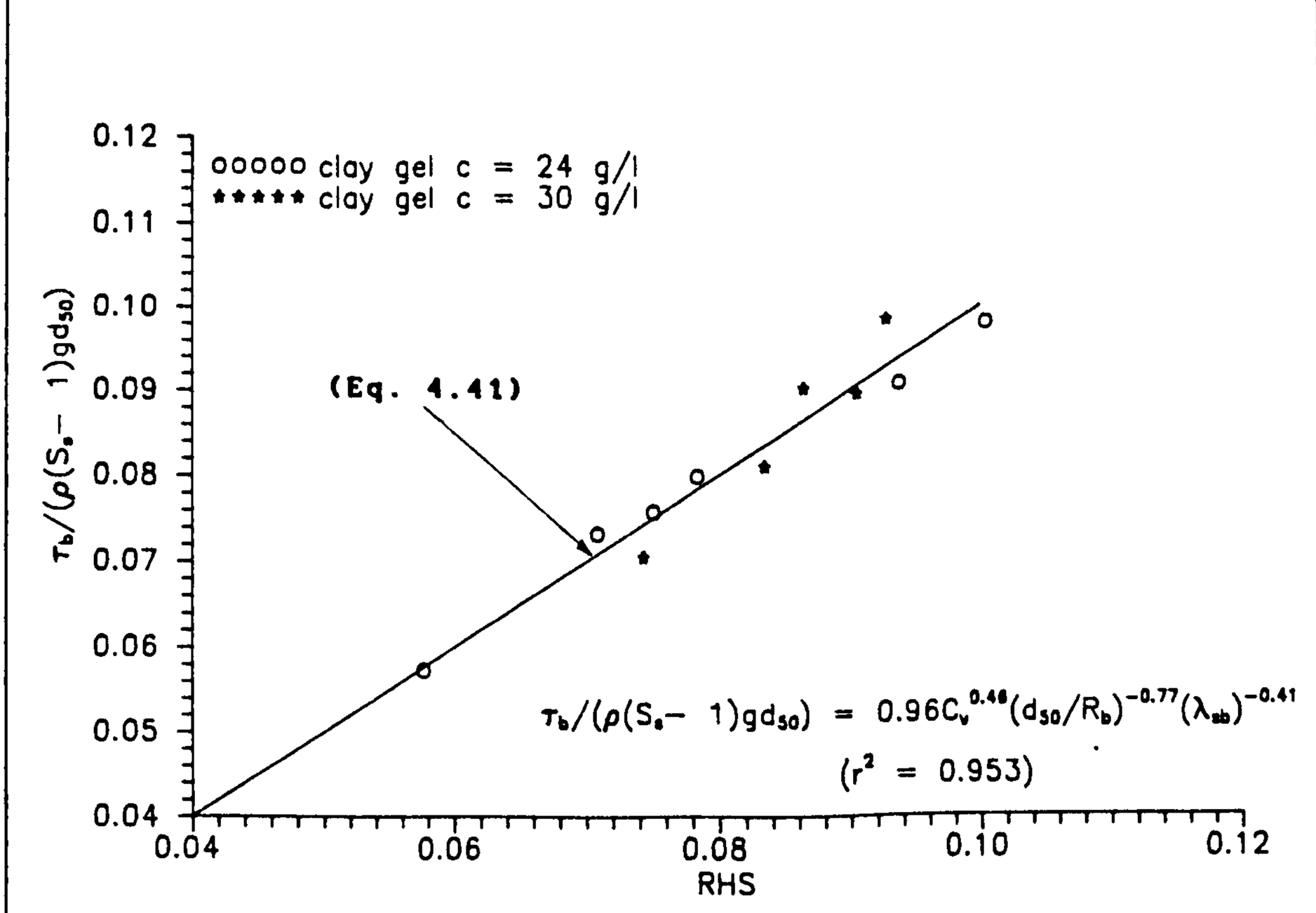

b) SEPARATED VALUES

FIGURE 4.51: SEDIMENT TRANSPORT OVER FIXED BEDS – ENTRAINMENT FUNCTION FOR LIMIT DEPOSITION CONDITION (Cohesive sediments)
154mm dia. flume (E=40.8mm), 20% clay gel– 80% sand (d_{50}=0.9mm)

4.3.4.4 Comparison of the Results

a) Einstein Bedload Diagram

The experimental results of the transport experiments (cohesive and non-cohesive sediments on loose beds and fixed beds) are shown in ϕ_b Vs. ψ_b plots (transport parameter Vs. flow intensity parameter) in figures 4.52 to 4.55.

On transport experiments over fixed beds the limit deposition criterion was employed. Figure 4.52 illustrates the influence of particle size on sediment transport over fixed beds. The limit deposition condition does not allow any deposition to occur in the pipe. Thus, the particles are in continuous motion (rolling and sliding) on the bed. The drag force exerted by the flowing water on each particle is proportional to the particle size (d) and to the relative local velocity (u_b) of the flow. Obviously for larger particles there is a higher local velocity and a larger exposed area, and this results in greater transport (see Fig. 4.52).

On rough beds part of the flow energy is spent in overcoming the friction between the particles and the rough bed. In alluvial channels the bed also has bedforms, which reduces the available energy even more. For this reason sediment transport over fixed smooth beds is higher than in the case of alluvial (Einstein curve) channels (see Fig. 4.52).

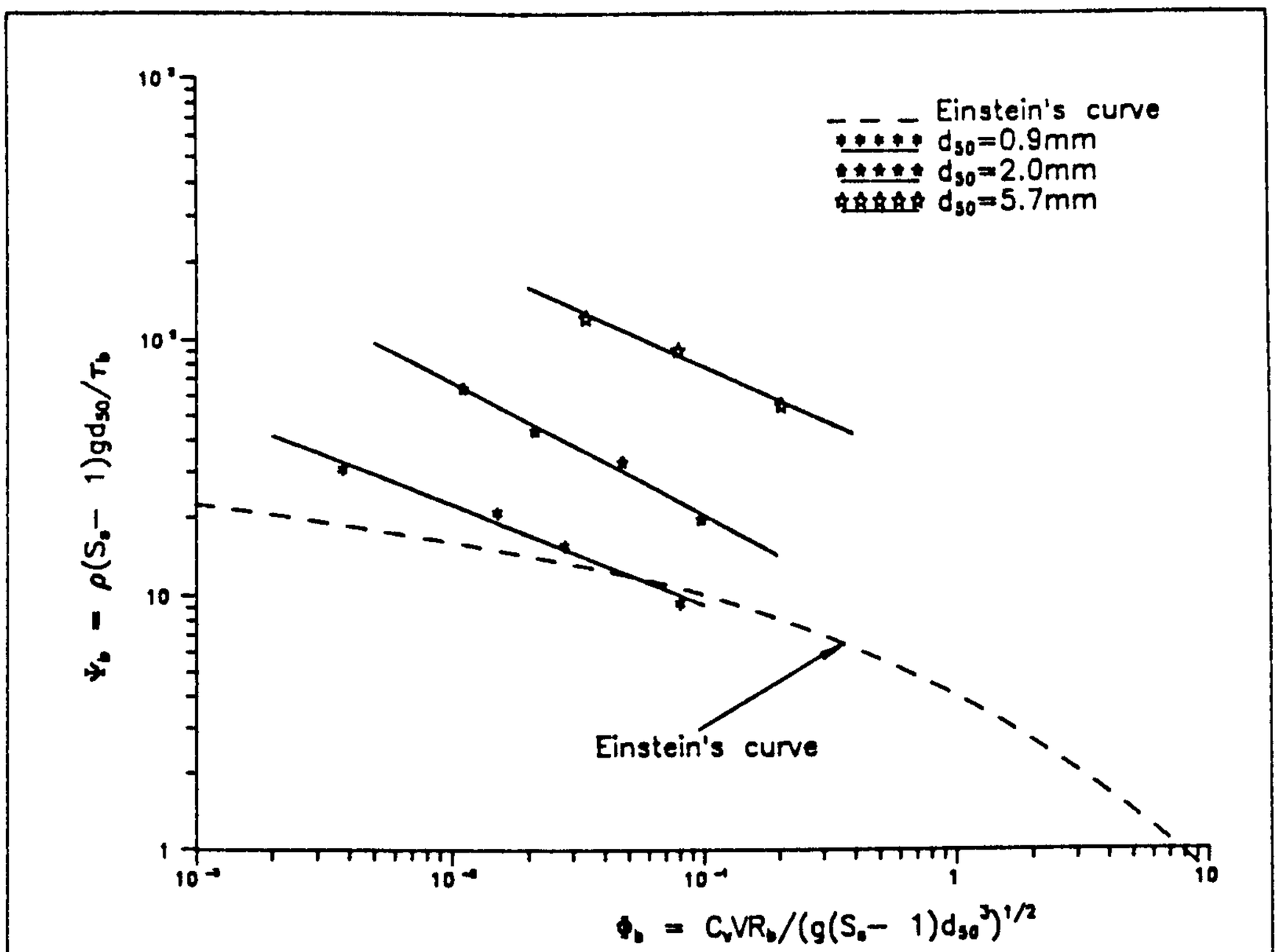

FIGURE 4.52: TRANSPORT EXPERIMENTS OVER FIXED BEDS
LIMIT DEPOSITION CONDITION – 154mm diameter flume
smooth bed (E=40.8mm) non–cohesive sediments

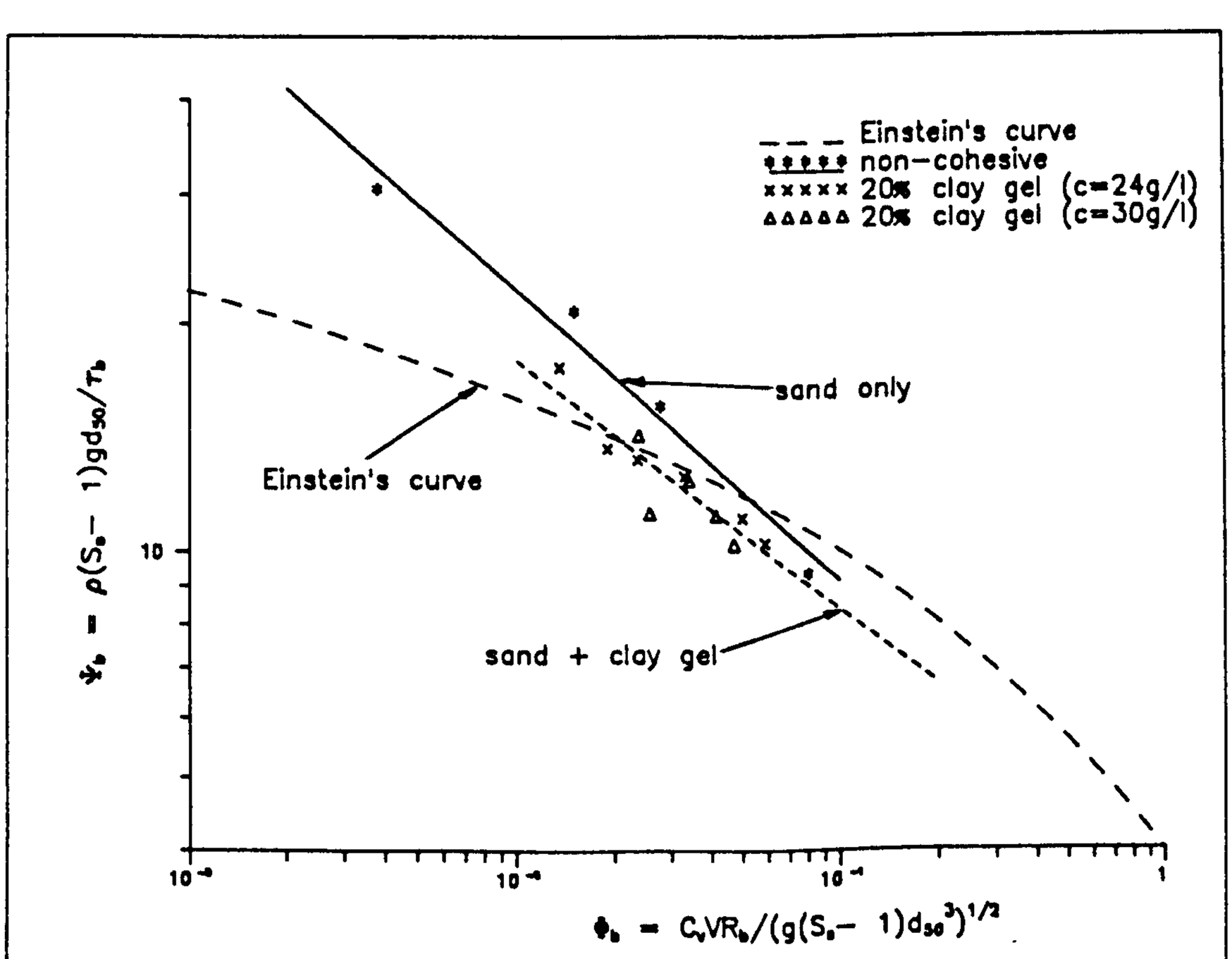

FIGURE 4.53: TRANSPORT EXPERIMENTS OVER FIXED BEDS
LIMIT DEPOSITION CONDITION – 154mm diameter flume
smooth bed (E=40.8mm) – sand (d_{50}=0.9mm) + clay gel

The influence of cohesion on sediment transport is not very noticeable, although in Fig. 4.53 it can be observed that the cohesive additive slightly reduces the transport capacity of a flow. For the same values of ψ_b , the values of ϕ_b (sediment transport) is thus smaller in the case of sand with clay.

In the transport experiments with cohesive sediments the cohesive additive was observed to be washed off from the particles as soon as the sediment entered the flow. The sediment was dispersed by the flowing water and it was observed to be transported as loose particles. However, the particles surface remains coated with cohesive additive for sometime after entering the flow, and this affected the transport (see Fig. 4.53).

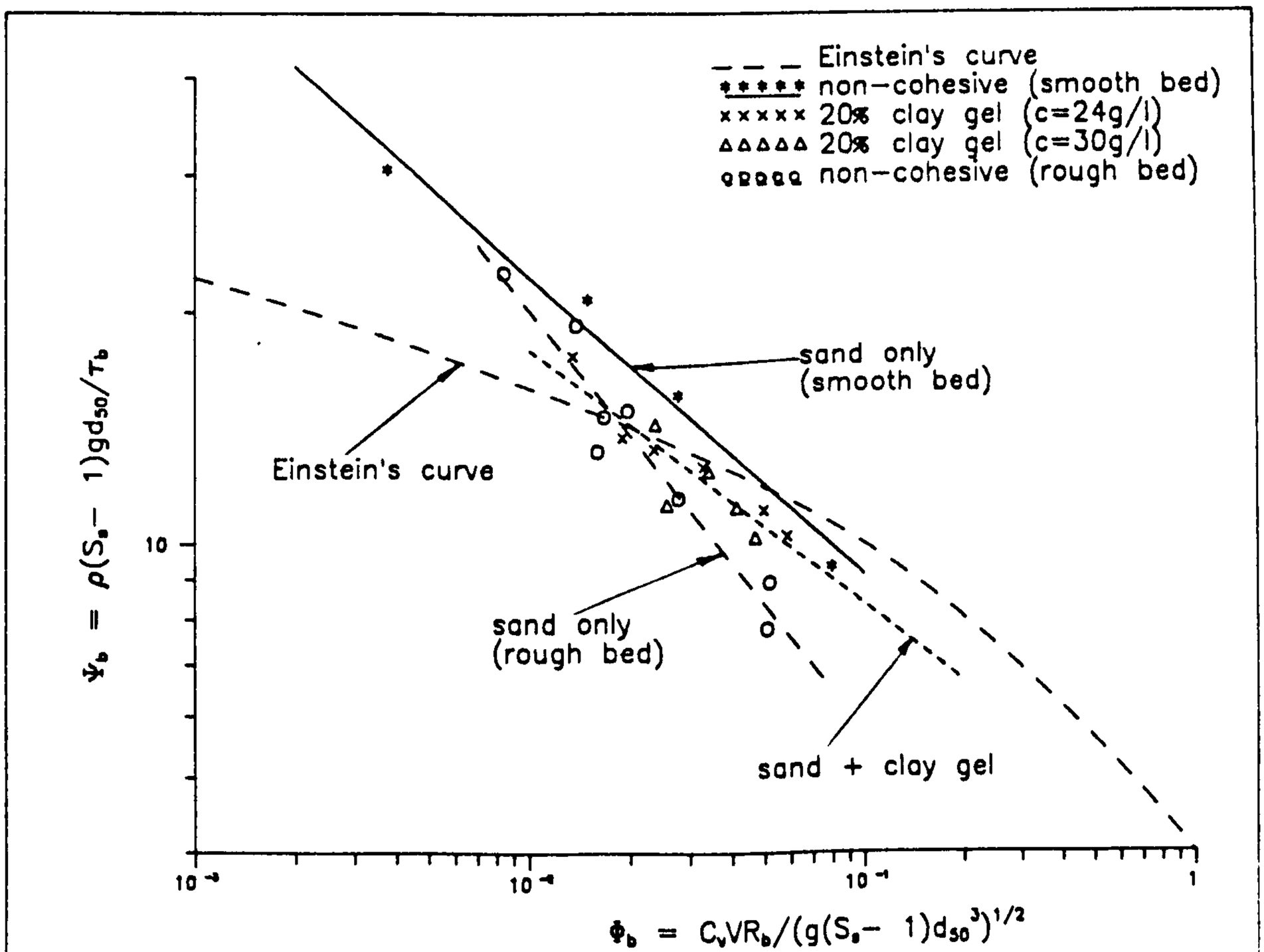

FIGURE 4.54: TRANSPORT EXPERIMENTS OVER FIXED BEDS
LIMIT DEPOSITION CONDITION – 154mm diameter flume
(E=40.8mm) – (sand d_{50}=0.9mm)

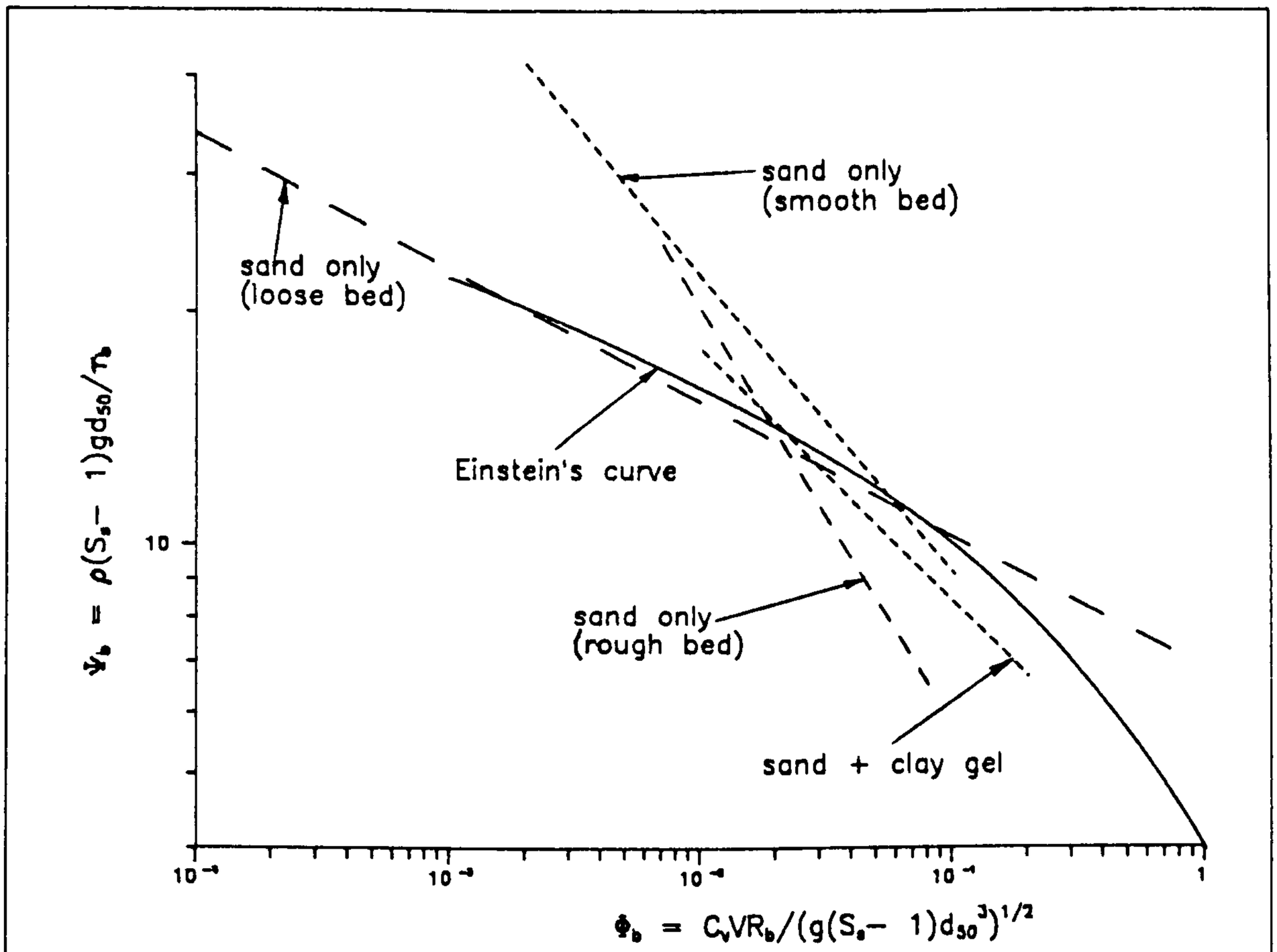

FIGURE 4.55: TRANSPORT EXPERIMENTS GENERAL COMPARISON
– 154mm diameter flume (E=40.8mm)
(sand d_{50}=0.9mm)

The results obtained with the two cohesive additives used did not show any clear difference in sediment transport for the two clay gel concentrations. As it can be observed (see Fig. 4.54) the effects of bed roughness are more noticeable than the effects of cohesive additives on the 0.9mm sand.

Finally in Fig. 4.55 the results for the same sand (d_{50}=0.9mm) and the same bed thickness (E=40.8mm) corresponding to loose bed experiments are plotted together with the fixed bed experimental results. The curve for loose bed shows lower levels of transport for higher values of the flow parameter (ψ_b). On the other hand, for the lower values of ψ_b (i.e. higher shear stresses), the ϕ_b values are larger (i.e. there is more sediment transport) than those corresponding to fixed beds. However, further experiments are needed to achieve more conclusive results.

b) Minimum Velocities Required for Limit Deposition Condition

In order to compare the results with those of Mayerle (1988) and Kithsiri (1990) multiregression analysis using Mayerle's format was carried out. The following equations were obtained:

$$\frac{V_L}{\sqrt{(S_s - 1)gd_{50}}} = 5.99\ (D_{gr})^{-0.08}(C_v)^{0.33}\left(\frac{d_{50}}{R}\right)^{-0.59}(\lambda_s)^{-0.19} \quad (4.43)$$

with r^2=0.978, for mean values, and

$$\frac{V_L}{\sqrt{(S_s - 1)gd_{50}}} = 7.53\ (D_{gr})^{-0.15}(C_v)^{0.32}\left(\frac{d_{50}}{R}\right)^{-0.52}(\lambda_s)^{-0.25} \quad (4.44)$$

with r^2=0.981, for separated bed values. In Fig. 4.56 equation 4.43 is plotted together with Mayerle's Eq. 2.46 for circular channels with no sediment bed. It is apparent that Eq. 2.46 (Mayerle, 1988) predicts higher velocities for non-deposition condition. This can be explained by the very narrow sediment width in Mayerle's experiments, as more velocity is required to avoid any deposition in the invert of the pipe.

However, Mayerle's equation for rectangular channels (Eq. 2.51) shows a better agreement with the data (see Fig. 4.57). This means that the presence of a sediment bed on the pipe invert makes the flow behave like rectangular channel flow. Obviously this is dependent on flow depths (shape effects), as for flows above half full a different behaviour occurs as seen in Sec. 4.3.3.2. Similar results are obtained when using Eq. 2.54 (Kithsiri, 1990) for rectangular flume (see Fig. 4.58).

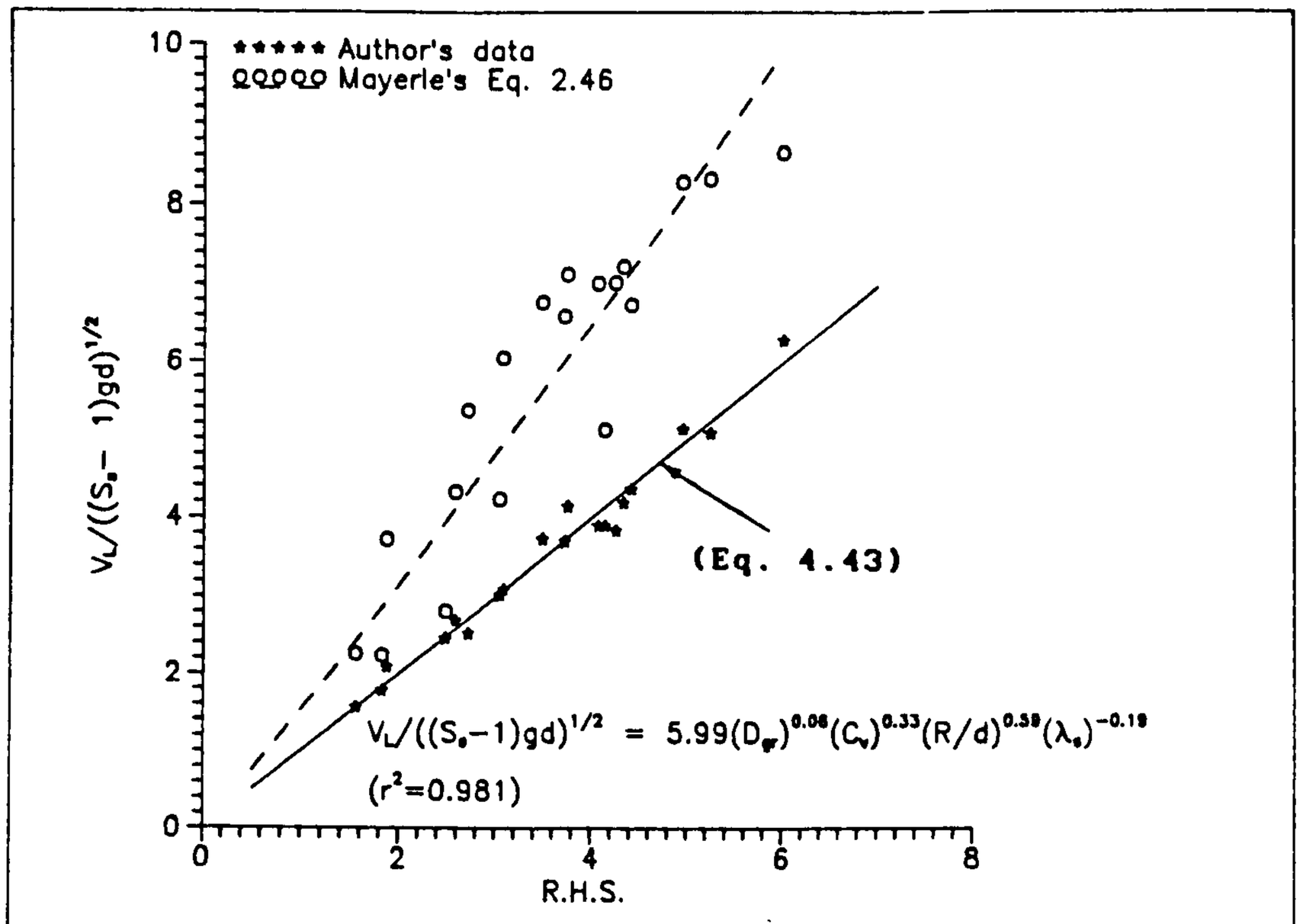

FIGURE 4.56: COMPARISON WITH MAYERLE'S EQ. FOR CIRC. CHANNELS
Transport Experiments Over Fixed Beds in Channels of circular Cross-section (D=154mm) with sediment bed (E=40.8mm)

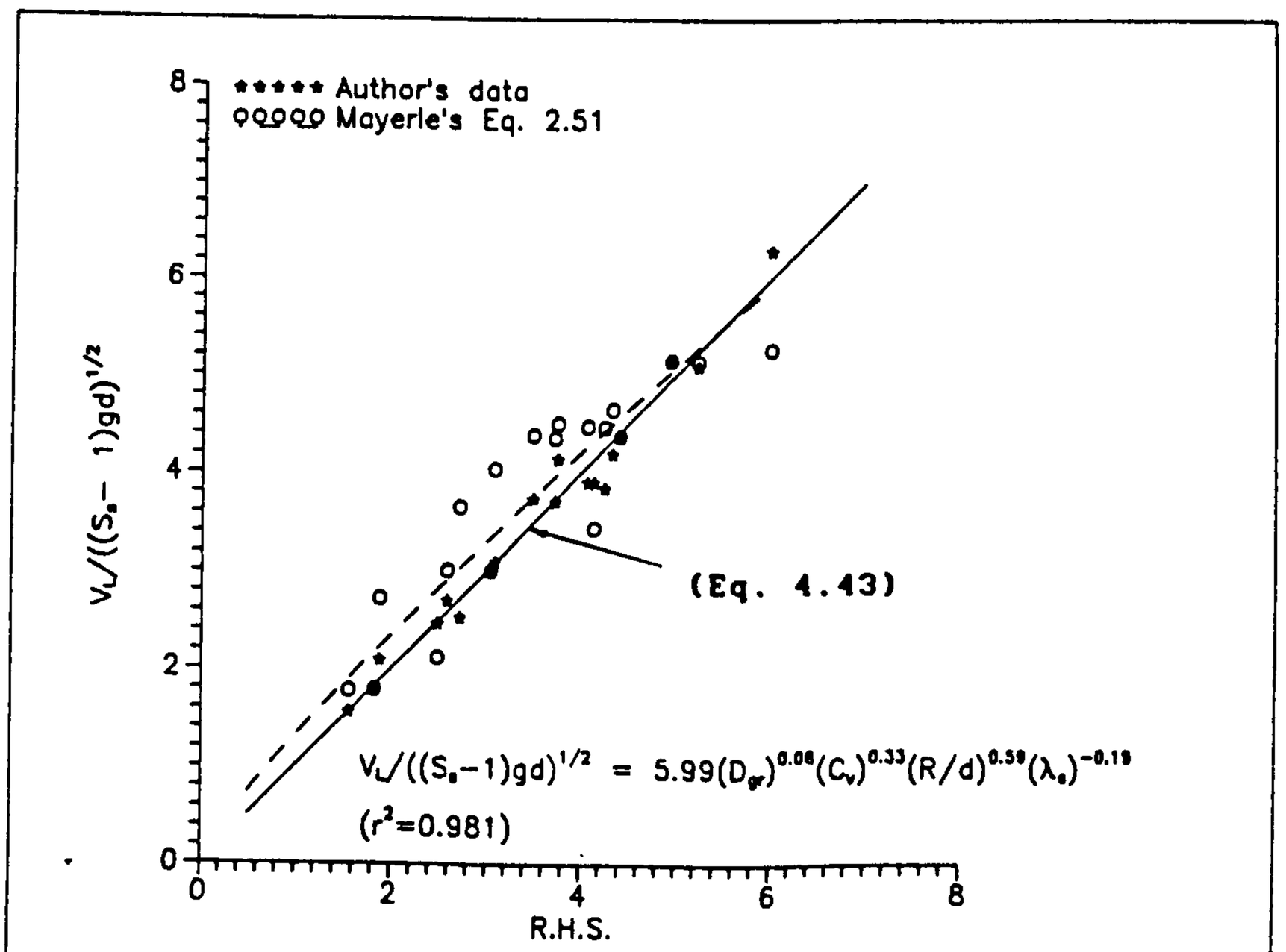

FIGURE 4.57: COMPARISON WITH MAYERLE'S EQ. FOR RECT. CHANNELS
Transport Experiments Over Fixed Beds in Channels of circular Cross-section (D=154mm) with sediment bed (E=40.8mm)

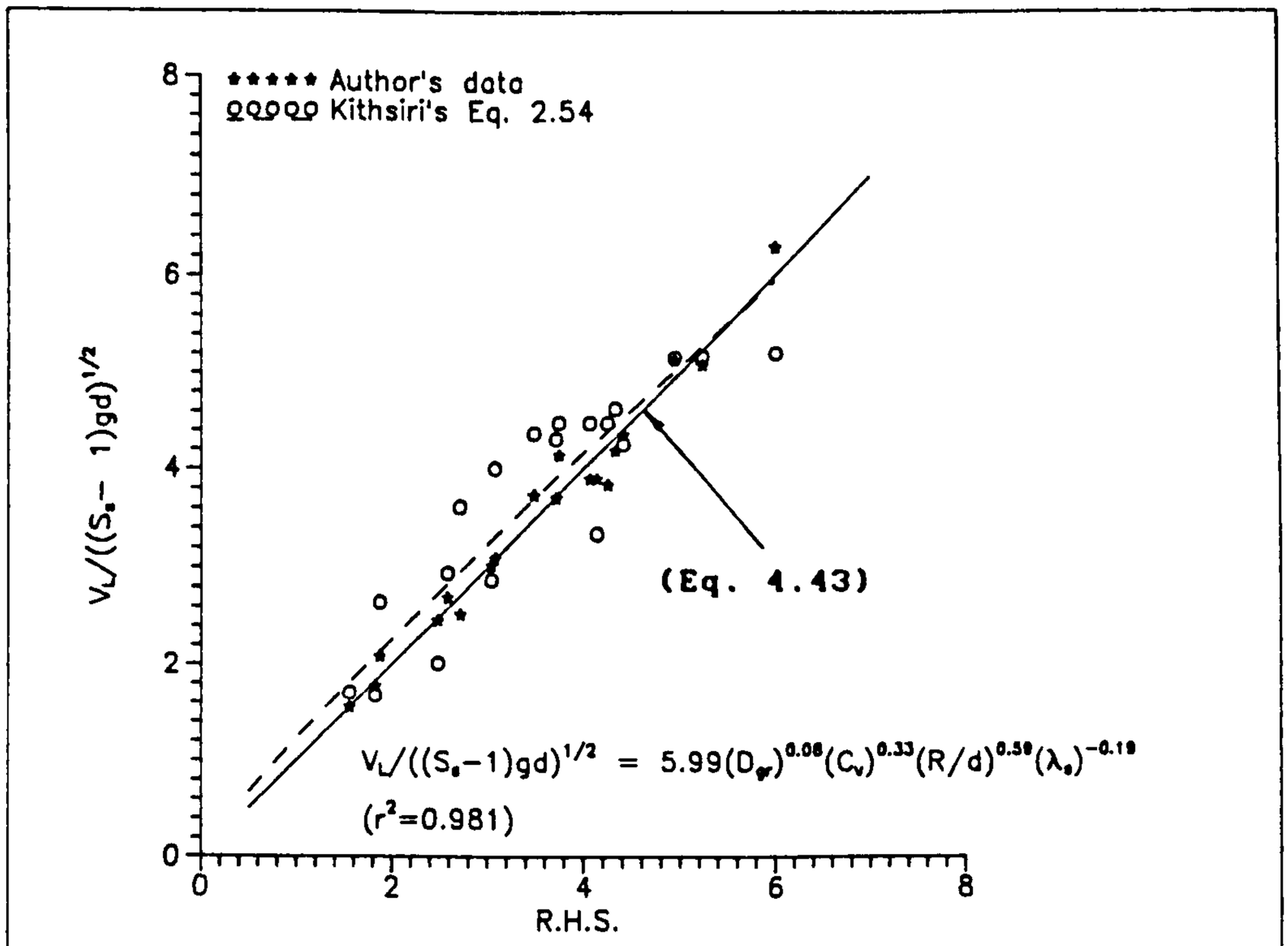

FIGURE 4.58: COMPARISON WITH KITHSIRI'S EQ. FOR RECT. CHANNELS
Transport Experiments Over Fixed Beds in Channels of circular Cross-section (D=154mm) with sediment bed (E=40.8mm)

c) Minimum Shear Stress Required for Limit Deposition Condition

In order to apply the minimum shear stress criterion to sewer design a multiregression was performed with the data, using Kithsiri's format, and the following equation was obtained:

$$\frac{\tau_b}{\rho(S_s-1)gd_{50}} = 6.42\,(D_{gr})^{-0.29}(C_v)^{0.64}\left(\frac{d_{50}}{R_b}\right)^{-1.03}(\lambda_{sb})^{0.5} \qquad (4.45)$$

with r^2=0.982, where τ_b is the separated bed shear stress, ρ is the water density, S_s is the relative density of the sediment, g is the acceleration due to gravity, d_{50} is the mean particle size, D_{gr} is the dimensionless grain size, C_v is the volumetric

sediment concentration, R_b is the hydraulic radius related to the bed only, and λ_{bs} is the separated bed friction factor with sediment. In Fig. 4.59 Mayerle's data, as analysed by Kithsiri (1990) and represented by Eq. 2.59 is plotted together with the author's data for comparison. It can be observed that Mayerle (1988) predicts higher values of minimum shear stress for limit deposition condition (on average ≅ 29% higher). The same thing can be observed when comparing with Kithsiri's Eq. 2.56 for rectangular channels (see Fig. 4.60).

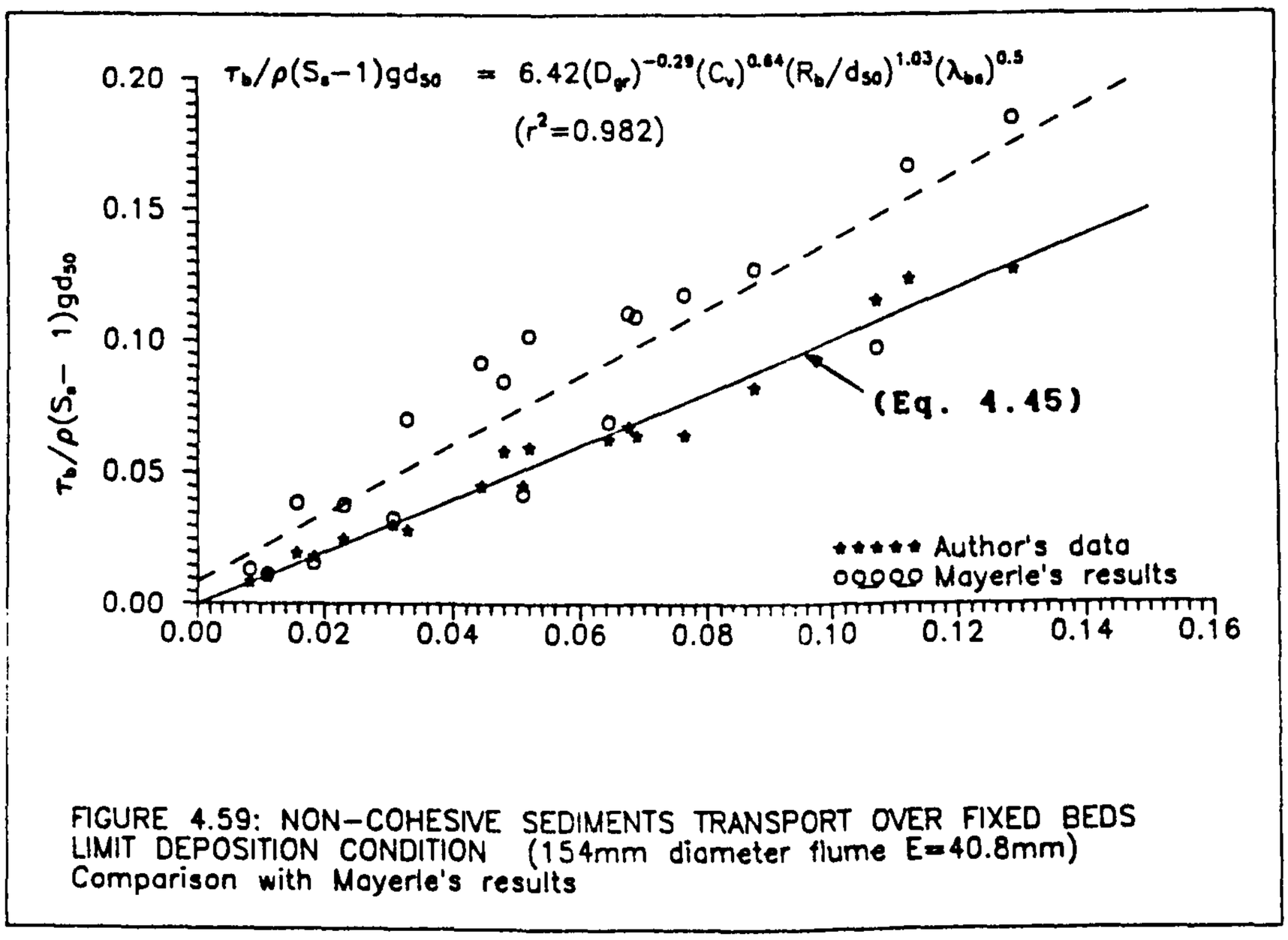

FIGURE 4.59: NON-COHESIVE SEDIMENTS TRANSPORT OVER FIXED BEDS LIMIT DEPOSITION CONDITION (154mm diameter flume E=40.8mm) Comparison with Mayerle's results

The above observations can be explained by the shear stress distribution. In case of smooth circular channels (with sediment bed separated bed) shear stresses were found to be 50 to 100% higher than mean shear stresses. In case of rectangular channels with smooth walls the separated bed shear stresses were higher than mean shear stress by no more than 20% (Kithsiri, 1990).

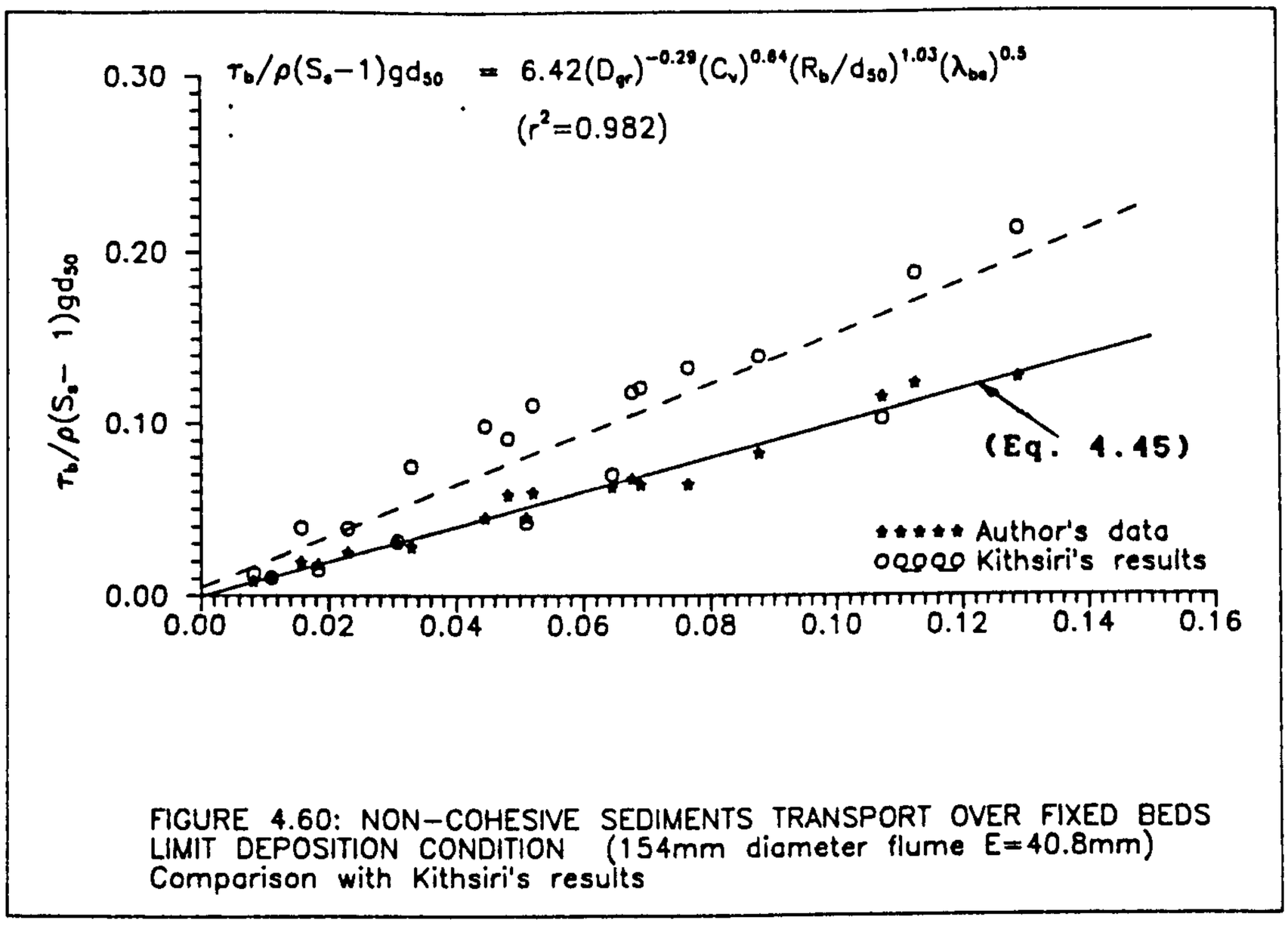

FIGURE 4.60: NON-COHESIVE SEDIMENTS TRANSPORT OVER FIXED BEDS LIMIT DEPOSITION CONDITION (154mm diameter flume E=40.8mm) Comparison with Kithsiri's results

TABLE 4.1: FULL PIPE FLOW ROUGHNESS EXPERIMENTS

(NO SEDIMENT BED)

154 mm diameter flume (smooth boundary)

	Q (l/s)	V (m/s)	T °C	R_e	S_f	λ	k_s (mm)
1	3.51	0.1884	20.1	2.86E+04	0.000297	0.025251	0.0593
2	6.58	0.3533	19.9	5.34E+04	0.000841	0.020358	-0.0280
3	8.27	0.4440	19.2	6.60E+04	0.001410	0.021606	0.0666
4	9.11	0.4891	19.4	7.31E+04	0.001534	0.019367	-0.0073
5	11.87	0.6373	19.0	9.43E+04	0.002548	0.018952	0.0144
6	11.91	0.6394	19.0	9.46E+04	0.002895	0.021383	0.1057
7	13.41	0.7199	18.7	1.06E+05	0.003290	0.019174	0.0352
8	13.87	0.7446	18.7	1.09E+05	0.003434	0.018704	0.0237
9	15.99	0.8585	18.3	1.25E+05	0.003983	0.016324	-0.0253
10	16.75	0.8993	17.4	1.28E+05	0.004750	0.017741	0.0136
11	17.51	0.9401	18.8	1.38E+05	0.005096	0.017418	0.0089
12	18.13	0.9733	18.7	1.43E+05	0.005408	0.017241	0.0073
13	20.12	1.0802	17.9	1.56E+05	0.006581	0.017035	0.0103
14	20.95	1.1247	18.5	1.64E+05	0.006912	0.016503	0.0011
15	21.03	1.1290	18.5	1.65E+05	0.007348	0.017410	0.0227
16	21.49	1.1537	18.0	1.67E+05	0.007595	0.017234	0.0198
17	21.66	1.1629	19.5	1.74E+05	0.007669	0.017130	0.0178
18	23.71	1.2729	18.5	1.86E+05	0.008808	0.016417	0.0076
19	23.85	1.2804	18.3	1.86E+05	0.008931	0.016453	0.0087
20	25.13	1.3492	18.9	1.99E+05	0.010045	0.016667	0.0166
21	25.59	1.3738	18.1	1.99E+05	0.009302	0.014885	-0.0166
22	26.77	1.4372	19.0	2.13E+05	0.009698	0.014181	-0.0247
23	27.24	1.4624	18.4	2.13E+05	0.010094	0.014255	-0.0226
24	28.20	1.5140	18.6	2.22E+05	0.011875	0.015648	0.0024
25	28.87	1.5499	18.6	2.27E+05	0.011826	0.014868	-0.0098
26	30.95	1.6616	17.5	2.37E+05	0.013904	0.015210	-0.0005
27	34.07	1.8291	17.7	2.62E+05	0.015280	0.013793	-0.0169
28	36.44	1.9564	18.0	2.82E+05	0.018535	0.014627	-0.0021
29	43.09	2.3134	18.2	3.36E+05	0.019654	0.011092	-0.0325

TABLE 4.2: OPEN CHANNEL FLOW ROUGHNESS EXPERIMENTS (NO SEDIMENT BED)

154 mm dia. flume (smooth boundary)

	S_o	Y_o (mm)	Q (l/s)	R_e	V (m/s)	λ	k_s (mm)	n
154 mm diameter flume								
1	0.004701	35.0	2.13	5.14E+04	0.669	0.01711	-0.0685	0.0077
2	0.004503	42.0	3.29	7.34E+04	0.799	0.01344	-0.0886	0.0070
3	0.004552	85.5	10.98	1.61E+05	1.034	0.01370	-0.0482	0.0078
4	0.004552	106.5	14.40	1.82E+05	1.048	0.01478	-0.0244	0.0082
5	0.005690	59.0	6.31	1.15E+05	0.961	0.01544	-0.0382	0.0079
6	0.005591	81.0	10.65	1.59E+05	1.073	0.01515	-0.0247	0.0081
7	0.005591	108.0	15.52	1.88E+05	1.112	0.01619	0.0083	0.0086
8	0.004998	47.3	3.69	7.98E+04	0.761	0.01815	-0.0156	0.0083
9	0.005047	59.8	5.82	1.10E+05	0.871	0.01682	-0.0176	0.0083
10	0.005047	78.8	9.25	1.46E+05	0.965	0.01659	-0.0011	0.0085
11	0.004998	93.3	12.07	1.70E+05	1.023	0.01609	-0.0015	0.0085
12	0.003859	49.0	3.4	7.06E+04	0.667	0.01880	-0.0137	0.0085
13	0.003835	72.3	6.7	1.09E+05	0.775	0.01850	0.0227	0.0089
14	0.003859	88.5	9.4	1.34E+05	0.848	0.01762	0.0185	0.0088
15	0.003859	113.0	13.7	1.62E+05	0.932	0.01612	-0.0046	0.0086
16	0.002128	54.0	3.12	6.14E+04	0.536	0.01736	-0.0662	0.0083
17	0.002350	71.8	5.6	9.35E+04	0.658	0.01563	-0.0623	0.0081
18	0.002152	98.3	8.6	1.17E+05	0.689	0.01567	-0.0454	0.0084
19	0.002152	121.3	11.9	1.37E+05	0.755	0.01385	-0.0688	0.0080
20	0.002721	45.0	2.3	5.01E+04	0.510	0.02116	0.0079	0.0089
21	0.002721	61.0	4.1	7.48E+04	0.603	0.01924	0.0031	0.0089
22	0.002672	81.5	6.8	1.02E+05	0.681	0.01805	0.0038	0.0089
23	0.002771	101.5	10.2	1.30E+05	0.781	0.01590	-0.0295	0.0085
		Averages					-0.024	0.008
302 mm diameter flume								
24	0.002000	44.7	2.9	4.86E+04	0.439	0.02257	0.05	0.0093
25	0.001423	110.3	16.0	1.63E+05	0.676	0.01474	-0.05	0.0086
26	0.000730	160.5	18.7	1.52E+05	0.484	0.01920	0.15	0.0102
27	0.000406	252.7	27.0	1.55E+05	0.422	0.01643	0.00	0.0097
		Averages					0.038	0.009

TABLE 4.3: FULL PIPE FLOW ROUGHNESS EXPERIMENTS (WITH SEDIMENT BED)

154 mm dia. flume (smooth wall, rough bed)

	Q (l/s)	T °C	V (m/s)	S_f	λ	λ_b	k_s (mm)	k_{sb} (mm)
	Bed thickness		18.4 mm					
	Sand bed		0.53 mm					
1	14.32	17.4	0.8245	0.00568	0.02395	0.04583	0.24	4.73
2	15.25	17.7	0.8780	0.00630	0.02345	0.04464	0.22	4.38
3	17.17	18.1	0.9886	0.00779	0.02287	0.04391	0.20	4.23
4	18.81	18.4	1.0830	0.00904	0.02211	0.04174	0.18	3.61
5	20.51	18.8	1.1809	0.01066	0.02193	0.04224	0.17	3.81
6	21.77	19.1	1.2534	0.01189	0.02170	0.04200	0.17	3.77
7	22.85	19.4	1.3156	0.01299	0.02153	0.04187	0.16	3.76
8	23.51	19.8	1.3536	0.01368	0.02141	0.04172	0.16	3.73
9	24.13	20.0	1.3893	0.01420	0.02110	0.04062	0.15	3.41
10	25.12	20.3	1.4463	0.01492	0.02046	0.03809	0.13	2.73
11	26.24	20.3	1.5108	0.01647	0.02070	0.03983	0.14	3.22
						Averages	0.175	3.762
	Bed thickness		12.46 mm					
	Sand bed		0.53 mm					
12	11.85	19.0	0.6614	0.00364	0.02443	0.05069	0.26	6.85
13	14.27	19.5	0.7965	0.00505	0.02335	0.04801	0.22	5.90
14	16.40	20.0	0.9153	0.00625	0.02191	0.04270	0.16	4.06
15	17.84	20.3	0.9957	0.00743	0.02198	0.04476	0.17	4.84
16	19.34	20.5	1.0794	0.00909	0.02289	0.05156	0.22	7.79
17	20.99	20.5	1.1715	0.01048	0.02241	0.05034	0.20	7.32
18	23.02	20.5	1.2848	0.01135	0.02018	0.03930	0.12	3.21
19	24.86	20.5	1.3875	0.01372	0.02091	0.04479	0.15	5.12
						Averages	0.186	5.634
	Bed thickness		20.0 mm					
	Sand bed		1.6 mm					
20	17.04	17.4	0.9904	0.00980	0.02846	0.06837	0.52	15.77
21	19.40	17.7	1.1275	0.01197	0.02683	0.06292	0.43	12.77
22	21.73	18.0	1.2630	0.01544	0.02757	0.06792	0.48	15.94
23	23.57	18.4	1.3699	0.01786	0.02712	0.06692	0.45	15.46
24	25.85	18.7	1.5024	0.02073	0.02617	0.06377	0.40	13.69
25	27.59	18.9	1.6035	0.02360	0.02615	0.06450	0.40	14.23
26	31.34	19.2	1.8215	0.02855	0.02451	0.05854	0.31	10.99
27	32.78	19.4	1.9052	0.03147	0.02470	0.05990	0.32	11.79
28	35.39	19.5	2.0569	0.03538	0.02382	0.05674	0.28	10.17
						Averages	0.400	13.424

TABLE 4.3: CONTINUATION

	Q (l/s)	T °C	V (m/s)	S_f	λ	λ_b	k_s (mm)	k_{sb} (mm)
	Bed thickness		60.3 mm					
	Sand bed		0.53 mm					
29	7.18	20.5	0.6052	0.005195	0.03100	0.04883	0.51	3.48
30	5.32	22.0	0.4484	0.003008	0.03270	0.05127	0.60	3.91
31	3.67	20.5	0.3093	0.001385	0.03163	0.04521	0.47	2.48
						Averages	0.524	3.291
	Bed thickness		40.8 mm					
	Sand bed		0.53 mm					
32	5.21	18.8	0.3550	0.001301	0.02623	0.03535	0.20	1.27
33	7.46	19.0	0.5083	0.003053	0.03001	0.05016	0.50	4.60
34	7.59	18.6	0.5172	0.002647	0.02514	0.03555	0.20	1.41
35	13.08	19.7	0.8913	0.007694	0.02460	0.03860	0.23	2.09
						Averages	0.280	2.344
	Bed thickness		40.8 mm					
	Sand bed		0.00 mm					
36	6.84	18.1	0.4661	0.002013	0.02354	0.02969	0.10	0.63
37	9.53	18.0	0.6494	0.003206	0.01931	0.02008	-0.01	0.04
38	12.64	19.2	0.8613	0.005329	0.01825	0.01927	0.00	0.046
39	16.12	19.0	1.0984	0.008876	0.01869	0.02224	0.03	0.194
						Averages	0.032	0.229

TABLE 4.4: ROUGHNESS EXPERIMENTS, OPEN CHANNEL FLOW
154 mm diameter flume (smooth wall, rough bed)

	S_o	Y_o (mm)	$\frac{(Yo+E)}{D}$	Q (l/s)	V (m/s)	λ	λ_b	k_s (mm)	k_{sb} (mm)	n	n_b
	Bed thickness			60.3 (mm)							
	Sand bed			0.53 (mm)							
1	0.001853	55.0	74.9	3.06	0.373	0.03239	0.03933	0.62	1.55	0.0114	0.0130
2	0.001685	35.1	61.9	1.53	0.286	0.03924	0.04532	0.91	1.70	0.0120	0.0132
3	0.002123	55.6	75.3	3.63	0.439	0.02699	0.03096	0.28	0.63	0.0104	0.0114
							Averages	0.603	1.294	0.01128	0.01254
	Bed thickness			40.8 (mm)							
	Sand bed			0.53 (mm)							
4	0.001704	76.1	75.9	5.07	0.452	0.02487	0.03002	0.25	0.76	0.0103	0.0117
5	0.002088	35.3	49.4	1.75	0.335	0.03630	0.04227	0.72	1.45	0.0116	0.0129
6	0.002377	35.1	49.3	2.28	0.439	0.02410	0.02522	0.08	0.14	0.0095	0.0098
7	0.001104	73.9	74.5	3.75	0.343	0.02769	0.03435	0.39	1.24	0.0109	0.0126
8	0.001104	39.2	51.9	1.53	0.263	0.03354	0.03832	0.54	1.08	0.0113	0.0124
9	0.001154	35.4	49.5	1.45	0.277	0.02945	0.03188	0.25	0.44	0.0105	0.0110
							Averages	0.373	0.852	0.01068	0.01172
	Bed thickness			20 (mm)							
	Sand bed			1.6 (mm)							
10	0.002851	46.5	43.2	2.53	0.403	0.04106	0.05864	1.38	5.33	0.0127	0.0162
11	0.002808	51.7	46.6	3.08	0.435	0.03719	0.05338	1.09	4.56	0.0123	0.0156
12	0.002806	66.6	56.2	4.65	0.496	0.03332	0.05038	0.90	4.86	0.0119	0.0157
13	0.003124	80.8	65.5	6.19	0.538	0.03469	0.05901	1.16	8.96	0.0123	0.0176
14	0.002867	95.1	74.7	8.02	0.594	0.02768	0.04421	0.54	4.21	0.0111	0.0152
15	0.002830	96.0	75.3	7.97	0.585	0.02822	0.04580	0.58	4.73	0.0112	0.0155
16	0.002862	52.1	46.8	3.15	0.441	0.03706	0.05330	1.09	4.58	0.0123	0.0156
17	0.002243	49.0	44.8	2.47	0.371	0.03952	0.05618	1.26	4.94	0.0126	0.0159
18	0.002184	64.9	55.1	3.87	0.425	0.03488	0.04276	1.02	2.44	0.0122	0.0139
19	0.002250	86.0	68.8	5.90	0.482	0.03200	0.05213	0.88	6.46	0.0119	0.0165
							Averages	0.991	5.105	0.01205	0.01577

TABLE 4.4: CONTINUATION

	S_o	Y_o (mm)	$\frac{(Yo+E)}{D}$	Q (l/s)	V (m/s)	λ	λ_b	k_s (mm)	k_{sb} (mm)	n	n_b
	Bed thickness		18.4 (mm)								
	Sand bed		0.53 (mm)								
20	0.001432	60.8	51.4	3.01	0.359	0.03082	0.04303	0.61	2.72	0.0114	0.0142
21	0.001520	26.8	29.4	0.76	0.230	0.04432	0.05481	1.06	2.49	0.0124	0.0142
22	0.002350	77.5	62.3	5.59	0.511	0.02844	0.04260	0.54	3.29	0.0112	0.0146
23	0.002070	105.4	80.4	7.71	0.521	0.02647	0.04317	0.45	4.12	0.0109	0.0151
24	0.002278	112.4	85.0	8.62	0.552	0.02596	0.04321	0.42	4.22	0.0108	0.0152
25	0.002290	53.5	46.7	3.10	0.426	0.03223	0.04475	0.67	2.80	0.0115	0.0143
26	0.002200	29.8	31.3	1.12	0.301	0.04088	0.05115	0.91	2.30	0.0120	0.0140
							Averages	0.666	3.134	0.01144	0.01451

TABLE 4.5: OPEN CHANNEL FLOW EXPERIMENTS (WITH SEDIMENT BED)
302 mm diameter flume (smooth walls, rough bed)

	S_o	Y_o (mm)	$\frac{(Yo+E)}{D}$ (%)	Q (l/s)	V (m/s)	λ	λ_b	k_s (mm)	k_b (mm)	Manning's Coef. n	Manning's Coef. n_b
	Bed thickness		47.6 mm								
	Sand bed		0.0 mm		(smooth)						
1	0.001100	65.4	38.2	8.70	0.505	0.01572	0.01417	-0.08	-0.08	0.0085	0.0079
2	0.002650	105.4	51.5	25.80	0.884	0.01720	0.01877	0.07	0.08	0.0094	0.0099
3	0.000460	155.0	67.9	22.19	0.506	0.01117	0.00392	-0.15	-0.17	0.0078	0.0039
4	0.000560	200.8	83.0	25.70	0.461	0.01752	0.01897	0.06	0.07	0.0099	0.0104
					Averages			-0.026	-0.024	0.00890	0.00803
	Bed thickness		47.6 mm								
	Sand bed		1.6 mm								
5	0.000936	49.4	32.9	2.82	0.223	0.05508	0.06963	3.92	8.57	0.0153	0.0179
6	0.000988	72.7	40.6	5.56	0.287	0.04720	0.06453	3.56	10.64	0.0149	0.0183
7	0.001052	98.1	49.0	9.40	0.349	0.04191	0.06238	3.17	13.28	0.0145	0.0189
8	0.000963	123.4	57.4	13.57	0.392	0.03480	0.05365	2.06	11.00	0.0135	0.0181
9	0.000951	149.8	66.2	18.21	0.430	0.03156	0.05089	1.65	11.12	0.0131	0.0180
10	0.001005	174.2	74.2	23.46	0.477	0.02856	0.04743	1.23	10.08	0.0126	0.0177
11	0.002190	101.2	50.0	14.69	0.527	0.03899	0.06010	2.64	12.95	0.0141	0.0188
12	0.002038	126.4	58.4	22.89	0.645	0.02760	0.04100	0.95	5.20	0.0121	0.0157
13	0.002034	152.7	67.1	27.58	0.638	0.03086	0.05248	1.58	12.89	0.0130	0.0185
14	0.002432	162.2	70.3	32.87	0.717	0.02997	0.05205	1.47	13.22	0.0128	0.0186
					Averages			2.224	10.894	0.0136	0.0181

TABLE 4.6: TYPICAL SHEAR STRESS DISTRIBUTION MEASUREMENT (14-10-88a)

a) FLOW CHARACTERISTICS

Flume Diameter	(D) =	154.00 (mm)	
Sand size	(d_{50})=	2.00 (mm)	
Bed Thickness	(E) =	18.40 (mm)	(E/D=0.119)
Effective Slope	(S) =	0.002350	
Discharge	(Q) =	5.59 (l/s)	
Normal Depth	(Y_o) =	77.45 (mm)	
(Y+E)/D	=	0.62	
Mean Velocity	(V) =	0.512 (m/s)	
Mean Shear Stress	(τ_o) =	0.929 (N/m^2)	
Predicted Bed Shear	(τ_b) =	1.386 (N/m^2)	(separated)

Current Meter: (No 1398-A)

V = 0.5096*N + 5.3654 (48.5 < N <267 Hz)

[cm/s] [Hz]

b) VELOCITY PROFILE A: (Position: X = 0 centreline)

y (mm)	N (Hz)	u (m/s)	umax-u (m/s)	umax-u regr.	$-5.75\text{Log}(\frac{y}{h})$
7.5	76.64	0.444	0.1331	0.1338	4.18
10.0	81.65	0.470	0.1075	0.1049	3.46
12.0	86.14	0.493	0.0847	0.0865	3.01
14.0	88.93	0.507	0.0705	0.0710	2.62
18.0	93.69	0.531	0.0462	0.0457	1.99
22.0	96.24	0.544	0.0332	0.0255	1.49
30.0	100.96	0.568	0.0091	-0.0058	0.72
40.0	102.75	0.577	0.0000	-0.0347	0.00
50.0	99.31	0.560	0.0175	-0.0572	-0.56
70.0	90.00	0.512	0.0650	-0.0911	-1.40

Regression Output:

Curve Gradient (Shear Velocity, u_*)	=	0.0403 (m/s)
Correlation Coef. (ρ^2)	=	0.9974
Measured Bed Shear Stress (τ_{bm})	=	1.626 (N/m)

TABLE 4.6: CONTINUATION

c) VELOCITY PROFILE B: X = 2 cm from centreline

Y (mm)	N (Hz)	u (m/s)	Umax-u (m/s)	Umax-u regr.	$-5.75\text{Log}(\frac{y}{h})$
7.5	74.99	0.436	0.1379	0.1395	4.18
10.0	79.95	0.461	0.1126	0.1111	3.46
12.0	83.64	0.480	0.0938	0.0931	3.01
14.0	86.70	0.495	0.0782	0.0779	2.62
18.0	91.59	0.520	0.0533	0.0531	1.99
22.0	95.70	0.541	0.0323	0.0333	1.49
30.0	100.85	0.568	0.0061	0.0027	0.72
40.0	102.04	0.574	0.0000	-0.0257	0.00
50.0	99.64	0.561	0.0122	-0.0477	-0.56
70.0	86.08	0.492	0.0813	-0.0809	-1.40

Regression Output:

Curve Gradient (Shear Velocity, u_*) = 0.03951 (m/s)

Correlation Coef. (ρ^2) = 0.9991

Measured Bed Shear Stress (τ_{bm}) = 1.561 (N/m^2)

d) VELOCITY PROFILE C: X = 4 cm from centreline

Y (mm)	N (Hz)	u (m/s)	Umax-u (m/s)	Umax-u regr.	$-5.75\text{Log}(\frac{y}{h})$
7.5	74.23	0.432	0.1140	0.1143	4.18
10.0	78.39	0.453	0.0928	0.0914	3.46
12.0	81.60	0.470	0.0764	0.0770	3.01
14.0	83.96	0.482	0.0644	0.0647	2.62
18.0	88.16	0.503	0.0430	0.0448	1.99
22.0	90.63	0.515	0.0304	0.0289	1.49
30.0	95.95	0.543	0.0033	0.0043	0.72
40.0	96.60	0.546	0.0000	-0.0185	0.00
50.0	94.30	0.534	0.0117	-0.0362	-0.56
70.0	77.00	0.446	0.0999	-0.0629	-1.40

Regression Output:

Curve Gradient (Shear Velocity, u_*) = 0.03176 (m/s)

Correlation Coef. (ρ^2) = 0.9983

Measured Bed Shear Stress (τ_{bm}) = 1.009 (N/m^2)

TABLE 4.6: CONTINUATION

e) VELOCITY PROFILE D: X = 5 cm from centreline

Y (mm)	N (Hz)	u (m/s)	$u_{max}-u$ (m/s)	$u_{max}-u$ regr.	$-5.75\text{Log}(\frac{y}{h})$
7.5	74.93	0.435	0.1019	0.1026	4.18
10.0	78.75	0.455	0.0824	0.0826	3.46
12.0	81.55	0.469	0.0682	0.0699	3.01
14.0	82.78	0.475	0.0619	0.0592	2.62
18.0	86.55	0.495	0.0427	0.0417	1.99
22.0	89.38	0.509	0.0283	0.0277	1.49
30.0	94.05	0.533	0.0045	0.0061	0.72
40.0	94.93	0.537	0.0000	-0.0139	0.00
50.0	92.53	0.525	0.0122	-0.0294	-0.56
70.0	75.21	0.437	0.1005	-0.0529	-1.40

Regression Output:

Curve Gradient (Shear Velocity, u_*) = 0.0279 (m/s)

Correlation Coef. (ρ^2) = 0.9977

Measured Bed Shear Stress (τ_{bm}) = 0.777 (N/m^2)

TABLE 4.7: SHEAR STRESS DETERMINATION

(FULL PIPE FLOW)

154 mm diameter flume (with sediment bed)

	Bed Thick-ness E (mm)	Pressure Gradient S	Discharge (l/s) Q	Shear Stress (N/m^2) mean τ_o	bed Predict. τ_b	bed Measured τ_{bm}	Trans Pos. (cm) X
1	12.5	0.001371	6.52	0.5029	1.1437	1.1670	0
2	12.5	0.004062	12.23	1.4900	3.2644	3.4250	0
3	12.5	0.006091	15.90	2.2343	4.4809	4.7580	0
4	12.5	0.011836	22.80	4.3417	9.2219	12.9940	0
5	18.4	0.006630	15.84	2.4339	4.7379	4.7540	0
6	18.4	0.002070	8.38	0.7429	1.3477	1.8130	0
7	18.4	0.000720	4.51	0.2573	0.4908	0.4730	0
8	18.4	0.003660	11.39	1.3129	2.4721	3.1310	0
9	18.4	0.001870	7.80	0.6706	1.2651	1.4570	0
10	18.4	0.009890	19.72	3.5448	6.7865	9.2570	0
11	18.4	0.006754	15.84	2.422	4.777	4.429	0
12	18.4	0.006754	15.84	2.422	4.777	3.667	2
13	18.4	0.006754	15.84	2.422	4.777	3.465	4
14	18.4	0.006754	15.84	2.422	4.777	2.181	5
15	40.8	0.001301	5.21	0.4131	0.5570	0.7340	0
16	40.8	0.003053	7.46	0.9691	1.6191	1.5340	0
17	60.3	0.005195	7.18	1.4193	2.2358	2.5130	0
18	60.3	0.003008	5.32	0.8921	1.4716	1.8950	0
19	60.3	0.003008	5.32	0.8921	1.4716	1.3940	2
20	60.3	0.003008	5.32	0.8921	1.4716	1.5920	4
21	60.3	0.001385	3.67	0.3783	0.5408	0.7610	0
22	60.3	0.001385	3.67	0.3783	0.5408	0.5650	2
23	60.3	0.001385	3.67	0.3783	0.5408	0.6060	4

TABLE 4.8: SHEAR STRESS COMPUTATIONS (OPEN CHANNEL FLOW)
154 mm diameter flume (with flat sediment bed)

	Bed Thick-ness E (mm)	Normal Depth Yo (mm)	Effect. Slope S	Flow rate Q (l/s)	Shear Stress (N/m^2) mean τ_o	bed Predic. τ_b	bed Measur. τ_{bm}	Trans Pos. X (cm)
1	60.3	55.0	0.001853	3.06	0.5629	0.6848	0.9540	0
2	60.3	55.0	0.001853	3.06	0.5629	0.6848	0.8730	2
3	60.3	55.0	0.001853	3.06	0.5629	0.6848	0.6280	4
4	60.3	35.1	0.001685	1.53	0.4002	0.4622	0.4990	0
5	60.3	35.1	0.001685	1.53	0.4002	0.4622	0.3720	2
6	60.3	35.1	0.001685	1.53	0.4002	0.4622	0.3520	4
7	60.3	55.6	0.002123	3.63	0.6489	0.7442	0.8730	0
8	60.3	55.6	0.002123	3.63	0.6489	0.7442	0.7240	2
9	60.3	55.6	0.002123	3.63	0.6489	0.7442	0.6870	4
10	40.8	76.1	0.001704	5.07	0.6351	0.7666	0.8590	0
11	40.8	35.3	0.002088	1.75	0.5102	0.5941	0.4610	0
12	40.8	35.1	0.002377	2.28	0.5793	0.6063	0.6460	0
13	40.8	73.9	0.001104	3.75	0.4078	0.5059	0.3760	0
14	40.8	39.2	0.001104	1.53	0.2900	0.3313	0.1650	0
15	40.8	35.4	0.001154	1.45	0.2825	0.3058	0.1830	0
16	20.0	46.5	0.002851	2.53	0.8349	1.1895	1.0810	0
17	20.0	51.7	0.002808	3.08	0.8806	1.2638	0.9020	0
18	20.0	66.6	0.002806	4.65	1.0263	1.5521	1.8330	0
19	20.0	80.8	0.003124	6.19	0.9620	1.3899	1.1980	0
20	20.0	80.8	0.003124	6.19	0.9620	1.3899	1.2700	2
21	20.0	80.8	0.003124	6.19	0.9620	1.3899	1.0750	4
22	20.0	95.1	0.002867	8.02	1.1379	1.7432	2.1230	0
23	20.0	95.1	0.002867	8.02	1.1379	1.7432	2.8570	2
24	20.0	95.1	0.002867	8.02	1.1379	1.7432	3.1840	4
25	20.0	95.1	0.002867	8.02	1.1379	1.7432	1.6900	5
26	20.0	96.0	0.002830	7.97	1.2060	1.9571	2.2340	0
27	20.0	52.1	0.002862	3.15	0.9023	1.2974	1.3840	0
28	20.0	49.0	0.002243	2.47	0.6790	0.9652	0.7420	0
29	20.0	64.9	0.002184	3.87	0.7877	0.9652	0.7420	0
30	20.0	86.0	0.002250	5.90	0.9277	1.5115	1.3380	0
31	18.4	67.2	0.001081	3.05	0.3972	0.5555	0.6210	0
32	18.4	57.7	0.001607	3.02	0.5396	0.7316	0.9790	0
33	18.4	60.8	0.001432	3.01	0.4961	0.6926	0.8410	0
34	18.4	26.8	0.001520	0.76	0.2937	0.3632	0.3500	0
35	18.4	26.8	0.001520	0.76	0.2934	0.3632	0.2990	3
36	18.4	26.8	0.001520	0.76	0.2934	0.3632	0.0800	5

TABLE 4.9: TURBULENCE MEASUREMENT EXPERIMENTS

FLOW CHARACTERISTICS - Open Channel Flow

154 mm diameter flume (E = 40.8 mm)

Series	Slope	Yo (mm)	$\frac{Yo+E}{D}$	Q (l/s)	V (m/s)	λ	λ_b
Rough Bed							
R1	0.002462	36.75	0.50	2.06	0.378	0.03463	0.04115
R2	0.002378	74.10	0.75	5.50	0.502	0.02789	0.03724
R3	0.001244	44.09	0.55	1.91	0.291	0.03348	0.03993
R4	0.001312	67.31	0.70	3.64	0.363	0.02838	0.03556
R5	0.003680	34.90	0.49	2.42	0.469	0.03249	0.03808
R6	0.003626	78.81	0.78	7.30	0.631	0.02742	0.03813
Smooth Bed							
S1	0.002466	36.58	0.50	2.15	0.397	0.03143	0.03628
S2	0.002329	78.69	0.78	6.35	0.549	0.02321	0.02807
S3	0.001499	36.96	0.50	1.73	0.316	0.03037	0.03393
S4	0.001361	72.79	0.74	4.26	0.395	0.02561	0.03097
S5	0.002195	35.49	0.50	2.08	0.396	0.02748	0.02998
S6	0.002206	73.47	0.74	5.74	0.528	0.02333	0.02767
S7	0.003507	34.81	0.49	2.57	0.499	0.02725	0.03021
S8	0.003500	76.37	0.76	8.21	0.729	0.01963	0.02143

Series	Equiv. Sand Roughness (mm)		Manning's Coef.		Shear Stress (N/m^2)		
					Mean	Bed	
						Predict. τ_b	Measur. τ_{bm}
	k_s	k_{sb}	n	n_b			
Rough Bed							
R1	0.48	1.28	0.01141	0.01280	0.6192	0.7358	1.158
R2	0.32	1.70	0.01092	0.01324	0.8795	1.1737	1.347
R3	0.40	1.25	0.01145	0.01288	0.3532	0.4213	0.414
R4	0.24	1.20	0.01095	0.01273	0.4685	0.5867	0.576
R5	0.37	0.95	0.01098	0.01221	0.8927	1.0462	1.333
R6	0.34	2.00	0.01086	0.01353	1.3644	1.8968	1.974
Smooth Bed							
S1	0.28	0.76	0.01086	0.01195	0.6181	0.7135	0.877
S2	0.05	0.49	0.00999	0.01134	0.8759	1.0593	0.945
S3	0.14	0.46	0.01069	0.01151	0.3784	0.4229	0.380
S4	0.09	0.67	0.01045	0.01186	0.5002	0.6048	0.453
S5	0.04	0.22	0.01012	0.01073	0.5387	0.5876	0.808
S6	0.04	0.41	0.00998	0.01119	0.8133	0.9648	1.058
S7	0.09	0.30	0.01006	0.01077	0.8490	0.9410	1.063
S8	0.05	0.04	0.00917	0.00973	1.3058	1.4257	1.522

TABLE 4.10: TURBULENCE MEASUREMENT EXPERIMENTS

FLOW CHARACTERISTICS - Full Pipe Flow

154 mm diameter flume (E = 40.8 mm)

Series	Pressure Gradient	Q (l/s)	V (m/s)	λ	λ_b	k_s (mm)
Rough						
RF1	0.007694	13.08	0.891	0.02925	0.05704	0.45
RF2	0.002647	7.59	0.517	0.02989	0.05412	0.40
Smooth						
SF1	0.002013	6.84	0.466	0.02800	0.04675	0.25
SF2	0.005329	12.64	0.861	0.02170	0.03156	0.04
SF3	0.003206	9.53	0.649	0.02296	0.03325	0.04
SF4	0.008876	16.12	1.098	0.01869	0.01909	0.01

Series	k_{sb} (mm)	Manning's Coef.		Shear Stress (N/m^2)		
				Mean	Bed	
					Predict. τ_b	Measur τ_{bm}
		n	n_b			
Rough						
RF1	8.88	0.01000	0.01751	2.4432	5.6642	3.8590
RF2	7.17	0.01011	0.01685	0.8406	1.8096	1.8649
Smooth						
SF1	4.46	0.00978	0.01545	0.6395	1.2695	0.7739
SF2	1.15	0.08610	0.01241	1.6921	2.9262	2.1068
SF3	1.35	0.00886	0.01273	1.0181	1.7530	1.4745
SF4	0.02	0.00870	0.00880	2.8184	2.8798	3.5132

TABLE 4.11: TYPICAL TURBULENCE INTENSITIES COMPUTATIONS

a) Flow Characteristics (R6)

Flume Diameter (D)	154.00 mm
Bed Thickness (E)	40.80 mm
Artificial Roughness	0.50 mm
Flume Slope (S_o)	0.003626
Discharge (Q)	7.30 l/s
Normal Depth (Y_o)	78.81 mm
Relative Depth $(Y_o+E)/D$	0.78
Mean Velocity (V)	0.631 m/s
Temperature (T)	18.5°C
Mean Shear Stress (τ_o)	1.364 (N/m^2)
Predicted Bed Shear Stress (τ_b)	1.897 (N/m^2)

b) Velocity and Turbulence Data

(1) Y (mm)	(2) u (m/s)	(3) RMS (m/s)	(4) TI (%)	(5) $u-u_{max}$ (m/s)	(6) Log(Y/h) x(-5.75)
3.0	0.551	0.066	11.98	0.225	7.4809
6.0	0.570	0.074	12.98	0.206	5.7500
10.0	0.627	0.066	10.53	0.149	4.4744
21.0	0.696	0.062	8.91	0.080	2.6216
30.0	0.762	0.038	4.99	0.014	1.7309
40.0	0.776	0.029	3.74	0.000	1.0125
50.0	0.766	0.029	3.79	0.010	0.4553
66.0	0.737	0.036	4.88	0.039	-0.2380
76.0	0.733	0.031	4.23	0.043	-0.5903

To obtain the shear velocity a regression analysis is performed between columns 5 and 6.

Regresion Output:

Constant	-0.049193	
Std Err of Y Est	0.0110513	
R Squared	0.9881474	Shear velocity
No. of Observations	5	u_x = 0.044579 (m/s)
Degrees of Freedom	3	
X Coefficient(s)	0.0445794	Bed Shear Stress
Std Err of Coef.	0.0028188	τ_b = 1.9873 (N/m^2)

TABLE 4.12: INITIATION OF EROSION EXPERIMENTS

(NON-COHESIVE SEDIMENT)

154 mm diameter flume E = 18.4 - 20 mm

	d_{50} (mm)	S_o	τ_o (N/m^2)	τ_b (N/m^2)	R_{e*}	R_{e*b}	$1/\Psi$	$1/\Psi_b$
a) Uniform size sand								
1	0.50	0.000938	0.16	0.21	5.6	6.4	0.02003	0.02636
2	0.50	0.001201	0.14	0.16	5.4	5.7	0.01825	0.02079
3	0.50	0.002074	0.14	0.15	5.3	5.5	0.01812	0.01901
4	0.90	0.001299	0.43	0.66	16.7	20.6	0.03058	0.04694
5	0.90	0.001963	0.38	0.54	15.7	18.7	0.02703	0.03841
6	0.90	0.002434	0.44	0.59	16.9	19.5	0.03129	0.04196
7	1.44	0.001981	0.43	0.55	26.7	30.2	0.01964	0.02513
8	1.44	0.003398	0.41	0.53	26.0	29.6	0.01873	0.02421
9	1.60	0.001441	0.53	0.82	32.9	40.9	0.02108	0.03262
10	1.60	0.002241	0.50	0.71	31.9	38.1	0.01989	0.02824
11	1.60	0.002802	0.51	0.68	32.1	37.3	0.02009	0.02705
12	2.00	0.001608	0.62	1.10	44.5	59.2	0.02098	0.03721
13	2.00	0.001855	0.55	0.73	41.8	48.2	0.01861	0.02470
14	2.00	0.002660	0.74	1.22	48.6	62.4	0.02504	0.04127
15	2.00	0.003358	0.57	0.75	42.7	49.0	0.01929	0.02538
16	2.00	0.003486	0.75	1.11	48.9	59.5	0.02537	0.03755
17	2.56	0.001317	0.85	1.45	66.6	87.0	0.02187	0.03731
18	2.56	0.002624	1.06	1.84	74.3	98.0	0.02717	0.04734
19	2.56	0.003243	1.10	1.92	75.8	100.2	0.02830	0.04940
20	2.56	0.003872	1.27	2.26	81.5	108.7	0.03268	0.05815
21	2.90	0.001805	0.84	1.30	75.0	93.4	0.01908	0.02953
22	2.90	0.002952	0.98	1.48	81.1	99.6	0.02226	0.03362
23	2.90	0.003962	0.90	1.25	77.7	91.5	0.02044	0.02839
24	4.10	0.001840	1.23	2.39	128.3	179.0	0.02030	0.03945
25	4.10	0.002953	1.37	2.23	135.6	172.8	0.02261	0.03681
26	4.10	0.003762	1.50	2.82	141.8	194.4	0.02522	0.04742
27	4.10	0.003937	1.26	1.82	130.1	156.2	0.02080	0.03004
28	4.10	0.004483	1.60	2.95	146.4	198.8	0.02690	0.04961
b) Mixed size sand								
29	0.90	0.001348	0.53	0.71	20.6	23.9	0.03840	0.05120
30	1.44	0.001746	0.56	0.77	32.4	37.9	0.04050	0.05510
31	2.00	0.001793	0.58	0.81	48.1	56.7	0.04190	0.05840
32	2.90	0.002712	0.75	1.04	75.0	88.7	0.05410	0.07520
33	4.10	0.002712	0.83	1.23	111.6	135.6	0.05990	0.08840

TABLE 4.12 a) INITIATION OF EROSION EXPERIMENTS

Non-cohesive sediments, 154mm diameter flume

	Sand size	Bed thick-ness	Channel slope	Corrected slope	Normal Depth	Disch.	Crit. Shear mean	Crit. Shear bed	Shape factors		Froude number	Mannings Coeff. mean	Mannings Coeff. bed	Part Reynolds number		Entrainment Function mean	Entrainment Function bed		Non-dim. Velocity
	d	E	S_o	S	Y_o	Q	τ_{oc}	τ_{bc}	Y_o/P	T/P	Fr	n	n_b	Re_*	Re_{*b}	$1/\psi$	$1/\psi_b$	V (m/s)	$\frac{V}{\sqrt{(S_s - 1)gd}}$
	(mm)	(mm)			(mm)	(l/s)	(N/m^2)	(N/m^2)											
1	0.50	18.4	0.000938	0.000971	21.6	0.44	0.16	0.21	0.139	0.866	0.394	0.01188	0.01325	5.6	6.4	0.02003	0.02636	0.171	1.92
2	0.50	18.4	0.001201	0.001326	15.4	0.28	0.14	0.16	0.109	0.902	0.434	0.01226	0.01394	5.4	5.7	0.01825	0.02079	0.160	1.80
3	0.50	18.4	0.002074	0.002100	7.0	0.10	0.14	0.15	0.058	0.953	0.526	0.01165	0.01250	5.3	5.5	0.01812	0.01901	0.134	1.51
4	0.90	20.0	0.001299	0.001682	41.8	1.56	0.43	0.66	0.210	0.754	0.475	0.01315	0.01689	16.7	20.6	0.03058	0.04694	0.285	2.40
5	0.90	20.0	0.001963	0.002070	31.6	1.05	0.38	0.54	0.178	0.811	0.507	0.01369	0.01775	15.7	18.7	0.02703	0.03841	0.264	2.23
6	0.90	20.0	0.002434	0.002365	26.3	0.86	0.44	0.59	0.158	0.840	0.560	0.01317	0.01609	16.9	19.5	0.03129	0.04196	0.267	2.25
7	1.44	18.4	0.001981	0.002058	29.5	1.10	0.43	0.55	0.170	0.822	0.591	0.01169	0.01362	26.7	30.2	0.01964	0.02513	0.298	2.01
8	1.44	18.4	0.003398	0.003497	14.8	0.44	0.41	0.53	0.106	0.905	0.716	0.01203	0.01343	26.0	29.6	0.01873	0.02421	0.259	1.75
9	1.60	20.0	0.001441	0.001454	67.8	3.23	0.53	0.82	0.271	0.611	0.449	0.01223	0.01663	32.9	40.9	0.02108	0.03262	0.347	2.19
10	1.60	20.0	0.002241	0.002008	42.4	1.75	0.50	0.71	0.213	0.756	0.543	0.01256	0.01628	31.9	38.1	0.01989	0.02624	0.323	2.03
11	1.60	20.0	0.002802	0.002514	28.5	0.95	0.51	0.68	0.168	0.834	0.580	0.01313	0.01655	32.1	37.3	0.02009	0.02705	0.280	1.77
12	2.00	18.4	0.001608	0.001678	69.7	3.22	0.62	1.10	0.273	0.597	0.416	0.01410	0.02116	44.5	59.2	0.02098	0.03721	0.330	1.92
13	2.00	18.4	0.002660	0.002476	43.8	1.85	0.74	1.22	0.215	0.743	0.522	0.01450	0.02038	48.6	62.4	0.02504	0.04127	0.320	1.86
14	2.00	18.4	0.003486	0.003294	33.4	1.41	0.75	1.11	0.184	0.801	0.622	0.01410	0.01893	48.9	59.5	0.02537	0.03755	0.333	1.93
15	2.00	18.4	0.001855	0.002038	41.8	1.92	0.55	0.73	0.210	0.754	0.583	0.01160	0.01450	41.8	48.2	0.01857	0.02463	0.349	2.03
16	2.00	18.4	0.003358	0.003462	22.2	0.83	0.57	0.75	0.141	0.863	0.709	0.01247	0.01427	42.7	49.0	0.01935	0.02544	0.311	1.81
17	2.56	20.0	0.001317	0.002056	86.9	5.63	0.85	1.45	0.300	0.494	0.506	0.01180	0.01582	66.6	87.0	0.02187	0.03731	0.464	2.35
18	2.56	20.0	0.002624	0.002648	77.2	5.30	1.06	1.84	0.266	0.555	0.589	0.01215	0.01720	74.3	96.0	0.02717	0.04734	0.494	2.50
19	2.56	20.0	0.003243	0.003127	72.4	5.08	1.10	1.92	0.279	0.584	0.631	0.01257	0.01800	75.8	100.2	0.02830	0.04940	0.508	2.57
20	2.56	20.0	0.003872	0.003785	43.0	2.23	1.27	2.26	0.214	0.752	0.676	0.01385	0.02020	81.5	108.7	0.03268	0.05815	0.404	2.05
21	2.90	18.4	0.001605	0.002038	88.7	6.14	0.84	1.30	0.301	0.481	0.524	0.01128	0.01498	75.0	93.4	0.01908	0.02953	0.488	2.33
22	2.90	18.4	0.002952	0.003231	49.6	3.14	0.98	1.48	0.231	0.711	0.720	0.01192	0.01537	81.1	99.6	0.02226	0.03362	0.471	2.24
23	2.90	18.4	0.003962	0.004244	31.7	1.65	0.90	1.25	0.178	0.810	0.791	0.01257	0.01537	77.7	91.5	0.02044	0.02839	0.412	1.97
24	4.10	18.4	0.001840	0.002427	87.3	6.75	1.23	2.39	0.299	0.490	0.592	0.01097	0.01473	128.3	179.0	0.02067	0.04019	0.546	2.24
25	4.10	18.4	0.002953	0.003212	64.4	7.18	1.37	2.23	0.295	0.506	0.669	0.01137	0.01503	135.6	172.8	0.02309	0.03745	0.601	2.46
26	4.10	18.4	0.003937	0.004243	49.5	3.57	1.26	1.82	0.230	0.712	0.821	0.01198	0.01580	130.1	156.2	0.02124	0.03060	0.537	2.20
27	4.10	20.0	0.003762	0.003636	80.3	6.49	1.50	2.62	0.290	0.533	0.658	0.01254	0.01926	141.8	194.4	0.02522	0.04742	0.571	2.34
28	4.10	20.0	0.004483	0.004200	73.9	5.97	1.60	2.95	0.260	0.572	0.699	0.01306	0.01985	148.4	198.8	0.02690	0.04961	0.575	2.36

TABLE 4.13: INITIATION OF EROSION EXPERIMENTS

(SYNTHETIC SEWER SEDIMENT)

(Laponite Clay-Sand-Water Mixtures)

Laponite clay gel concentration c = 24 g/l
154 mm diameter flume E = 18.4 mm (smooth bed)

Sand size (mm)	Clay gel %	Sand prop. %	Density ρ (Kg/m^3)	Crit.Shear Stress τ_{01} (N/m^2)	Crit.Shear Stress τ_{02} (N/m^2)
0.36	0	100	1618	0.120	0.120
	20	80	1907	0.940	1.233
	25	75	1848	2.555	3.522
	30	70	1814	3.247	3.513
	35	65	1797	4.044	4.844
	40	60	1757	5.243	5.456
	60	40	1345	2.778	2.945
0.53	0	100	1648	0.160	0.160
	20	80	1920	0.851	0.976
	30	70	1750	3.300	3.956
	40	60	1618	3.814	3.921
0.89	0	100	1630	0.400	0.400
	15	85	1911	0.408	0.656
	20	80	1932	1.659	2.599
	30	70	1760	2.723	3.513
	40	60	1603	2.253	2.856
	60	40	1352	1.721	2.359
1.44	0	100	1570	0.430	0.430
	15	85	1816	1.008	1.437
	20	80	1567	1.591	1.987
	40	60	1607	2.365	2.588

TABLE 4.14: INITIATION OF EROSION EXPERIMENTS

(SYNTHETIC SEWER SEDIMENT)

(Laponite Clay-Sand-Water Mixtures)

Sand size 600-1180 um (0.89 mm)
154 mm diameter flume E = 18.4 mm (smooth bed)

Clay conc. (g/l)	Clay gel prop. % (wt)	Sand prop. % (wt)	Density ρ (Kg/m^3)	Crit.Shear Stress τ_{01} (N/m^2)	Crit.Shear Stress τ_{02} (N/m^2)
24	0	100	1630	0.245	0.245
	15	85	1911	0.408	0.656
	20	80	1932	2.111	2.599
	30	70	1768	2.723	3.513
	40	60	1603	2.253	2.856
	60	40	1352	1.721	2.359
27	0	100	1630	0.245	0.245
	20	80	1910	2.033	2.706
	30	70	1770	5.178	5.403
	40	60	1611	4.693	5.207
	50	50	1467	3.520	4.194
	60	40	1377	2.186	2.910
30	0	100	1630	0.245	0.245
	20	80	1935	1.991	2.910
	30	70	1771	4.799	5.266
	35	65	1658	4.592	5.051
	40	60	1585	4.551	5.039
	50	50	1460	2.895	3.335
33	0	100	1630	0.245	0.245
	20	80	1916	2.092	2.830
	30	70	1766	5.766	6.032
	40	60	1610	5.250	5.599
	50	50	1418	4.702	5.136
36	30	70	1738	5.773	6.697
40	30	70	1755	6.325	6.955

TABLE 4.15: INITIATION OF EROSION EXPERIMENTS

(SYNTHETIC SEWER SEDIMENT)

(Laponite Clay-Sand-Water Mixtures)

Sand size 90-150 um (0.12 mm)
154 mm diameter flume E = 18.4 mm (smooth bed)

Clay conc. (g/l)	Clay gel prop. % (wt)	Sand prop. % (wt)	Density ρ (Kg/m^3)	Crit.Shear Stress τ_{01} (N/m^2)	τ_{02} (N/m^2)
18	85.5	14.5	1103	1.082	1.428
	74.5	25.5	1191	1.428	1.740
	62.2	37.8	1312	1.485	1.747
	53.0	47.0	1418	2.097	2.541
	47.0	53.0	1480	2.194	2.463
	40.0	60.0	1688	1.959	2.225
22	85.5	14.5	1121	1.976	2.317
	80.5	19.5	1157	2.028	2.544
	74.5	25.5	1209	2.156	-
	62.2	37.8	1308	2.714	3.568
	53.0	47.0	1408	3.053	3.916
	40.0	60.0	1606	3.300	3.699
	31.6	68.4	1744	3.146	3.486
25	85.5	14.5	1112	2.159	2.494
	80.5	19.5	-	2.235	2.787
	74.5	25.5	1209	2.289	2.720
	62.2	37.8	1375	2.544	3.092
	50.0	50.0	1449	4.086	4.551
	40.0	60.0	1687	5.305	5.970
	30.0	70.0	1752	3.046	3.623

TABLE 4.16: SUMMARY OF SYNTHETIC SEWER SEDIMENT EXPERIMENTS

Laponite clay-sand-water mixtures

154 mm diameter flume E = 18.4 mm (smooth bed)

sand size d_{50} (mm)	Clay conc. c (g/l)	Clay prop. % (wt)	Sand prop. % (wt)	Density ρ (Kg/m^3)	Critical Shear Stress	
					τ_{01} (N/m^2)	τ_{02} (N/m^2)
0.12	18	53	47	1418	2.097	2.541
	22	40	60	1606	3.300	3.699
(type C)	22	40	60	1581	(1.8)	(2.4)
	25	40	60	1687	5.305	5.970
(type C)	25	40	60	1579	(3.6)	(4.6)
0.89	24	30	70	1768	2.723	3.513
	27	30	70	1770	5.178	5.403
	30	30	70	1771	4.799	5.266
	33	30	70	1766	5.766	6.032
	36	30	70	1738	5.773	6.697
	40	30	70	1755	6.325	6.955
1.44	30	30	70	1783	4.826	5.501
	33	30	70	1795	5.415	5.842
	36	30	70	1773	5.798	6.476
	40	30	70	1777	6.667	7.327
2.03	30	20	80	1804	4.059	4.476
(type A)	30	20	80	1943	(4.9)	(5.9)
	33	20	80	1822	4.553	5.787
	36	20	80	1850	4.879	6.050
(type A)	36	20	80	1967	(6.4)	(8.9)
	40	20	80	1805	5.211	7.567
2.86	33	20	80	1805	4.132	5.203
	36	20	80	1805	4.521	5.548
	40	20	80	1821	4.707	7.726

NOTE: τ_{01} = first spots of erosion

τ_{02} = bed collapse

Only optimum sand clay gel ratio values shown.

TABLE 4.17: TRANSPORT EXPERIMENTS OVER LOOSE BED (NON-COHESIVE SEDIMENT)

154 mm diameter flume with sediment bed

E (mm)	d_{50} (mm)	S_o	Q (l/s)	Y_o (mm)	τ_o (N/m^2)	q_s (g/min)	Bed Formation (Y,L)
16.3	0.53	0.001190	0.92	30.3	0.251	0.03	no
		0.001129	1.68	43.4	0.311	1.33	no
		0.000969	2.75	62.2	0.340	2.55	no
		0.001093	2.75	60.0	0.375	5.48	no
		0.001315	4.70	84.8	0.541	20.30	dune (8.7mm, 0.3m)
		0.001697	5.65	92.0	0.720	55.57	dune (12.2mm, 0.4m)
	0.89	0.001550	1.02	32.4	0.344	0.00	no
		0.001449	1.88	46.6	0.420	0.69	no
		0.001530	3.23	62.6	0.538	10.32	no
		0.001561	6.44	100.1	0.678	38.21	dune (7.1mm, 0.3m)
	1.7	0.002984	1.28	30.2	0.629	0.01	no
		0.003081	2.62	45.4	0.877	16.69	no
		0.002043	7.65	102.1	0.891	30.35	wave (10mm, 1.7m)
		0.003055	3.94	58.3	1.029	78.50	not measured
	2.9	0.003731	1.41	32.9	0.832	0.00	no
		0.003096	4.14	60.4	1.065	0.23	no
		0.003073	8.55	95.7	1.320	35.87	no
		0.003777	3.02	49.0	1.134	0.36	no
		0.003855	4.51	60.2	1.324	8.18	not measured
40.8	0.53	0.001023	1.50	35.9	0.253	0.77	no
		0.001121	1.47	35.7	0.276	0.84	no
		0.001105	3.81	73.1	0.407	10.67	dune (6.8mm, 0.62m)
		0.001814	1.95	39.7	0.481	16.35	dune (4.5mm, 0.30m)
		0.001581	4.66	72.8	0.581	75.59	dune (7.3mm, 0.26m)
	0.89	0.000945	1.25	36.4	0.236	0.00	no
		0.001453	1.49	35.2	0.355	0.08	no
		0.001686	4.61	76.5	0.630	26.32	no
		0.002845	2.21	39.0	0.746	30.99	wave (4.0 mm, 0.3 m)
		0.002579	5.66	80.7	0.976	108.41	dune (11.3mm, 0.64m)
		0.003199	5.47	76.2	1.193	111.39	dune (9.8mm, 0.31m)
60.3	0.53	0.001902	0.72	19.2	0.292	0.02	no
		0.001762	1.05	23.9	0.319	2.63	no
		0.001725	1.64	33.6	0.399	17.53	dune (4.2mm, 0.15m)
		0.001972	2.39	43.4	0.533	33.36	dune (4.0mm, 0.12m)
	0.89	0.001779	1.54	33.0	0.406	0.98	no
		0.001694	1.61	35.3	0.404	1.41	no
		0.001819	2.32	43.2	0.491	16.01	no
		0.001720	3.69	61.0	0.544	37.41	dune (7.5mm, 0.88m)
		0.002293	2.56	44.6	0.630	28.96	dune (7.0mm, 1.09m)

TABLE 4.18: TRANSPORT EXPERIMENTS OVER FIXED BED

NO DEPOSITION CONDITION NON-COHESIVE SEDIMENT

154 mm diameter flume E = 18.4 mm (smooth bed)

	S_o	Y_o (mm)	Q (l/s)	$\frac{Y_o+E}{D}$	τ_o (N/m^2)	d_{50} (mm)	q_s (g/s)	C_v
1	0.003524	76.6	8.04	0.76	1.3159	0.9	5.70	2.73E-04
2	0.003440	35.5	2.75	0.56	0.8444	0.9	1.50	2.10E-04
3	0.001555	76.2	4.99	0.76	0.5798	0.9	1.05	8.11E-05
4	0.001605	37.1	1.77	0.51	0.4063	0.9	0.20	4.25E-05
5	0.003524	76.6	8.04	0.76	1.3159	2.0	6.55	3.25E-04
6	0.003440	35.5	2.75	0.56	0.8444	2.0	2.40	3.48E-04
7	0.001555	76.2	4.99	0.76	0.5798	2.0	1.40	1.12E-04
8	0.001605	37.1	1.77	0.51	0.4063	2.0	0.54	1.22E-04
9	0.003524	76.6	8.04	0.76	1.3159	5.7	13.50	6.77E-04
10	0.003440	35.5	2.75	0.56	0.8444	5.7	3.95	5.79E-04
11	0.001555	76.2	4.99	0.76	0.5798	5.7	2.20	1.78E-04

TABLE 4.19: TRANSPORT EXPERIMENTS OVER FIXED BED

NO DEPOSITION CONDITION NON-COHESIVE SEDIMENT

154 mm diameter flume E = 18.4 mm (k_s = 2.3 mm)

	S_o	Y_o (mm)	Q (l/s)	$\frac{Y_o+E}{D}$	τ_o (N/m^2)	d_{50} (mm)	q_s (g/s)	C_v
12	0.003479	79.1	7.21	0.7785	1.3101	0.9	3.08	1.64E-04
13	0.003573	61.1	5.36	0.6616	1.2207	0.9	2.90	2.09E-04
14	0.003596	43.6	3.34	0.5480	1.0136	0.9	1.43	1.65E-04
15	0.003590	32.0	2.08	0.4727	0.8182	0.9	0.95	1.76E-04
16	0.002163	36.4	1.97	0.5012	0.5403	0.9	0.43	8.32E-05
17	0.002032	49.1	3.04	0.5837	0.6165	0.9	0.77	9.70E-05
18	0.002273	62.1	4.47	0.6681	0.7826	0.9	0.99	8.54E-05
19	0.002169	81.2	5.99	0.7922	0.8216	0.9	1.04	6.70E-05

TABLE 4.20: CONSTANTS IN EQUATION 4.33

Flume Bed	Sand Size	Mean Values		Separated Values	
		a	b	a	b
smooth	0.9	3.990	-0.389	3.740	-0.387
	2.0	3.576	-0.526	3.227	-0.524
	5.7	9.010	-0.452	7.960	-0.449
rough	0.9	2.120	-0.505	1.625	-0.546

TABLE 4.21: TRANSPORT EXPERIMENTS OVER FIXED BED
NO DEPOSITION CONDITION COHESIVE SEDIMENT

20% clay gel c = 24 g/l
80% sand d = 0.9 mm

154 mm diameter flume E = 40.8 mm (smooth bed)

	S_o	Y_o (mm)	Q (l/s)	$\frac{Y_o+E}{D}$	τ_o (N/m^2)	d_{50} (mm)	q_s (g/s)	C_v
1	0.002169	81.29	6.04	0.79	0.822	0.9	1.54958	9.90E-05
2	0.002214	68.84	4.92	0.71	0.797	0.9	1.13639	8.91E-05
3	0.002159	51.43	3.37	0.60	0.673	0.9	0.75889	8.69E-05
4	0.003599	39.69	2.98	0.52	0.954	0.9	1.69389	2.19E-04
5	0.003509	54.16	4.68	0.62	1.127	0.9	3.29000	2.71E-04
6	0.003547	47.80	3.92	0.58	1.059	0.9	2.69167	2.65E-04

TABLE 4.22: TRANSPORT EXPERIMENTS OVER FIXED BED - NO DEPOSITION

CONDITION COHESIVE SEDIMENT 20% clay gel c = 30 g/l

80% sand d = 0.9 mm

Flume 154 mm dia. E = 40.8 mm (smooth bed)

	S_o	Y_o (mm)	Q (l/s)	$\frac{Y_o+E}{D}$	τ_o (N/m^2)	d_{50} (mm)	q_s (g/s)	C_v
1	0.003562	47.14	3.85	0.57	1.054	0.9	2.65278	2.66E-04
2	0.003609	39.49	2.89	0.52	0.953	0.9	2.04333	2.72E-04
3	0.003529	53.59	4.59	0.61	1.126	0.9	3.20556	2.70E-04
4	0.002288	63.96	4.68	0.68	0.799	0.9	1.75833	1.45E-04
5	0.002304	86.17	6.19	0.82	0.881	0.9	2.27167	1.42E-04

CHAPTER FIVE

SUMMARY OF CONCLUSIONS AND RECOMMENDATIONS FOR FURTHER WORK

The present study has covered hydraulics, initiation of erosion and transport of cohesive and non-cohesive sediments in channels of circular cross-section with sediment bed. Comparisons were made between cohesive and non-cohesive sediment behaviour and between wide channels and channels of circular cross-section.

5.1 HYDRAULIC CHARACTERISTICS

a) Flow Resistance

The Colebrook-White formula was used to determine the value of the absolute channel roughness (k_s) in sediment-free conditions, from the calculated values of friction factor (Darcy-Weisbach formula). The resulting k_s values for $Re \leq 200{,}000$ indicated the channels to be smooth.

Flow resistance in full pipe flow conditions for $Re \leq 200{,}000$ conforms to the von Karman-Prandt equation (see Fig. 4.1) for smooth pipes. However, the open channel flow results showed a large degree of scatter (see Fig. 4.2). This can be attributed to the substitution of D=4R in Darcy-Weisbach and Colebrook-White formulae, which assume that the shear stress is uniformly distributed around the section.

In channels of circular cross-section with sediment bed the friction factor of the bed (λ_b) is dependent on bed roughness, bed thickness (E) and on flow depth (Y_o). The relative friction

factor (λ_b/λ) increases with bed roughness and flow depth (Fig. 4.7a).

There are indications (see Fig. 4.7b) that λ_b/λ decreases with sediment bed thickness. As the sediment bed level increases there is a greater bed width and the wall effects are thus diminished. This trend is likely to be valid up to 50% of the diameter. For sediment bed levels above 50% of the diameter the bed width decreases with bed level and a different trend may be expected.

b) Velocity Distribution

Velocity distributions over the flat beds of channels of circular cross-section are found to be dependent on flow depth (channel shape) and bed roughness. Two dimensional flow was observed for shallow flow depths and three dimensional flow for deeper flows (i.e., $(Y_o+E)/D \geq 0.62$, see Fig. 4.14). In full pipe flow conditions, the flow was observed to revert to two dimensional flow. However, in the largest sediment bed used, the velocity and shear stress distributions showed the effects of secondary currents even in the full pipe flow case (see Fig. 4.15).

c) Shear Stress Distribution

Shear stress distribution measurements corroborated the applicability of the Einstein-Vanoni separation technique, which gives realistic average values of bed shear stresses. The shear stress distribution measurements showed the effects of secondary currents as not only one but several peaks were observed across

the bed. For $0.62 \leq (Y_o+E)/D < 1$ the maximum values of bed shear stress were observed at both sides of the centerline (see Fig. 4.14). For full pipe flow conditions the maximum shear stress was always located at the centerline of the channel.

d) Turbulence Intensities

Distributions of turbulence intensities over the flat bed of channel of circular cross-section were found to be dependent on flow depth and bed roughness. Maximum levels of turbulence were always observed near the bed. The turbulence intensities on rough beds are found to be higher than those of smooth beds. Minimum levels of turbulence were found near the center point of the flow area for deep flow depths and near the water surface for shallow flow depths.

The dependence of turbulence intensity on bed roughness is an important feature in the erosion process of cohesive sediment beds. An increase in roughness (first spots of erosion) causes an increase in the turbulence level, which in turn is responsible for the growth of the spots of erosion. This is the phenomena that triggers off the collapse of the cohesive bed.

5.2 INITIATION OF EROSION

a) Non-cohesive Sediments

The critical shear stresses for sand particles, in channels of circular cross-section with sediment bed, were found to be lower

than the corresponding values of wide channels (i.e., Shields' curve). However, when bed shear stresses (Einstein-Vanoni separation technique) are used there is a better agreement with Shields' prediction (see Fig. 4.27).

The influence of the channel shape on critical conditions is noticeable for flow depths above half full pipe. Results from experiments using mixed size sands suggest the existence of sheltering and armouring of the particles on the bed.

b) Cohesive Sediments

Initiation of erosion of cohesive sediment is largely dependent on the proportion and concentration of the cohesive additive. The erosion studies show that even a low level of cohesion can increase the critical shear stress significantly.

The size of the aggregates (sand size) has no significant effect on the critical shear stress of cohesive sediments. For a given sand size and laponite clay gel concentration, there is an optimum proportion of sand to clay-gel to achieve maximum critical shear stress (see Figs. 4.34 and 4.36).

The synthetic sewer sediment (Laponite clay + sand + water) mixtures used to represent freshly deposited sewer sediment with slight consolidation (Type A sewer sediment) required a maximum critical shear stress of around 6 to 7 N/m^2 for complete erosion. The Laponite clay gel concentrations in this case ranged from 30 to 40 g/l and the sand sizes used ranged from 0.89 to 2.86 mm.

The synthetic sewer sediment representing the weak cohesive sewer sediment (Type C sewer sediment) showed maximum critical shear stresses of around 2.5 N/m^2. Laponite clay gel concentration, in this case, was limited to 18 g/l, and the sand size was 0.12 mm. The optimum proportion of clay-gel to sand was 0.47 by weight.

5.3 SEDIMENT TRANSPORT OVER LOOSE BEDS

a) Non-cohesive Sediments

Results from transport experiments showed that in channels of circular cross-section with loose sediment bed there is more transport (see Figs. 4.39 and 4.40) than for similar flows in alluvial channels. Although when using the separated bed values the difference is reduced, the channels of circular cross-section show still more transport capacity.

Indications (see Fig. 4.41 and 4.42) are that the transport capacity of a uniform flow increases with sediment bed thickness. As there is more space (width) for the particles to move, the transport process is more effective and as a result a greater bedload (sediment rate per unit width) is obtained. However, as it was mentioned above, the sediment bed width will start decreasing after the sediment bed level exceeds half full pipe. As the experiments covered sediment bed thickness only up to 39%, it can only be speculated that a different trend may occur for sediment bed levels above half full pipe (50%).

Bedforms were also observed in the channel of circular cross-section with sediment bed. According to various bedform classifications (Shields 1936, Simmons 1963 and Van Rijn 1988) the measured bedforms correspond to dunes in wide channels. Bedform dimensions were found to be dependent on flow depth (shape effect) and particle size.

b) Cohesive Sediments

A rapid collapse of the bed was observed soon after the critical conditions were exceeded. The cohesive sediment was detached from the bed in clusters, which were rapidly disunited by the flowing water and then behaved like non-cohesive sediment as they were transported by the flow.

The characteristic behaviour (see Fig. 4.47) of the cohesive sediment bed when the shear stress exceeds the critical conditions, does not make possible the establishment of equilibrium conditions of sediment transport. Because the cohesive sediment during transport behaves like non-cohesive sediment, the actual shear stress during the critical conditions is much higher than the required shear stress to initiate this "non-cohesive" sediment. Thus the detached cohesive clusters are transported very rapidly almost in suspension.

The same happens to any cohesive sediment being fed into the flow at the upstream end of the test section. Thus no deposition is possible and the sediment bed is unavoidably disintegrated.

A similar phenomenon takes place in sewers during storm events. A "first foul flush" of pollutants is generally observed at the onset of the storm flow. The cohesive sediments bed (deposited during dry weather flow, DWF) is disintegrated as the critical conditions are exceeded, and the materials (pollutants) are transported downstream and discharged through the storm sewage overflows (SSO) to the receiving stream.

5.4 SEDIMENT TRANSPORT OVER FIXED BEDS

a) Non-cohesive Sediments

The results from transport experiments over fixed beds (limit deposition condition) showed that in channels of circular cross-section with sediment bed there is more transport than in alluvial channels (see Fig. 4.48). The results also showed that for a given uniform flow sediment transport increases with particle size, which can be attributed to the increase in exposed area of the particles.

Bed roughness was also found to affect the transport capacity of a given uniform flow as more energy has to be used to overcome the higher friction resistance, apart from the increase in turbulence intensities, which also dissipate more energy. This also explains why there is less transport in alluvial channels where there is not only grain roughness but also bed formation.

Minimum mean velocities to maintain non-deposition condition were found to be lower than those of channels of circular

cross-section without sediment bed (see Fig. 4.56).

Minimum mean velocities to maintain non-deposition condition were found to be similar to those of channels of rectangular cross-section (see Figs. 4.57 and 4.58).

Minimum shear stresses required to maintain non-deposition conditions were found to be lower than those corresponding to rectangular channels (see Figs. 4.59 and 4.60).

b) Cohesive Sediments

The results from experiments with cohesive sediment show only a slight decrease in sediment transport, compared to the non-cohesive sediments experiments. This corroborates the observations made during the initiation of erosion experiments, that the detached cohesive sediment particles behave like non-cohesive sediment when transported by a uniform flow in a channel of circular cross-section.

However, only two different cohesive sediment mixtures were used in transport experiments. In order to achieve more conclusive results more transport experiments, covering a wide combination of cohesive sediment mixtures, are needed.

5.5 RECOMMENDATION FOR FURTHER WORK

The main objective of the present study was to determine the influence of cohesion on sediment movement in channels in order

to describe the transition from non-cohesive to cohesive behaviour of sediments. A synthetic sewer sediment (Williams and Williams, 1988), which is rheologically suitable has been extensively investigated in the hydraulics laboratory.

The point of initiation of erosion was found to be highly dependent on the concentration and proportion of the cohesive additive (Laponite clay). However, transport experiments with the synthetic sewer sediment were not successful due to the drop in cohesive strength once the sediment is detached from the bed.

In order to obtain more conclusive results it is necessary to carry out more experimental work such as:

a) <u>Hydraulics of the circular cross-section with sediment bed</u>

Further investigation of the velocity and shear stress distributions on the channel cross-section are needed in order to relate these distributions to sediment movement. Turbulence intensities also need to be investigated in depth across the entire flow section of the flume. Measurements of Reynolds stresses for various bed configurations would be very helpful in quantifying the effect of turbulence on sediment movement.

The relationship between bed shear stress and mean shear stress should be studied for a wider range of sediment bed thicknesses. Therefore extensive measurements of velocity profiles to determine velocity and shear stress distributions are needed. It would be interesting to see how the mechanism of deposition takes

place just before the pipe is blocked with sediment (i.e., sediment bed thicknesses above half full), and how the mechanism of erosion (as soon as there is enough pressure gradient) takes place in a channel section partially blocked with sediment.

b) Sediment Movement in Pipe Channels

Systematic investigation of non-cohesive sediment transport in channels of circular cross-section is required in order to obtain reliable relations between hydraulic and sediment parameters. This should consider several channel bed thicknesses and flow depths.

Initially very low concentration additives (laponite clay gel) should be used in order to detect the departure from non-cohesive behaviour. The size range of aggregate (sand) should be extended to the lower end as rheological tests can only be carried out for suspensions with very small particle size.

Experimental investigations should also contemplate the possibility of putting the additive directly into the flume water, and see how the initiation of erosion and transport of non-cohesive sediments is affected by this change in fluid properties.

Unsteady flow conditions should also be considered in order to study the influence of consolidation time, which occurs during low flows (DWF). Furthermore as it is essential to relate

properly laboratory and field (sewers sediment). Therefore parallel studies in real sewers should be carried out for various flow dephs and bed configurations. It is also necessary to maintain a record of rheological parameters from both laboratory and field experiments, so that adequate links can be esbablished between laboratory (synthetic sediment) and field (real sewer sediment) results.

APPENDIX A

NOTATION

APPENDIX A NOTATION

A cross-sectional area of the flow

d_{50} median diameter of particles in a mixture

C Chezy roughness coefficient

C' Chezy roughness coefficient related to grains

C_v sediment concentration by dry volume

c clay gel concentration

c_B rate of displacement of the bedforms

D internal diameter of pipe channel

D_{gr} , D_* dimensionless particle number $((S_s - 1)g/\nu^2)^{1/3}\ d_{50}$

E sediment bed thickness

F_d Froude number of particle ($= V/\sqrt{(S_s-1)gd}$)

F_{dc} Froude number of particle for incipient motion

G rigidity modulus, correction factor density distribution

g gravitational constant

g_s' bedload in weight per unit time per unit width

h location of maximum velocity in channel section

K_D coefficient in dimensionless transport parameter φ_D

k_s overall Nikuradse's equivalent sand roughness

k_{ss} overall Nikuradse's equivalent sand roughness with sediment

k_{sb} bed Nikuradse's equivalent sand roughness

I_w Plasticity index

n overall Manning roughness coefficient

n_b bed Manning roughness coefficient

P wetted perimeter of the flow

q_s bedload in volume per unit time and unit width

Q flow rate

Q_s^* transport parameter ($= Q_s \rho g(S_s - 1)w_s^{3/2}$)

Q_s absolute volume rate of sand

R overall hydraulic radius (A/P)

R' overall hydraulic radius (A/P) related to grains

R" overall hydraulic radius (A/P) related to bedforms

R_b bed hydraulic radius

R_w wall hydraulic radius

S_o channel longitudinal bed slope

S_f water surface slope (pressure gradient)

S_s relative density of sediment (ρ_s/ρ)

SF_p shape factor of particle

SF_c shape factor of channel

T transport parameter (= $(u_*'^2 - u_{*cr}'^2)/(u_{*cr}'^2)$)

u local velocity

u_{max} maximum local velocity

u' turbulent velocity fluctuation

u_* shear velocity

u_{*b} bed shear velocity

V mean velocity

V_c mean velocity for incipient motion

V_L mean velocity at limit deposition criterion

Y_o depth of uniform flow

w_s settling velocity of particle

γ specific weight of water

γ_s specific weight of sediment

Δ bedform height

θ half angle subtended by the water-line at the centre of pipe channel

θ_o half angle subtended by the sediment bed surface at the centre of a pipe channel

Ξ dimensionless particle number (= $((S_s - 1)/\nu^2)gd_{50}^3$)

λ overall friction factor (clear water)

λ_b bed friction factor (clear water)

λ_s overall friction factor with sediment transport

λ_{sb} bed friction factor with sediment transport

μ dynamic viscocity of water

ν kinematic viscosity of water(= μ/ρ)

ρ density of water

ρ_s density of sediment

τ_o mean shear stress (= ρgRS_o)

τ_{oc} critical mean shear stress

τ_b computed bed shear stress (= ρgR_bS_o)

τ_{bc} critical mean shear stress

τ_{bm} measured bed shear stress

τ_{01} mean shear stress at first spots of erosion

τ_{02} mean shear stress at collapse of cohesive bed

τ_y yield stress

φ_D dimensionless transport parameter $= K_D \left(\frac{V^2}{gD} \sqrt{\frac{gd}{w_s^2}} \right)^{-3/2}$

Φ non-dimensional transport parameter ($= C_v VR / \sqrt{gd_{50}^3 (S_s - 1)}$)

ψ non-dimensional shear stress ($= \tau_o / (\rho_s - \rho) g d_{50}$)
(flow intensity parameter)
(shear intensity parameter)

Φ_b non-dim. bed transport parameter ($= C_v VR_b / \sqrt{gd_{50}^3 (S_s - 1)}$)

ψ_b non-dim. bed shear stress ($= \tau_b / (\rho_s - \rho) g d_{50}$)

APPENDIX B

REFERENCES

REFERENCES

1. *Abdel-Rahman, N.M., 1982,* "The Effect of Flowing Water on Cohesive Beds", Thesis presented to Hydraulic Research and Soil Mechanics Laboratory, Swiss Federal Institute of Technology, Zurich, Switzerland.

2. *Ackers, P and White, W.R. 1973,* "Sediment Transport New Approach and Analysis", Proc. A.S.C.E., Vol. 99, HY11.

3. *Ariathurai, R. and Krone, R.B., 1976,* "Finite Element Model for Cohesive Sediment Transport", Journal of the Hydr. Div., Proc. of the A.S.C.E., Vol. 102, No. HY3.

4. *Ariathurai, R., MacArthur, R. and Krone, R.B., 1977,* "Mathematical Model of Estuarial Sediment Transport", Technical Report D-77-12, U.S. Army Corps of Engineers.

5. *Asaeda, Takashi et al., 1989,* "Sediment Entrainment in Channel with Rippled Bed", Journal of Hydraulic Engineering, Proc. of the A.S.C.E. Vol. 115, No. 3.

6. *Bagnold, R.A., 1956,* "Flow of Cohesionless Grains in Fluids", Proc. Roy. Soc., Phil. Trans. Ser. A, Vol. 249,, No. 964.

7. *Burt, T.N. and Game, A.C., 1985,* "The Carrousel", Report No. SR33, Hydraulics Research Limited, Wallingford.

8. *CIRIA, 1987,* "Sediment Movement in Combined Sewerage and Storm-Water Drainage Systems", Construction Industry Research and Information Association, Project Report 1

9. *Coles, P. and Miles, G.V., 1983,* "Two Dimensional Model of Mud Transport", Journal of Hydraulic Engineering, Proc. of the A.S.C.E. Vol. 109, No. 1, pp 1-12.

10. *Craven, J.P. and Ambrose, H.H., 1953,* "The Transportation of Sand in Pipes", Proc. of the Fifth Hydr. Conf., Bull. 34, State Univ. of Iowa Studies in Engineering.

11. *Crabtree, R. W., 1988,* "A Classification of Combined Sewer Sediment Types and Characteristics", WRc, Swindon, .

12. *Crabtree, R. W., Foster, C.F., Nalluri, C. and Williams, D.J.A., 1989,* "Recommendations for Further Research into Combined Sewer Sediment Deposits", WRc Report No. FR 0040 for Foundation for Water Research, Swindon.

13. *Chow, V.T., 1985,* "Open Channel Hydraulics". McGraw Hill International Book Company, 21st printing.

14. *Davies, J.T., 1972,* "Turbulence Phenomena", Academic Press Inc., London.

15. *Dunn, I.S., 1959,* "Tractive Resistance of Cohesive Channels" Proc. A.S.C.E. Vol. 85 No SM3.

16. *Engelund, F., 1966,* "Hydraulic Resistance of Alluvial Streams", Journal of the Hydr. Div., Proc. of the A.S.C.E., Vol. 92, No. HY2.

17. *Engelund, F. and Hansen, E., 1967,* "A Monograph on Sediment Transport in Alluvial Streams", Teknisk Forlag, Copenhagen.

18. *Enger, P.F., 1963,* "Canal Erosion and Tractive Force Study", US Recl. Report No. Hydr. 532.

19. *Espey, W.H., 1963,* "A new Test to Measure the Scour of Cohesive Sediment", Hydr. Eng. Lab., Dept. of Civil Eng., Technical Report HYD01-6301. The University of Texas.

20. *Einstein, H. A., 1942,* "Formulas for the Transportation of Bed Load". Trans. A.S.C.E., Vol. 107, pp 561-567.

21. *Flaxman, E.M., 1963,* "Channel Stability in Undisturbed Cohesive Soils", Proc. A.S.C.E., Vol. 89, No. HY2 pp 87-96

22. *Fukuda, M.K., 1980,* "The Entrainment of Cohesive Sediments in Fresh Water", Journal of Geoph. Research, Vol. 85, No. C5, pp 2813-2824.

23. *Graf, W. H., 1971,* "Hydraulics of Sediment Transport". McGraw Hill series in Water Resources and Enviromental Engineering.

24. *Grass, A.J., 1967,* "Boundary layer Turbulence in Open Channel Flow", PhD thesis, London University.

25. *Grass, A.J., 1970,* "Initial Instability of Fine Bed Sand", Proc. of the A.S.C.E., Journal of Hydr. Eng., Vol. 96, No HY3.

26. *Grissinger, E.H., 1966,* "Resistance on Selected Clay Systems to Erosion by Water", Water Resources Research, Vol. 2 No 1.

27. *Hare, G.H., 1988,* "Sediment Movement in Sewers", Hydraulics Research Ltd., SR Report 179.

28. *Hayter, E.J. and Mehta, A.J., 1984,* "Modeling Estuarine Cohesive Sediment Transport", Abstract of the 19th Coastal Eng. Conf. , A.S.C.E., pp. 362-363.

29. *Jayaraman, V.V., 1970,* "Resistance Studies on Smooth Open Channels", Journal of the Hydr. Div., Proc. of the A.S.C.E., Vol. 96, No.HY5.

30. *Kampuis, J.W. and Hall, K.R., 1983,* "Cohesive Material Erosion by Unidirectional Current", Journal of Hydr. Eng., Proc. A.S.C.E. Vol. 109, No. 1 pp.49-61.

31. *Kandula, V.N., et Al. 1983,* "Velocity Distribution in Smooth Rectangular Open Channels", Journal of Hydr. Eng., Proc. A.S.C.E. Vol. 109, No. HY7.

32. *Kelly, W.E. and Gularte, R.C., 1981,* "Erosion Resistance of Cohesive Soils", Journal of Hydr. Eng., Proc. of the A.S.C.E., Vol. 107, pp.1211-1214.

33. *Kithsiri, M.M.A.U., 1990,* "Sediment Transport in Rectangular channels with rigid beds", M-Phil thesis, Dept. of Civil Engineering, University of Newcastle upon Tyne.

34. *Kleijwegt, R.A., Veldkamp, R.G. and Nalluri, C., 1989,* "Sediments in Sewers: Initiation of Transport", 2nd Int. Conference on Urban Storm Water Quality and Ecological Effects upon Receiving Waters, Wageningen, The Netherlands.

35. *Kolar, V., 1988,* "Hydraulic Transport of Solid Particles in Pipes", Technical Papers Faculty of Civil Engineering, Technical University of Prague.

36. *Lau, Y.L., 1988,* "Hydraulic Resistance of Ripples", Journal of the Hydr. Div., Proc. of the A.S.C.E., Vol. 114, No.10.

37. *Loveless, J. H.,1986,* "Sediment Transport in Circular and Non-circular Conduits", Proc. of Conference in Hydraulic design in Water Resources, Southampton, U.K..

38. *Lyle, W.M. and Smerdon, E.T., 1965,* "Relation of Compaction and Other Soil Properties to Erosion and Resistance of Soils", Trans. Am. Soc. of Agr. Eng., Vol. 8, No. 3.

39. *Macke, E., 1983,* "Sizing of Flow Conditions that prevent the Formation of Deposits in Sewer Systems", Korrespondenz Abwasser, Vol. 30.

40. *Mash, F.D. et al., 1968,* "Erosion of Cohesive Sediments", Task Committee Report Proc. of the A.S.C.E., Vol. 94, No. HY4.

41. *May, R., 1982,* "Sediment Transport in Sewers". Hydraulic Research Station, Report IT 222.

42. *May, R. et al., 1989,* "Self-cleansing Conditions for Sewer Carrying Sediment". Report SR 221, Hydraulic Research, Wallingford.

43. *Mayerle, R., 1988,* "Sediment Transport in Rigid Boundary Channels", PhD Thesis, Dept. of Civil Eng., University of Newcastle upon Tyne.

44. *Moore, W.L. and Mash, F.D., 1962,* "Experiments on the Scour Resistance of Cohesive Sediments", Journal of Geoph. Research, Vol. 67, No. 4, pp. 1437-1449.

45. *Nalluri, C., 1985,* "Sediment Transport in Rigid Boundary Channels", Euromech 192: Transport of Suspended Solids in Open Channels, Munich, Neubiberg.

46. *Nalluri, C. and Novak, P., 1973,* "Turbulence Characte ristics in a Smooth Open Channel of Circular Cross-section",Journal of Hydraulic Research 11 , No. 4.

47. *Nalluri, C. and Adepoju, B.A., 1985,* "Shape effects on Resistance to Flow in Smooth Channels of Circular Cross-section". Journal of Hydraulic Research, vol. 23, No. 1.

48. *Nalluri, C. and Alvarez, E., 1987,* "Erosion of Cohesive Sediment Beds in Open Channels", Euromech 215: Mechanics of Sediment Transport in Fluvial and Marine Enviroment, Genoa, Italy.

49. *Nalluri, C., Alvarez, E. and Kleijwegt, R., 1989,* "Initiation of Sediment Movement in Sewers", IAHR XXIII Congress, Ottawa, Canada.

50. *Nalluri, C. and Mayerle, R., 1989,* "Sediment Transport with no Deposition in Rigid Boundary Channels", IAHR XXIII Congress, Ottawa, Canada.

51. *Nalluri, C. and Alvarez, E., 1990,* "The Influence of Cohesion on Sediment Behaviour in Pipes and Open Channels", Final Report, Department of Civil Engineering, University of Newcastle upon Tyne, U.K.

52. *Nicholson, J.M.C., 1983,* "Three Dimensional Models of Particulate and Cohesive Suspended Sediment Transport", PhD Thesis, University of Manchester.

53. *Nicholson, J.M.C. and O'Connor B., 1986,* "Cohesive Sediment transport Model", Journal of the Hydr. Div., Proc. of the A.S.C.E., Vol. 112, No.7.

54. *Novak, P. and Nalluri, C., 1975,* "Sediment Transport in Smooth Fixed Bed Channels", Journal of the Hydraulics Division, ASCE,Vol. 101, No. HY9, pp. 1139-1154.

55. *Novak, P. and Nalluri, C., 1984,* "Incipient Motion of Sediment Particles over Fixed beds", Journal of Hydr. Research, Vol. 22, No. 3.

56. *Novak, P. and Nalluri, C.,1987,* "Sediment Transport in Sewers and their Sea Outfalls", IAHR XXII Congress and IV Int. Conference in Urban Storm Drainage, Lausanne, Switzerland.

57. *Odd, N.V.M., and Owen, M.W., 1972,* "A Two-Layer Model of Mud Transport in the Thames Estuary", Proc. Institution of Civil Engineers, London, Supplementary Paper 7517S.

58. *Olphen, van H., 1963,* "An Introduction to Clay Colloid Chemistry", for clay technologists, geologists and soil scientists. Interscience Publishers, John Wileys & Son N.Y..

59. *Onishi, Y., 1981,* "Sediment-Contaminant Transport Model", Journal of the Hydraulics Division, A.S.C.E., Vol. 107, No. HY9, pp. 1089-1107.

60. *Otsubo, K. and Mukaora, K., 1985,* "Resuspension Rate Function for Cohesive Sediments in Stream", Journal of HydroScience and Hydr. Engineering, Vol. 3, No. 2, pp. 1-13.

61. *Otsubo, K. and Mukaora, K., 1988,* "Critical Shear Stress of Cohesive Bottom Sediments", Journal of Hydraulic Engineering, October, Vol. 114, No. 10.

62. *Parchure, T.M. and Metha, A.J, 1985,* "Cohesive Sediment Deposits", Journal of Hydr. Eng. Proc. of the A.S.C.E., Vol. 111, No. 10, pp.1308-1326.

63. *Partheniades, E. 1965,* "Erosion and Deposition of Cohesive Soils", Journal of the Hydraulic Division, Proc. of the A.S.C.E., Vol. 91, No. HY1.

64. *Partheniades, E. and Paaswell, R.E. 1970,* "Erodibility of Channels with Cohesive Boundary", Journal of the Hydraulic Division, Proc. of the A.S.C.E., Vol. 96, No. HY3.

65. *Pedroli,* R, 1963, "Bed Load Transportation in Channels with Fixed and Smooth Inverts", Mitteilung des Eidg. Amtes fur Wasserwirtschaft, Dienst Exemplar, No 43, Bern, Switzerland.

66. *Perrusquia, G.S. et al., 1987,* "Flow capacity of Sewer with a Sediment Bed", 4th International Conference on Urban Storm Drainage, IAHR XXII Congress, Lausanne, Switzerland.

67. *Perrusquia, G.S., 1988,* "Part Full Flow in Pipes with a Sediment Bed", Report Series A:17, Department of Hydraulics, Chalmers University of Technology.

68. *Raudkivi, A.J., and Hutchinson, D.L., 1974,* "Erosion of Kaolinite Clay by Flowing Water", Proc. of the Royal Soc. London, A337, pp. 537-544.

69. *Raudkivi, A.J., and Tan, S.K., 1984,* "Erosion of Cohesive Soils", Journal of Hydr. Research, Vol. 22, No. 4, pp.217-233.

70. *Replogle, A. and Chow, V. T., 1966,* "Tractive Force Distribution in Open Channels". Journal of the Hydraulics Division, Proc. of the A.S.C.E., HY2, March , pp. 169-191.

71. *Reynolds, A.J., 1974,* "Turbulent Flows in Engineering", John Wiley & Sons, London.

72. *Robinson, M.P. and Graf, W.H., 1972,* "Pipelining of Low Concentration Sand-water Mixtures", Journal of the Hydraulics Division, Proc. of the A.S.C.E., Vol. 98, HY7, pp. 1221-1241.

73. *Rodger, J.G., 1980,* "Simulation of Stratified Flows in Estuaries", Proc. of the 2nd Symp. on Stratified Flows, I.A.H.R., pp. 707-718.

74. *Smerdon, E.T., and Beasley, R.P., 1959,* "The Tractive Force Applied to Stability of Open Channels in Cohesive Soils", University of Missouri, Agric. Exp. Station, Bull. 715.

75. *Smith, T.J., O'Connor, B.A., Longden, S.D., Summers, I.G.S. and McDowell, D.M., 1980,* "A Multi-Channel, Electro-Optical Turbidity Meter", J. Phys. E: Sci. Instrum., Vol. 13, U.K.

76. *Sonnen, M. B. and Field, R., 1977,* "Deposition and Scour in Sewers", Int. Symposium on Urban Hydrology, Hydraulics and Sediment Control, University of Lexington, kentucky , USA.

77. *The Task Committee for Preparation of the Sedimentation Manual, 1970,* "Sediment Transportation Mechanics: J. Transportation of Sediment in Pipes", Journal of the Hydr. Div., Proc. of the A.S.C.E., Vol. 96, No. HY7, pp. 1503-1538.

78. *Terzaghi, K. and Peck, R., 1967,* "Soil Mechanics in Engineering Practice". Second edition. John Wiley and Sons Inc., New York, USA.

79. *Thorn, M.F.C., 1981,* "Physical Processes of Siltation in Tidal Channels", Proc. of the Conf. on Hydr. Modelling Applied to Maritime Eng. Problems, I.C.E., London, pp.47-55.

80. *Van Olphen, 1963,* "An Introduction to Clay Colloid Chemistry", Interscience Publishers, John Wiley & Son, New York.

81. *Van Rijn, L.C., 1984,* "Sediment transport", Journal of the Hydr. Div., Proc. of the A.S.C.E., Vol. 110, Nos.10, 11 and 12, December, 1984. Part I: Bedload transport
Part II: Suspended Load Transport
Part III: Bedforms and Alluvial Roughness

82. *Van Rijn, L.C., 1987,* "Mathematical Modelling of Morphological Processes in the Case of Suspended Sediment Transport", DELFT Hydraulics Communication No. 382.

83. *Vanoni, V.A., 1964,* "Measurements of Critical Shear Stress", California Inst. Tech., Report No. KH-R-7.

84. *Vanoni, V. and Brooks, N., 1957,* "Laboratory Studies of the Roughness and Suspended Load of Alluvial Streams", Final Report No. E68, Sedimentation Laboratory, California Institute of Technology, Pasadena, California.

85. *Velde, B, 1985,* "Developments in Sedimentology, Clay Minerals" a physico-chemical explanation of their occurrence. Elsevier.

86. *Viswanathan, C.K. and Leutheusser, H., 1970,* "Distribution of Tractive Force in Open Channels", Journal of Hydr. Eng., Proc. A.S.C.E. Vol. 96, No. HY7.

87. *Water Research Centre, 1986,* "Reentrainment of Cohesive Sediments in Combined Sewers", Report of the Geotechnical Consulting Group, WRc, Swindon.

88. *Williams, D. J. A., Williams, P. R. and Crabtree R. W. 1989,* "Preliminary Investigation Into the Rheological Properties of Sewer Sediment Deposits and the Development of a Synthetic Sewer Sediment Material for Laboratory Studies". FR 0016, Foundation for Water Research, Medmeham.

89. *Wilcock, P. R. and Southard, J.B., 1988,* "Experimental Study of Incipient Motion in Mixed Size Sediment", Water Resources Research, July, Vol.24, No. 7. pp 1137-1151.

90. *Wilcock, P. R., 1988,* "Methods for Estimating the critical Shear Stress of Individual Fractions in Mixed Size Sediment", Water Resources Research, July, Vol. 24, No. 7, pp. 1127-1135.

91. *Yalin, M. S., 1963,* "An Expression for Bed-Load transportation", Journal of Hydr. Eng., Proc. A.S.C.E. Vol. 89, No. HY3.

92. *Yalin, M. S., 1972,* "Mechanics of Sediment Transport",Pergamon Press,Ltd., Headington Hill Hall, Oxford.

93. *Yang, C. Ted, 1973,* "Incipient Motion and Sediment Transport", Journal of the Hydr. Div., Proc. of the A.S.C.E., Vol.99, No. HY10.

APPENDIX C

PLATES

LIST OF PLATES

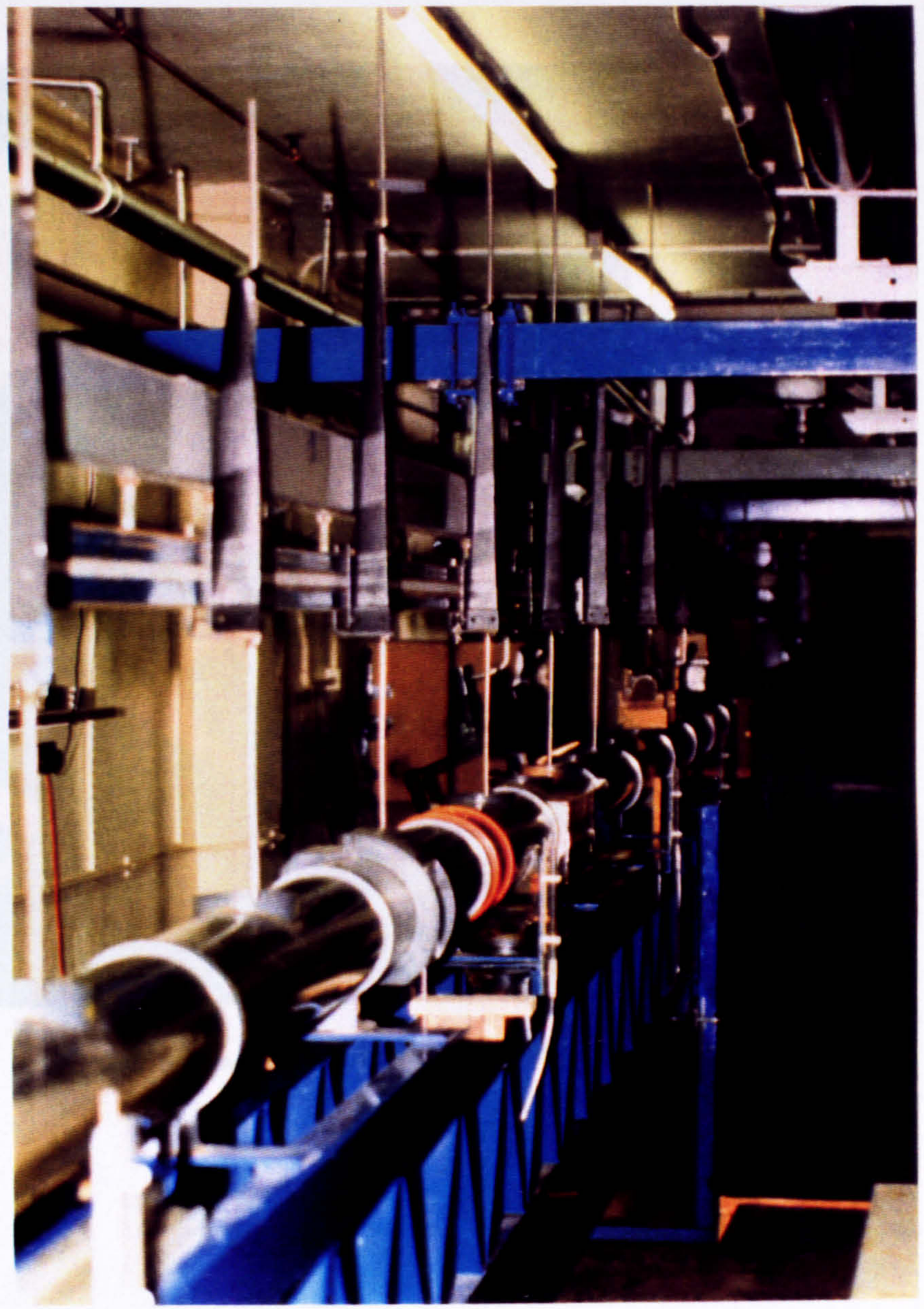

a) 154mm diameter flume
(Length = 20.5m)

b) 302mm diameter flume
(Length = 12m)

PLATE 1: Flumes of circular cross-section

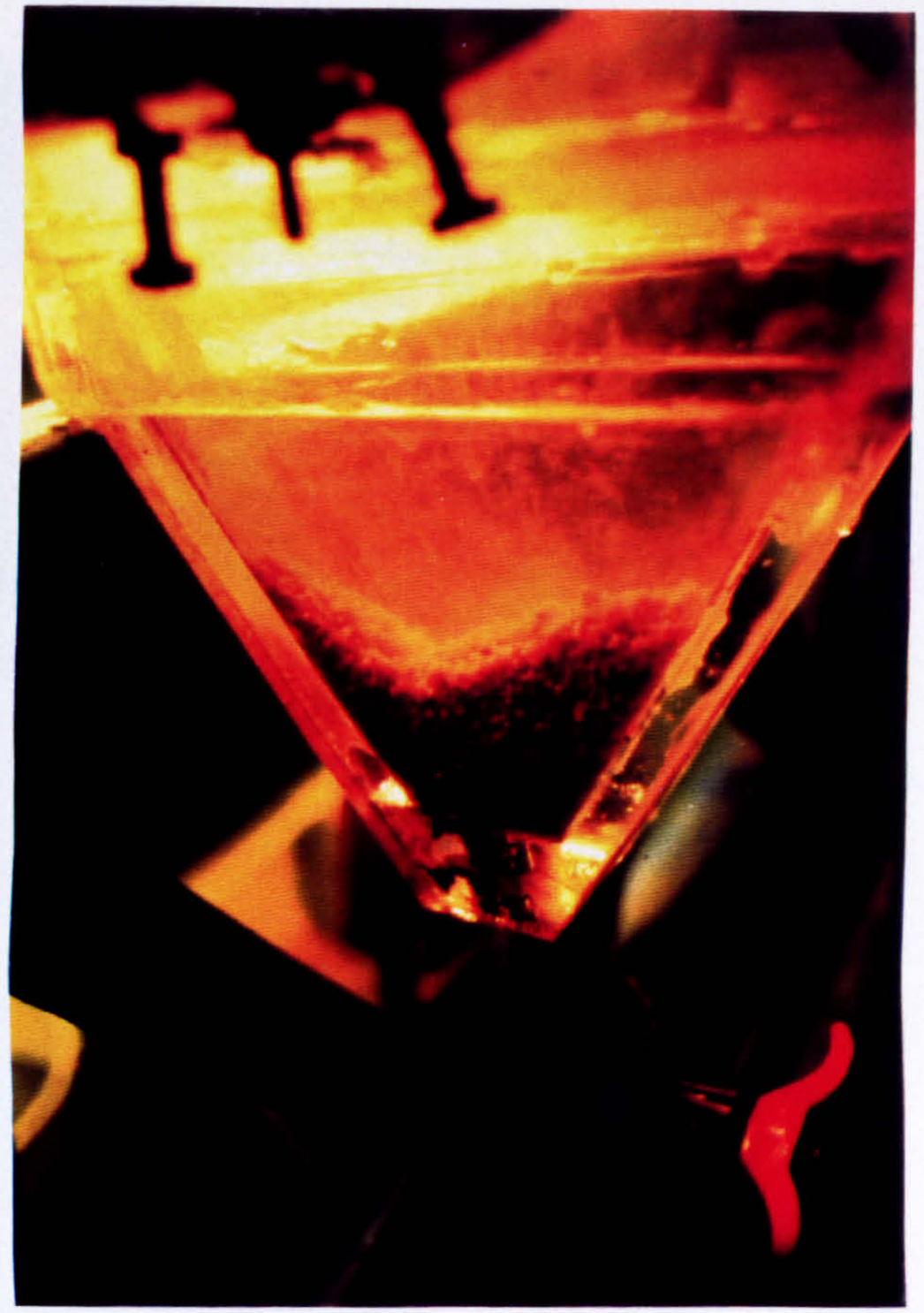

PLATE 2: Sediment trap during operation

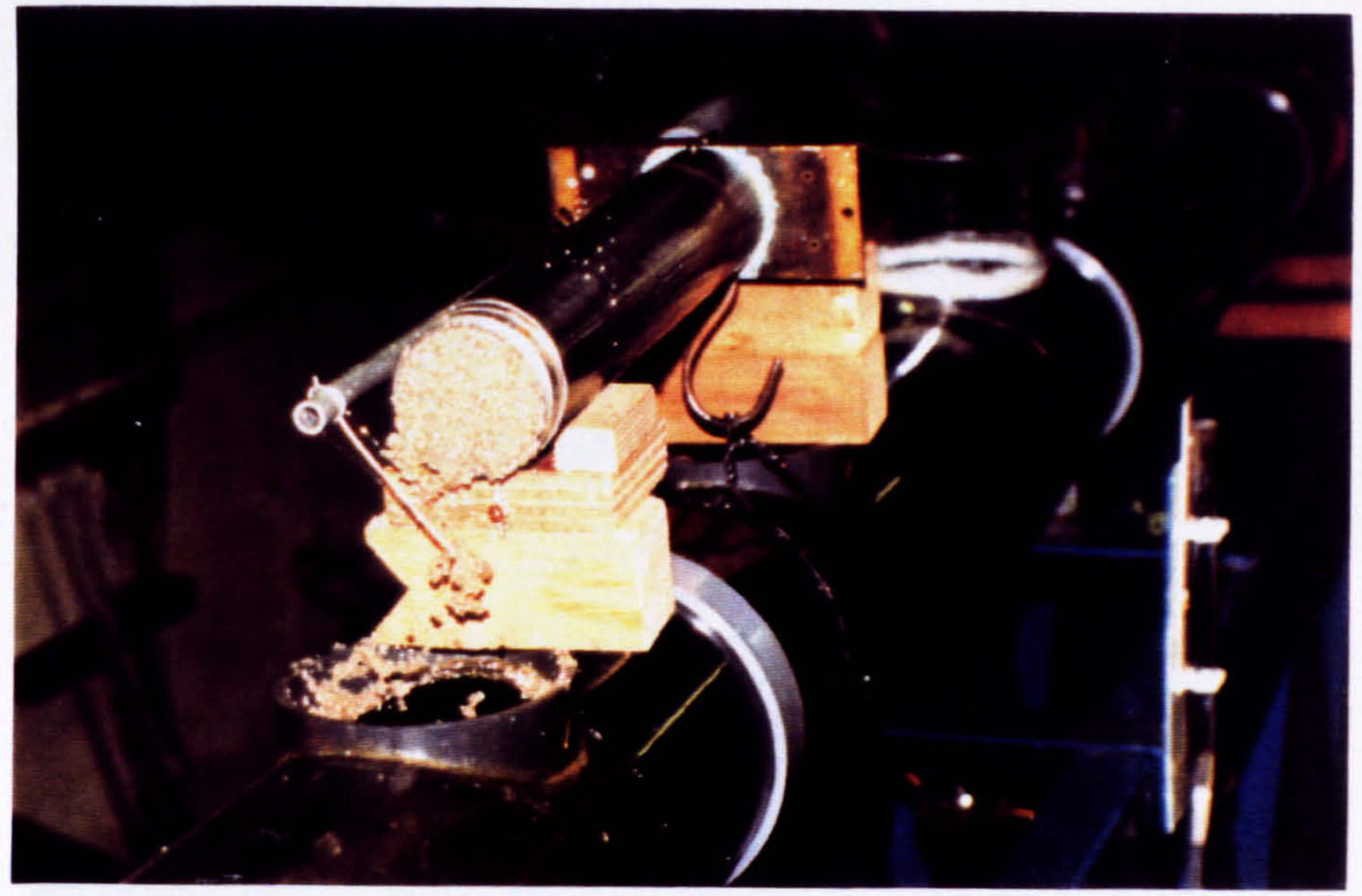

PLATE 3: Cohesive sediment feeder during operation

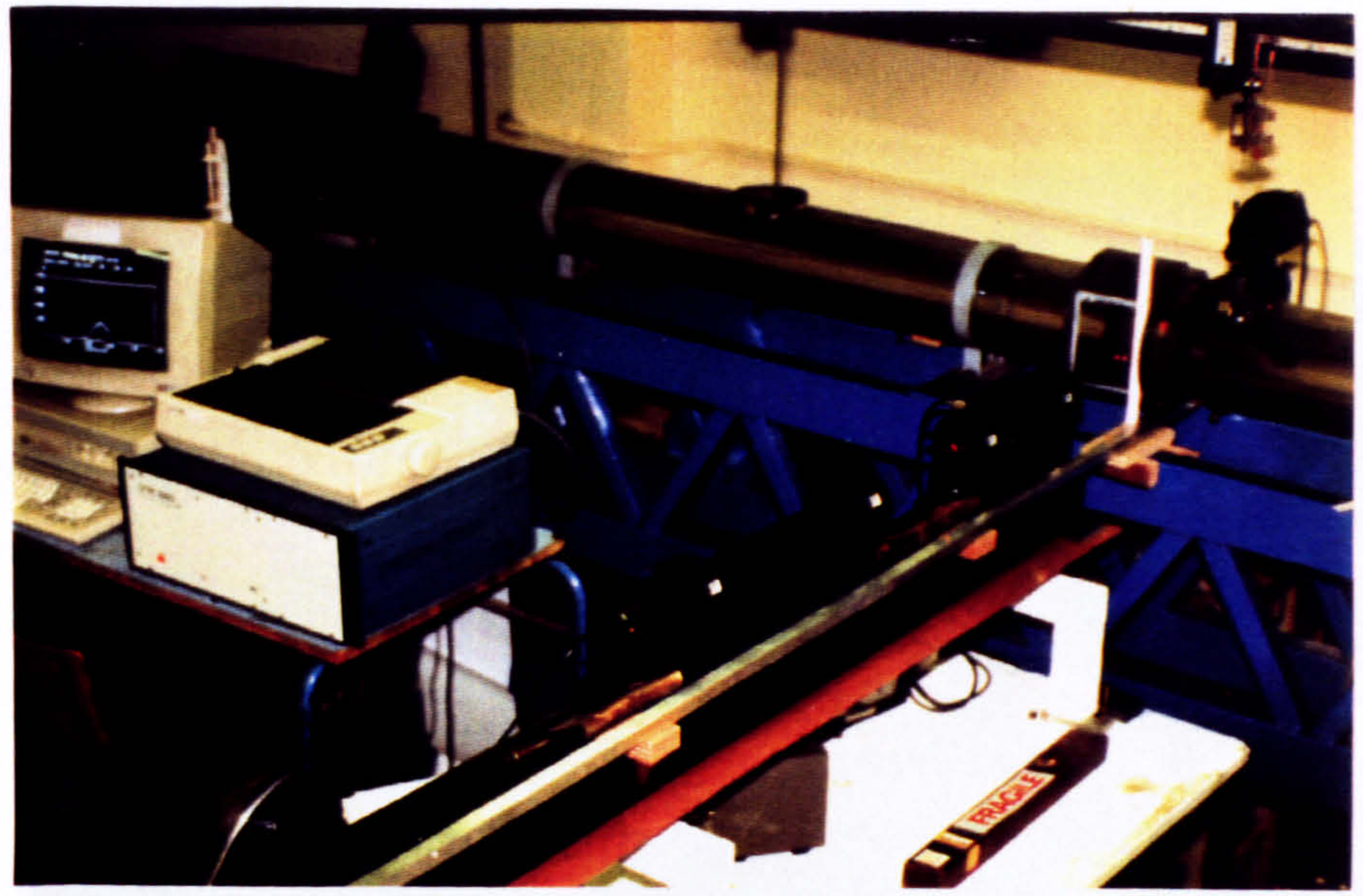

PLATE 4: Laser Doppler Velocimeter

PLATE 5: Synthetic sewer sediment being placed in the flume

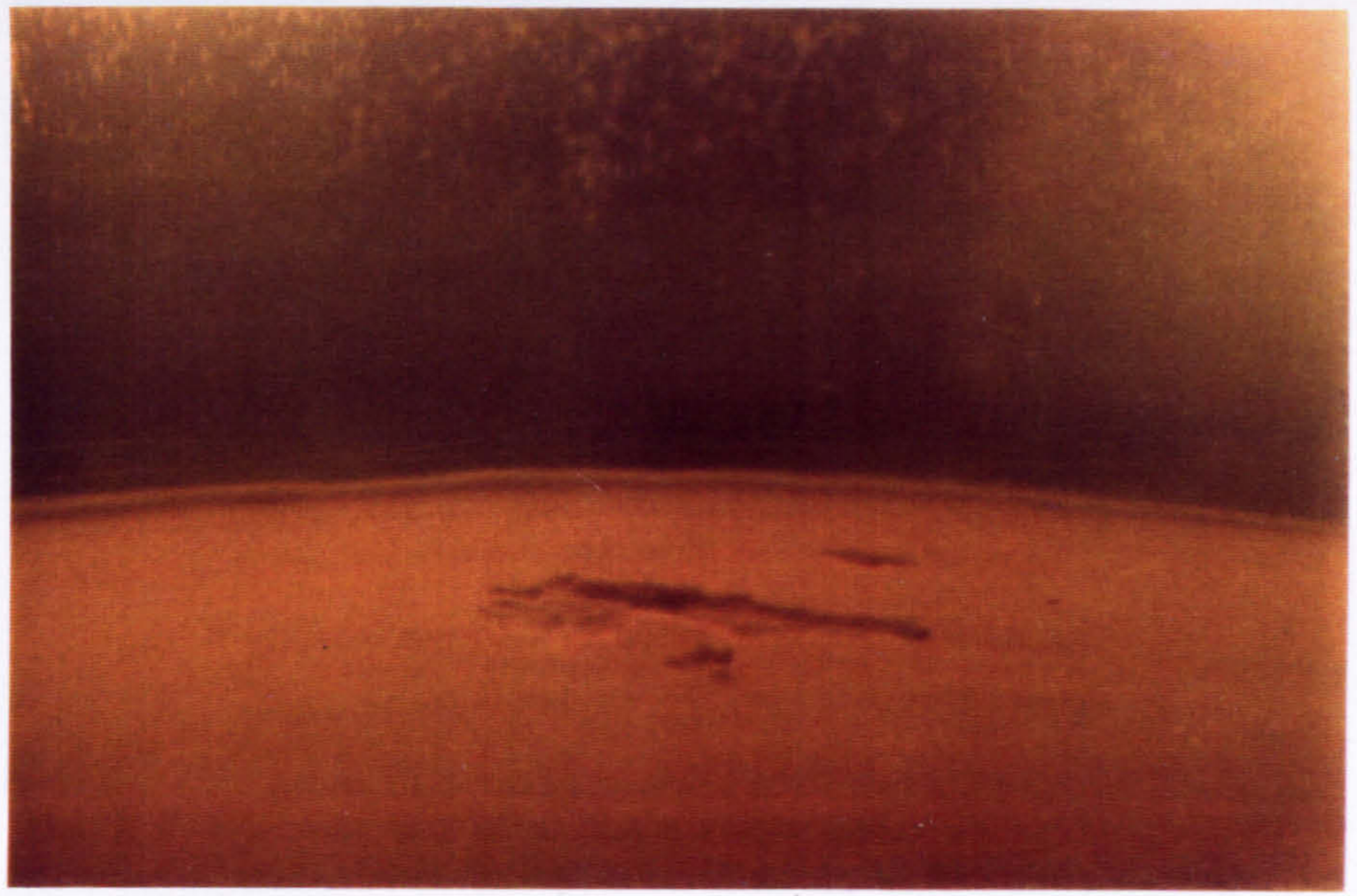

PLATE 6: First spots of erosion appearing on the bed surface (τ_{01})

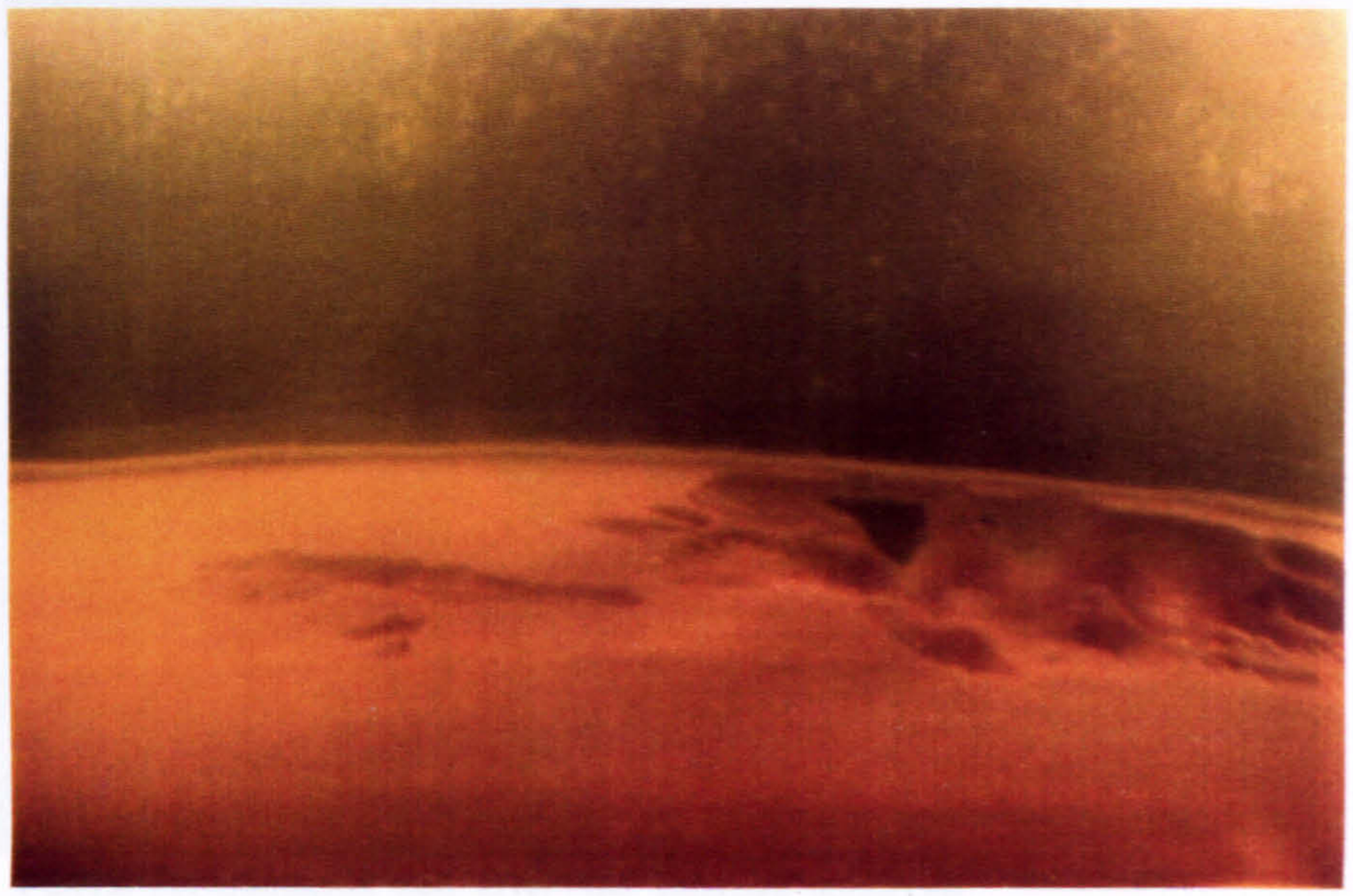

PLATE 7: Bed collapse, erosion progressing very rapidly (τ_{02})

PLATE 8: Bed formation (85% sand (d_{50}=0.12mm)
15% clay gel (18 g/l)

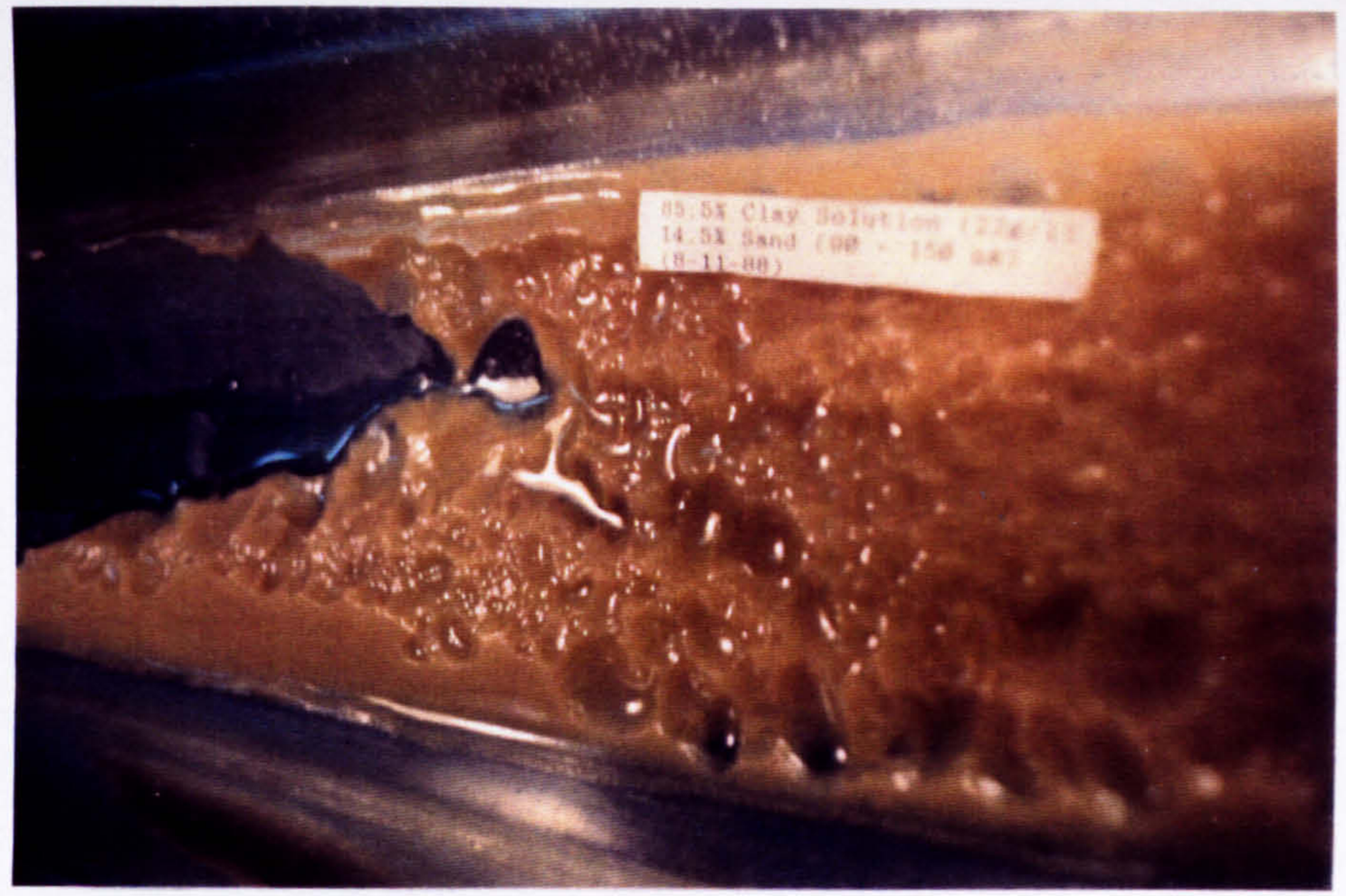

PLATE 9: Sediment bed after the collapse occurred
Mixture: 85.5% Clay gel (22 g/l), 14.5% Sand (0.12mm)

PLATE 10: Sediment bed after the collapse occurred
Mixture: 53% Clay gel (22 g/l), 47% Sand (0.12mm)

APPENDIX D

VELOCITY PROFILES MEASUREMENTS

MEASUREMENTS OF VELOCITY PROFILES

D = 154 mm (with sediment flat bed)

	Bed Thickness	Normal Depth	Energy Gradient	Discharge	Shear Stress (N/m^2) mean		bed		Trans Pos.
	E (mm)	Y_o (mm)	S	Q (l/s)	τ_o		τ_b	τ_{bm}	X (cm)
1	60.3	full	0.005195	7.18	1.4193		2.2358	2.5130	0
2	60.3	full	0.003008	5.32	0.8921		1.4716	1.8950	0
3	60.3	full	0.003008	5.32	0.8921		1.4716	1.3940	2
4	60.3	full	0.003008	5.32	0.8921		1.4716	1.5920	4
5	60.3	full	0.001385	3.67	0.3783		0.5408	0.6060	0
6	60.3	full	0.001385	3.67	0.3783		0.5408	0.5650	2
7	60.3	full	0.001385	3.67	0.3783		0.5408	0.7610	4
8	60.3	55.0	0.001853	3.06	0.5629		0.6848	0.9540	0
9	60.3	55.0	0.001853	3.06	0.5629		0.6848	0.8730	2
10	60.3	55.0	0.001853	3.06	0.5629		0.6848	0.6280	4
11	60.3	35.1	0.001685	1.53	0.4002		0.4622	0.4990	0
12	60.3	35.1	0.001685	1.53	0.4002		0.4622	0.3720	2
13	60.3	35.1	0.001685	1.53	0.4002		0.4622	0.3520	4
14	60.3	55.6	0.002123	3.63	0.6489		0.7442	0.8730	0
15	60.3	55.6	0.002123	3.63	0.6489		0.7442	0.7240	2
16	60.3	55.6	0.002123	3.63	0.6489		0.7442	0.6870	4
17	40.8	full	0.001301	5.21	0.4131		0.5570	0.7340	0
18	40.8	full	0.003053	7.46	0.9691		1.6191	1.5340	0
19	40.8	76.1	0.001704	5.07	0.6351		0.7666	0.8590	0
20	40.8	35.3	0.002088	1.75	0.5102		0.5941	0.4610	0
21	40.8	35.1	0.002377	2.28	0.5793		0.6063	0.6460	0
22	40.8	73.9	0.001104	3.75	0.4078		0.5059	0.3760	0
23	40.8	39.2	0.001104	1.53	0.2900		0.3313	0.1650	0
24	40.8	35.4	0.001154	1.45	0.2825		0.3058	0.1830	0
25	20.0	46.5	0.002851	2.53	0.8349		1.1895	1.0810	0
26	20.0	51.7	0.002808	3.08	0.8806		1.2638	0.9020	0
27	20.0	66.6	0.002806	4.65	1.0263		1.5521	1.8330	0
28	20.0	80.8	0.003124	6.19	1.2569		2.1376	1.1980	0
29	20.0	80.8	0.003124	6.19	1.2569		2.1376	1.2700	2
30	20.0	80.8	0.003124	6.19	1.2569		2.1376	1.0750	4

MEASUREMENTS OF VELOCITY PROFILES (CONT.)

D = 154 mm (with sediment flat bed)

	Bed Thickness E (mm)	Normal Depth Y_o (mm)	Energy Gradient S	Discharge Q (l/s)	Shear Stress (N/m^2) mean τ_o	bed τ_b	τ_{bm}	Trans Pos. X (cm)
31	20.0	95.1	0.002867	8.02	1.2191	1.9471	1.5680	0
32	20.0	95.1	0.002867	8.02	1.2191	1.9471	2.1610	2
33	20.0	95.1	0.002867	8.02	1.2191	1.9471	2.8960	4
34	20.0	95.1	0.002867	8.02	1.2191	1.9471	0.6690	5
35	20.0	96.0	0.002830	7.97	1.2060	1.9571	2.2340	0
36	20.0	52.1	0.002862	3.15	0.9023	1.2974	1.3840	0
37	20.0	49.0	0.002243	2.47	0.6790	0.9652	0.7420	0
38	20.0	64.9	0.002184	3.87	0.7877	0.9652	0.7420	0
39	20.0	86.0	0.002250	5.90	0.9277	1.5115	1.3380	0
40	18.4	67.2	0.001081	3.05	0.3972	0.5555	0.6210	0
41	18.4	57.7	0.001607	3.02	0.5396	0.7316	0.9790	0
42	18.4	60.8	0.001432	3.01	0.4961	0.6926	0.8410	0
43	18.4	26.8	0.001520	0.76	0.2937	0.3632	0.3500	0
44	18.4	26.8	0.001520	0.76	0.2934	0.3632	0.2990	3
45	18.4	26.8	0.001520	0.76	0.2934	0.3632	0.0800	5
46	18.4	77.5	0.002350	5.59	0.9287	1.3913	1.6260	0
47	18.4	77.5	0.002350	5.59	0.9287	1.3913	1.5610	2
48	18.4	77.5	0.002350	5.59	0.9287	1.3913	1.0090	4
49	18.4	77.5	0.002350	5.59	0.9287	1.3913	0.7770	5
50	18.4	105.4	0.002070	7.71	0.9009	1.4674	1.4010	0
51	18.4	105.4	0.002070	7.71	0.9009	1.4674	1.4750	2
52	18.4	105.4	0.002070	7.71	0.9009	1.4674	1.2710	4
53	18.4	105.4	0.002070	7.71	0.9009	1.4674	0.8260	5
54	18.4	112.4	0.002278	8.62	0.9931	1.6472	1.4710	0
55	18.4	112.4	0.002278	8.62	0.9931	1.6472	1.5780	2
56	18.4	112.4	0.002278	8.62	0.9931	1.6472	0.9720	4
57	18.4	112.4	0.002278	8.62	0.9931	1.6472	0.6870	5
58	18.4	full	0.006754	15.84	2.422	4.777	4.429	0
59	18.4	full	0.006754	15.84	2.422	4.777	3.667	2
60	18.4	full	0.006754	15.84	2.422	4.777	3.465	4
61	18.4	full	0.006754	15.84	2.422	4.777	2.181	5

MEASUREMENTS OF VELOCITY PROFILES

D = 154 mm (with sediment flat bed)

	Bed Thickness	Normal Depth	Energy Gradient	Discharge	Shear Stress (N/m^2) mean	bed		Trans Pos.
	E (mm)	Y_o (mm)	S	Q (l/s)	τ_o	τ_b	τ_{bm}	X (cm)
62	18.4	53.5	0.002290	3.10	0.7311	1.0171	0.8390	0
63	18.4	53.5	0.002290	3.10	0.7311	1.0171	0.8140	2
64	18.4	53.5	0.002290	3.10	0.7311	1.0171	0.6940	3
65	18.4	53.5	0.002290	3.10	0.7311	1.0171	0.7310	4
66	18.4	53.5	0.002290	3.10	0.7311	1.0171	0.4890	5
67	18.4	29.8	0.002200	1.12	0.4639	0.5778	0.3970	0
68	18.4	29.8	0.002200	1.12	0.4639	0.5778	0.1720	2
69	18.4	29.8	0.002200	1.12	0.4639	0.5778	0.2030	4
70	18.4	29.8	0.002200	1.12	0.4639	0.5778	0.1200	5
71	18.4	full	0.006630	15.84	2.4339	4.7379	4.7540	0
72	18.4	full	0.002070	8.38	0.7429	1.3477	1.8130	0
73	18.4	full	0.000720	4.51	0.2573	0.4908	0.4730	0
74	18.4	full	0.003660	11.39	1.3129	2.4721	3.1310	0
75	18.4	full	0.001870	7.80	0.6706	1.2651	1.4570	0
76	18.4	full	0.003490	11.35	1.2508	2.2005	2.6730	0
77	18.4	full	0.009890	19.72	3.5448	6.7865	9.2570	0
78	12.5	full	0.001371	6.52	0.5029	1.1437	1.1670	0
79	12.5	full	0.004062	12.23	1.4900	3.2644	3.4250	0
80	12.5	full	0.006091	15.90	2.2343	4.4809	4.7580	0
81	12.5	full	0.011836	22.80	4.3417	9.2219	12.9940	0
82	0.0	105.5	0.002137	8.84	0.9490	-	1.4210	0
83	0.0	103.8	0.002137	8.77	0.9430	-	1.4700	0
84	0.0	103.8	0.002137	8.77	0.9430	-	1.3920	0
85	0.0	80.7	0.002137	5.58	0.8310	-	1.3470	0
86	0.0	80.3	0.002137	5.45	0.8280	-	1.2650	0
87	0.0	80.3	0.002137	5.45	0.8280	-	1.2800	0
88	0.0	126.4	0.002137	12.28	0.9820	-	1.7470	0
89	0.0	125.9	0.002137	12.09	0.9820	-	1.9160	0
90	0.0	123.0	0.002137	12.30	0.9820	-	1.8170	0
91	0.0	124.1	0.002137	12.17	0.9820	-	1.7850	0

APPENDIX E

TURBULENCE INTENSITY DATA

VELOCITY AND TURBULENCE INTENSITY PROFILES

Channel of circular cross-section

LASER DOPPLER ANEMOMETRY R1

Flume Diameter	D = 154	(mm)
Bed Thickness	E = 40.8	(mm)
Discharge	Q = 2.06	(l/s)
Slope	S = 0.002462	
Mean Shear Stress	τ_o = 0.6192	(N/m^2)
Bed Shear Stress	τ_{bm} = 1.1580	(N/m^2)
Mean Velocity	V = 0.378	(m/s)
Normal Depth	Y_o = 36.75	(mm)
	(Y+E)/D = 0.50	
Temperature	T = 17.8 - 18.4 C°	

y (mm)	$\frac{y}{Y_o}$	u (m/s)	$\sqrt{\overline{u'^2}}$ (m/s)	$\frac{\sqrt{\overline{u'^2}}}{u}$ (%)	$u-u_{max}$ (m/s)	-Log(y/h) x5.75
4.5	0.122	0.335	0.038	11.34	0.164	5.05003
6.0	0.163	0.357	0.041	11.48	0.142	4.33163
9.0	0.245	0.391	0.042	10.74	0.108	3.31911
15.0	0.408	0.452	0.035	7.74	0.047	2.04348
24.0	0.653	0.477	0.024	5.03	0.022	0.86979
30.0	0.816	0.490	0.023	4.69	0.009	0.31256
34.0	0.925	0.499	0.023	4.61	0.000	0.00000

Regression Output:

Constant	-0.00832
Std Err of Y Est	0.008177
R Squared	0.987356
No. of Observations	6
Degrees of Freedom	4
X Coefficient(s)	0.034029
Std Err of Coef.	0.001925

Shear velocity

$u_* = 0.034$ (m/s)

Bed Shear Stress

$\tau_b = 1.158$ (N/m^2)

VELOCITY AND TURBULENCE INTENSITY PROFILES

Channel of circular cross-section

LASER DOPPLER ANEMOMETRY R2

Flume Diameter D = 154 (mm)

Bed Thickness E = 40.80 (mm)

Discharge Q = 5.5 (l/s)

Slope S = 0.002378

Mean Shear Stress τ_o = 0.8795 (N/m^2)

Bed Shear Stress τ_{bm} = 1.3477 ($N//m^2$)

Mean Velocity V = 0.502 (m/s)

Normal Depth Y_o = 74.1 (mm)

(Y+E)/D = 0.746

Temperature T = 18.4 - 19.0 °C

y (mm)	$\frac{y}{Y_o}$	u (m/s)	$\sqrt{\overline{u'^2}}$ (m/s)	$\frac{\sqrt{\overline{u'^2}}}{u}$ (%)	$u-u_{max}$ (m/s)	-Log(y/h) x5.75
4.0	0.054	0.393	0.057	14.50	0.219	6.04413
8.0	0.108	0.450	0.065	14.44	0.162	4.31320
14.0	0.189	0.509	0.048	9.43	0.103	2.91574
24.0	0.324	0.545	0.042	7.71	0.067	1.56976
34.0	0.459	0.594	0.035	5.89	0.018	0.69997
45.0	0.607	0.612	0.023	3.76	0.000	0.00000
55.0	0.742	0.597	0.024	4.02	0.015	-0.50111
70.0	0.945	0.558	0.027	4.84	0.054	-1.10334

Regression Output:

Constant	-0.00026
Std Err of Y Est	0.006795
R Squared	0.994821
No. of Observations	6
Degrees of Freedom	4
X Coefficient(s)	0.036711
Std Err of Coef.	0.001324

Shear velocity

u_* = 0.0367 (m/s)

Bed Shear Stress

τ_b = 1.3477 (N/m^2)

VELOCITY AND TURBULENCE INTENSITY PROFILES

Channel of circular cross-section

LASER DOPPLER ANEMOMETRY R3

Flume Diameter D = 154 (mm)

Bed Thickness E = 40.80 (mm)

Discharge Q = 1.91 (l/s)

Slope S = 0.001244

Mean Shear Stress τ_o = 0.3532 (N/m^2)

Bed Shear Stress τ_{bm} = 0.4148 (N/m^2)

Mean Velocity V = 0.290 (m/s)

Normal Depth Y_o = 44.09 (mm)

(Y+E)/D = 0.55

Temperature T = 18.5 - 18.8 C°

y (mm)	$\frac{y}{Y_o}$	u (m/s)	$\sqrt{\overline{u'^2}}$ (m/s)	$\frac{\sqrt{\overline{u'^2}}}{u}$ (%)	$u-u_{max}$ (m/s)	-Log(y/h) x5.75
4.0	0.091	0.275	0.026	9.45	0.100	5.03160
8.0	0.181	0.297	0.028	9.43	0.078	3.30068
12.0	0.272	0.331	0.027	8.16	0.044	2.28816
21.0	0.476	0.354	0.026	7.34	0.021	0.89069
30.0	0.680	0.375	0.017	4.53	0.000	0.00000
40.0	0.907	0.373	0.019	5.09	0.000	-0.71840

Regression Output:

Constant	0.001711
Std Err of Y Est	0.006391
R Squared	0.981572
No. of Observations	5
Degrees of Freedom	3
X Coefficient(s)	0.020366
Std Err of Coef.	0.001611

Shear velocity

u_* = 0.02036660 (m/s)

Bed Shear Stress

τ_b = 0.4148 (N/m^2)

VELOCITY AND TURBULENCE INTENSITY PROFILES

Channel of circular cross-section

LASER DOPPLER ANEMOMETRY R4

Flume Diameter D = 154 (mm)

Bed Thickness E = 40.80 (mm)

Discharge Q = 3.64 (l/s))

Slope S = 0.001312

Mean Shear Stress τ_o = 0.4685 ((N/m^2)

Bed Shear Stress τ_{bm} = 0.5769 (N/m^2)

Mean Velocity V = 0.363 (m/s)

Normal Depth Y_o = 67.31 (mm)

(Y+E)/D = 0.440

Temperature T = 18.8 - 18.9 °C

y (mm)	$\frac{y}{Y_o}$	u (m/s)	$\sqrt{\overline{u'^2}}$ (m/s)	$\frac{\sqrt{\overline{u'^2}}}{u}$ (%)	$u-u_{max}$ (m/s)	-Log(y/h) x5.75
2.0	0.030	0.284	0.045	15.85	0.154	7.48092
4.0	0.059	0.316	0.035	11.08	0.122	5.75000
8.0	0.119	0.352	0.035	9.94	0.086	4.01908
13.5	0.201	0.378	0.030	7.94	0.060	2.71243
28.0	0.416	0.434	0.028	6.45	0.004	0.89069
40.0	0.594	0.438	0.020	4.57	0.000	0.00000
61.5	0.914	0.425	0.020	4.71	0.000	-1.07419

Regression Output:

Constant	-0.01229
Std Err of Y Est	0.006881
R Squared	0.987203
No. of Observations	4
Degrees of Freedom	2
X Coefficient(s)	0.024019
Std Err of Coef.	0.001933

Shear velocity

u_* = 0.0240 (m/s)

Bed Shear Stress

τ_b = 0.5769 (N/m^2)

VELOCITY AND TURBULENCE INTENSITY PROFILES

Channel of circular cross-section

LASER DOPPLER ANEMOMETRY R5

Flume Diameter D = 154 (mm)

Bed Thickness E = 40.80 (mm)

Discharge Q = 2.42 (l/s)

Slope S = 0.00368

Mean Shear Stress τ_o = 0.8927 (N/m^2)

Bed Shear Stress τ_{bm} = 1.3334 (N/m^2)

Mean Velocity V = 0.469 (m/s)

Normal Depth Y_o = 34.9 (mm)

(Y+E)/D = 0.49

Temperature T = 17.3 - 17.°C

y (mm)	$\frac{y}{Y_o}$	u (m/s)	$\sqrt{\overline{u'^2}}$ (m/s)	$\frac{\sqrt{\overline{u'^2}}}{u}$ (%)	$u-u_{max}$ (m/s)	-Log(y/h) x5.75
4.0	0.115	0.460	0.060	13.04	0.179	5.19277
6.5	0.186	0.506	0.050	9.88	0.133	3.98036
9.5	0.272	0.538	0.046	8.55	0.101	3.03270
13.5	0.387	0.564	0.044	7.80	0.075	2.15519
23.0	0.659	0.623	0.032	5.14	0.016	0.82468
32.0	0.917	0.639	0.028	4.38	0.000	0.00000

Regression Output:

Constant	-0.01010
Std Err of Y Est	0.004565
R Squared	0.995833
No. of Observations	5
Degrees of Freedom	3
X Coefficient(s)	0.036515
Std Err of Coef.	0.001363

Shear velocity

u_* = 0.0365 (m/s)

Bed Shear Stress

τ_b = 1.3334 (N/m^2)

VELOCITY AND TURBULENCE INTENSITY PROFILES

Channel of circular cross-section

LASER DOPPLER ANEMOMETRY R6

Flume Diameter	D = 154	(mm)
Bed Thickness	E = 40.80	(mm)
Discharge	Q = 7.30	(l/s)
Slope	S = 0.003626	
Mean Shear Stress	τ_o = 1.3644	(N/m^2)
Bed Shear Stress	τ_{bm} = 1.9749	(N/m^2)
Mean Velocity	V = 0.631	(m/s)
Normal Depth	Y_o = 78.81	(mm)
	(Y+E)/D = 0.78	
Temperature	T = 17.3 - 18.0	°C

Laser Doppler Anemometry (TSI IFA 550)

angle	11.66 degrees
Freq. shift	0.1 Mhz
Lens	243 degrees
Conversion Factor	3.115 (Mhz/(m/s))

y (mm)	$\frac{y}{Y_o}$	u (m/s)	$\sqrt{\overline{u'^2}}$ (m/s)	$\frac{\sqrt{\overline{u'^2}}}{u}$ (%)	$u-u_{max}$ (m/s)	-Log(y/h) x5.75
3.0	0.038	0.551	0.066	11.98	0.225	6.4684
6.0	0.076	0.570	0.074	12.98	0.206	4.7375
10.0	0.127	0.627	0.066	10.53	0.149	3.4618
21.5	0.272	0.696	0.062	8.91	0.080	1.5503
30.0	0.381	0.762	0.038	4.99	0.014	0.7184
40.0	0.508	0.776	0.029	3.74	0.000	0.0000
50.0	0.634	0.766	0.029	3.79	0.010	-0.5572
66.0	0.837	0.737	0.036	4.88	0.039	-1.2505
75.0	0.952	0.733	0.031	4.23	0.043	-1.5698

Regression Output:	
Constant	-0.00324
Std Err of Y Est	0.012057
R Squared	0.985890
No. of Observations	5
Degrees of Freedom	3
X Coefficient(s)	0.044440

Shear velocity

$u_* = 0.0444$ (m/s)

Bed Shear Stress

$\tau_b = 1.9749$ (N/m^2)

VELOCITY AND TURBULENCE INTENSITY PROFILES

Channel of circular cross-section

LASER DOPPLER ANEMOMETRY RF1

Flume Diameter D = 154 (mm)

Bed Thickness E = 40.80 (mm)

Discharge Q = 13.08 (l/s)

Slope S = 0.007626

Mean Shear Stress τ_o = 2.4432 (N/m^2)

Bed Shear Stress τ_{bm} = 3.859 (N/m^2)

Mean Velocity V = 0.891 (m/s)

Normal Depth Y_o = 113.2 (mm)

(Y+E)/D = 1.00 (full pipe flow)

Temperature T = 19.4 - 19.9 °C

y (mm)	$\frac{y}{Y_o}$	u (m/s)	$\sqrt{\overline{u'^2}}$ (m/s)	$\frac{\sqrt{\overline{u'^2}}}{u}$ (%)	$u-u_{max}$ (m/s)	-Log(y/h) x5.75
4.0	0.035	0.758	0.110	14.51	0.343	6.76252
8.0	0.071	0.835	0.104	12.46	0.266	5.03160
15.5	0.137	0.944	0.088	9.32	0.157	3.37996
25.0	0.221	1.006	0.071	7.06	0.095	2.18621
32.0	0.283	1.056	0.067	6.34	0.045	1.56975
40.7	0.359	1.088	0.060	5.51	0.013	0.96920
50.0	0.442	1.100	0.044	4.00	0.001	0.45529
60.0	0.530	1.101	0.047	4.27	0.000	0.00000
70.0	0.618	1.054	0.056	5.31	0.047	-0.3849
80.0	0.707	1.027	0.060	5.84	0.074	-0.7183

Regression Output:

Constant	-0.0480
Std Err of Y Est	0.00575
R Squared	0.99753
No. of Observations	5
Degrees of Freedom	3
X Coefficient(0.06212	
Std Err of Coe0.00178	

Shear velocity

u_* = 0.06212 (m/s)

Shear stress

τ_b = 3.859 (N/m^2)

VELOCITY AND TURBULENCE INTENSITY PROFILES

Channel of circular cross-section

LASER DOPPLER ANEMOMETRY RF2

Flume Diameter D = 154 (mm)

Bed Thickness E = 40.80 (mm)

Discharge Q = 7.59 (l/s)

Slope S = 0.002647

Mean Shear Stress τ_o = 0.8406 (N/m^2)

Bed Shear Stress τ_{bm} = 1.8649 (N/m^2)

Mean Velocity V = 0.517 (m/s)

Normal Depth Y_o = 113.2 (mm)

(Y+E)/D = 1.00

Temperature T = 18.2 - 18.9 °C

Laser Doppler Anemometry (TSI IFA 550)

angle 11.66 degrees

Freq. shift 0.1 MHz

Lens 243 degrees

Conversion Factor 3.115 (MHz/ m/s)

y (mm)	$\frac{y}{Y_o}$	u (m/s)	$\sqrt{\overline{u'^2}}$ (m/s)	$\frac{\sqrt{\overline{u'^2}}}{u}$ (%)	$u-u_{max}$ (m/s)	-Log(y/h) x5.75
4.0	0.035	0.461	0.061	13.23	0.190	6.3072
8.0	0.071	0.508	0.060	11.81	0.143	4.5763
14.3	0.126	0.527	0.054	10.25	0.124	3.1259
20.0	0.177	0.568	0.050	8.80	0.083	2.2882
30.0	0.265	0.604	0.049	8.11	0.047	1.2756
40.0	0.353	0.641	0.033	5.15	0.010	0.5572
50.0	0.442	0.651	0.036	5.53	0.000	0.0000
60.0	0.530	0.650	0.029	4.46	0.001	-0.4553
75.0	0.663	0.640	0.029	4.53	0.011	-1.0125
84.0	0.742	0.602	0.038	6.31	0.049	-1.2955

Regression Output:

Constant	-0.01223
Std Err of Y Est	0.004177
R Squared	0.995119
No. of Observations	4
Degrees of Freedom	2
X Coefficient(s)	0.043185
Std Err of Coef.	0.002138

Shear Velocity

u_* = 0.0432 (m/s)

Bed Shear Stress

τ_b = 1.8649 (N/m2)

VELOCITY AND TURBULENCE INTENSITY PROFILES

Channel of circular cross-section

(11-12-89) S1

Flume Diameter D = 154 (mm)

Bed Thickness E = 40.80 (mm)

Discharge Q = 2.15 (l/s)

Slope S = 0.002466

Mean Shear Stress τ_o = 0.618 (N/m^2)

Bed Shear Stress τ_{bm} = 0.878 (N/m^2)

Mean Velocity V = 0.396 (m/s)

Normal Depth Y_o = 36.58 (mm)

(Y+E)/D = 0.50

Temperature T = 20.5 °C

y (mm)	$\frac{y}{Y_o}$	u (m/s)	$\sqrt{\overline{u'^2}}$ (m/s)	$\frac{\sqrt{\overline{u'^2}}}{u}$ (%)	$u-u_{max}$ (m/s)	-Log(y/h) x5.75
3.0	0.082	0.347	0.035	10.1	0.174	5.75
6.0	0.164	0.391	0.042	10.7	0.130	4.02
10.0	0.273	0.421	0.039	9.3	0.100	2.74
15.0	0.410	0.471	0.037	7.9	0.050	1.73
25.0	0.683	0.506	0.024	4.7	0.015	0.46
30.0	0.820	0.521	0.021	4.0	0.000	0.00

Regression Output:

Constant	0.007990
Std Err of Y Est	0.010691
R Squared	0.971939
No. of Observations	4
Degrees of Freedom	2
X Coefficient(s)	0.029630
Std Err of Coef.	0.003559

Shear Velocity

u_x = 0.0296 (m/s)

Bed Shear Stress

τ_b = 0.878 (N/m2)

VELOCITY AND TURBULENCE INTENSITY PROFILES

Channel of circular cross-section

(12-12-89) S2

Flume Diameter D = 154 (mm)

Bed Thickness E = 40.80 (mm)

Discharge Q = 6.35 (l/s)

Slope S = 0.002329

Mean Shear Stress τ_o = 0.876 (N/m^2)

Bed Shear Stress τ_{bm} = 0.945 (N/m^2)

Mean Velocity V = 0.550 (m/s)

Normal Depth Y_o = 78.69 (mm)

$(Y+E)/D$ = 0.78

Temperature T = 19.1 - 20.3°C

y (mm)	$\frac{y}{Y_o}$	u (m/s)	$\sqrt{\overline{u'^2}}$ (m/s)	$\frac{\sqrt{\overline{u'^2}}}{u}$ (%)	$u-u_{max}$ (m/s)	-Log(y/h) x5.75
5.0	0.064	0.495	0.046	9.3	0.157	5.19
10.0	0.127	0.548	0.049	8.9	0.104	3.46
15.0	0.191	0.559	0.053	9.5	0.093	2.45
22.0	0.280	0.611	0.046	7.5	0.041	1.49
30.0	0.381	0.632	0.040	6.3	0.020	0.72
40.0	0.508	0.652	0.026	4.0	0.000	0.00
50.0	0.635	0.647	0.026	4.0	0.005	-0.56
75.0	0.953	0.612	0.027	4.4	0.040	-1.57

Regression Output:

Constant	0.000955
Std Err of Y Est	0.009343
R Squared	0.980036
No. of Observations	6
Degrees of Freedom	4
X Coefficient(s)	0.030736
Std Err of Coef.	0.002193

Shear Velocity

u_* = 0.0307 (m/s)

Bed Shear Stress

τ_b = 0.945 (N/m^2)

VELOCITY AND TURBULENCE INTENSITY PROFILES

Channel of circular cross-section

(15-12-89) S3

Flume Diameter D = 154 (mm)

Bed Thickness E = 40.80 (mm)

Discharge Q = 1.73 (l/s)

Slope S = 0.001499

Mean Shear Stress τ_o = 0.379 (N/m^2)

Bed Shear Stress τ_{bm} = 0.380 (N/m^2)

Mean Velocity V = 0.316 (m/s)

Normal Depth Y_o = 36.96 (mm)

(Y+E)/D = 0.50

Temperature T = 20.5 °C

y (mm)	$\frac{y}{Y_o}$	u (m/s)	$\sqrt{\overline{u'^2}}$ (m/s)	$\frac{\sqrt{\overline{u'^2}}}{u}$ (%)	$u-u_{max}$ (m/s)	-Log(y/h) x5.75
3.0	0.081	0.279	0.036	12.9	0.122	6.13
6.0	0.162	0.305	0.034	11.1	0.096	4.40
9.0	0.244	0.314	0.029	9.2	0.087	3.39
15.0	0.406	0.339	0.030	8.8	0.062	2.12
22.0	0.595	0.372	0.027	7.3	0.029	1.16
30.0	0.812	0.392	0.020	5.1	0.009	0.38
35.0	0.947	0.401	0.020	5.0	0.000	0.00

LDA Regression Output:

Constant	0.0103
Std Err of Y Est	0.0097
R Squared	0.9586
No. of Observations	6.0000
Degrees of Freedom	4.0000
X Coefficient(s)	0.019501
Std Err of Coef.	0.002025

Shear Velocity

u_* = 0.0195 (m/s)

Bed Shear Stress

τ_b = 0.380 (N/m^2)

VELOCITY AND TURBULENCE INTENSITY PROFILES

Channel of circular cross-section

(17-12-89) S4

Flume Diameter D = 154 (mm)

Bed Thickness E = 40.80 (mm)

Bed Thickness E = 40.80 (mm)

Discharge Q = 4.26 (l/s)

Slope S = 0.001361

Mean Shear Stress τ_o = 0.500 ($N//m^2$)

Bed Shear Stress τ_{bm} = 0.453 ($N//m^2$)

Mean Velocity V = 0.395 (m/s)

Normal Depth Y_o = 72.79 (mm)

(Y+E)/D = 0.74

Temperature T = 19 - 20.4 °C

y (mm)	$\frac{y}{Y_o}$	u (m/s)	$\sqrt{\overline{u'^2}}$ (m/s)	$\frac{\sqrt{\overline{u'^2}}}{u}$ (%)	$u-u_{max}$ (m/s)	-Log(y/h) x5.75
3.0	0.041	0.331	0.043	13.0	0.142	7.48
6.0	0.082	0.361	0.039	10.8	0.112	5.75
9.0	0.124	0.383	0.039	10.2	0.090	4.74
15.0	0.206	0.413	0.035	8.5	0.060	3.46
25.0	0.343	0.436	0.030	6.9	0.037	2.19
35.0	0.481	0.473	0.017	3.6	0.000	1.35
50.0	0.687	0.464	0.018	3.9	0.009	0.46
60.0	0.824	0.452	0.023	5.1	0.021	0.00

Regression Output:

Constant	-0.0248
Std Err of Y Est	0.0070
R Squared	0.9811
No. of Observations	5.0000
Degrees of Freedom	3.0000
X Coefficient(s)	0.024193
Std Err of Coef.	0.001938

Shear Velocity

u_* = 0.0242 (m/s)

Bed Shear S res

τ_{bm} = 0.585 (N/m^2)

VELOCITY AND TURBULENCE INTENSITY PROFILES

Channel of circular cross-section

(18-12-89) S5

Flume Diameter D = 154 (mm)

Bed Thickness E = 40.80 (mm)

Discharge Q = 2.08 (l/s)

Slope S = 0.002195

Mean Shear Stress τ_o = 0.539 (N/m^2)

Bed Shear Stress τ_{bm} = 0.809 (N/m^2)

Mean Velocity V = 0.396 (m/s)

Normal Depth Y_o = 35.49 (mm)

(Y+E)/D = 0.50

Temperature T = 18.7 - 19.2 C°

y (mm)	$\frac{y}{Y_o}$	u (m/s)	$\sqrt{\overline{u'^2}}$ (m/s)	$\frac{\sqrt{\overline{u'^2}}}{u}$ (%)	$u-u_{max}$ (m/s)	-Log(y/h) x5.75
3.0	0.085	0.359	0.045	12.5	0.146	5.91
6.0	0.169	0.387	0.042	10.9	0.118	4.18
10.0	0.282	0.425	0.038	8.9	0.080	2.90
15.0	0.423	0.450	0.039	8.7	0.055	1.89
25.0	0.704	0.491	0.030	6.1	0.014	0.62
32.0	0.902	0.505	0.021	4.2	0.000	0.00

Regression Output:

Constant	-0.0012
Std Err of Y Est	0.0022
R Squared	0.9984
No. of Observations	5.0000
Degrees of Freedom	3.0000
X Coefficient(s)	0.028439
Std Err of Coef.	0.000652

Shear Velocity

u_* = 0.0284 (m/s)

Bed Shear Stress

τ_{bm} = 0.809 (N/m^2)

VELOCITY AND TURBULENCE INTENSITY PROFILES

Channel of circular cross-section

(19-12-89) S6

Flume Diameter D = 154 (mm)

Bed Thickness E = 40.80 (mm)

Discharge Q = 5.74 (l/s)

Slope S = 0.002196

Mean Shear Stress τ_o = 0.814 ($N//m^2$)

Bed Shear Stress τ_{bm} = 1.058 ($N//m^2$)

Mean Velocity V = 0.521 (m/s)

Normal Depth Y_o = 74.68 (mm)

$(Y+E)/D$ = 0.75

Temperature T = 18.2 - 19.8 °C

y (mm)	$\frac{y}{Y_o}$	u (m/s)	$\sqrt{\overline{u'^2}}$ (m/s)	$\frac{\sqrt{\overline{u'^2}}}{u}$ (%)	$u-u_{max}$ (m/s)	-Log(y/h) x5.75
3.0	0.040	0.426	0.055	12.9	0.194	7.03
6.0	0.080	0.476	0.048	10.1	0.144	5.29
10.0	0.134	0.494	0.054	10.9	0.126	4.02
15.0	0.201	0.542	0.049	9.0	0.078	3.01
25.0	0.335	0.583	0.036	6.2	0.037	1.73
35.0	0.469	0.613	0.030	4.9	0.007	0.89
50.0	0.669	0.620	0.022	3.5	0.000	0.00
60.0	0.803	0.603	0.024	4.0	0.017	-0.46

Regression Output:

Constant	-0.0188
Std Err of Y Est	0.0100
R Squared	0.9777
No. of Observations	5.0000
Degrees of Freedom	3.0000
X Coefficient(s)	0.032530
Std Err of Coef.	0.002834

Shear Velocity

u_x = 0.0325 (m/s)

Bed Shear Stress

τ_{bm} = 1.058 (N/m^2)

VELOCITY AND TURBULENCE INTENSITY PROFILES

Channel of circular cross-section

(20-12-89) S7

Flume Diameter D = 154 (mm)

Bed Thickness E = 40.80 (mm)

Discharge Q = 2.57 (l/s)

Slope S = 0.003507

Mean Shear Stress τ_o = 0.849 (N/m^2)

Bed Shear Stress τ_{bm} = 1.063 (N/m^2)

Mean Velocity V = 0.500 (m/s)

Normal Depth Y_o = 34.81 (mm)

(Y+E)/D = 0.49

Temperature T = 19 - 20.3 °C

y (mm)	$\frac{y}{Y_o}$	u (m/s)	$\sqrt{\overline{u'^2}}$ (m/s)	$\frac{\sqrt{\overline{u'^2}}}{u}$ (%)	$u-u_{max}$ (m/s)	-Log(y/h) x5.75
3.0	0.086	0.535	0.059	11.0	0.173	5.29
8.0	0.230	0.612	0.049	8.0	0.096	2.85
15.0	0.431	0.664	0.049	7.4	0.044	1.28
25.0	0.718	0.708	0.028	4.0	0.000	0.00

Regression Output:

Constant	0.0015
Std Err of Y Est	0.0019
R Squared	0.9996
No. of Observations	4.0000
Degrees of Freedom	2.0000
X Coefficient(s)	0.032609
Std Err of Coef.	0.000485

Shear Velocity

u_* = 0.0326 (m/s)

Bed Shear Stress

τ_{bm} = 1.063 (N/m^2)

VELOCITY AND TURBULENCE INTENSITY PROFILES

Channel of circular cross-section

(21-12-89) S8

Flume Diameter D = 154 (mm)

Bed Thickness E = 40.80 (mm)

Discharge Q = 8.21 (l/s)

Slope S = 0.003500

Mean Shear Stress τ_o = 1.306 (N/m^2)

Bed Shear Stress τ_{bm} = 1.522 (N/m^2)

Mean Velocity V = 0.729 (m/s)

Normal Depth Y_o = 76.37 (mm)

(Y+E)/D = 0.76

Temperature T = 19.6 - 20.9 °C

y (mm)	$\frac{y}{Y_o}$	u (m/s)	$\sqrt{\overline{u'^2}}$ (m/s)	$\frac{\sqrt{\overline{u'^2}}}{u}$ (%)	$u-u_{max}$ (m/s)	-Log(y/h) x5.75
3.0	0.039	0.607	0.073	12.0	0.250	6.47
10.0	0.131	0.687	0.063	9.2	0.170	3.46
15.0	0.196	0.749	0.063	8.4	0.108	2.45
25.0	0.327	0.802	0.063	7.9	0.055	1.17
40.0	0.524	0.857	0.036	4.2	0.000	0.00
55.0	0.720	0.846	0.031	3.7	0.011	-0.80
70.0	0.917	0.810	0.039	4.8	0.047	-1.40

Regression Output:

Constant	0.0108
Std Err of Y Est	0.0171
R Squared	0.9770
No. of Observations	5.0000
Degrees of Freedom	3.0000
X Coefficient(s)	0.039013
Std Err of Coef.	0.003458

Shear Velocity

u_x = 0.0390 (m/s)

Bed Shear stress

τ_{bm} = 1.522 (N/m^2)

VELOCITY AND TURBULENCE INTENSITY PROFILES

Channel of circular cross-section

LASER DOPPLER ANEMOMETRY SF1

Flume Diameter D = 154 (mm)

Bed Thickness E = 40.80 (mm)

Discharge Q = 6.84 (l/s)

Slope S = 0.002013

Mean Shear Stress τ_o = 0.6395 (N/m^2)

Bed Shear Stress τ_{bm} = 0.7739 (N/m^2)

Mean Velocity V = 0.466 (m/s)

Normal Depth Y_o = 113.2 (mm)

(Y+E)/D = 1.00 (full pipe flow)

Temperature T =

y (mm)	$\frac{y}{Y_o}$	u (m/s)	$\sqrt{\overline{u'^2}}$ (m/s)	$\frac{\sqrt{\overline{u'^2}}}{u}$ (%)	$u-u_{max}$ (m/s)	-Log(y/h) x5.75
4	0.035	0.379	0.045	11.87	0.205	6.76252
9	0.080	0.420	0.047	11.19	0.164	4.73748
15	0.133	0.441	0.043	9.75	0.143	3.46184
25	0.221	0.496	0.039	7.86	0.088	2.18621
35	0.309	0.524	0.033	6.30	0.060	1.34598
45	0.398	0.543	0.033	6.08	0.041	0.71840
60	0.530	0.584	0.022	3.77	0.000	0.00000
78	0.689	0.548	0.031	5.66	0.036	-0.65517

Regression Output:

Constant	0.027756
Std Err of Y Est	0.011934
R Squared	0.972200
No. of Observations	6
Degrees of Freedom	4
X Coefficient(s)	0.027818
Std Err of Coef.	0.002352

Shear velocity

u_* = 0.0278 (m/s)

Bed Shear Stress

τ_{bm} = 0.7739 (N/m^2)

VELOCITY AND TURBULENCE INTENSITY PROFILES

Channel of circular cross-section

LASER DOPPLER ANEMOMETRY SF2

Flume Diameter	D = 154	(mm)
Bed Thickness	E = 40.80	(mm)
Discharge	Q = 12.64	(l/s
Slope	S = 0.0053	
Mean Shear Stress	τ_o = 1.692	(N/m^2)
Bed Shear Stress	τ_{bm} = 2.108	(N/m^2)
Mean Velocity	V = 0.861	(m/s)
Normal Depth	Y_o = 113.2	(mm)
	(Y+E)/D = 1.00	
Temperature	T = 18.9 - 19.4	

y (mm)	$\frac{y}{Y_o}$	u (m/s)	$\sqrt{\overline{u'^2}}$ (m/s)	$\frac{\sqrt{\overline{u'^2}}}{u}$ (%)	$u-u_{max}$ (m/s)	-Log(y/h) x5.75
3.0	0.027	0.694	0.075	10.81	0.321	7.4809
6.0	0.053	0.767	0.077	10.04	0.248	5.7500
10.0	0.088	0.786	0.083	10.56	0.229	4.4744
14.0	0.124	0.843	0.071	8.42	0.172	3.6341
18.0	0.159	0.880	0.062	7.05	0.135	3.0066
24.0	0.212	0.911	0.062	6.81	0.104	2.2882
30.0	0.265	0.938	0.067	7.14	0.077	1.7309
40.0	0.353	1.003	0.060	5.98	0.012	1.0125
65.0	0.574	1.015	0.047	4.63	0.000	-0.1999
85.0	0.751	0.923	0.065	7.04	0.092	-0.8698

Regression Output:

Constant	-0.00
Std Err of Y Est	0.019
R Squared	0.968
No. of Observations	8
Degrees of Freedom	6
X Coefficien	0.0459
Std Err of C	0.0033

Shear velocity

$u_* = 0.0459$ (m/s)

Bed Shear Stress

$\tau_{bm} = 2.1077$ (N/m^2)

VELOCITY AND TURBULENCE INTENSITY PROFILES

Channel of circular cross-section

LASER DOPPLER ANEMOMETRY SF3

Flume Diameter D = 154 (mm)

Bed Thickness E = 40.80 (mm)

Discharge Q = 9.7 (l/s)

Slope S = 0.003572

Mean Shear Stress τ_o = 1.1344 (N/m^2)

Bed Shear Stress τ_{bm} = 1.4745 (N/m^2)

Mean Velocity V = 0.661 (m/s)

Normal Depth Y_o = 113.2 (mm)

(Y+E)/D = 1.00

Temperature T = 17.4 ± 18.6

y (mm)	$\frac{y}{Y_o}$	u (m/s)	$\sqrt{\overline{u'^2}}$ (m/s)	$\frac{\sqrt{\overline{u'^2}}}{u}$ (%)	$u-u_{max}$ (m/s)	-Log(y/h) x5.75
3.0	0.027	0.536	0.058	10.82	0.259	7.48092
6.0	0.053	0.590	0.058	9.83	0.205	5.75000
10.0	0.088	0.634	0.056	8.83	0.161	4.47437
14.0	0.124	0.643	0.060	9.33	0.152	3.63413
18.0	0.159	0.675	0.058	8.59	0.120	3.00655
24.0	0.212	0.721	0.061	8.46	0.074	2.28816
30.0	0.265	0.744	0.058	7.80	0.051	1.73092
40.0	0.353	0.795	0.035	4.40	0.000	1.01252
65.0	0.574	0.786	0.035	4.45	0.009	-0.19988
83.5	0.738	0.741	0.047	6.34	0.054	-0.82533

Regression Output:

Constant	-0.01325
Std Err of Y Est	0.017689
R Squared	0.962487
No. of Observations	8
Degrees of Freedom	6
X Coefficient(s)	0.038398
Std Err of Coef.	0.003094

Shear velocity

u_* = 0.03839869 (m/s)

Bed Shear Stress

τ_{bm} = 1.4745 (N/m2)

VELOCITY AND TURBULENCE INTENSITY PROFILES

Channel of circular cross-section

(31-1-90) SF4

Flume Diameter D = 154 (mm)

Bed Thickness E = 40.80 (mm)

Discharge Q = 16.12 (l/s)

Slope S = 0.008876

Mean Shear Stress τ_o = 2.8187 (N/m^2)

Bed Shear Stress τ_{bm} = 3.5132 (N/m^2)

Mean Velocity V = 1.098 (m/s)

Normal Depth Y_o = 36.58 (mm)

(Y+E)/D = 1.00

Temperature T = 18.3 - 19.0 °C

y (mm)	$\frac{y}{Y_o}$	u (m/s)	$\sqrt{\overline{u'^2}}$ (m/s)	$\frac{\sqrt{\overline{u'^2}}}{u}$ (%)	$u-u_{max}$ (m/s)	-Log(y/h) x5.75
3	0.027	0.872	0.092	10.55	0.461	7.4809
6	0.053	0.946	0.095	10.04	0.387	5.7500
10	0.088	1.024	0.095	9.28	0.309	4.4744
14	0.124	1.085	0.100	9.22	0.248	3.6341
18	0.159	1.117	0.097	8.68	0.216	3.0066
24	0.212	1.181	0.096	8.13	0.152	2.2882
30	0.265	1.219	0.089	7.30	0.114	1.7309
40	0.353	1.293	0.063	4.87	0.040	1.0125
65	0.574	1.333	0.054	4.05	0.000	-0.1999
85	0.751	1.234	0.084	6.81	0.099	-0.8698

Regression Output:

Constant	0.032389
Std Err of Y Est	0.014362
R Squared	0.987327
No. of Observations	6
Degrees of Freedom	4
X Coefficient(s)	0.059272
Std Err of Coef.	0.003357

Shear velocity

u_* = 0.0593 (m/s)

Bed Shear Stress

τ_{bm} = 3.5132 (N/m^2)

APPENDIX F

INITIATION OF EROSION DATA
NON-COHESIVE SEDIMENT

TABLE F1: INITIATION OF EROSION EXPERIMENTS

Sediment Size	(d)	0.50 (mm)
Flume Diameter	(D)	154 (mm)
Sediment Thickness	(E)	18.4 (mm)
Density	(ρ)	2609 (Kg/m^3)
Bed width	(B)	99.9 (mm)

	S_o	Y_o (mm)	$\frac{(Y_o+E)}{D}$	Q (l/s)	τ_o (N/m^2)	τ_b (N/m^2)	g_* (g/min)	C_v
1	0.001076	15.80	0.22	0.26	0.135	0.1511	0.00000	0.00E+00
2	0.000937	26.00	0.29	0.56	0.177	0.2513	0.00094	1.07E-08
3	0.000937	32.10	0.33	0.88	0.208	0.2451	0.00266	1.93E-08
4	0.000937	37.90	0.37	1.18	0.236	0.2808	0.25056	1.35E-06
5	0.001364	15.28	0.22	0.27	0.166	0.1889	0.00058	1.35E-08
6	0.001228	20.30	0.25	0.43	0.190	0.2214	0.00029	4.33E-09
7	0.001330	23.87	0.27	0.59	0.234	0.2823	0.00816	8.89E-08
8	0.001351	33.93	0.34	1.10	0.317	0.3980	0.05248	3.04E-07
9	0.001356	34.31	0.34	1.12	0.313	0.4046	0.00055	3.12E-09
10	0.002096	10.12	0.19	0.17	0.179	0.1895	0.00180	6.66E-08
11	0.002156	14.40	0.21	0.33	0.250	0.2793	0.01727	3.33E-07
12	0.002073	17.95	0.24	0.51	0.290	0.3198	0.17224	2.16E-06
13	0.002073	21.20	0.26	0.68	0.332	0.3733	1.34010	1.26E-05

	u_* (m/s)	Re_*	$\frac{\tau_o}{\rho g(Ss-1)d}$	u_{*b} (m/s)	Re_{*b}	$\frac{\tau_b}{\rho g(Ss-1)d}$
1	0.0116	5.19	0.0171	0.0123	5.49	0.0192
2	0.0133	5.94	0.0224	0.0159	7.08	0.0319
3	0.0144	6.45	0.0264	0.0157	6.99	0.0311
4	0.0154	6.86	0.0299	0.0168	7.48	0.0356
5	0.0129	5.76	0.0211	0.0137	6.14	0.0239
6	0.0138	6.15	0.0241	0.0149	6.64	0.0281
7	0.0153	6.84	0.0297	0.0168	7.50	0.0358
8	0.0178	7.95	0.0402	0.0199	8.91	0.0505
9	0.0177	7.90	0.0397	0.0201	8.98	0.0513
10	0.0134	5.97	0.0227	0.0138	6.15	0.0240
11	0.0158	7.06	0.0317	0.0167	7.46	0.0354
12	0.0170	7.60	0.0367	0.0179	7.98	0.0405
13	0.0182	8.13	0.0421	0.0193	8.63	0.0473

TABLE F1: CONTINUATION

	k_s (mm)	k_{sb} (mm)	$\frac{V}{\sqrt{(S_s - 1)gd}}$	λ	λ_b
1	0.64	1.28	1.5946	0.05299	0.05931
2	0.77	2.15	1.9793	0.04591	0.05585
3	0.23	0.93	2.4386	0.03543	0.04167
4	0.17	0.87	2.7164	0.03264	0.03884
5	0.86	1.66	1.7585	0.05622	0.06383
6	0.66	1.57	1.9899	0.04770	0.05563
7	0.70	1.86	2.2815	0.04512	0.05433
8	0.59	2.10	2.8813	0.03867	0.04915
9	0.60	2.17	2.8680	0.03873	0.04944
10	0.18	0.36	1.7418	0.04951	0.05240
11	0.53	1.03	2.2679	0.04960	0.05541
12	0.20	0.51	2.7258	0.03924	0.04335
13	0.19	0.57	3.0176	0.03678	0.04137

TABLE F2: INITIATION OF EROSION EXPERIMENTS

Sediment Size	(d)	0.89 (mm)
Flume Diameter	(D)	154 (mm)
Sediment Thickness	(E)	20.0 (mm)
Density	(ρ)	2593 (Kg/m^3)
Bed width	(B)	103.5 (mm)

	S_o	Y_o (mm)	$\frac{(Y_o+E)}{D}$	Q (l/s)	τ_o (N/m^2)	τ_b (N/m^2)	g_s (g/min)	C_v
1	0.001512	34.82	0.36	0.96	0.3591	0.5246	0.000000	0.00E+00
2	0.001556	38.66	0.38	1.21	0.3990	0.5902	0.000748	3.98E-09
3	0.001639	45.05	0.42	1.65	0.4686	0.7144	0.345144	1.35E-06
4	0.001653	49.95	0.45	2.01	0.5068	0.7857	2.896233	9.25E-06
5	0.002051	54.53	0.48	2.39	0.6660	1.1189	8.378691	2.26E-05
6	0.001728	31.80	0.34	0.94	0.3833	0.5344	0.001198	8.21E-09
7	0.002044	40.18	0.39	1.49	0.5391	0.8091	0.410777	1.78E-06
8	0.002226	43.31	0.41	1.69	0.6191	0.9737	2.133009	8.09E-06
9	0.002282	47.43	0.44	2.02	0.6758	1.0863	8.009409	2.55E-05
10	0.002279	23.90	0.29	0.65	0.4043	0.5357	0.000000	0.00E+00
11	0.002323	30.35	0.33	1.03	0.4971	0.6857	0.013738	8.56E-08
12	0.002388	32.59	0.34	1.16	0.5394	0.7631	0.138441	7.64E-07
13	0.002468	38.76	0.38	1.60	0.6342	0.9343	5.883867	2.37E-05

	$\frac{\tau_o}{\rho g(Ss-1)d}$	u_* (m/s)	Re_*	$\frac{\tau_b}{\rho g(Ss-1)d}$	u_{*b} (m/s)	Re_{*b}
1	0.0258	0.0189	15.06	0.0377	0.0189	14.99
2	0.0287	0.0200	15.87	0.0425	0.0195	15.51
3	0.0337	0.0216	17.20	0.0514	0.0206	16.33
4	0.0365	0.0225	17.89	0.0565	0.0213	16.94
5	0.0479	0.0258	20.51	0.0805	0.0220	17.48
6	0.0276	0.0196	15.56	0.0384	0.0183	14.57
7	0.0388	0.0232	18.45	0.0582	0.0198	15.71
8	0.0445	0.0249	19.77	0.0700	0.0203	16.11
9	0.0486	0.0260	20.66	0.0781	0.0209	16.63
10	0.0291	0.0201	15.98	0.0385	0.0169	13.42
11	0.0358	0.0223	17.72	0.0493	0.0181	14.37
12	0.0388	0.0232	18.46	0.0549	0.0185	14.68
13	0.0456	0.0252	20.01	0.0672	0.0195	15.52

TABLE F2: CONTINUATION

	k_s (mm)	k_{sb} (mm)	$\frac{V}{\sqrt{(S_s - 1)gd}}$	λ	λ_b
1	3.37	11.74	1.8069	0.06378	0.09323
2	2.69	10.41	2.0120	0.05659	0.08372
3	2.24	10.13	2.3037	0.05054	0.07708
4	1.90	9.60	2.5074	0.04651	0.07211
5	2.95	16.93	2.6947	0.05261	0.08843
6	2.41	7.78	1.9485	0.05780	0.08062
7	2.61	10.64	2.3699	0.05491	0.08261
8	3.26	14.48	2.4802	0.05823	0.09160
9	2.96	14.55	2.6670	0.05464	0.08785
10	2.76	7.11	1.8552	0.06691	0.08867
11	2.18	6.85	2.2588	0.05618	0.07751
12	2.37	7.95	2.3520	0.05649	0.07993
13	2.16	8.59	2.6521	0.05173	0.07624

TABLE F3: INITIATION OF EROSION EXPERIMENTS

Sediment Size	(d)	1.44 (mm)
Flume Diameter	(D)	154 (mm)
Sediment Thickness	(E)	18.4 (mm)
Density	(ρ)	2550 (Kg/m^3)
Bed width	(B)	99.9 (mm)

	S_o	Y_o (mm)	$\frac{(Y_o+E)}{D}$	Q (l/s)	τ_o (N/m^2)	τ_b (N/m^2)	g_s (g/min)	C_v
1	0.002126	25.22	0.28	0.82	0.392	0.4869	0.00048	3.84E-09
2	0.002001	36.22	0.35	1.52	0.487	0.6331	0.00635	2.73E-08
3	0.002032	40.09	0.38	1.83	0.533	0.7029	0.03862	1.38E-07
4	0.001981	43.73	0.40	2.11	0.553	0.7339	0.08037	2.49E-07
5	0.002148	47.28	0.43	2.44	0.633	0.8777	0.45165	1.21E-06
6	0.003459	10.78	0.19	0.27	0.312	0.3366	0.00000	0.00E-00
7	0.003505	16.47	0.23	0.53	0.455	0.6235	0.00158	1.95E-08
8	0.003541	20.65	0.25	0.65	0.555	0.7183	0.02911	2.93E-07
9	0.003510	23.20	0.27	0.94	0.605	0.7455	0.10633	7.39E-07
10	0.003509	25.88	0.29	1.13	0.660	0.8304	0.28986	1.68E-06

	u_* (m/s)	Re_*	$\frac{\tau_o}{\rho g(Ss-1)d}$	u_{*b} (m/s)	Re_{*b}	$\frac{\tau_b}{\rho g(Ss-1)d}$
1	0.0198	25.44	0.0179	0.0221	28.37	0.0222
2	0.0221	28.38	0.0223	0.0252	32.35	0.0289
3	0.0231	29.68	0.0244	0.0265	34.09	0.0321
4	0.0235	30.22	0.0252	0.0271	34.83	0.0335
5	0.0252	32.34	0.0289	0.0296	38.09	0.0401
6	0.0177	22.73	0.0143	0.0183	23.59	0.0154
7	0.0213	27.44	0.0208	0.0250	32.10	0.0285
8	0.0236	30.29	0.0254	0.0268	34.46	0.0328
9	0.0246	31.62	0.0276	0.0273	35.10	0.0341
10	0.0257	33.02	0.0301	0.0288	37.05	0.0379

TABLE F3: CONTINUATION

	k_s (mm)	k_{sb} (mm)	$\frac{V}{\sqrt{(S_s - 1)gd}}$	λ	λ_b
1	0.79	2.21	1.7943	0.04420	0.05497
2	0.56	2.14	2.2086	0.03658	0.04756
3	0.51	2.15	2.3685	0.03484	0.04597
4	0.44	2.05	2.4672	0.03317	0.04405
5	0.57	2.81	2.6109	0.03393	0.04708
6	0.34	0.58	1.5137	0.04906	0.05287
7			1.8769		
8	2.13	5.23	1.7841	0.06343	0.08210
9	0.71	1.89	2.2622	0.04298	0.05300
10	0.72	2.08	2.3968	0.04158	0.05236

TABLE F4: INITIATION OF EROSION EXPERIMENTS

Sediment Size	(d)	1.60 (mm)
Flume Diameter	(D)	154 (mm)
Sediment Thickness	(E)	20.0 (mm)
Density	(ρ)	2602 (Kg/m^3)
Bed width	(B)	103.5 (mm)

	S_o	Y_o (mm)	$\frac{(Y_o+E)}{D}$	Q (l/s)	τ_o (N/m^2)	τ_b (N/m^2)	g_s (g/min)	C_v
1	0.001449	81.48	0.66	4.67	0.5852	0.8890	0.11505	1.58E-07
2	0.001531	77.98	0.64	4.20	0.6066	1.0005	0.06318	9.64E-08
3	0.001515	75.70	0.62	3.96	0.5919	0.9785	0.05294	8.56E-08
4	0.001467	74.19	0.61	3.86	0.5679	0.9115	0.05969	9.91E-08
5	0.001367	55.73	0.49	2.43	0.4501	0.6588	-	-
6	0.001396	50.28	0.46	2.00	0.4299	0.6347	-	-
7	0.001799	41.93	0.40	1.71	0.4890	0.6905	0.00010	3.75E-10
8	0.001993	46.68	0.43	2.15	0.5837	0.8523	0.02152	6.41E-08
9	0.001841	62.85	0.54	3.48	0.6517	0.9804	0.08677	1.60E-07
10	0.002299	57.00	0.50	3.00	0.7674	1.2441	0.06078	1.30E-07
11	0.002110	35.89	0.36	1.46	0.5123	0.6944	0.00000	0.00E+00
12	0.002469	32.20	0.34	1.28	0.5526	0.7478	0.00578	2.89E-08
13	0.002546	34.89	0.36	1.45	0.6055	0.8468	0.01239	5.47E-08
14	0.002529	37.81	0.38	1.62	0.6381	0.9202	0.01184	4.67E-08
15	0.002511	41.30	0.40	1.92	0.6752	0.9814	0.09055	3.02E-07

	u_* (m/s)	Re_*	$\frac{\tau_o}{\rho g(Ss-1)d}$	u_{*b} (m/s)	Re_{*b}	$\frac{\tau_b}{\rho g(Ss-1)d}$
1	0.0242	34.56	0.0233	0.0298	42.59	0.0354
2	0.0246	35.18	0.0241	0.0316	45.19	0.0398
3	0.0243	34.76	0.0235	0.0313	44.69	0.0389
4	0.0238	34.04	0.0226	0.0302	43.13	0.0363
5	0.0212	30.31	0.0179	0.0257	36.67	0.0262
6	0.0207	29.62	0.0171	0.0252	35.99	0.0253
7	0.0221	31.59	0.0195	0.0263	37.54	0.0275
8	0.0242	34.51	0.0232	0.0292	41.71	0.0339
9	0.0255	36.47	0.0259	0.0313	44.73	0.0390
10	0.0277	39.57	0.0305	0.0353	50.39	0.0495
11	0.0226	32.33	0.0204	0.0264	37.64	0.0276
12	0.0235	33.58	0.0220	0.0273	39.07	0.0298
13	0.0246	35.15	0.0241	0.0291	41.57	0.0337
14	0.0253	36.09	0.0254	0.0303	43.34	0.0366
15	0.0260	37.12	0.0269	0.0313	44.75	0.0390

TABLE F4: CONTINUATION

	k_s (mm)	k_{sb} (mm)	$\frac{V}{\sqrt{(S_s - 1)gd}}$	λ	λ_b
1	0.39	3.55	2.5401	0.02886	0.04386
2	0.84	7.28	2.3898	0.03378	0.05573
3	0.93	7.82	2.3243	0.03485	0.05762
4	0.80	6.41	2.3134	0.03371	0.05414
5	0.81	4.58	1.9905	0.03611	0.05288
6	1.16	5.88	1.8387	0.04044	0.05971
7	1.12	4.75	1.9277		
8	1.12	5.33	2.1523		
9	0.67	4.43	2.4935		
10	1.62	9.95	2.3937		
11	1.02	3.74	1.9731	0.04216	0.05714
12	1.29	4.32	1.9505	0.04626	0.06259
13	1.51	5.48	2.0179	0.04736	0.06626
14	1.70	6.67	2.0628	0.04800	0.06923
15	1.41	6.04	2.2037	0.04180	0.06423

TABLE F5: INITIATION OF EROSION EXPERIMENTS

Sediment Size	(d)	2.00 (mm)
Flume Diameter	(D)	154 (mm)
Sediment Thickness	(E)	18.4 (mm)
Density	(ρ)	2507 (Kg/m^3)
Bed width	(B)	99.9 (mm)

	S_o	Y_o (mm)	$\frac{(Y_o+E)}{D}$	Q (l/s)	τ_o (N/m^2)	τ_b (N/m^2)	g_s (g/min)	C_v
1	0.003068	14.13	0.21	0.38	0.3502	0.3946	0.00000	0.00E+00
2	0.003732	25.16	0.28	1.03	0.6860	0.8737	0.00760	4.91E-08
3	0.003587	30.26	0.32	1.43	0.7619	0.9912	0.06952	3.23E-07
4	0.003804	22.27	0.26	0.80	0.6341	0.8047	0.00447	3.71E-08
5	0.003762	28.76	0.31	1.26	0.7682	1.0181	0.04180	2.21E-07
6	0.003673	32.81	0.33	1.59	0.8300	1.1205	0.24999	1.05E-06
7	0.003770	35.13	0.35	1.81	0.8971	1.2300	0.77081	2.83E-06
8	0.002043	41.58	0.39	1.85	0.5498	0.7416	0.00271	9.74E-09
9	0.002016	46.23	0.42	2.28	0.5847	0.7848	0.00798	2.33E-08
10	0.002055	53.83	0.47	2.91	0.6602	0.9724	0.04356	9.95E-08
11	0.002796	39.89	0.38	1.62	0.7306	1.2446	0.00000	0.00E+00
12	0.003576	33.90	0.34	1.43	0.8284	1.3094	0.00356	1.66E-08
13	0.003226	40.46	0.38	1.94	0.8516	1.4424	0.00559	1.91E-08
14	0.003079	46.84	0.42	2.43	0.9010	1.0397	0.01043	2.85E-08
15	0.001830	55.48	0.48	2.25	0.5992	1.1029	0.00030	8.86E-10
16	0.001671	67.16	0.56	3.05	0.6138	1.1268	0.00023	5.01E-10
17	0.001616	73.73	0.60	3.58	0.6236	1.3071	0.00121	2.25E-09
18	0.001561	90.24	0.71	4.56	0.6563	1.7879	0.00108	1.57E-09
19	0.001713	112.48	0.85	5.62	0.7444	1.1507	0.00203	2.40E-09
20	0.002536	46.91	0.42	2.07	0.7429	1.2148	0.00066	2.12E-09
21	0.002427	62.46	0.53	3.20	0.8548	1.5454	0.00180	3.74E-09
22	0.002143	85.53	0.67	4.96	0.8840	1.7552	0.00618	8.28E-09

TABLE F5: CONTINUATION

	u_* (m/s)	Re_*	$\frac{\tau_o}{\rho g(Ss-1)d}$	u_{*b} (m/s)	Re_{*b}	$\frac{\tau_b}{\rho g(Ss-1)d}$
1	0.0187	37.20	0.0118	0.0199	39.49	0.0134
2	0.0262	53.44	0.0232	0.0296	60.31	0.0296
3	0.0276	58.07	0.0258	0.0315	66.23	0.0335
4	0.0252	50.78	0.0215	0.0284	57.20	0.0272
5	0.0277	56.89	0.0260	0.0319	65.49	0.0344
6	0.0288	59.35	0.0281	0.0335	68.95	0.0379
7	0.0300	61.84	0.0304	0.0351	72.41	0.0416
8	0.0234	41.87	0.0186	0.0272	48.63	0.0251
9	0.0242	43.18	0.0198	0.0280	50.03	0.0266
10	0.0257	45.88	0.0223	0.0312	55.68	0.0329
11	0.0288	51.40	0.0280	0.0353	63.00	0.0421
12	0.0292	52.11	0.0288	0.0362	64.62	0.0443
13	0.0300	53.60	0.0305	0.0380	67.82	0.0488
14	0.0245	43.71	0.0203	0.0322	57.58	0.0352
15	0.0248	44.24	0.0208	0.0332	59.30	0.0373
16	0.0250	44.59	0.0211	0.0336	59.94	0.0381
17	0.0256	45.75	0.0222	0.0362	64.56	0.0442
18	0.0273	48.72	0.0252	0.0423	75.51	0.0605
19	0.0270	48.27	0.0247	0.0339	60.57	0.0389
20	0.0273	48.67	0.0251	0.0349	62.24	0.0411
21	0.0292	52.21	0.0289	0.0393	70.20	0.0523
22	0.0297	53.09	0.0299	0.0419	74.81	0.0594

TABLE F5: CONTINUATION

	k_s (mm)	k_{sb} (mm)	$\frac{V}{\sqrt{(S_s - 1)gd}}$	λ	λ_b
1	0.66	1.21	1.3612	0.05023	0.05662
2	1.27	3.28	1.9525	0.04882	0.06219
3	1.01	2.98	2.1871	0.04284	0.05575
4	1.74	4.14	1.7343	0.05672	0.07200
5	1.52	4.37	2.0567	0.04954	0.06566
6	1.32	4.22	2.2268	0.04543	0.06133
7	1.30	4.43	2.3462	0.04430	0.06076
8	0.85	3.20	1.9759	0.03825	0.05159
9	0.60	2.48	2.1491	0.03412	0.04581
10	0.65	3.15	2.3113	0.03342	0.04696
11	3.00	11.32	1.9280	0.06040	0.09077
12	2.16	9.70	2.1324	0.05060	0.07782
13	2.05	10.80	2.2636	0.04770	0.07637
14	3.24	19.95	1.7272	0.05433	0.09427
15	2.34	18.22	1.8917	0.04633	0.08328
16	1.80	15.78	2.0058	0.04185	0.07564
17	1.91	22.59	2.0733	0.04127	0.08222
18	2.78	49.10	2.0944	0.04595	0.11041
19	3.35	14.59	1.8132	0.06026	0.09493
20	2.90	15.01	1.9274	0.05438	0.08893
21	2.83	20.66	2.1541	0.04996	0.09032
22	2.04	22.98	2.3802	0.04219	0.08379

TABLE F6: INITIATION OF EROSION EXPERIMENTS

Sediment Size	(d)	2.56 (mm)
Flume Diameter	(D)	154 (mm)
Sediment Thickness	(E)	20.0 (mm)
Density	(ρ)	2548 (Kg/m^3)
Bed width	(B)	103.5 (mm)

	S_o	Y_o (mm)	$\frac{(Y_o+E)}{D}$	Q (l/s)	τ_o (N/m^2)	τ_b (N/m^2)	g_s (g/min)	C_v
1	0.001350	46.45	0.43	1.76	0.394	0.5614	0.00000	0.00E+00
2	0.001543	52.25	0.47	2.19	0.487	0.7426	0.00000	0.00E+00
3	0.001646	59.93	0.52	2.88	0.567	0.8841	0.00000	0.00E+00
4	0.001903	74.34	0.61	4.29	0.737	1.2390	0.00000	0.00E+00
5	0.001763	105.08	0.81	6.54	0.761	1.4027	0.00010	1.00E-10
6	0.001976	83.84	0.67	5.34	0.807	1.3681	0.00100	1.22E-09
7	0.002136	92.78	0.73	6.39	0.903	1.5727	0.13594	1.39E-07
8	0.002584	84.18	0.68	6.10	1.057	1.8411	0.00100	1.07E-09
9	0.002711	82.69	0.67	5.95	1.101	1.9609	0.25798	2.84E-07
10	0.002955	73.75	0.61	5.18	1.140	1.9954	0.36140	4.56E-07
11	0.003098	78.55	0.64	5.90	1.231	2.1778	0.97332	1.08E-06
12	0.003328	82.94	0.67	6.49	1.353	2.4872	1.77333	1.79E-06
13	0.003924	60.91	0.53	4.00	1.364	2.4313	-	-
14	0.003853	66.18	0.56	4.50	1.404	2.5828	0.23635	3.43E-07
15	0.003673	73.00	0.60	5.38	1.410	2.5935	0.73945	8.99E-07
16	0.003690	76.08	0.62	5.76	1.445	2.6897	1.63896	1.86E-06

	u_* (m/s)	Re_*	$\frac{\tau_o}{\rho g(Ss-1)d}$	u_{*b} (m/s)	Re_{*b}	$\frac{\tau_b}{\rho g(Ss-1)d}$
1	0.0199	45.39	0.0101	0.0237	54.16	0.0144
2	0.0221	50.46	0.0125	0.0273	62.29	0.0191
3	0.0238	54.41	0.0146	0.0297	67.96	0.0228
4	0.0272	62.06	0.0190	0.0352	80.46	0.0319
5	0.0284	64.93	0.0208	0.0375	85.61	0.0361
6	0.0276	63.07	0.0196	0.0370	84.54	0.0352
7	0.0300	68.67	0.0232	0.0397	90.65	0.0405
8	0.0322	73.62	0.0267	0.0429	98.08	0.0474
9	0.0332	75.86	0.0283	0.0443	101.22	0.0505
10	0.0338	77.19	0.0293	0.0447	102.10	0.0513
11	0.0351	80.21	0.0317	0.0467	106.67	0.0560
12	0.0368	84.09	0.0348	0.0499	113.99	0.0640
13	0.0369	84.40	0.0351	0.0493	112.70	0.0626
14	0.0375	85.65	0.0361	0.0508	116.16	0.0665
15	0.0376	85.83	0.0363	0.0509	116.40	0.0667
16	0.0380	86.89	0.0372	0.0519	118.54	0.0692

TABLE F6: CONTINUATION

	k_s (mm)	k_{sb} (mm)	$\frac{V}{\sqrt{(S_s - 1)gd}}$	λ	λ_b
1	1.03	4.75	1.4209	0.04005	0.05705
2	1.36	7.27	1.5498	0.04168	0.06353
3	1.11	6.94	1.7483	0.03803	0.05936
4	1.04	8.67	2.0672	0.03559	0.05983
5	0.69	9.60	2.2453	0.03111	0.05733
6	0.76	7.42	2.2696	0.03228	0.05472
7	0.66	7.53	2.4569	0.03079	0.05367
8	0.83	8.45	2.5791	0.03266	0.05690
9	1.02	10.32	2.3935	0.03449	0.06143
10	1.26	10.98	2.5162	0.03713	0.06499
11	1.10	10.42	2.6792	0.03528	0.06242
12	1.20	12.57	2.7866	0.03585	0.06589
13	2.72	19.02	2.3887	0.04919	0.08771
14	2.68	20.87	2.4553	0.04801	0.08830
15	1.86	16.50	2.6392	0.04165	0.07662
16	1.76	16.59	2.7037	0.04064	0.07565

TABLE F7: INITIATION OF EROSION EXPERIMENTS

Sediment Size	(d)	2.90 (mm)
Flume Diameter	(D)	154 (mm)
Sediment Thickness	(E)	18.4 (mm)
Density	(ρ)	2548 (Kg/m^3)
Bed width	(B)	99.9 (mm)

	S_o	Y_o (mm)	$\frac{(Y_o+E)}{D}$	Q (l/s)	τ_o (N/m^2)	τ_b (N/m^2)	g_s (g/min)	C_v
1	0.002095	69.98	0.57	4.46	0.787	1.2050	0.00000	0.00E+00
2	0.002018	78.22	0.63	5.08	0.801	1.2836	0.00258	3.33E-09
3	0.002083	85.86	0.68	5.91	0.861	1.4078	0.01831	2.03E-08
4	0.002000	94.05	0.73	6.60	0.852	1.3974	0.01539	1.53E-08
5	0.001992	104.22	0.80	7.45	0.865	1.4480	0.01704	1.50E-08
6	0.003365	52.16	0.46	3.40	1.059	1.6148	0.02617	5.03E-08
7	0.003110	46.65	0.42	2.80	0.908	1.3100	0.00038	8.96E-10
8	0.003490	58.38	0.50	4.20	1.180	1.8420	0.16747	2.61E-07
9	0.003394	58.92	0.50	4.21	1.154	1.8007	0.11495	1.79E-07
10	0.003144	60.21	0.51	4.18	1.083	1.6980	0.18013	2.82E-07
11	0.002880	63.85	0.53	4.50	1.028	1.5884	0.03015	4.38E-08
12	0.004432	32.16	0.33	1.71	0.986	1.3629	0.03977	1.52E-07
13	0.004419	32.15	0.33	1.68	0.983	1.3693	0.01397	5.43E-08
14	0.003908	32.80	0.33	1.50	0.883	1.2808	0.00141	6.15E-09
15	0.004216	41.95	0.39	2.71	1.142	1.6407	0.18053	4.36E-07

	u_* (m/s)	Re_*	$\frac{\tau_o}{\rho g(Ss-1)d}$	u_{*b} (m/s)	Re_{*b}	$\frac{\tau_b}{\rho g(Ss-1)d}$
1	0.0280	72.63	0.0179	0.0347	89.88	0.0274
2	0.0283	73.29	0.0182	0.0358	92.77	0.0292
3	0.0293	75.96	0.0195	0.0375	97.15	0.0320
4	0.0292	75.56	0.0193	0.0374	96.79	0.0317
5	0.0294	76.15	0.0196	0.0381	98.53	0.0329
6	0.0325	84.25	0.0241	0.0402	104.05	0.0367
7	0.0301	78.01	0.0206	0.0362	93.72	0.0298
8	0.0344	88.94	0.0268	0.0429	111.13	0.0418
9	0.0340	87.96	0.0262	0.0424	109.88	0.0409
10	0.0329	85.22	0.0246	0.0412	106.70	0.0386
11	0.0321	83.01	0.0233	0.0399	103.20	0.0361
12	0.0314	81.32	0.0224	0.0369	95.59	0.0310
13	0.0314	81.19	0.0223	0.0370	95.81	0.0311
14	0.0297	76.94	0.0201	0.0358	92.67	0.0291
15	0.0338	87.50	0.0259	0.0405	104.88	0.0373

TABLE F7: CONTINUATION

	k_s (mm)	$k_{s,b}$ (mm)	$\frac{V}{\sqrt{(S_s - 1)gd}}$	λ	λ_b
1	0.51	3.97	2.1678	0.03040	0.04656
2	0.54	4.95	2.1909	0.03029	0.04853
3	0.48	5.05	2.3162	0.02915	0.04771
4	0.39	4.58	2.3619	0.02772	0.04550
5	0.32	4.56	2.4249	0.02674	0.04476
6	0.93	5.35	2.2942	0.03656	0.05577
7	0.76	3.83	2.1414	0.03585	0.05176
8	0.82	5.38	2.4949	0.03443	0.05375
9	0.80	5.32	2.4755	0.03421	0.05338
10	0.80	5.46	2.3980	0.03419	0.04282
11	0.62	4.47	2.4212	0.03189	0.04929
12	1.21	4.29	2.0089	0.04459	0.06161
13	1.33	4.75	1.9734	0.04601	0.06409
14	2.19	7.96	1.7182	0.05426	0.07882
15	0.88	4.01	2.3429	0.03778	0.05428

TABLE F8: INITIATION OF EROSION EXPERIMENTS

Sediment Size	(d)	4.10 (mm)
Flume Diameter	(D)	154 (mm)
Sediment Thickness	(E)	18.4 - 20 (mm)
Density	(ρ)	2479 (Kg/m^3)
Bed width	(B)	99.9 (mm)

	S_o	Y_o (mm)	$\frac{(Y_o+E)}{D}$	Q (l/s)	τ_o (N/m^2)	τ_b (N/m^2)	g_s (g/min)	C_v
1	0.002739	86.18	0.68	6.97	1.1329	1.7640	0.01754	1.69E-08
2	0.002246	91.16	0.71	6.92	0.9472	1.4384	0.00254	2.47E-09
3	0.002297	104.75	0.80	8.11	0.9978	1.6136	0.00010	8.29E-11
4	0.003118	61.50	0.52	4.51	1.0883	1.5856	0.00010	1.49E-10
5	0.003262	70.46	0.58	5.63	1.2297	1.8790	0.00215	2.57E-09
6	0.003256	79.00	0.63	6.65	1.2989	2.0615	0.00847	8.56E-09
7	0.004142	50.53	0.45	3.65	1.2759	1.8461	0.01945	3.58E-08
8	0.004281	57.00	0.49	4.44	1.4261	2.1600	0.03668	5.56E-08
9	0.004522	62.08	0.52	5.14	1.5869	2.5277	0.12538	1.64E-07
10	0.004027	66.10	0.55	5.62	1.4656	2.2583	0.09740	1.17E-07
11	0.004234	73.35	0.61	5.82	1.629	3.0195	0.01000	1.16E-08
12	0.004166	83.31	0.67	7.18	1.697	3.2093	0.13207	1.24E-07
13	0.003678	74.56	0.61	5.58	1.427	2.6362	0.01000	1.21E-08
14	0.003792	85.65	0.69	7.01	1.561	3.0064	0.09199	8.82E-08
15	0.003439	87.34	0.70	7.27	1.426	2.6064	0.00100	9.25E-10
16	0.004111	102.53	0.80	9.52	1.772	3.5355	0.29435	2.08E-07
17	0.004647	111.71	0.86	10.80	2.003	4.2772	1.44089	8.97E-07

	u_* (m/s)	Re_*	$\frac{\tau_o}{\rho g(Ss-1)d}$	u_{*b} (m/s)	Re_{*b}	$\frac{\tau_b}{\rho g(Ss-1)d}$
1	0.0337	123.22	0.0191	0.0420	153.75	0.0297
2	0.0308	112.66	0.0159	0.0379	138.84	0.0242
3	0.0316	115.64	0.0168	0.0402	147.05	0.0271
4	0.0330	120.77	0.0183	0.0398	145.77	0.0267
5	0.0351	128.37	0.0207	0.0433	158.68	0.0316
6	0.0360	131.93	0.0218	0.0454	166.21	0.0347
7	0.0357	130.76	0.0215	0.0430	157.29	0.0310
8	0.0378	138.24	0.0240	0.0465	170.13	0.0363
9	0.0398	145.83	0.0267	0.0503	184.05	0.0425
10	0.0383	140.15	0.0246	0.0475	173.96	0.0380
11	0.0404	147.76	0.0274	0.0549	201.16	0.0508
12	0.0412	150.81	0.0285	0.0567	207.38	0.0540
13	0.0378	138.27	0.0240	0.0513	187.96	0.0443
14	0.0395	144.65	0.0263	0.0548	200.72	0.0506
15	0.0378	138.23	0.0240	0.0511	186.89	0.0438
16	0.0421	154.08	0.0298	0.0595	217.67	0.0595
17	0.0448	163.84	0.0337	0.0654	239.41	0.0719

TABLE F8: CONTINUATION

	k_s (mm)	k_{sb} (mm)	$\frac{V}{\sqrt{(S_s - 1)gd}}$	λ	λ_b
1	0.43	3.69	1.9240	0.02781	0.04331
2	0.32	2.90	1.8074	0.02640	0.04009
3	0.33	3.88	1.8593	0.02626	0.04247
4	0.56	3.23	1.7902	0.03093	0.04507
5	0.58	3.96	1.9220	0.03025	0.04624
6	0.54	4.43	2.0106	0.02926	0.04644
7	0.85	4.05	1.8058	0.03558	0.05148
8	0.92	5.09	1.9157	0.03528	0.05345
9	1.01	6.51	2.0161	0.03546	0.05649
10	0.66	4.40	2.0565	0.03148	0.04850
11	1.86	16.85	1.8887	0.04154	0.07700
12	1.38	14.90	2.0418	0.03707	0.07010
13	1.79	16.34	1.7789	0.04097	0.07572
14	1.48	16.67	1.9373	0.03783	0.07285
15	0.95	10.69	1.9711	0.03340	0.06106
16	0.95	14.25	2.2179	0.03274	0.06535
17	1.01	18.27	2.3425	0.03729	0.05325

APPENDIX G

INITIATION OF EROSION DATA
COHESIVE SEDIMENTS

TABLE G-1: INITIATION OF EROSION EXPERIMENTS

(SYNTHETIC SEWER SEDIMENT)

(Laponite Clay-Sand-Water Mixtures)

Laponite clay gel concentration 24 g/l
154 mm diameter flume E = 18.4 mm (smooth bed)

Sand size (mm)	Clay gel %	Sand prop. %	Density ρ (Kg/m^3)	Crit.Shear Stress τ_{01} (N/m^2)	Crit.Shear Stress τ_{02} (N/m^2)
0.36	0	100	1618	0.120	0.120
	20	80	1907	0.940	1.233
	25	75	1848	2.555	3.522
	30	70	1814	3.247	3.513
	35	65	1797	4.044	4.844
	40	60	1757	5.243	5.456
	60	40	1345	2.778	2.945
0.53	0	100	1648	0.160	0.160
	20	80	1920	0.851	0.976
	30	70	1750	3.300	3.956
	40	60	1618	3.814	3.921
0.89	0	100	1630	0.400	0.400
	15	85	1911	0.408	0.656
	20	80	1932	1.659	2.599
	30	70	1760	2.723	3.513
	40	60	1603	2.253	2.856
	60	40	1352	1.721	2.359
1.44	0	100	1570	0.430	0.430
	15	85	1816	1.008	1.437
	20	80	1567	1.591	1.987
	40	60	1607	2.365	2.588

TABLE G-2: INITIATION OF EROSION EXPERIMENTS (SYNTHETIC SEWER SEDIMENT)

(Laponite Clay-Sand-Water Mixtures)

Sand size 90-150 um (0.12 mm)
154 mm diameter flume E = 18.4 mm (smooth bed)

Clay concent. (g/l)	Clay prop. %	Sand prop. %	Density ρ (Kg/m^3)	Crit. Shear Stress τ_{01} (N/m^2)	Crit. Shear Stress τ_{02} (N/m^2)
18	85.5	14.5	1103	1.082	1.428
	74.5	25.5	1191	1.428	1.740
	62.2	37.8	1312	1.485	1.747
	53.0	47.0	1418	2.097	2.541
	47.0	53.0	1480	2.194	2.463
	40.0	60.0	1688	1.959	2.225
22	85.5	14.5	1121	1.976	2.317
	80.5	19.5	1157	2.028	2.544
	74.5	25.5	1209	2.156	-
	62.2	37.8	1308	2.714	3.568
	53.0	47.0	1408	3.053	3.916
	40.0	60.0	1606	3.300	3.699
	31.6	68.4	1744	3.146	3.486
25	85.5	14.5	1112	2.159	2.494
	80.5	19.5	-	2.235	2.787
	74.5	25.5	1209	2.289	2.720
	62.2	37.8	1375	2.544	3.092
	50.0	50.0	1449	4.086	4.551
	40.0	60.0	1687	5.305	5.970
	30.0	70.0	1752	3.046	3.623

TABLE G-3: INITIATION OF EROSION EXPERIMENTS (SYNTHETIC SEWER SEDIMENT)

(Laponite Clay-Sand-Water Mixtures)

Sand size 600-1180 um (0.89 mm)
154 mm diameter flume E = 18.4 mm (smooth bed)

Clay conc. (g/l)	Clay gel %	Sand prop. %	Density ρ (Kg/m^3)	Crit. Shear Stress τ_{01} (N/m^2)	Crit. Shear Stress τ_{02} (N/m^2)
24	0	100	1630	0.245	0.245
	15	85	1911	0.408	0.656
	20	80	1932	2.111	2.599
	30	70	1768	2.723	3.513
	40	60	1603	2.253	2.856
	60	40	1352	1.721	2.359
27	0	100	1630	0.245	0.245
	20	80	1910	2.033	2.706
	30	70	1770	5.178	5.403
	40	60	1611	4.693	5.207
	50	50	1467	3.520	4.194
	60	40	1377	2.186	2.910
30	0	100	1630	0.245	0.245
	20	80	1935	1.991	2.910
	30	70	1771	4.799	5.266
	35	65	1658	4.592	5.051
	40	60	1585	4.551	5.039
	50	50	1460	2.895	3.335
33	0	100	1630	0.245	0.245
	20	80	1916	2.092	2.830
	30	70	1766	5.766	6.032
	40	60	1610	5.250	5.599
	50	50	1418	4.702	5.136
36	30	70	1738	5.773	6.697
40	30	70	1755	6.325	6.955

TABLE G-4: INITIATION OF EROSION EXPERIMENTS (SYNTHETIC SEWER SEDIMENT)

(Laponite Clay-Sand-Water Mixtures)

Sand size 1180-1700 um (1.44 mm)
154 mm diameter flume E = 18.4 mm (smooth bed)

Clay concent. (g/l)	Clay prop. %	Sand prop. %	Density ρ (Kg/m^3)	Crit. Shear Stress τ_{01} (N/m^2)	Crit. Shear Stress τ_{02} (N/m^2)
30	0	100	1581	0.335	0.335
	20	80	1832	3.190	3.807
	25	75	1867	4.409	5.470
	30	70	1783	4.826	5.501
	40	60	1639	3.791	4.535
	50	50	1445	2.823	3.633
33	30	70	1795	5.415	5.842
36	30	70	1773	5.798	6.476
40	30	70	1777	6.667	7.327

TABLE G-5: INITIATION OF EROSION EXPERIMENTS (SYNTHETIC SEWER SEDIMENT)

(Laponite Clay-Sand-Water Mixtures)

Sand size 1.7 - 2.36 mm (2.0 mm)
154 mm diameter flume E = 18.4 mm (smooth bed)

Clay concent. (g/l)	Clay prop. %	Sand prop. %	Density ρ (Kg/m^3)	Crit. Shear Stress	
				τ_{01} (N/m^2)	τ_{02} (N/m^2)
30	0	100	1551	0.480	0.480
	15	85	1741	3.078	3.859
	20	80	1804	4.059	4.476
	25	75	1899	3.648	4.222
	30	70	1788	3.575	4.116
	40	60	1609	3.451	3.841
33	20	80	1822	4.553	5.787
36	20	80	1850	4.879	6.050
40	20	80	1805	5.211	7.567

TABLE G-6: INITIATION OF EROSION EXPERIMENTS (SYNTHETIC SEWER SEDIMENT)

(Laponite Clay-Sand-Water Mixtures)

Sand size 2.36 - 3.35 mm (2.9 mm)
154 mm diameter flume E = 18.4 mm (smooth bed)

Clay concent. (g/l)	Clay prop. %	Sand prop. %	Density ρ (Kg/m^3)	Crit. Shear Stress τ_{01} (N/m^2)	Crit. Shear Stress τ_{02} (N/m^2)
33	0	100	1517	0.690	0.690
	10	90	1615	3.726	5.450
	15	85	1720	3.894	5.447
	20	80	1805	4.132	5.203
	25	75	1890	3.974	5.176
	30	70	1793	3.506	5.393
36	20	80	1805	4.521	5.548
40	20	80	1821	4.707	7.726

APPENDIX H

LASER DOPPLER VELOCIMETRY
OPERATION OF THE IFA-550

APPENDIX H

LASER DOPPLER VELOCIMETER

H.1 Introduction

The advantage of non-intrusive measurement, high accuracy and repeatability make the Laser Doppler Velocimetry (LDV) technique specially suited for turbulence measurements.

The distinct properties of the gas laser are the spatial and temporal coherence. The spatial coherence describes the ability of the light field to form interference fringes in space. The temporal coherence on the other hand, describes the purity of the laser light.

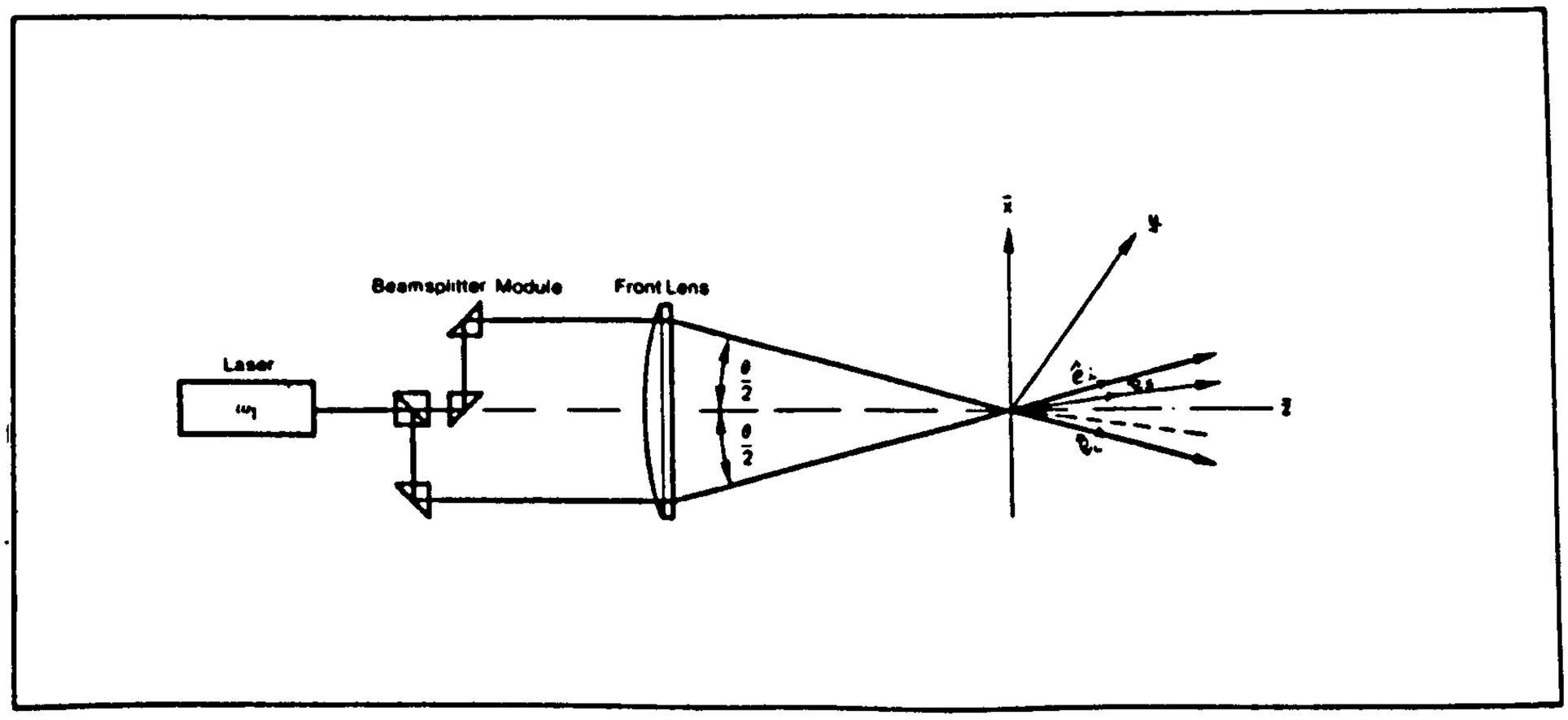

FIGURE H.1: LASER DOPPLER VELOCIMETER REPRESENTATION

A LDV consists of an optical system and an electronic processor. The optical system takes the laser beam and divides it into two

beams that intersect each other in the flow under investigation (see Fig. H.1) in what is known as the measuring volume. The light scattered from the small particles, moving with the flow through the measuring volume, is detected by the optical system (photodetector).

Because of the movement of the particles, the scattered light is of another frequency (Doppler effect). After finding the frequency shift of the detected signal, the processor converts it into velocity.

H.2 Theoretical Basis

The simplest way of explaining the nature of the laser Doppler signal is the fringe model. The two intersecting beam make up a fringe pattern (see Fig. H.2). Particles moving across the fringe scatter the light and a signal, consisting of light and dark regions, is detected. The time difference between the light peaks

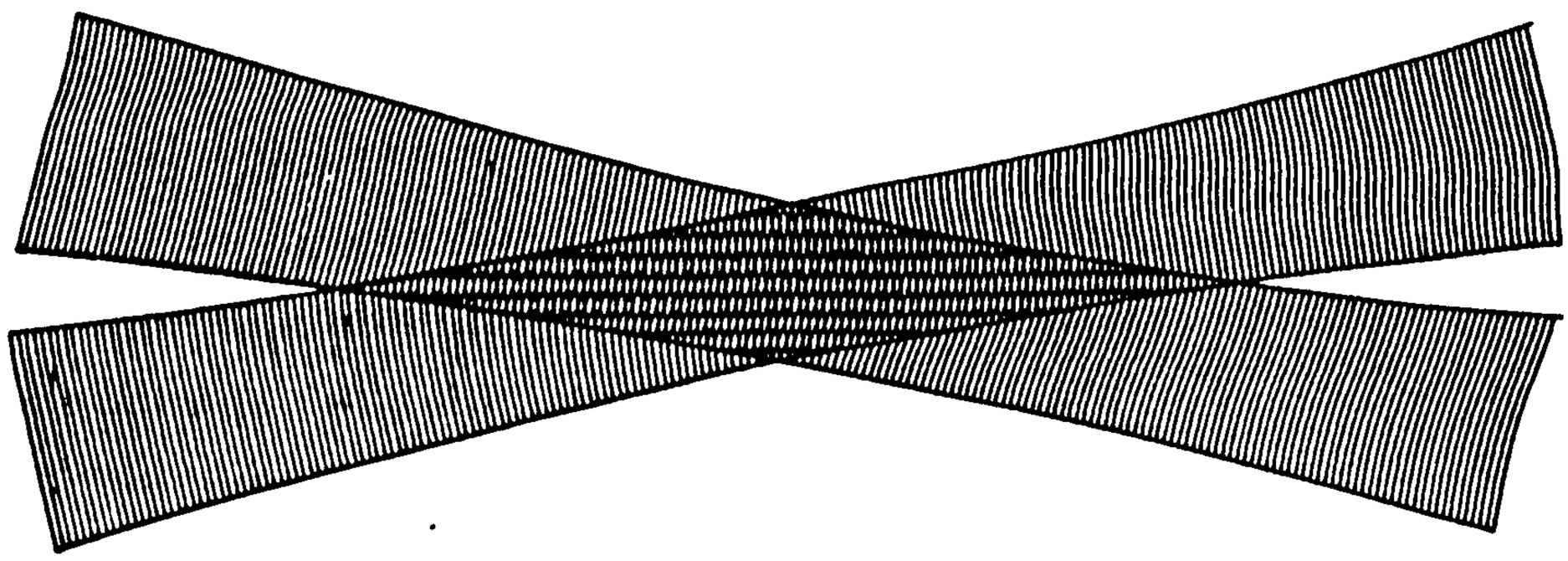

FIGURE H.2: FRINGE MODEL

is dependent on the velocity of the particles and the fringe spacing. The latter being determined by the optical setup, the laser light wavelength and the angle between the two incident beams. The fringe spacing is given by:

$$\delta_f = \frac{\lambda}{2} \sin(\theta/2) \qquad \text{(H.1)}$$

where λ is the laser light wavelength, θ the angle extended by the two incident beams. The Doppler frequency (f_D) is given by:

$$f_D = f_s - f_i = \frac{1}{\lambda} \vec{V} \cdot (\hat{e}_s - \hat{e}_i) \qquad \text{(H.2)}$$

where f_s and f_i are the frequencies of the scattered and incident beams respectively, $\vec{V}$ is the velocity vector of the particle passing through the measuring volume, and $\hat{e}_s$ and $\hat{e}_i$ are the unit vectors of the scattered and incident beam respectively.

By considering the velocity component in the direction of the flow f_D can be written as:

$$f_D = \frac{2Vx}{\lambda} \sin(\theta/2) \qquad \text{(H.3)}$$

and the velocity is given by:

$$Vx = \frac{\lambda \, f_D}{2 \sin(\theta/2)} \qquad \text{(H.4)}$$

where θ and λ are known parameters of the system and f_D is measured from the signal.

In practical situations there are other factors to take into consideration. For instance if there is more than one particle in the measuring volume the signal will not be the well defined dark and light regions. Or, for example to determine whether the particle is moving in the reverse direction, a frequency shift is added into one of the incident beams. Thus particles moving in one direction will show a Doppler frequency higher than the added frequency and particles moving in the opposite direction will show a lower frequency.

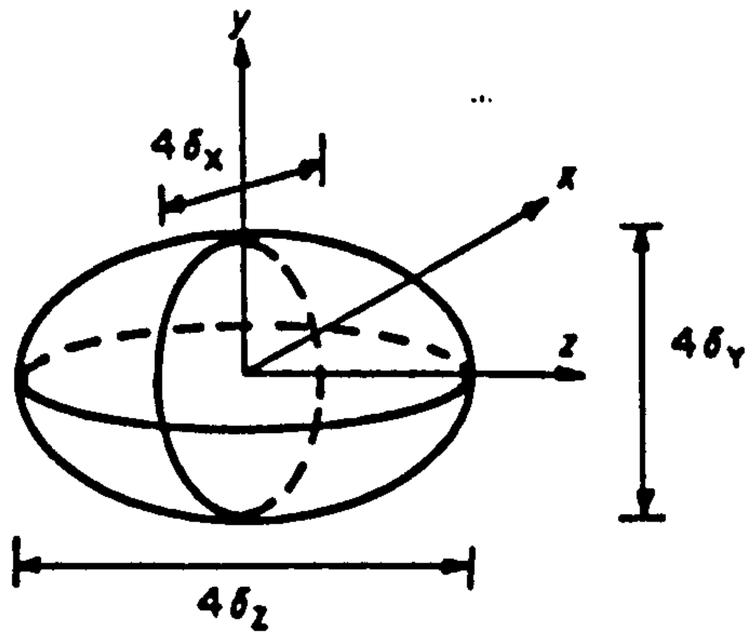

FIGURE A.3: PROBE VOLUME (ELLIPSOID)

In a laser beam operating in the fundamental optical mode Transverse Electromagnetic Mode (TEM), the measuring volume is an ellipsoid (see Fig. A.3). The TEM means that the laser may be focused to the smallest spot and the energy can be concentrated in a small measuring volume (i.e., the laser beam has a Gaussian intensity distribution). The probe volume parameters according to Fig. A.3 are:

$$2a = 4\delta_x = \frac{d_w}{\cos(\theta/2)} \qquad \text{(H.5)}$$

$$2b = 4\delta_y = d_w \qquad \text{(H.6)}$$

$$2c = 4\delta_z = \frac{d_w}{\sin(\theta/2)} \qquad \text{(H.7)}$$

where d_w is the diameter of the laser beam waist, which is

given by:

$$d_w = (4/\pi)(f\lambda/d_2) = (4/\pi)(f\lambda/(Ed_1)) \qquad (H.8)$$

where f is the focal distance of the optical system, d_1 is the beam waist diameter, d_2 is the expanded beam waist diameter, and E is the beam expansion ratio.

The number of fringes (N_f) is given by:

$$N_f = \frac{4D_2}{\pi d_2} = \frac{4ED_1}{\pi E d_1} \qquad (H.9)$$

where D_1 is the beams separation at front of lens and D_2 is the beams separation in the optics.

The performance of the LDA is described by the same parameters. It is related to the calibration constant, to the dimensions of the measuring volume and to the number and separation of the interference fringe lines in the measuring volume, and to the fixed characteristics of the LDA system such as laser beams separation, laser wavelength, beam expansion ratio and the measuring distance.

A3 Signal Processing

The main output of a LDV is a current pulse from the photodetector. The velocity information is present in the Doppler signal as a frequency modulation of the detector current. Thus the signal processing electronics work essentially as a frequency demodulator.

Two extreme type of signal can be encountered in practice. One is a quasi continuous signal due to multiple particles passing through the measuring volume. The envelope and phase of the signal contain random fluctuations as a result of the random number and positioning of the particles in the measuring volume. On the other extreme there is a burst of signal resulting from a single particle transversing the measuring volume.

Nevertheless, the processor must be able to detect real time information containing high frequency components in the presence of wide bandwidth noise (primary shot noise, from reflected and ambient light, noise from the photodetector and thermal noise from the processor).

H.4 Processor Used in the Experimental Work

A signal processor employed was a TSI intelligent flow analyzer for Laser Velocimetry model IFA-550. This processor was designed to extract velocity information from noisy signals derived from a LDA. A new approach for separating the signal from the noise, is applied in the operation of the processor. This gives the following features:

a) It makes only "good" (valid) measurements or makes no measurements at all.
b) It operates fully automatically and validates the maximum number of data possible.
c) It can process individual burst of Doppler signal as well as continuous signal with multiple changes in phase.

The processor accomplishes these features by using autocorrelation (i.e., autocorrelating the zero-crossings of the doppler signal); accurate time measurements (based on a counter type processor); and the feed-forward mechanism similar to that of a phase-locked-loop.

Operating principle
The processor determines the frequency of the Doppler signal produced by a LDV system by measuring the duration of eight continuous cycles of the Doppler signal. Then it divides the time by eight to obtain the period for one cycle of the Doppler signal and thus the frequency is determined. The processor then applies a special mathematical algorithm to test each zero-crossing of the signal. the test determines whether the signal meets the

predetermined minimum signal-to-noise ratio and satisfies the coherency conditions demanded by the properties of an autocorrelation of zero-crossings of Doppler signals. Only when 16 contiguous half-cycles have been validated by a comparison function a valid measurement is output.

The validated measurement is also fed back to the processor to be used as a criterion for measuring the next measurement. A search function is also available, which takes over when the processor looses the signal. Therefore the processor (IFA-550) gives only good measurements, selected according to a predetermined signal-to-noise ratio.

Because the processor operates on the zero-crossing of the signal is independent of its amplitude. And very often this means that it can validate a higher data rate compared to a counter-type-processor.

APPENDIX I

EINSTEIN-VANONI-BROOK WALL SEPARATION TECHNIQUE

APPENDIX I:

EINSTEIN-VANONI-BROOK WALL SEPARATION TECHNIQUE

I.1. Hydraulic Characteristics of Channels of Circular Cross-section with Flat Bed

a) Geometry of the Cross-section

The hydraulics of a channel of circular cross-section is characterised by the internal diameter (D), the longitudinal slope (S_o), the flow rate (Q), the flow depth (Y_o) and the roughness of the internal walls (k_s).

Assuming a channel of circular cross-section with a flat deposited sediment bed flowing part full under uniform flow conditions (see Fig. I.1) the geometric properties of the cross-section may be expressed in term of the angle 2θ and the thickness (E) of the deposited bed.

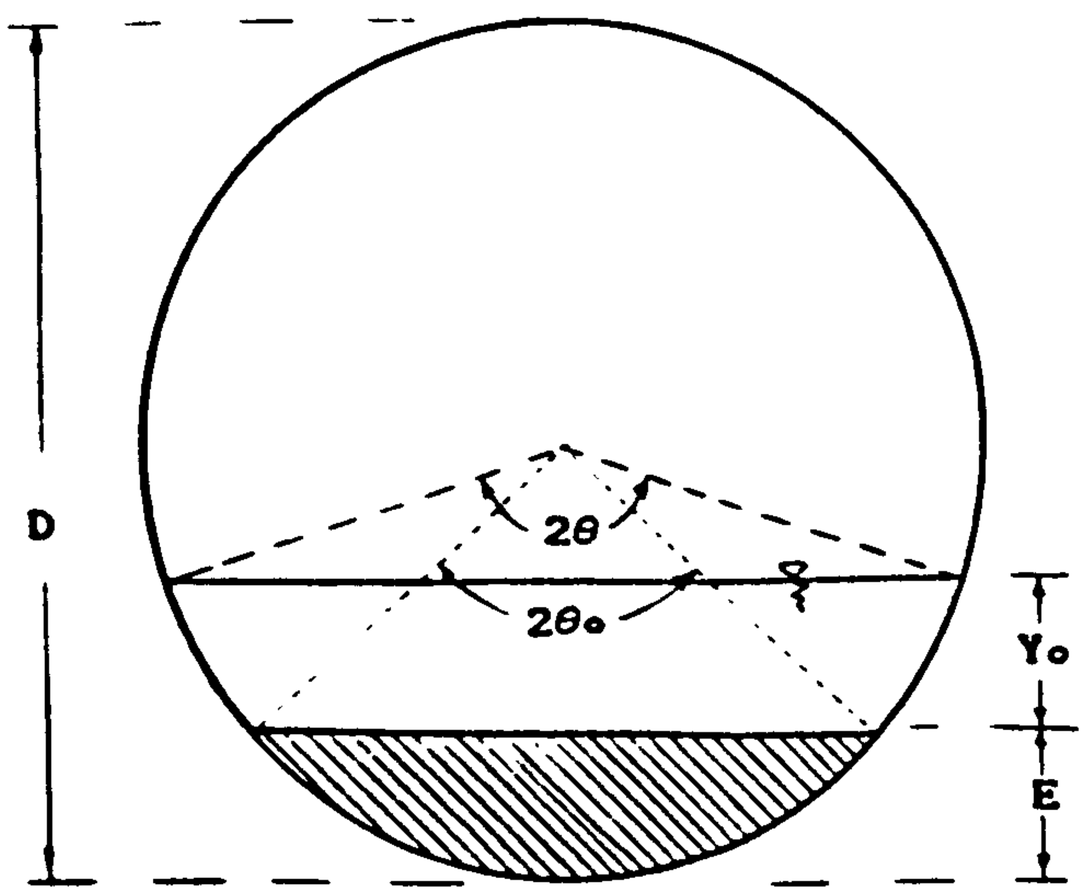

Figure I.1: Channel of circular cross-section with a flat sediment bed

the area is given by,

$$A = \frac{D^2}{4}\left(\theta - \frac{\mathrm{Sin}(2\theta)}{2}\right) - \frac{D^2}{4}\left(\theta_o - \frac{\mathrm{Sin}(2\theta_o)}{2}\right) \qquad (I.1)$$

and the wetted perimeter by

$$P = D(\theta - \theta_o + \sin\theta) \qquad (I.2)$$

thus, the hydraulic radius is given by:

$$R = A/P = \frac{D^2}{4}\left(\theta - \theta_o + \frac{\mathrm{Sin}(2\theta_o)}{2} - \frac{\mathrm{Sin}(2\theta)}{2}\right) \qquad (I.3)$$

b) Uniform Flow equations

In uniform flow the bed slope (S_o) is equal to the energy gradient (S_f). Combining Darcy-Weisbach and ColeBrook -White equations the following expression can be obtained:

$$V = -\sqrt{32\ g\ R\ S_o}\ \log\left(\frac{k_s}{14.8\ R} + \frac{2.51\ \nu}{2\ R\sqrt{32\ g\ R\ S_o}}\right) \qquad (I.4)$$

which can be used to compute the mean velocity of a given uniform flow . Manning's equation (1890) for uniform flow is

$$V = \frac{1}{n}\ R^{2/3}\ S_o^{1/2} \qquad (I.5)$$

and Chezy's equation (1768) is:

$$V = C\sqrt{R\ S_o} \qquad (I.6)$$

c) Shear stress exerted by the moving fluid

The basic mechanism responsible for sediment motion is the drag force exerted by the fluid flow on individual grains. This is the motivating force acting in the direction of flow. The shear stress restraining the fluid is distributed round the boundary of the cross-section and because of the shape of the cross-section and the presence of a free surface (on which the shear stress is negligibly small) the shear stress distribution is not uniform round the cross-section.

d) Channel of Composite Roughness

It is common to find in laboratory flumes that the wall surface is not as rough as the bed especially in dealing with sand beds. In order to minimize the effect of the wall a correction becomes necessary. In the literature several side-wall correction methods are available (Einstein 1942, Johnson 1942, Vanoni and Brook 1957).

Vanoni and Brook modified Johnson approach based on Darcy-Weisbach friction factor and made the following assumptions:

a) The channel cross-section can be divided into two sections (bed and wall) with corresponding wetted perimeter P_b and P_w being the boundary between the two section a surface of zero shear.

b) The mean velocities in the two sections are equal

c) Each section is considered independently.

d) The roughness in each section is homogeneous.

Assuming the pipe wall to be smooth Colebrook-White expression for smooth pipes,

$$\frac{1}{\sqrt{\lambda_w}} = 2 \text{ Log } \left\{ \frac{R_{ew} \sqrt{\lambda_w}}{2.51} \right\} \qquad \text{(I.7)}$$

can be used. Darcy's equation for head loss can be written as:

$$\frac{h_f}{L} = S_o = \frac{\lambda V^2}{8 g R} \qquad \text{(I.8)}$$

the velocity may be expressed as:

$$V^2 = \frac{8 g R S_o}{\lambda} \qquad \text{(I.9)}$$

Reynolds' number of the flow is:

$$R_e = \frac{4 R V}{\nu} \qquad \text{(I.10)}$$

combining equations I.9 and I.10 yields

$$V^3 = \left(\frac{8 g \nu S_o}{4} \right) \frac{R_e}{\lambda} \qquad \text{(I.11)}$$

Assuming equal velocities in the cross-section Eq. I.11 for the wall becomes:

$$V_w^3 = \left(\frac{8 g \nu S_o}{4} \right) \frac{R_{ew}}{\lambda_w} \qquad \text{(I.12)}$$

and for the bed:

$$V_b^3 = \left(\frac{8 g \nu S_o}{4} \right) \frac{R_{eb}}{\lambda_b} \qquad \text{(I.13)}$$

Thus from Eqs. I.11, I.12 & I.13 the following expression is obtained:

$$\frac{R_e}{\lambda} = \frac{R_{ew}}{\lambda_w} = \frac{R_{eb}}{\lambda_b} \qquad (I.14)$$

similarly substituting the corresponding values for the bed and for the wall in equation I.9 and equating the velocities yields,

$$\frac{A}{P\,\lambda} = \frac{A_w}{P_w\,\lambda_w} = \frac{A_b}{P_b\,\lambda_b} \qquad (I.15)$$

substituting $A = A_w + A_b$ and re-arranging terms equation I.15 becomes:

$$P\,\lambda = P_w\,\lambda_w + P_b\,\lambda_b \qquad (I.16)$$

For a given uniform flow generally the known parameters are:

$$V\ ,\ S_o\ ,\ g\ ,\ \nu\ ,\ P_w\ ,\ P_b\ ,\ A \text{ and } \lambda$$

and the main unknown

$$\lambda_b\ ,\ \lambda_w\ ,\ R_b \text{ and } R_w$$

This can be easily solved with a computer program using the above equations. With equations I.7 and I.14 a value for λ_w and R_{ew} can be found by iteration and then by using equation I.14 the value for λ_b is obtained. From Eq. I.9 the the hydraulic radius of the bed can be written as

$$R_b = \frac{\lambda_b\ V^2}{8\ g\ S_o} \qquad (I.17)$$

Therefore the shear stress exerted on the bed can be expressed as

$$\tau_b = \rho\ g\ R_b\ S_o \tag{I.18}$$

where R_b is the hydraulic radius corresponding to the channel bed (i.e. without the side wall effect).